frontiers | Research Topics

Value of a multidisciplinary approach for modern diagnosis of infectious diseases

Edited by
Stefano Marletta, Stefano Stracquadanio and Andrea Marino

Published in
Frontiers in Cellular and Infection Microbiology

ISSN 1664-8714
ISBN 978-2-8325-5738-9
DOI 10.3389/978-2-8325-5738-9

About Frontiers

Frontiers is more than just an open access publisher of scholarly articles: it is a pioneering approach to the world of academia, radically improving the way scholarly research is managed. The grand vision of Frontiers is a world where all people have an equal opportunity to seek, share and generate knowledge. Frontiers provides immediate and permanent online open access to all its publications, but this alone is not enough to realize our grand goals.

Frontiers journal series

The Frontiers journal series is a multi-tier and interdisciplinary set of open-access, online journals, promising a paradigm shift from the current review, selection and dissemination processes in academic publishing. All Frontiers journals are driven by researchers for researchers; therefore, they constitute a service to the scholarly community. At the same time, the *Frontiers journal series* operates on a revolutionary invention, the tiered publishing system, initially addressing specific communities of scholars, and gradually climbing up to broader public understanding, thus serving the interests of the lay society, too.

Dedication to quality

Each Frontiers article is a landmark of the highest quality, thanks to genuinely collaborative interactions between authors and review editors, who include some of the world's best academicians. Research must be certified by peers before entering a stream of knowledge that may eventually reach the public - and shape society; therefore, Frontiers only applies the most rigorous and unbiased reviews. Frontiers revolutionizes research publishing by freely delivering the most outstanding research, evaluated with no bias from both the academic and social point of view. By applying the most advanced information technologies, Frontiers is catapulting scholarly publishing into a new generation.

What are Frontiers Research Topics?

Frontiers Research Topics are very popular trademarks of the *Frontiers journals series*: they are collections of at least ten articles, all centered on a particular subject. With their unique mix of varied contributions from Original Research to Review Articles, Frontiers Research Topics unify the most influential researchers, the latest key findings and historical advances in a hot research area.

Find out more on how to host your own Frontiers Research Topic or contribute to one as an author by contacting the Frontiers editorial office: frontiersin.org/about/contact

Value of a multidisciplinary approach for modern diagnosis of infectious diseases

Topic editors

Stefano Marletta — University of Verona, Italy

Stefano Stracquadanio — University of Catania, Italy

Andrea Marino — University of Catania, Italy

Citation

Marletta, S., Stracquadanio, S., Marino, A., eds. (2024). *Value of a multidisciplinary approach for modern diagnosis of infectious diseases*. Lausanne: Frontiers Media SA. doi: 10.3389/978-2-8325-5738-9

Table of contents

05 Editorial: Value of a multidisciplinary approach for modern diagnosis of infectious diseases
Andrea Marino, Stefano Stracquadanio and Stefano Marletta

08 Diagnostic value of inflammatory indicators for surgical site infection in patients with breast cancer
Dongmei Li, Shanshan Ding, Jie Li, Xianglu Liao, Kun Ru, Lisheng Liu and Wenjing Shang

22 Diagnostic value of chemiluminescence for urinary lipoarabinomannan antigen assay in active tuberculosis: insights from a retrospective study
Luyi Huang, Yayan Niu, Li Zhang, Rong Yang and Meiying Wu

32 Comparison of metagenomic next-generation sequencing and blood culture for diagnosis of bloodstream infections
Juan Yu, Li Zhang, Deyu Gao, Jie Wang, Yi Li and Ning Sun

45 Sonication protocols and their contributions to the microbiological diagnosis of implant-associated infections: a review of the current scenario
Natally Dos Santos Silva, Beatriz Souza Toscano De Melo, Alessandra Oliva and Paulo Sérgio Ramos de Araújo

60 Weathering the storm: diagnosis and treatment of a life-threatening disseminated *Nocardia otitidiscaviarum* infection
Li-Yan Zhang, Liang Wang, Zeeshan Umar, Yuan-Hong Huang and Bing Gu

66 Real-time fluorescent multiple cross displacement amplification for rapid and sensitive *Mycoplasma pneumoniae* detection
Fei Xiao, Yu Zhang, Wenjian Xu, Jin Fu, Xiaolan Huang, Nan Jia, Chunrong Sun, Zheng Xu, Baoying Zheng, Juan Zhou, Yi Wang and Lihui Meng

80 Development of a novel sandwich immunoassay based on targeting recombinant Francisella outer membrane protein A for the diagnosis of tularemia
Jieun Jang, Do Hyung Kwon, Ju-Hong Jang, Dong-Gwang Lee, Seo-Hyuk Chang, Min-Young Jeon, Young-Su Jeong, Dong-Hyun Song, Jeong-Ki Min, Jong-Gil Park, Moo-Seung Lee, Baek-Soo Han, Wonjun Yang, Nam-Kyung Lee and Jangwook Lee

93 Comprehensive insights into UTIs: from pathophysiology to precision diagnosis and management
Swathi Sujith, Adline Princy Solomon and John Bosco Balaguru Rayappan

120 Aptamers: precision tools for diagnosing and treating infectious diseases
Swathi Sujith, Rajalakshmi Naresh, B. U. Srivisanth, Anusree Sajeevan, Shobana Rajaramon, Helma David and Adline Princy Solomon

152 Carbapenem-resistant *Klebsiella oxytoca* transmission linked to preoperative shaving in emergency neurosurgery, tracked by rapid detection via chromogenic medium and whole genome sequencing
Yun-Lan Jiang, Yi-Yu Lyu, Li-Li Liu, Zhi-Ping Li, Dan Liu, Jie-Hao Tai, Xiao-Qian Hu, Wen-Hui Zhang, Wen-Wen Chu, Xue Zhao, Wei Huang and Yi-Le Wu

frontiers | Frontiers in Cellular and Infection Microbiology

TYPE Editorial
PUBLISHED 15 November 2024
DOI 10.3389/fcimb.2024.1514207

OPEN ACCESS

EDITED AND REVIEWED BY
Sherry Dunbar,
Luminex, United States

*CORRESPONDENCE
Stefano Marletta
stefano.marletta92@gmail.com

†These authors have contributed equally to this work and share first authorship

RECEIVED 20 October 2024
ACCEPTED 23 October 2024
PUBLISHED 15 November 2024

CITATION
Marino A, Stracquadanio S and Marletta S (2024) Editorial: Value of a multidisciplinary approach for modern diagnosis of infectious diseases.
Front. Cell. Infect. Microbiol. 14:1514207.
doi: 10.3389/fcimb.2024.1514207

Editorial: Value of a multidisciplinary approach for modern diagnosis of infectious diseases

Andrea Marino[1†], Stefano Stracquadanio[2†] and Stefano Marletta[3,4*]

[1]Department of Clinical and Experimental Medicine, Unit of Infectious Diseases, ARNAS Garibaldi Hospital, University of Catania, Catania, Italy, [2]Department of Biomedical and Biotechnological Sciences, Section of Microbiology, University of Catania, Catania, Italy, [3]Division of Pathology, Humanitas Cancer Center, Catania, Italy, [4]Department of Diagnostics and Public Health, Section of Pathology, University of Verona, Verona, Italy

KEYWORDS

precision medicine, artificial intelligence, infectious disease, microbiology, pathology

Editorial on the Research Topic
Value of a multidisciplinary approach for modern diagnosis of infectious diseases

Editorial

Infectious diseases continue to pose significant challenges to global public health, exacerbating the burden on healthcare systems worldwide (Naghavi et al., 2024; La Via et al., 2024). The rise of antimicrobial resistance (AMR), the emergence of new pathogens, and the re-emergence of familiar ones have created an urgent need for innovative solutions in diagnosis and treatment. Infectious agents such as bacteria, viruses, fungi, and parasites cause a broad spectrum of diseases that account for a considerable percentage of global morbidity and mortality (Charalampous et al., 2023). Early and accurate diagnosis is essential for controlling outbreaks, improving patient outcomes, and curbing the misuse of antibiotics, which fuels resistance (Hahn et al., 2020; Saydam et al., 2021).

Traditional diagnostic methods, though valuable, often struggle to keep pace with the rapid evolution of pathogens and the complexity of infectious diseases (Vidyarthi et al., 2022). Techniques such as culture-based tests, even if reliable, are slow and can lack the sensitivity needed for early detection (Miller et al., 2024). Empirical treatments, frequently employed due to diagnostic delays, may be ineffective and contribute to resistance. In this context, precision diagnostics and novel therapeutic strategies have emerged as pivotal tools in infectious disease management, offering faster, more accurate, and more individualized approaches to tackling infections (Devrim et al., 2022).

Recent advances in molecular biology, bioinformatics, and biotechnology have given rise to precision diagnostic tools capable of addressing the shortcomings of conventional methods (Liu et al., 2023). Technologies like next-generation sequencing (NGS), aptamer-based diagnostics, and advanced immunoassays are revolutionizing the way we diagnose infections. These tools can detect pathogens with greater sensitivity and specificity, even in

cases where traditional methods fall short. Furthermore, the advent of real-time, point-of-care diagnostic systems (Stracquadanio et al., 2021) has made it possible to deliver rapid, actionable results, transforming the way clinicians approach treatment.

At the intersection of diagnostics and therapeutics, precision tools are also playing a crucial role in developing targeted treatments. Aptamers, for example, are nucleic acid-based molecules that can be engineered to bind specific pathogens or toxins, offering a highly selective and effective means of both diagnosing and neutralizing infections. Additionally, technologies such as metagenomics and sonication protocols are expanding our understanding of microbial communities and biofilms, leading to more effective interventions against chronic and resistant infections.

This Research Topic brings together ten articles that explore cutting-edge developments in the use of precision tools for diagnosing and treating infectious diseases. From advancements in rapid diagnostic assays to innovative approaches in therapeutic intervention, the contributions in this Research Topic illustrate the potential of these tools to reshape the landscape of infectious disease management. Whether addressing the diagnostic challenges of bloodstream infections, optimizing the identification of pathogens in surgical site infections, or exploring novel diagnostic markers for rare diseases, the research presented here is a testament to the progress being made in the field.

By integrating precision diagnostics and targeted therapies, we are entering a new era in infectious disease management—one where personalized care can lead to better outcomes, reduced transmission, and more efficient use of resources. As we move forward, continued research and innovation in this domain will be critical in our ongoing efforts to control and eventually eliminate the global threat of infectious diseases.

Advancements in diagnostic technologies

The shift toward rapid, accurate diagnostic techniques is a focal point of this Research Topic. Aptamer-based technologies, as discussed by Sujith et al., offer a promising approach by providing high specificity and sensitivity, surpassing traditional antibody-based methods. Their structural robustness makes them highly suitable for long-term storage and application in molecular diagnostics. Similarly, the study by Xiao et al. presents a novel real-time fluorescent multiple cross displacement amplification technique for *Mycoplasma pneumoniae* detection, providing a rapid and sensitive alternative for point-of-care settings, which could prove invaluable in resource-limited regions.

Next-generation sequencing and metagenomics

Metagenomic next-generation sequencing (mNGS) is revolutionizing the way bloodstream infections (BSIs) are diagnosed. Yu et al. highlight the advantages of mNGS in detecting pathogens in plasma samples, showing superior performance compared to traditional blood cultures, particularly for gram-negative bacteria. This method represents a critical step forward in reducing diagnostic delays and improving outcomes in sepsis management.

Therapeutic implications and resistance challenges

The emergence of drug-resistant pathogens, such as carbapenem-resistant *Klebsiella oxytoca* in emergency neurosurgical settings, as explored by Jiang et al., underscores the importance of timely and precise interventions. The study traces the transmission of resistant bacteria, identifying the contamination source and advocating for standardized infection control procedures (El-Sokkary et al., 2022; Marino et al., 2023).

Similarly, the research by Zhang et al. on *Nocardia otitidiscaviarum* infection demonstrates the life-saving potential of early diagnosis and tailored treatments in managing rare but deadly infections. This case further emphasizes the role of advanced laboratory techniques, such as metagenomic sequencing and mass spectrometry, in diagnosing complex infectious diseases.

Emerging diagnostic tools

Innovative diagnostic assays, such as the chemiluminescence-based urinary lipoarabinomannan (LAM) antigen assay for tuberculosis detection, are advancing the field. Huang et al. report the assay's high specificity for extrapulmonary tuberculosis (EPTB), offering a non-invasive and efficient diagnostic tool that could reduce mortality, especially in settings where conventional methods fall short.

Moreover, the development of a sandwich immunoassay targeting *Francisella tularensis* outer membrane protein A for tularemia diagnosis, as described by Jang et al., represents a leap forward in addressing bioterrorism-related pathogens. This assay's high sensitivity and specificity could have far-reaching applications in public health and biodefense.

Future directions and broader implications

The articles in this Research Topic collectively highlight the necessity of adopting precision tools in diagnosing and treating infectious diseases. From real-time diagnostics to the identification of resistance mechanisms, the work presented here advances our understanding of pathogen detection and management. Looking ahead, the integration of these novel technologies with further technological developments such as artificial intelligence-based tools (Marletta et al., 2023) into clinical practice will be crucial in

addressing the growing threat of infectious diseases and antimicrobial resistance.

We extend our sincere gratitude to all the contributors for their valuable insights and groundbreaking research, and we hope this Research Topic will inspire further advancements in the fight against infectious diseases.

Author contributions

AM: Conceptualization, Methodology, Writing – original draft. SS: Conceptualization, Methodology, Writing – original draft. SM: Conceptualization, Methodology, Writing – original draft.

Conflict of interest

The authors declare that the research was conducted in the absence of any commercial or financial relationships that could be construed as a potential conflict of interest.

Publisher's note

References

Charalampous, P., Haagsma, J. A., Jakobsen, L. S., Gorasso, V., Noguer, I., Padron-Monedero, A., et al. (2023). Burden of infectious disease studies in Europe and the United Kingdom: a review of methodological design choices. *Epidemiol. Infect.* 151, e19. doi: 10.1017/S0950268823000031

Devrim, I., Erdem, H., El-Kholy, A., Almohaizeie, A., Logar, M., Rahimi, B. A., et al. (2022). Analyzing central-line associated bloodstream infection prevention bundles in 22 countries: The results of ID-IRI survey. *Am. J. Infect. Control* 50, 1327–1332. doi: 10.1016/j.ajic.2022.02.031

El-Sokkary, R., Erdem, H., Kullar, R., Pekok, A. U., Amer, F., Grgić, S., et al. (2022). Self-reported antibiotic stewardship and infection control measures from 57 intensive care units: An international ID-IRI survey. *J. Infect. Public Health* 15, 950-954. doi: 10.1016/j.jiph.2022.07.009

Hahn, A., Podbielski, A., Meyer, T., Zautner, A. E., Loderstädt, U., Schwarz, N. G., et al. (2020). On detection thresholds-a review on diagnostic approaches in the infectious disease laboratory and the interpretation of their results. *Acta Trop.* 205, 105377. doi: 10.1016/j.actatropica.2020.105377

La Via, L., Sangiorgio, G., Stefani, S., Marino, A., Nunnari, G., Cocuzza, S., et al. (2024). The global burden of sepsis and septic shock. *Epidemiol. (Basel Switzerland)* 5, 456–478. doi: 10.3390/epidemiologia5030032

Liu, Q., Jin, X., Cheng, J., Zhou, H., Zhang, Y., and Dai, Y. (2023). Advances in the application of molecular diagnostic techniques for the detection of infectious disease pathogens (Review). *Mol. Med. Rep.* 27, 104. doi: 10.3892/mmr.2023.12991

Marino, A., Stracquadanio, S., Campanella, E., Munafò, A., Gussio, M., Ceccarelli, M., et al. (2023). Intravenous fosfomycin: A potential good partner for cefiderocol. Clinical experience and considerations. *Antibiotics* 12 (1), 49. doi: 10.3390/antibiotics12010049

Marletta, S., L'Imperio, V., Eccher, A., Antonini, P., Santonicco, N., Girolami, I., et al. (2023). Artificial intelligence-based tools applied to pathological diagnosis of microbiological diseases. *Pathol. Res. Pract.* 243, 154362. doi: 10.1016/j.prp.2023.154362

Miller, J. M., Binnicker, M. J., Campbell, S., Carroll, K. C., Chapin, K. C., Gonzalez, M. D., et al. (2024). Guide to utilization of the microbiology laboratory for diagnosis of infectious diseases: 2024 update by the infectious diseases society of america (IDSA) and the american society for microbiology (ASM). *Clin. Infect. Dis.* 5, ciae104. doi: 10.1093/cid/ciae104

Naghavi, M., Vollset, S. E., Ikuta, K. S., Swetschinski, L. R., Gray, A. P., Wool, E. E., et al. (2024). Global burden of bacterial antimicrobial resistance 1990-2021: a systematic analysis with forecasts to 2050. *Lancet (London England)* 404, 1199–1226.

Saydam, F. N., Erdem, H., Ankarali, H., El-Arab Ramadan, M. E., El-Sayed, N. M., Civljak, R., et al. (2021). Vector-borne and zoonotic infections and their relationships with regional and socioeconomic statuses: An ID-IRI survey in 24 countries of Europe, Africa and Asia. *Travel Med. Infect. Dis.* 44, 102174. doi: 10.1016/j.tmaid.2021.102174

Stracquadanio, S., Di Gaudio, F., Giunta, E., Falliti, G., Caruso, D., Pinzone, C., et al. (2021). Reverse transcriptase loop-mediated isothermal amplification (RT-LAMP) as a user-friendly system to detect SARS-CoV-2 infection: a multicentric study. *New Microbiol.* 44, 181–183. Available at.

Vidyarthi, A. J., Das, A., and Gupta, A. (2022). Revisiting conventional microbiology techniques in the era of molecular testing. *Curr. Med. Res. Pract.* 12, 274–279. doi: 10.4103/cmrp.cmrp_60_22

frontiers | Frontiers in Cellular and Infection Microbiology

TYPE Original Research
PUBLISHED 25 October 2023
DOI 10.3389/fcimb.2023.1286313

OPEN ACCESS

EDITED BY
Stefano Marletta,
University of Verona, Italy

REVIEWED BY
Paola Chiara Rizzo,
Integrated University Hospital Verona, Italy
Nicoló Caldonazzi,
University of Verona, Italy
Vittoria Moscatt,
Garibaldi Hospital, Italy

*CORRESPONDENCE
Wenjing Shang
17865136693@163.com

RECEIVED 31 August 2023
ACCEPTED 05 October 2023
PUBLISHED 25 October 2023

CITATION
Li D, Ding S, Li J, Liao X, Ru K, Liu L and Shang W (2023) Diagnostic value of inflammatory indicators for surgical site infection in patients with breast cancer. *Front. Cell. Infect. Microbiol.* 13:1286313. doi: 10.3389/fcimb.2023.1286313

Diagnostic value of inflammatory indicators for surgical site infection in patients with breast cancer

Dongmei Li, Shanshan Ding, Jie Li, Xianglu Liao, Kun Ru, Lisheng Liu and Wenjing Shang*

Department of Clinical Laboratory, Shandong Cancer Hospital and Institute, Shandong First Medical University and Shandong Academy of Medical Sciences, Jinan, Shandong, China

Background: Breast cancer is the most commonly diagnostic cancer in women worldwide. The main treatment for these patients is surgery. However, there is a high incidence of surgical site infection (SSI) in breast cancer patients. The aim of this study was to identify effective infection-related diagnostic markers for timely diagnosis and treatment of SSI.

Methods: This retrospective study included 263 breast cancer patients who were treated between July 2018 and March 2023 at the Shandong Cancer Hospital and Institute. We analyzed differences between the SSI group and control group and differences before and during infection in the SSI group. Finally, we tested the distribution of pathogenic microorganisms and their susceptibility to antibiotics.

Results: Compared with preoperative inflammatory indicators, white blood cells (WBC), neutrophils (NEU), absolute neutrophil count to the absolute lymphocyte count (NLR), D2 polymers (D-Dimer) and fibrinogen (FIB) were significantly increased, while lymphocytes (LYM), albumin (ALB) and prealbumin (PA) were significantly decreased in the SSI group. Compared with uninfected patients, WBC, NEU, NLR and FIB were significantly increased, ALB and PA were significantly decreased in SSI patients, while LYM and D-Dimer did not differ significantly. The distribution of infection bacteria in SSI patients showed that the proportion of patients with *Staphylococcus aureus* infection was as high as 70.41%; of those patients, 19.33% had methicillin-resistant *Staphylococcus aureus* (MRSA) infection. The area under the curves (AUCs) of the receiver operating curves (ROCs) for WBC, NEU, NLR, FIB, ALB and PA were 0.807, 0.811, 0.730, 0.705, 0.663 and 0.796, respectively. The AUCs for other inflammatory indicators were not statistically significant. There was no significant difference in antibiotic resistance for *Staphylococcus aureus* when compared to that of gram-positive bacteria. The resistance of gram-positive bacteria to ceftriaxone (CRO), cefoxitin (FOX), chloramphenicol (CHL), minocycline (MNO) and tetracycline (TCY) was lower than that of gram-negative bacteria, while the resistance to gentamicin (GEN) was higher.

Conclusion: This study demonstrated that WBC, NEU, NLR, FIB and PA have good predictive value for identifying patients at risk of SSI. The cut-off values of inflammatory indicators can be helpful in the prevention and diagnosis of SSI.

KEYWORDS

SSI, inflammatory indicators, *Staphylococcus aureus*, antibiotic resistance, breast cancer, diagnostic value

1 Introduction

Female breast cancer is the leading cause of global cancer incidence, with an estimated 2.3 million new cases each year, thus representing 11.7% of all new cancer cases (Sung et al., 2021). Effective treatments are critical for the prognosis and survival of patients with breast cancer (Maajani et al., 2019). Mastectomy is regarded as a routine surgical procedure for patients with breast cancer. However, SSI after breast surgery can lead to very poor consequences, such as poor outcomes and delayed access to chemotherapy and radiation therapy (Tejirian et al., 2006; Bernier, 2015). The factors influencing SSI have been classified into patient characteristics and surgical related-process, including age, body mass index (BMI), smoking, diabetes mellitus, preoperative treatment, the size of the resection site, prosthesis implantation, tumor progression and metastasis (El-Tamer et al., 2007; Committee on Gynecological Practice, 2015; Zhang et al., 2020). Moreover, evidence has shown that the five-year risk of breast cancer recurrence may be higher in case of SSI (Savioli et al., 2020; Wu et al., 2022). Therefore, it is necessary to identify rapid and effective inflammatory indicators for diagnosing SSI if we are to manage the treatment of patients with breast cancer in a timely manner.

Blood samples have several advantages for the analysis of biomarkers; for example, the blood can be assessed easily in a manner that is not traumatic for the patient. Therefore, the identification of relevant biomarkers of infection in blood samples represents a particularly exciting focus for research (Li et al., 2023). There are several classic infection-related indicators, particularly are procalcitonin (PCT) and C-reactive-protein (CRP) (Ruan et al., 2018; Stocker et al., 2021). Under normal conditions, thyroid C cells and adipose cells secrete and produce hormonally active PCT (Tan et al., 2021). The plasma levels of PCT are known to be increased in severe bacterial, fungal, and parasitic infections, as well as in sepsis and multiple organ failure (Kyriazopoulou et al., 2021). The levels of CRP are known to increase rapidly in blood plasma during infection or tissue damage (Sheinenzon et al., 2021; Cooper et al., 2023). CRP can activate complement and strengthen phagocytic cells, thus increasing the body's ability to remove pathogenic microorganisms and damaged, necrotic, apoptosis cells. Thus, CRP plays an important protective role in the natural immune process of the body (Ngwa and Agrawal, 2019). It is also possible that WBC, NEU, and NLR in blood plasma could represent informative biomarkers for patients with infection (Christensen et al., 2013; Russell et al., 2019). In addition, indicators related to blood clotting function have also been closely linked to infection. For example, the levels of D-Dimer in patients with *Mycoplasma pneumoniae* pneumonia are known to increase; furthermore, patients with high levels of D-Dimer had more severe clinical manifestations and required longer duration of treatment (Zheng et al., 2021). Fibrinogen is an acute phase reaction proteins and is known to be elevated during infection (Engelmann and Massberg, 2013). Moreover, nutritional indicators including PA and ALB can play an important role in reducing the risk of SSI and postoperative complications (Zhou et al., 2017; Roche et al., 2018).

The distribution of microflora exhibits unique characteristics in breast cancer patients with SSI. Gram-positive bacteria have a higher rate of infection than Gram-negative bacteria, and *Staphylococcus aureus* has the highest probability of infection (Felippe et al., 2007; O'Connor et al., 2020). Prior to surgery for breast cancer, clinicians routinely prescribe antibiotics to prevent SSI. However, some studies have shown that the preoperative use of antibiotics has no direct benefit in reducing the risk of SSI in breast cancer patients (Zhang et al., 2020; Stallard et al., 2022). Furthermore, the overuse of antibiotics can increase bacterial resistance and leads to infections that are more difficult to treat; this can lead to poor outcome for the patients involved (Segura-Egea et al., 2017). Therefore, diagnosing or predicting SSI early and accurately will significantly improve clinical outcomes and reduce the overuse of antibiotics (Celik et al., 2022).

In this study, we analyzed changes in the levels of inflammatory indicators before and during SSI in a cohort of patients undergoing surgery for breast cancer. In addition, we also compared changes of inflammatory markers in breast cancer patients with surgical infection and those without surgical infection. By performing these analyses, we were able to explore the diagnostic efficacy of inflammatory indicators in SSI. Next, we analyzed different types of bacteria, the changes of inflammatory indicators caused by different

Abbreviations: SSI, surgical site infection; WBC, white blood cells; NEU, neutrophils; LYM, lymphocytes; NLR, absolute neutrophil count to the absolute lymphocyte count; D-Dimer, D2 polymers; FIB, fibrinogen; ALB, albumin; PA, prealbumin; MRSA, methicillin-resistant *Staphylococcus aureus*; ROC, the receiver operating curve; AUC, the area under the curve; CRO, ceftriaxone; FOX, cefoxitin; CHL, chloramphenicol; MNO, minocycline; TCY, tetracycline; OXA, oxacillin; CIP, ciprofloxacin; LVX, levofloxacin; GEN, gentamicin; BMI, body mass index.

bacteria, and the antibiotic resistance of different bacteria. Our overall goal was to provide timely and effective treatment for breast cancer patients with SSI.

2 Materials and methods

2.1 Participants

We conducted a retrospective study of breast cancer patients who underwent breast surgery between July 2018 and March 2023 at the Shandong Cancer Hospital and Institute. Electronic medical records and the Ruimei Laboratory Information System version 6.0 (rmlis, Huangpu District, Shanghai, China) were used to collect clinical information. SSIs were identified by the Centers for Disease Control and Prevention/National Healthcare Safety Network (CDC/NHSN) surveillance definition of health care-associated infections (Horan et al., 2008). SSI occurred within 30 days after surgery. SSI needs to meet at least one of the following conditions (1): pathogenic microorganisms isolated from cultures (2); purulent drainage from the incision (3); presence of at least one of the following symptoms of infection: localized swelling, heat, pain or erythema (4); diagnosis of SSI by the surgeon. This study involved 466 breast cancer patients. 153 patients were excluded because duplicate or insufficient data. Another 50 patients were excluded due to the infection was not at the surgical site or was not caused by the surgery. Finally, 169 patients were classified into SSI group and 94 patients were classified into control group. SSI was diagnosed on the basis of information from electronic medical records, including clinical symptoms, histopathology, microbiological culture, sensitivity results and medication charts. The studies involving human participants were reviewed and approved by the Ethics Committee of the Shandong Cancer Hospital and Institute. The patients/participants provided their written informed consent to participate in this study.

2.2 Analysis of inflammatory indicators

The data used in this study were collected from electronic medical records and the Ruimei Laboratory Information System. An automatic hematological analyzer Sysmex XN9000 (Sysmex Corporation, Kobe, Japan) was utilized to analyze blood cells. The normal reference ranges of WBC, NEU, LYM and NLR were 3.5 - 9.5×10^9, 1.8 - 6.3×10^9, 1.1 - 3.2×10^9 and 1.0 - 2.0, respectively. D-Dimer and FIB was analyzed with an ACL 750 system (Chicago, IL, USA). The reference ranges of D-Dimer and FIB were 0 - 1 mg/L and 2 - 4 g/L, respectively. ALB, PA and hsCRP were analyzed using a Beckman Coulter analyzer AU5800 (Beckman Coulter, CA, USA). The reference ranges of ALB and PA were 40 - 55 g/L and 0.25 - 0.4 g/L, respectively. An hsCRP level < 10 mg/L was considered to indicate no systemic infection. A COBAS E801 immunoassay analyzer (Roche Diagnostics GmbH, Mannheim, Germany) was used to quantify PCT. The levels of PCT should be < 0.05 μg/L in healthy individuals. Blood tests were performed when the patient had signs and symptoms of infection. All the above tests were carried out according to the manufacturer's instructions.

2.3 Culture and identification of microorganisms

Samples used for culture included puncture fluid, drainage fluid, tissue, wound secretion, pus and wound swab. Samples were inoculated on Columbia Blood Agar Plates, Chocolate Agar Plates and MacConkey Agar Plates and a BRUKER microflex MALDI TOF/TOF Mass Spectrometer (BRUKER Corporation, Massachusetts, USA) was used to identify microorganism from cultured samples. A BD Phoenix M50 automated microbial system (Becton, Dickinson and Company, New Jersey, USA) was used to perform antimicrobial susceptibility tests. The procedures were performed in accordance with the manufacturer's instructions and the BC standards of the Clinical Laboratory Standards Institute.

2.4 Statistical analysis

Statistical analyses were performed using SPSS software version 23.0 (SPSS, IL, USA) and GraphPad Prism version 9.0 (GraphPad Software, CA, USA). Comparisons of non-normally distributed data were analyzed by Mann-Whitney U tests. Comparisons of normally distributed data were performed by t tests. ROC curves were used to estimate the diagnostic value of inflammatory indicators. Youden's index was used to determine cut-off points by optimally balancing sensitivity and specificity. $p < 0.05$ was considered statistically significant.

3 Results

3.1 Demographics and clinical characteristics of the study population

A total of 466 breast cancer patients who underwent breast surgery were included in this study. Of the eligible patients, 169 were classified into SSI group and 94 were classified into control group Figure 1. More than 70% of patients were under the age of 60 years. 262 females and 1 male were included in this study. We found that arterial hypertension, diabetes mellitus, preoperative therapy, excision mode, prosthesis implantation, tumor histopathological feature and prophylactic antibiotics were not significantly correlated with SSI. However, we did find that BMI was significantly correlated with SSI. Detailed characteristics of the subjects are shown in Table 1.

3.2 Changes of inflammatory indicators before and during SSI in the same breast cancer patients

First, we identified inflammatory indicators associated with SSI by assessing a range of indicators before and during SSI in the same

10.3389/fcimb.2023.1286313

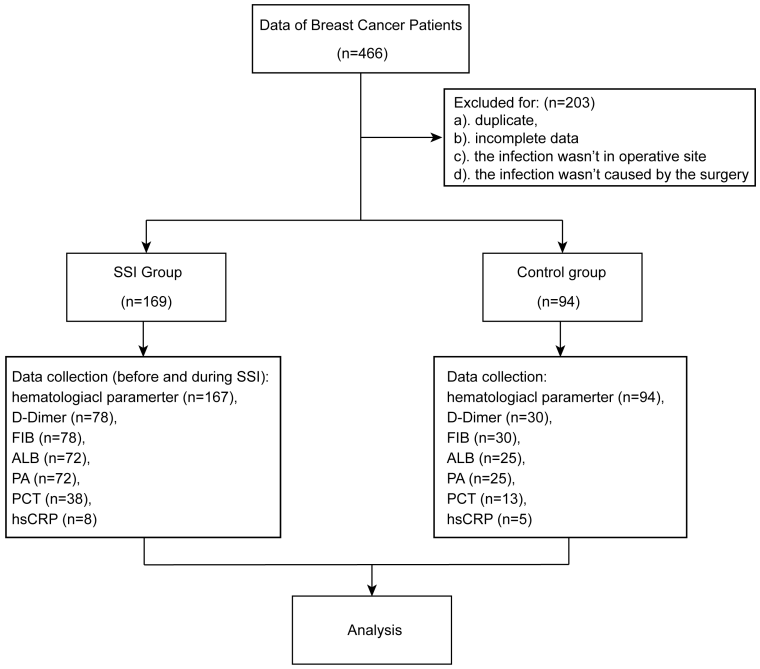

FIGURE 1
Flow diagram of case collection.

TABLE 1 Clinical parameters of breast cancer patients.

Clinical parameters	SSI (n=169)	Control group (n=94)	*p*-Value
Age, years, n (%)			0.1376
<60	122 (72.19)	71 (75.53)	
≥60	47 (27.81)	23 (24.47)	
Gender, n (%)			0.1736
Male	1 (0.59)	0 (0)	
Female	168 (99.41)	94 (100)	
Arterial hypertension, n (%)			0.1709
Yes	37 (21.89)	20 (21.28)	
No	132 (78.11)	74 (78.72)	
Body Mass Index, n (%)			0.0141
>25	119 (70.41)	80 (85.11)	
<25	50 (29.59)	14 (14.89)	
Diabetes mellitus			0.1538
Yes	20 (11.83)	8 (8.51)	
No	149 (88.17)	86 (91.49)	
Preoperative therapy			0.1935
Yes	29 (17.16)	18 (19.15)	
No	140 (82.84)	76 (80.85)	
Excision mode			0.1439

(Continued)

10.3389/fcimb.2023.1286313

TABLE 1 Continued

Clinical parameters	SSI (n=169)	Control group (n=94)	*p*-Value
Partial excision	19 (11.24)	6 (6.38)	
Total excision	150 (88.76)	88 (93.62)	
Surgery			0.2029
Unilateral surgery	19 (11.24)	14 (14.89)	
Bilateral surgery	150 (88.76)	80 (85.11)	
Prosthesis implantation			0.1863
Yes	10 (5.92)	7 (7.45)	
No	159 (94.08)	87 (92.55)	
Lymphatic metastasis			0.5000
Yes	96 (56.80)	47 (50.00)	
No	73 (43.20)	47 (50.00)	
Carcinoma histology			0.1912
Invasive ductal	147 (86.98)	81 (86.17)	
Non-invasive	18 (10.65)	13 (13.83)	
Invasive lobular	4 (2.37)	0	
ASA Score			0.0720
I or II	136 (80.47)	88 (93.62)	
≥ III	33 (19.53)	6 (6.38)	
Tumor size(cm)			0.3767
≤2	36 (21.30)	37 (39.36)	
2-5	41 (24.26)	20 (21.28)	
>5	92 (54.44)	37 (39.36)	
Prophylactic antibiotics			0.2174
Yes	156 (92.31)	81 (86.17)	
No	13 (7.69)	13 (13.83)	

patients with breast cancer. Analysis showed that the levels of WBC, NEU, NLR, D-Dimer and FIB were significantly higher during SSI than in control subjects (Figures 2A-E). However, the levels of LYM, ALB and PA were lower during SSI than the non-infected control subjects (Figures 2F-H). Detailed information, including the median levels and ranges of inflammatory indicators are presented in Table 2.

3.3 Changes of inflammatory indicators in SSI and control groups

In order to better explore the changes of inflammatory indicators in breast patients undergoing surgery, we divided patients into SSI group and a postoperative control group according to whether they developed surgery site infection or not. We found that the levels of WBC, NEU, NLR and FIB were significantly higher, while ALB and PA were lower in the SSI group than those in the control group (Figures 3A-F). There were no significant between-group differences for the levels of LYM and D-Dimer (Figures 3G, H). The median levels and ranges of inflammatory indicators are shown in Table 3. Only a small amount of PCT and hsCRP data were available; however, analysis showed that there was no significant difference between the SSI and control groups in terms of PCT and hsCRP (Figure S1).

3.4 Pathogenic microorganisms and infections

Next, we analyzed the distribution of pathogenic microorganisms responsible for infected in the breast patients with SSI. Analysis showed that *Staphylococcus aureus* accounted for the highest proportion (up to 70.41%), followed by *Staphylococcus epidermidis* (11.24%); gram-negative bacteria accounted for only 11.24%. In addition, 2.37% of patients had

10.3389/fcimb.2023.1286313

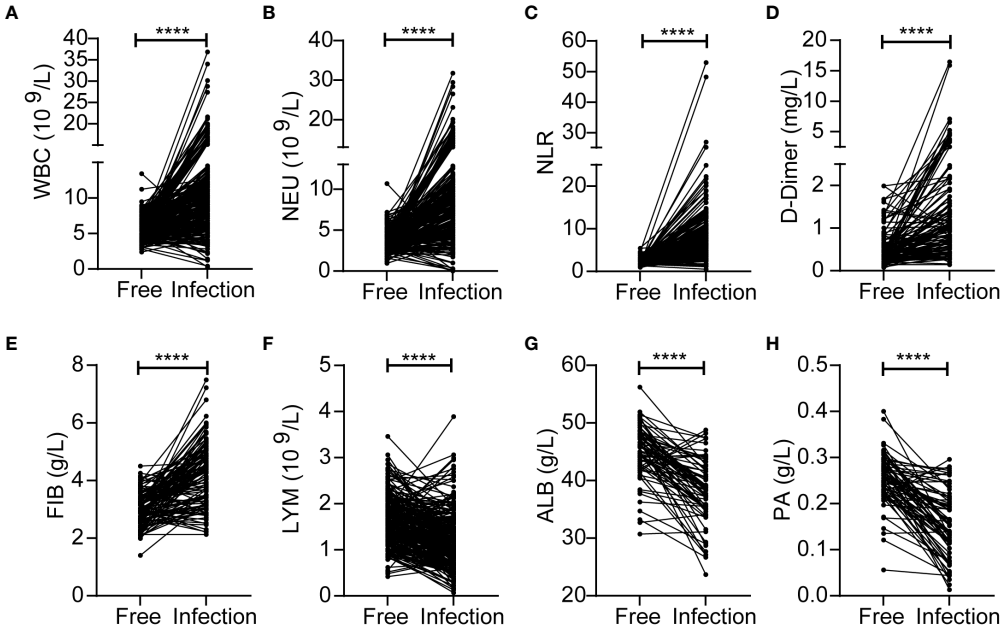

FIGURE 2
Changes of inflammatory indicators before and during SSI in the breast cancer patients with SSI. The levels of WBC **(A)**, NEU **(B)**, NLR **(C)**, D-Dimer **(D)**, FIB **(E)**, LYM **(F)**, ALB **(G)**, PA **(H)**. ****$p < 0.0001$.

infections caused by two different types of bacteria (Figure 4A). Details of bacterial distribution are shown in Table 4. Importantly, of the patients infected with *Staphylococcus aureus*, 19.32% had MRSA (Figure 4B), thus highlighting the urgent need to develop methods to diagnose and treat infection as early as possible.

Next, we analyzed the effects of different types of bacterial infections on various inflammatory indicators. The increase of WBC, NEU and FIB after infection with *Staphylococcus aureus* was greater than that of coagulase-negative *Staphylococcus* and gram-negative bacteria (Figures 5A-C). The increase of NLR after infection with *Staphylococcus aureus* was greater than that of gram-negative bacteria (Figure 5D). In addition, PA levels were significantly higher after infection with gram-negative bacteria than after infection with *Staphylococcus aureus* (Figure 5E). Distinct types of bacterial infection had no significant effects on the levels of LMY, D-Dimer and ALB (Figures 5F-H). The changes and ranges of various inflammatory indicators between different bacterial infections are shown in Table 5. Due to the small amount of data available for PCT and hsCRP, we were unable to identify any significant changes associated with *Staphylococcus aureus* and other bacterial infections (Figure S2).

3.5 Diagnostic utility of inflammatory indicators

We constructed ROC curves to evaluate the diagnostic utility of inflammatory indicators in breast cancer patients. The results showed that in the SSI group, WBC and NEU had discriminative power, with AUCs of 0.807 and 0.811, respectively, when compared with the control group (Figures 6A, B). For NLR, FIB, ALB and PA, the AUCs were 0.73, 0.705, 0.663 and 0.796, respectively

TABLE 2 Comparison of inflammatory indicators before and during bacterial infection in the same breast cancer patients.

Variable	germ-free	bacteria-infected group	*p*-value
WBC median (range) (10^9/L)	5.58 (2.38-11.22)	10.30 (0.43-21.65)	<0.0001
NEU median (range) (10^9/L)	3.42 (0.94-7.19)	8.29 (0.15-20.06)	<0.0001
NLR median (range)	2.07 (0.89-5.53)	6.61 (0.51-52.93)	<0.0001
D-Dimer (range) (mg/L)	0.34 (0.06-1.99)	1.04 (0.14-15.87)	<0.0001
FIB median (range) (g/L)	2.95 (1.4-4.5)	4.15 (2.13-7.49)	<0.0001
LYM median (range) (10^9/L)	1.61 (0.52-3.46)	1.25 (0.13-3.89)	<0.0001
ALB (range) (g/L)	45.9 (30.7-56.2)	38.7 (23.7-48.8)	<0.0001
PA (range) (g/L)	0.26 (0.06-0.40)	0.15 (0.01-0.30)	<0.0001

10.3389/fcimb.2023.1286313

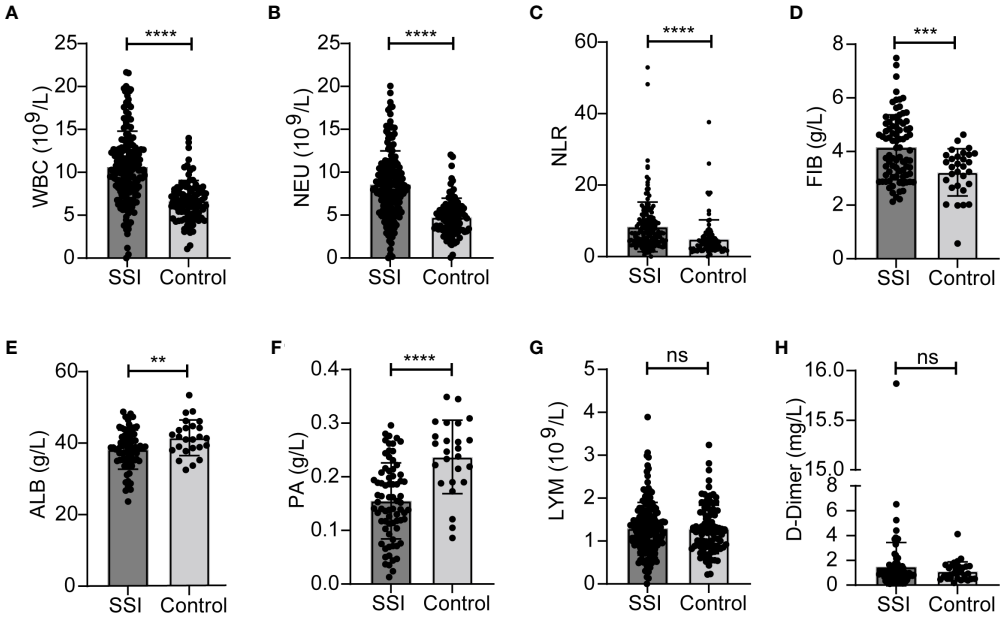

FIGURE 3
Changes of inflammatory indicators in SSI and control groups. The levels of WBC **(A)**, NEU **(B)**, NLR **(C)**, FIB **(D)**, ALB **(E)**, PA **(F)**, LYM **(G)**, D-Dimer **(H)**. $^{**}p < 0.01$, $^{***}P < 0.001$, $^{****}p < 0.0001$. ns, significance.

(Figures 6C-F). The confidence interval (CI), sensitivity and specificity analysis of various inflammatory indicators are shown in Figure 6G and Table 6. Meanwhile, we constructed ROC curves for LYM, D-Dimer, PCT and hsCPR, however, their AUCs for these parameters were small and were not statistically significant (Figures S3, Table S1). We calculated cut-off values for WBC (8.57×109/L), NEU (6.48×109/L), NLR (5.27), FIB (4.13 g/L), ALB (40.7 g/L), and PA (0.214 mg/L). The cut-off values of NEU, NLR and FIB were higher than the normal range. The cut-off value of WBC was within the normal range, but close to the maximum reference value. The cut-off value of ALB was also within the normal range, but close to the minimum reference value. The cut-off value of PA was lower than the normal range. We think that these cut-off values could better help clinicians determine whether a breast cancer patient has SSI. More information relating to ROC curve analysis is shown in Table 6.

3.6 Analysis of the drug resistance of pathogenic bacteria

Finally, we analyzed the drug resistance of different type of bacteria. We found that the drug resistance rates of *Staphylococcus aureus* to oxacillin (OXA), ciprofloxacin (CIP) and levofloxacin (LVX) were 19.13%, 11.30% and 8.7%, while the drug resistance rates of gram-positive bacteria were 23.19%, 15.22% and 13.67%, respectively (Figures 7A, B). Because *Staphylococcus aureus* accounted for 81.5% of gram-positive bacteria, the resistance rate of gram-positive bacteria was not significantly different when compared to *Staphylococcus aureus*. Compared with gram-positive bacteria, gram-negative bacteria showed higher resistance to CRO (0 vs 33.33%), FOX (23.53 vs 55.56%), CHL (2.97 vs 20%), MNO (0 vs 9.09%) and TCY (6.52 vs 25%); furthermore, gram-negative bacteria showed lower resistance to GEN (23.91 vs 8.7%)

TABLE 3 Comparison of inflammatory indicators in Surgical site infection (SSI) and control group.

Variable	SSI	Control group	*p*-value
WBC median (range) (10^9/L)	10.30 (0.43-21.65)	6.61 (1.07-13.98)	<0.0001
NEU median (range) (10^9/L)	8.29 (0.15-20.06)	4.64 (0.06-12.04)	<0.0001
NLR median (range)	6.61 (0.51-52.94)	3.63 (0.08-37.61)	<0.0001
FIB median (range) (g/L)	4.14 (2.13-7.49)	3.44 (0.57-4.63)	0.0002
ALB (range) (g/L)	40.0 (23.7-48.8)	41.4 (32.5-53.4)	0.0097
PA (range) (g/L)	0.15 (0.01-0.30)	0.25 (0.09-0.35)	<0.0001
LYM median (range) (10^9/L)	1.25 (0.13-3.89)	1.24 (0.22-3.24)	0.9516
D-Dimer (range) (mg/L)	0.99 (0.11-15.87)	0.96 (0.18-4.12)	0.3303

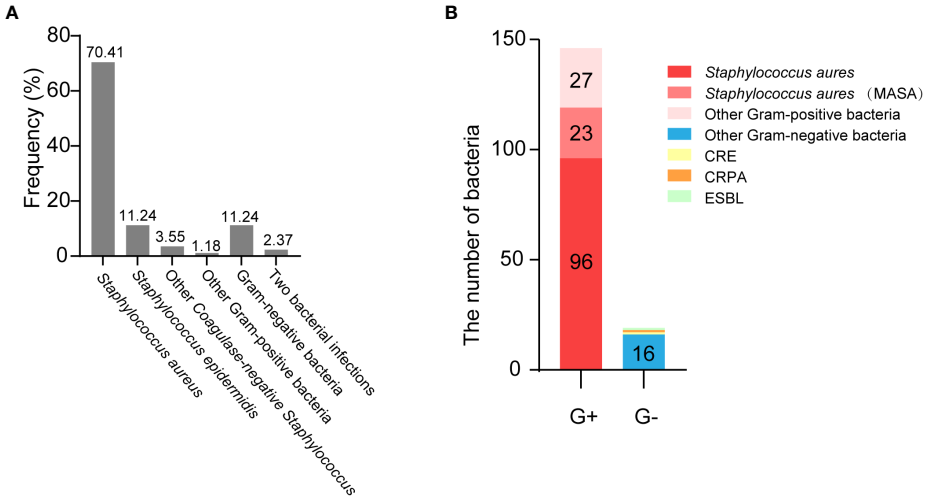

FIGURE 4
The distribution of pathogenic microorganisms responsible for infected in the breast cancer patients with SSI. **(A)** The frequency of isolates in breast cancer patients with SSI. **(B)** The distribution of muti-drug resistant bacteria.

(Figures 7B, C). Detailed information relating to the resistance rates of pathogenic microorganisms are given in Tables 7 and 8.

4 Discussion

Cancer is a leading cause of death and a significant barrier to longer life expectancy for every country in the world (Bray et al., 2021). Female breast cancer is the main cause of global cancer incidence and the fifth leading cause of cancer mortality worldwide, with 685,000 deaths annually (Sung et al., 2021). Surgery is still the standard treatment for breast cancer (O'Connor et al., 2020). However, SSI has become an important factor that affects the prognosis of patients with breast cancer. SSI can increase the financial burden to patients, delay postoperative radiotherapy, increase metastatic relapse and reduced survival exist rates (Zukowska and Zukowski, 2022). In our analysis, we found that the use of antibiotic prophylaxis could not reduce the likelihood of SSI; this finding was in line with previous studies (Prudencio et al., 2020). The relevant data of patients with a local recurrence were not included in this paper. Therefore, we did not analyze whether SSI was associated with a local recurrence, which suggests that we need to further track the patients' disease course and analyze the relationship between SSI and breast cancer recurrence in the future.

TABLE 4 Distribution of infection-associated bacteria.

Microorganism	n (%)
Gram-positive bacteria	146 (86.39)
Staphylococcus aures	119 (70.41%)
Staphylococcus epidermidis	19 (11.24%)
Other *Coagulase-negative Staphylococcus*	6 (3.55%)
Others	2 (1.18%)
Gram-negative bacteria	19 (11.24%)
Pseudomonas aeruginosa	7 (4.14%)
Escherichia coli	3 (1.78%)
Enterobacter cloacae	2 (1.18%)
Serratia marcescens	2 (1.18%)
Acinetobacter	2 (1.18%)
Others	3 (1.78%)
Two bacterial infections	4 (2.37%)

The levels of many inflammatory indicators change when SSI occurs. Therefore, it is important to find effective indicators to ensure that SSI is diagnosed and treated in a timely. In this study, we analyzed a range of inflammatory markers including blood-related indicators (WBC, NEU, LYM, NLR, D-Dimer, FIB, ALB, PA) and classical inflammatory markers (PCT and hsCRP). WBC, NEU and NLR all increased significantly in SSI (Figure 2A-C, 3A-C); these findings were consistent with previous research (Huh et al., 2019; Inose et al., 2019). Blood clotting related indicators were also closely associated with infection (King et al., 2014). Consistent with these findings, we found that FIB was also significantly increased in patients with SSI (Figure 3D). Previous studies have found that patients with low PA and ALB levels prior to surgery have an increased risk of SSI (Salvetti et al., 2018; Mentor et al., 2020); our present findings concurred with these previous data (Figure 3E, F). PCT and CRP have received increasing levels of attention with regards to the diagnosis of infection (Tang et al., 2018; Giannini et al., 2019). However, the amount of data related to PCT and CRP in these cases was insufficient to allow us to analyze their correlation with SSI; this requires further investigation. In addition to the analysis of inflammatory indicators, we also analyzed the clinical characteristics of our patients. We found that BMI was correlated with the SSI in breast cancer patients (Table 1). Other research also shown that obesity may increase the risk of breast cancer and that losing weight can reduce the risk of breast cancer (Lee et al., 2019;

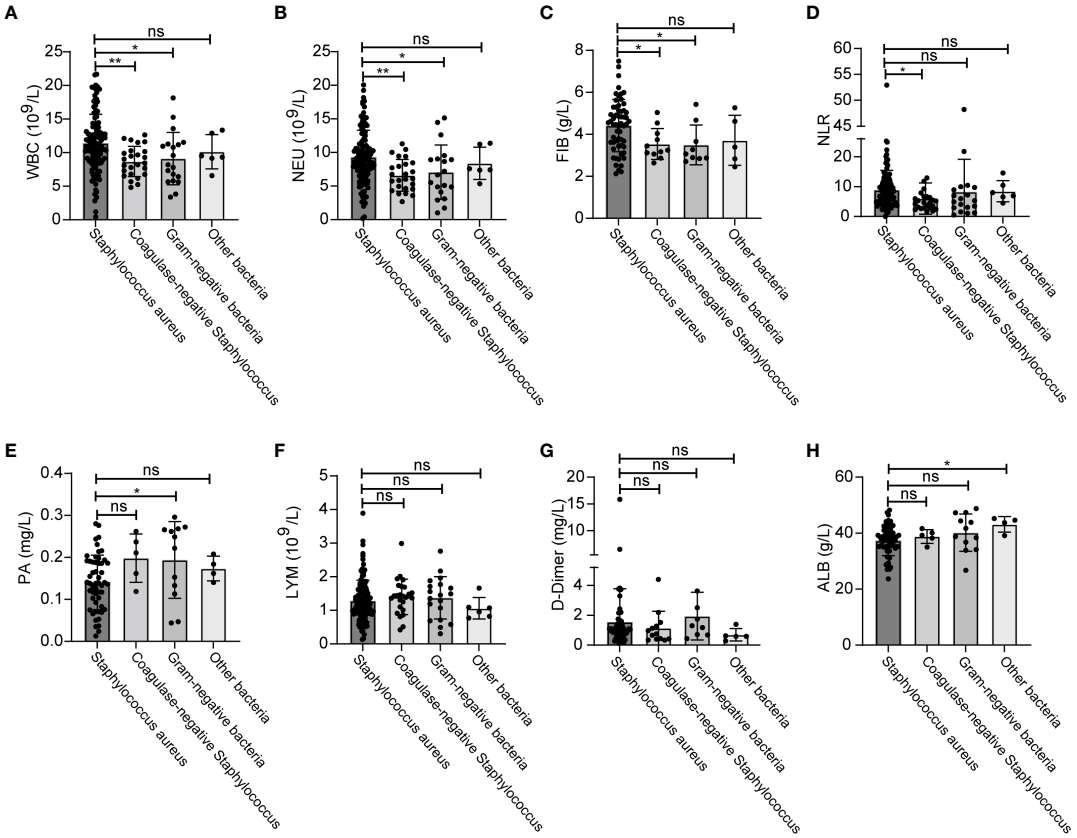

FIGURE 5
Changes of inflammatory indicators after infection with different bacteria. The levels of WBC **(A)**, NEU **(B)**, FIB **(C)**, NLR **(D)**, PA **(E)**, LYM **(F)**, D-Dimer **(G)**, ALB **(H)**. *$p < 0.5$, **$p < 0.01$. ns, significance.

Crafts et al., 2022). This highlights the fact that exercise and weight control are important for the prevention of cancer.

In order to further explore the changes of inflammatory indicators caused by different types of bacterial infections in SSI, we first classified the infectious bacteria. Growing evidence shows that *Staphylococcus aureus*, including MRSA, is the main cause of SSI (Saadatian-Elahi et al., 2008; Patel et al., 2017). In our study, we found that the infection rate caused by *Staphylococcus aureus* reached as high as 70.41% in breast cancer patients with SSI (Figure 4A). In addition, our analysis also showed that WBC and NEU increased more significantly with *Staphylococcus aureus* infection than with any other bacterial infection (Figures 5A, B). Consistent with these results, the AUCs for WBC and NEU were both > 0.8, thus indicating that they had superior diagnostic value for SSI (Figures 6A, B). Finally, we analyzed the drug sensitivity of *Staphylococcus aureus*, gram-positive bacteria and gram-negative

TABLE 5 Comparison of inflammatory indicators between different bacterial infection.

Variable	*Staphylococcus aureus*	Coagulase-negative *Staphylococcus*	Gram-negative bacteria	Other bacteria
WBC median (range) (10^9/L)	11.0 (0.43-21.65)	8.44 (4.82-12.63)	8.2 (3.39-18.14)	9.52 (6.58-13.35)
NEU median (range) (10^9/L)	8.89 (0.15-20.06)	6.12 (2.67-11.29)	6.66 (1.00-15.13)	7.58 (5.34-11.36)
FIB median (range) (g/L)	4.52 (2.13-7.49)	3.25 (2.64-5.04)	3.07 (2.71-5.43)	3.40 (2.46-5.27)
NLR median (range)	7.39 (1.15-52.94)	4.68 (1.66-26.88)	5.28 (0.51-48.23)	7.98 (4.46-14.56)
PA median (range) (g/L)	0.14 (0.01-0.28)	0.21 (0.12-0.26)	0.25 (0.04-0.30)	0.18 (0.14-0.21)
LYM median (range) (10^9/L)	1.41 (0.13-1.55)	1.42 (0.42-2.99)	1.45 (0.30-2.76)	1.07 (0.77-1.66)
D-Dimer (mg/L)	1.04 (0.11-15.87)	0.75 (0.33-4.40)	1.30 (0.44-5.24)	0.59 (0.28-1.39)
ALB (g/L)	37.7 (23.7-48.2)	39.2 (35.0-41.6)	41.7 (26.7-48.8)	44.6 (39.1-45.2)

10.3389/fcimb.2023.1286313

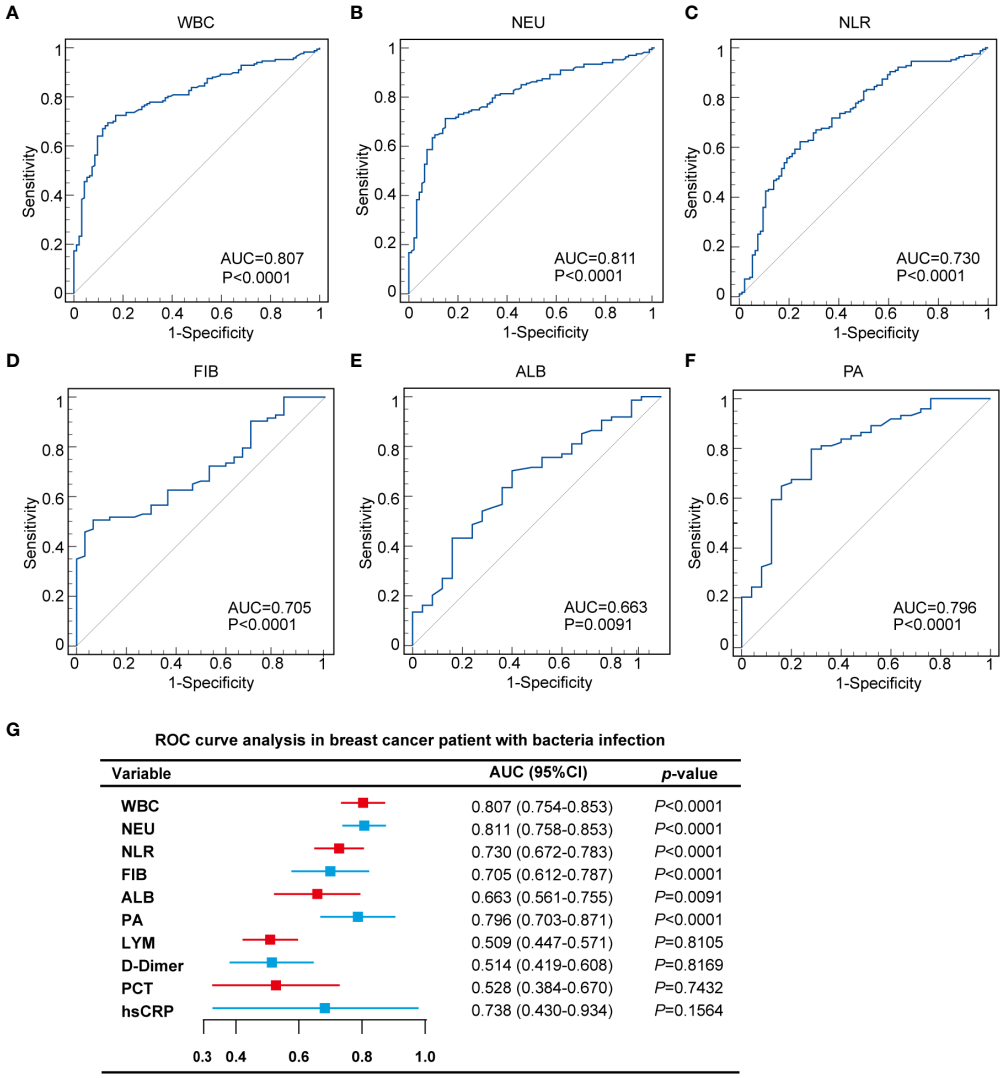

FIGURE 6
Diagnostic utility of inflammatory indicators in breast cancer patients with SSI. **(A)** ROC curves analyzed that the AUC of WBC was 0.807. **(B)** ROC curves analyzed that the AUC of NEU was 0.811. **(C)** ROC curves analyzed that the AUC of NLR was 0.730. **(D)** ROC curves analyzed that the AUC of FIB was 0.705. **(E)** ROC curves analyzed that the AUC of ALB was 0.663. **(F)** ROC curves analyzed that the AUC of PA was 0.796. **(G)** 95% CI and *p*-value of ROC curves.

TABLE 6 The diagnostic performance comparison of WBC, NEU, NLR ALB and PA between SSI and control group in breast cancer patients.

Diagnostic performance	WBC	NEU	NLR	FIB	ALB	PA
AUC	0.807	0.811	0.730	0.705	0.663	0.796
95% CI	0.754-0.853	0.758-0.856	0.672-0.783	0.612-0.787	0.561-0.755	0.703-0.871
Cut-off value	8.57×10^9/L	6.48×10^9/L	5.27	4.13 g/L	40.7 g/L	0.214 g/L
Sensitivity	0.69	0.71	0.62	0.51	0.70	0.80
Specificity	0.86	0.85	0.75	0.93	0.60	0.72
PPV	0.89	0.89	0.81	0.93	0.84	0.89
NPV	0.39	0.38	0.47	0.60	0.61	0.47
Youden index	0.5563	0.5636	0.3781	0.4394	0.3027	0.5173
p-value	<0.0001	<0.0001	<0.0001	<0.0001	0.0091	<0.0001

10.3389/fcimb.2023.1286313

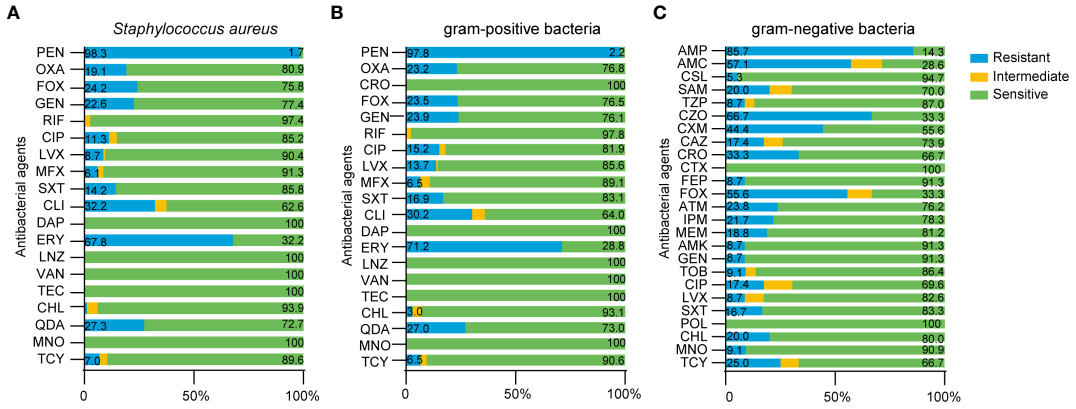

FIGURE 7
Drug resistance of pathogenic microorganism in breast cancer patients with SSI. **(A)** Antimicrobial susceptibility results of *Staphylococcus aureus*, **(B)** gram-positive bacteria, **(C)** gram-negative bacteria.

bacteria (Figures 7A-C), hoping that our results could provide reference guidelines for the timely and accurate drug treatment of SSI in breast cancer patients.

With the continuous development of detection technology, an increasing number of inflammatory markers have been developed and utilized. The levels of cytokines, especially IL-6 and IL-10, usually increase during bacterial infection and are considered to represent early biomarkers to assist in the diagnosis of bacterial infections (Ye et al., 2020; Zhu et al., 2022). Acute-phase reactant serum amyloid A (A-SAA) is used in clinical laboratories as an indicator of inflammation and is more conclusive than the detection of CRP in patients with viral infections, and severe acute pancreatitis (Ye et al., 2020; Zhu et al., 2021). Human neutrophil lipocalin (HNL) is a novel inflammatory marker; the diagnostic

TABLE 7 Comparison of drug resistance of gram-positive bacteria and *Staphylococcus aureus* in breast cancer patients.

Antimicrobial agents	Drug resistance rate	
	gram-positive bacteria (%)	*Staphylococcus aureus* (%)
PEN (penicillin)	97.84	98.26
OXA (oxacillin)	23.19	19.13
FOX (cefoxitin)	23.53	24.24
GEN (gentamicin)	23.91	22.61
RIF (rifampin)	0	0
CIP (ciprofloxacin)	15.22	11.30
LVX (levofloxacin)	13.67	8.70
MFX (moxifloxacin)	6.52	6.09
SXT (Sulfamethoxazole Tablets)	16.91	14.16
CLI (clindamycin)	30.22	32.17
DAP (daptomycin)	0	0
ERY (erythromycin)	71.22	67.83
LNZ (linezolid)	0	0
VAN (vancomycin)	0	0
TEC (teicoplanin)	0	0
CHL (chloramphenicol)	2.97	1.22
QDA (Quinuputin/Dafuputin)	27.03	27.27
MNO (minocycline)	0	0
TCY (tetracycline)	6.52	6.96

TABLE 8 Compare of drug resistance of gram-positive bacteria and gram-negative bacteria in breast cancer patients.

Antimicrobial agents	Drug resistance rate	
	gram-positive bacteria (%)	gram-negative bacteria (%)
CRO (ceftriaxone)	0	33.33
FOX (cefoxitin)	23.53	55.56
GEN (penicillin)	23.91	8.70
CIP (ciprofloxacin)	15.22	17.39
LVX (levofloxacin)	13.67	8.70
SXT (Sulfamethoxazole Tablets)	16.91	16.67
CHL (chloramphenicol)	2.97	20
MNO (minocycline)	0	9.09
TCY (tetracycline)	6.52	25

efficacy of HNL is not affected by the site of infection or by the pathogenic bacterial species involved (Fang et al., 2020). Heparin-binding protein (HBP) is another novel inflammatory factor released from neutrophils (Wang et al., 2022). HBP can directly kill bacteria and enhance bacterial clearance by attracting immune cells to the site of infection and is considered to represent a novel and valuable biomarker for infectious disease (Katsaros et al., 2022; Xue et al., 2022). This study revealed that WBC, NEU, NLR, FIB and PA have good predictive value for identifying SSI in breast cancer patients. Meanwhile, the test of antimicrobial susceptibility could be helpful in the treatment of SSI caused by different type of bacteria. In order to improve diagnosis and treatment times of SSI, we need to expand the number of specimens and increase new inflammatory markers in the future research.

Data availability statement

The raw data supporting the conclusions of this article will be made available by the authors, without undue reservation.

Ethics statement

The studies involving humans were approved by Ethics Committee of the Shandong Cancer Hospital and Institute. The studies were conducted in accordance with the local legislation and institutional requirements. The participants provided their written informed consent to participate in this study. Written informed consent was obtained from the individual(s) for the publication of any potentially identifiable images or data included in this article.

Author contributions

DL: Conceptualization, Writing – original draft. SD: Writing – original draft. JL: Writing – original draft. XL: Writing – original draft. KR: Writing – review & editing. LL: Writing – review & editing. WS: Conceptualization, Formal Analysis, Writing – original draft, Writing – review & editing.

Funding

The author(s) declare financial support was received for the research, authorship, and/or publication of this article. This work was supported by the Natural Science Foundation of Shandong Province (ZR2021QH069).

Conflict of interest

The authors declare that the research was conducted in the absence of any commercial or financial relationships that could be construed as a potential conflict of interest.

Publisher's note

Supplementary material

The Supplementary Material for this article can be found online at: https://www.frontiersin.org/articles/10.3389/fcimb.2023.1286313/full#supplementary-material

References

Bernier, J. (2015). Post-mastectomy radiotherapy after neodjuvant chemotherapy in breast cancer patients: A review. *Crit. Rev. Oncol. Hematol.* 93 (3), 180–189. doi: 10.1016/j.critrevonc.2014.10.011

Bray, F., Laversanne, M., Weiderpass, E., and Soerjomataram, I. (2021). The ever-increasing importance of cancer as a leading cause of premature death worldwide. *Cancer* 127 (16), 3029–3030. doi: 10.1002/cncr.33587

Celik, I. H., Hanna, M., Canpolat, F. E., and Mohan, P. (2022). Diagnosis of neonatal sepsis: the past, present and future. *Pediatr. Res.* 91 (2), 337–350. doi: 10.1038/s41390-021-01696-z

Christensen, C. P., Bedair, H., Della Valle, C. J., Parvizi, J., Schurko, B., and Jacobs, C. A. (2013). The natural progression of synovial fluid white blood-cell counts and the percentage of polymorphonuclear cells after primary total knee arthroplasty: a multicenter study. *J. Bone Joint Surg. Am.* 95 (23), 2081–2087. doi: 10.2106/JBJS.L.01646

Committee on Gynecological Practice. (2015). Committee opinion no. 619: Gynecologic surgery in the obese woman. *Obstet Gynecol* 125 (1), 274–278. doi: 10.1097/01.AOG.0000459870.06491.71

Cooper, J., Pastorello, Y., and Slevin, M. (2023). A meta-analysis investigating the relationship between inflammation in autoimmune disease, elevated CRP, and the risk of dementia. *Front. Immunol.* 14. doi: 10.3389/fimmu.2023.1087571

Crafts, T. D., Tonneson, J. E., Wolfe, B. M., and Stroud, A. M. (2022). Obesity and breast cancer: Preventive and therapeutic possibilities for bariatric surgery. *Obes. (Silver Spring)* 30 (3), 587–598. doi: 10.1002/oby.23369

El-Tamer, M. B., Ward, B. M., Schifftner, T., Neumayer, L., Khuri, S., and Henderson, W. (2007). Morbidity and mortality following breast cancer surgery in women: national benchmarks for standards of care. *Ann. Surg.* 245 (5), 665–671. doi: 10.1097/01.sla.0000245833.48399.9a

Engelmann, B., and Massberg, S. (2013). Thrombosis as an intravascular effector of innate immunity. *Nat. Rev. Immunol.* 13 (1), 34–45. doi: 10.1038/nri3345

Fang, C., Wang, Z., Dai, Y., Chang, W., Sun, L., and Ma, X. (2020). Serum human neutrophil lipocalin: An effective biomarker for diagnosing bacterial infections. *Clin. Biochem.* 75, 23–29. doi: 10.1016/j.clinbiochem.2019.10.003

Felippe, W. A., Werneck, G. L., and Santoro-Lopes, G. (2007). Surgical site infection among women discharged with a drain in *situ* after breast cancer surgery. *World J. Surg.* 31 (12), 2293–2299. doi: 10.1007/s00268-007-9248-3

Giannini, O., Del Giorno, R., Zasa, A., and Gabutti, L. (2019). Comparative impact of C-reactive protein testing in hospitalized patients with acute respiratory tract infection: A retrospective cohort study. *Adv. Ther.* 36 (11), 3186–3195. doi: 10.1007/s12325-019-01090-6

Horan, T. C., Andrus, M., and Dudeck, M. A. (2008). CDC/NHSN surveillance definition of health care-associated infection and criteria for specific types of infections in the acute care setting. *Am. J. Infect. Control* 36 (5), 309–332. doi: 10.1016/j.ajic.2008.03.002

Huh, J. W., Lee, W. Y., Park, Y. A., Cho, Y. B., Kim, H. C., Yun, S. H., et al. (2019). Oncological outcome of surgical site infection after colorectal cancer surgery. *Int. J. Colorectal Dis.* 34 (2), 277–283. doi: 10.1007/s00384-018-3194-4

Inose, H., Kobayashi, Y., Yuasa, M., Hirai, T., Yoshii, T., and Okawa, A. (2019). Procalcitonin and neutrophil lymphocyte ratio after spinal instrumentation surgery. *Spine (Phila Pa 1976)* 44 (23), E1356–E1E61. doi: 10.1097/BRS.0000000000003157

Katsaros, K., Renieris, G., Safarika, A., Adami, E. M., Gkavogianni, T., Giannikopoulos, G., et al. (2022). Heparin binding protein for the early diagnosis and prognosis of sepsis in the emergency department: the prompt multicenter study. *Shock* 57 (4), 518–525. doi: 10.1097/SHK.0000000000001900

King, C., Aylin, P., Moore, L. S., Pavlu, J., and Holmes, A. (2014). Syndromic surveillance of surgical site infections–a case study in coronary artery bypass graft patients. *J. Infect.* 68 (1), 23–31. doi: 10.1016/j.jinf.2013.08.017

Kyriazopoulou, E., Liaskou-Antoniou, L., Adamis, G., Panagaki, A., Melachroinopoulos, N., Drakou, E., et al. (2021). Procalcitonin to reduce long-term infection-associated adverse events in sepsis. A randomized trial. *Am. J. Respir. Crit. Care Med.* 203 (2), 202–210. doi: 10.1164/rccm.202004-1201OC

Lee, K., Kruper, L., Dieli-Conwright, C. M., and Mortimer, J. E. (2019). The impact of obesity on breast cancer diagnosis and treatment. *Curr. Oncol. Rep.* 21 (5), 41. doi: 10.1007/s11912-019-0787-1

Li, D., Li, J., Zhao, C., Liao, X., Liu, L., Xie, L., et al. (2023). Diagnostic value of procalcitonin, hypersensitive C-reactive protein and neutrophil-to-lymphocyte ratio for bloodstream infections in pediatric tumor patients. *Clin. Chem. Lab. Med.* 61 (2), 366–376. doi: 10.1515/cclm-2022-0801

Maajani, K., Jalali, A., Alipour, S., Khodadost, M., Tohidinik, H. R., and Yazdani, K. (2019). The global and regional survival rate of women with breast cancer: A systematic review and meta-analysis. *Clin. Breast Cancer* 19 (3), 165–177. doi: 10.1016/j.clbc.2019.01.006

Mentor, K., Ratnayake, B., Akter, N., Alessandri, G., Sen, G., French, J. J., et al. (2020). Meta-analysis and meta-regression of risk factors for surgical site infections in hepatic and pancreatic resection. *World J. Surg.* 44 (12), 4221–4230. doi: 10.1007/s00268-020-05741-6

Ngwa, D. N., and Agrawal, A. (2019). Structure-function relationships of C-reactive protein in bacterial infection. *Front. Immunol.* 10. doi: 10.3389/fimmu.2019.00166

O'Connor, R. I., Kiely, P. A., and Dunne, C. P. (2020). The relationship between post-surgery infection and breast cancer recurrence. *J. Hosp Infect.* 106 (3), 522–535. doi: 10.1016/j.jhin.2020.08.004

Patel, H., Khoury, H., Girgenti, D., Welner, S., and Yu, H. (2017). Burden of surgical site infections associated with select spine operations and involvement of staphylococcus aureus. *Surg. Infect. (Larchmt)* 18 (4), 461–473. doi: 10.1089/sur.2016.186

Prudencio, R. M. A., Campos, F. S. M., Loyola, A., Archangelo Junior, I., Novo, N. F., Ferreira, L. M., et al. (2020). Antibiotic prophylaxis in breast cancer surgery. A randomized controlled trial. *Acta Cir Bras.* 35 (9), e202000907. doi: 10.1590/s0102-865020200090000007

Roche, M., Law, T. Y., Kurowicki, J., Sodhi, N., Rosas, S., Elson, L., et al. (2018). Albumin, prealbumin, and transferrin may be predictive of wound complications following total knee arthroplasty. *J. Knee Surg.* 31 (10), 946–951. doi: 10.1055/s-0038-1672122

Ruan, L., Chen, G. Y., Liu, Z., Zhao, Y., Xu, G. Y., Li, S. F., et al. (2018). The combination of procalcitonin and C-reactive protein or presepsin alone improves the accuracy of diagnosis of neonatal sepsis: a meta-analysis and systematic review. *Crit. Care* 22 (1), 316. doi: 10.1186/s13054-018-2236-1

Russell, C. D., Parajuli, A., Gale, H. J., Bulteel, N. S., Schuetz, P., de Jager, C. P. C., et al. (2019). The utility of peripheral blood leucocyte ratios as biomarkers in infectious diseases: A systematic review and meta-analysis. *J. Infect.* 78 (5), 339–348. doi: 10.1016/j.jinf.2019.02.006

Saadatian-Elahi, M., Teyssou, R., and Vanhems, P. (2008). Staphylococcus aureus, the major pathogen in orthopaedic and cardiac surgical site infections: a literature review. *Int. J. Surg.* 6 (3), 238–245. doi: 10.1016/j.ijsu.2007.05.001

Salvetti, D. J., Tempel, Z. J., Goldschmidt, E., Colwell, N. A., Angriman, F., Panczykowski, D. M., et al. (2018). Low preoperative serum prealbumin levels and the postoperative surgical site infection risk in elective spine surgery: a consecutive series. *J. Neurosurg. Spine* 29 (5), 549–552. doi: 10.3171/2018.3.SPINE171183

Savioli, F., Edwards, J., McMillan, D., Stallard, S., Doughty, J., and Romics, L. (2020). The effect of postoperative complications on survival and recurrence after surgery for breast cancer: A systematic review and meta-analysis. *Crit. Rev. Oncol. Hematol.* 155, 103075. doi: 10.1016/j.critrevonc.2020.103075

Segura-Egea, J. J., Gould, K., Sen, B. H., Jonasson, P., Cotti, E., Mazzoni, A., et al. (2017). Antibiotics in endodontics: a review. *Int. Endod. J.* 50 (12), 1169–1184. doi: 10.1111/iej.12741

Sheinenzon, A., Shehadeh, M., Michelis, R., Shaoul, E., and Ronen, O. (2021). Serum albumin levels and inflammation. *Int. J. Biol. Macromol* 184, 857–862. doi: 10.1016/j.ijbiomac.2021.06.140

Stallard, S., Savioli, F., McConnachie, A., Norrie, J., Dudman, K., Morrow, E. S., et al. (2022). Antibiotic prophylaxis in breast cancer surgery (PAUS trial): randomised clinical double-blind parallel-group multicentre superiority trial. *Br. J. Surg.* 109 (12), 1224–1231. doi: 10.1093/bjs/znac280

Stocker, M., van Herk, W., El Helou, S., Dutta, S., Schuerman, F., van den Tooren-de Groot, R. K., et al. (2021). C-reactive protein, procalcitonin, and white blood count to rule out neonatal early-onset sepsis within 36 hours: A secondary analysis of the neonatal procalcitonin intervention study. *Clin. Infect. Dis.* 73 (2), e383–ee90. doi: 10.1093/cid/ciaa876

Sung, H., Ferlay, J., Siegel, R. L., Laversanne, M., Soerjomataram, I., Jemal, A., et al. (2021). Global cancer statistics 2020: GLOBOCAN estimates of incidence and mortality worldwide for 36 cancers in 185 countries. *CA Cancer J. Clin.* 71 (3), 209–249. doi: 10.3322/caac.21660

Tan, T. L., Kang, C. W., Ooi, K. S., Tan, S. T., Ahmad, N. S., Nasuruddin, D. N., et al. (2021). Comparison of sPLA2IIA performance with high-sensitive CRP neutrophil percentage PCT and lactate to identify bacterial infection. *Sci. Rep.* 11 (1), 11369. doi: 10.1038/s41598-021-90894-0

Tang, J. H., Gao, D. P., and Zou, P. F. (2018). Comparison of serum PCT and CRP levels in patients infected by different pathogenic microorganisms: a systematic review and meta-analysis. *Braz. J. Med. Biol. Res.* 51 (7), e6783. doi: 10.1590/1414-431x20176783

Tejirian, T., DiFronzo, L. A., and Haigh, P. I. (2006). Antibiotic prophylaxis for preventing wound infection after breast surgery: a systematic review and metaanalysis. *J. Am. Coll. Surg.* 203 (5), 729–734. doi: 10.1016/j.jamcollsurg.2006.07.013

Wang, Z., Chang, B., Zhang, Y., Chen, J., Xie, F., Xiang, Y., et al. (2022). Clinical value of serum sTREM-1 and HBP levels in combination with traditional inflammatory markers in diagnosing hospital-acquired pneumonia in elderly. *BMC Infect. Dis.* 22 (1), 773. doi: 10.1186/s12879-022-07758-9

Wu, Y., Yao, Y., Zhang, J., Gui, H., Liu, J., and Liu, J. (2022). Tumor-targeted injectable double-network hydrogel for prevention of breast cancer recurrence and wound infection *via* synergistic photothermal and brachytherapy. *Adv. Sci. (Weinh)* 9 (24), e2200681. doi: 10.1002/advs.202200681

Xue, M., Zhang, T., Lin, R., Zeng, Y., Cheng, Z. J., Li, N., et al. (2022). Clinical utility of heparin-binding protein as an acute-phase inflammatory marker in interstitial lung disease. *J. Leukoc. Biol.* 112 (4), 861–873. doi: 10.1002/JLB.3MA1221-489R

Ye, M., Joosse, M. E., Liu, L., Sun, Y., Dong, Y., Cai, C., et al. (2020). Deletion of IL-6 exacerbates colitis and induces systemic inflammation in IL-10-deficient mice. *J. Crohns Colitis* 14 (6), 831–840. doi: 10.1093/ecco-jcc/jjz176

Zhang, H., Wang, Y., Yang, S., and Zhang, Y. (2020). Peri-operative antibiotic prophylaxis does not reduce surgical site infection in breast cancer. *Surg. Infect. (Larchmt)* 21 (3), 268–274. doi: 10.1089/sur.2019.116

Zheng, Y., Hua, L., Zhao, Q., Li, M., Huang, M., Zhou, Y., et al. (2021). The level of D-dimer is positively correlated with the severity of mycoplasma pneumoniae pneumonia in children. *Front. Cell Infect. Microbiol.* 11. doi: 10.3389/fcimb.2021.687391

Zhou, J., Hiki, N., Mine, S., Kumagai, K., Ida, S., Jiang, X., et al. (2017). Role of prealbumin as a powerful and simple index for predicting postoperative complications after gastric cancer surgery. *Ann. Surg. Oncol.* 24 (2), 510–517. doi: 10.1245/s10434-016-5548-x

Zhu, Q., Li, H., Zheng, S., Wang, B., Li, M., Zeng, W., et al. (2022). IL-6 and IL-10 are associated with gram-negative and gram-positive bacteria infection in lymphoma. *Front. Immunol.* 13. doi: 10.3389/fimmu.2022.856039

Zhu, S., Zeng, C., Zou, Y., Hu, Y., Tang, C., Liu, C., et al. (2021). The clinical diagnostic values of SAA PCT, CRP and IL-6 in children with bacterial, viral, or co-infections. *Int. J. Gen. Med.* 14, 7107–7113. doi: 10.2147/IJGM.S327958

Zukowska, A., and Zukowski, M. (2022). Surgical site infection in cardiac surgery. *J. Clin. Med.* 11 (23), 6991. doi: 10.3390/jcm11236991

frontiers | Frontiers in Cellular and Infection Microbiology

TYPE Original Research
PUBLISHED 08 December 2023
DOI 10.3389/fcimb.2023.1291974

OPEN ACCESS

EDITED BY
Stefano Stracquadanio,
University of Catania, Italy

REVIEWED BY
Afsal Kolloli,
Rutgers University, Newark, United States
Nanying Che,
Capital Medical University, China

*CORRESPONDENCE
Meiying Wu
wu_my@126.com

†These authors have contributed equally to this work and share first authorship

RECEIVED 10 September 2023
ACCEPTED 09 November 2023
PUBLISHED 08 December 2023

CITATION
Huang L, Niu Y, Zhang L, Yang R and Wu M (2023) Diagnostic value of chemiluminescence for urinary lipoarabinomannan antigen assay in active tuberculosis: insights from a retrospective study. *Front. Cell. Infect. Microbiol.* 13:1291974. doi: 10.3389/fcimb.2023.1291974

Diagnostic value of chemiluminescence for urinary lipoarabinomannan antigen assay in active tuberculosis: insights from a retrospective study

Luyi Huang[1†], Yayan Niu[2†], Li Zhang[1], Rong Yang[1] and Meiying Wu[2*]

[1]Department of Infectious, Zhangjiagang First Peoples Hospital, Suzhou, China, [2]Department of Tuberculosis, The Fifth People's Hospital of Suzhou, The Affiliated Infectious Diseases Hospital of Soochow University, Suzhou, China

Purpose: This study aimed to assess the efficacy of chemiluminescence-based urinary lipoarabinomannan (LAM) antigen assay as a diagnostic tool for identifying active tuberculosis.

Methods: A retrospective study was conducted on 166 Tuberculosis (TB), 22 Non-Tuberculous Mycobacteria (NTM), 69 Non-TB cases, and 73 healthy controls from Zhangjiagang First Peoples Hospital between July 2022 and November 2022. Clinical and laboratory data were collected, including urine samples for LAM antigen detection, sputum samples and pleural effusion for GeneXpert, TB-DNA, and culture.

Results: TB group exhibited a higher LAM positivity rate ($P < 0.001$). CD4 count and diabetes as independent factors influencing the diagnostic accuracy of LAM. The LAM assay showed a sensitivity of 50.6% and a specificity of 95.65%. Notably, LAM's sensitivity was superior to TB-DNA (50.60% vs. 38.16%, $P < 0.05$). LAM's PTB detection rate was 51.7%, superior to TB-DNA ($P = 0.047$). Moreover, in EPTB cases, the LAM detection rate was 42.11%, surpassing Gene Xpert ($P = 0.042$), as well as exceeding the detection rates of TB-DNA and sputum culture.

Conclusion: LAM antigen detection using chemiluminescence has demonstrated outstanding clinical diagnostic value for active TB, especially in the diagnosis of extrapulmonary TB. The convenience of sample collection in this diagnostic approach allows for widespread application in the clinical diagnosis of active tuberculosis, particularly in cases of EPTB and sputum-negative patients.

KEYWORDS

urine LAM antigen detection, active tuberculosis, chemiluminescence method, diagnostic value, retrospective study

Introduction

Tuberculosis (TB) remains one of the major infectious diseases that poses a serious threat to human health (Fernandes et al., 2022). According to the World Health Organization (WHO) report, the estimated number of new TB cases globally reached 10.6 million in the period from 2020 to 2021 (Bagcchi, 2023). Extrapulmonary tuberculosis (EPTB) accounts for approximately 13.37% to 53.00% of all TB cases globally, which is noteworthy (Ohene et al., 2019; Pang et al., 2019). Among the 30 countries worldwide with a high burden of TB, China currently ranks second and is also one of the countries with a high burden of drug-resistant TB (Bagcchi, 2023). Due to the coexistence of pulmonary tuberculosis (PTB) and EPTB (Ohene et al., 2019), as well as the higher drug resistance rate in EPTB compared to PTB alone (Boonsarngsuk et al., 2018), the diagnosis of these conditions is more challenging. The End TB global project proposes that the design of new diagnosis methods or the improvement of the current diagnostic tests are a priority to accelerate the efforts to stop TB (Uplekar et al., 2015).

The Common clinical tests for TB infection include Mycobacterium TB culture (Azadi et al., 2018), acid-fast smear (Azadi et al., 2018), interferon-γ release assay (IGRA) (Goletti et al., 2022), and polymerase chain reaction (PCR) (Steingart et al., 2014). Despite their advantages, these strategies have limitations, including long turnaround time, the need for sputum or invasive blood samples, reliance on specific instruments, and low sensitivity (Franzblau et al., 2012). The limitations of sputum-based TB diagnosis are particularly pronounced for individuals with EPTB or those co-infected with HIV (Franzblau et al., 2012; Zhao et al., 2012). Thus, the development of sensitive and easy-to-use urine tests for this pathogen challenge has significant implications.

The detection of lipoarabinomannan (LAM) levels in the urine represents one such possible test. LAM is a heat-stable glycolipid that is found in the outer cell wall of Mycobacterium (Brennan, 2003; Lawn et al., 2012). It is released by metabolically active mycobacteria, which makes it a valuable marker for TB detection (Minion et al., 2011). Moreover, LAM is filtered by the kidneys (Lawn et al., 2009; Minion et al., 2011), and therefore, it can be detected in urine, which overcomes the limitations of testing in patients who are unable to produce sputum. As a result, it has been recommended by the WHO (Organization, 2022). These tests have shown higher sensitivity in populations that are HIV-positive. Lawn (Lawn et al., 2012) has shown that TB-LAM testing was performed on HIV-positive patients with a CD4 cell count less than 200 cells/μL. The results showed a sensitivity of 52.5% (39.1–65.7). Another study (Székely et al., 2022) shown that Overall FujiLAM sensitivity was 54.8% (95% CI: 49.1–60.4), and overall specificity was 85.1% (83.1–86.9). However, it is disappointing that the sensitivity of this test in HIV-negative patients is low, approximately 10-20% (Achkar et al., 2011). Research on chemiluminescence platforms offering heightened sensitivity has yet to be reported.

In this study, we evaluated a novel diagnostic approach using chemiluminescence to detect the presence of LAM in the urine of HIV-negative individuals. We conducted a comprehensive analysis of the clinical factors that could influence LAM detection and performed a thorough comparison between urine LAM detection and other laboratory TB diagnostic methods, specifically focusing on the diagnosis of PTB and EPTB. The purpose of this study was to provide a new TB diagnostic method for clinical through comprehensively analyzing the clinical value of urine LAM detection and contribute to the goal of End TB.

Materials and methods

Study design and study population

This retrospective study aimed to evaluate the diagnostic performance of urinary LAM in diagnosing TB compared to Gene Xpert, TB-DNA, and sputum culture. Between July and November 2022, a total of 400 HIV-negative suspected tuberculosis patients visited the infectious department of Zhangjiagang First People Hospital. Of these, 275 patients underwent LAM testing, and after excluding 18 individuals currently undergoing tuberculosis treatment, 257 suspected patients were included in the study. Among them, 166 were confirmed to have tuberculosis (including 147 cases of PTB and 19 cases of EPTB), 22 had NTM, and 69 were Non-TB patients. In addition, 76 individuals without TB symptoms or a history of exposure to tuberculosis were collected from the physical examination department as healthy controls and underwent LAM testing on urine samples. Three participants were excluded due to unqualified samples, leaving 73 individuals included in the healthy control group. In total, 330 participants were included in the study, all of whom were HIV-negative individuals (Figure 1). The diagnostic criteria outlined in the "Diagnosis for pulmonary tuberculosis (WS 288-2017)" (National Health Commission of the People's Republic of China (2017a)) and "Classification of Tuberculosis (WS196-2017)" (National Health Commission of the People's Republic of China (2017b)), We also referred to the "WHO consolidated guidelines on tuberculosis. Module 3: diagnosis-rapid diagnostics for tuberculosis detection" (Organization, 2020). NTM diagnostic criteria outlined in "Guidelines for Diagnosis and Treatment of Non-Tuberculous Mycobacterial Diseases (2020 Edition)" and "Consensus management recommendations for less common non-tuberculous mycobacterial pulmonary diseases" (Lange et al., 2022), The inclusion criteria for the healthy control group were individuals who underwent routine physical examinations and had no history of exposure to tuberculosis or any symptoms of tuberculosis. The study adhered to the principles outlined in the Declaration of Helsinki and received approval from the Ethics Committee of Zhangjiagang First Peoples Hospital (No. ZJGYYLL-2022-11-021). Written informed consent was obtained from all participants, allowing the utilization of their data for research purposes (Table 1).

Sample collection

Sputum samples

Sputum samples were collected from the patients through spontaneous expectoration. Fresh sputum was obtained from the patients' first-morning expectoration after rinsing their mouths with water. The patients were instructed to forcefully expectorate from deep within their lungs into a glass or plastic cup or onto wax-coated paper. In cases where patients had no or minimal sputum,

10.3389/fcimb.2023.1291974

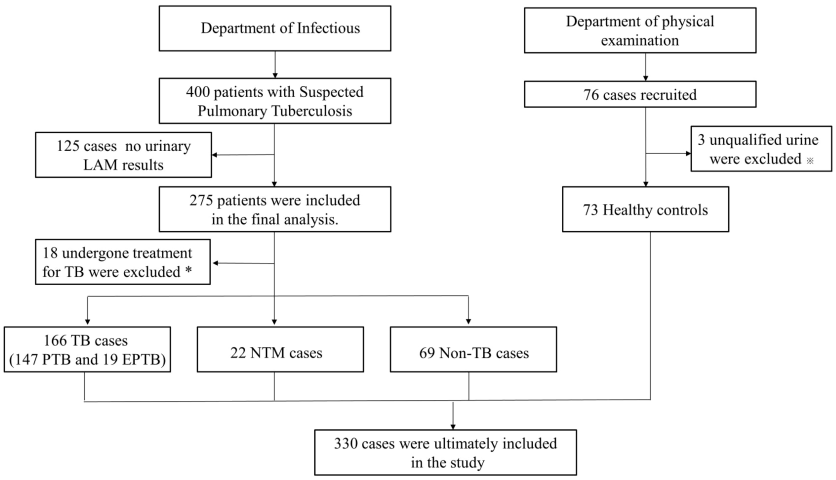

FIGURE 1
Study selection for patients flow chart. TB, tuberculosis; PTB, pulmonary tuberculosis; EPTB, extrapulmonary tuberculosis; NTM, nontuberculosis mycobacteria; Non-TB, non-tuberculosis. *Patients with previously diagnosed tuberculosis were excluded from analyses. ※Urine samples that contain suspended particles or are cloudy are at risk of contamination.

they underwent inhalation of a mist of saline solution (100 g/L) heated to 45°C to aid in the expectoration of sputum.

Three sputum samples were collected from each patient, including one in the evening, one in the early morning, and one at the time of collection. These three samples were combined and thoroughly mixed to form a single specimen. Subsequently, the sputum specimen was mixed with 5 mL of 0.9% saline solution to ensure uniformity and facilitate laboratory processing. The prepared specimen was then sent to the laboratory for further analysis.

TABLE 1 Baseline characteristics of participants.

Variables	TB					NTM	Non-TB	Healthy controls	χ^2/Z	P
	LAM+	LAM-	χ^2/Z	P	Total	n=22 (6.67%)	n=69 (20.91%)	n=73(22.12%)		
	n=84	n=82			n=166 (50.30%)					
Gender			3.699	0.054					1.948[a]	0.378[a]
									3.246[b]	0.355[b]
Male	62 (73.81%)	49 (59.76%)			111(66.87%)	14 (63.64%)	52(75.36%)	45(61.64%)		
Female	22 (26.19%)	33 (40.24%)			55(33.13%)	8 (36.36%)	17(24.64%)	28(38.36%)		
Age (years)	56(33-67)	36.5(27-66)	-2.417	0.016	50.5(29.75-67.00)	62.82 ± 14.99	66.10 ± 17.28	57.48 ± 16.90	40.59[a]	<0.0001[a]
Other pre-existing comorbidities										
Diabetes	17 (20.24%)	5(6.10%)	5.185	0.023	22(13.25%)	2(9.09%)	13(18.84%)	_	1.78[a]	0.410[a]
Hypertension	14 (16.67%)	8(9.76%)	1.229	0.268	22(13.25%)	1(4.55%)	24(34.78%)	_	18.16[a]	<0.0001[a]
COPD	5(5.95%)	2(2.44%)	1.268	0.26	7(4.22%)	1(4.55%)	25(36.33%)	_	46.12[a]	<0.0001[a]
Autoimmune disease	0	1(1.22%)	1.031	0.31	1(0.6%)	0	0	_	0.55[a]	0.759[a]
Clinical symptom								_		

(Continued)

10.3389/fcimb.2023.1291974

TABLE 1 Continued

Variables	TB					NTM	Non-TB	Healthy controls	χ^2/Z	P
	LAM+	LAM-	χ^2/Z	P	Total	n=22 (6.67%)	n=69 (20.91%)	n=73(22.12%)		
	n=84	n=82			n=166 (50.30%)					
Cough	69 (82.14%)	60 (73.17%)	1.928	0.165	129(77.71%)	19(86.36%)	66(95.65%)	_	11.43[a]	0.003[a]
Hemoptysis	8(9.52%)	12 (14.63%)	1.108	0.292	20(12.05%)	0	7(10.14%)	_	3.01[a]	0.222[a]
Hyperthermia	9 (10.71%)	9 (10.98%)	0.095	0.758	18(10.84%)	1(4.55%)	17(24.64%)	_	9.49[a]	0.009[a]
Methods										
LAM	84 (100%)	82 (100%)	0.024	0.877	166(100%)	22(100%)	69(100%)	73(100%)		
Gene Xpert	78 (92.86%)	78 (95.12%)	0.376	0.54	156(93.98%)	22(100%)	67(97.10%)	_		
TB-DNA	75 (89.29%)	77 (93.90%)	1.145	0.285	152(91.57%)	22(100%)	67(97.10%)	_		
Sputum culture	75 (89.29%)	77 (93.90%)	1.145	0.285	152(91.57%)	18(81.82%)	68(98.55%)	_		
CD4 count (*10^9 cells/L)	0.46 ± 0.24	0.52 ± 0.24	0.616	0.003	0.51 ± 0.25	0.46 ± 0.19	0.57 ± 0.26	_	2.04[a]	0.361[a]
CD8 count (*10^9 cells/L)	0.38 ± 0.22	0.41 ± 0.22	0.621	0.05	0.41 ± 0.22	0.38 ± 0.17	0.46 ± 0.21	_	1.67[a]	0.434[a]
CD4/CD8	1.43 ± 0.70	1.61 ± 1.51	1.397	0.317	1.52 ± 1.17	1.36 ± 0.64	1.38 ± 0.83	_	0.64[a]	0.726[a]

TB, tuberculosis; NTM, nontuberculosis mycobacteria; Non-TB, non-tuberculosis; LAM, Liboarabinomannan; CPOD, Chronic Obstructive Pulmonary Disease; TB-DNA, Mycobacterium tuberculosis gene amplification assay; _, not collected; [a], compared among TB, NTM and Non-TB groups; [b], compared among TB, NTM, Non-TB and Healthy controls groups; P<0.05, significant difference.

Urine samples

When collecting urine samples from patients, we should adhere to the following conditions: Each test sample should have a total urine volume of no less than 10 mL. When selecting midstream urine samples, it is important to avoid samples with high protein content, fat, or other interfering substances in order to ensure sample accuracy. After sample collection, the specimens should be stored at room temperature, and the storage time should not exceed 72 hours. If testing cannot be completed promptly, the samples should be refrigerated at 2°C.~8°C for a maximum of 7 days. If long-term testing is delayed, the samples should be stored at -15°C or below. Additionally, to prevent damage to the sample, it is recommended to minimize the number of freeze-thaw cycles, and the number of freeze-thaw cycles should not exceed three.

Pleural effusion

Before performing thoracentesis, healthcare professionals communicate with the patient, explaining the purpose, steps, and potential risks of the procedure, and obtain the patient's consent. Clinicians typically use clinical examinations and imaging studies, such as chest X-rays or ultrasounds, to determine the location and nature of the pleural effusion. Local anesthesia and disinfection are applied at the sampling site to alleviate the patient's pain and minimize the risk of infection. A fine needle or catheter is used by the doctor to puncture the site of the pleural effusion, and the pleural fluid is aspirated into a collection container through the needle or catheter. Once the fluid is collected, the needle or catheter is carefully removed, and the sampling site is treated appropriately.

Laboratory TB diagnostic methods

GeneXpert

According to the instructions, the processing solution was mixed with the sputum sample or pleural effusion at a ratio of 1:2. The mixture was then placed on a vortex mixer and vortexed for 0.5 minutes. After incubating at a specific temperature for 15 minutes, the specimen was vortexed again for 0.5 minutes and then incubated for an additional 5 minutes until it was fully liquefied. The mixed solution was then added to the detection cartridge and placed in the GeneXpert instrument for testing. The GeneXpert detection system and accompanying reagents were provided by Cepheid, USA.

TB-DNA-PCR

The drainage of Sputum or pleural effusion were placed in a sterile sputum box for examination. The TB-DNA detection kit from Sun Yat-sen University Da'an gene Co., Ltd. was used, and the detection process was carried out following the provided instructions.

Mycobacterium tuberculosis culture

Sputum specimens or pleural effusion underwent a decontamination process using N-acetyl-L-cysteine-sodium hydroxide (NALC-NaOH) solution. Subsequently, the specimens were washed with a phosphate buffer at pH 6.8. A volume of 0.5 mL from each specimen was then inoculated into MGIT (Mycobacteria Growth Indicator Tube) culture tubes, which contained nutrient supplements and antimicrobial agents. To facilitate culture and detection, the culture tubes were placed in a BACTEC MGIT 960 Mycobacterial Detection System. The process of mycobacterial isolation and culture examination followed the guidelines outlined in the "Laboratory Testing Guidelines for Tuberculosis Diagnosis." The MGIT 960 detection system and its associated reagents were provided by BD, USA.

Urinary LAM detection (chemiluminescence)

For urinary LAM detection, 4 mL of midstream urine was collected from the patient, and the test was performed following the instructions provided by the manufacturer (Guangzhou Leide Biotechnology Co., LTD., China). 1.5 mL of the test sample was transferred to a 10 mL centrifuge tube. Then, 50 μL of the magnetic bead reagent, which contains LAM-capturing antibodies, was added to the centrifuge tube and mixed. The tube was labeled for identification. The labeled centrifuge tube was placed in a rotating mixer and incubated at room temperature with a rotation speed of 30-50 rpm for 2 hours. After incubation, the centrifuge tube was placed on a magnetic rack for adsorption. Once the components were fully separated, the liquid above the sediment was discarded. The mixture was thoroughly mixed using a vortex mixer. Within 5 minutes, the sample was processed following the operation manual of the LAM detection chemiluminescence analyzer. If the time exceeds 5 minutes, the sample needs to be mixed again before testing. The LAM detection system and accompanying reagents were provided by Leide Biosciences Co., Ltd, China.

Statistical analysis

Statistical analysis was conducted using SPSS 20.0. Baseline characteristics are presented as means ± standard deviation (SD) or as medians [interquartile ranges (IQRs)] for continuous variables, as appropriate. Categorical variables are presented as numbers (percentages). For categorical variables in the clinical and demographic data, the chi-squared test, Student's t-test, and Mann-Whitney U test were employed to compare differences between categorical variables, normally distributed continuous variables, and non-normally distributed continuous variables, respectively. Logistic regression analysis was utilized to evaluate the relationship between measured variables and the diagnosis of LAM.

Results

Patient characteristics

In our study, we analyzed a total of 330 cases. The demographics and clinical characteristics of the final study population were presented in Table 1. Among these cases, 166 (50.30%) were diagnosed with TB, 22 patients (6.67%) had NTM infections, 69 (20.91%) had Non-TB conditions (pulmonary diseases other than TB), and 73 patients (22.12%) formed the healthy control group without pulmonary diseases (Table 1). The gender distribution was similar across the TB, NTM, Non-TB, and healthy control groups (P=0.355), as well as within the TB, NTM, and Non-TB groups. The TB group had a significantly younger age compared to the other groups (P<0.0001). We also examined the prevalence of other existing conditions among the TB, NTM, and Non-TB groups, and found that the rates of diabetes (P=0.410) and autoimmune disease (P=0.759) were similar. However, hypertension (P<0.0001) and COPD (P<0.0001) were significantly more common in the Non-TB group than in the other groups. Analyzing clinical symptoms, we noted that the occurrence of cough (P=0.003) and hyperthermia (P=0.009) was notably higher in the Non-TB group compared to the TB and NTM groups. CD4 count(P=0.361), CD8 count (P=0.434), and CD4/CD8 ratio (P=0.726) showed no significant differences among the TB, NTM, and Non-TB groups.

In the TB group, 84 cases were LAM+ (50.6%), while 82 were LAM- (49.4%). The LAM+ group had a higher average age (56 (33–67) vs 36.5 (27–66), P=0.016) and a greater prevalence of diabetes (20.24% vs 6.10%, P=0.023) compared to the LAM- group. However, the CD4 count in the LAM+ group was significantly lower than in the LAM- group (0.46 ± 0.24 vs 0.52 ± 0.24, P=0.003).

Diagnostic performance of LAM

Based on the reference range provided by the test kit (S/CO>1 is positive), we compared the LAM positive and negative rate among these groups. Among TB, NTM, Non-TB and healthy control group, the positive rate of LAM in TB group significantly higher than other groups (50.6% vs. 36.36% vs. 4.35% vs. 5.48%, P<0.0001, Figure 2A). Next, we compared the S/CO level among these groups, and found that the S/CO level in TB group was significantly higher than that in non-TB group (2.22 ± 3.33 vs 0.78 ± 0.19, P=0.0079, Figure 2B) and healthy group (2.22 ± 3.33 vs 0.76 ± 0.14, P=0.0062, Figure 2B), the S/CO level in NTM group was significantly higher than that in non-TB group (2.78 ± 7.43 vs 0.78 ± 0.19, P=0.0338, Figure 2B) and healthy group (2.78 ± 7.43 vs 0.76 ± 0.14,P=0.0310, Figure 2B), but have no difference between TB group and NTM group (2.22 ± 3.33 vs 2.78 ± 7.43,P=0.7977, Figure 2B). We divided

the TB group into LAM- and LAM+ groups based on the reference range and found that the S/CO levels of LAM+ were significantly higher than those of LAM-(Figure 2C).

Analysis of risk factors of LAM

To clarify the risk factors that influence the diagnostic results of LAM, we conducted a univariate logistic regression analysis on the significant variables that showed differences between the LAM- and LAM+ subgroups in TB patients (Table 2). The univariate analysis revealed that age (Odds Ratio [OR]: 1.021, 95% Confidence Interval [CI]: 1.01-1.04, P=0.011), diabetes (OR: 3.91, 95%CI:1.37-11.16, P=0.011), and CD4 count (OR: 0.13, 95%CI:0.03-0.54, P=0.005) were significantly associated with the LAM diagnostic results. But CD8 counts have no correlation with LAM diagnostic (OR: 0.24, 95% CI:0.05-1.02, P=0.054). After for confounders (age, diabetes and CD4 count), patients with diabetes exhibited a three-fold probability of LAM-positive (OR: 3.14, 95%CI:1.06-9.29, P=0.039), and patient with increase in CD4 count, the probability of being LAM-positive decrease (OR: 0.197, 95%CI:0.046-0.85, P=0.029).

Comparison the diagnostic performance of 4 methods in TB

To assess the diagnostic accuracy of LAM, we compared LAM with Gene Xpert, TB-DNA, and sputum culture. According to the composite reference standard (CRS), the sensitivity, specificity, positive predictive value (PPV), negative predictive value (NPV), and Kappa value of Gene Xpert for detecting active pulmonary tuberculosis were 55.13%, 100%, 100%, 48.91%, and 0.425, respectively. The corresponding values of TB-DNA were 38.16%, 100%,100%, 41.61%, and 0.274, respectively. The corresponding values of Sputum culture were 46.71%, 100%, 100%, 45.64%, and 0.351, respectively. The corresponding values of LAM detection were 50.6%, 95.65%, 95.55%, 44.59%, and 0.347, respectively. The sensitivity of LAM was significantly higher than TB-DNA (50.60% vs 38.16%, P<0.05), slightly higher than Sputum culture (50.60% vs 46.71%) and slightly lower than GeneXpert (50.60% vs 55.13%) (Table 3). We also investigated the diagnostic accuracy of four methods for NTM and found that sputum culture had the highest sensitivity for NTM diagnosis (72.22%), followed by LAM (36.36%), as shown in Supplementary Table 1.

Comparison the detection rates of 4 methods in PTB and EPTB

Simultaneously, we compared the detection rates of these four diagnostic methods in PTB and EPTB (Table 4). In PTB, the detection rate of LAM was significantly higher than that of TB-DNA (51.7% vs 40%, P=0.047), and have no significant difference with Gene Xpert (51.7% vs 60.43%, P=0.137) and sputum culture (51.7% vs 48.57%, P=0.596). In EPTB, the detection rate of LAM was significantly higher than that of Gene Xpert (42.11% vs 11.76%, P=0.047), and slightly higher than that of TB-DNA (42.11% vs 16.67%, P=0.129) and sputum culture (42.11% vs 25%, P=0.326). However, due to the relatively small sample size, no significant differences were observed.

A

LAM	TB	NTM	Non-TB	Healthy controls	χ^2 76.449	P <0.0001
Total	166	22	69	73		
Positive	84(50.60%)	8(36.36%)	3(4.35%)	4(5.48%)		
Negative	82(49.40%)	14(63.64%)	66(95.65%)	69(94.52%)		

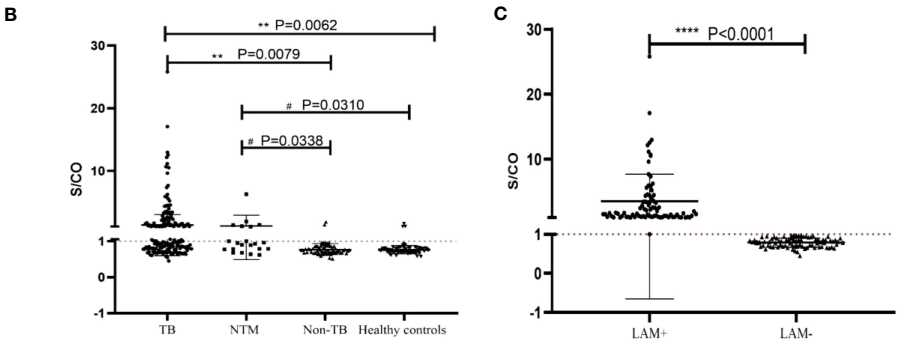

FIGURE 2
Analysis of the diagnostic performance of LAM. **(A)** The diagnostic results of LAM in the four study groups. **(B, C)** Statistical analysis of S/CO. S/CO, S represents the optical density of sample, with CO referring to the Cut Off, which is the critical value. If the S/CO value is greater than 1, it indicates that the specimen produced a result higher than the critical value, and therefore it is considered positive. Conversely, if the S/CO value is less than 1, it indicates that the specimen produced a result lower than the critical value, and therefore it is considered negative. **, P<0.01; ****, P<0.0001, compared to TB Group; #, P<0.05, compared to NTM Group; significant difference.

TABLE 2 Univariate and multivariable analysis of the diagnosis of LAM in TB.

Variables	Univariate analysis			Multivariate analysis		
	β	OR [95% CI]	P	β	OR [95% CI]	P
Age	0.02	1.021(1.01-1.04)	0.011	0.014	1.015(1.00-1.03)	0.096
Diabetes (yes vs no)	-1.117	3.91(1.37-11.16)	0.011	1.144	3.14(1.06-9.29)	0.039
CD4 count	-2.02	0.13(0.03-0.54)	0.005	-1.624	0.197(0.046-0.85)	0.029
CD8 count	-1.44	0.24(0.05-1.02)	0.054			

Variables with P≤ 0.05 in univariate models were analyzed in the multivariate analysis model. OR, Odds ratio; CI, Confidence interval.

Discussion

Currently, it is necessary to perform several tests to have a TB diagnosis. Despite the availability of new diagnostic techniques, the smear test and the culture of the microorganism are the gold-standard tests, but these are delivering late diagnoses (Broger et al., 2023). The LAM urine assay was seen as a potentially revolutionary diagnostic for active TB (Flores et al., 2021). With its potential to be used as a simple point-of-care test, lack of bio-safety concerns, and use of a noninvasive, convenient patient specimen, the LAM assay was fast-tracked for commercial development (Flores et al., 2021). The existing commercial LAM detection kits, due to the limitations of detection methodology (colloidal gold method), lead to insufficient sensitivity, and can only be applied to HIV positive patients, which greatly limits the promotion and application of this technology (Broger et al., 2020).

In this study, we aim to investigate the accuracy of LAM detection using a chemiluminescence assay. Therefore, we conducted LAM testing in patients diagnosed with TB (contain PTB and EPTB), non-TB, NTM and healthy control. The results showed that the positive rates in the four groups were 50.5%, 4.35%, 36.36%, and 5.48%, respectively (Figure 2). Moreover, the specificity of LAM in patients with Non-TB was 95.65%. Compared to previous studies, where LAM sensitivity in HIV-negative individuals ranged from 10% to 20% (van Crevel and Critchley, 2021; Liu et al., 2022), our study demonstrated significantly improved sensitivity. Our study also found that LAM had a sensitivity of 36.36% to NTM infection. These findings suggest that urine LAM testing for NTM infection may serve as a valuable adjunctive diagnostic tool but cannot differentiate between tuberculosis and NTM infections (De et al., 2020; Liu et al., 2022).

To determine potential factors affecting LAM detection results, we conducted univariate and multivariate logistic regression analysis on these risk factors, which have significant differences between LAM+ and LAM- groups. We found that diabetes and CD4 count were independent factors that influenced the results of LAM. Diabetes, a chronic metabolic disorder, the prevalence of PTB in the diabetic population is 2-3 times higher than in the normal population (van Crevel and Critchley, 2021), and diabetes mellitus may increase the risk of TB, with a 3.11-fold increase in the risk of PTB and a 1.18-fold increase in latent tuberculosis infection (LTBI) (Al-Rifai et al., 2017). Studies have reported that LAM enters the urine in the form of immune complexes (Sakamuri et al., 2013), with higher concentrations observed when renal filtration function is impaired (Lawn and Gupta-Wright, 2016). This phenomenon may explain why LAM is more easily detectable in individuals with tuberculosis and concomitant diabetes, as prolonged exposure to elevated blood glucose levels in diabetic patients can impair glomerular and tubular function (Oshima et al., 2021). Additionally, it has been suggested that impaired immune

TABLE 3 The diagnostic performance of four methods in TB.

Methods	Results	CRS		Sensitivity	Specificity	PPV	NPV	Kappa
		TB	Non-TB					
LAM	positive	84	3	50.60%	95.65%	95.55%	44.59%	0.347
	negative	82	66					
Gene Xpert	positive	86	0	55.13%	100%	100%	48.91%	0.425
	negative	70	67					
TB-DNA	positive	58	0	38.16%*	100%	100%	41.61%	0.274
	negative	94	67					
Sputum culture	positive	71	0	46.71%	100%	100%	45.64%	0.351
	negative	81	68					

CRS, composite reference standard; TB, tuberculosis; Non-TB, non-tuberculosis; LAM, Liboarabinomannan; TB-DNA, Mycobacterium tuberculosis gene amplification assay; PPV, positive predictive value; NPV, negative predictive value. Sensitivity = True Positive Cases/(True Positive Cases + False Negative Cases) × 100%; Specificity = True Negative Cases/(True Negative Cases + False Positive Cases) × 100%; PPV = True Positive Cases/(True Positive Cases + False Positive Cases) × 100%; NPV = True Negative Cases/(True Negative Cases + False Negative Cases) × 100%; *, P<0.05, compared to LAM detection.

TABLE 4 The detection rate of four methods in PTB and EPTB.

Methods	PTB			EPTB		
	n	Detection rate	P	n	Detection rate	P
LAM	147	76 (51.70%)	-	19	8 (42.11%)	-
Gene Xpert	139	84 (60.43%)	0.137	17	2 (11.76%)	0.042*
TB-DNA	140	56 (40.00%)	0.047*	12	2 (16.67%)	0.129
Sputum culture	140	68 (48.57%)	0.596	12	3 (25.00%)	0.326

PTB, pulmonary tuberculosis; EPTB, extrapulmonary tuberculosis; LAM, Liboarabinomannan;TB-DNA, Mycobacterium tuberculosis gene amplification assay; *, P<0.05, compared to LAM assay.

function in diabetic individuals may render them less capable of resisting the invasion and dissemination of Mtb (Birhanu et al., 2019). Since LAM concentration is closely related to bacterial load (Shah et al., 2010), this could contribute to the increased detectability of LAM in tuberculosis patients with diabetes. Furthermore, the association between a higher rate of LAM detection and a lower CD4 count has been extensively demonstrated in studies involving HIV-infected individuals (Huerga et al., 2019a). This may be attributed to the diminished anti-tuberculosis immune response associated with a low CD4 count, which leads to increased invasion and dissemination of Mtb, resulting in elevated LAM levels in the body (Huerga et al., 2019a). The WHO recommends the use of the Lateral Flow urine lipoarabinomannan (LF-LAM) assay as a rapid point-of-care test to assist in the diagnosis of tuberculosis in patients with advanced HIV-induced immunosuppression (Organization, 2019). Additional research also demonstrated that LAM exhibits higher sensitivity in patients with lower CD4 counts (Achkar et al., 2011) (Huerga et al., 2019b). Our study demonstrates that, when sensitivity is sufficient, LAM testing can also be applicable to HIV-negative populations and immunocompromised individuals.

We also compared LAM with other laboratory diagnostic methods. Our results showed that GeneXpert had a sensitivity of 55.13% and a specificity of 100%, The sensitivity of the two methods is in line with literature reports 57.4% (Zhang et al., 2018). TB-DNA had a sensitivity of 38.16% and a specificity of 100%; sputum culture had a sensitivity of 46.71% and a specificity of 100%. The sensitivity of the two methods is in line with literature reports (Horne et al., 2010; Inoue et al., 2011). Notably, the sensitivity of the urinary LAM assay (chemiluminescence) was determined to be 50.6%, which is significantly higher than that of TB-DNA(P<0.05), and higher than that of the sputum culture but lower than that of the GeneXpert method. These results suggest that the urinary LAM test may be a valuable tool for the diagnosis of tuberculosis, particularly in cases where GeneXpert or TB-DNA may not be readily available or suitable.

In addition, we also investigated the detection rates of the four diagnostic methods for pulmonary and extra pulmonary tuberculosis. Previous research has indicated that the incidence and prevalence of extrapulmonary tuberculosis may be underestimated due to several factors, including inadequate attention to extrapulmonary tuberculosis, insufficient diagnostic methods, and low rates of confirmation. This situation has led to a consistently lower cure rate for EPTB compared to PTB, posing challenges to global tuberculosis control efforts (Gambhir et al., 2017; Raghuvanshi et al., 2018). In this study, the detection rates of Gene Xpert, TB-DNA, and sputum culture for extrapulmonary tuberculosis are as follows: 11.76%, 16.67%, and 25%. Consistent with our findings, other studies have also observed that conventional methods are not very effective in detecting extrapulmonary tuberculosis, with a positivity rate ranging from 17.3% to 33.2% (Liu et al., 2020). The low sensitivity of these diagnostic tests may be attributed to the low number of mycobacteria present in peritoneal effusion (Rufai et al., 2015). In contrast, LAM showed detection rates of 51.7% for pulmonary tuberculosis and 42.11% for extrapulmonary tuberculosis. LAM's detection rate in extrapulmonary tuberculosis was higher than the other three diagnostic methods, particularly significantly higher than Gene Xpert (P<0.05). This highlights the significant advantage of LAM in diagnosing EPTB compared to existing clinical diagnostic methods. It is non-invasive, simple, rapid, and accurate.

Our study has limitations that indicate further research is warranted. Firstly, it is a single-center study and did not cover data from multiple centers or a large sample size. Therefore, further research is needed to expand to broader regions and include a larger number of samples. Second, as a retrospective study, patients were not consequently recruited to complete the evaluation of multiple diagnostics. The bias in the selection of the participants may weaken confidence in results. Lastly, LAM testing cannot distinguish between TB and NTM, which is consistent with previous findings (Broger et al., 2020; van Crevel and Critchley, 2021). Overall, despite these limitations, our study highlights the potential for further investigation. Future research should encompass multiple centers, larger sample sizes, and prospective designs to ensure more comprehensive and robust results.

Conclusion

In conclusion, urinary LAM antigen detection using chemiluminescence represents a significant advancement in the clinical diagnosis of active TB. It can be widely used in both HIV-negative and HIV-positive populations of tuberculosis patients. The superior diagnostic performance of LAM, combined with its convenience in acquiring samples from individuals who cannot produce sputum or have difficulties in sputum collection, makes it a

promising approach. That can contribute to global efforts in controlling and managing tuberculosis. However, further research and validation are necessary to fully harness the potential of LAM detection and to optimize its integration into tuberculosis (TB) diagnostic algorithms worldwide.

Data availability statement

The original contributions presented in the study are included in the article/Supplementary Material. Further inquiries can be directed to the corresponding author.

Ethics statement

The studies involving humans were approved by Zhangjiagang Hospital (No. ZJGYYLL -2022-11-021). The studies were conducted in accordance with the local legislation and institutional requirements. Written informed consent for participation in this study was provided by the participants' legal guardians/next of kin.

Author contributions

LH: Writing – original draft. YN: Writing – review & editing. LZ: Writing – original draft. RY: Writing – original draft. MW: Writing – review & editing.

Funding

The author(s) declare financial support was received for the research, authorship, and/or publication of this article. This work was supported in part by grants from the Respiratory Infectious Diseases Clinical Medical Center of Suzhou, China (Szlcyxzx202108); Youth Science and Technology Project of Suzhou, China (KJXW2022046) and Zhangjiagang Medical and Health Technology Innovation Guidance Project, China (ZKYL2233).

Acknowledgments

The authors would like to thank Leide Biosciences Co., Ltd for providing kits and testing services. Special appreciation goes to Juanjuan Peng and Hongxia Wei for their collaboration and support, which greatly contributed to the success of this study.

Conflict of interest

The authors declare that the research was conducted in the absence of any commercial or financial relationships that could be construed as a potential conflict of interest.

Publisher's note

Supplementary material

The Supplementary Material for this article can be found online at: https://www.frontiersin.org/articles/10.3389/fcimb.2023.1291974/full#supplementary-material

SUPPLEMENTARY TABLE 1
The diagnostic performance of four methods in NTM CRS, composite reference standard; NTM, nontuberculosis mycobacteria; Non-TB, non-tuberculosis; LAM, Liboarabinomannan;TB-DNA, *Mycobacterium tuberculosis* gene amplification assay; PPV, positive predictive value; NPV, negative predictive value. Sensitivity = True Positive Cases/(True Positive Cases + False Negative Cases) × 100%; Specificity = True Negative Cases/(True Negative Cases + False Positive Cases) × 100%; PPV = True Positive Cases/(True Positive Cases + False Positive Cases) × 100%; NPV = True Negative Cases/(True Negative Cases + False Negative Cases) × 100%.

References

Achkar, J. M., Lawn, S. D., Moosa, M. Y., Wright, C. A., and Kasprowicz, V. O. (2011). Adjunctive tests for diagnosis of tuberculosis: serology, ELISPOT for site-specific lymphocytes, urinary lipoarabinomannan, string test, and fine needle aspiration. *J. Infect. Dis.* 204 (suppl_4), S1130–S1141. doi: 10.1093/infdis/jir450

Al-Rifai, R. H., Pearson, F., Critchley, J. A., and Abu-Raddad, L. J. (2017). Association between diabetes mellitus and active tuberculosis: A systematic review and meta-analysis. *PloS One* 12 (11), e0187967. doi: 10.1371/journal.pone.0187967

Azadi, D., Motallebirad, T., Ghaffari, K., and Shojaei, H. (2018). Mycobacteriosis and tuberculosis: laboratory diagnosis. *Open Microbiol. J.* 12, 41. doi: 10.2174/1874285801812010041

Bagcchi, S. (2023). WHO's global tuberculosis report 2022. *Lancet Microbe* 4 (1), e20. doi: 10.1016/S2666-5247(22)00359-7

Birhanu, A., Negash, M., Genetu, M., Wondmagegn, T., and Shibabaw, T. (2019). Immunological impacts of diabetes on the susceptibility of mycobacterium tuberculosis. *J. Immunol. Res.* 2019, 6196532–6196532. doi: 10.1155/2019/6196532

Bjerrum, S., Schiller, I., Dendukuri, N., Kohli, M., Nathavitharana, R. R., Zwerling, A. A., et al (2019). Lateral flow urine lipoarabinomannan assay for detecting active tuberculosis in people living with HIV. *Cochrane Database Syst Rev.* 10 (10), CD011420. doi: 10.1002/14651858

Boonsarngsuk, V., Mangkang, K., and Santanirand, P. (2018). Prevalence and risk factors of drug-resistant extrapulmonary tuberculosis. *Clin. Respir. J.* 12 (6), 2101–2109. doi: 10.1111/crj.12779

Brennan, P. J. (2003). Structure, function, and biogenesis of the cell wall of *Mycobacterium tuberculosis*. *Tuberculosis* 83 (1-3), 91–97. doi: 10.1016/S1472-9792(02)00089-6

Broger, T., Nicol, M. P., Sigal, G. B., Gotuzzo, E., Zimmer, A. J., Surtie, S., et al. (2020). Diagnostic accuracy of 3 urine lipoarabinomannan tuberculosis assays in HIV-negative outpatients. *J. Clin. Invest.* 130 (11), 5756–5764. doi: 10.1172/JCI140461

Broger, T., Koeppel, L., Huerga, H., Miller, P., Gupta-Wright, A., Blanc, F. X., et al. (2023). Diagnostic yield of urine lipoarabinomannan and sputum tuberculosis tests in

people living with HIV: a systematic review and meta-analysis of individual participant data. *Lancet Global Health* 11 (6), e903–e916. doi: 10.1016/S2214-109X(23)00135-3

De, P., Amin, A. G., Graham, B., Martiniano, S. L., Caceres, S. M., Poch, K. R., et al. (2020). Urine lipoarabinomannan as a marker for low-risk of NTM infection in the CF airway. *J. Cystic Fibrosis* 19 (5), 801–807. doi: 10.1016/j.jcf.2020.06.016

Fernandes, G. F. S., Thompson, A. M., Castagnolo, D., Denny, W. A., and Dos Santos, J. L. (2022). Tuberculosis drug discovery: challenges and new horizons. *J. Medicinal Chem.* 65 (11), 7489–7531. doi: 10.1021/acs.jmedchem.2c00227

Flores, J., Cancino, J. C., and Chavez-Galan, L. (2021). Lipoarabinomannan as a point-of-care assay for diagnosis of tuberculosis: how far are we to use it? *Front. Microbiol.* 12, 638047. doi: 10.3389/fmicb.2021.638047

Franzblau, S. G., DeGroote, M. A., Cho, S. H., Andries, K., Nuermberger, E., Orme, I. M., et al. (2012). Comprehensive analysis of methods used for the evaluation of compounds against Mycobacterium tuberculosis. *Tuberculosis* 92 (6), 453–488. doi: 10.1016/j.tube.2012.07.003

Gambhir, S., Ravina, M., Rangan, K., Dixit, M., Barai, S., Bomanji, J., et al. (2017). Imaging in extrapulmonary tuberculosis. *Int. J. Infect. Dis.* 56, 237–247. doi: 10.1016/j.ijid.2016.11.003

Goletti, D., Delogu, G., Matteelli, A., and Migliori, G. B. (2022). The role of IGRA in the diagnosis of tuberculosis infection, differentiating from active tuberculosis, and decision making for initiating treatment or preventive therapy of tuberculosis infection. *Int. J. Infect. Dis.* 124, S12–S19. doi: 10.1016/j.ijid.2022.02.047

Health, N (2018). China, Diagnosis for pulmonary tuberculosis (WS288-2017). *Electr J. Emerg. Infect. Dis.* 3, 59–61F.P.C.O.t.P.S.R.O

Health, P.S.R.O.C.S and F.P. Commission (2018). Tuberculosis classification (WS196-2017). *Electronic J. Emerging Infect. Dis.* 3 (03), 191–192.

Horne, D. J., Royce, S. E., Gooze, L., Narita, M., Hopewell, P. C., Nahid, P., et al. (2010). Sputum monitoring during tuberculosis treatment for predicting outcome: systematic review and meta-analysis. *Lancet Infect. Dis.* 10 (6), 387–394. doi: 10.1016/S1473-3099(10)70071-2

Huerga, H., Rucker, S. C. M., Bastard, M., Dimba, A., Kamba, C., Amoros, I., et al. (2019a). Should urine-LAM tests be used in TB symptomatic HIV-positive patients when no CD4 count is available? A prospective observational cohort study from Malawi. *JAIDS J. Acquired Immune Deficiency Syndromes* 83 (1), 1. doi: 10.1097/QAI.0000000000002206

Huerga, H., Mathabire Rucker, S. C., Cossa, L., Bastard, M., Amoros, I., Manhiça, I., et al. (2019b). Diagnostic value of the urine lipoarabinomannan assay in HIV-positive, ambulatory patients with CD4 below 200 cells/µl in 2 low-resource settings: a prospective observational study. *PloS Med.* 16 (4), e1002792. doi: 10.1371/journal.pmed.1002792

Inoue, M., Tang, W. Y., Wee, S. Y., and Barkham, T. (2011). Audit and improve! Evaluation of a real-time probe-based PCR assay with internal control for the direct detection of *Mycobacterium tuberculosis* complex. *Eur. J. Clin. Microbiol. Infect. Dis.* 30, 131–135. doi: 10.1007/s10096-010-1059-z

Lange, C., Böttger, E. C., Cambau, E., Griffith, D. E., Guglielmetti, L., van Ingen, J., et al. (2022). Consensus management recommendations for less common non-tuberculous mycobacterial pulmonary diseases. *Lancet Infect. Dis.* 22 (7), e178–e190. doi: 10.1016/S1473-3099(21)00586-7

Lawn, S. D., and Gupta-Wright, A. (2016). Detection of lipoarabinomannan (LAM) in urine is indicative of disseminated TB with renal involvement in patients living with HIV and advanced immunodeficiency: evidence and implications. *Trans. R. Soc. Trop. Med. Hygiene* 3), 180. doi: 10.1093/trstmh/trw008

Lawn, S. D., Edwards, D. J., Kranzer, K., Vogt, M., Bekker, L. G., and Wood, R. (2009). Urine lipoarabinomannan assay for tuberculosis screening before antiretroviral therapy diagnostic yield and association with immune reconstitution disease. *Aids* 23 (14), 1875–1880. doi: 10.1097/QAD.0b013e32832e05c8

Lawn, S. D., Kerkhoff, A. D., Vogt, M., and Wood, R. (2012). Diagnostic accuracy of a low-cost, urine antigen, point-of-care screening assay for HIV-associated pulmonary tuberculosis before antiretroviral therapy: a descriptive study. *Lancet Infect. Dis.* 12 (3), 201–209. doi: 10.1016/S1473-3099(11)70251-1

Liu, D., Gu, L., Zhang, R., Liu, L., Shen, Y., Shao, Y., et al. (2022). Utility of urine lipoarabinomannan (LAM) in diagnosing mycobacteria infection among hospitalized HIV-positive patients. *Int. J. Infect. Dis.* 118, 65–70. doi: 10.1016/j.ijid.2022.02.046

Liu, R., Li, J., Tan, Y., Shang, Y., Li, Y., Su, B., et al. (2020). Multicenter evaluation of the acid-fast bacillus smear, mycobacterial culture, Xpert MTB/RIF assay, and adenosine deaminase for the diagnosis of tuberculous peritonitis in China. *Int. J. Infect. Dis.* 90, 119–124. doi: 10.1016/j.ijid.2019.10.036

Minion, J., Leung, E., Talbot, E., Dheda, K., Pai, M., and Menzies, D. (2011). Diagnosing tuberculosis with urine lipoarabinomannan: systematic review and meta-analysis. *Eur. Respir. J.* 38 (6), 1398–1405. doi: 10.1183/09031936.00025711

National Health Commission of the People's Republic of China (2017a). *WS 288-2017 Diagnosis for Pulmonary Tuberculosis Standards*.

National Health Commission of the People's Republic of China (2017b). *WS 196-2017 Classification of Tuberculosis*.

Ohene, S.-A., Bakker, M. I., Ojo, J., Toonstra, A., Awudi, D., and Klatser, P. (2019). Extra-pulmonary tuberculosis: a retrospective study of patients in Accra, Ghana. *PloS One* 14 (1), e0209650. doi: 10.1371/journal.pone.0209650

Organization, W. H. (2020). *WHO consolidated guidelines on tuberculosis. Module 3: diagnosis-rapid diagnostics for tuberculosis detection* (Geneva: World Health Organization).

Organization, W. H. (2022). *WHO consolidated guidelines on tuberculosis. Module 3: diagnosis. Tests for TB infection* (Geneva: World Health Organization).

Oshima, M., Shimizu, M., Yamanouchi, M., Toyama, T., Hara, A., Furuichi, K., et al. (2021). Trajectories of kidney function in diabetes: a clinicopathological update. *Nat. Rev. Nephrol.* 17 (11), 740–750. doi: 10.1038/s41581-021-00462-y

Pang, Y., An, J., Shu, W., Huo, F., Chu, N., Gao, M., et al. (2019). Epidemiology of extrapulmonary tuberculosis among inpatients, China, 2008–2017. *Emerging Infect. Dis.* 25 (3), 457. doi: 10.3201/eid2503.180572

Raghuvanshi, S., Kotwal, A., Maheshwari, R., and Sindhwani, G. (2018). Evaluation of line-probe assay for molecular analysis and drug susceptibility of extra-pulmonary tuberculosis. *Int. J. Tuberculosis Lung Dis.* 22 (9), 1077–1081. doi: 10.5588/ijtld.17.0802

Rufai, S. B., Singh, A., Kumar, P., Singh, J., and Singh, S. (2015). Performance of Xpert MTB/RIF assay in diagnosis of pleural tuberculosis by use of pleural fluid samples. *J. Clin. Microbiol.* 53 (11), 3636–3638. doi: 10.1128/JCM.02182-15

Sakamuri, R. M., Price, D.N., Lee, M., Cho, S. N., Barry, C. E. 3rd, Via, L. E., et al. (2013). Association of lipoarabinomannan with high density lipoprotein in blood: Implications for diagnostics. *Tuberculosis* 93 (3), 301–307. doi: 10.1016/j.tube.2013.02.015

Shah, M., Martinson, N. A., Chaisson, R. E., Martin, D. J., Variava, E., and Dorman, S. E. (2010). Quantitative analysis of a urine-based assay for detection of lipoarabinomannan in patients with tuberculosis. *J. Clin. Microbiol.* 48 (8), 2972–2974. doi: 10.1128/JCM.00363-10

Steingart, K. R., Schiller, I., Horne, D. J., Pai, M., Boehme, C. C., and Dendukuri, N. (2014). Xpert® MTB/RIF assay for pulmonary tuberculosis and rifampicin resistance in adults. *Cochrane Database systematic Rev.* 2014 (1), CD009593. doi: 10.1002/14651858.CD009593.pub3

Székely, R., Sossen, B., Mukoka, M., Muyoyeta, M., Nakabugo, E., Hella, J., et al. (2022). Multicentre accuracy trial of FUJIFILM SILVAMP TB LAM test in people with HIV reveals lot variability. *medRxiv*. doi: 10.1101/2022.09.07.22278961

Uplekar, M., Weil, D., Lonnroth, K., Jaramillo, E., Lienhardt, C., Dias, H. M., et al. (2015). WHO's new end TB strategy. *Lancet* 385 (9979), 1799–1801. doi: 10.1016/S0140-6736(15)60570-0

van Crevel, R., and Critchley, J. A. (2021). The interaction of diabetes and tuberculosis: translating research to policy and practice. *Trop. Med. Infect. Dis.* 6 (1), 8. doi: 10.3390/tropicalmed6010008

Zhang, Q., Zhang, Q., Sun, B. Q., Liu, C., Su, A. N., Wang, X. H., et al. (2018). GeneXpert MTB/RIF for rapid diagnosis and rifampin resistance detection of endobronchial tuberculosis. *Respirology* 23 (10), 950–955. doi: 10.1111/resp.13316

Zhao, D., Yang, X. M., Chen, Q. Y., Zhang, X. S., Guo, C. J., and Che, XY. (2012). A modified acid-fast staining method for rapid detection of Mycobacterium tuberculosis. *J. microbiological Methods* 91 (1), 128–132. doi: 10.1016/j.mimet.2012.07.024

frontiers | Frontiers in Cellular and Infection Microbiology

TYPE Original Research
PUBLISHED 24 January 2024
DOI 10.3389/fcimb.2024.1338861

OPEN ACCESS

EDITED BY
Stefano Stracquadanio,
University of Catania, Italy

REVIEWED BY
Nikhil Ram Mohan,
Stanford University, United States
Hua Jiang,
Guangzhou Medical University, China

*CORRESPONDENCE
Ning Sun
steamsn@163.com

†These authors have contributed equally to this work

RECEIVED 15 November 2023
ACCEPTED 08 January 2024
PUBLISHED 24 January 2024

CITATION
Yu J, Zhang L, Gao D, Wang J, Li Y and Sun N (2024) Comparison of metagenomic next-generation sequencing and blood culture for diagnosis of bloodstream infections. *Front. Cell. Infect. Microbiol.* 14:1338861. doi: 10.3389/fcimb.2024.1338861

Comparison of metagenomic next-generation sequencing and blood culture for diagnosis of bloodstream infections

Juan Yu[1,2†], Li Zhang[1†], Deyu Gao[2], Jie Wang[3], Yi Li[2] and Ning Sun[2*]

[1]Department of Clinical Laboratory, Nanjing Lishui People's Hospital, Nanjing, China, [2]Department of Clinical Laboratory Science, Jinling Hospital, Affiliated Hospital of Medical School, Nanjing University, Nanjing, China, [3]Clinical Medicine Research Center, The Affiliated Suqian First People's Hospital of Nanjing Medical University, Suqian, China

Objectives: This study aimed to evaluate the clinical performance of plasma cell-free DNA (cfDNA) next-generation sequencing (NGS) for pathogen detection in patients with sepsis.

Methods: A total of 43 pairs of blood and plasma samples form 33 blood culture-positive patients were used as testing samples in metagenomic NGS (mNGS) and NGS of 16S ribosomal RNA gene amplicons (16S rRNA NGS). The results of routine tests, including microbial culture, complete blood count, and biochemical tests, were collected from electronic medical records.

Results: Using blood as an mNGS testing sample, the proportion of host DNA was 99.9%, with only three bacteria and no fungi detected. When using plasma in mNGS, the proportion of host DNA was approximately 97%, with 84 bacteria and two fungi detected. Notably, 16S rRNA NGS detected 15 and 16 bacteria in 43 pairs of blood and plasma samples, respectively. Blood culture detected 49 bacteria (23 gram-negative bacilli and 26 gram-positive cocci) and four fungi, with 14 bacteria considered contaminants by clinical microbiologists. For all blood cultures, plasma cfDNA mNGS detected 78.26% (19/23) gram-negative rods, 17% (2/12) gram-positive cocci, and no fungi. Compared to blood cultures, the sensitivity and specificity of plasma cfDNA mNGS for detecting bacteria and fungi were 62.07% and 57.14%, respectively.

Conclusion: Compared to blood, plasma is more suitable for the detection of bloodstream infections using mNGS and is less affected by host DNA. The positive detection rate of plasma cfDNA mNGS for bloodstream infections caused by gram-negative bacteria was higher than that caused by gram-positive cocci.

KEYWORDS

bloodstream infections, plasma cell-free DNA, metagenomic next-generation sequencing, 16S rRNA, diagnosis

1 Introduction

Bloodstream infection (BSI) is a serious disease caused by various pathogens, such as bacteria, fungi, and viruses, which enter and reproduce in the bloodstream (Martinez and Wolk, 2016; Lamy et al., 2020). It usually occurs in compromised patients, such as those in intensive care units or those with long-term hospital stays, organ transplant recipients, and patients with tumors, and often lead to severe complications, such as sepsis, shock, and even death (Martinez and Wolk, 2016; Lamy et al., 2020). The sources of BSIs are diverse and include surgical incision, lung, catheter-related, and abdominal infection. An early and accurate diagnosis is crucial for timely and appropriate treatment.

BSIs can be diagnosed based on clinical symptoms, blood biochemical markers, blood cultures, and nucleic acid amplification tests (Martinez and Wolk, 2016; Gu et al., 2019; Lamy et al., 2020; Gu et al., 2021; Yan et al., 2023). Blood culture is the most common method for the detection and identification of bacteria and fungi in patients with sepsis and can also optimize the use of antimicrobial drugs and evaluate treatment effectiveness (Garcia et al., 2015; Opota et al., 2015; Fabre et al., 2022). However, the turnaround time for blood cultures is usually over 24 hours and is prone to false positives and negatives (Garcia et al., 2015). Recently, metagenomic next-generation sequencing (mNGS) has attracted widespread attention for use in pathogen detection (Gu et al., 2019; Gu et al., 2021; Yan et al., 2021). It is a culture-independent detection method that can detect all pathogens and identify rare or unknown pathogens. However, mNGS also has disadvantages, such as complex sample preparation, cumbersome sequencing procedures, and the effect of host DNA. Several studies have shown that plasma cell-free DNA (cfDNA) mNGS (plasma mNGS) has significant value in the BSI detection and can significantly reduce the adverse effects of host DNA (Grumaz et al., 2016; Blauwkamp et al., 2019; Barrett et al., 2020; Yan et al., 2021; Park et al., 2023; Xu et al., 2023). cfDNA in the plasma is fragmented DNA derived from dead microorganisms, whereas whole blood samples may contain live pathogens and higher concentrations of microbial genomic DNA. Direct evidence is needed to confirm that detecting cfDNA in the plasma using mNGS is a good choice for clinical performance. Additionally, BSIs can also be identified using the NGS-targeted 16S rRNA gene (16S rRNA NGS), which can not only alleviate the impact of host DNA, but also significantly reduce the cost of testing (Rutanga et al., 2018). Similar to mNGS, the detection and identification of BSIs using 16S rRNA NGS can be performed directly on whole blood or plasma samples (El Gawhary et al., 2016; Lelouvier et al., 2016; Moore et al., 2016; Païssé et al., 2016; Fida et al., 2021). More data are required to compare and evaluate the clinical performance of 16S rRNA NGS in the diagnosis of BSIs.

In this study, we aimed to evaluate the clinical performance of 16S rRNA NGS and mNGS (plasma mNGS, blood mNGS, plasma 16S RNA NGS, and blood 16S RNA NGS) in the detection and identification of pathogens in patients with sepsis using plasma and blood as test samples.

2 Materials and methods

2.1 Study overviews and subjects

This is a non-interventional and retrospective study. Between April 2023 and June 2023, 198 residual peripheral venous blood samples were collected after routine testing from 170 patients who underwent blood culture testing on the same day. Samples with positive blood cultures were retained for mNGS and 16S rRNA NGS, whereas those with negative blood cultures were excluded. The sources of BSIs were determined based on microbiological culture, clinical symptoms, imaging examination, and treatment response. Any remaining blood samples were stored in standard EDTA tubes, with an approximate volume of 2 ml. One microliter of peripheral venous blood samples was immediately stored at -80°. The remaining samples were centrifuged at 16000×g for 10 min, and 800 µl of plasma was collected and stored at -80°. This study was approved by the Ethics Committee of Jinling Hospital and People's Hospital of Lishui (Nanjing, China), and informed consent was not required because patient information was anonymized and residual samples were obtained after routine testing.

2.2 Blood cultures

In our clinical microbiology laboratory, the standard blood culture involved two sets: one set included a pair of BD BACTEC Plus Aerobic/F bottles and BD BACTEC Lytic Anaerobic/F bottles (Becton Dickinson, Heidelberg, Germany), and the other set consisted of a pair of aerobic and anaerobic blood culture bottles (BacT/ALERT FA/FN Plus, bioMérieux, Marcy-l'Etoile, France). The blood culture bottles were incubated for 5 days. Cultures from positive blood culture bottles were inoculated onto blood, chocolate, and MacConkey agars, followed by microscopic testing. Biochemical identification was performed using the VITEK2 COMPACT system (bioMérieux, Marcy-l'Etoile, France).

2.3 Nucleic acid extraction

Nucleic acid was extracted from 600 µl of peripheral venous blood and plasma using a modified RNA/DNA Purification Kit (Magnetic Bead) in a Stream SP96 Automatic Nucleic Acid Extraction System (DaAnGene, Guangzhou, China). Finally, nucleic acid was eluted in 50 µl of sterile deionized water.

2.4 Metagenomic NGS

Reverse transcription of RNA was performed using PrimeScript™ 1st Strand cDNA Synthesis Kit (Takara, Dalian, China). Subsequently, double-stranded cDNA was synthesized using RNase H and DNA Polymerase I (Takara, Dalian, China) and purified using TaKaRa MiniBEST DNA Fragment Purification Kit Ver.4.0 (Takara, Dalian, China). Double-stranded cDNA was mixed with equal volume of

nucleic acid elution. DNA was randomly fragmented using Covaris S220 (Covaris, Woburn, MA, USA) to an average size of 300–350 bp. The fragmented DNA was quantified using a Qubit@ 2.0 Fluorometer (Thermo Fisher Scientific Inc., USA). Library preparation, including end repair, adaptor linking, purification, and PCR amplification, was performed using the VAHTS Universal Pro DNA Library Prep Kit for Illumina (Vazyme Biotech Co., Ltd., Nanjing, China). The library was determined and quantified by Agilent 2100 Bioanalyzer and Qubit@ 2.0 Fluorometer (Thermo Fisher Scientific Inc., USA). NGS was performed using the NovaSeq platform (Illumina, San Diego, CA, US) with 2×150 paired ends.

2.5 16S rRNA NGS

As described in our previous study (Sun et al., 2023), the V3–V4 region of the 16S rRNA gene was amplified using two universal primers with adaptor (341F and 806R), and NGS was performed using a NovaSeq platform (Illumina, San Diego, CA, US) with 2×250 paired ends.

2.6 Negative and internal controls

Sterile deionized water and three paired samples of peripheral venous blood and plasma collected from healthy individuals after routine testing were used as the blank and negative controls, respectively. Artificial synthetic DNA (7.5×10^4 copies) was used as an internal control and spiked into all samples and controls to serve as a quality control. All controls were processed in parallel with all the samples.

2.7 Bioinformatic analysis

Raw data obtained from mNGS were analyzed using a previously-described protocol (Lu et al., 2022), and data obtained from 16S rRNA NGS were analyzed using the Basic Local Alignment Search Tool (BLAST, version 2.12.0+, https://blast.ncbi.nlm.nih.gov/Blast.cgi) (Rognes et al., 2016). Low-quality mNGS and 16S rRNA NGS data were removed using Fastp software (Chen et al., 2018). Host DNA reads were removed after alignment with the human reference genome GRCh38 using BWA-MEM (Li, 2013). The clean data were annotated with a prebuilt database (https://genome-idx.s3.amazonaws.com/kraken/k2_standard_eupath_ 20201202.tar.gz) using kraken2 software. The clean reads from16S rRNA NGS were clustered using VSEARCH with 100% identity (Rognes et al., 2016). Operational taxonomic units were annotated using BLAST+ against the National Center for Biotechnology Information 16S rRNA database.

2.8 Criteria for pathogen identification

The criteria for pathogen identification were developed as described in the previous studies (Blauwkamp et al., 2019; Gu et al., 2019; Barrett et al., 2020; Gu et al., 2021; Wang et al., 2021; Yan et al., 2021; Xu et al., 2023). For mNGS, the reads per million (RPM) and Z-scores of each species per sample were calculated using Pavian (https://fbreitwieser.shinyapps.io/pavian/) and compared with negative controls. Because of the concentration of host DNA, we compared the mNGS results with the corresponding sample types of negative controls, for example, plasma samples versus plasma negative controls. The criteria were as follows: 1) The Z-score of pathogens in the sample was three-fold higher than that in negative controls; 2) the reads were strictly mapped to three different regions of the genome; and 3) the species with the highest abundance were retained when the RPM was more than five times. Furthermore, each species was considered a pathogen when it was considered clinically relevant by clinicians or had been reported in the literature. The detection and identification of pathogens using 16S rRNA NGS was based on our previous study (Sun et al., 2023).

2.9 Statistical analysis

Statistical analysis was performed using R software (Version 4.3.0). Continuous variables are presented as means and standard deviations, and categorical variables are presented as counts and percentages. The results of blood and plasma mNGS were compared using the non-parametric Mann-Whitney U test. Clinical sensitivity and specificity were calculated using standard formulas and evaluated using Fisher's exact test.

3 Results

3.1 Patient characteristics

Of the 198 samples, 43 blood culture-positive samples collected from 33 hospitalized patients were screened to evaluate the clinical performance of NGS in the detection and identification of pathogens. The mean age was 50 years old, and 76% (25/33) of patients were men. The patients included in the study presented with signs and symptoms of infection, including respiratory and abdominal infections. They were promptly treated with empirical anti-microbial therapies, such as piperacillin/tazobactam or biapenem. Blood culture testing was administered when their body temperature exceeded 38°. The mean length of the hospital stay was 31 days. The median white blood cell count was 11.7 × 10^9 cells/l, median lymphocyte count was 0.67 × 10^9 cells/l, and median neutrophils were 9.6 × 10^9 cells/l. The median values of C-reactive protein and procalcitonin were 91.6 mg/l and 1.525 μg/l, respectively, with the levels exceeding the normal range. The hospitalization diagnoses included three cases of intestinal fistula, one case of abdominal injury, two cases of lung infection, one case of abdominal pain, one case of rapidly progressive nephritis, 20 cases of acute severe pancreatitis, one case of Crohn's disease, one case of chronic renal insufficiency, one case of duodenal fistula, one case of gastrointestinal bleeding, and one case of tremor.

3.2 Comparison of blood and plasma mNGS in the detection of pathogen

The influence of host DNA on the detection and identification of pathogens using mNGS was analyzed using DNA extracted from

the blood and plasma. After removing host DNA reads, the mean number of reads of plasma mNGS accounted for 3.04% (95% CI: 2.21% to 3.86%; reads: 9.83 × 10^5), whereas the mean number of reads of blood mNGS is 0.05% (95% CI: 0.045% to 0.050%; reads: 7.96 × 10^3). There was a significant difference between the two groups (Figures 1A, B). We compared the reads of the internal controls spiked with plasma and blood samples. The results showed that no reads were determined in the three blood samples, and the mean number of reads in all blood samples were five (relative abundance was 0.059%; 95% CI: 0.044% to 0.073%). For plasma mNGS, the mean number of reads are 2 × 10^3 (relative abundance of 0.22%; 95% CI: 0.17% to 0.27%). A significant difference was observed in the detection of internal controls between the two methods (Figures 1C, D). Therefore, plasma is a better choice for the detection and identification of pathogens in BSIs using mNGS.

3.3 Comparison of mNGS and 16S rRNA NGS using blood and plasma as test samples

Blood mNGS detected only three bacteria in there samples (sample ID: B02, B12, and B43), which were also detected by plasma mNGS (Figure 2A). However, plasma mNGS detected 84 bacteria belonging to 26 genera and 40 species, as well as two fungi (Figure 2A), of which 22% (19/86) were *Klebsiella pneumoniae* (Figure 2C). The median RPM of bacteria and fungi were 3.29 (range: 0.11 to 10801.45; Figure 2D). Notably, various DNA viruses were detected (Figure 2E), such as human betaherpesvirus 5 (CMV), human alphaherpesvirus 1 (HSV1), human alphaherpesvirus 2 (HSV2), torque teno virus (TTV), human gammaherpesvirus (EBV), and hepatitis B virus (HBV), and the median RPM was 0.91 (range: 0.07 to 10958.91; Figure 2F). No RNA viruses were detected using mNGS. The types and abundance of DNA viruses detected in the plasma were higher than those in the blood samples (Figures 2B, E). The results of 16S rRNA NGS for detecting bacteria in the blood and plasma samples showed that there were only 10 consistent bacteria between the two methods (Figure 2A), and there was no significant difference in read counts (Figures 2G, H). By comparing mNGS and 16S rRNA NGS, we found that plasma mNGS could detect more potential pathogens.

3.4 Comparison of plasma cell-free mNGS with blood cultures

Of the 43 samples, blood culture detected 49 bacteria (23 gram-negative bacilli and 26 gram-positive cocci) and four fungi, and 14 gram-positive cocci were determined to be contaminants by clinical microbiologists (Figure 3A; Supplementary Table S1). After removing the contaminating strains, 31 blood culture-positive samples (72%) were obtained, with 24 samples showing bacteremia caused by a

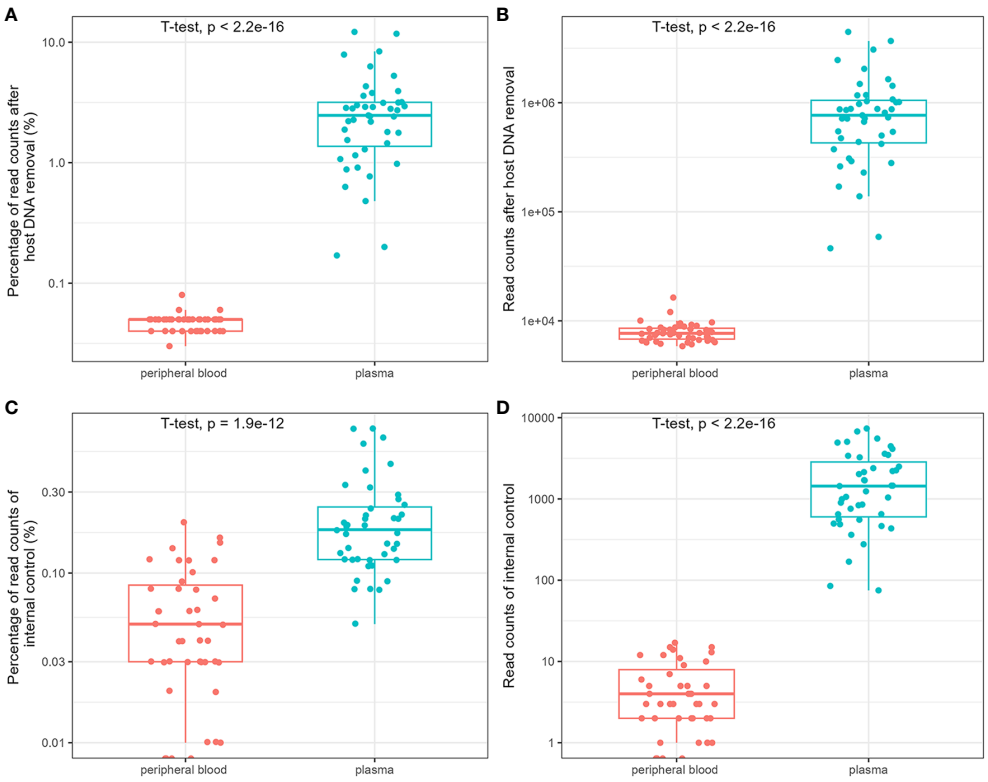

FIGURE 1
Comparison of the influence of host DNA on detection and identification of pathogens using metagenomic next-generation sequencing (mNGS). The relative abundance and reads of non-host DNA **(A, B)** and internal controls **(C, D)**.

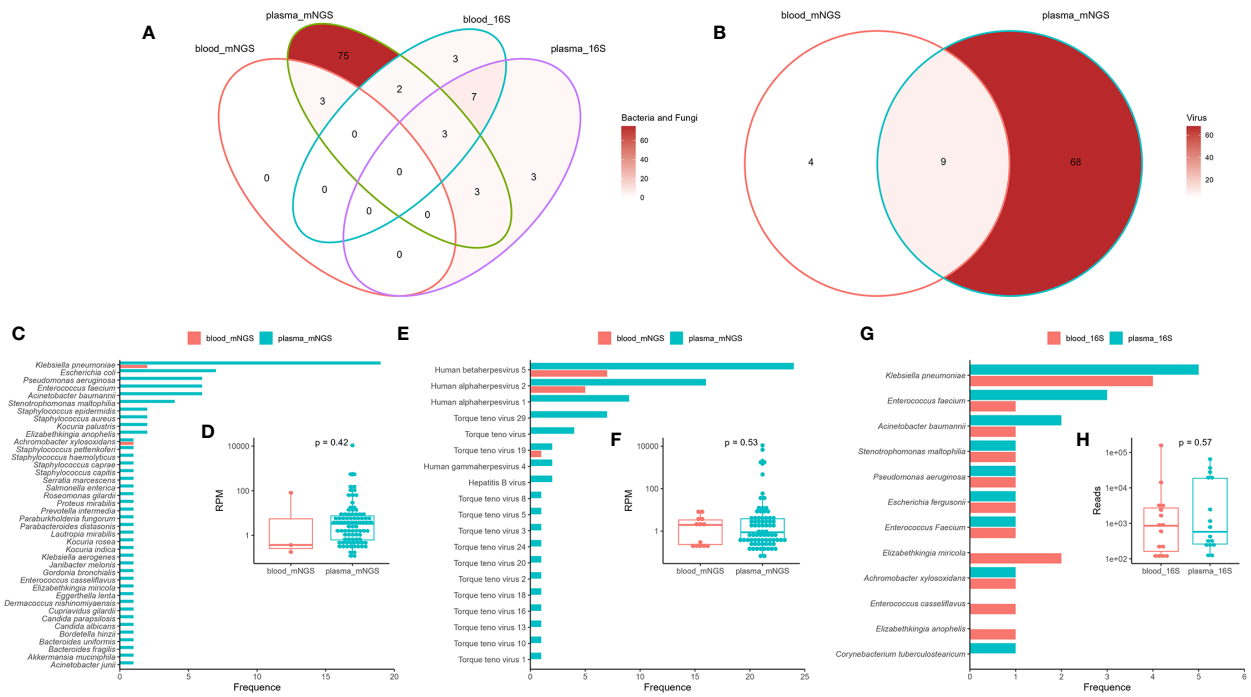

FIGURE 2
Comparison of mNGS and 16S rRNA gene next-generation sequencing (16S rRNA NGS) in detection of bloodstream infections using blood and plasma as test samples. Venn diagram analysis of the consistency of the detection results (**A**: bacteria and fungi; **B**: viruses) using mNGS and 16S rRNA NGS. Distribution and reads per million (RPM) of microbes (**C**, **D**: bacteria and fungi; **E**, **F**: virus) detected by mNGS. Distribution **(G)** and reads **(H)** of bacteria detected by 16S rRNA NGS. Plasma_mNGS, mNGS using plasma as a test sample. Blood_mNGS, mNGS using blood as a test sample. Plasma_16S, 16S rRNA NGS using plasma as a test sample. Blood_16S, 16S rRNA NGS using blood as a test sample.

single bacterium and seven samples containing two or more pathogens (Figure 3B). Analysis of the source of BSIs showed that 16 were catheter-related infections, nine were abdominal infections, eight were pancreatic infections, five were respiratory tract infections, and one was a urinary tract infection (Figure 3C). The comparison between plasma mNGS and blood culture showed a consistency rate of 78.26% (19/23) for gram-negative bacteria and only 17% (2/12) for gram-positive cocci (Figure 3D). Both fungi were detected by blood culture, whereas the 14 gram-positive contaminants were not detected by plasma mNGS. The mean time of positivity to detect gram-positive bacteria was 19.4 hours, which was longer than the mean time of positivity to detect gram-negative bacteria (15.1 hours); however, there was no significant difference ($p = 0.473$, Figure 3E). There was no significant correlation between the number of positive blood culture bottles and plasma mNGS results (Figure 3F). The type of bacteria had a significant influence on plasma mNGS, with higher positivity for gram-negative bacteria than for gram-positive bacteria and fungi.

The plasma mNGS results were consistent with the blood culture results for 26 samples, including 18 blood culture-positive samples and eight false-positive samples (Table 1, Supplementary Table S1). However, there were differences between the blood culture and plasma mNGS results for 17 samples (Table 2). Thirteen samples were positive for blood culture, whereas four samples were false positives. The source of BSIs in the 13 samples from 11 patients included seven catheter-related BSIs, two respiratory tract infections, three pancreatic infections, and one intra-abdominal infection. In sample B10, *Enterococcus faecium* was not detected by plasma mNGS; however, consecutive blood and catheter tip cultures indicated catheter-related BSIs. In sample B12, *Candida auris* was not detected by plasma mNGS; however, infection source analysis showed that the patient had respiratory tract-, pancreatic-, and catheter-related infections. Case P17 (samples B19 and B20) involved pancreatic infection and catheter-related BSI, with catheter tip culture results showing *Enterococcus faecalis* and *C. parapsilosis*, and pancreatic fluid culture showing *K. pneumoniae* and *E. faecalis*. *Acinetobacter baumannii* was not detected in two samples by plasma mNGS. In case P03 (sample B03), the aerobic bottle in the lower left quadrant of the blood culture showed a positive result with a positivity time of 10 hours. The other three bottles were negative after 5 days of incubation. The patient's pancreatic fluid culture revealed *K. pneumoniae*, which was also detected by plasma mNGS. In case P18 (sample B21), blood cultures revealed *A. baumannii* by blood culture, whereas plasma mNGS detected *Acinetobacter junii*. *Staphylococcus aureus* was not detected in two cases. Patient P06 had glomerulonephritis and developed a catheter-related BSI. However, the culture results of the catheter tip, pus, and blood revealed *S. aureus*. Plasma mNGS detected *Kocuria rosea* and *Janibacter melonis*, which are skin surface colonizers and potential pathogens that cause BSIs. In case P24 (samples B25 and B28, blood cultures 24 hours interview), *Staphylococcus hominis*, a common skin surface commensal and an unusual pathogen causing catheter-related BSI, was detected, whereas

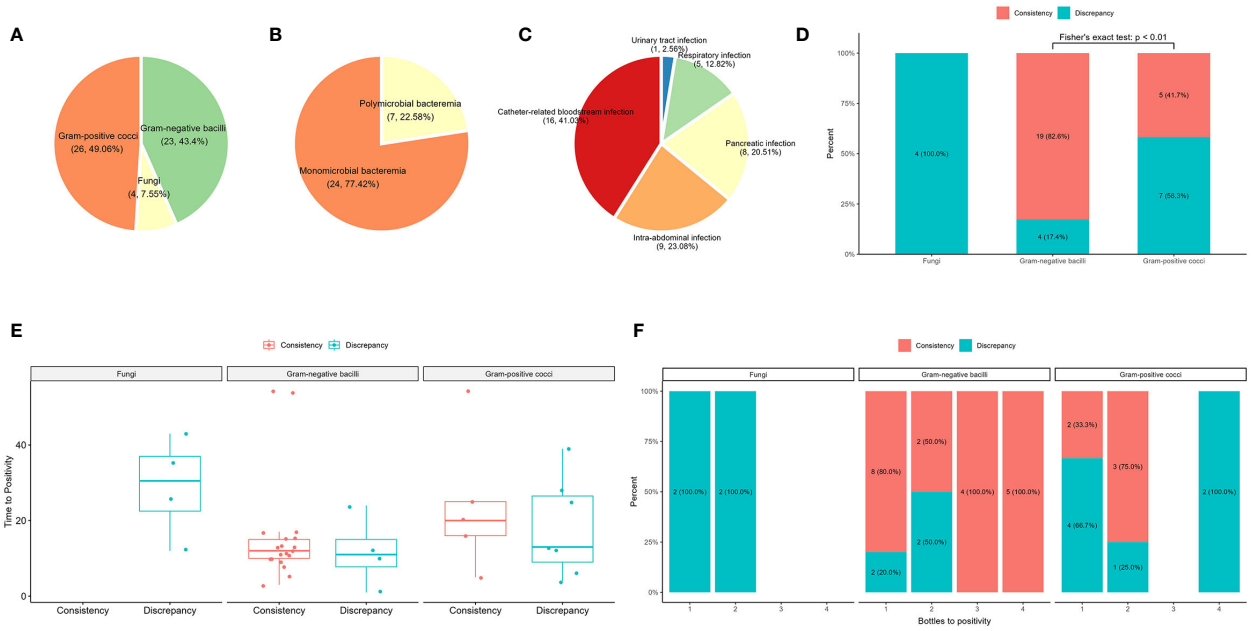

FIGURE 3
Comparison of plasma mNGS and blood culture in the detection of bacteria and fungi. **(A)** Distribution of blood culture. **(B)** Composite of monomicrobial and polymicrobial bacteremia after removal of the contaminating strains. **(C)** The source of bloodstream infections. **(D)** The influence of the type of pathogen detected by plasma mNGS versus blood culture. **(E)** Effect of time of positivity of blood culture on plasma mNGS. **(F)** Number of bottles of blood culture used in plasma mNGS.

plasma mNGS detected *K. pneumoniae* and *E. faecium*, which were also detected by pancreatic fluid culture. Case P11 (sample B13) presented with a gastrointestinal hemorrhage. During hospitalization, respiratory tract infection and catheter-related BSI were observed. *Candida parapsilosis* was cultured from aerobic bottles for 12 hours on both sides. Plasma mNGS detected *Pseudomonas aeruginosa*, which was consistent with the culture of sputum and bronchoalveolar lavage before 24 hours. In Case P21 (sample B25), *Burkholderia cepacia* was detected by blood culture, with all four bottles showing positive results after 24 hours. However, plasma mNGS only detected *Staphylococcus epidermidis* and *Elizabethkingia miricola*, which were also detected by plasma 16S rRNA NGS. Case P09 (B33) had a catheter-related BSI. *E. faecalis* and *Stenotrophomonas maltophilia* were cultured from the blood culture after 2 days and from catheter tip culture after 1day. Notably, the plasma mNGS did not detect any pathogens on the same day. However, both *E. faecalis* and *S. maltophilia* were detected by plasma mNGS after 2 days.

3.5 Clinical performance of plasma mNGS

We evaluated the clinical performance of plasma mNGS for bacterial and fungal detection using blood cultures as a reference method. Of the 43 samples, plasma mNGS was considered positive only when all pathogens detected by blood culture were detected. The sensitivity and specificity of plasma mNGS were 62.07% (95% CI: 42% to 79%) and 57.14% (95% CI: 29% to 82%), respectively, and the agreement between the two methods was 60% (Table 3). Plasma mNGS detected two cases of HBV, nine cases of HSV1, 16 cases of HSV2, 24 cases of CMV, two cases of human gammaherpesvirus 4, and 11 cases of TTV among the 43 samples. Since TTV is also widely present in healthy individuals, and the results of real-time PCR showed that TTV DNA was positive in all 43 samples, TTV was excluded. Using the results of real-time PCR as a reference method, the sensitivity and specificity of plasma mNGS for virus detection were 66.67%–85.71% and 58.62%–100%, respectively (Table 3).

4 Discussion

In this study, we carried out a retrospective study comparing 16S rRNA NGS and mNGS using whole blood and plasma as testing samples for detecting pathogens causing BSIs and compared the results with those of blood culture and viral real-time PCR. We found that, at a fixed depth, the proportion of host reads in whole blood samples exceeded 99%, making it ineffective for the detection and identification of pathogens in patients with sepsis. Compared with 16S rRNA NGS, mNGS could detect more potentially pathogenic bacteria in BSIs. Additionally, a novel finding was that mNGS had a higher detection consistency with blood culture for BSIs caused by gram-negative bacteria, whereas the detection consistency results for catheter-related BSIs caused by gram-positive bacteria was low.

We tested 43 pairs of blood culture-positive samples, with a mean of 64 million (range: 34–70 million) reads. Using whole blood and plasma as testing samples for mNGS, the proportions of host reads were 0.05% and 3.04%, respectively. Internal controls were added to all samples; however, owing to the influence of host DNA,

TABLE 1 Concordant results between blood culture and plasma cell-free DNA mNGS.

Patient ID	sample ID	Gender	Disease[a]	Age	Admission date	Discharge date	Sampling date	Bottle positives	Time to positivity	Results of blood culture	Results of plasma mNGS	Source of blood culture
P01	B01	male	SAP	37	2023/3/9	2023/4/30	2023/4/25	1/4	10	*Acinetobacter baumannii*	*Staphylococcus aureus*, *Klebsiella pneumoniae*, *Acinetobacter baumannii*	Catheter-related bloodstream infection
P02	B02	male	SAP	47	2023/4/21	2023/4/28	2023/4/26	4/4, 2/4	11, 25	*Klebsiella pneumoniae*, *Enterococcus faecium*	*Klebsiella pneumoniae*, *Acinetobacter baumannii*, *Enterococcus faecium*	Intra-abdominal infection
P04	B04	male	SAP	53	2023/3/24	2023/5/11	2023/4/27	4/4	13	*Pseudomonas aeruginosa*	*Pseudomonas aeruginosa*, Human alphaherpesvirus 1, *Staphylococcus haemolyticus*, Human betaherpesvirus 5	Catheter-related bloodstream infection
P04	B09	male	SAP	53	2023/3/24	2023/5/11	2023/5/6	1/4	17	*Pseudomonas aeruginosa*	*Pseudomonas aeruginosa*, *Stenotrophomonas maltophilia*, Human betaherpesvirus 5, Human alphaherpesvirus 1	Catheter-related bloodstream infection
P05	B05	female	AP	50	2023/4/10	2023/5/10	2023/5/3	3/4, 1/4, 3/4	9, 13, 15	*Pseudomonas aeruginosa*, *Klebsiella pneumoniae*, *Stenotrophomonas maltophilia*	*Pseudomonas aeruginosa*, *Stenotrophomonas maltophilia*, *Klebsiella pneumoniae*, Human betaherpesvirus 5	Catheter-related bloodstream infection
P08	B08	male	Pulmonary infection	87	2023/4/18	2023/6/2	2023/5/5	1/4	13	*Klebsiella pneumoniae*	Human betaherpesvirus 5, *Klebsiella pneumoniae*	Urinary tract infection
P10	B11	female	intestinal fistula	48	2023/4/26	2023/5/15	2023/5/6	3/4, 1/4	3, 54	*Klebsiella pneumoniae*, *Escherichia coli*	*Klebsiella pneumoniae*, *Pseudomonas aeruginosa*, *Bacteroides uniformis*, *Parabacteroides distasonis*, *Akkermansia muciniphila*, *Eggerthella lenta*, *Escherichia coli*, Human betaherpesvirus 5	Intra-abdominal infection
P12	B14	male	abdominal pain	53	2023/5/10	2023/5/11	2023/5/10	4/4	12	*Escherichia coli*	*Escherichia coli*, *Enterococcus casseliflavus*, Human betaherpesvirus 5	Intra-abdominal infection
P13	B15	male	pulmonary infection	35	2023/5/10	2023/5/18	2023/5/11	1/4	15	*Klebsiella pneumoniae*	*Klebsiella pneumoniae*, *Dermacoccus nishinomiyaensis*, *Acinetobacter baumannii*, Human betaherpesvirus 5	Respiratory infection

(Continued)

10.3389/fcimb.2024.1338861

TABLE 1 Continued

Patient ID	sample ID	Gender	Disease[a]	Age	Admission date	Discharge date	Sampling date	Bottle positives	Time to positivity	Results of blood culture	Results of plasma mNGS	Source of blood culture
P13	B22	male	pulmonary infection	35	2023/5/10	2023/5/18	2023/5/11	1/4	15	*Acinetobacter baumannii*	*Klebsiella pneumoniae*, *Acinetobacter baumannii*	Respiratory infection
P14	B16	male	AP	43	2023/4/3	2023/5/20	2023/5/11	1/4	17	*Klebsiella pneumoniae*	*Klebsiella pneumoniae*, Human betaherpesvirus 5	Pancreatic infection
P15	B17	male	SAP	55	2023/5/4	2023/5/22	2023/5/11	2/4	11	*Acinetobacter baumannii*	*Escherichia coli*, *Klebsiella pneumoniae*, *Cupriavidus gilardii*, *Salmonella enterica*, *Acinetobacter baumannii*, *Pantoea ananatis*, Human betaherpesvirus 5	Intra-abdominal infection
P15	B35	male	SAP	55	2023/5/4	2023/5/22	2023/5/11	2/4	11	*Enterococcus faecium*	*Elizabethkingia anophelis*, *Escherichia coli*, *Enterococcus faecium*	Intra-abdominal infection
P16	B18	male	SAP	38	2023/5/12	2023/6/8	2023/5/12	1/4	11	*Klebsiella pneumoniae*	*Klebsiella pneumoniae*	Pancreatic infection
P19	B23	female	AP	50	2023/3/20	2023/5/18	2023/5/16	1/4	12	*Acinetobacter baumannii*	*Staphylococcus aureus*, *Escherichia coli*, *Proteus mirabilis*, *Acinetobacter baumannii*	Catheter-related bloodstream infection
P20	B24	male	duodenal fistula	53	2023/5/15	2023/5/26	2023/5/17	3/4	5	*Klebsiella pneumoniae*	*Klebsiella pneumoniae*, *Escherichia coli*, Human betaherpesvirus 5	Intra-abdominal infection
P25	B29	female	AP	66	2023/4/26	2023/6/10	2023/4/27	2/4	16	*Enterococcus faecium*	*Enterococcus faecium*	Pancreatic infection
P28	B36	female	psychogenic tremor	88	2023/5/9	2023/5/16	2023/5/6	2/4	12, 23	*Staphylococcus epidermidis*	*Paraburkholderia fungorum*, *Escherichia coli*, *Roseomonas gilardii*, *Kocuria indica*, *Staphylococcus epidermidis*	Respiratory infection

[a]SAP, Severe acute pancreatitis; AP, acute pancreatitis.

10.3389/fcimb.2024.1338861

TABLE 2 Discordant Culture and mNGS results.

Patient ID	Sample ID	Gender	Disease[a]	Age	Admission date	Discharge date	Sampling date	Bottle positives	Time to positivity	Results of blood culture	Results of plasma mNGS (reads)	Source of blood culture
P03	B03	male	SAP	32	2023/2/18	2023/5/17	2023/4/26	1/4	10	*Acinetobacter baumannii*	Human betaherpesvirus 5	Pancreatic infection
P04	B12	male	SAP	53	2023/3/24	2023/5/11	2023/5/8	1/4, 4/4	26	*Candida auris*, *Achromobacter xylosoxidans*	*Achromobacter xylosoxidans*, Human betaherpesvirus 5, *Pseudomonas aeruginosa*, *Serratia marcescens*, *Bordetella hinzii*, *Stenotrophomonas maltophilia*, *Klebsiella pneumoniae*, *Candida parapsilosis*	Catheter-related bloodstream infection
P06	B06	male	Glomerulonephritis	67	2023/4/27	2023/5/11	2023/5/3	4/4	4	*Staphylococcus aureus*	Human betaherpesvirus 5, *Kocuria rosea*, *Janibacter melonis*	Catheter-related bloodstream infection
P07	B07	male	AP	36	2023/4/14	2023/5/12	2023/5/4	1/4	39	*Staphylococcus aureus*	Human betaherpesvirus 5, *Klebsiella aerogenes*, *Kocuria palustris*	Intra-abdominal infection
P09	B33	male	SAP	38	2023/3/27	2023/5/19	2023/5/4	1/4	13	*Enterococcus*	Human betaherpesvirus 5	Catheter-related bloodstream infection
P09	B10	male	SAP	38	2023/3/27	2023/5/19	2023/5/6	4/4, 2/4	6, 10	*Enterococcus faecium*, *Stenotrophomonas maltophilia*	*Lautropia mirabilis*, Human betaherpesvirus 5, *Prevotella intermedia*, *Stenotrophomonas maltophilia*, *Bacteroides fragilis*	Catheter-related bloodstream infection
P11	B13	male	Gastrointestinal hemorrhage	74	2023/5/5	2023/5/10	2023/5/9	2/4	12	*Candida parapsilosis*	*Pseudomonas aeruginosa*, Human betaherpesvirus 5	Respiratory infection
P17	B19	male	SAP	37	2023/5/11	2023/5/22	2023/5/12	2/4, 1/4	35, 54	*Candida parapsilosis*, *Enterococcus*	*Klebsiella pneumoniae*, *Enterococcus faecium*, Human alphaherpesvirus 2, Human betaherpesvirus 5, Human alphaherpesvirus 1	Pancreatic infection
P17	B20	male	SAP	37	2023/5/11	2023/5/22	2023/5/14	2/4, 1/4	20, 43	*Enterococcus faecium*, *Candida parapsilosis*	*Gordonia bronchialis*, *Enterococcus faecium*, *Klebsiella pneumoniae*, Human alphaherpesvirus 2, Human	Pancreatic infection

(Continued)

10.3389/fcimb.2024.1338861

TABLE 2 Continued

Patient ID	Sample ID	Gender	Disease[a]	Age	Admission date	Discharge date	Sampling date	Bottle positives	Time to positivity	Results of blood culture	Results of plasma mNGS (reads)	Source of blood culture
											betaherpesvirus 5, Human alphaherpesvirus 1	
P18	B21	male	SAP	33	2023/5/5	2023/5/28	2023/5/14	4/4	1	*Acinetobacter baumannii*	*Acinetobacter junii*, Human betaherpesvirus 5, Human alphaherpesvirus 1	Catheter-related bloodstream infection
P21	B25	female	SAP	51	2023/5/15	2023/6/19	2023/5/17	4/4	24	*Burkholderia cepacia*	*Staphylococcus epidermidis*, *Elizabethkingia miricola*, Human betaherpesvirus 5	Respiratory infection
P23	B27	male	Chronic renal insufficiency	44	2023/4/25	2023/5/8	2023/4/25	1/4	17	Staphylococcus haemolyticus	*Staphylococcus epidermidis*, Human alphaherpesvirus 2	Contaminant
P24	B28	male	AP	38	2023/4/23	2023/5/5	2023/4/27	1/4	28	Staphylococcus hominis	*Klebsiella pneumoniae*, *Enterococcus faecium*, Human alphaherpesvirus 2, Hepatitis B virus, Human betaherpesvirus, Torque teno virus, Human alphaherpesvirus 2	Catheter-related bloodstream infection
P24	B31	male	AP	38	2023/4/23	2023/5/5	2023/4/28	1/4	25	Staphylococcus hominis	*Klebsiella pneumoniae*, Hepatitis B virus, Torque teno virus	Catheter-related bloodstream infection
P26	B32	female	Crohn's disease	68	2023/4/27	2023/5/26	2023/5/3	1/4	46	Enterococcus	*Elizabethkingia anopheles*, *Kocuria palustris*, *Klebsiella pneumoniae*, *Candida albicans*	Contaminant
P30	B43	male	SAP	47	2023/5/9	2023/6/2	2023/5/17	2/4	21	Staphylococcus hominis	*Klebsiella pneumoniae*, Human betaherpesvirus 5, Human alphaherpesvirus 1, Human alphaherpesvirus 2, Human gammaherpesvirus 4	Contaminant
P31	B39	female	AP	38	2023/3/8	2023/5/16	2023/5/11	1/4	25	Staphylococcus epidermidis	Staphylococcus capitis, Staphylococcus caprae, Staphylococcus pettenkoferi	Contaminant

[a]SAP, Severe acute pancreatitis; AP, acute pancreatitis.

10.3389/fcimb.2024.1338861

TABLE 3 The agreement of plasma mNGS results versus those of blood culture and real-time PCR virus test.

		Plasma mNGS								
		Positive	Negative	Sensitivity (%)	Specificity (%)	PPV (%)	NPV (%)	*p*-value	Kappa	Agreement
Blood culture	Positive	18	11	62.07	57.14	75.00	42.11	0.33	0.18	0.60
	Negative	6	8							
CMV real-time PCR	Positive	12	2	85.71	58.62	50.00	89.47	< 0.05	0.37	0.67
	Negative	12	17							
EBV real-time PCR	Positive	2	1	66.67	100.00	100.00	97.56	< 0.05	0.79	0.98
	Negative	0	40							
HSV1 real-time PCR	Positive	9	3	75.00	96.77	90.00	90.91	< 0.05	0.76	0.91
	Negative	1	30							
HSV2 real-time PCR	Positive	16	5	76.19	90.91	88.89	80.00	< 0.05	0.67	0.84
	Negative	2	20							

CMV, human betaherpesvirus 5; EBV, human gammaherpesvirus; HSV1, human alphaherpesvirus 1; HSV2, human alphaherpesvirus 2.

no internal control reads were detected in any of the three samples. The presence of host DNA is unfavorable for the detection and identification of pathogenic microorganisms that cause BSIs (Blauwkamp et al., 2019; Gu et al., 2019; Gu et al., 2021). Although the sequencing depth can be increased, this can significantly increase sequencing costs and the difficulty of data analysis. Using plasma as a testing sample for the metagenomic detection of pathogenic microorganisms causing BSIs is an effective way to reduce detection costs.

While several studies have demonstrated that combining 16S rRNA NGS with blood culture can enhance the sensitivity and specificity of detecting bloodstream infections (BSIs), it is worth noting that in some cases, whole blood and plasma samples were directly used without prior blood culture (El Gawhary et al., 2016; Lelouvier et al., 2016; Moore et al., 2016; Païssé et al., 2016; Rutanga et al., 2018; Fida et al., 2021). Using 16S rRNA NGS with whole blood and plasma as testing samples, 15 and 16 bacteria were detected, respectively, with 10 bacteria identical between the samples and accounting for 67% and 63% of the detections, respectively. This may be because fragmented pathogenic bacterial DNA exists in plasma, whereas intact bacteria may exist in whole blood, resulting in a few differences in the types of bacteria present in the two types of samples. Furthermore, the sensitivity and specificity of 16S rRNA NGS can be significantly impacted by the low pathogenic bacterial load, which can be as low as 1-10 colony-forming units per microliter in whole blood. To improve the detection of BSIs, it is beneficial to use a larger volume of blood (Rutanga et al., 2018). Compared with 16S rRNA NGS for BSIs, plasma mNGS can detect more potentially pathogenic microorganisms, including viruses and fungi (Rodriguez et al., 2020). 16S rRNA NGS is a high-throughput sequencing method targeting the 16S rRNA gene. The copy number of the 16S rRNA gene in plasma or whole blood samples is much lower than that of fragmented pathogenic bacterial DNA. Furthermore, the 16S rRNA gene is not effective in distinguishing certain bacteria (Muhamad Rizal et al., 2020; Stebner et al., 2021; Sun et al., 2023), such as Enterobacteriaceae, *Staphylococcus*. In conclusion, 16S rRNA NGS is not suitable for detecting pathogenic bacteria that cause BSIs.

We screened positive blood culture samples to evaluate the clinical performance of mNGS. The results showed that the sensitivity and specificity of plasma mNGS were 62.07% and 57.14%, respectively, which were lower than those reported in previous studies (Blauwkamp et al., 2019; Wang et al., 2021; Xu et al., 2023). This may be because the proportion of true-positive blood cultures was 67.44% (29/43), which is higher than that reported in previous studies (Hogan et al., 2021; Wang et al., 2021; Falabello De Luca et al., 2023), resulting in a lower sensitivity and specificity of detection. The sources of BSIs were classified, and it was found that the detection rate of gram-negative bacteria, mostly originating from gastrointestinal infections, was higher than that of gram-positive cocci causing catheter-related infections. It has been proposed that the gram-positive bacteria responsible for catheter-related BSIs may have a relatively low abundance. In fact, the average bacterial reads detected in peripheral blood samples were found to be approximately 1/200th of the reads observed in the catheter tip (Yan et al., 2023). When conducting mNGS to detect BSIs, analyzing the potential sources of infection could be more effective, especially for catheter-related infections. This approach can lead to a faster and more accurate diagnosis, allowing timely and appropriate treatment interventions to reduce the burden on patients. No RNA viruses were detected; however, multiple DNA viruses, including CMV, EBV, and HSV, were detected in these patients. These viruses proliferate easily in immunocompromised patients, thereby affecting their prognosis. The positivity rate of CMV detection with plasma mNGS was higher than that with real-time PCR, which may be due to the mismatch of primers and probes for CMV, resulting in the omission of some subtypes. Alternatively, it may be due to the low copy number of the amplification region in real-time PCR, which may have affected CMV detection.

This study has some limitations. First, the sample size was not particularly large, especially regarding the variety of sources of BSIs in patients. Second, the results of blood cultures for some samples may have been affected by sampling issues, leading to some positive blood cultures being considered contaminants, thus affecting our comparative analysis of a large number of positive results. Finally, some mNGS results were not effectively validated, and whether the free DNA of pathogenic microorganisms in the plasma causes BSIs, or is released into the bloodstream from the site of infection after the death of the pathogenic microorganisms remains unclear.

In conclusion, we found that using mNGS with plasma samples is more suitable for detecting BSIs, is less affected by host DNA, and can detect more potential pathogens than 16S rRNA NGS. More importantly, the detection of BSIs caused by gram-negative bacteria was more consistent with blood cultures than with those caused by gram-positive bacteria.

Data availability statement

The data presented in the study are deposited in the repository of National Genomics Data Center of China (http://ngdc.cncb.ac.cn), with the accession number of PRJCA021184 (https://ngdc.cncb.ac.cn/gsa/s/Am54C9dr).

Ethics statement

The studies involving humans were approved by the ethical standards of Jinling Hospital of China. The studies were conducted in accordance with the local legislation and institutional requirements. Written informed consent for participation was not required from the participants or the participants' legal guardians/next of kin because patient information was anonymized and the samples were residual after routine testing.

Author contributions

JY: Writing – original draft, Conceptualization, Formal Analysis, Investigation, Methodology, Resources. LZ: Conceptualization, Formal Analysis, Resources, Funding acquisition, Writing – original draft. DG: Formal Analysis, Resources, Investigation, Methodology, Writing – original draft. JW: Investigation, Methodology, Writing – original draft. YL: Investigation, Methodology, Writing – original draft. NS: Writing – original draft, Writing – review & editing.

Funding

The author(s) declare financial support was received for the research, authorship, and/or publication of this article. This study was funded by the Health Technology Development Special Foundation of Nanjing City (No. YKK18216), the Suqian Sci&Tech Program (SY202214), and the National Key Clinical Program of China (grant no. 2014ZDZK003).

Conflict of interest

The authors declare that the research was conducted in the absence of any commercial or financial relationships that could be construed as a potential conflict of interest.

Publisher's note

Supplementary material

The Supplementary Material for this article can be found online at: https://www.frontiersin.org/articles/10.3389/fcimb.2024.1338861/full#supplementary-material

References

Barrett, S. L. R., Holmes, E. A., Long, D. R., Shean, R. C., Bautista, G. E., Ravishankar, S., et al. (2020). Cell free DNA from respiratory pathogens is detectable in the blood plasma of Cystic Fibrosis patients. *Sci. Rep.* 10, 6903. doi: 10.1038/s41598-020-63970-0

Blauwkamp, T. A., Thair, S., Rosen, M. J., Blair, L., Lindner, M. S., Vilfan, I. D., et al. (2019). Analytical and clinical validation of a microbial cell-free DNA sequencing test for infectious disease. *Nat. Microbiol.* 4, 663–674. doi: 10.1038/s41564-018-0349-6

Chen, S., Zhou, Y., Chen, Y., and Gu, J. (2018). fastp: an ultra-fast all-in-one FASTQ preprocessor. *Bioinformatics* 34, i884–i890. doi: 10.1093/bioinformatics/bty560

El Gawhary, S., El-Anany, M., Hassan, R., Ali, D., and El Gameel, E. Q. (2016). The role of 16S rRNA gene sequencing in confirmation of suspected neonatal sepsis. *J. Trop. Pediatr.* 62, 75–80. doi: 10.1093/tropej/fmv066

Fabre, V., Carroll, K. C., and Cosgrove, S. E. (2022). Blood culture utilization in the hospital setting: a call for diagnostic stewardship. *J. Clin. Microbiol.* 60, e01005–e01021. doi: 10.1128/jcm.01005-21

Falabello De Luca, A. C., Marinho, G. B., Franco, J. B., Tenório, J. D. R., Andrade, N. S., Batista, A. M., et al. (2023). Quantification of Torque Teno Virus (TTV) in plasma and saliva of individuals with liver cirrhosis: a cross sectional study. *Front. Med.* 10. doi: 10.3389/fmed.2023.1184353

Fida, M., Wolf, M. J., Hamdi, A., Vijayvargiya, P., Esquer Garrigos, Z., Khalil, S., et al. (2021). Detection of pathogenic bacteria from septic patients using 16S ribosomal RNA gene–targeted metagenomic sequencing. *Clin. Infect. Dis.* 73, 1165–1172. doi: 10.1093/cid/ciab349

Garcia, R. A., Spitzer, E. D., Beaudry, J., Beck, C., Diblasi, R., Gilleeny-Blabac, M., et al. (2015). Multidisciplinary team review of best practices for collection and handling

of blood cultures to determine effective interventions for increasing the yield of true-positive bacteremias, reducing contamination, and eliminating false-positive central line–associated bloodstream infections. *Am. J. Infection Control* 43, 1222–1237. doi: 10.1016/j.ajic.2015.06.030

Grumaz, S., Stevens, P., Grumaz, C., Decker, S. O., Weigand, M. A., Hofer, S., et al. (2016). Next-generation sequencing diagnostics of bacteremia in septic patients. *Genome Med.* 8, 73. doi: 10.1186/s13073-016-0326-8

Gu, W., Deng, X., Lee, M., Sucu, Y. D., Arevalo, S., Stryke, D., et al. (2021). Rapid pathogen detection by metagenomic next-generation sequencing of infected body fluids. *Nat. Med.* 27, 115–124. doi: 10.1038/s41591-020-1105-z

Gu, W., Miller, S., and Chiu, C. Y. (2019). Clinical metagenomic next-generation sequencing for pathogen detection. *Annu. Rev. Pathol. Mech. Dis.* 14, 319–338. doi: 10.1146/annurev-pathmechdis-012418-012751

Hogan, C. A., Yang, S., Garner, O. B., Green, D. A., Gomez, C. A., Dien Bard, J., et al. (2021). Clinical impact of metagenomic next-generation sequencing of plasma cell-free DNA for the diagnosis of infectious diseases: A multicenter retrospective cohort study. *Clin. Infect. Dis.* 72, 239–245. doi: 10.1093/cid/ciaa035

Lamy, B., Sundqvist, M., and Idelevich, E. A. (2020). Bloodstream infections – Standard and progress in pathogen diagnostics. *Clin. Microbiol. Infection* 26, 142–150. doi: 10.1016/j.cmi.2019.11.017

Lelouvier, B., Servant, F., Païssé, S., Brunet, A.-C., Benyahya, S., Serino, M., et al. (2016). Changes in blood microbiota profiles associated with liver fibrosis in obese patients: A pilot analysis. *Hepatology* 64, 2015–2027. doi: 10.1002/hep.28829

Li, H. (2013) *Aligning sequence reads, clone sequences and assembly contigs with BWA-MEM*. Available at: http://arxiv.org/abs/1303.3997 (Accessed April 4, 2023).

Lu, J., Rincon, N., Wood, D. E., Breitwieser, F. P., Pockrandt, C., Langmead, B., et al. (2022). Metagenome analysis using the Kraken software suite. *Nat. Protoc.* 17, 2815–2839. doi: 10.1038/s41596-022-00738-y

Martinez, R. M., and Wolk, D. M. (2016). Bloodstream infections. *Microbiol. Spectr.* 4, 4.4.42. doi: 10.1128/microbiolspec.DMIH2-0031-2016

Moore, M. S., McCarroll, M. G., McCann, C. D., May, L., Younes, N., and Jordan, J. A. (2016). Direct screening of blood by PCR and pyrosequencing for a 16S rRNA gene target from emergency department and intensive care unit patients being evaluated for bloodstream infection. *J. Clin. Microbiol.* 54, 99–105. doi: 10.1128/JCM.02394-15

Muhamad Rizal, N. S., Neoh, H., Ramli, R., A/L K Periyasamy, P. R., Hanafiah, A., Abdul Samat, M. N., et al. (2020). Advantages and limitations of 16S rRNA next-generation sequencing for pathogen identification in the diagnostic microbiology laboratory: perspectives from a middle-income country. *Diagnostics* 10, 816. doi: 10.3390/diagnostics10100816

Opota, O., Croxatto, A., Prod'hom, G., and Greub, G. (2015). Blood culture-based diagnosis of bacteraemia: state of the art. *Clin. Microbiol. Infection* 21, 313–322. doi: 10.1016/j.cmi.2015.01.003

Païssé, S., Valle, C., Servant, F., Courtney, M., Burcelin, R., Amar, J., et al. (2016). Comprehensive description of blood microbiome from healthy donors assessed by 16S targeted metagenomic sequencing. *Transfusion* 56, 1138–1147. doi: 10.1111/trf.13477

Park, S. Y., Chang, E. J., Ledeboer, N., Messacar, K., Lindner, M. S., Venkatasubrahmanyam, S., et al. (2023). Plasma microbial cell-free DNA sequencing from over 15,000 patients identified a broad spectrum of pathogens. *J. Clin. Microbiol.* 61, e01855–e01822. doi: 10.1128/jcm.01855-22

Rodriguez, C., Jary, A., Hua, C., Woerther, P.-L., Bosc, R., Desroches, M., et al. (2020). Pathogen identification by shotgun metagenomics of patients with necrotizing soft-tissue infections. *Br. J. Dermatol.* 183, 105–113. doi: 10.1111/bjd.18611

Rognes, T., Flouri, T., Nichols, B., Quince, C., and Mahé, F. (2016). VSEARCH: a versatile open source tool for metagenomics. *PeerJ* 4, e2584. doi: 10.7717/peerj.2584

Rutanga, J. P., Van Puyvelde, S., Heroes, A.-S., Muvunyi, C. M., Jacobs, J., and Deborggraeve, S. (2018). 16S metagenomics for diagnosis of bloodstream infections: opportunities and pitfalls. *Expert Rev. Mol. Diagn.* 18, 749–759. doi: 10.1080/14737159.2018.1498786

Stebner, A., Ensser, A., Geißdörfer, W., Bozhkov, Y., and Lang, R. (2021). Molecular diagnosis of polymicrobial brain abscesses with 16S-rDNA-based next-generation sequencing. *Clin. Microbiol. Infection* 27, 76–82. doi: 10.1016/j.cmi.2020.03.028

Sun, N., Chen, Y., Zhang, J., Cao, J., Huang, H., Wang, J., et al. (2023). Identification and characterization of pancreatic infections in severe and critical acute pancreatitis patients using 16S rRNA gene next generation sequencing. *Front. Microbiol.* 14. doi: 10.3389/fmicb.2023.1185216

Wang, L., Guo, W., Shen, H., Guo, J., Wen, D., Yu, Y., et al. (2021). Plasma microbial cell-free DNA sequencing technology for the diagnosis of sepsis in the ICU. *Front. Mol. Biosci.* 8. doi: 10.3389/fmolb.2021.659390

Xu, C., Chen, X., Zhu, G., Yi, H., Chen, S., Yu, Y., et al. (2023). Utility of plasma cell-free DNA next-generation sequencing for diagnosis of infectious diseases in patients with hematological disorders. *J. Infection* 86, 14–23. doi: 10.1016/j.jinf.2022.11.020

Yan, G., Liu, J., Chen, W., Chen, Y., Cheng, Y., Tao, J., et al. (2021). Metagenomic next-generation sequencing of bloodstream microbial cell-free nucleic acid in children with suspected sepsis in pediatric intensive care unit. *Front. Cell. Infect. Microbiol.* 11. doi: 10.3389/fcimb.2021.665226

Yan, Z., Wang, Y., Zeng, W., Xia, R., Liu, Y., Wu, Z., et al. (2023). Microbiota of long-term indwelling hemodialysis catheters during renal transplantation perioperative period: a cross-sectional metagenomic microbial community analysis. *Ren Fail* 45, 2256421. doi: 10.1080/0886022X.2023.2256421

frontiers | Frontiers in Cellular and Infection Microbiology

TYPE Review
PUBLISHED 13 May 2024
DOI 10.3389/fcimb.2024.1398461

OPEN ACCESS

EDITED BY
Stefano Marletta,
University of Verona, Italy

REVIEWED BY
Andrea Marino,
University of Catania, Italy
Alexis Rodríguez,
Autonomous University of the State of Morelos, Mexico

*CORRESPONDENCE
Natally Dos Santos Silva
natallydossantos8@gmail.com

RECEIVED 09 March 2024
ACCEPTED 29 April 2024
PUBLISHED 13 May 2024

CITATION
Silva NS, De Melo BST, Oliva A and de Araújo PSR (2024) Sonication protocols and their contributions to the microbiological diagnosis of implant-associated infections: a review of the current scenario.
Front. Cell. Infect. Microbiol. 14:1398461.
doi: 10.3389/fcimb.2024.1398461

Sonication protocols and their contributions to the microbiological diagnosis of implant-associated infections: a review of the current scenario

Natally Dos Santos Silva [1*], Beatriz Souza Toscano De Melo [2], Alessandra Oliva [3] and Paulo Sérgio Ramos de Araújo [1]

[1]Departamento de Medicina Tropical - Universidade Federal de Pernambuco – UFPE, Recife, Brazil, [2]Departamento de Microbiologia - Instituto Aggeu Magalhães – Fiocruz, Recife, Brazil, [3]Dipartimento di Sanità Pubblica e Malattie Infettive - Sapienza University of Rome, Rome, Italy

Addressing the existing problem in the microbiological diagnosis of infections associated with implants and the current debate about the real power of precision of sonicated fluid culture (SFC), the objective of this review is to describe the methodology and analyze and compare the results obtained in current studies on the subject. Furthermore, the present study also discusses and suggests the best parameters for performing sonication. A search was carried out for recent studies in the literature (2019-2023) that addressed this research topic. As a result, different sonication protocols were adopted in the studies analyzed, as expected, and consequently, there was significant variability between the results obtained regarding the sensitivity and specificity of the technique in relation to the traditional culture method (periprosthetic tissue culture – PTC). Coagulase-negative *Staphylococcus* (CoNS) and *Staphylococcus aureus* were identified as the main etiological agents by SFC and PTC, with SFC being important for the identification of pathogens of low virulence that are difficult to detect. Compared to chemical biofilm displacement methods, EDTA and DTT, SFC also produced variable results. In this context, this review provided an overview of the most current scenarios on the topic and theoretical support to improve sonication performance, especially with regard to sensitivity and specificity, by scoring the best parameters from various aspects, including sample collection, storage conditions, cultivation methods, microorganism identification techniques (both phenotypic and molecular) and the cutoff point for colony forming unit (CFU) counts. This study demonstrated the need for standardization of the technique and provided a theoretical basis for a sonication protocol that aims to achieve the highest levels of sensitivity and specificity for the reliable microbiological diagnosis of infections associated with implants and prosthetic devices, such as prosthetic joint infections (PJIs). However, practical application and additional complementary studies are still needed.

KEYWORDS

infections, review, sonication, diagnostic, microbiology

1 Introduction

Joint replacement surgeries, known as arthroplasties, are increasingly frequent and widely used procedures with the aim of replacing, remodeling or realigning a joint (Torres et al., 2015; Filho et al., 2020). Taking into account projections on certain orthopedic procedures, for example, by 2030 in the United States, a significant increase in the number of primary hip (174%) and knee (673%) arthroplasties is expected; for the same period, the United Kingdom expects a 400% increase in demand for arthroplasty (Torres et al., 2015; Ahmed and Haddad, 2019; Filho et al., 2020).

This increasing use of implantable technology has also increased the risk of deep surgical site infections (SSIs) (Torres et al., 2015). In this context, prosthetic joint infections (PJIs) occur in the joint area up to two years after surgery and are generally acquired during the implant procedure (Filho et al., 2020). They are classified according to the time interval between surgery and the onset of symptoms, which can be classified as follows: early, if it occurs within a time interval of < 3 months after the placement of the prosthesis; early late, if it occurs within a time interval of 3 to 12 months; and chronic delay, if it occurs within a time interval of >12 months. This classification also involves the way the disease is presented, whether it is acute or chronic (Beam and Osmon, 2018; Zardi and Franceschi, 2020).

Among the most common pathogens associated with PJI are *Staphylococcus* coagulase-negative and *Staphylococcus aureus*, two of which are the most common etiological agents of the disease, followed by *Streptococcus* sp., *Enterococcus* sp., gram-negative bacilli, anaerobes and yeasts. These agents are also known as good biofilm formers and are bacterial structures that are favored in PJI because of the abiotic surface of the implant and the lack of a local immunological response, resulting in persistent and progressive infection during treatment (Karbysheva et al., 2020; Zardi and Franceschi, 2020).

PJI is still considered the second most common complication, second only to aseptic loosening, and is the most important complication in arthroplasty. It may be responsible for loosening, chronic pain and instability of the prosthesis and is thus associated with a high rate of morbidity, in addition to the risk of death and the need for complex treatment strategies that involve surgical interventions and prolonged antibiotic therapy (Flurin et al., 2021; Zhang et al., 2021b). The long-term impacts on patients' quality of life are negative; even following successful clearance of the infection, failure to control the disease can lead to the need for joint fusion and even amputation (Xu et al., 2023).

In addition to causing serious problems for the physical and mental health of patients, PJI also causes relevant economic problems. Hospital fees are generally significantly greater for the treatment of infected joints than for the treatment of noninfected joints. In the United States, the average total cost for revision knee arthroplasty is estimated at US$75,028.07, without considering the costs of prolonged antibiotic therapy at home. Similar patterns have been reported in other developed countries (Zardi and Franceschi, 2020; Xu et al., 2023).

According to statistics from the National Healthcare Safety Network (NHSN), which was released in 2017, joint infections are responsible for 1.9% of all surgical site infections (SSIs) worldwide (Moore et al., 2015). However, despite the widespread use of well-established infection prevention measures, these data on the occurrence of PJI may be underestimated due to one of the greatest challenges of this infection: diagnosis. Since there is no single test or finding for safe and accurate diagnosis, a combination of clinical findings, laboratory results of peripheral blood and synovial fluid, histological evaluations, imaging and molecular studies is performed, in addition to the important and necessary microbiological findings. In this scenario, several standardized diagnostic criteria for PJI have been proposed by different groups and societies, such as the Musculoskeletal Infection Society (MSIS), the Infectious Diseases Society of America (IDSA), the International Consensus Meeting (ICM), and the European Bone and Joint Infection Society (EBJIS), each of which adopts different definitions and cutoff points for the same infection (Trebse and Roskar, 2021).

In the process of diagnosing PJI, periprosthetic tissue culture (PTC) is considered the gold standard diagnostic technique because it allows the identification of infectious pathogen(s) and the determination of antimicrobial susceptibility, and this method can be used to determine the best and most targeted therapeutic approach (Tande and Patel, 2014; Salar et al., 2021). However, the sensitivity of tissue cultures varies from 65 to 94% and presents high false-negative rates, possibly due to the biofilm formation characteristic of this infection, which makes it difficult to obtain viable loose bacteria (planktonic) for cultivation, especially in chronic and low-grade infections preventing an accurate diagnosis from being made, causing treatment failures and prolonging the patient's suffering (Moore et al., 2015; Shen et al., 2015).

Therefore, Trampuz et al. (2007) (Trampuz et al., 2007) popularized the use of the sonication technique to process removed knee and hip prostheses (Trampuz et al., 2007; Shen et al., 2015). Since then, sonication has been suggested as a useful method for sample processing, aiming to physically displace biofilms prior to standard culture. Organizations such as the Swiss Orthopedics and Swiss Society for Infectious Diseases (SOSSID) and EBJIS have supported its use based on studies that reported greater sensitivity and specificity of sonicated fluid culture (SFC) from explanted prostheses compared to standard culture (Shen et al., 2015; Bellova et al., 2019).

However, despite most studies in the literature indicating superior results with sonication, several studies observed a variable effect on the physical displacement of the biofilm (Bellova et al., 2019), and some even showed greater sensitivity of PTC (Oliva et al., 2016). Consequently, these discrepancies raise doubts about the reliability of the sonication technique for more accurate diagnosis of PJI (Oliva et al., 2016; Bellova et al., 2019). These variations can be attributed to the different protocols used for sonication (Oliva et al., 2016; Bellova et al., 2019).

Therefore, this report proposes an analysis of the literature on the subject in a similar way to other recent studies that reviewed the diagnostic methods available for infections associated with implants and their advances, including an overview of sonication (Birlutiu et al., 2017; Portillo and Sancho, 2023; Yilmaz et al., 2023; Azad and

Patel, 2024). However, this review sought to analyze and describe the sonication protocols used in studies published in the last five years, with emphasis on the sensitivity and specificity rates achieved by these methods in comparison with PTC. Furthermore, this review also aimed to identify, in depth, the best parameters that should be considered for potential standardization of sonication protocols based on the most recent published studies.

1.1 Literature search

For the literature search, the following terms were used: "prosthetic joint infection," "sonication," "tissue culture," "biofilm," "sensitivity," "specificity," "diagnosis" and combinations of these terms. The search was conducted in the National Center for Biotechnology Information (NCBI) search engine, PubMed®. To comprehensively examine recent literature, the inclusion criteria for this analysis were original articles that were available electronically, published within the last five years (2019-2023) and written in English. Exclusion criteria included research such as case reports, letters, editorials and books. Furthermore, studies that addressed the microbiological diagnosis of infections other than PJI were excluded.

2 Sonication method

The sonication technique is performed using a device called a sonicator. This device emits sound waves in the ultrasound spectrum, creating high-intensity pressure waves in a liquid medium and causing the formation and collapse of tiny bubbles. When these bubbles collapse, they release energy capable of disrupting intercellular connections on the device's surface, dislodging the bacteria. Additionally, sonication causes the deagglomeration and lysis of cell adhesion proteins, disrupting the physical structure of the biofilm (Oliva et al., 2016).

Due to these characteristics, sonication has been increasingly utilized to increase the yield of bacterial cultures by releasing organisms embedded in biofilms associated with implants and prostheses, particularly in joints. The sonication technique, apart from dislodging bacteria from the biofilm structure, can also lead to the lysis of bacterial cells. However, this outcome depends on various protocol factors, such as the acoustic frequency, energy, temperature, duration of exposure to ultrasound, and shape of the bacteria (Oliva et al., 2021).

2.1 Review/search results

We identified a total of 11 studies that met the established inclusion criteria, and these studies are described in Table 1.

After conducting an exploratory reading of the material obtained, the following points were discussed: 1- the sonication protocol used and the results obtained regarding the sensitivity and specificity compared with those of periprosthetic tissue culture; 2- the main microorganisms isolated; and 3- the ability of sonication protocols to displace biofilm structure compared to other displacement techniques.

3 The sensitivity and specificity of sonication protocols are greater than those of periprosthetic tissue culture

Differences in the parameters of the sonication protocols adopted in the selected studies were observed. These differences include the use and duration of vortexing, the use of centrifugation as a method for determining sample concentration after vortex agitation, and variations in the sonication bath concerning frequency, power density, and time. Additionally, cutoff values for microbial count to define infection differed among the studies (Table 2).

The studies analyzed also calculated the sensitivity and specificity percentages of their sonication protocols and standard cultures. Sensitivity is defined as the ability of the diagnostic test to detect individuals who are truly positive and is calculated according to the number of true positives divided by the number of true positives added to the number of false negatives (TP/(TP+FN)), using the gold standard test as a reference. Specificity is defined as the ability of the diagnostic test to detect true negatives and is calculated according to the number of true negatives divided by the number of true negatives plus the number of false positives (TN/(TN+FP)) using the gold standard test as a reference (Ueda et al., 2019).

The first analyzed sonication protocol included vortex mixing of the container with the implant immersed in sterile saline solution for 30 s, an ultrasound bath at a frequency of 40 ± 2 kHz, and 0.22 ± 0.04 W/cm^2 for 1 min, followed by vortexing for another 30 s. Then, 50 mL of sonicated fluid was centrifuged at 2600 rpm for 15 minutes and cultured. The cutoff for a positive result was ≥1 CFU/plate, calculated as CFU/mL based on CFU/plate. For statistical tests, 2x2 contingency tables were constructed consisting of true-positive (TP), false-positive (FP), false-negative (FN) and true-negative (TN) results, taking positive results for the disease as a reference according to MSIS criteria. Ninety-five percent confidence intervals were calculated as exact binomial confidence intervals. The sensitivity and specificity of the different diagnostic culture methods were compared by McNemar's test of paired proportions. All testing was conducted using SPSS v22.0 software (SPSS, Inc., Chicago, IL), with a p value < 0.05 (in 2-sided testing) considered to indicate statistical significance (Ueda et al., 2019).

The reported sensitivity for SFC was 71%, 95% CI (44.0-88.6), while PTC achieved a sensitivity of 59%, 95% CI (33.5-80.6) at a cutoff point of 1 colony-forming unit/plate and 1 positive culture. Furthermore, the detection rate of orthopedic implant-associated infection (OIAI) attributed to sonicated fluid culture was significantly greater than that attributed to tissue culture (61% vs. 36%; p = 0.02). Using the cutoff point of 2 positive culture, the combination of the two methods (PTC and SFC) showed better sensitivity than the conventional method (94%, 95% CI (69.2-99.7) vs. 82%, 95% CI (55.8-95.3); p = 0.25) (Ueda et al., 2019).

TABLE 1 Details of selected studies.

Author / year	Type of study	Aim of the study	Methodology	Comparator	Main results
(Ueda et al., 2019)	Prospective study.	Assess whether combining the conventional culture and implant sonicate fluid culture (SFC) methods increased the diagnostic accuracy of orthopedic implant-associated infection (OIAI).	Consecutive patients (n = 66) undergoing implant removal (OIAI, 17; non-OIAI, 49) were evaluated. The total of 493 samples were analysed (39 preoperative joint aspirates, 243 peri-implant tissue specimens, 124 implant sonication, 67 controls, and 20 water bath samples). OIAI was preoperatively evaluated based on clinical evidence of infection or aspirate culture (AC). Conventional methods required positive results in either preoperative ACs or intraoperative tissue cultures (TC), whereas the combination method required at least 1 positive culture among 3 sources (AC, TC, or SFC). The application of SFC and the detection rate, sensitivity, and specificity of the diagnostic methods were assessed.	Conventional culture (Aspirate culture and Tissue cultures).	SFC alone detected OIAI in three patients (18%), with *Peptostreptococcus* and *Corynebacterium* species also exclusively isolated by SFC. The attributable detection rate of CFS infection was significantly higher than that of TC (61% vs 36%; P = 0.02). Sensitivities for AC, TC, and SFC with a cutoff of 1 colony forming unit/ plaque and 1 positive culture were 60%, 59%, and 71%, respectively. When using a cutoff point of 2 positive cultures, the combined method (vs conventional) demonstrated significantly higher sensitivity (71% vs 47%; P = 0.008).
(Bellova et al., 2019)	Retrospectively study.	Determine the diagnostic performance (specificity, sensitivity) of SFC against PTC, when using European Bone and Joint Infection Society (EBJIS) criteria.	From March 2017 to April 2018, 257 implants were submitted for sonication. PJI was defined according to the EBJIS criteria as well as according to the International Consensus Meeting criteria of 2018 (ICM 2018). Only cases with at least one corresponding tissue sample were included. Samples were cultured using traditional microbiological plating techniques.	Periprosthetic tissue culture (PTC).	When using the EBJIS criteria, the sensitivity of SFC and PTC was 69.0 and 62.8%, respectively (p = .04). Meanwhile, the specificity was 90.2 and 92.9%, respectively (p = .65). When adopting ICM 2018 criteria, the sensitivity of SFC and PTC was 87.5 and 84.4% (p = .63) respectively, while the specificity was 85.1 and 92.5% (p = .05), respectively. The most commonly identified pathogens were coagulase-negative *Staphylococci* (26% overall).
(Akgün et al., 2020)	Retrospectively study.	Investigate the validity of implant sonication fluid cultures in the diagnosis of shoulder PJI compared with tissue culture.	Analyzing all patients who underwent a revision surgery for any kind of suspected septic or aseptic event due to failed shoulder arthroplasty at our institution between July 2014 and December 2018. The diagnostic validity of implant sonication was analyzed on the basis of the last proposed definition criteria of the International Consensus Meeting and compared with standard tissue cultures.	Periprosthetic tissue culture (PTC).	Of the 28 infected patients, 20 (71.4%) had an identified organism by tissue cultures, and *Cutibacterium acnes* was the most commonly isolated pathogen. The sensitivities of sonicate fluid (≥50 CFU/mL) and periprosthetic tissue culture for the diagnosis of periprosthetic shoulder infection were 36% and 61% (P = 0.016), and the specificities were 97.7% and 100% (P > .99), respectively. If no cutoff value was used in sonication culture, the sensitivity increased to 75% whereas the specificity dropped to 82%. Although there was no significant difference in sensitivity between tissue culture and the no-cutoff sonication fluid culture (61% vs. 75%, P = .125), the specificity of tissue culture was significantly higher (100% vs. 82%, P = .01).
(Hoekstra et al., 2020)	Retrospectively study.	Assess the clinical importance of a standardized sonication protocol in detecting PJI.	All patients with revision surgery of a hip or knee prosthesis between 2011 and 2016 were retrospectively reviewed and divided in two groups: clinically suspected of infection or not suspected of infection. For both tissue culture and implant sonication, calculations of sensitivity and specificity were performed. Clinical relevance of sonication was evaluated by calculating in which percentage of patients' sonication influenced clinical treatment.	Periprosthetic tissue culture (PTC).	Sensitivity of perioperatively taken tissue cultures was 94.3% and specificity was 99.3%. For sonication sensitivity was 80.5% and specificity was 97.8%. In the infection group eight patients (9%) with only one positive tissue culture and a positive sonication fluid culture with the same pathogen were found.
(Torrens et al., 2020)	Retrospectively study.	Determine whether sonication yields	Includes 99 shoulder surgeries with implants explanted. The inclusion criteria required at least four tissue cultures,	Periprosthetic tissue culture (PTC).	Considering the cases with a definitive infection, the sensitivity of the tissue culture was 87.09% and the sensitivity of sonication

(Continued)

TABLE 1 Continued

Author / year	Type of study	Aim of the study	Methodology	Comparator	Main results
		greater sensitivity when compared with the traditional tissue culture in detecting periimplant infections in shoulder surgery.	sonication of the material explanted, and a minimum follow-up of two years. Patients were classified according to the definition of periprosthetic shoulder infection of the ICM 2018 on Orthopedic Infections. The classifications are definitive infection, probable infection, possible infection, and unlikely infection.		stood at 80.64% (p = 0.406). Analyzing the cases with a definitive infection and those having a possible/ probable infection together and comparing them with those with unlikely infection, the sensitivity of sonication was 80.4% and the sensitivity of the tissue culture came to 91.4%. The specificity of the sonication was 98.1% and the specificity of the tissue culture was 99.6%.
(Randau et al. 2021)	Retrospectively study.	Assess the performance of a commercially available dithiothreitol (DTT) kit for routine use in diagnosing PJIs in comparison to conventional microbiological tissue specimens and sonication procedures in a maximal care hospital.	Applied the DTT system in 40 consecutive cases of revision arthroplasty (23 PJIs and 17 aseptic revisions), with an exchange or a removal of components. The hardware components were split between the DTT system and the conventional sonication procedure. At least three tissue biopsies and a joint fluid specimen were sent for microbiological and histopathological analysis.	Dithiothreitol (DTT)	Cultures of the DTT fluid showed a sensitivity of 65% and specificity of 100%, as referenced to conventional microbiological cultures. Sonication had better sensitivity (75%) but lower specificity (85%). The categorical agreement of DTT cultures compared to sonication fluid cultures was 78% (31/40).
(Rieber et al., 2021)	Retrospectively study.	Analyze the accuracy of our culture techniques for the diagnosis of PJI.	Tissue samples and components from 258 patients after revision arthroplasty of the hip, knee, and shoulder were investigated, and the results of TC were compared to those of SFC. Furthermore, an evaluation was performed of the influence of different culture media on the detection rate.	Periprosthetic tissue culture (PTC).	The overall sensitivity of TC was no different to that of SFC (91.3% vs 90.8%, P = 1). In 153 cases (82.3%), TC and SFC showed concordant positive results. Results were discordant in 33 cases (17.7%). When differentiated according to the type of infection, TC showed significantly better results than SFC in detecting polymicrobial infections (97.0% vs 67.0%, P = 0.004).
(Stephan et al., 2021)	Retrospectively study.	Assess the influence of preoperative antibiotic prophylaxis (PAP) and antibiotic therapy (AT) on sonicated fluid cultures in patients with implantassociated infection compared to conventional tissue culture.	Three groups were compared: (I) standard PAP, (II) AT for at least one day, and (III) no antibiotics before surgery. For the inclusion criteria, an established diagnostic protocol for implantassociated infection was used. Sonicate fluid cultures were validated by corresponding microbiological and histopathological samples.	Periprosthetic tissue culture (PTC), in three different groups: (I) standard PAP, (II) AT for at least one day, and (III) no antibiotics before surgery.	The detection rate by sonicate fluid cultures in patients receiving PAP (n = 27, 29 pathogens), AT before surgery (n = 33, 48 pathogens) and no antibiotics before surgery (n = 30, 37 pathogens) were 86.2%, 81.3%, and 86.5% (p = .778), respectively. Eleven of 114 infectious agents were detected exclusively by sonicate fluid cultures, while conventional tissue culture failed in these cases.
(Flurin et al., 2021)	Retrospectively study.	Assess sonication for PJI diagnosis after Total Elbow Arthroplasty (TEA).	Retrospectively analyzed 112 sonicate fluid cultures from patients who underwent revision of a TEA at a single institution between 2007 and 2019, comparing results to those of tissue cultures. Excluded patients who had fewer than 2 tissues submitted for culture. Used the Infectious Diseases Society of America guidelines to define PJI. In addition, compared the sensitivity of tissue culture to the combination of tissue and sonicate fluid culture.	Periprosthetic tissue culture (PTC).	The most common pathogens were coagulase-negative *Staphylococcus* sp (49%), followed by *Staphylococcus aureus* (12%). Sensitivity of tissue culture was 63%, and sensitivity of sonicate fluid culture was 76% (P = .109). Specificity of tissue culture was 94% and specificity of sonicate fluid culture was 100%. Sensitivity of sonicate fluid culture in combination with tissue culture was 84% (P = .002 compared to tissue culture alone).

(Continued)

TABLE 1 Continued

Author / year	Type of study	Aim of the study	Methodology	Comparator	Main results
(Sebastian et al., 2021)	Prospective study.	Evaluate the diagnostic utility of DTT treatment of periprosthetic tissue and explanted implants, as compared to the normal saline treatment of periprosthetic tissues and sonication of explanted implants for the diagnosis of PJI.	Seventy-three revision arthroplasty cases were prospectively included in this study. Three to five tissue specimens and the explanted implants were collected from each patient. Periprosthetic tissue samples were processed by both normal saline and DTT treatments. Explanted implants were subjected to both DTT treatment and sonication.	Dithiothreitol (DTT).	The sensitivity of DTT treated periprosthetic tissue culture (PTC) and saline treated PTC was similar (66.6% vs 58.8%, P = 0.25). The specificity of both was 100%. Sonication and DTT treatment of explanted implants showed comparable sensitivity (85.3% vs 82.4%) and specificity (100% vs 97.4%), P > 0.99. Compared to DTT treated PTC, culture of DTT treated explanted implants significantly improved the diagnosis of PJI (P = 0.03).
(Aliyev et al., 2022)	Prospective study.	Evaluate the sensitivity and specificity of the sonication cultures and to evaluate the effect of sonication on the antibiotic treatment of patients.	Sixty-four patients who were scheduled for revision hip or knee arthroplasties were included in the study. Aspiration fluid, tissue, and sonication cultures were performed from all patients and compared in terms of sensitivity, specificity, positive predictive value (PPV), negative predictive value (NPV), and overall accuracy. Other targets of the study were to investigate the rate of change in the antibiotic treatment.	Aspiration fluid and periprosthetic tissue cultura (PTC).	The sensitivity, specificity, PPV, NPV, and overall accuracy of the fluid culture obtained by the sonication method were 71.4%, 96.6%, 96.2%, 73.7%, and 82.8%, respectively. The sensitivity, specificity, PPV, NPV, and overall accuracy of the fluid culture obtained after tissue sampling were 68.6%, 100%, 100.0%, 72.5%, and 82.8%, respectively. There was no statistically significant difference between the sonication method and tissue culture in terms of sensitivity and specificity (p = 1.0). The sensitivity, specificity, PPV, NPV, and overall accuracy of the fluid culture obtained by the aspiration method were 28.6%, 93.1%, 83.3%, 51.9%, and 57.8%, respectively.
(Karbysheva et al. 2022)	Prospective study.	Compare the biofilm dislodgement efficacy of chemical method (DTT) compared to the sonication procedure in the diagnosis of PJI.	187 patients undergoing hip and knee prostheses explantation were included, of whom 94 were assigned for sonication and 93 for DTT group.	Dithiothreitol (DTT).	Sonication demonstrated superior sensitivity (73.8%) compared to DTT (43.2%) in diagnosing PJI, with comparable specificity levels (98% and 94.6%, respectively).

The 12 selected articles are detailed by author, type of study, objective of the study, methodology, comparator and tabulated in ascending order according to the year of publication.

A second study used the sonication protocol proposed by Trampuz et al., 2007 (Trampuz et al., 2007). The container with the prosthetic components was filled with Ringer's solution (an isotonic solution containing sodium, chloride, potassium, calcium and sodium lactate used to prevent osmotic shock in bacteria in procedures intended for the preparation of suspensions), vortexed (30 s), sonicated at a frequency of 40 ± 2 kHz and 0.22 ± 0.04 W/cm^2 (Aquasonic Model 750T - VWR Scientific Products) for 5 min, vortexed for an additional 30 s, and then cultured. Sensitivities and specificities were also calculated using a 2×2 contingency table for both methods, as well as their 95% confidence intervals. To compare the sensitivities and specificities of the different tests, the McNemar test was used to compare paired proportions (p value < 0.05) (Flurin et al., 2021).

For sonicate fluids, was considered a culture positive if there was growth of greater than 20 CFU/10 mL of sonicate fluid, with the exception of virulent microorganisms such as *S. aureus*, for which any growth was considered positive. The sensitivity and specificity of SFC were 76%, 95% CI (62-85), and 100%, 95% IC (94-100), respectively, while for PTC, these values decreased by 63%, 95% CI (49-75), and 94%, 95% IC (85-98), respectively. The sensitivity of both tests combined (84%, 95% CI 71-91) was significantly greater than the sensitivity of tissue culture alone (63%, p = 0.002) (Flurin et al., 2021).

In another study, the explanted prostheses were immersed in Ampuwa® solution (a highly pure hypotonic water that does not contain dissolved substances) followed by an ultrasonic bath for 1 min at 80% power (P=160 W) (BactoSonic; Bandelin, Berlim, Alemanha), and no vortex was used before culture. Sensitivity and specificity were determined (2x2 contingency tables for SFC and PTC and their proportions calculated using the McNemar test, using SPSS software - IBM Corporation; Armonk, NY, United

TABLE 2 Characterization of the studies employing sonication.

Author/ Year	Number of samples/ patients	Type of infection	Infection Criteria	Vortex use	Sample centrifugation	Sensitivity and Specificity of SFC and TC	CFU cut off points (culture positivity)
(Ueda et al., 2019)	493 cultures.	Orthopedic ImplantAssociated Infection (OIAI)	Musculoskeletal Infection Society (MSIS).	Yes Before and after sonication	Yes	Sonication: 70.6% (44.0-88.6 CI 95%)/ 100% (91.1-100 CI 95%). Tissue culture: 58.8% (33.5-80.6 CI 95%)/98.0% (88.099.9 CI 95%).	1 CFU/plate.
(Flurin et al., 2021)	112 patients.	49 with PJI and 63 with aseptic failure	Infectious Diseases Society of America (IDSA).	Yes Before sonication	No	Sonication: 76%/ 100% Tissue culture: 63%/94%.	≥ 20 CFU/mL, except for virulent microorganisms such as *S. aureus*, for which any growth was considered positive.
(Bellova et al., 2019)	257 of potentially infected prostheses	Periprosthetic joint infection (PJI)	European Bone and Joint Infection Society (EBJIS) and International Consensus Meeting (ICM) criteria.	No	No	EBJIS criteria: Sonication: 69.0% (p = 0.04)/100% (p = 0.65). Tissue culture: 63% (p = 0.04)/94% (p = 0.65). ICM criteria: Sonication: 87,5% (p = 0.63)/ 85.1% (p=0.05). Tissue culture: 84,4% (p = 0.63)/92.5% (p = 0.05).	>50 CFU/mL, except for virulent microorganisms such as *S. aureus* and anaerobes for which any growth was considered positive.
(Rieber et al., 2021)	258 patients	Periprosthetic joint infection (PJI).	Musculoskeletal Infection Society (MSIS) updated by Parvizi et al., 2018 (Parvizi et al., 2018)	Yes Before and after sonication	No	Sonication: 90.8% (p = 1) Tissue culture: 91.3% (p = 1).	Isolation of the same organism by culture from two or more separate tissue or fluid samples from the prosthesis.
(Akgün et al., 2020)	80 patients	Periprosthetic joint infection (PJI) of shoulder	International Consensus Meeting (ICM).	Yes Before and after sonication	No	Sonication: 36% (p = 0.016)/97.7% (p > 0.99). Tissue culture: 61% (p = 0.016)/ 100% (p > 0.99).	Sonication: ≥ 50 CFU/mL of a low virulent organism or any growth of a high-virulent organism was present. Tissue culture: ≥ 2 CFU/mL.
(Torrens et al., 2020)	99 shoulder surgeries with implants explanted	Periprosthetic Joint Infection (PJI) of shoulder	International Consensus Meeting (ICM).	Yes Before and after sonication	No	Sonication: 80.04% (p = 0.406)/98.1% (p = 0.027) Tissue culture: 87.09% (p = 0.406)/ 99.6% (p =0.027).	50 CFU/mL.
(Hoekstra et al., 2020)	226 patients	Periprosthetic Joint Infection (PJI) of Hip or Knee.	International Consensus Meeting (ICM).	Yes Before and after sonication	No	Sonication: 80,5% (71-88 CI 95%)/ 97.7% (94-99). Tissue culture: 94,3% (87-98 95% CI)/ 99,3% (96-99 95% CI).	Any growth observed in the sonication fluid that were not contaminants, based on the discretion of the attending clinical microbiologist, was considered positive.

The methodology of the studies selected in topic 1 is outlined in Table 2, with a focus on the parameters employed in their sonication protocols.

States) for the diagnosis of PJI defined according to the EBJIS criteria, which considers a count of > 50 CFU/mL of any organism as positive for PJI, and in accordance with the criteria of the ICM 2018, which considers two positive cultures of the same organism as the major criterion for the diagnosis of PJI and a single positive culture as the minor criterion (Bellova et al., 2019).

Based on the EBJIS infection criteria, there was a statistically significant difference in sensitivity between sonication fluid culture and tissue culture (p = 0.04). SFC exhibited a sensitivity of 69.0% (100/145 patients were accurately identified by the SFC as positive) and a specificity of 90.2% (101/112 patients were accurately identified by the SFC as negative), while PTC demonstrated a

sensitivity of 62.8% (91/145) and a specificity of 92.9% (104/112). However, when the ICM 2018 criteria were adopted, the sensitivities of SFC and PTC were 87.5% (84/96) and 84.4% (81/96) ($p = 0.63$), respectively, while the specificities were 85.1% (137/161) and 92.5% (149/161) ($p = 0.05$), respectively (Bellova et al., 2019).

On the other hand, even when using a standardized protocol (Trampuz et al., 2007) that has already shown positive results (Flurin et al., 2021), the general sensitivity obtained was not significantly different between PTC and SFC (91.3%, 170/186 vs 90.8%, 169/186; $p = 1$), considering isolation of the same organism by culture from two or more separate tissue or fluid samples from the prosthesis as positive. However, examining the results based on infection type, PTC demonstrated better performance in detecting polymicrobial infections than did SFC (97.0%, 32/33 vs 67.0%, 22/33; $p = 0.004$), as determined by the two-proportion Z test using RStudio software (version 1.2.5042) ($p < 0.05$) (Rieber et al., 2021).

Better results for PTC were also observed using a proposed sonication protocol (Renz et al., 2018) that included the addition of saline solution to the container with the prosthesis to cover most of the implant, then an initial vortex shaking (30 s) of the container, followed by a sonication bath for 1 min at 40 kHz (BactoSonic; Bandelin Electronic, Berlin, Germany), and another 30 seconds of vortex mixing. A cutoff point of ≥ 50 CFU/mL was used to determine positivity by sonication of the fluid and isolation of the same organism from 2 or more tissue samples to determine positivity by standard culture (ICM 2018) (Akgün et al., 2020).

Using a 2x2 contingency table, McNemar comparison test, chi-square test and Fisher's exact test to determine significant differences between categorical variables ($p < 0.05$) (SPSS version 20 - IBM, Armonk, NY, USA) resulted in a sensitivity of 36% for SFC (≥ 50 CFU/mL), while it was 61% for PTC (≥ 2 tissue samples with the same organism) ($p = 0.016$). The specificity was 97.7% for SFC and 100% for PTC ($p > 0.99$). However, when the cutoff value was eliminated in sonication culture, the sensitivity increased to 75%. Nevertheless, this increase in sensitivity came at the expense of decreased specificity, which decreased to 82%. These changes did not result in a statistically significant difference in the diagnostic benefits of SFC compared to PTC (Akgün et al., 2020).

Similar findings were reported when assessing the sensitivity of SFC compared to that of PTC in detecting peri-implant infections in shoulder surgery using a similar reported protocol (Akgün et al., 2020). After the removed components were transported in a polyethylene container with approximately 200–400 ml of sterile saline, the container was first vortexed for 30 seconds and then sonicated for one minute at a frequency of 40 ± 5 kHz in a Bransonic® SM25E-MT ultrasound bath (Branson Ultrasonics Corporation, Geneva, Switzerland) after vortexing again for 30 seconds. Sonication was considered positive if at least 50 CFU/mL was detected (ICM 2018). PTC achieved 87.09% sensitivity, and SFC reached 80.64% ($p = 0.406$). The specificity of PTC was 99.6%, and that of SFC was 98.1% ($p = 0.175$) ($p < 0.05$) (sensitivity, specificity, ROC area and Delong comparison test calculated in STATA 15.1). No statistically significant difference was found between the results obtained by the two methods (Torrens et al., 2020).

The sonication procedure, which involved immersing the prosthetic container (90%) in Ringer's solution, followed by 30 seconds of shaking, a 1-minute sonication bath at 100% power (200 W, 0.22 W/cm^2) (Bandelin Bactosonic), and another 30 seconds of shaking before fluid culture, also yielded favorable results for PTC compared to SFC. Using this protocol and ICM 2018 criteria, the PTC sensitivity was 94.3%, 95% CI (87-98), and the specificity was 99.3%, 95% CI (96-99). The sensitivity for SFC was 81%, 95% CI (71-88), and the specificity was 97.8%, 95% CI (94-99), which were considerably lower than the results observed for PTC (2x2 contingency table using SPSS version 22.0). Although the sensitivity and specificity of SFC were lower than those of PTC, it is worth noting that 8 patients (9% of the total) suspected of having a periprosthetic joint infection could be definitively diagnosed based on a positive result from SFC (Hoekstra et al., 2020).

Sonication has shown variable diagnostic accuracy in these studies. It was possible to observe that the best sensitivity and specificity indices, compared to those of PTC, were achieved by sonication protocols that used sterile saline solution for immersion of the prosthesis, low frequencies of ultrasound waves (40 kHz) for a period of 1 or 5 minutes, the use of a vortex (before and after sonication) and centrifugation and even lower cutoff points (≥1 CFU/mL) than the 50 CFU/mL recommended by some consensuses.

In general, the results obtained with SFC were better for diagnosing PJI. Even in some studies in which its sensitivity and specificity were lower than those of PTC, it was possible to observe a small significant difference or even no significant difference. This superiority is magnified when we analyze the cost-benefit of the technique, which presents potential improvement in culture results, in a simple technique with lower recurrence rates (associated with the diagnostic inaccuracy of traditional tissue culture) and costs. Therefore, it is easily applicable in clinical practice from surgical and microbiological points of view (Flurin et al., 2021). However, considering the positive contribution that PTC can add to the diagnosis (Rieber et al., 2021), it is still possible to perform a combination of SFC and PTC (Ueda et al., 2019).

4 Microorganism detection capacities of SFC and PTC and the main microorganisms isolated

Among the predominant microorganisms identified in the OIAI, coagulase-negative *Staphylococcus* species (CoNS) were the primary causative agents of infections in 24 isolates detected by both the SFC and PTC methods. However, 18% of the positive diagnoses were exclusively identified using sonication. In these cases, less virulent species, such as *Streptococcus* of the *viridans* group, *Peptostreptococcus*, and *Corynebacterium* spp., were also isolated. *Peptostreptococcus* and *Corynebacterium* spp. were isolated by SFC only. Among patients who had prior antibiotic therapy, 67% of those who received SFC had infections (Ueda et al., 2019).

In a recent study, the most common pathogen isolated from periprosthetic elbow infection using both methods was CoNS (49%), followed by *Staphylococcus aureus* (12%), gram-negative *Enterobacter cloacae* (3%) and *Klebsiella pneumoniae* (2%). The authors observed that among the positive cultures, 78% exhibited monomicrobial cultures, while 22% had polymicrobial cultures. The SFC method played a crucial role in identifying the majority of polymicrobial infections, leading to treatment modifications in 4 out of 5 patients. However, it is worth noting that SFC failed to detect *Corynebacterium amycolatum*, a species that was only identified through tissue culture, but it did not have any impact on the choice of antibiotic regimen. In 10 patients, only sonicate cultures were positive: 7 for *S. epidermidis*, 1 for coagulase-negative *Staphylococcus* sp., 1 for *S. aureus* and 1 for *Parvimonas micra* (Flurin et al., 2021).

In cases of PJI, the primary pathogens were also CoNS. The SFC method successfully isolated 38 of these microorganisms, whereas the PTC method yielded only 30 isolates. The second most frequently isolated microorganism was *S. aureus*, which was further classified as *methicillin-susceptible Staphylococcus aureus* (MSSA) *or methicillin-resistant Staphylococcus aureus* (MRSA). There were more SFC isolates than PTC isolates for both MSSA (14 vs. 12) and MRSA (5 vs. 4). They also observed that in early PJI detected using sonication, 48.9% of the cases were attributed to high-virulence pathogens, while 51.1% were associated with low-virulence pathogens. A similar pattern was observed for delayed and late infections combined, with 35.7% classified as having high virulence and 64.3% as having low virulence. Significantly, 7.8% of delayed or late infections detected using SFC were positive for anaerobes, with *Cutibacterium acnes* identified as the predominant species. In comparison, only 2.6% of infections were detected through PTC (Bellova et al., 2019).

In addition, for the microbiological diagnosis of PJI, 220 microorganisms were isolated from the PTC and SFC methods, and concordant positive results were obtained for 153 out of 186 patients (82.3%). The CoNS (n= 60) were also the main group of bacteria isolated, with *Staphylococcus epidermidis* (n = 43) as the main species. The second most prevalent pathogen was *S. aureus* (n= 55), followed by anaerobic bacteria (n=43), and members of the Enterobacterales family (n= 27), *Streptococcus* spp. (n= 17) and *Enterococcus* spp. (n= 14) were also isolated in this study (Rieber et al., 2021).

However, in periprosthetic elbow infections, the most frequently isolated pathogen by tissue culture was *C. acnes*, accounting for 46% of the cases. The second most isolated pathogen was CoNS, accounting for 17.9% of the cases, followed by *S. aureus*, accounting for 7%. Other bacteria isolated included *Finegoldia magna* (3.6%), *Streptococcus agalactiae* (13.6%), *Enterococcus faecalis* (3.6%), and *Peptoniphilus asaccharolyticus* (3.6%). In 75% of patients, at least one organism was successfully isolated by sonication. However, it is noteworthy that there were discordant results between SFC and PTC in 32% of the patients (Akgün et al., 2020).

This microbial identification was also observed in patients with confirmed infection in hip or knee prostheses. Among these patients, only eight individuals (9%) had positive cultures for the same pathogen using both the SFC and PTC methods. Certain pathogens could only be identified using the SFC method. These pathogens are typically low in virulence and are known to produce biofilms, making them particularly difficult to detect. Examples of such pathogens include *Streptococcus mitis*, *S. epidermidis*, *Aggregatibacter* species, *C. acnes*, and *Corynebacterium striatum* (Hoekstra et al., 2020).

Considering that peri-implant infections in the shoulder were definitively diagnosed, *S. epidermidis* was present in 42% of the patients, followed by *C. acnes* in 22.5%. Among these cases, 22.6% were classified as polymicrobial infections, with *C. acnes* being involved in most of these cases (71%) (Torrens et al., 2020).

When evaluating the influence of preoperative antibiotic prophylaxis (PAP) and antibiotic therapy (AT) on SFC in patients with implant-associated infections, 114 important infectious agents were detected, 11 of which were detected exclusively after the use of SFC. The main microorganisms isolated included CoNS, *S. aureus*, *Streptococcus* spp., and *Enterococcus* spp. Microorganisms were identified despite prior antibiotic therapy; therefore, they do not recommend omitting antibiotic prophylaxis in patients with implant-associated infections (Stephan et al., 2021).

Moreover, although the SFC technique did not enhance the sensitivity of microbiological diagnosis for PJIs in this study, it did demonstrate the ability to identify distinct microorganisms compared to other methods. This finding contributed to changes in the strategy of antibiotic therapy for infected patients, as it relies on antimicrobial sensitivities derived from microbiological culture results (Aliyev et al., 2022).

Sonicated fluid culture plays an important role in the detection of particular microorganisms, such as *Peptostreptococcus, Streptococcus mitis, S. epidermidis, Aggregatibacter* species, *Corynebacterium* spp. and *Cutibacterium acnes*. C. acnes is responsible for chronic and low-grade infections that represent an additional challenge to the diagnosis of PJI, with an emphasis on *C. acnes*, which decreases the sensitivity of traditional diagnostic tests for infections associated with orthopedic implants (Renz et al., 2018; Hoekstra et al., 2020). In addition to the aforementioned bacteria, fungal PJI, although rare (1% to 2%), can be difficult to control and identify because the isolation of organisms by traditional culture can take a long time, resulting in false negatives (Chisari et al., 2022). It is believed that fungi and mycobacteria are responsible for more than 85% of cases of negative cultures in PJI (7%-15%). In this context, sonication is a low-cost method capable of increasing the chances of identifying the causative agent (Palan et al., 2019).

The ability of CFS to identify diverse and especially low-virulence microorganisms, even in the face of preoperative antibiotic prophylaxis, can affect the antibiotic therapy strategy adopted (Aliyev et al., 2022). This characteristic has the potential to increase the effectiveness of treatment, reduce costs associated with prolonged use of antibiotics and longer hospital stays, often requiring multiple surgical procedures, thus reducing unnecessary exposure to antibiotics; consequently, bacterial resistance has increased dramatically in the last ten years, probably due to the excessive and often inappropriate use of antibiotics (Drago and De Vecchi, 2017).

This ability may further permit the use of an antibiotic-loaded bone cement spacer sonication fluid culture technique to confirm the eradication of infection or two-stage revision reinfection prior to reimplantation of new prostheses. It can be used accurately as a complement to evaluate the therapeutic effect of IAP (Zhang et al., 2021a).

5 The ability of sonication protocols to dislodge biofilm structure compared to that of other displacement methods

Dislodging of bacterial cells from the biofilm structure can be achieved by mechanical means or chemical or physical methods. Mechanical methods such as scraping the prosthesis or vortices have rarely been evaluated; when studied, they have shown low performance (Bjerkan et al., 2009; Drago and De Vecchi, 2017), and in the current literature, they are scarce (Drago and De Vecchi, 2017). The use of chemical substances in explanted implants and periprosthetic tissues is suggested as a possible biofilm dislodgement method with possible applicability in the diagnosis of infections associated with implants. Among the proposed agents are the metal chelator ethylenediaminetetraacetic acid (EDTA) and the strong reducing agent dithiothreitol (DTT) (Karbysheva et al., 2020).

It was suggested that the activity of EDTA against biofilm cells occurs through the chelation of magnesium, calcium, and iron, enhancing the detachment of cells from the biofilm matrix (Banin et al., 2006). Additional observations included that the mean colony count (logCFU/mL) after DTT treatment was comparable to that achieved after sonication or physical methods and greater than the count obtained using the scraping technique (Drago et al., 2012).

Compared with DTT treatments for the diagnosis of PJI, the explanted implants were immersed in 0.1% w/v TDT (Promega, Madison, WI, USA) in sterile saline and kept in an incubator with shaking for 15 minutes at room temperature, followed by centrifugation at 3,000 rpm for 10 minutes before standard cultivation. With a sonication protocol for explanted implants, 90% of the prosthesis was immersed in sterile saline solution, followed by vigorous manual shaking for 30 seconds before and after the sonicated bath, which was programmed for 7 min at 40 kHz in BactoSonic (Bandelin GmbH, Berlin, Germany). The procedure was finished with centrifugation at 4,000 rpm for 20 minutes. Using the MSIS definition of IAP, both methods, SFC and DTT, demonstrated similar sensitivity rates of 85.3% (29/34) and 82.4% (28/34) ($p > 0.05$) (analysis performed with STATA software version 14.2 - Stata Corp LLC; Texas, USA), respectively. Although not statistically significant, the specificity was greater when using the SFC technique (100%, 39/39 vs. 97.4%, 38/39 $p > 0.99$) (Sebastian et al., 2021).

In another study, DTT treatment involved the use of a MicroDTTect closed system for biofilm processing via this chemical method. Explant samples were collected from the sterile system itself, and then, in the laboratory, the chamber valve containing TDT (150 mL, 0.1% p/v) was broken, allowing DTT to flow into the explant. The device was subsequently mechanically stirred for 15 minutes at room temperature, after which standard cultivation continued. For the sonication protocol, the explanted implants were collected in sterile plastic bags that were subsequently filled with sterile saline solution, vortexed for 30 seconds and sonicated in a Bactosonic 14.2 device (Bactosonic, Bandelin, Berlin, Germany) for 5 minutes with a frequency of 40 ± 2 kHz and a power density of 0.22 ± 0.04 W/cm2 followed by 30 seconds of vortexing (Randau et al., 2021).

Using the MSIS criteria to define PJI, the authors found a sensitivity of 65% (13/20) and specificity of 100% (20/20) for DTT fluid culture compared to conventional microbiological cultures. Sonication had better sensitivity (75%, 15/20) but lower specificity (85%, 17/20) than conventional microbiological culture ($p > 0.05$) (statistical significance between groups was assessed by the Mann-Whitney test). Fisher's exact test was used for contingency, sensitivity and specificity analysis. The analysis was performed using GraphPad Prism 8.0.2 (GraphPad Software, La Jolla, CA, USA). The categorical concordance of DTT cultures with that of SFC cultures was 78% (31/40) (Randau et al., 2021).

Based on these results, sonication has been shown to be the main assay for biofilm detection in the microbiological diagnosis of implant-associated infection (Karbysheva et al., 2020). Even in one study that showed a loss of specificity, sonication provided a more reliable diagnosis of PJI, as it identified more pathogens than DTT treatment (Karbysheva et al., 2022). However, given the positive impacts that chemical methods can have on the diagnosis of these infections, especially on culture specificity, DTT treatment could be used as a biofilm displacement technique in situations where sonication is not viable or possible (Sebastian et al., 2021). It is also possible to evaluate the potential additive effect of chemical shift on sonication (Karbysheva et al., 2020).

6 Proposal for a standardized sonication protocol

To propose the best parameters for establishing a sonication protocol, studies by Cieslinski et al., 2021, Trampuz et al., 2006, Oliva et al., 2021, Rosa et al., 2019, Ueda et al., 2019, Dudek et al., 2020, Li et al., 2018, Ribeiro et al., 2022, Beguiristain et al., 2023, Borens et al., 2013 and Morgenstern et al., 2020 (Trampuz et al., 2006; Borens et al., 2013; Rosa et al., 2019; Ueda et al., 2019; Dudek et al., 2020; Morgenstern et al., 2020; Cieslinski et al., 2021; Oliva et al., 2021; Ribeiro et al., 2022; Beguiristain et al., 2023), were also reviewed in addition to the abovementioned studies (Figure 1).

6.1 Material collection

After revision surgery, it is recommended that all prosthetic components, periprosthetic cement or osteosynthesis devices, including polyethylene (PE) materials and metal and polymethylmethacrylate (PMMA) components, be carefully

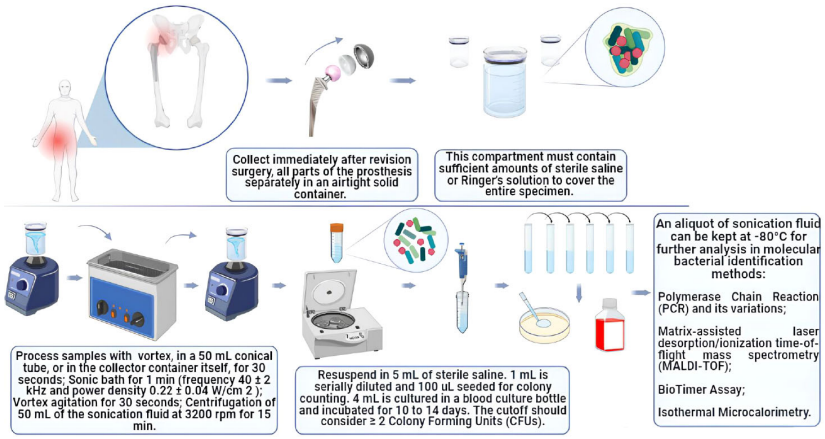

FIGURE 1
Diagram of the sonication protocol according to the parameters reviewed in this study.

removed to avoid direct contact with the patient's skin. These items should be collected separately. To ensure the integrity of the collected samples and preserve the viability of microorganisms, it is important to use airtight containers. It has already been demonstrated that storing samples in plastic bags can significantly reduce colony-forming unit (CFU) counts and is associated with the risk of contamination (Rosa et al., 2019; Cieslinski et al., 2021).

The use of plastic bags for storage promotes the desiccation of microorganisms, which can lead to changes in their biophysical properties, such as surface tension. This desiccation can disrupt physiological processes, including the growth of microorganisms (Cieslinski et al., 2021).

Thus, physical containers with thicker, completely sealed (hermetic) surfaces can serve as a protective measure by preventing water loss and helping to maintain microbial viability while reducing the risk of contamination. It is important for the entire sample to be covered, so these compartments should contain an adequate amount of sterile saline or Ringer's solution. By ensuring a sealed and moist environment, physical containers can help preserve the viability of microorganisms and maintain their physiological state during storage. This is crucial for accurate microbiological analysis and for reducing the potential for false-negative results or alterations in microbial characteristics.

6.2 Sample storage

The samples should be processed soon after removal, ideally within 2 to 4 hours. However, if immediate processing is not feasible, the samples can be stored at -4°C without liquid. Refrigerated samples can be stored for 7 days, and although there may be a minor decrease in the bacterial load over time, this decrease is unlikely to have a significant impact on the culture's positivity. This is particularly true when molecular methods are employed for bacterial identification of sonicated fluid (Cieslinski et al., 2021).

6.3 Vortex-sonication-vortex method

In this proposed protocol, the processing of the samples involves the following steps:

1. Sample vortex: The sample is vortexed for 30 seconds in the collection container, ensuring that the prosthesis is completely submerged in a sterile saline solution (the amount of solution depends on the sample size).
2. Sonication bath: The sample was immersed in a sonication bath for 1 min at a frequency of approximately 40 ± 2 kHz and a power density of 0.22 ± 0.04 W/cm^2.
3. Vortex Agitation: After sonication, the sample was vortexed again for 30 seconds.
4. Centrifugation: Approximately 15 mL of sonication fluid (without the prosthesis) was centrifuged at 3200 rpm for 15 minutes to concentrate the sample (bacterial cells, probably present in the sonication fluid) for later culturing.

As a standard procedure to minimize the risk of contamination in subsequent protocol steps, it is important to change the water in the ultrasonic bath after each round of sonication.

The use of vortex stirring and centrifugation has been shown to contribute to enhancing specificity (Rosa et al., 2019; Oliva et al., 2021). With respect to the duration of sonication, a 1-minute duration produced good results. This short period of sonication helps to avoid potential bactericidal effects of the procedure (Ueda et al., 2019).

The ideal ultrasound frequencies for sonication to identify etiological agents of implant-associated infections, particularly PJI caused by pathogens such as *S. aureus*, *P. aeruginosa*, and *E. coli*, are 35 kHz and 40 kHz (Dudek et al., 2020). These frequencies were effective in displacing bacteria from biofilms, and they had a significant impact on the survival of bacteria, particularly those in a planktonic state.

The majority of studies describing the use of the sonication technique for explant prostheses use a sonication bath, often due to sample size constraints. However, it is worth noting that recently, an article demonstrated greater sensitivity with direct intraoperative sonication culture of implants and soft tissues than with conventional synovial fluid culture utilizing a portable probe sonicator (Shanghai Weimi Ultrasonic Co., Ltd.) (Ji et al., 2023).

6.4 Microbiological analysis

1- The sediment obtained from the centrifuged solution must be resuspended in 5 mL of sterile saline solution. 2- To determine the microbial cell count and viability, 1 mL of the resuspension was serially diluted 10 times at a ratio of 1:10, resulting in a total volume of 1 mL. Between 3-100 µL of the last three dilutions were plated on Mueller Hinton agar plates and incubated for 18-24 hours at 37°C to facilitate bacterial growth. 4- The remaining 4 mL of the resuspension was inoculated into blood culture bottles. The bottles are subsequently incubated for 10 to 14 days to facilitate the detection of slow-growing or fastidious microorganisms that might be present in the sample. In cases where there is clinical evidence of infection but standard microbiological cultures yield negative results, it is advisable to conduct additional fungal and mycobacterial cultures.

The advantages of inoculation into blood culture bottles have recently been highlighted. Among them are the increased sensitivity and specificity of culture, even in patients who received prior antibiotic therapy, due to the presence of antimicrobial removal systems and lytic agents in blood bottles that further promote the release of intracellular microorganisms. In this context, the use of blood culture bottles to inoculate joint fluids directly at the patient's bedside can be valuable. Additionally, the application of an innovative version of the sonication culture method involves direct sonication of the retrieved implant and soft tissue, without a sonication tube, intraoperatively. This method utilizes a BACT/ALERT 3D blood culture system, contributing to the increased effectiveness of microbiological diagnosis for PJI (Drago et al., 2019; Ji et al., 2023).

The incubation period should be extended to up to two weeks to enhance the likelihood of identifying causative agents comprehensively. For instance, species such as *Staphylococcus* spp. are more likely to emerge during the initial week of incubation, while *Cutibacterium* spp. are typically detected during the second week (Oliva et al., 2021). Once the etiological agent is accurately identified, it becomes possible to prescribe the most suitable treatment. In regard to antibiotics, selecting the appropriate type and dosage is crucial. Notably, the cure rate for patients with culture-negative PJI is generally low (Li et al., 2018).

6.5 Bacterial phenotypic identification and quantification from sonication fluid

A positive culture result for sonication fluid was determined by a bacterial concentration ≥ 2 CFU/mL in ≥ 2 cultures. In this context, a monomicrobial PJI is considered if only one bacterial species grows above the cutoff in sonicated fluid cultures. Conversely, polymicrobial PJI is diagnosed if more than one species is isolated following the same criteria. Following a positive blood culture, phenotypic identification should be conducted using culture media supporting the growth of both aerobic and anaerobic bacteria. It is important to note that for diagnosis, the identified species are more relevant than the CFU count.

Some studies used cutoff points ≥ 1 and ≥ 5 CFU, as the sensitivity of sonicated liquid cultures can be significantly reduced, especially in patients who have received previous antibiotic therapy or still have chronic, low-grade infection. It is worth mentioning that the cutoff point of 50 CFU/mL, which is defended by most medical societies and widely used in clinical practice, may not be ideal in these cases, despite its ability to distinguish effective infections (Ueda et al., 2019; Oliva et al., 2021).

The growth of any virulent microorganism responsible for high-grade acute infections, such as *Staphylococcus aureus* and gram-negative bacilli, will also be considered. However, the growth of low-virulence microorganisms responsible for chronic and low-grade infections, such as coagulase-negative *Staphylococcus, Enterococcus* spp., *Corynebacterium* spp. and *Cutibacterium acnes*, in a single sample must be evaluated in conjunction with the patient's clinical context (Drago et al., 2019; Romanò et al., 2019; Ueda et al., 2019; Oliva et al., 2021). This is where sonication presents one of its greatest advantages, which is its ability to more efficiently identify bacteria responsible for chronic, low-grade and difficult-to-detect infections, as previously mentioned, helping to improve the poor performance of conventional microbiological methods for identifying these pathogens (Renz et al., 2018; Hoekstra et al., 2020).

According to our suggested protocol, any growth detected in the sonicated fluid culture from patients who received antibiotics within two weeks prior to sample collection should be regarded as a positive result (Ueda et al., 2019; Oliva et al., 2021).

6.6 Bacterial identification by molecular methods

The sonication protocol, involving the use of a vortex-sonication vortex followed by CFU counts, may have several limitations. These include the inability to dislodge all adherent microorganisms in the biofilm and the potential for sonication to affect microbial viability, leading to inaccurate CFU counts. Molecular methods can be employed to address these limitations and contribute to the identification of difficult-to-cultivate bacteria, anaerobes, and noncultivable bacteria (Rosa et al., 2019).

These molecular methods include polymerase chain reaction (PCR), such as bacterial identification based on the amplification of 16S ribosomal RNA, and various methods, such as multiplex PCR (mPCR), which can amplify the genetic material of different targets in a single process, thus allowing bacterial identification, as performed in commercial panels of multiplex PCR for IAP (Schoenmakers et al., 2023). It exhibits good sensitivity and requires less sample material and time than culture-based

methods. Broad-range PCR can identify the predominant bacterial strain at infection sites of various cultural origins, even in patients undergoing antibiotic therapy. The main limitations of PCR-based diagnosis include the inability to discriminate between live and dead bacteria and DNA contamination. However, when used in conjunction with sonication, it has great diagnostic value for PJI, especially for routine clinical practice when used in panels, as already mentioned (Liu et al., 2018; Schoenmakers et al., 2023; Tsikopoulos and Meroni, 2023).

Another method is identification by matrix-assisted laser desorption/ionization time-of-flight mass spectrometry (MALDI-TOF), which allows direct identification of aerobic and anaerobic bacteria from positive blood cultures. MALDI-TOF has been successfully employed for detecting microorganisms in biological samples, whether from colonies or fluids. Several studies support the feasibility of using this technique for bacterial identification in sonicated fluid as well as direct identification in blood culture bottles. This approach facilitates early and reliable identification, serving as an alternative to culture methods (Cieslinski et al., 2021; Ribeiro et al., 2022; Beguiristain et al., 2023).

As additional techniques, we can also perform fluorescence *in situ* hybridization (FISH), in which fluorescent probes bind to complementary nucleic acid sequences to identify the presence or absence of these target sequences. The ability to identify bacteria in negative cultures reduces false positives through better identification of environmental contamination and the ability to exclude dead bacteria with a viability stain. Another technique that can help with pathogen identification is DNA microarrays, where microarrays allow the simultaneous measurement of large numbers of genes involving thousands of microscopic DNA sequences (probes) complementary to specific gene fragments of the microorganisms studied. However, both of these methods have the disadvantages of high cost, the need for specialized equipment, the potential for contamination and a lack of probes relevant for diagnosing PJI (Shoji and Chen, 2020).

We can also mention the use of identification methods based on specific bacteriophages for the pathogens studied, where DNA detection by qPCR and adenosine triphosphate (ATP) detection are performed after bacteriophage lysis. This technique aims to contribute to the development of a faster, more sensitive, specific and, at the same time, economical and practical system to establish an accurate diagnosis of PJI, with applicability in sonicated fluid (Šuster and Cör, 2022).

6.7 Alternative identification methods

Among the alternative methods of bacterial identification that have been suggested for the diagnosis of infections associated with implants, the BioTimer Assay (BTA), which indirectly identifies microorganisms through the detection of microbial metabolic products, uses an original reagent containing red phenol or resazurin as indicators. Phenol red changes from red to yellow, indicating the presence of fermenting microorganisms, while resazurin changes from violet to pink, indicating the presence of nonfermenting microorganisms (Rosa et al., 2019).

Another method is isothermal microcalorimetry, which is considered a new method for real-time detection of heat production related to the growth of reproductive microorganisms in biological fluid. This detection method has proven to be highly sensitive and rapid in synovial fluid samples for the diagnosis of septic arthritis. Likewise, sonication fluid microcalorimetry was useful for diagnosing PJI with a considerably faster detection time than conventional microbial culture (Borens et al., 2013; Morgenstern et al., 2020).

These methods have the advantages of easy execution and accessibility for the identification process. However, they present important limitations compared to molecular methods, which perform more precise identification. BTA is incapable of identifying microbial genera and species, a problem that can be remedied with sonication, as BTA has good sensitivity for microbial analysis (Rosa et al., 2019).. Microcalorimetry has reduced sensitivity due to the same challenge that culture faces with the presence of biofilms for diagnosing PJI but could complement cultures and support rapid, real-time decisions in orthopedic device-related infections (Morgenstern et al., 2020).

Additionally, imaging techniques to visualize biofilms can also be applied. Confocal laser scanning microscopy and scanning electron microscopy provide imaging of the biofilm without compromising the biofilm structure; in some cases, confocal laser microscopy makes it possible to visualize viable biofilm bacteria in joint fluid, wound tissue and bone cement. Scanning electron microscopy can be used to visualize the coaggregation of microbial cells, but the preparation often results in the loss of the biofilm matrix. The cost and training requirements for obtaining the best images limit the use of these techniques (56).

7 Conclusion

One of the primary challenges in the management of implant-associated infections is microbiological diagnosis. To ensure a reliable diagnosis and successful treatment, complete removal of the implant and dislodgment of the microorganisms causing the infection, which are predominantly present in biofilm structures, are necessary. For this purpose, the sonication technique was successfully proposed, although its diagnostic accuracy is still questioned in the current literature.

When reviewing the literature, it was possible to observe the adoption of different protocols, as expected, and consequently different results regarding the sensitivity and specificity of sonicated fluid cultures compared to those of periprosthetic tissue cultures. It was possible to observe an even greater prevalence of coagulase-negative *Staphylococcus* species, followed by *Staphylococcus aureus*, identified as etiological agents of infections associated with implants, by both culture methods, but sonication proved to be important for the identification of low-virulence pathogens that produce biofilms, which are notoriously difficult to detect, such as the species *Peptostreptococcus* and *Corynebacterium* spp.

In the analysis of the studies that compared SFC and chemical methods of biofilm displacement, EDTA and DTT, it was observed that the results varied between the superior sensitivity and

specificity of SFC, and there was no significant difference between the SFC and chemical methods.

In this context, we conducted an analysis of various aspects, including sample collection, storage conditions, cultivation methods, microorganism identification techniques (both phenotypic and molecular), and the cutoff point for CFU counts. Additionally, we propose optimal parameters for programming the sonication bath and sample processing.

In conclusion, based on our analysis and review of the current literature, we have established a theoretical foundation for standardizing sonication protocols. The aim of this study was to achieve the highest sensitivity and specificity indices for the reliable microbiological diagnosis of infections associated with implants and prosthetic devices, such as PJIs. However, practical application and further complementary studies are still necessary.

Author contributions

ND: Data curation, Methodology, Project administration, Writing – original draft, Writing – review & editing. BS: Data curation, Methodology, Writing – original draft, Writing – review & editing. AO: Formal Analysis, Supervision, Validation, Writing – review & editing. PR: Formal Analysis, Resources, Supervision, Validation, Writing – original draft, Writing – review & editing.

Funding

The author(s) declare financial support was received for the research, authorship, and/or publication of this article. The financial resources to carry out this research were provided through *Conselho Nacional de Desenvolvimento Científico e Tecnológico* - CNPq (CNPq/MCTI No. 10/2023 – UNIVERSAL).

Conflict of interest

The authors declare that the research was conducted in the absence of any commercial or financial relationships that could be construed as a potential conflict of interest.

The author(s) declared that they were an editorial board member of Frontiers, at the time of submission. This had no impact on the peer review process and the final decision.

Publisher's note

References

Ahmed, S. S., and Haddad, F. S. (2019). Prosthetic joint infection. *Bone Joint Res.* 8, 570–572. doi: 10.1302/2046-3758.812.BJR-2019-0340

Akgün, D., Maziak, N., Plachel, F., Siegert, P., Minkus, M., Thiele, K., et al. (2020). The role of implant sonication in the diagnosis of periprosthetic shoulder infection. *J. Shoulder. Elbow. Surg.* 29, e222–e228. doi: 10.1016/j.jse.2019.10.011

Aliyev, O., Yıldız, F., Kaya, H. B., Aghazada, A., Sümbül, B., Citak, M., et al. (2022). Sonication of explants enhances the diagnostic accuracy of synovial fluid and tissue cultures and can help determine the appropriate antibiotic therapy for prosthetic joint infections. *Int. Orthop.* 46, 415–422. doi: 10.1007/s00264-021-05286-w

Azad, M. A., and Patel, R. (2024). Practical Guidance for Clinical Microbiology Laboratories: Microbiologic diagnosis of implant-associated infections. *Clin. Microbiol. Rev.* 20, e0010423. doi: 10.1128/cmr.00104-23

Banin, E., Brady, K. M., and Greenberg, E. P. (2006). Chelator-Induced Dispersal and Killing of *Pseudomonas aeruginosa* cells in a biofilm. *Society* 72, 2064–2069. doi: 10.1128/AEM.72.3.2064

Beam, E., and Osmon, D. (2018). Prosthetic joint infection update. *Infect. Dis. Clin. North Am.* 32, 843–859. doi: 10.1016/j.idc.2018.06.005

Beguiristain, I., Henriquez, L., Sancho, I., Martin, C., Hidalgo-Ovejero, A., Ezpeleta, C., et al. (2023). Direct prosthetic joint infection diagnosis from sonication fluid inoculated in blood culture bottles by direct MALDI-TOF mass spectrometry. *Diagnostics* 13. doi: 10.3390/diagnostics13050942

Bellova, P., Knop-Hammad, V., Königshausen, M., Mempel, E., Frieler, S., Gessmann, J., et al. (2019). Sonication of retrieved implants improves sensitivity in the diagnosis of periprosthetic joint infection. *BMC Musculoskelet. Disord.* 20, 1–9. doi: 10.1186/s12891-019-3006-1

Birlutiu, R. M., Birlutiu, V., Mihalache, M., Mihalache, C., and Cismasiu, R. S. (2017). Diagnosis and management of orthopedic implant-associated infection: a comprehensive review of the literature. *Biomed. Research-tokyo.* 28, 5063–5073.

Bjerkan, G., Witsø, E., and Bergh, K. (2009). Sonication is superior to scraping for retrieval of bacteria in biofilm on titanium and steel surfaces in vitro. *Acta Orthop.* 80, 245–250. doi: 10.3109/17453670902947457

Borens, O., Yusuf, E., Steinrücken, J., and Trampuz, A. (2013). Accurate and early diagnosis of orthopedic device-related infection by microbial heat production and sonication. *J. Orthopedic. Res.* 31, 1700–1703. doi: 10.1002/jor.22419

Chisari, E., Lin, F., Fei, J., and Parvizi, J. (2022). Fungal periprosthetic joint infection: Rare but challenging problem. *Chin. J. Traumatol.* 25, 63–66. doi: 10.1016/j.cjtee.2021.12.006

Cieslinski, J., Ribeiro, V. S. T., Kraft, L., Suss, P. H., Rosa, E., Morello, L. G., et al. (2021). Direct detection of microorganisms in sonicated orthopedic devices after in *vitro* biofilm production and different processing conditions. *Eur. J. Orthopedic. Surg. Traumato.* 31, 1113–1120. doi: 10.1007/s00590-020-02856-3

Drago, L., Clerici, P., Morelli, I., Ashok, J., Benzakour, T., Bozhkova, S., et al. (2019). The world association against infection in orthopedics and trauma (WAIOT) procedures for microbiological sampling and processing for periprosthetic joint infections (PJIs) and other implant-related infections. *J. Clin. Med.* 1, 8. doi: 10.3390/jcm8070933

Drago, L., and De Vecchi, E. (2017). Microbiological Diagnosis of Implant-Related Infections: Scientific Evidence and Cost/Benefit Analysis of Routine Antibiofilm Processing [published correction appears in Adv Exp Med Biol. 2017; 971:113]. *Adv. Exp. Med. Biol.* 971, 51–67. doi: 10.1007/5584_2016_154

Drago, L., Romanò, C. L., Mattina, R., Signori, V., and De Vecchi, E. (2012). Does dithiothreitol improve bacterial detection from infected prostheses? A pilot study infection. *Clin. Orthop. Relat. Res.* 470, 2915–2925. doi: 10.1007/s11999-012-2415-3

Dudek, P., Grajek, A., Kowalczewski, J., Madycki, G., and Marczak, D. (2020). Ultrasound frequency of sonication applied in microbiological diagnostics has a major impact on viability of bacteria causing periprosthetic joint infection. *Int. J. Infect. Dis.* 100, 158–163. doi: 10.1016/j.ijid.2020.08.038

Filho, C. A. M., Aragão, M. T., and Santos, R. S. (2020). Clinical and epidemiological profile of infections related to joint prostheses. *Arch. Health* 1, 7–16. doi: 10.46919/archv1n1-002

Flurin, L., Greenwood-Quaintance, K. E., Esper, R. N., Sanchez-Sotelo, J., and Patel, R. (2021). Sonication improves microbiologic diagnosis of periprosthetic elbow infection. *J. Shoulder. Elbow. Surg.* 30, 1741–1749. doi: 10.1016/j.jse.2021.01.023

Hoekstra, M., Veltman, E. S., Nurmohamed, RFRHA, van Dijk, B., Rentenaar, R. J., Vogely, H. C., et al. (2020). Sonication leads to clinically relevant changes in treatment of periprosthetic hip or knee joint infection. *J. Bone Jt. Infect.* 5, 128–132. doi: 10.7150/jbji.45006

Ji, B., Aimaiti, A., Wang, F., Maimaitiyiming, A., Zhang, X., Li, G., et al. (2023). Intraoperative direct sonication of implants and soft tissue for the diagnosis of periprosthetic joint infection. *J. Bone Joint Surg.* 105, 855–874. doi: 10.2106/JBJS.22.00446

Karbysheva, S., Cabric, S., Koliszak, A., Bervar, M., Kirschbaum, S., Hardt, S., et al. (2022). Clinical evaluation of dithiothreitol in comparison with sonication for biofilm dislodgement in the microbiological diagnosis of periprosthetic joint infection. *Diagn. Microbiol. Infect. Dis.* 103, 115679. doi: 10.1016/j.arth.2017.11.049

Karbysheva, S., Di Luca, M., Butini, M. E., Winkler, T., Schütz, M., and Trampuz, A. (2020). Comparison of sonication with chemical biofilm dislodgement methods using chelating and reducing agents: Implications for the microbiological diagnosis of implant associated infection. *PloS One* 15, 1–15. doi: 10.1371/journal.pone.0231389

Li, C., Renz, N., Thies, C. O., and Trampuz, A. (2018). Meta-analysis of sonicate fluid in blood culture bottles for diagnosing periprosthetic joint infection. *J. Bone Jt. Infect.* 3, 273–279. doi: 10.7150/jbji.29731

Liu, K., Fu, J., Yu, B., Sun, W., Chen, J., and Hao, L. (2018). Meta-analysis of sonication prosthetic fluid PCR for diagnosing periprosthetic joint infection. *PloS One* 1, 13. doi: 10.1371/journal.pone.0196418

Moore, A. J., Blom, A. W., Whitehouse, M. R., and Gooberman-Hill, R. (2015). Deep prosthetic joint infection: A qualitative study of the impact on patients and their experiences of revision surgery. *BMJ Open* 5, 1–13. doi: 10.1136/bmjopen-2015-009495

Morgenstern, C., Renz, N., Cabric, S., Maiolo, E., Perka, C., and Trampuz, A. (2020). Thermogenic diagnosis of periprosthetic joint infection by microcalorimetry of synovial fluid. *BMC Musculoskelet. Disord.* 21, 1–7. doi: 10.1186/s12891-020-03366-3

Oliva, A., Miele, M. C., Al Ismail, D., Di Timoteo, F., De Angelis, M., Rosa, L., et al. (2021). Challenges in the microbiological diagnosis of implant-associated infections: A summary of the current knowledge. *Front. Microbiol.* 12. doi: 10.3389/fmicb.2021.750460

Oliva, A., Pavone, P., D'Abramo, A., Iannetta, M., Mastroianni, C. M., and Vullo, V. (2016). Role of sonication in the microbiological diagnosis of implant-associated infections: Beyond the orthopedic prosthesis. *Adv. Exp. Med. Biol.* 897, 85–102. doi: 10.1007/5584_2015_5007

Palan, J., Nolan, C., Sarantos, K., Westerman, R., King, R., and Foguet, P. (2019). Culture-negative periprosthetic joint infections. *EFORT. Open Rev.* 4, 585–594. doi: 10.1302/2058-5241.4.180067

Parvizi, J., Tan, T. L., Goswami, K., Higuera, C., Della Valle, C., Chen, A. F., et al. (2018). The 2018 definition of periprosthetic hip and knee infection: an evidence-based and validated criteria. *J. Arthroplasty.* 33, 1309–1314.e2. doi: 10.1016/j.arth.2018.02.078

Portillo, M. E., and Sancho, I. (2023). Advances in the microbiological diagnosis of prosthetic joint infections. *Diagn. (Basel).* 13, 809. doi: 10.3390/diagnostics13040809

Randau, T. M., Molitor, E., Fröschen, F. S., Hörauf, A., Kohlhof, H., Scheidt, S., et al. (2021). The performance of a dithiothreitol-based diagnostic system in diagnosing periprosthetic joint infection compared to sonication fluid cultures and tissue biopsies. *Z. Orthop. Unfall.* 159, 447–453. doi: 10.1055/a-1150-8396

Renz, N., Mudrovcic, S., Perka, C., and Trampuz, A. (2018). Orthopedic implant-associated infections caused by Cutibacterium spp. – A remaining diagnostic challenge. *PloS One* 13. doi: 10.1371/journal.pone.0202639

Ribeiro, V. S. T., Cieslinski, J., Bertol, J., Schumacher, A. L., Telles, J. P., and Tuon, F. F. (2022). Detection of microorganisms in clinical sonicated orthopedic devices using conventional culture and qPCR. *Rev. Bras. Ortop. (Sao. Paulo).* 57, 689–696. doi: 10.1055/s-0041-1732386

Rieber, H., Frontzek, A., Heinrich, S., Breil-Wirth, A., Messler, J., Hegermann, S., et al. (2021). Microbiological diagnosis of polymicrobial periprosthetic joint infection revealed superiority of investigated tissue samples compared to sonicate fluid generated from the implant surface. *Int. J. Infect. Dis.* 106, 302–307. doi: 10.1016/j.ijid.2021.03.085

Romanò, C. L., Al Khawashki, H., Benzakour, T., Bozhkova, S., del Sel, H., Hafez, M., et al. (2019). The W.A.I.O.T. definition of high-grade and low-grade peri-prosthetic joint infection. *J. Clin. Med.* 1, 8. doi: 10.3390/jcm8050650

Rosa, L., Lepanto, M. S., Cutone, A., Berlutti, F., De Angelis, M., Vullo, V., et al. (2019). BioTimer assay as complementary method to vortex-sonication-vortex technique for the microbiological diagnosis of implant associated infections. *Sci. Rep.* 9, 1–10. doi: 10.1038/s41598-01944045-1

Salar, O., Phillips, J., and Porter, R. (2021). Diagnosis of knee prosthetic joint infection; aspiration and biopsy. *Knee* 30, 249–253. doi: 10.1016/j.knee.2020.12.023

Schoenmakers, J. W. A., de Boer, R., Gard, L., Kampinga, G. A., van Oosten, M., van Dijl, J. M., et al. (2023). First evaluation of a commercial multiplex PCR panel for rapid detection of pathogens associated with acute joint infections. *J. Bone Jt. Infect.* 8, 45–50. doi: 10.5194/jbji-8-45-2023

Sebastian, S., Malhotra, R., Sreenivas, V., Kapil, A., and Dhawan, B. (2021). The utility of dithiothreitol treatment of periprosthetic tissues and explanted implants in the diagnosis of prosthetic joint infection. *Indian J. Med. Microbiol.* 39, 179–183. doi: 10.1016/j.ijmmb.2020.12.004

Shen, H., Tang, J., Wang, Q., Jiang, Y., and Zhang, X. (2015). Sonication of explanted prosthesis combined with incubation in BD Bactec bottles for pathogen-based diagnosis of prosthetic joint infection. *J. Clin. Microbiol.* 53, 777–781. doi: 10.1128/JCM.02863-14

Shoji, M. M., and Chen, A. F. (2020). Biofilms in periprosthetic joint infections: A review of diagnostic modalities, current treatments, and future directions. *J. Knee. Surg.* 33, 119–131. doi: 10.1055/s-0040-1701214

Stephan, A., Thürmer, A., Glauche, I., Nowotny, J., Zwingenberger, S., and Stiehler, M. (2021). Does preoperative antibiotic prophylaxis affect sonication-based diagnosis in implant-associated infection? *J. Orthopedic. Res.* 39, 2646–2652. doi: 10.1002/jor.25015

Šuster, K., and Cör, A. (2022). Fast and specific detection of staphylococcal PJI with bacteriophage-based methods within 104 sonicate fluid samples. *J. Orthop. Res.* 40, 1358–1364. doi: 10.1002/jor.25167

Tande, A. J., and Patel, R. (2014). Prosthetic joint infection. *Clin. Microbiol. Rev.* 27, 302–345. doi: 10.1128/CMR.00111-13

Torrens, C., Fraile, A., Santana, F., Puig, L., and Alier, A. (2020). Sonication in shoulder surgery: is it necessary? *Int. Orthop.* 44, 1755–1759. doi: 10.1007/s00264-020-04543-8

Torres, L. M., Turrini, N. R., Merighi, A. M. B., and Cruz, A. G. (2015). Readmissão por infecção do sítio cirúrgico ortopédico: uma revisão integrativa Readmission from orthopedic surgical site infections: an integrative review Reingreso por infección del sitio quirúrgico ortopédico: una revisión integradora. *Rev. Esc. Enferm. USP.* 49, 1004–1011. doi: 10.1590/S0080-623420150000600018

Trampuz, A., Piper, K. E., Hanssen, A. D., Osmon, D. R., Cockerill, F. R., Steckelberg, J. M., et al. (2006). Sonication of explanted prosthetic components in bags for diagnosis of prosthetic joint infection is associated with risk of contamination. *J. Clin. Microbiol.* 44, 628–631. doi: 10.1128/JCM.44.2.628-631.2006

Trampuz, A., Piper, K. E., Jacobson, M. J., Hanssen, A. D., Unni, K. K., Osmon, D. R., et al. (2007). Sonication of removed hip and knee prostheses for diagnosis of infection. *New Engl. J. Med.* 357, 654–663. doi: 10.1056/nejmoa061588

Trebse, R., and Roskar, S. (2021). Evaluation and interpretation of prosthetic joint infection diagnostic investigations. *Int. Orthop.* 45, 847–855. doi: 10.1007/s00264-021-04958-x

Tsikopoulos, K., and Meroni, G. (2023). Periprosthetic joint infection diagnosis: A narrative review. *Antibiotics* 1, 12. doi: 10.3390/antibiotics12101485

Ueda, N., Oe, K., Nakamura, T., Tsuta, K., Iida, H., and Saito, T. (2019). Sonication of extracted implants improves microbial detection in patients with orthopedic implant-associated infections. *J. Arthroplasty.* 34, 1189–1196. doi: 10.1016/j.arth.2019.02.020

Xu, Y., Huang, T. B., Schuetz, M. A., and Choong, P. F. M. (2023). Mortality, patient-reported outcome measures, and the health economic burden of prosthetic joint infection. *EFORT. Open Rev.* 8, 690–697. doi: 10.1530/EOR-23-0078

Yilmaz, M. K., Abbaszadeh, A., Tarabichi, S., Azboy, I., and Parvizi, J. (2023). Diagnosis of periprosthetic joint infection: the utility of biomarkers in 2023. *Antibiotics. (Basel).* 12, 1054. doi: 10.3390/antibiotics12061054

Zardi, E. M., and Franceschi, F. (2020). Prosthetic joint infection. A relevant public health issue. *J. Infect. Public Health* 13, 1888–1891. doi: 10.1016/j.jiph.2020.09.006

Zhang, Q., Ding, B., Wu, J., Dong, J., and Liu, F. (2021a). Sonication fluid culture of antibiotic-loaded bone cement spacer has high accuracy to confirm eradication of infection before reimplantation of new prostheses. *J. Orthop. Surg. Res.* 16, 377. doi: 10.1186/s13018-021-02520-4

Zhang, Q., Xi, Y., Li, D., Yuan, Z., and Dong, J. (2021b). The yield of sonication fluid culture for presumed aseptic loosening of orthopedic devices: a meta-analysis. *Ann. Palliat. Med.* 10, 1792–1808. doi: 10.21037/apm-20-1228

frontiers | Frontiers in Cellular and Infection Microbiology

TYPE Brief Research Report
PUBLISHED 31 May 2024
DOI 10.3389/fcimb.2024.1397847

OPEN ACCESS

EDITED BY
Stefano Marletta,
University of Verona, Italy

REVIEWED BY
Nicholas Geremia,
Ospedale dell'Angelo, Italy
Michael John Calcutt,
University of Missouri, United States
Andrea Marino,
University of Catania, Italy

*CORRESPONDENCE
Bing Gu
gubing@gdph.org.cn
Liang Wang
wangliang@gdph.org.cn

†These authors have contributed equally to this work

RECEIVED 08 March 2024
ACCEPTED 16 May 2024
PUBLISHED 31 May 2024

CITATION
Zhang L-Y, Wang L, Umar Z, Huang Y-H and Gu B (2024) Weathering the storm: diagnosis and treatment of a life-threatening disseminated *Nocardia otitidiscaviarum* infection.
Front. Cell. Infect. Microbiol. 14:1397847.
doi: 10.3389/fcimb.2024.1397847

Weathering the storm: diagnosis and treatment of a life-threatening disseminated *Nocardia otitidiscaviarum* infection

Li-Yan Zhang[1,2†], Liang Wang[2,3*†], Zeeshan Umar[2], Yuan-Hong Huang[1] and Bing Gu[2*]

[1]Laboratory Medicine, Ganzhou Municipal Hospital, Guangdong Provincial People's Hospital Ganzhou Hospital, Ganzhou, Guangdong, China, [2]Laboratory Medicine, Guangdong Provincial People's Hospital (Guangdong Academy of Medical Sciences), Southern Medical University, Guangzhou, Guangdong, China, [3]Centre for Precision Health, School of Medical and Health Sciences, Edith Cowan University, Perth, WA, Australia

Nocardiosis demonstrates a temporal categorization that includes acute, subacute, and chronic stages alongside distinct typical localizations such as pulmonary, cutaneous, and disseminated forms. Disseminated nocardiosis, commonly caused by *Nocardia asteroides*, *N. brasiliensis*, and *N. farcinica*, continues to result in substantial morbidity and mortality. Herein, we report a life-threatening disseminated nocardiosis caused by *Nocardia otitidiscaviarum* in a patient with minimal change disease. This study emphasizes the difficulty in the diagnosis and treatment of unknown infections in clinical settings and highlights the important role played by laboratories in solving infectious diseases caused by rare pathogens.

KEYWORDS

***Nocardia otitidiscaviarum*, nocardiosis, minimal change disease, microscopic examination, mass spectrometry, metagenomic sequencing**

Introduction

Nocardiosis in humans was first reported in Vienna, Austria, by Eppinger in 1890 in a man with pulmonary disease with "pseudotuberculosis" of lungs and pleura (Eppinger, 1890), as well as the presence of caseous peribronchial lymph nodes, meningitis, and multiple brain abscesses (Lee et al., 2021). The disease is caused by a group of opportunistic bacterial pathogens belonging to the genus *Nocardia* that are slow-growing, Gram-variable, partially acid-fast, with filamentous branching and environmental ubiquity (Sah et al., 2020). *Nocardia* enters the human body via the respiratory tract (pulmonary infection) or

skin (superficial cutaneous and subcutaneous infection) and usually causes damage in immunocompromised hosts (Sah et al., 2020). Of all *Nocardia* species, *Nocardia otitidiscaviarum* (formerly *N. caviae*) is a rarely reported pathogen with less known pathogenicity and incidence than other *Nocardia* species such as *N. asteroides*, *N. brasiliensis*, and *N. farcinica* (Clark et al., 1995; Sah et al., 2020). In a recent epidemiological study, it was found that among the 441 non-repetitive *Nocardia* strains reported in China from 2009 to 2021, only 26 strains (5.9%) were identified as *N. otitidiscaviarum* (Wang et al., 2022). Similarly, in Australia, the isolation percentage of *N. otitidiscaviarum* was reported to be 4.9% (Georghiou and Blacklock, 1992). Additionally, Beaman et al. reported that 1 out of 347 *Nocardia* isolates (2.9%) was *N. otitidiscaviarum* in the United States from 1972 to 1974 (Beaman et al., 1976). In another study by Kageyama et al., 14 out of 303 pathogenic *Nocardia* strains (4.62%) were identified as *N. otitidiscaviarum* from 1992 to 2001 in Japan (Kageyama et al., 2003).

N. otitidiscaviarum was initially identified from the middle ear infection of a guinea pig and reported by Snijders as a novel species in 1924 (Snijders, 1924; Sah et al., 2020). However, the first human infection was not reported until 1974, when two fatal systematic nocardiosis infections were recorded (Causey et al., 1974). Currently, it is still very challenging to make an early diagnosis of *Nocardia* infections in clinical settings. Because of the insufficient specificity of clinical features and strict requirement of laboratory detection, a 2- to 3-week duration could be required from specimen collection to *Nocardia* identification (Li et al., 2021).

To get a better understanding of nocardiosis infection caused by *N. otitidiscaviarum*, we reviewed several representative studies published recently, which investigated the infection by the bacterial pathogen with a focus on epidemiology, drug resistance, and detection. In particular, Wang et al. report on the species distribution and antimicrobial susceptibility of 441 *Nocardia* strains collected from various regions in China over 13 years, among which *N. farcinica* was the most commonly isolated species, primarily from lower respiratory tract specimens while *N. otitidiscaviarum* represented 5.9% of isolates, with the majority obtained from the lower respiratory tract (Wang et al., 2022). Interestingly, all strains of *N. otitidiscaviarum* were susceptible to linezolid, amikacin, and trimethoprim-sulfamethoxazole (TMP-SMX), highlighting the importance of accurate species identification and antibiotic susceptibility testing for effective management of nocardiosis (Wang et al., 2022). Different from the epidemiological study, drug-resistant *N. otitidiscaviarum* is not uncommon and can often cause serious infections, which have been frequently reported in clinical cases. For example, Barry et al. underscore the significance of considering *N. otitidiscaviarum* in at-risk patients with relevant occupational exposure, while highlighting the TMP-SMX resistance and the importance of suspecting it when clinical response is lacking, which may have significant implications for clinical management of similar infections (Barry et al., 2022). In addition, Saksena et al. present two cases of fatal pulmonary infection caused by the rare *N. otitidiscaviarum* in elderly patients (Saksena et al., 2020). Both cases exhibited drug resistance, particularly to TMP-SMX, despite empirical treatment with it, while the isolates were susceptible to amikacin, linezolid, ciprofloxacin, and gentamicin (Saksena et al., 2020). In addition, Ranjan reported that, in a case of pleural nocardiosis in a 38-year-old man with immune thrombocytopenia (ITP) and HIV, pleural fluid analysis revealed *N. otitidiscaviarum* growth resistant to multiple antibiotics but susceptible to amikacin, linezolid, and levofloxacin; despite aggressive treatment, including steroid therapy for ITP, the patient succumbed to sepsis and concurrent infections with *Candida guilliermondii*, *Escherichia coli*, and *Stenotrophomonas maltophilia*, underscoring the challenge of managing nocardiosis in immunocompromised individuals (Ranjan et al., 2024).

In early 2024, several case reports have described the rare infection by the bacterial pathogen *N. otitidiscaviarum*, indicating that more and more researchers and clinical doctors pay attention to this bacterial infection. For example, Srivastava and colleagues reported *N. otitidiscaviarum* causing pulmonary nocardiosis in India (Srivastava et al., 2024), while Lin et al. reported a pulmonary co-infection with *N. otitidiscaviarum* and *Aspergillus* (Lin et al., 2024). In another study, Erbaş et al. reported a rare case of a newborn with branchial cleft cyst infection due to *N. otitidiscaviarum* (Erbaş et al., 2024). In addition, two studies reported multidrug-resistant *N. otitidiscaviarum* causing fatal pleural nocardiosis in an immunosuppressed patient (Ranjan et al., 2024) and empyema thoracis in an elderly patient (Pérez Ramos et al., 2023), strengthening that special attention should be paid to both bacterial drug resistance and vulnerable populations (Zhang et al., 2023).

Taken together, early identification of *Nocardia* to species level, facilitated by mass spectrometry (MS), is crucial for improving treatment outcomes, particularly in critically ill patients, emphasizing the need for integrating MS into diagnostic algorithms for nocardiosis to guide appropriate therapy. In addition, the necessity of initiating combination therapy, including trimethoprim/sulfamethoxazole, with the assistance of tests of drug susceptibilities, is important, as resistance patterns differ among species, potentially leading to fatal outcomes without precision treatment.

In this brief research report, we present a rapid diagnosis and successful treatment of a life-threatening disseminated nocardiosis infection caused by *N. otitidiscaviarum* in a patient with minimal change disease (MCD) who underwent long-term hormone therapy. This case strengthens the important role laboratory medicine equipped with comprehensively analytical techniques plays in solving a clinical mystery caused by an unusual pathogen.

Case presentation

A 66-year-old Chinese man was initially diagnosed with nephrotic syndrome due to proteinuria in the 1st Affiliated Hospital of Gan'nan Medical College in 2019. Because of the recurrent proteinuria symptom, the patient was admitted to Ganzhou Municipal Hospital in July 2020, where he was diagnosed with MCD via percutaneous biopsy. The patient

received long-term, high-dose prednisone treatment to avoid the recurrence of proteinuria. On 1 December 2021, the patient presented with a worsening cough, thick yellow-green sputum, right scrotal swelling, and bilateral testicular redness without inducement. On 6 December, the patient was diagnosed with inflammatory changes in the right epididymis and right testicular hydrocele in Longnan County People's Hospital and was given oral amoxicillin but failed to improve and started to show worsening symptoms.

The patient was then admitted to Ganzhou Municipal Hospital for hospitalization. On 8 December, the medical laboratory reported critical values of white blood cell count at 31.71×10^9/L and a neutrophil count at 30.13×10^9/L, indicating a serious infection despite unknown sites and reasons. Pain in the swollen epididymis rules out testicular torsion, abscess, scrotal hydrops, seminal cyst, hernia, trauma, and testicular cancer. Color ultrasound suggested that the inflammatory changes of the right epididymis and hydrocele of the right testis should be considered. Amoxicillin capsules were taken orally, but the testicular swelling and pain did not improve significantly, and the symptoms gradually worsened. Clinical symptoms of epididymitis include pain, swelling, and severe scrotal pain, which are often unilateral. Therefore, the patient was finally diagnosed with epididymitis, received ceftriaxone for anti-infective therapy, and was transferred to the urology department for further observation. On 9 December, the patient was given Sulperazon due to an unknown fever (38.7°C) and durative right scrotal pain. On physical examination, it was found that the patient had rales in the left lower lung, and weakened breath sounds in both lower lungs. Computed tomography (CT) showed infiltrative consolidation with cavitation, which suggested pneumonia. Finally, the multidisciplinary team (MDT) diagnosis recommended the transfer of the patient to the respiratory department for pulmonary infection treatment.

On 13 December, the patient developed a high fever and breathing difficulty with 90% blood oxygen saturation. Physical examination revealed that the skin on the pulp of the little finger was black and fluctuating, and multiple pus spots were scattered on the whole body with local skin redness. Chest CT showed an unknown infection in the upper lobes of both lungs and the lower lobe of the left lung. To identify the pathogenic bacteria, the MDT consisting of respiratory physicians, pharmacists, medical laboratory specialists, and medical imaging experts from Guangdong Provincial People's Hospital was invited to investigate the case. Specimens of skin lesions were collected from the bedside for a 3-day culture inoculation on Columbia blood agar plates at 35 ± 2°C and smear microscopic examination. Combined with the patient's medical history, laboratory tests, and chest CT, preliminary diagnosis was given as bacterial and fungal co-infection in bilateral lungs, which was accompanied by systemic spread. Further brain magnetic resonance imaging (MRI) was recommended, which confirmed intracranial infection. In particular, *Nocardia* culture in cerebrospinal fluid was positive. Head MRI showed space-occupying lesions. Clinical manifestations were worsening for consciousness, fever, and atypical clinical symptoms. No intracranial hypertension and no headache were reported. On 15 December, VITECK® MS (bioMérieux, France) confirmed that the pathogenic bacterium was *N. otitidiscaviarum* with 99.9% confidence. Targeted next-generation sequencing (tNGS) was conducted on bronchoalveolar lavage fluid (BLF) on 16 December and the results came back on 17 December, in which two bacterial pathogens *N. otitidiscaviarum* (9×10^4 copies/mL) and *Klebsiella aerogenes* (<100 copies/mL) were reported. For specific information and general procedures of the tNGS analysis, please refer to the Supplementary Materials . The tNGS result matched with clinical symptoms and the MS result. Taking all the evidence together, the final diagnosis of this intriguing case was disseminated nocardiosis.

Susceptibility testing was conducted via the Kirby–Bauer method. Since the patient had underlying kidney disease, hence vancomycin intolerance, the combined therapy of linezolid/compound sulfamethoxazole for *N. otitidiscaviarum* and piperacillin/tazobactam for *K. aerogenes* was adopted for disseminated nocardiosis. It is noteworthy that on 22 December, during anti-infective therapy, the patient developed renal failure with hyperkalemia (serum potassium concentration >7.5 mmol/L) and oliguria, and also bore the risk of cardiac arrest at any time. Because the drug effect of potassium excretion was poor, the patient was treated with emergency hemodialysis. On 2 January 2022, the serum potassium concentration of the patient returned to 4.8 mmol/L with increased urine output and recovery of renal function. For a schematic illustration of the timeline of clinical events, please refer to Figure 1.

Discussion

Infection with *N. otitidiscaviarum* is rarely reported in China and worldwide, making its diagnosis extremely difficult since it is less likely to be suspected during infection investigation (Liu et al., 2017; Zheng, 2019). Cutaneous infection by *N. otitidiscaviarum* is almost indistinguishable from skin diseases by common pyogenic organisms, which can seriously delay the diagnosis and treatment procedures (Clark et al., 1995). In this case, although we confirmed the infectious agent as *N. otitidiscaviarum* and successfully eradicated the bacterial pathogen via a timely antibiotic treatment, there were still a series of unanswered questions about when, where, and how the patient acquired the rare bacterium due to the very low prevalence of *N. otitidiscaviarum* in the environment when compared with other *Nocardia* species and other opportunistic pathogens (Liu et al., 2017). Since nocardiosis normally develops in immunocompetent and immunosuppressed patients and individuals receiving long-term or large-dose corticosteroid therapy (Zheng, 2019), it was well understandable that the patient with MCD in this study was susceptible to the infection of *N. otitidiscaviarum* due to long-term prednisone usage. During the diagnosis of the infection, non-typical clinical features also made it difficult to determine the infectious cause. A variety of traditional and advanced analytical techniques in the medical laboratory, such as culture, smear, MS, and metagenomics, were conducted to confirm the infectious agent rapidly and accurately, which led to the discovery of *N. otitidiscaviarum* infection in this case. Therefore, applying novel techniques and combining them with traditional methods for clinical diagnosis of infrequent infectious diseases is crucial. It is also worth emphasizing that,

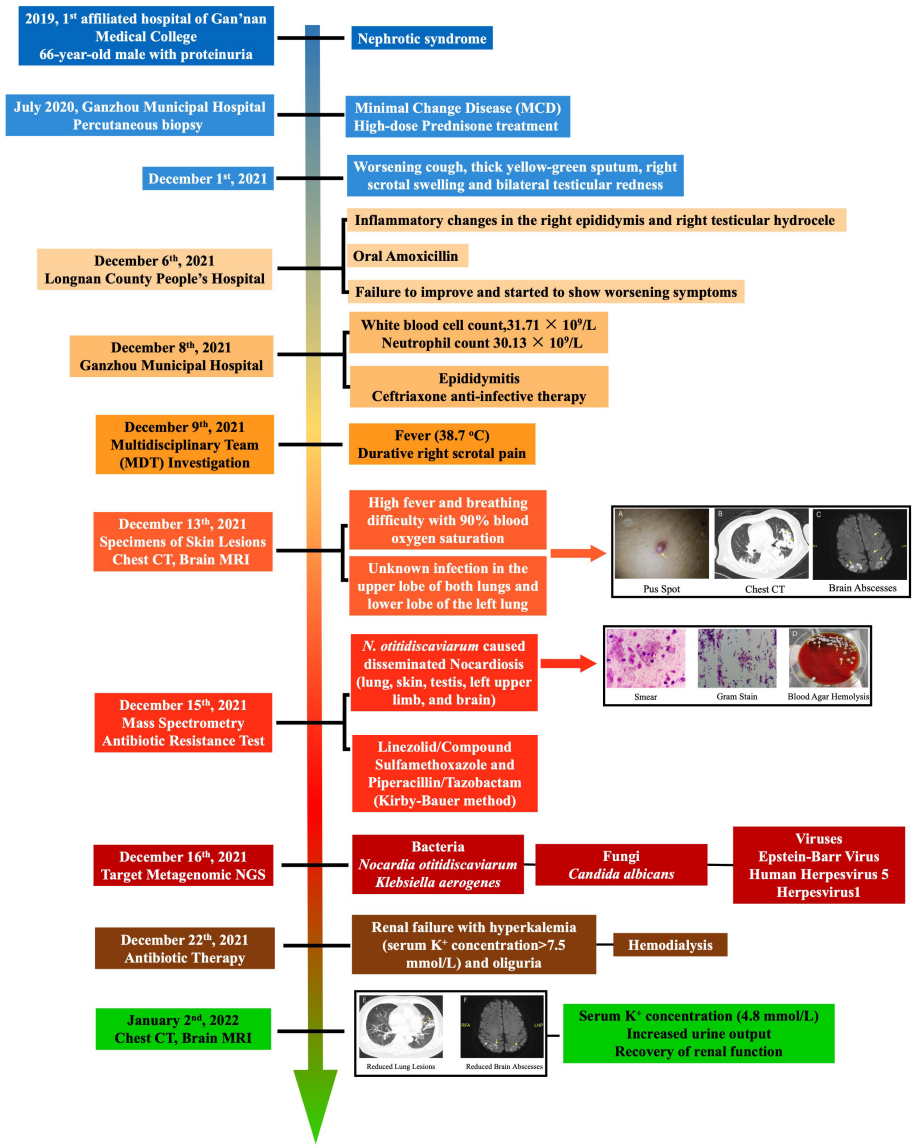

FIGURE 1
Timeline of clinical events summarizing the diagnosis and treatment of the patient from hormone therapy to infection presentation and eventually to treatment regimen. Enlarged images of pub spot, chest CT, smear and Gram stain slides, blood agar plates, and brain abscesses were available in the Supplementary Materials.

after confirming the causal pathogens, rapid determination of bacterial antibiotic resistance was also essential in the efficient treatment of the rare infection, especially when the patient had underlying diseases. In sum, we demonstrated a rare disseminated nocardiosis case caused by *N. otitidiscaviarum* in a patient with MCD with long-term hormone therapy, which showed that nocardiosis could present in various manners and involve multiple organs. According to the report, to achieve the early identification of the causative species and provide an appropriate treatment regimen for *Nocardia* infection, possible risk factors of the disease should be recognized, and the application of advanced analytical techniques is crucial.

Data availability statement

The raw data supporting the conclusions of this article will be made available by the authors, without undue reservation.

Ethics statement

The studies involving humans were approved by Ganzhou Municipal Hospital (Approval No. 2022041H). The studies were conducted in accordance with the local legislation and institutional requirements. The participants provided their

written informed consent to participate in this study. Written informed consent was obtained from the individual(s) for the publication of any potentially identifiable images or data included in this article.

Author contributions

LW: Investigation, Methodology, Validation, Visualization, Writing – original draft, Writing – review & editing. L-YZ: Data curation, Formal analysis, Investigation, Methodology, Validation, Visualization, Writing – original draft, Writing – review & editing. ZU: Formal analysis, Methodology, Validation, Visualization, Writing – original draft, Writing – review & editing. Y-HH: Formal analysis, Investigation, Methodology, Validation, Visualization, Writing – original draft, Writing – review & editing. BG: Conceptualization, Funding acquisition, Methodology, Project administration, Resources, Supervision, Validation, Writing – original draft, Writing – review & editing.

Funding

The author(s) declare financial support was received for the research, authorship, and/or publication of this article. This study was supported by the Guangdong Basic and Applied Basic Research Foundation (Grant No. 2021A1515220022) and the Ganzhou Science and Technology Bureau Project (Grant No. GZ2022ZSF252). The funders had no role in study design, data collection and analysis, decision to publish, or preparation of the manuscript.

Acknowledgments

The authors thank the laboratory staff for their assistance with handling, processing, and analyzing specimens at Ganzhou Municipal Hospital and Guangdong Provincial People's Hospital.

Conflict of interest

The authors declare that the research was conducted in the absence of any commercial or financial relationships that could be construed as a potential conflict of interest.

The author(s) declared that they were an editorial board member of Frontiers, at the time of submission. This had no impact on the peer review process and the final decision.

Publisher's note

Supplementary material

The Supplementary Material for this article can be found online at: https://www.frontiersin.org/articles/10.3389/fcimb.2024.1397847/full#supplementary-material

References

Barry, M., Alshehri, S., Alguhani, A., Barry, M., Alhijji, A., Binkhamis, K., et al. (2022). A fatal case of disseminated nocardiosis due to Nocardia otitidiscaviarum resistant to trimethoprim–sulfamethoxazole: case report and literature review. *Ann. Clin. Microbiol. Antimicrob.* 21, 1–8. doi: 10.1186/s12941-022-00511-9

Beaman, B. L., Burnside, J., Edwards, B., and Causey, W. (1976). Nocardial infections in the United States 1972–1974. *J. Infect. Dis.* 134, 286–289. doi: 10.1093/infdis/134.3.286

Causey, W. A., Amell, P., and Brinker, J. (1974). Systemic nocardia caviae infection. *Chest* 65, 360–362. doi: 10.1378/chest.65.3.360

Clark, N. M., Braun, D. K., Pasternak, A., and Chenoweth, C. E. (1995). Primary cutaneous nocardia otitidiscaviarum infection: case report and review. *Clin. Infect. Dis.* 20, 1266–1270. doi: 10.1093/clinids/20.5.1266

Eppinger, H. (1890). Uber eine Neue Pathogene Cladothrix und eine durch sie Hervorgerufene Pseudotuberculosis. *Wien Klin Wschr* 3, 3.

Erbaş, I. C., Çakil Güzin, A., Özdem Alataş, Ş., Akyildiz, C., Üçüncü Egeli, T., and Belet, N. (2024). Newborn with branchial cleft cyst infection due to nocardia otitidiscaviarum. *Pediatr. Infect. Dis. J.* 43 (6), e222–e224. doi: 10.1097/INF.0000000000004296

Georghiou, P. R., and Blacklock, Z. M. (1992). Infection with Nocardia species in Queensland: A review of 102 clinical isolates. *Med. J. Aust.* 156, 692–697. doi: 10.5694/j.1326-5377.1992.tb121509.x

Kageyama, A., Yazawa, K., Ishikawa, J., Hotta, K., Nishimura, K., and Kageyama, A. (2003). Nocardial infections in Japan from 1992 to 2001, including the first report of infection by nocardia transvalensis. *Eur. J. Epidemiol.* 19, 383–389. doi: 10.1023/B:EJEP.0000024706.02325.c0

Lee, E. K., Kim, J., Park, D.-H., Lee, C. K., Kim, S. B., Sohn, J. W., et al. (2021). Disseminated nocardiosis caused by Nocardia farcinica in a patient with colon cancer. *Medicine* 100, 1–6. doi: 10.1097/MD.0000000000026682

Li, Y., Tang, T., Xiao, J., Wang, J., Li, B., Ma, L., et al. (2021). Clinical analysis of 11 cases of nocardiosis. *Open Med.* 16, 610–617. doi: 10.1515/med-2020-0196

Lin, C., Wang, S. S., An, R., Feng, T., and Huang, S. M. (2024). Pulmonary co-infection with Nocardia otitidiscaviarum and Aspergillus: a case report. *Zhonghua Jie He He Hu Xi Za Zhi* 47, 237–240. doi: 10.3760/cma.j.cn112147-20230714-00008

Liu, C., Feng, M., Zhu, J., Tao, Y., Kang, M., and Chen, L. (2017). Severe pneumonia due to Nocardia otitidiscaviarum identified by mass spectroscopy in a cotton farmer. *Medicine* 96, 1–3. doi: 10.1097/MD.0000000000006526

Pérez Ramos, I. S., Gurruchaga Yanes, M. L., Fernández Vecilla, D., Oiartzabal Elorriaga, U., Unzaga Barañano, M. J., and Díaz De Tuesta Del Arco, J. L. (2023). Cavitary pneumonia and empyema thoracis caused by multidrug resistant Nocardia otitidiscaviarum in an elderly patient. *Rev. Española Quimioterapia* 37, 97–99. doi: 10.37201/req/042.2023

Ranjan, R., Bir, R., Gunasekaran, J., Yadav, V. S., and Gupta, R. M. (2024). A fatal case of multidrug-resistant pleural nocardiosis by nocardia otitidiscaviarum in an immunosuppressed patient: A case report and literature review. *Cureus.* 16 (1), 1–9. doi: 10.7759/cureus.52071

Sah, R., Khadka, S., Neupane, S., Nepal, G., Singla, S., Kumari, P., et al. (2020). Disseminated infection with Nocardia otitidiscaviarum in a patient under steroid therapy. *Clin. Case Rep.* 8, 369–373. doi: 10.1002/ccr3.2640

Saksena, R., Rynga, D., Rajan, S., Gaind, R., Dawar, R., Sardana, R., et al. (2020). Fatal pulmonary infection by trimethoprim-sulfamethoxazole resistant Nocardia otitidiscaviarum: report of two cases and review. *J. Infect. Develop. Countries* 14, 214–222. doi: 10.3855/jidc.10169

Snijders, N. L. (1924). Cavia-scheefkopperij, een nocardiose. *Geneeskundig TUdschrift voor Nederlandsch-Indie* 64, 3.

Srivastava, S., Samaddar, A., Khan, S., Tak, V., Bohra, G. K., Sharma, D., et al. (2024). Nocardia otitidiscaviarum causing pulmonary nocardiosis: a case report and its review of the literature. *Access Microbiol.* 6, 1–7. doi: 10.1099/acmi.0.000530.v5

Wang, H., Zhu, Y., Cui, Q., Wu, W., Li, G., Chen, D., et al. (2022). Epidemiology and antimicrobial resistance profiles of the nocardia species in China 2009 to 2021. *Microbiol. Spectr.* 10, 1–14. doi: 10.1128/spectrum.01560-21

Zhang, L. Z., Shan, C. T., Zhang, S. Z., Pei, H. Y., and Wang, X. W. (2023). [Disseminated nocardiosis caused by Nocardia otitidiscaviarum in an immunocompetent host: a case report]. *Zhonghua Jie He He Hu Xi Za Zhi* 46, 1127–1130. doi: 10.3760/cma.j.cn112147-20230516-00243

Zheng, S.-W. (2019). Disseminated nocardiosis due to Nocardia otitidiscaviarum: A case report and literature review. *Asian Pacific J. Trop. Med.* 12, 185–194. doi: 10.4103/1995-7645.257120

frontiers | Frontiers in Cellular and Infection Microbiology

TYPE Original Research
PUBLISHED 08 August 2024
DOI 10.3389/fcimb.2024.1423155

OPEN ACCESS

EDITED BY
Stefano Stracquadanio,
University of Catania, Italy

REVIEWED BY
Dimitra K. Toubanaki,
Pasteur Hellenic Institute, Greece
Jun He,
University of South China, China

*CORRESPONDENCE
Yi Wang
wildwolf0101@163.com
Juan Zhou
zhoujuan2015@126.com
Baoying Zheng
zbaoy1981@163.com
Lihui Meng
mengmlh@163.com

RECEIVED 25 April 2024
ACCEPTED 19 July 2024
PUBLISHED 08 August 2024

CITATION
Xiao F, Zhang Y, Xu W, Fu J, Huang X, Jia N, Sun C, Xu Z, Zheng B, Zhou J, Wang Y and Meng L (2024) Real-time fluorescent multiple cross displacement amplification for rapid and sensitive *Mycoplasma pneumoniae* detection.
Front. Cell. Infect. Microbiol. 14:1423155.
doi: 10.3389/fcimb.2024.1423155

Real-time fluorescent multiple cross displacement amplification for rapid and sensitive *Mycoplasma pneumoniae* detection

Fei Xiao[1], Yu Zhang[1], Wenjian Xu[2], Jin Fu[1], Xiaolan Huang[1], Nan Jia[1], Chunrong Sun[1], Zheng Xu[1], Baoying Zheng[3]*, Juan Zhou[1]*, Yi Wang[1]* and Lihui Meng[4]*

[1]Experiment Research Center, Capital Institute of Pediatrics, Beijing, China, [2]Laboratory Center, Children's Hospital Affiliated to the Capital Institute of Pediatrics, Beijing, China, [3]Respiratory Medicine, Children's Hospital Affiliated to the Capital Institute of Pediatrics, Beijing, China, [4]Department of Infectious Diseases, Children's Hospital Affiliated to Capital Institute of Pediatrics, Beijing, China

Mycoplasma pneumoniae is a significant pathogen responsible for community-acquired pneumonia, predominantly affecting children and adolescents. Here, we devised a rapid method for *M. pneumoniae* that combined multiple cross displacement amplification (MCDA) with real-time fluorescence technology. A set of ten primers, which were specifically designed for *M. pneumoniae* detection, were employed in a real-time fluorescence MCDA reaction. Of these, one primer incorporated a restriction endonuclease recognition sequence, a fluorophore, and a quencher, facilitating real-time fluorescence detection. The real-time (RT)-MCDA reactions were monitored in a simple real-time fluorescence instrument and conducted under optimised conditions (64°C for 40 min). The detection limit of the *M. pneumoniae* RT-MCDA assay for genomic DNA extracted from *M. pneumoniae* culture was down to 43 fg/μl. This assay accurately identified *M. pneumoniae* strains without cross-reacting with other bacteria. To validate its practical application, we tested the *M. pneumoniae* RT-MCDA assay using genomic DNA extracted from clinical samples. The assay's detection capability proved comparable with real-time PCR, MCDA-based biosensor detection, and visual inspection under blue light. The entire process, including rapid DNA extraction and real-time MCDA detection, was completed within 1 h. Overall, the *M. pneumoniae* RT-MCDA assay reported here is a simple and effective diagnostic tool for rapid *M. pneumoniae* detection, which holds significant potential for point-of-care testing and in resource-limited regions.

KEYWORDS

***Mycoplasma pneumoniae*, real-time detection, multiple cross displacement amplification, restriction endonuclease, rapid diagnosis**

Introduction

Mycoplasma pneumoniae is a prevalent cause of community-acquired pneumonia (Hammerschlag, 2001; Lee, 2008; Kumar and Kumar, 2023). This infectious agent can affect individuals of all ages but is most common among children and adolescents, with its incidence rising annually (Chang et al., 2014; Chen et al., 2024; Liu et al., 2024). Infections with *M. pneumoniae* typically manifest with respiratory symptoms but it can also lead to complications outside the respiratory system, such as cardiovascular and neurological complications (Kumar and Kumar, 2023). The clinical signs of *M. pneumoniae* infection are non-specific and coupled with diagnostic complexities, making early and rapid identification challenging (Hammerschlag, 2001; Kumar and Kumar, 2023). Therefore, improving the accuracy of *M. pneumoniae* detection is particularly important for clinical diagnosis and management.

There is no significant difference in clinical symptoms and imaging between *M. pneumonia* infection-associated pneumonia and pneumonia caused by other pathogens. Thus, the identification and diagnosis of *M. pneumoniae* infection mainly relies on laboratory diagnosis (Hammerschlag, 2001; Daxboeck et al., 2003; Kumar and Kumar, 2023). Currently, the main techniques for detecting *M. pneumoniae* are the culture-based method, serological tests, and polymerase chain reaction (PCR) (Kumar and Kumar, 2023). The culture-based method is regarded as the "gold standard" for confirming *M. pneumoniae* infections (Daxboeck et al., 2003; Chang et al., 2014; Kumar and Kumar, 2023). However, it is time-consuming (2–6 weeks for results), labour-intensive, and costly, limiting its practical use in clinical settings (Chang et al., 2014; Kumar and Kumar, 2023). Serological testing is commonly used due to its ease of use (Daxboeck et al., 2003; Chang et al., 2014). However, challenges in producing highly specific *M. pneumoniae* antibodies, due to numerous stop codons in the *M. pneumoniae* gene sequence and difficulties in recombinant antigen production via prokaryotic expression, affect the sensitivity and specificity of this method. Factors such as patient age, immune status, and the quality of test kits also impact results (Daxboeck et al., 2003; Chang et al., 2014). In addition, the requirement for paired serum samples taken 1–2 weeks apart makes serological testing less accessible and generally retrospective (Chang et al., 2014). A PCR-based detection assay is emerging as a rapid and reliable diagnostic method, often regarded as the new "gold standard" for detecting *M. pneumoniae* due to its high sensitivity and specificity (Chang et al., 2014; Park, 2022). However, its widespread adoption is hampered by the need for sophisticated equipment and skilled operators, particularly in primary healthcare settings (Chang et al., 2014; Park, 2022). To address these limitations presented by PCR-based methods, various isothermal amplification techniques have been developed since the early 1990s as alternatives to PCR (Zhao et al., 2015; Park, 2022; Srivastava and Prasad, 2023). These methods allow for the rapid and efficient amplification of nucleic acids at a constant temperature, offering advantages such as lower equipment costs, quicker results, simpler procedures, and greater specificity and sensitivity, making them suitable for immediate clinical use (Wang et al., 2015, 2016).

In recent years, the use of multiple cross displacement amplification (MCDA) technology within the realm of isothermal amplification has proven effective for detecting numerous pathogens (Zhao et al., 2019; Li et al., 2020; Jiang et al., 2022; Jia et al., 2023; Zhou et al., 2023). MCDA is a novel amplification strategy based on isothermal chain displacement polymerisation reactions, in which a set of 10 specific primers is designed for each target, spanning 10 different regions of the target sequence, achieving sensitivity in the femtogram range (Wang et al., 2015). At the operational temperatures (58°C–70°C), the dynamic interaction between primer-template hybridisation facilitates the annealing of a high concentration of primers onto the DNA template without requiring a denaturation phase, thus initiating synthesis (Wang et al., 2015). This leads to exponential amplification of the DNA products through chain displacement reactions. The MCDA reactions can be monitored through three primary methods: colorimetric analysis, agarose gel electrophoresis, and real-time turbidimetry. Therefore, the MCDA technique not only offers rapid results, high specificity, and sensitivity, but also has the added benefits of low equipment demands and simplicity in execution.

In this study, we successfully incorporated MCDA technology into the real-time PCR platform, creating a novel real-time MCDA detection method specifically tailored for *M. pneumoniae*. This approach enables direct monitoring of fluorescence signals and allows results to be read directly through the instrument without having to open the reaction tube, significantly reducing the risk of contamination. This rapid, sensitive, specific, and contamination-free method proves highly effective in diagnosing *M. pneumoniae* infection. During the establishment of this technique, we also assessed its clinical accuracy in detecting *M. pneumoniae* infection. The results of our study indicate that *M. pneumoniae* RT-MCDA is particularly useful in regions lacking dedicated product testing laboratories.

Materials and methods

Reagents and instruments

A DNA Isothermal Amplification Kit, biotin-14-dCTP, visual detection reagent (VDR), and a nanoparticle-based lateral flow biosensor (LFB) were obtained from Huidexin Biotech Co., Ltd (Tianjin, China). Restriction endonuclease (*Nb.BsrDI*) was purchased from New England BioLabs (Beijing, China). A nucleic acid extraction kit was obtained from Beijing Transgen Biotech Co., Ltd (Beijing, China) and real-time PCR kits were procured from HuNan SX Bio-Tech Co., Ltd (HuNan, China). The BluSight Pro (GD50502) was obtained from Manod Biotech. Co, Ltd (Suzhou, China). The real-time turbidimeter (LA-320C) was purchased from Eiken Chemical Co., Ltd, Japan. A fluorescence quantitative PCR instrument ABI 7500 was purchased from Applied Biosystem Inc., USA.

Primer design

A set of ten primers targeting the community-acquired respiratory distress syndrome (CARDS) toxin gene (LR214945.1) of *M. pneumoniae* were designed using primer premier 5.0 (https://primerexplorer.jp). The primer set includes two displacement primers (F1 and F2), two cross primers (CP1 and CP2), and six amplification primers (C1, C2, D1, D2, R1, and R2). The amplification primer D1 used in the *M. pneumonia* MCDA-LFB assay (termed D1$^{\#}$) was modified by assigning a fluorophore (FAM) at the 5' end, whereas the amplification primer C1 employed in the *M. pneumoniae* RT-MCDA assay (termed C1*) was modified by additionally adding a short sequence (Ss, TGCAATG) at the 5′ end and assigning a fluorophore and black hole quencher 1 (BHQ1) at the 5′ end and the middle of new primer. Primers and labelled primers used in this study were synthesised by AoKe Biotech Co., Ltd (Beijing, China). The sequences, location, and the modification of the primers are shown in Table 1 and Figure 1.

DNA preparation

Genomic DNA of all the strains was extracted and purified using an EasyPure® Genomic DNA kit (TransGen Biotech, Beijing, China) according to the manufacturer's instructions. Purity and concentration were determined using a Nanodrop 2000 (Thermo Fisher, Waltham, MA, USA) at A260/280. Before usage, the extracted DNA was kept at −20°C.

TABLE 1 The primers used in the study.

Gene	Primer[a]	Sequence and modifications (5′-3′)	Length[b]
CARDs toxin	F1	CTAAGGGGAATTAAAACGCAA	21nt
	F2	GTGCACTTTGAGCTGACC	18nt
	CP1	GACTTTTGTTTGGGGTTTACTTCGA AACCTTTATGTTACAAGCAGAT	47mer
	CP2	TGTCTCAAGGATTTAACTGGTGCATA CTGAGTAGTAAAGGCAGT	44mer
	C1	GACTTTTGTTTGGGGTTTACTTCGA	25nt
	C2	TGTCTCAAGGATTTAACTGGTGC	23nt
	D1	CCAAAAAGACATTGTTATTTTGC	23nt
	D2	ACAAATCAGTCTTTCGCTT	19nt
	R1	AAGAAGATGGTTTGGGGAA	19nt
	R2	TGGGATGTTTATCAACGA	18nt
	D1$^{\#}$	FAM-CCAAAAAGACATTGTTATT TTGC	23nt
	C1*	FAM-TGCAATG-GACT (BHQ1)TTTGTTTGGGGTTTACTTCGA	25nt

[a]F1 and F2, displacement primers; CP1 and CP2, cross primers; C1, C2, D1, D2, R1, and R2, amplification primers; C1*, 5′-labelled with FAM and BHQ1 when used in an M. pneumoniae RT- MCDA assay; D1$^{\#}$, 5′-labelled with FAM when used in an M. pneumoniae-MCDA-LFB assay.
[b]nt, nucleotide; mer, monomeric unit.

Standard *M. pneumoniae* -MCDA-LFB reaction

The volume of the MCDA reaction system was 25 µl, containing 12.5 µl of 2 × isothermal reaction buffer, 0.1 µmol/L each of displacement primers (F1 and F2), 0.4 µmol/L each of cross primers (CP1 and CP2), 0.2 µmol/L each of amplification primers [C1, C2, D1$^{\#}$(FAM labelled), D2, R1, and R2], 1.0 µl of *Bst* 2.0 DNA polymerase (8 U), 0.5 µl of biotin-14-dCTP, and 1 µl of DNA template from *M. pneumoniae* pure culture or 5 µl from clinical samples. In addition, 1 µl of DNA template of *Klebsiella pneumoniae* was employed as a negative control, and 1 µl of double distilled water (DW) was used as a blank control. The reaction mixtures were incubated at 64°C for 1 h using a real-time turbidimeter or traditional PCR instrument. The results were monitored using a real-time turbidimeter, VDR, and LFB test. For real-time turbidimeter, reaction with turbidity >0.1 was considered as positive, otherwise as negative. For VDR, reaction with a light blue colour was deemed as positive, while the colourless one was negative. For result interpretation by LFB, 5 µl of MCDA reaction products were added to the sample pad of LFB, followed by 100 µl of running buffer [10 mM PBS (PH 7.4) with 1% Tween 20]. The results were indicated within 2 min, with two red lines at the control line (CL) and testing line (TL) representing a positive result and one red line at the CL representing a negative result. In parallel, results of the *M. pneumoniae* MCDA reaction were real-time monitored by real-time turbidimeter and visually inspected by naked eye with VDR.

Standard *M. pneumoniae* RT-MCDA reaction

The RT-MCDA assay was conducted in a 25 µl reaction system consisting of 12.5 µl of buffer, 0.1 µmol/L each of displacement primers (F1 and F2), 0.4 µmol/L each of cross primers (CP1and CP2), 0.2 µmol/L each of amplification primers [C1* (restriction endonuclease recognition sequence, FAM and BHQ1 labelled), C2, D1, D2, R1, and R2], 1.0 µl of Bst DNA polymerase (8 U), 1.0 µl of *Nb.BsrDI* restriction endonuclease, and 1 µl of template from pure culture (5 µl from the clinical sample). The reaction was carried out using real-time PCR instruments for 40 cycles with a setting mode of 5 s at 64°C for reaction and 55 s at 64°C for fluorescence monitoring. Reaction with apparent fluorescence generation indicated a positive result, while that with trace or none fluorescent signal implied a negative one. The positive threshold value was obtained by testing plenty of positive, negative, and blank reactions.

Optimisation of the *M. pneumoniae* RT-MCDA assay

The optimal reaction temperature for the *M. pneumoniae* MCDA reaction was determined by performing an *M.*

10.3389/fcimb.2024.1423155

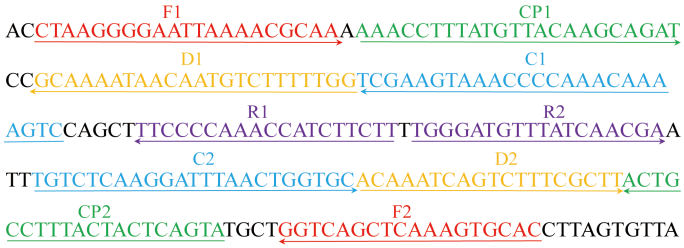

FIGURE 1
Primers for the *CARDS* toxin gene used in the *M. pneumoniae* RT-MCDA assay in this study. The location of the primer sequences used in this study on the targeting *CARDS* toxin gene of *M. pneumoniae*. Right and left arrows show sense and complementary sequences, respectively. The coloured text indicates the position of the primers, including two displacement primers (F1 and F2), two cross primers (CP1 and CP2), and six amplification primers (C1, C2, D1, D2, R1, and R2).

pneumoniae MCDA reaction at temperatures from 60 to 67°C with a 1°C interval for 40 min followed by incubation at 85°C to stop the reaction. The amplification process was real-time monitored using a real-time turbidimeter. DNA templates from *M. pneumoniae* were used as a positive control and DW as a blank control. The temperature generating the best reaction performance was considered as the optimal one. Meanwhile, assays with different reaction times from 10 min to 40 min (with 10 min intervals) were conducted to determine the optimal reaction time. The shortest time required for the MCDA reaction was regarded as the optimal reaction time. All the tests were repeated three times. The obtained optimum reaction temperature and time were employed for the following tests.

Sensitivity and specificity evaluation of the *M. pneumoniae* RT-MCDA assay

To determine the sensitivity of the *M. pneumoniae* RT-MCDA assay, DNA templates from cultured *M. pneumoniae* were serially diluted to 4.3 ng/μl, 430 pg/μl, 43 pg/μl, 4.3 pg/μl, 430 fg/μl, 43 fg/μl, and 4.3 fg/μl. Accordingly, 1 μl or 2 μl each of the serial templates was added into the *M. pneumoniae* RT-MCDA reaction systems to test the limit of detection (LoD) of the assay. Each reaction was repeatedly tested in triplicate. For the specificity assessment of the *M. pneumoniae* RT-MCDA assay, DNA templates from three *M. pneumoniae* strains and 29 non-*M. pneumoniae* strains (Table 2) were examined by this assay with three replicates. Similarly, all the samples were tested by the MCDA-LFB assay for comparison.

Clinical application assessment of the *M. pneumoniae* RT-MCDA assay

For evaluation of the clinical feasibility, DNA templates extracted from 48 sputum samples were retrospectively tested by the *M. pneumoniae* RT-MCDA assay and MCDA-LFB test. Particularly, 1 μl, 3 μl, 5 μl, and 7 μl of clinical sample template were examined separately to identify the appropriate volume for clinical evaluation. The 48 samples were collected from children hospitalised in the Children's Hospital Affiliated to Capital Institute of Pediatrics from 12 October 2023 to 20 December 2023 and had been examined using the real-time PCR method for clinical diagnosis. All the samples were obtained with informed consent signed by the guardians of the participants.

Results

Principle of the *M. pneumoniae* RT-MCDA assay

The *M. pneumoniae* RT-MCDA assay was devised by combining an MCDA reaction with restriction endonuclease cleavage, which will generate fluorescent readouts for result interpretation. As illustrated in Figure 2, using primers (C1* in this study) adding a short sequence 5′-TGCAATG-3′, which could be specifically recognised and cleaved by restriction endonuclease *Nb.BsrDI*, the RT-MCDA reaction will produce plenty of products containing the *Nb.BsrDI* recognition sequence. Once the generated products were cleaved by *Nb.BsrDI*, fluorescent signals were yielded due to the separation of FAM and BHQ1, which flanked the *Nb.BsrDI* recognition sequence. It is worth mentioning that owing to the addition of the short sequence (Ss, TGCAATG) at the 5′ end of the amplification primer C1 (C1*), *Nb.BsrDI* accurately identified the target double-stranded DNA sequences and cut them to generate fluorescence signals, which will not be interfered with by the excess (single-stranded) primer cleavage. The fluorescent signals could be visually inspected with the naked eye under blue light in addition to a real-time PCR instrument. Thus, the presence or absence of target pathogen will be reported only with the naked eye rather than complicated instruments.

In this study, an *M. pneumoniae*-MCDA-LFB assay was conducted in parallel for comparison. The principle of the MCDA-LFB assay is shown in Figure 3. Unlike the RT-MCDA assay, the MCDA-LFB assay was devised on the basis of the MCDA reaction and LFB detection. Using a FAM-labelled primer and biotin-14-dCTP, the MCDA reaction could produce abundant FAM/biotin-labelled amplicons, which could be transformed into a colorimetric readout with LFB. Particularly, the immobilised anti-FAM of LFB captured FAM-containing target amplification products and SA-GNPs (streptavidi-coated dyed polymer nanoparticles) enabled

10.3389/fcimb.2024.1423155

TABLE 2 Strains for specificity confirmation of *M. pneumoniae* RT-MCDA assay.

Pathogen	Strain no. (source of the strains)[a]	No. of strains	*M. pneumoniae* real-time MCDA[b]
Mycoplasma pneumonia	Isolated strains (CDC)	3	P
Acinetobacter baumannii	Isolated strains (CIP)	1	N
Bacillus cereus	Isolated strains (CIP)	1	N
Citrobacter spp.	Isolated strains (CIP)	1	N
Corynebacterium striatum	Isolated strains (CIP)	1	N
Enteroinvasive Escherichia coli	Isolated strains (CIP)	1	N
Enterotoxigenic Escherichia coli	Isolated strains (CIP)	1	N
Haemophilus influenza	Isolated strains (CIP)	2	N
Klebsiella pneumonia	Isolated strains (CIP)	2	N
Listeria innocua	Isolated strains (CIP)	1	N
Listeria monocytogenes	Isolated strains (CIP)	1	N
Monilia albican	Isolated strains (CIP)	1	N
Moraxella catarrhalis	Isolated strains (CIP)	1	N
Mycobacterium tuberculosis	Isolated strains (CIP)	1	N
Neisseria meningitides	Isolated strains (CIP)	1	N
Nocardia asteroids	Isolated strains (CIP)	1	N
Pseudomonas aeruginosa	Isolated strains (CIP)	1	N
Shigella sonnei	Isolated strains (CIP)	1	N
Staphylococcus amber	Isolated strains (CIP)	1	N
Staphylococcus haemolyticus	Isolated strains (CIP)	1	N
Steptococcus salivarius	Isolated strains (CIP)	1	N
Streptococcus aureus	Isolated strains (CIP)	1	N
Streptococcus pneumoniae	Isolated strains (CIP)	2	N
Streptococcus pyogenes	Isolated strains (CIP)	1	N
Mycoplasma genitalium	Isolated strains (CIP)	1	N
Mycoplasma genitalium	Isolated strains (CIP)	1	N
Mycoplasma urealyticum	Isolated strains (CIP)	1	N

[a]CIP, Capital Institute of Pediatrics; CDC, Chinese Center for Disease Control and prevention.
[b]P, positive; N, negative.

products containing biotin to be visualised, resulting in a red line occurring in the TL region of LFB. The remaining SA-GNPs were captured by the biotinylated bovine serum albumin (biotin-BSA) in the CL region, resulting in a red line in the CL region, indicating the effectiveness of the LFB (Figure 3).

Effectiveness of the primer set for the *M. pneumoniae* RT-MCDA assay

The effectiveness of the primer set (Figure 1, Table 1) for the *M. pneumoniae* MCDA assay was confirmed by performing an MCDA reaction with the selected primer set and monitoring results using three methods (real-time turbidity, VDR, and LFB). Using a real-time turbidimeter, the positive reaction (the reactions of *M. pneumoniae*) displayed a sharp increase in turbidity, whereas the negative (the reaction of *K. pneumoniae*) and blank control (the reaction of DW) reactions did not generate any turbidity (Figure 4A). Using VDR, the colour of the positive control changed into light green, whereas the others were colourless (Figure 4B). With LFB, two visible red lines in the CL and TL regions were observed with the positive control products, whereas only one line in CL was observed when the negative and blank control products were examined (Figure 4C). Thus, the primer set was determined to establish the *M. pneumoniae* RT-MCDA assay.

Subsequently, the primer set was used for *M. pneumoniae* RT-MCDA assay confirmation. As shown in Figure 4D, positive reactions released fluorescent signals that showed an obvious fluorescence value in the real-time PCR platform and a light yellow colour under blue light, whereas the negative and blank controls did not present a fluorescent signal either in the real-time PCR platform or under blue light. These data indicated that the selected primer set was suitable for the *M. pneumoniae* RT-MCDA assay and *M. pneumoniae* detection.

Optimal reaction condition for the *M. pneumoniae* RT-MCDA assay

Temperatures ranging from 60°C to 67°C with a 1°C interval were employed to conduct the MCDA reactions for the

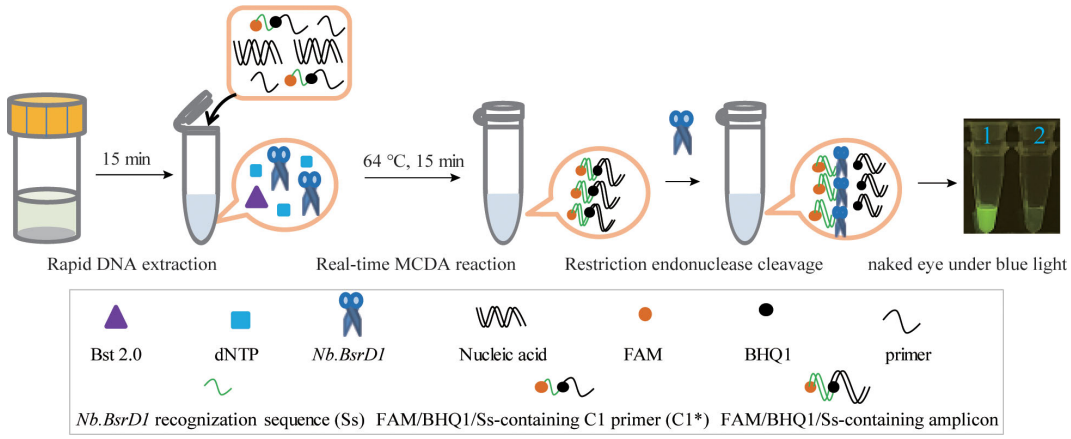

FIGURE 2
Schematic illustration of the *M. pneumoniae* RT-MCDA assay. In the *M. pneumoniae* RT- MCDA system, the primer C1* was modified by adding a short sequence (TGCAATG) at 5′ end that could be recognised by restriction endonuclease *Nb.BsrDI*. When reacted with C1*, the *M. pneumoniae* real-time MCDA system generated plenty of Ss-containing target amplicons that were then cleaved by restriction endonuclease *Nb.BsrDI*, which could separate the fluorophore FAM from BHQ1, resulting in the emission of fluorescence signals that could be visually inspected with the naked eye under blue light, in addition to a real-time PCR instrument.

optimisation of the reaction temperature. As shown in Figure 5, 64° C was the optimal reaction temperature for the primer set, as the faster peak was obtained under this condition. Therefore, 64°C was subsequently used as the optimal temperature for the *M. pneumoniae* MCDA assay. In addition, the *M. pneumoniae* MCDA assay was conducted at 64°C for 10 min, 20 min, 30 min, and 40 min to reveal the optimal reaction time. As shown in Figure 6, it was concluded that the LoD level (determined by sensitivity analysis as 43 fg/μl) of the genomic DNA of *M. pneumoniae* could be detected only after amplification at 64°C for 40 min. Thus, a reaction temperature of 64°C and a reaction time of 40 min were employed in the following tests, and the whole diagnostic procedure, from template extraction to result reporting, was finished within 1 h (Figure 2).

Sensitivity and specificity of the *M. pneumoniae* RT- MCDA assay

To assess the sensitivity of the *M. pneumoniae* RT-MCDA assay, an RT-MCDA assay was performed with serial dilutions of genomic DNA templates from *M. pneumoniae* strains. The detection limits of the *M. pneumoniae* RT-MCDA assay with 1 μl or 2 μl of pure culture template were both 43 fg/μl (Figures 7A, B), which was in complete accordance with those observed with the naked eye under blue light (Figure 7C) and that when using an MCDA-LFB assay (Figure 7D). Considering the risk of carryover contamination, a reaction volume of 1 μl was recommended.

To estimate the analytical specificity, the *M. pneumoniae* RT-MCDA assay was conducted using genomic DNA templates extracted

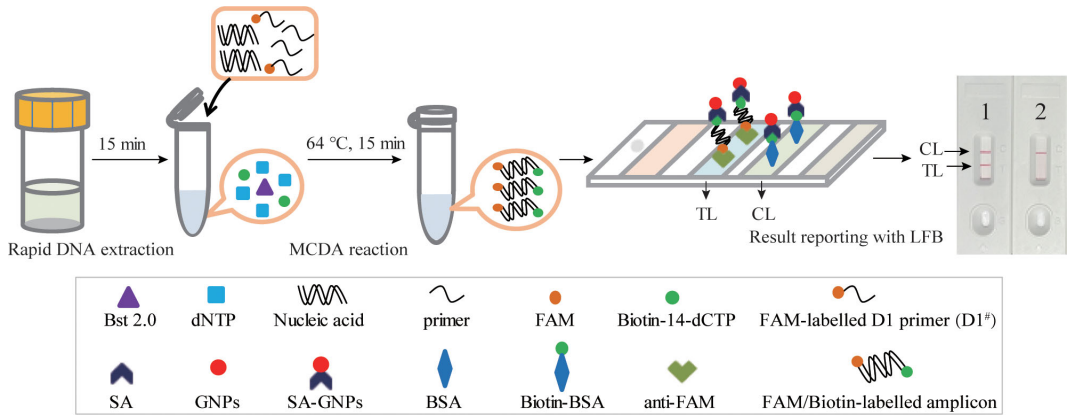

FIGURE 3
Schematic illustration of the *M. pneumoniae*-MCDA-LFB assay. In the *M. pneumoniae* -MCDA-LFB system, anti-FAM immobilised on LFB can capture the double-labelled amplicon (produced by FAM-labelled amplification primer D1# and biotin-14-dCTP) in the reaction and is visualised by the reaction of biotin and SA-GNPs (dark red), resulting in a red line occurring in the TL region of the LFB. The remaining SA-GNPs were captured by the immobilised biotin-BSA at the CL region, leading to a red line occurring in the CL region, which indicated the effectiveness of the LFB.

10.3389/fcimb.2024.1423155

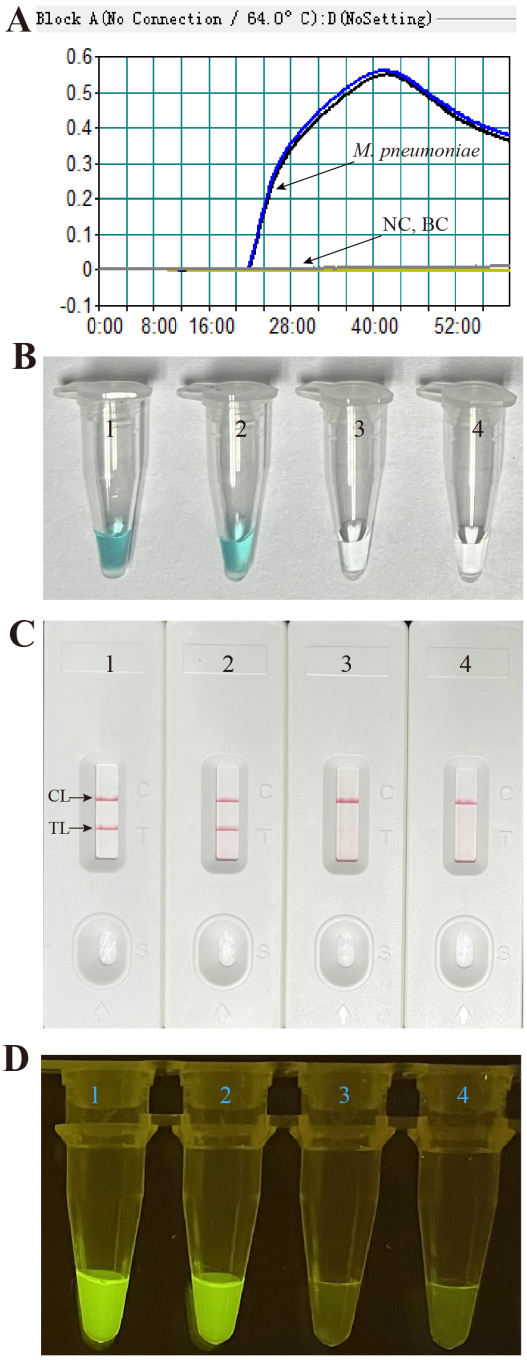

FIGURE 4
Effectiveness of the primer set for the *M. pneumoniae* RT-MCDA reaction. The DNA templates extracted from *M. pneumoniae* strains were effectively amplified with MCDA reactions at 64°C for 1 h, and there was no obvious amplification in the negative and blank controls. The products were indicated by real-time turbidity **(A)**, the VDR **(B)**, and the nanoparticle-based LFB test **(C)**, and observed with the naked eye under blue light **(D)**. Tubes/strips 1–2 represent DNA templates extracted from *M. pneumoniae* strains. Tube/strip 3 represents DNA template extracted from a *Klebsiella pneumoniae* strain, Tube/strip 4 represents the blank control. CL, control line; TL, test line.

from *M. pneumoniae* strains and non-*M. pneumoniae* strains (Table 2). When analysed using a real-time fluorometer, the positive results were only acquired from the reactions with DNA templates of *M. pneumoniae* strains; the non-*M. pneumoniae* strains were negative (Figure 8A). When observed under blue light, a light yellow colour was only observed with the products of three *M. pneumoniae* strains and not with those of the 29 non-*M. pneumoniae* pathogens (Figure 8B). When monitored by LFB, the three *M. pneumoniae* strains displayed two red lines at both TL and CL of LFB, whereas all the 29 non-*M. pneumoniae* pathogens displayed only one red line in CL of LFB (Figure 8C). All the above results proved that the specificity of the *M. pneumoniae* RT-MCDA assay was 100%.

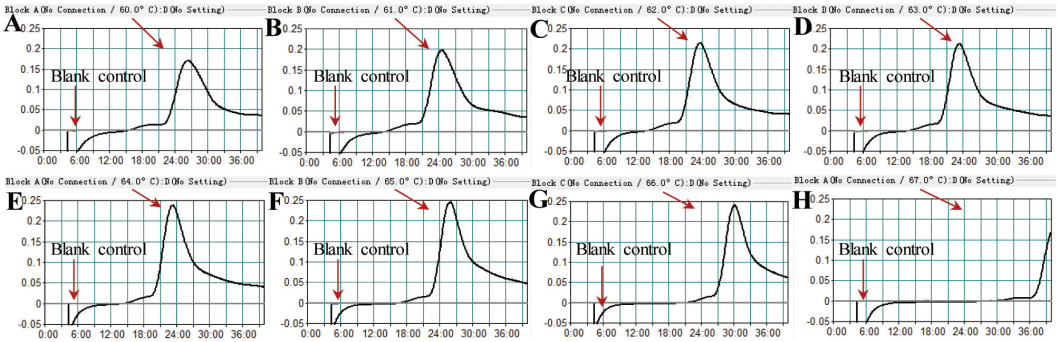

FIGURE 5
Temperature optimisation for the *M. pneumoniae* RT-MCDA assay. MCDA reactions detecting *M. pneumoniae* were conducted using a real-time turbidimeter. Turbidity >0.1 was considered a positive result. The kinetic curves at different temperatures ranging from 60 to 67°C **(A–H)** were acquired, showing that 64°C was the optimal temperature.

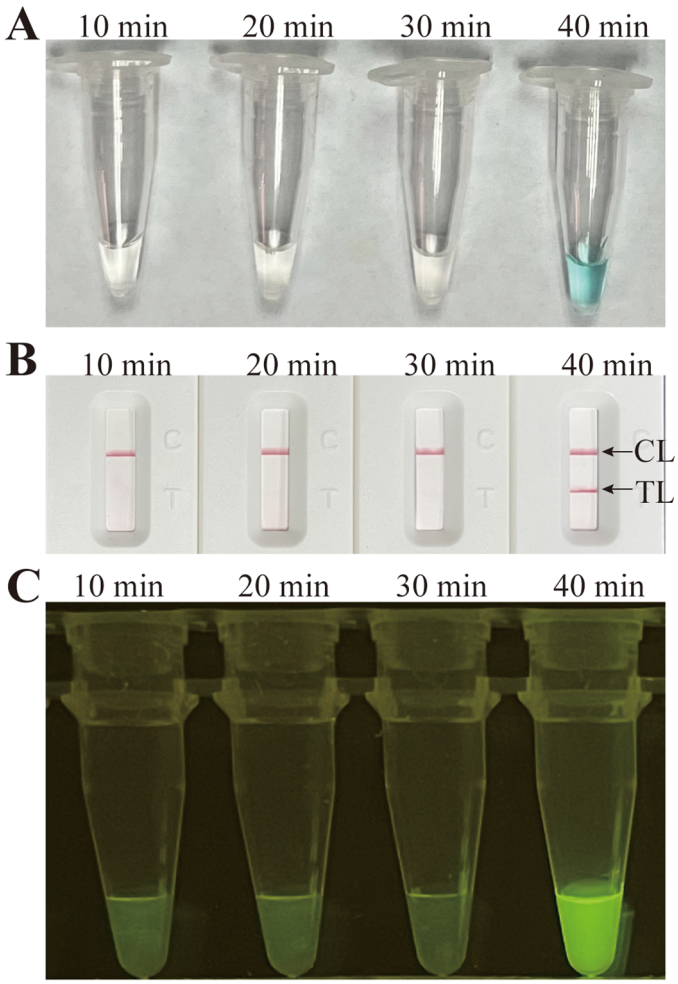

FIGURE 6
Time optimisation for the *M. pneumoniae* RT-MCDA assay. The standard MCDA reaction with four distinct times, 10 min, 20 min, 30 min, and 40 min, was tested and analysed by VDR **(A)**, LFB **(B)**, and the naked eye under blue light **(C)** at the optimal temperature of 64°C. The LoD level of *M. pneumoniae* genomic DNA could be detected only after amplification for 40 min. Strips/tubes 1–7, DNA templates extracted from serial dilutions (4.3 ng–4.3 fg/μl); strip/tube 8, blank control. CL, control line; TL, test line.

10.3389/fcimb.2024.1423155

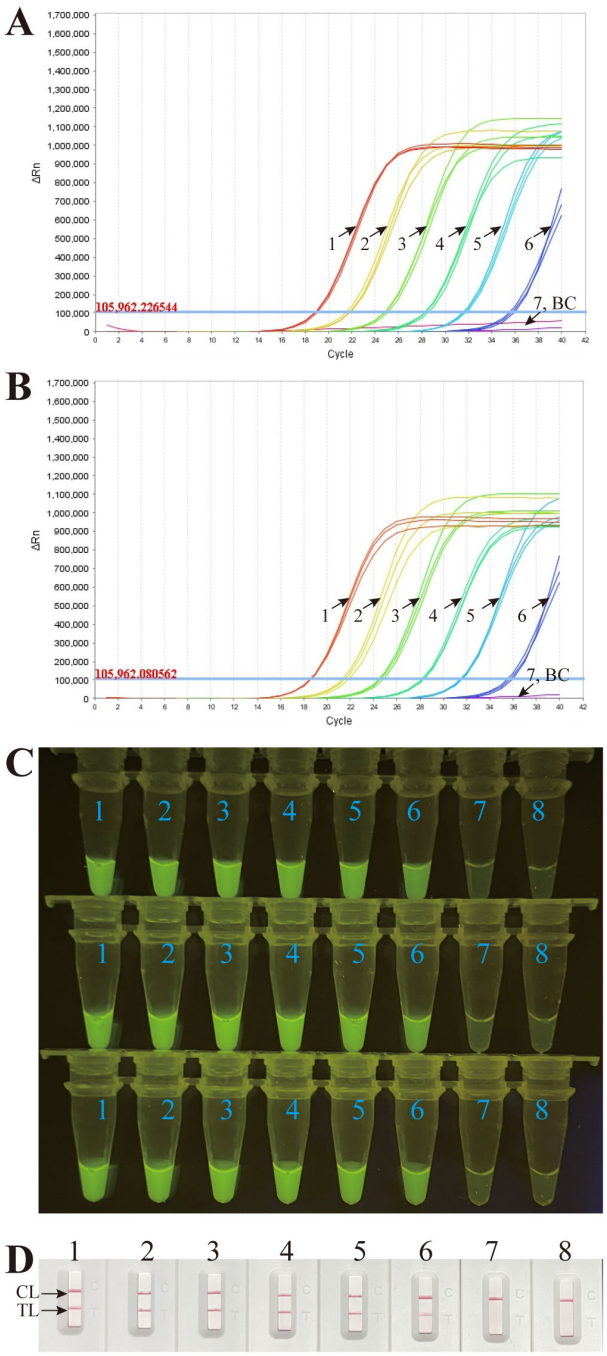

FIGURE 7
Sensitivity confirmation of the *M. pneumoniae* RT-MCDA assay. Sensitivity of the *M. pneumoniae* RT-MCDA assay was analysed using DNA templates extracted from serial dilutions (4.3 ng, 430 pg, 43 pg, 4.3 pg, 430 fg, 43 fg, and 4.3 fg/μl) of cultured *M. pneumoniae*. Three detection formats were used for amplification products analysis: **(A)** real-time fluorescence with 1 μl of template; **(B)** real-time fluorescence with 2 μl of template; **(C)** visual detection with the naked eye under blue light; and **(D)** an LFB test. The results of the three tests showed that the lowest detection limit of the *M. pneumoniae* RT-MCDA was 43 fg/μl. The sensitivity was also confirmed through visual detection with the naked eye under blue light **(C)** and an LFB test **(D)**. TL, test line; CL, control line.

Application of the *M. pneumoniae* RT-MCDA assay in clinical specimens

To further validate the feasibility of the *M. pneumoniae* RT-MCDA assay in clinical application, the optimised process was used to detect the retrospectively collected DNA templates extracted from 48 sputum samples, which were previously detected using the real-time PCR method. Among the 48 samples, 26 tested positive for the *M. pneumoniae* RT-MCDA assay and 22 samples tested negative, regardless of whether the reaction volume was 1 μl, 3 μl, 5 μl, or 7 μl (Figures 9A-D). However, reactions with 1 μl and 3 μl of clinical sample template displayed more threshold results, which

10.3389/fcimb.2024.1423155

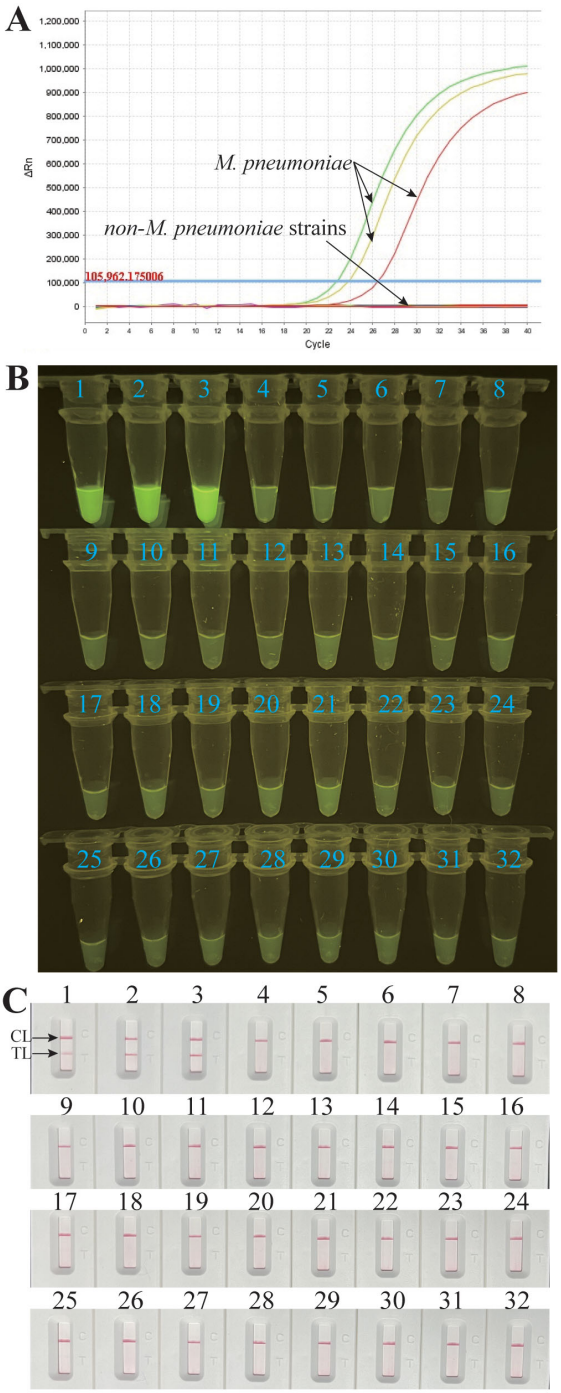

FIGURE 8
Analytical specificity of the *M. pneumoniae* RT-MCDA assay. DNA templates from three *M. pneumoniae* strains and 29 non-*M. pneumoniae* strains were tested using the *M. pneumoniae* RT-MCDA assay. No reactions were recorded with the non-*M. pneumoniae* strains. The generated fluorescence signals were recorded by the real-time PCR platform **(A)** and visually interpreted with the naked eye under blue light **(B)**. The results were also confirmed by an LFB test **(C)**. Signals/tubes/strips 1–3 represent the three *M. pneumoniae* strains, and the others represent the non-*M. pneumoniae* strains (Table 2). TL, test line; CL, control line.

may be difficult to read with the naked eye, thus 5 μl of clinical sample template was selected for clinical evaluation analysis. Of note, the results obtained by the *M. pneumoniae* RT-MCDA assay (with 5 μl of template) (Figures 9C, E) were identical to that obtained by the *M. pneumoniae* MCDA-LFB assay (Figure 9F). In terms of the results obtained using the real-time PCR method, 26 positive specimens were previously determined positive and 22 specimens were negative. The complete accordance between the *M.*

10.3389/fcimb.2024.1423155

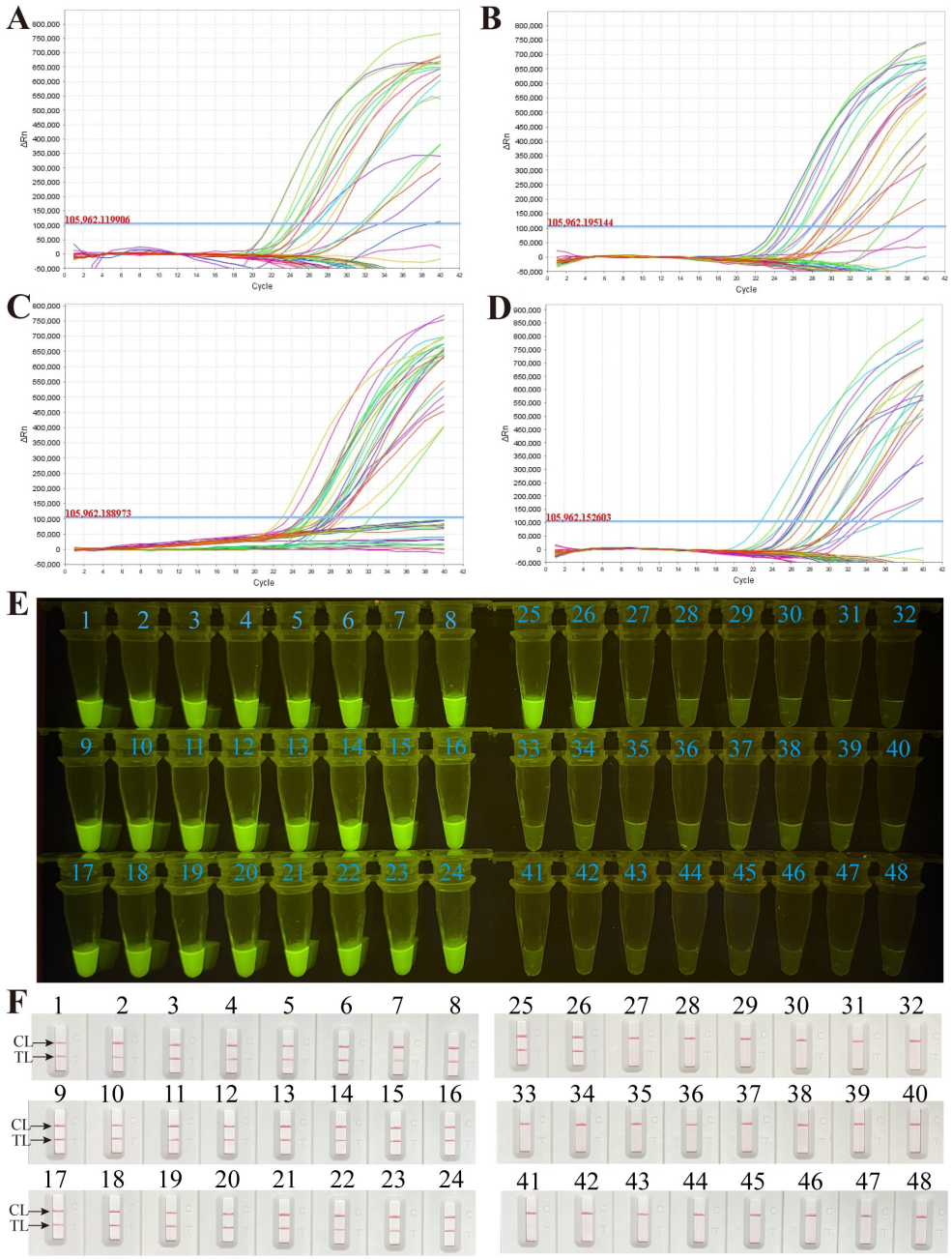

FIGURE 9
Application of the *M. pneumoniae* RT- MCDA assay in clinical specimens. DNA templates from 48 sputum samples were detected by the *M. pneumoniae* RT-MCDA assay. The produced fluorescent signals were documented by the real-time PCR system with 1 μl of template **(A)**, 3 μl of template **(B)**, 5 μl of template **(C)**, and 7 μl of template **(D)**, and visually interpreted with the naked eye under blue light **(E)**. The results were also confirmed by *M. pneumoniae*-MCDA-LFB **(F)**. Signals/tubes/strips 1–26 represent the results of the templates from the positive samples, and tubes/strips 27–48 represent the results of the *M. pneumoniae* negative samples. TL, test line; CL, control line.

pneumoniae RT-MCDA assay and real-time PCR method implied the feasibility of the *M. pneumoniae* RT-MCDA assay in clinical practice.

Discussion

In recent years, the global surge in macrolide resistance among *M. pneumoniae* strains has been particularly pronounced in China, where resistance levels have approached nearly 90%. This alarming trend has led to an increase in cases of severe pneumonia among patients who do not receive timely and effective treatment, posing a serious threat to public health (Kumar and Kumar, 2023; Chen et al., 2024). Furthermore, *M. pneumoniae* infections are characterised by non-specific clinical and imaging features, along with limited microbial diagnostic options, complicating the clinical diagnosis and increasing the likelihood of missing optimal treatment windows. This often exacerbates the patient's

disease burden (Kumar and Kumar, 2023). Consequently, there is a critical need for rapid and precise detection methods to identify and diagnose *M. pneumoniae* infections early and effectively.

Numerous isothermal amplification techniques have been developed for diagnosing pathogen infections, including nucleic acid sequence-based amplification, self-sustained sequence replication, strand displacement amplification, exponential amplification reaction, helicase-dependent amplification, recombinase polymerase amplification, single primer isothermal amplification, rolling circle amplification, loop-mediated isothermal amplification (LAMP), and cross priming amplification (Wang et al., 2016). However, these methods face technical challenges and do not entirely fulfill the point-of-care detection standards set by the World Health Organization (Srivastava and Prasad, 2023). MCDA is a relatively recent advancement in this area and addresses many limitations of earlier techniques (Wang et al., 2015). MCDA has gained broad application in fields such as basic research, medical diagnostics, and food safety (Qi et al., 2018; Boonbanjong et al., 2022; Li et al., 2022). Here, we introduce a novel real-time fluorescence MCDA method for *M. pneumoniae* that integrates real-time PCR technology with MCDA for efficient clinical detection. This approach uses a set of 10 sequence-specific primers that target 10 distinct regions (F1, F2, C1, C2, P1, P2, R1, R2, D1, and D2), ensuring high specificity (Wang et al., 2015, 2016). Critically, our technique employs the 5′ endonuclease recognition sites and fluorophore labelling to achieve precise cleavage of double-stranded DNA by the restriction enzyme *Nb.BsrDI*, releasing a fluorescence signal. Thus, the new real-time fluorescence MCDA method enables rapid multiplex detection and identification in a single isothermal step without the need for thermal cycling or subsequent analysis (Wang et al., 2015, 2016; Srivastava and Prasad, 2023). Additionally, the early high expression of the *CARDS* toxin gene during infection and the critical role of CARDS toxin in the pathogenesis of *M. pneumoniae* facilitate the *CARDS* toxin gene as a preferable biomarker for early and accurate *M. pneumoniae* detection (Chaudhry et al., 2016; Su et al., 2021). It was reported that detection assays targeting the *CARDS* toxin gene exhibited superior sensitivity compared with those targeting other genes such as the ATPase (Mp3 and Mp7) gene (Winchell et al., 2008). Thus, the real-time MCDA targeting the *CARDS* toxin gene in this study offers a more timely and efficient diagnosis, increasing early detection capabilities. In addition, a real-time PCR method targeting the P1 gene was used for clinical feasibility comparison.

In this study, we employed the restriction enzyme *Nb.BsrDI* and a modified primer, C1*, to detect MCDA reaction products through fluorescence. Additionally, another modified primer, D1$^{\#}$, and biotin-14-dCTP were used in a local feedback mechanism to monitor these products. We evaluated the sensitivity and specificity of these two methods through detailed analytical comparisons, finding both to be equally effective in detecting *M. pneumoniae*. Furthermore, the optimised real-time fluorescence MCDA detection process we developed can complete the identification of *M. pneumoniae* within 1 h, allowing for prompt treatment and control of the infection. Given its efficiency and reliability, the real-time MCDA detection method introduced in this study is highly recommended for the early diagnosis and management of *M. pneumoniae* infections.

The newly developed RT-MCDA assay demonstrated high sensitivity in detecting *M. pneumoniae*, with a LoD of 43 fg (approximately 47 copies) genomic DNA per reaction. This sensitivity is comparable with that achieved by real-time PCR (approximately 10 copies) (Morozumi et al., 2006) and slightly higher than that achieved by LAMP assays (50–600 fg) (Saito et al., 2005; Zhao et al., 2013; Wang et al., 2019; Xiao et al., 2022). A comparison of different methods for *M. pneumoniae* infection diagnosis is summarised in Table 3 (Daxboeck et al., 2003; Templeton et al., 2003; Saito et al., 2005; Morozumi et al., 2006; Loens et al., 2010; Zhao et al., 2013; Wang et al., 2019; Xiao et al., 2022). Table 3 conclusively shows that the RT-MCDA assay had superior sensitivity and timeliness but a relatively higher cost in *M. pneumoniae* detection; the LAMP-based assay displayed moderate sensitivity and timeliness as well as a relatively high cost; the real-time PCR method exhibited superior sensitivity and moderate timeliness and cost; the serological test displayed poor sensitivity but was superior in timeliness and cost; and the culture method showed poor sensitivity and timeliness but was the least costly. As a conclusion, the RT-MCDA assay was a superior option for *M. pneumoniae* detection with a further optimisation of sensitivity and cost. Moreover, the RT-MCDA assay exhibited no cross-reactivity with non-*M. pneumoniae* pathogens, achieving a specificity of 100%. To assess the clinical applicability of this method, we analysed 48 suspect samples, confirming *M. pneumoniae* in 26 cases (54.17%)—a rate consistent with that of real-time PCR. Although there were no significant statistical differences between the RT-MCDA method and conventional real-time PCR, further validation with a larger sample set is warranted. Additionally, the outcomes of the *M. pneumoniae* RT-MCDA assay are not only trackable through a real-time fluorescence monitoring system but can also be visually confirmed under blue light, significantly reducing the contamination risks typically associated with opening the reaction container. Given its robust performance and operational flexibility, this novel method holds promise for its widespread use in clinical diagnostics, field testing, and resource-constrained environments.

In summary, this study successfully developed a real-time MCDA detection method for *M. pneumoniae* that offers timely, simple, and reliable testing. This novel assay represents a promising

TABLE 3 Sensitivity, time, and cost comparison of different methods for *M. pneumoniae* detection.

Methods	LoD	Time (min)	Cost (RMB)
RT-MCDA assay	43 fg (~47 copies)/reaction	~40 min	~60
LAMP-based assay	50~600 fg (55~660 copies)/reaction	40~60 min	~60
Real-time PCR	~10 copies/reaction	~90 min	~50
Serological test	17 U/ml	~15 min	~30
Culture	10^5 cfu/ml	2~6 week	~20

tool for the rapid, sensitive, and specific identification of *M. pneumoniae* infections and stands as a viable option for increasing diagnostic capabilities.

Data availability statement

The original contributions presented in the study are included in the article/supplementary material. Further inquiries can be directed to the corresponding authors.

Ethics statement

The studies involving human participants were reviewed and approved by the ethic committee of Capital Institute of Pediatrics (Ethical approval number: SHERLLM2021010). The patients/participants [legal guardian/next of kin] provided written informed consent to participate in the study.

Author contributions

FX: Writing – original draft, Conceptualization, Data curation, Formal Analysis, Investigation, Methodology, Validation, Writing – review & editing. YZ: Data curation, Formal Analysis, Writing – original draft. WX: Conceptualization, Writing – original draft. JF: Project administration, Writing – review & editing. XH: Project administration, Writing – review & editing. NJ: Formal Analysis, Writing – review & editing. CS: Software, Writing – review & editing. ZX: Data curation, Writing – original draft. BZ: Conceptualization, Resources, Writing – review & editing. JZ: Formal Analysis, Supervision, Writing – review & editing. YW: Data curation, Formal Analysis, Funding acquisition, Methodology, Project administration, Resources, Software, Writing – review & editing. LM: Project administration, Resources, Supervision, Validation, Writing – review & editing.

Funding

The author(s) declare that financial support was received for the research, authorship, and/or publication of this article. This study was funded by Beijing Nova Program (Grant No. Z211100002121042), National Natural Science Foundation of China (82200115), National Key Research and Development Program of China (Grant No. 2021YFC2301101 and 2021YFC2301102), Special Innovation and Promotion Project of Beijing Medical Administration (Grant No. XTCX201820) and the Research Foundation of Capital Institute of Pediatrics (Grant No. PX2021050).

Conflict of interest

The authors declare that the research was conducted in the absence of any commercial or financial relationships that could be construed as a potential conflict of interest.

Publisher's note

References

Boonbanjong, P., Treerattrakoon, K., Waiwinya, W., Pitikultham, P., and Japrung, D. (2022). Isothermal amplification technology for disease diagnosis. *Biosensors (Basel)* 12 (9):677. doi: 10.3390/bios12090677

Chang, H. Y., Chang, L. Y., Shao, P. L., Lee, P. I., Chen, J. M., Lee, C. Y., et al. (2014). Comparison of real-time polymerase chain reaction and serological tests for the confirmation of Mycoplasma pneumoniae infection in children with clinical diagnosis of atypical pneumonia. *J. Microbiol. Immunol. Infect.* 47, 137–144. doi: 10.1016/j.jmii.2013.03.015

Chaudhry, R., Ghosh, A., and Chandolia, A. (2016). Pathogenesis of Mycoplasma pneumoniae: An update. *Indian J. Med. Microbiol.* 34, 7–16. doi: 10.4103/0255-0857.174112

Chen, Y., Zhang, Y., Tang, Q. N., and Shi, H. B. (2024). Efficacy of doxycycline therapy for macrolide-resistant Mycoplasma pneumoniae pneumonia in children at different periods. *Ital. J. Pediatr.* 50, 38. doi: 10.1186/s13052-024-01615-y

Daxboeck, F., Krause, R., and Wenisch, C. (2003). Laboratory diagnosis of Mycoplasma pneumoniae infection. *Clin. Microbiol. Infect.* 9, 263–273. doi: 10.1046/j.1469-0691.2003.00590.x

Hammerschlag, M. R. (2001). Mycoplasma pneumoniae infections. *Curr. Opin. Infect. Dis.* 14, 181–186. doi: 10.1097/00001432-200104000-00012

Jia, N., Wang, C., Liu, X., Huang, X., Xiao, F., Fu, J., et al. (2023). A CRISPR-Cas12a-based platform for ultrasensitive rapid highly specific detection of Mycobacterium tuberculosis in clinical application. *Front. Cell Infect. Microbiol.* 13. doi: 10.3389/fcimb.2023.1192134

Jiang, L., Gu, R., Li, X., Song, M., Huang, X., and Mu, D. (2022). Multiple Cross Displacement Amplification Coupled with Lateral Flow Biosensor (MCDA-LFB) for rapid detection of Legionella pneumophila. *BMC Microbiol.* 22, 20. doi: 10.1186/s12866-021-02363-3

Kumar, S., and Kumar, S. (2023). Mycoplasma pneumoniae: Among the smallest bacterial pathogens with great clinical significance in children. *Indian J. Med. Microbiol.* 46, 100480. doi: 10.1016/j.ijmmb.2023.100480

Lee, K. Y. (2008). Pediatric respiratory infections by Mycoplasma pneumoniae. *Expert Rev. Anti Infect. Ther.* 6, 509–521. doi: 10.1586/14787210.6.4.509

Li, S., Liu, C., Liu, Y., Ma, Q., Wang, Y., and Wang, Y. (2020). Establishment and application of a multiple cross displacement amplification combined with nanoparticles-based biosensor method for the detection of Bordetella pertussis. *BMC Microbiol.* 20, 263. doi: 10.1186/s12866-020-01945-x

Li, X., Zhang, X., Shi, X., Shi, H., Wang, Z., and Peng, C. (2022). Review in isothermal amplification technology in food microbiological detection. *Food Sci. Biotechnol.* 31, 1501–1511. doi: 10.1007/s10068-022-01160-6

Liu, X., Zhang, Q., Chen, H., Hao, Y., Zhang, J., Zha, S., et al. (2024). Comparison of the clinical characteristics in parents and their children in a series of family clustered Mycoplasma pneumoniae infections. *BMC Pulm. Med.* 24, 107. doi: 10.1186/s12890-024-02922-0

Loens, K., Goossens, H., and Ieven, M. (2010). Acute respiratory infection due to Mycoplasma pneumoniae: current status of diagnostic methods. *Eur. J. Clin. Microbiol. Infect. Dis.* 29, 1055–1069. doi: 10.1007/s10096-010-0975-2

Morozumi, M., Ito, A., Murayama, S. Y., Hasegawa, K., Kobayashi, R., Iwata, S., et al. (2006). Assessment of real-time PCR for diagnosis of Mycoplasma pneumoniae pneumonia in pediatric patients. *Can. J. Microbiol.* 52, 125–129. doi: 10.1139/w05-118

Park, J. W. (2022). Principles and applications of loop-mediated isothermal amplification to point-of-care tests. *Biosensors (Basel)* 12 (10), 857. doi: 10.3390/bios12100857

Qi, H., Yue, S., Bi, S., Ding, C., and Song, W. (2018). Isothermal exponential amplification techniques: From basic principles to applications in electrochemical biosensors. *Biosens. Bioelectron.* 110, 207–217. doi: 10.1016/j.bios.2018.03.065

Saito, R., Misawa, Y., Moriya, K., Koike, K., Ubukata, K., and Okamura, N. (2005). Development and evaluation of a loop-mediated isothermal amplification assay for rapid detection of Mycoplasma pneumoniae. *J. Med. Microbiol.* 54, 1037–1041. doi: 10.1099/jmm.0.46071-0

Srivastava, P., and Prasad, D. (2023). Isothermal nucleic acid amplification and its uses in modern diagnostic technologies. *3 Biotech.* 13, 200. doi: 10.1007/s13205-023-03628-6

Su, X., You, X., Luo, H., Liang, K., Chen, L., Tian, W., et al. (2021). Community-acquired respiratory distress syndrome toxin: unique exotoxin for M. pneumoniae. *Front. Microbiol.* 12. doi: 10.3389/fmicb.2021.766591

Templeton, K. E., Scheltinga, S. A., Graffelman, A. W., Van Schie, J. M., Crielaard, J. W., Sillekens, P., et al. (2003). Comparison and evaluation of real-time PCR, real-time nucleic acid sequence-based amplification, conventional PCR, and serology for diagnosis of Mycoplasma pneumoniae. *J. Clin. Microbiol.* 41, 4366–4371. doi: 10.1128/JCM.41.9.4366-4371.2003

Wang, Y., Wang, Y., Jiao, W., Li, J., Quan, S., Sun, L., et al. (2019). Development of loop-mediated isothermal amplification coupled with nanoparticle-based lateral flow biosensor assay for Mycoplasma pneumoniae detection. *AMB Express* 9, 196. doi: 10.1186/s13568-019-0921-3

Wang, Y., Wang, Y., Ma, A. J., Li, D. X., Luo, L. J., Liu, D. X., et al. (2015). Rapid and sensitive isothermal detection of nucleic-acid sequence by multiple cross displacement amplification. *Sci. Rep.* 5, 11902. doi: 10.1038/srep11902

Wang, Y., Wang, Y., Zhang, L., Liu, D., Luo, L., Li, H., et al. (2016). Multiplex, rapid, and sensitive isothermal detection of nucleic-acid sequence by endonuclease restriction-mediated real-time multiple cross displacement amplification. *Front. Microbiol.* 7. doi: 10.3389/fmicb.2016.00753

Winchell, J. M., Thurman, K. A., Mitchell, S. L., Thacker, W. L., and Fields, B. S. (2008). Evaluation of three real-time PCR assays for detection of Mycoplasma pneumoniae in an outbreak investigation. *J. Clin. Microbiol.* 46, 3116–3118. doi: 10.1128/JCM.00440-08

Xiao, F., Zhou, J., Sun, C., Huang, X., Zheng, B., Fu, J., et al. (2022). Loop-mediated isothermal amplification coupled with nanoparticle-based biosensor: A rapid and sensitive method to detect mycoplasma pneumoniae. *Front. Cell Infect. Microbiol.* 12. doi: 10.3389/fcimb.2022.882855

Zhao, F., Liu, Z., Gu, Y., Yang, Y., Xiao, D., Tao, X., et al. (2013). Detection of Mycoplasma pneumoniae by colorimetric loop-mediated isothermal amplification. *Acta Microbiol. Immunol. Hung* 60, 1–9. doi: 10.1556/AMicr.60.2013.1.1

Zhao, F., Niu, L., Yan, L., Nong, J., Wang, C., Wang, J., et al. (2019). Establishment and application of multiple cross displacement amplification coupled with lateral flow biosensor (MCDA-LFB) for visual and rapid detection of candida albicans in clinical samples. *Front. Cell Infect. Microbiol.* 9. doi: 10.3389/fcimb.2019.00102

Zhao, Y., Chen, F., Li, Q., Wang, L., and Fan, C. (2015). Isothermal amplification of nucleic acids. *Chem. Rev.* 115, 12491–12545. doi: 10.1021/acs.chemrev.5b00428

Zhou, J., Xiao, F., Fu, J., Jia, N., Huang, X., Sun, C., et al. (2023). Rapid detection of monkeypox virus by multiple cross displacement amplification combined with nanoparticle-based biosensor platform. *J. Med. Virol.* 95, e28479. doi: 10.1002/jmv.28479

frontiers | Frontiers in Cellular and Infection Microbiology

TYPE Original Research
PUBLISHED 20 August 2024
DOI 10.3389/fcimb.2024.1455259

OPEN ACCESS

EDITED BY
Andrea Marino,
University of Catania, Italy

REVIEWED BY
E. Diane Williamson,
Defence Science and Technology Laboratory, United Kingdom
Matthew L. Nilles,
University of North Dakota, United States

*CORRESPONDENCE
Wonjun Yang
wonjun@kribb.re.kr
Nam-Kyung Lee
nklee@kribb.re.kr
Jangwook Lee
jlee@kribb.re.kr

†These authors have contributed equally to this work

RECEIVED 26 June 2024
ACCEPTED 01 August 2024
PUBLISHED 20 August 2024

CITATION
Jang J, Kwon DH, Jang J-H, Lee D-G, Chang S-H, Jeon M-Y, Jeong Y-S, Song D-H, Min J-K, Park J-G, Lee M-S, Han B-S, Yang W, Lee N-K and Lee J (2024) Development of a novel sandwich immunoassay based on targeting recombinant Francisella outer membrane protein A for the diagnosis of tularemia. *Front. Cell. Infect. Microbiol.* 14:1455259. doi: 10.3389/fcimb.2024.1455259

Development of a novel sandwich immunoassay based on targeting recombinant Francisella outer membrane protein A for the diagnosis of tularemia

Jieun Jang[1,2†], Do Hyung Kwon[1,2†], Ju-Hong Jang[1], Dong-Gwang Lee[1], Seo-Hyuk Chang[1], Min-Young Jeon[1], Young-Su Jeong[3], Dong-Hyun Song[3], Jeong-Ki Min[1], Jong-Gil Park[1,2], Moo-Seung Lee[4], Baek-Soo Han[5], Wonjun Yang[1*], Nam-Kyung Lee[1*] and Jangwook Lee[1,2*]

[1]Biotherapeutics Translational Research Center, Korea Research Institute of Bioscience and Biotechnology, Daejeon, Republic of Korea, [2]Department of Biomolecular Science, Korea Research Institute of Bioscience and Biotechnology, School of Bioscience, Korea University of Science and Technology, Daejeon, Republic of Korea, [3]Chem-Bio Technology Center, Agency for Defense Development, Daejeon, Republic of Korea, [4]Environmental Diseases Research Center, Korea Research Institute of Bioscience and Biotechnology, Daejeon, Republic of Korea, [5]Biodefense Research Center, Korea Research Institute of Bioscience and Biotechnology, Daejeon, Republic of Korea

Introduction: Tularemia, caused by the bacterium *Francisella tularensis*, poses health risks to humans and can spread through a variety of routes. It has also been classified as a Tier 1 Select agent by the CDC, highlighting its potential as a bioterrorism agent. Moreover, it is difficult to diagnose in a timely fashion, owing to the non-specific nature of tularemia infections. Rapid, sensitive, and accurate detection methods are required to reduce mortality rates. We aimed to develop antibodies directed against the outer membrane protein A of *F. tularensis* (FopA) for rapid and accurate diagnosis of tularemia.

Methods: We used a baculovirus insect cell expression vector system to produce the FopA antigen and generate anti-FopA antibodies through immunization of BALB/c mice. We then employed hybridoma and phage display technologies to screen for antibodies that could recognize unique epitopes on FopA.

Result: Two monoclonal antibodies, 6B12 and 3C1, identified through phage display screening specifically bound to recombinant FopA in a dose-dependent manner. The binding affinity of the anti-FopA 6B12 and 3C1 antibodies was observed to have an equilibrium dissociation constant of 1.76 × 10-10 M and 1.32 × 10-9 M, respectively. These antibodies were used to develop a sandwich ELISA system for the diagnosis of tularemia. This assay was found to be highly specific and sensitive, with detection limits ranging from 0.062 ng/mL in PBS to 0.064 ng/mL in skim milk matrices.

Discussion: Our findings demonstrate the feasibility of a novel diagnostic approach for detecting *F. tularensis* based on targeting FopA, as opposed to existing tests that target the bacterial lipopolysaccharide.

KEYWORDS

tularemia, *Francisella tularensis*, FopA, tier 1 select agent, sandwich immunoassay

1 Introduction

Tularemia is a disease that affects humans and animals and is caused by the bacterium *Francisella tularensis* (*F. tularensis*) (Çelebi et al., 2006). Infection can occur through direct contact with infected animals or their tissues, bites from infected ticks or flies, or exposure to contaminated water or soil (Hickey et al., 2011; Sharma et al., 2023). According to the U.S. Centers for Disease Control and Prevention (CDC), approximately 200 cases of human infections are reported annually in the United States, with a consistently increasing trend having occurred (Bishop et al., 2023). The disease is widespread in the Northern Hemisphere and is found in a few countries in the Southern Hemisphere. Although it is generally considered to be a rare disease, it is frequently found in Northern and Central Europe and in countries of the former Soviet Union, which have reported the highest number of human cases (Hestvik et al., 2015; Lindgren et al., 2024). The disease exhibits significant annual and seasonal variation, with most outbreaks being local and sporadic but mostly occurring during late summer and autumn (Maurin and Gyuranecz, 2016). Research on tularemia has gained increased attention over the past two decades because of the classification of *F. tularensis* as a Tier 1 Select agent by the CDC, which highlights its high morbidity and mortality, ease of aerosolization, and low infectious dose (Genchi et al., 2015; Nelson and Sjöstedt, 2024). *F. tularensis* poses a significant threat as a Category A potential agent of bioterrorism, along with *Bacillus anthracis*, *Yersinia pestis*, smallpox virus, and botulinum neurotoxin (Altman and Wachs, 2002; Lamps et al., 2004).

The clinical manifestations of tularemia often make clinical diagnosis challenging owing to its non-specific nature, which frequently mimics that of influenza or other respiratory infections (Lamps et al., 2004). In some cases, patients develop systemic illnesses. Inhalation of infectious aerosols can lead to severe pneumonia, with mortality rates as high as 60% (Boisset et al., 2014; Zellner and Huntley, 2019). The lack of available vaccines and the limited effectiveness of a small group of antibiotics in treating tularemia further underscore the importance of administering appropriate treatment in the early stages of the disease (Maurin et al., 2024). Although efficient antibiotic therapy is available, delayed diagnosis can result in increased mortality rates. Therefore, rapid, sensitive, and accurate detection methods are required (Lamps et al., 2004).

Various diagnostic methods for *F. tularensis* infection in humans and animals, including serological and molecular biological procedures, are available (Yang and Rothman, 2004; Walker, 2014). Although bacterial culture-based diagnosis is considered the gold standard, it is time-consuming, laborious, and poses a risk of infection to operators (Wiesinger-Mayr et al., 2007; Yao et al., 2022). Molecular biological methods, such as real-time polymerase chain reaction (RT-PCR), are safe, reliable, highly sensitive, and specific, but are conversely time-consuming, difficult to operate, and require precise equipment (Kim et al., 2015; Liu et al., 2019). Another method for detecting *F. tularensis* infections involves immunological techniques, which employ antibodies to detect specific antigens, thereby revealing the presence of bacteria (Maurin, 2020; Hannah et al., 2021). To date, various diagnostic kits have been commercialized for sensitive and specific detection of *F. tularensis* using molecular biological and immunological techniques (Table 1). Despite the availability of these kits, information on their target antigens and detection ranges is lacking. Lipopolysaccharide (LPS) is the predominant outer membrane component of Gram-negative bacteria. Employing LPS as a diagnostic antigen is insufficient for differentiating between infections caused by cross-reactive species, such as *Brucella*, *Yersinia enterocolitica*, *Vibrio cholerae*, and *Escherichia coli*, which often leads to false positives (Pelletier et al., 2009; Yanes et al., 2018). Owing to the predominance of LPS in the outer membrane of bacteria, which is targeted by most commercial *F. tularensis* detection kits, cross-reactivity with undesired bacteria is possible (Yanes et al., 2018). Many studies have reported that bacterial outer membrane proteins (Omp) have strong immunogenicity and can be substituted for LPS (Ahmed et al., 2015; Nagaratnam et al., 2022). Furthermore, Omp antigens can significantly reduce false-positive results caused by cross-reactive bacteria (Yao et al., 2022). Therefore, it is important to develop new detection methods that can specifically and sensitively identify *F. tularensis* antigens rather than relying on LPS targeting.

This study aimed to develop antibodies that can bind to the outer membrane protein A of *F. tularensis* (FopA) for diagnostic purposes. FopA is a protein consisting of 393 amino acids with less

TABLE 1 Commercial *Francisella tularensis* detection kit.

Product	Method	Company	Target	Characteristics	Reference
VIRAPID® TULAREMIA	LFA[a]	Vircell	LPS[b]	99.1% sensitivity and 98.6% specificity	(Kılıç et al., 2012; Chaignat et al., 2014)
BADD Tularemia Biowarfare Detection Test Kit	LFA[a]	ADVNT biotechnologies	Not reported	1.48 x 10^6 cfu/mL of LoD[c]	https://advnt.org
Raid™ 8	LFA[a]	Alexeter Technologies	Not reported	1.6 x 10^6 cfu/mL of LoD[c]	https://www.alexeter.com
Tularemia BioThreat Alert® Kit	LFA[a]	Tetracore	Not reported	1.0 x 10^7~ 1 x10^8 cfu/mL of LoD[c]	(Pillai et al., 2020)
SERION ELISA classic Francisella tularensis	ELISA	SERION diagnostics	LPS[b]	86.3% sensitivity and 95.5% specificity	(Yanes et al., 2018)
Tularemia test kit Biotoxis	RT-PCR	Bertin	Not reported	90.32~96.55% sensitivity, 1,000 cfu/L LoD/49 copies	(Hennebique et al., 2020)
Francisella tularensis RT-PCR Kit	RT-PCR	BioPerfectus	Not reported	5 copies/reaction of LoD[c]	https://www.bioperfectus.com

[a]Lateral Flow Assay.
[b]Lipopolysaccharide.
[c]Limit of Detection.

than 40% sequence identity to known bacterial outer membrane proteins, and is highly immunogenic (Nagaratnam et al., 2022). Several studies have shown that FopA functions as a protective antigen against tularemia. In this study, we utilized recombinant FopA antigen produced by an insect cell-based expression system to immunize mice and identified high-affinity and sensitive antibodies that bind to FopA through two distinct screening methods. We then assessed the limit of detection of a sandwich immunoassay established using two selected antibodies for detecting FopA in various buffer matrices. Our findings demonstrate the feasibility of a novel diagnostic approach for detecting *F. tularensis*.

2 Materials and methods

2.1 Cell lines

Expi293F™ cells were grown in suspension culture with expression medium (Gibco, A14351-02) at 37°C in a 70% humid, 5% CO_2 incubator. For hybridoma fusion, Sp2/0-Ag14 (ATCC) cells were grown in Medium A (STEMCELL Technologies) and DMEM supplemented with 10% Fetal Bovine Serum (R&D systems), 1% Antibiotic-Antimycotic (Gibco) at 37°C in a 5% CO_2 incubator.

2.2 Generation of FopA-encoding bacmid

The *fopA* gene (FTT0583) was synthesized by Gene-art (Thermo Fisher Scientific). The pFastBac-FopA donor plasmid was constructed using the pFastBac™ vector in the Bac-to-Bac™ Vector Kit (Gibco). DH10Bac Competent Cells (Gibco, 10361012) were transformed to generate bacmid containing FopA gene following the manufacturer's instructions. The bacmid was analyzed with pUC/M13 primers by PCR as previously described (Jang et al., 2022) to verify the FopA encoding sequence.

2.3 Preparation of FopA-encoding baculovirus

ExpiSf9™ cells were transfected with a recombinant bacmid encoding the *fopA* gene for 120 hours. Following this, the recombinant baculovirus was collected through centrifugation and the isolation of supernatants. A 24-well plate containing ExpiSf9™ cells at 1.25 × 10^6 cells/well in ExpiSf9™ CD medium was used to determine the baculovirus titer. The baculovirus was serially diluted in ExpiSf™ CD medium (1:1,000 to 1:100,000), and incubated for 14 – 16 hours at 28°C. The cells in each well were then transferred to a flow cytometry tube, and stained with an APC conjugated anti-Baculovirus envelope gp64 antibody (Thermo Fisher Scientific, 17-6991-80) for 30 minutes at room temperature. The samples were then washed, centrifuged, and analyzed using the NovoSampler Pro flow cytometer (Agilent). Data was then analyzed using NovoExpress software (Agilent), and the viral titer was calculated using the equation described below by selecting the dilution sample that yields a percent of gp64-positive cells of < 10%.

$$\text{Viral Titer}\left(\frac{\text{ivp}}{\text{mL}}\right) = \left(\frac{\text{Cell number} \times \text{Percent gp64 positive cells}}{\text{Dilution of virus stock}}\right) \times 0.01$$

2.4 Recombinant FopA production

Protein expression was performed with ExpiSf9™ cells at a density of 5 × 10^6 cells/mL and ≥ 90% viability. Following seeding,

ExpiSf™ Enhancer (Gibco) was added to the cells. 18-24 hours later, the cells were infected with a recombinant baculovirus stock having a MOI of 5. After 120 hours post of infection, the supernatants were harvested through centrifugation at 4,000 rpm for 30 minutes and then filtered using a 0.22-μm bottle top vaccum filter. Recombinant FopA from the filtered supernatants was purified using a cOmplete™ His-Tag Purification Column (Roche) equipped with NGC QUEST 100 Chromatography Systems (Bio-Rad). Recombinant FopA was eluted with 80mM imidazole PBS buffer and then dialyzed in PBS (pH 7.4)

2.5 Hybridoma generation and antibody selection

5-week-old female BALB/c were immunized with recombinant FopA antigen produced using baculovirus, and hybridomas were generated as previously described (Jang et al., 2022). The hybridomas were screened to identify mAbs against recombinant FopA by ELISA. The cDNA of hybridoma cells was synthesized using a random hexamer primer and the gene identification of the antibody VH or VL chain with PCR method, forward and reverse primer sets were designed and employed as previously described (Babrak et al., 2017). The Animal Research Ethics Committee of the Korea Research Institute of Bioscience and Biotechnology reviewed and authorized the use of animals and experimental protocols (IACUC approval no. KRIBB-AEC-21119).

2.6 Construction of a single chain variable fragment library

The construction of the single chain variable fragment library was carried out in three stages of PCR as previously described (Lee et al., 2018) with some modifications. Initially, the variable heavy (VH) and variable light (VL) chain sequences of the cDNA were amplified during the first PCR. In the second PCR, the flanking region containing the partial glycine and serine (G4S) linker and the SfiI enzyme site was bound to the amplified VH and VL sequences. A third PCR was performed to assemble the VH and VL thereby generating single-chain variable fragment (scFv). Each PCR product was analyzed on a 2.0% TAE agarose gel using electrophoresis. The purified gels were cleansed using the NucleoSpin® Gel and PCR Clean-up kit (MACHEREY–NAGEL). The third PCR product and phagemid vector (pComb3XSS) were then digested by SfiI (NEB) at 50°C for 16 hours. The digested phagemid vector was analyzed using 0.7% agarose gel electrophoresis, and the digested vector and PCR products were purified. These products were then ligated with T4 DNA ligase (NEB) at 16°C overnight and inactivated at 65°C for 10 minutes. The ligates were then desalted using the Microcon-10kDa Centrifugal Filter Unit with Ultracel-10 membrane (Millipore). They were centrifuged at 14,000 × g for 20 minutes at room temperature, and this process was repeated two more times. The desalted and concentrated ligates were collected in a new tube by centrifuging at 3,000 × g for 3 minutes and electro-transformed into *E. coli* TG1 competent cells (Lucigen), as described previously (Lee et al., 2018). Constructed sub-libraries were titrated, mixed together, and used for phage display panning.

2.7 Antibody selection using phage display technology

The selection of scFv antibodies to the FopA antigen was achieved through phage display technology, as previously described (Jeon et al., 2023). Briefly, anti-FopA scFv antibodies were selected through two sets of phage display panning using immunotubes (Thermo Fisher Scientific, 444202) or Dynabeads™ M-270 Epoxy (Thermo Fisher Scientific, 14301) coated with recombinant FopA. Three rounds of bio-panning were performed, and individual scFvs binding to FopA in the third round output were screened by ELISA. To produce immunoglobulin G (IgG) antibodies, the DNA sequence of the selected scFv clones was used to clone each variable heavy and light chain genes into the pcDNA3.4-based expression vector. The anti-FopA IgG antibody was produced and purified following previously described methods (Jeon et al., 2023).

2.8 Indirect ELISA

Recombinant FopA protein (100 ng/well) was immobilized on a 96-well Maxisorp plate (Thermo Fisher Scientific, 439454) at 4 °C overnight. Following this, the plates were washed with PBS-T (PBS with 0.05% Tween20) and blocked with 3% (w/v) bovine serum albumin (BSA)/PBS for 1 hour 30 minutes at room temperature. For binding analysis of purified antibodies that were serially diluted in PBS, the diluted solution was added to each well, followed by incubation for 1 hour at room temperature. For hybridoma screening, supernatants of hybridoma culture media served as the primary antibody. After washing with PBS-T, a Goat anti-Human IgG F(ab')2 - HRP (Invitrogen, 31414) was added, and incubated for 1 hour at room temperature. For supernatants of hybridoma ELISA, goat anti-Mouse IgG (Fab specific)–Peroxidase antibody (Sigma Aldrich, A9917) was used as a secondary antibody. Following another round of washing with PBS-T, tetramethylbenzidine (TMB) substrate reagent (BD Biosciences, 555214) was added to each well, and the plate was incubated. The reaction was then terminated using a stop solution, and absorbance was measured at 450 nm using a SpectraMAX ABS Plus plate reader (Molecular Devices). Supernatants collected by periplasm extraction were utilized as an alternative to the primary antibody in the ELISA assay for periplasm extraction. In this case, Anti-HA-Peroxidase (Roche, 12013819001) was employed as a secondary antibody. Curve-fitting analysis for ELISA data was performed using Prism 9 software (GraphPad Software, USA).

2.9 Affinity measurement using BLI

An amine-reactive second-generation (AR2G) biosensor (Sartorius) was employed to immobilize recombinant FopA, as

described in prior research (Jang et al., 2022). The biosensors were treated with 1 M ethanolamine-HCl (pH 8.5) for 300 seconds to quench them, and a baseline was established using PBS for 120 seconds. The Octet K2 system (Sartorius) was used for kinetic analysis by measuring the association (K_{on}) and dissociation (K_{off}) of anti-FopA antibodies for 600 seconds. The equilibrium dissociation constant (KD) of each antibody was calculated using data analysis software (HT 12.0; Sartorius) based on K_{on} and K_{off}.

2.10 Competitive ELISA

A 96-well plate coated with recombinant FopA was prepared and blocked according to the procedures outlined in the indirect ELISA method section. Subsequently, biotinylated mAbs were added to each well at a concentration of 20 nM using the EZ-Link™ Sulfo-NHS-LC-biotinylation kit (Thermo Fisher Scientific). Non-biotinylated mAbs were serially diluted from 100 nM and added to the wells along with the biotinylated mAbs. The mixture was incubated for 1 hour at room temperature, and then the wells were washed with PBST. HRP-conjugated streptavidin (Sigma Aldrich) was added to the wells and incubated for 30 minutes at room temperature. The wells were washed again, and then TMB was added and reacted as described above.

2.11 Sandwich ELISA

The validation of 3C1 and 6B12 mAbs was carried out using a capture mAb (50 nM) that was coated on a 96-well plate and left overnight at 4°C. Following this, the plate was blocked with 3% BSA/PBS for an hour, after which serial dilutions of recombinant FopA in 3% BSA/PBS were added to each well, and the plate was incubated for an hour at room temperature. After washing the plate, 20 nM biotinylated detector mAb was added to each well and incubated for an hour at room temperature. The plate was then washed with PBST and incubated with HRP-conjugated streptavidin (Sigma Aldrich) for 30 minutes at room temperature. This process was duplicated to assess the impact of the evaluation matrix, using bovine serum albumin (Sigma Aldrich), skimmed milk powder (Gibco), human serum (Sigma Aldrich), mouse urine, and soil water to dilute recombinant FopA at different concentrations in various matrices directly. These matrices were then transferred to 96-well plates coated with capture mAb. The detection of FopA in the other matrices was carried out as previously described.

2.12 Evaluation of limit of detection

The definition of LoD is the lowest concentration of FopA antigen that produces a detectable colorimetric signal, exceeding non-specific binding. For determining the LoD, linear regression analysis was executed using GraphPad Prism 9.0 (GraphPad Software, USA), and the standard deviation of the response (σ) and the slope (S) of the calibration curve were employed following the equation provided below.

$$LoD = 3.3 \times \sigma / s$$

2.13 Statistical analysis

Data were analyzed using the means ± the standard deviation (SD) of the means, and statistical data analyses were performed by GraphPad Prism 9.0 (GraphPad Software, USA).

3 Results

3.1 Recombinant FopA antigen production and mouse immunization

To produce the FopA antigen and generate FopA antibodies, we utilized a Baculovirus-insect cell expression vector system (Jang et al., 2022). The *fopA* gene containing the 6 × His tag was inserted into the pFastBac donor plasmid, transformed into competent cells, and bacmid DNA was isolated and confirmed by agarose gel electrophoresis (Figure 1A; Supplementary Figures 1A, B). Pure recombinant FopA protein, corresponding to approximately 44 kDa, was purified using a Ni-NTA column and analyzed by SDS-PAGE and Coomassie Brilliant Blue staining (Figure 1B). BALB/c mice were immunized with recombinant FopA for hybridoma and phage display screening using a single-chain variable fragment (scFv) library. Initially, 5-week-old BALB/c mice were immunized with the antigen with complete Freund's adjuvant by intraperitoneal injection, followed by three subcutaneous injections of the antigen with incomplete Freund's adjuvant fortnightly for boost immunization. The final booster immunization was performed by intravenous injection to increase the intensity of the booster (Figure 1C).

3.2 Screening of antibodies binding to FopA antigen by immune library and hybridoma

To select highly specific and diverse antibodies that bind to FopA, we used the hybridoma method and phage display in conjunction with an immune library (Figure 2A). This involved fusing Sp2/0 myeloma cells and splenocytes isolated from FopA-immunized mice to generate and screen hybridoma clones based on their binding activity to recombinant FopA using ELISA. After screening, two candidate mAbs were selected for DNA sequencing (Figure 2B). To construct an immune scFv library against FopA, total RNA was isolated from the splenocytes of immunized mice and cDNA was synthesized via reverse transcription PCR. The VH and VL regions were amplified using multiple primers to generate the scFv genes (Supplementary Figure 2). Biopanning was performed three times using the FopA antigen, and polyclonal

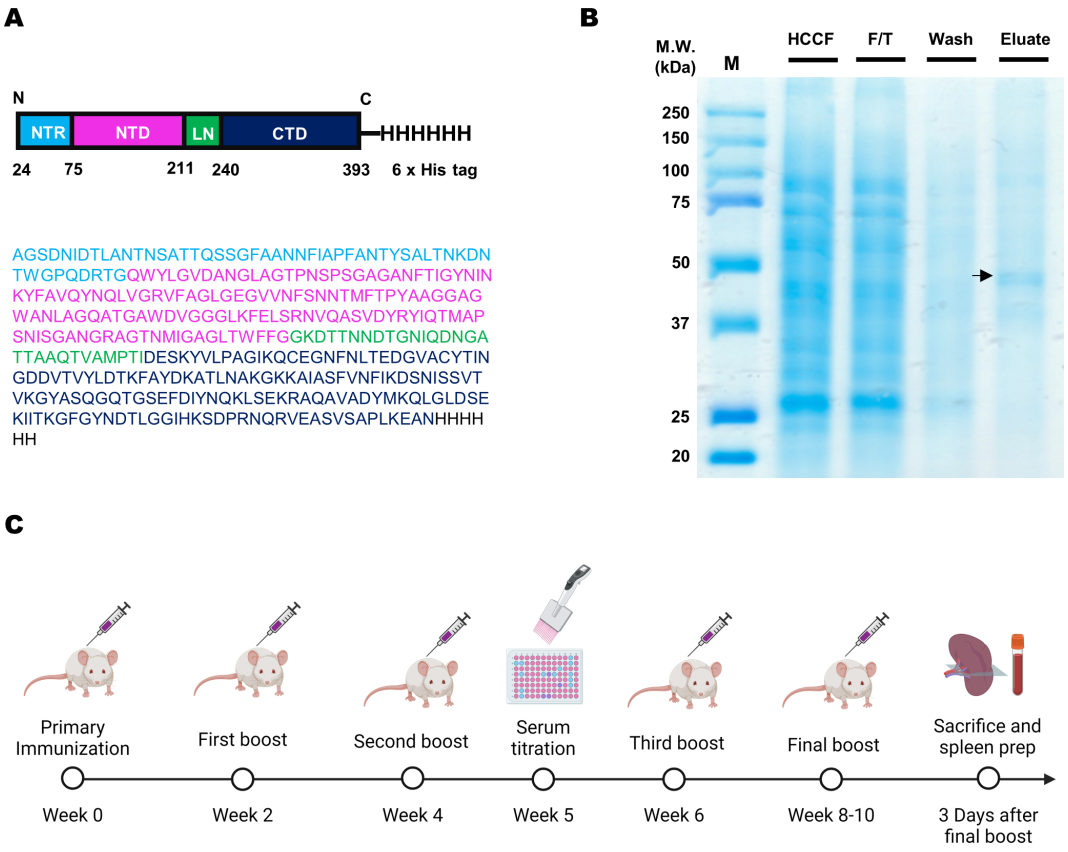

FIGURE 1
Recombinant FopA protein expression and mouse immunization. **(A)** Schematic illustration of the expressed domains of FopA protein with polyhistidine tags and amino acid sequence of FopA. **(B)** The production of recombinant FopA protein was analyzed using SDS-PAGE. The harvested cell culture fluid (Lane 1), flow-through fraction (Lane 2), washed fraction (Lane 3), and elution fraction (Lane 4). **(C)** Schematic representation of the mouse immunization protocol. The mice were immunized four to five times at 2-week intervals, and serum was collected after the second boost step for serum antibody titration. The spleen was collected 3 days after the final boost. Created with BioRender.com.

antibodies from each round were expressed by IPTG induction (Supplementary Figures 3A, B). The antigen-binding activity of these antibodies was evaluated by ELISA. The binding of polyclonal anti-FopA antibodies from the third-round output was significantly greater than that observed in previous rounds or in the initial immune library (Supplementary Figures 3C, D). This suggests that the panning rounds successfully amplified the target-binding clones. To further analyze the output of the third round, we screened individual scFv clones and identified 16 positive binders for the antigen (Figure 2C). By analyzing DNA sequences of anti-FopA antibodies, we finally determined the complementarity-determining regions (CDRs) in the variable heavy (VH) and variable light (VL) chain sequences of two (Figure 2D) and six (Figure 2E) antibodies derived from hybridomas and phage display panning, respectively.

3.3 Production and characterization of monoclonal antibodies against FopA

To evaluate the binding affinity of the antibodies, scFvs obtained from the immune library were converted into IgG, transfected into Expi293F cells, transiently expressed, and purified for measurement (Jeon et al., 2023). In contrast, 6H6 and 6D10 hybridoma clones were not produced as an intact IgG form (data not shown). Therefore, the VH and VL chains of these clones were individually cloned into heavy chain (HC) and light chain (LC) expression vectors containing the constant region. HC and LC expression vectors were generated for each antibody and were transiently expressed in Expi293F cells. The antibodies were verified under both non-reducing and reducing conditions and their size and purity were determined using SDS-PAGE (Figures 3A, B). The binding activity of IgGs was initially validated by ELISA, which demonstrated that 6B12, 3H7, and 3C1 clones specifically bound to FopA in a dose-dependent manner (Figure 3C). Biolayer interferometry (BLI) was used to determine the affinity of these antibodies. Recombinant FopA was immobilized on a biosensor tip and 100 nM of each antibody was allowed to bind to the antigen (Figure 3D). Our results revealed that the anti-FopA 6B12 and 3C1 antibodies exhibited the highest binding affinity among the tested antibodies, with apparent K_D of 1.76×10^{-10} M and 1.32×10^{-9} M, respectively. Therefore, these two antibodies were selected for further analyses. For detailed examination, either 6B12 or 3C1 IgG was immobilized on a biosensor tip and subjected to varying concentrations of the FopA antigen. The binding affinities were calculated for their association and dissociation values at six different concentrations of antigen, and the K_D value of 6B12 was

10.3389/fcimb.2024.1455259

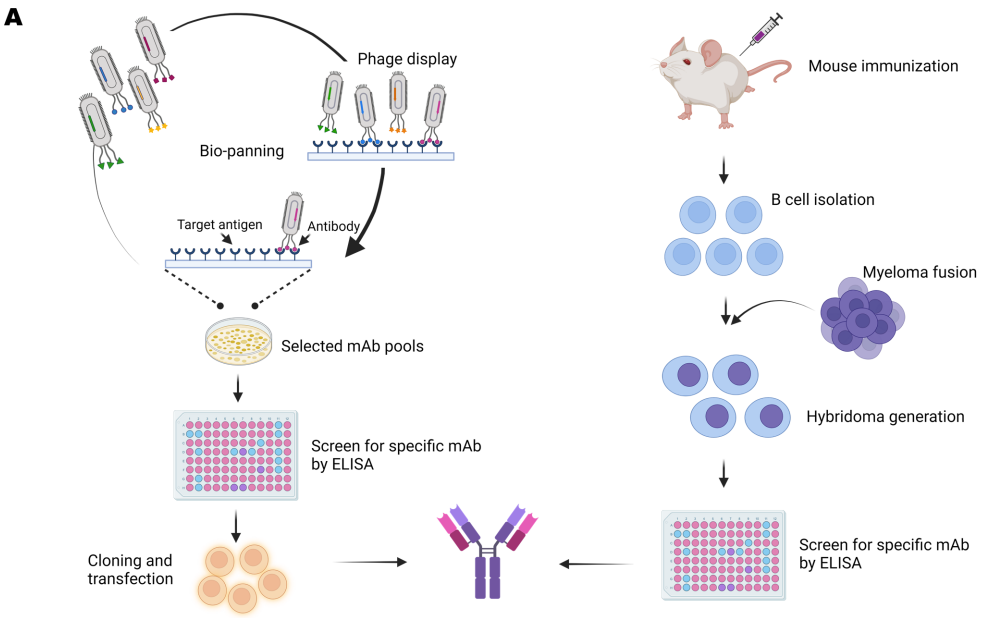

D

Clone ID	VH			VL		
	HCDR1	HCDR2	HCDR3	LCDR1	LCDR2	LCDR3
6H6	GYTFTSYN	IYPGNGGT	ARGGDWFAY	QSLVHSNGNTY	KVS	SQSTHVPWT
6D10	GYTFTNHH	INPYNDYT	ARSGRYGYERAMDY	SSVSY	ATS	QQWSSNPLT

E

Clone ID	VH			VL		
	HCDR1	HCDR2	HCDR3	LCDR1	LCDR2	LCDR3
1A9	GFNIKDYY	IDPENGDT	NAVYHDYDGSFFDV	QSLVHSNGDTY	KVS	SQSTHFPLT
3C1	GFTFSSYG	ISSGGSYT	ARHPLFYDYDGWYFDV	QSLENSNGNTY	KVS	FQGSHVPYT
3H5	GFNIKDTY	IDPANGNT	ARPPIPMDWYLDV	QNINVW	KAS	QQGQSYPYT
3H7	GFSLTSYG	IWGDGST	ARRDYAMDY	QSLVHSNGNTY	KVS	SQSTHVPYT
3F7	GFNIKDTY	INPGTGYT	ARDDGIYAMDY	QSLVHSNGNTY	KVS	FQGSHVPYT
6B12	GFTFSYFG	ISSDSSTI	ARQELLRPPWFAY	QSVSND	YAS	QQDYSSPLT

FIGURE 2
Antibody screening with Immune library and Hybridoma technology. **(A)** Schematic representation of the Hybridoma antibody screening method and phage display screening method with immune antibody library. **(B, C)** Screening of antibodies against the FopA recombinant protein. Out of the 954 antibody clones produced from hybridoma screening, 6H6 and 6D10 (O.D. 450nm > 1.0) were selected. 16 positive clones (O.D. 450nm > 1.0) were selected from the total of 672 scFv clones produced by the immune library. **(D, E)** Sequence identification of the variable heavy (VH) and light (VL) chains of anti-FopA antibodies. The VH and VL regions of each antibody were sequenced to identify the complementarity-determining regions (CDRs). Created with BioRender.com.

5.06×10^{-9} M, and 3C1 was 5.62×10^{-9} M (Figures 3E, F). These findings demonstrate that anti-FopA 6B12 and 3C1 antibodies are produced purely in IgG form and have a prominent binding affinity for a specific antigen, making them promising candidates for immunoassays.

3.4 Development of a sandwich ELISA method for the detection of FopA

It is vital to ensure that a suitable combination of antibodies is selected for the development of a sandwich ELISA-based detection

10.3389/fcimb.2024.1455259

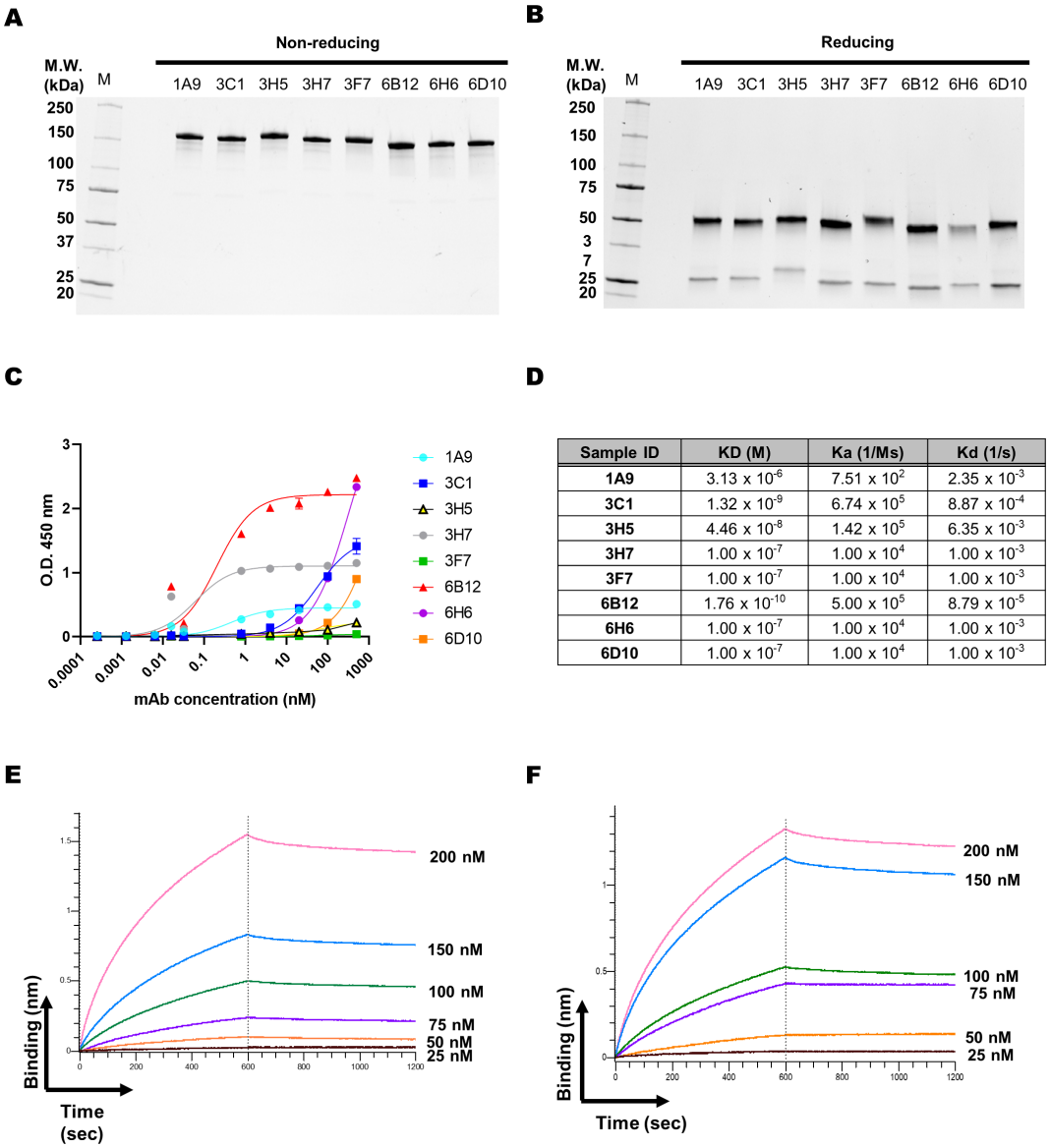

Sample ID	KD (M)	Ka (1/Ms)	Kd (1/s)
1A9	3.13×10^{-6}	7.51×10^{2}	2.35×10^{-3}
3C1	1.32×10^{-9}	6.74×10^{5}	8.87×10^{-4}
3H5	4.46×10^{-8}	1.42×10^{5}	6.35×10^{-3}
3H7	1.00×10^{-7}	1.00×10^{4}	1.00×10^{-3}
3F7	1.00×10^{-7}	1.00×10^{4}	1.00×10^{-3}
6B12	1.76×10^{-10}	5.00×10^{5}	8.79×10^{-5}
6H6	1.00×10^{-7}	1.00×10^{4}	1.00×10^{-3}
6D10	1.00×10^{-7}	1.00×10^{4}	1.00×10^{-3}

FIGURE 3
Antibody production and characterization. Two IgG antibodies were purified from hybridoma and six IgG antibodies from an immune library. The expressed antibodies were purified using a protein A column and analyzed by SDS-PAGE to determine their sizes and purity. **(A)** The non-reducing condition showed an intact size of approximately 150 kDa, while **(B)** the reducing condition showed sizes of 50 kDa (Heavy chain) and 25 kDa (Light chain). **(C)** The binding activity of the eight IgG antibodies was validated using recombinant FopA protein. ELISA assessed the dose-dependent binding of 6B12, 3H7, and 3C1 IgGs. **(D)** The binding affinity of the eight antibodies was measured using biolayer interferometry. Recombinant FopA was immobilized on an AR2G biosensor and allowed to bind to the antibodies. **(E, F)** For detailed analysis, the antibodies were immobilized on an AR2G biosensor and subsequently permitted to bind with the FopA antigen diluted to various concentrations (25, 50, 75, 100, 150, and 200 nM). Kinetic rates and equilibrium binding constants were analyzed using global fitting analysis of the binding curves. Values represent the mean ± SD for a duplicate **(C)**.

system, considering that different antibody sequences may possess distinct epitopes on the target (Jang et al., 2022). To this end, we conducted a competitive binding assay to evaluate the efficacy of biotinylated and non-biotinylated antibodies in detecting the FopA antigen.

As depicted in Figure 4A, our results demonstrated that, regardless of the concentration of the naked 3C1 antibody, the biotinylated 6B12 antibody was able to bind to the antigen. In contrast, when a biotinylated 3C1 antibody was used, its binding to the antigen was hindered by the naked 6B12 antibody. These findings were confirmed using sandwich ELISA, in which the 3C1 antibody was used as the capture antibody, and the 6B12 antibody was used as the detector antibody. As the concentration of the FopA antigen increased, so did the absorbance, indicating that 6B12 is a suitable candidate as a detector antibody, whereas 3C1 is suitable as a capture antibody in a sandwich ELISA configuration (Figure 4B). Furthermore, analysis of the limit of detection (LoD) demonstrated that this pair of antibodies was highly specific and sensitive, exhibiting detection limits of 0.062 ng/mL in PBS and 0.064 ng/mL in skim milk matrices (Figures 4C, D).

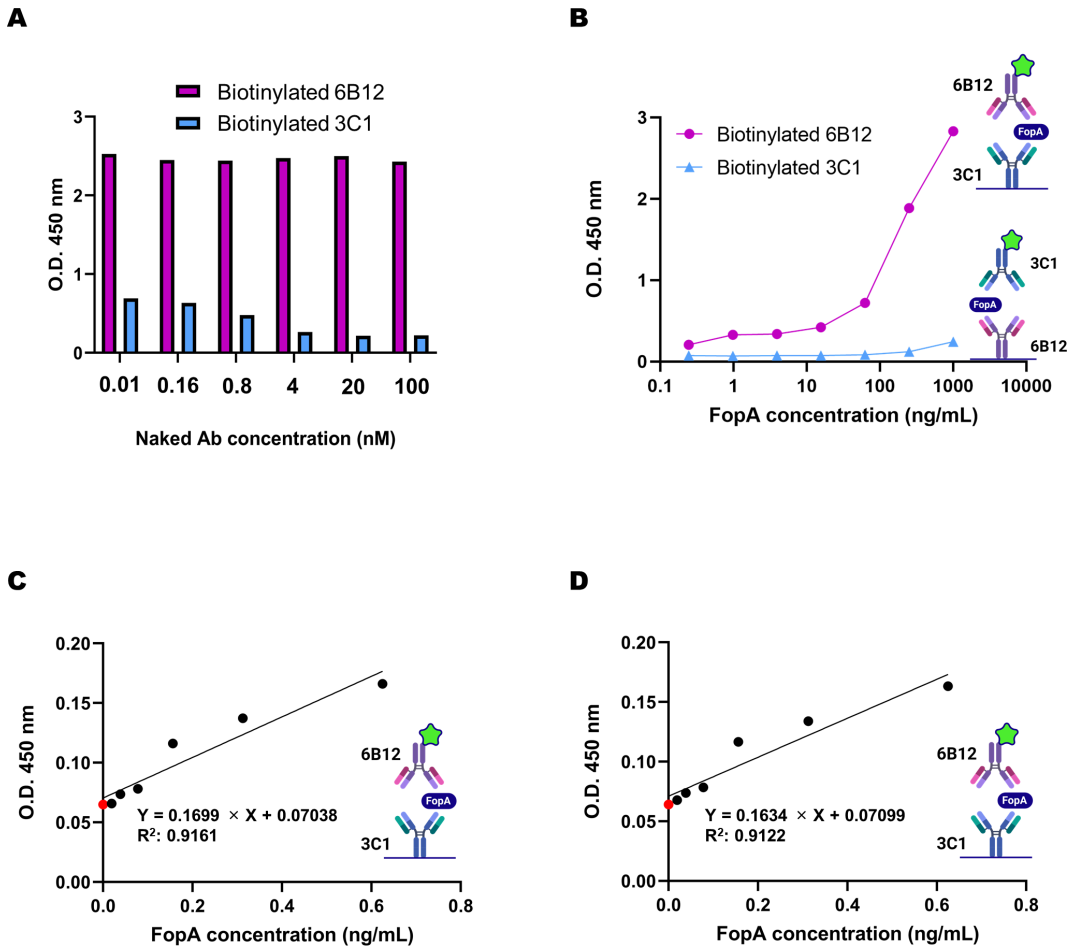

FIGURE 4
Development of a method for detecting FopA antigen using a sandwich ELISA. **(A)** Two combinations of antibodies were evaluated for competitive ELISA using recombinant FopA. Each biotinylated antibody was fixed at 20 nM concentration, and each naked antibody diluted one-fifth serially from 100 nM concentration was incubated with the antigen. **(B)** The detection efficiency of the two combinations of antibodies, 3C1 (capture) and biotinylated 6B12 (detector), or biotinylated 3C1 (detector) and 6B12 (capture), was assessed using the sandwich ELISA method. **(C, D)** The limit of detection was determined by incubating each capture mAb (50 nM) coated on a 96-well ELISA plate and using a biotinylated detector mAb (20 nM) to detect 0.062 ng/mL of FopA in PBS, 0.064 ng/mL in 3% skim milk, and a red dot indicating the background signal. The limit of detection value was calculated as described method section. Values represent the mean ± SD for a duplicate **(A)** and a triplicate **(B–D)**. Created with BioRender.com.

3.5 Validation of sandwich ELISA for detecting FopA in diverse matrices

We evaluated the potential of our immunoassay method to diagnose *F. turalensis* in clinical and contaminated samples using FopA protein in various matrices. As shown in Figure 5A, recombinant FopA was successfully detected at a range of 0.3–20 ng/mL when diluted in PBS, skim milk, human serum, bovine serum albumin (BSA), mouse urine, and soil water. Our results indicated that recombinant FopA protein could be sensitively detected at an approximate 0.3 ng/mL concentration across all matrices. To the impact of various matrices on the detection of FopA protein, we conducted linear regression analyses and found that human serum, BSA, mouse urine, and soil water had little to no effect on the LoD values, which were determined in the range of 0.066 to 0.074 ng/mL (Figures 5B–E). Therefore, an immunoassay method utilizing anti-FopA monoclonal antibodies is capable of detecting FopA without interference from different matrices, including human sera, and effectively identifying pathogens in contaminated samples across various environments.

4 Discussion

Given its status as a potentially infectious disease, it is essential to promptly and accurately diagnose tularemia, a disease with a range of clinical symptoms and potentially fatal consequences. This is particularly crucial in situations of widespread exposure, such as during a pandemic, where quick and accurate diagnosis can save lives (Hannah et al., 2021). To provide a more precise and prompt diagnosis of *F. tularensis*, we developed a sandwich ELISA test that employs a novel antibody designed to bind FopA, a distinctive outer membrane protein antigen of *F. tularensis*. While most existing antibody-based immunoassays target the LPS found in *F. tularensis*, this method raises concerns regarding false-positive results. We developed a novel diagnostic method that has not been previously

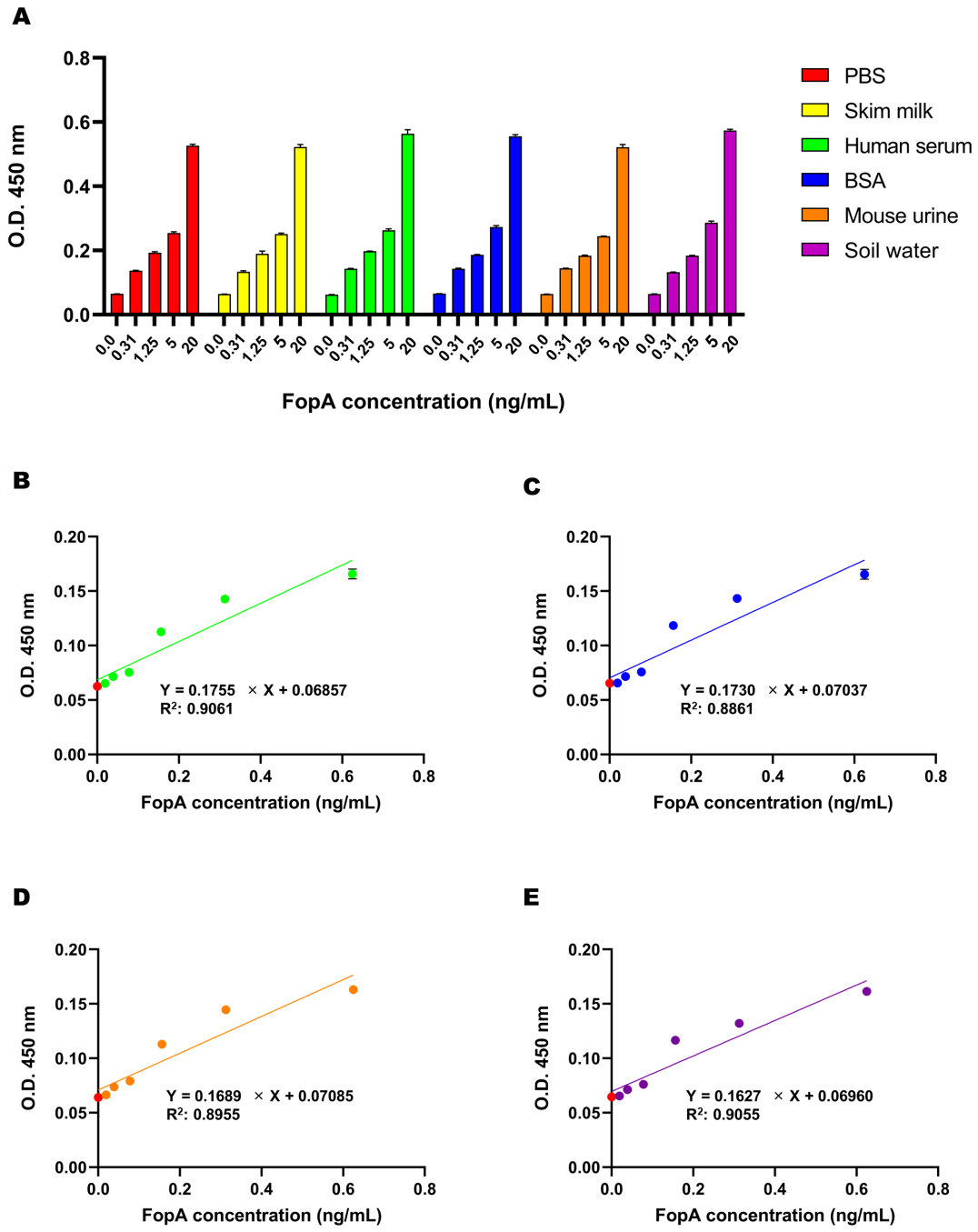

FIGURE 5
Detection of FopA using the sandwich ELISA in various matrices. The evaluation of a pair of antibodies for detecting recombinant FopA using sandwich ELISA in various matrices, including 3% human serum, 3% bovine serum albumin (BSA), mouse urine, and soil water. **(A)** The capture monoclonal antibody (50 nM) coated on a 96-well ELISA plate and biotinylated detector monoclonal antibody (20 nM) were employed to assess the FopA concentration serially diluted from 20 ng/mL. The detection sensitivity of FopA was evaluated by serial dilution of the sample, resulting in a determined limit of detection (LoD) of 0.066 ng/mL for 3% human serum **(B)**, 0.074 ng/mL for 3% BSA **(C)**, 0.071 ng/mL for mouse urine **(D)**, and 0.067 ng/mL for soil water **(E)**, and a red dot indicating the background signal. Error bars represent standard deviations from a triplicate.

reported, utilizing antibodies that specifically bind to FopA. The protein used in our new diagnostic method is a member of the OmpA family and exhibits low sequence homology with that of other gram-negative bacteria (Nagaratnam et al., 2022). Moreover, FopA has a high copy number on the outer membrane of bacteria and is immunogenic, making it a suitable target for antibody development (Confer and Ayalew, 2013). Previous studies have suggested that monoclonal antibodies against FopA can inhibit *F. tularensis* pathogenicity. However, they have not been used for diagnosis or to provide detailed information on their sensitivity and specificity (Savitt et al., 2009).

Immunoassays are capable of providing quick and precise diagnoses compared to PCR based-or cell culture-based diagnostic methods (Liu et al., 2021). To achieve optimal results using immunoassays, it is

important to develop antibodies with high specificity and sensitivity (Cox et al., 2019). To this end, we utilized an insect cell based expression system to produce high-purity recombinant FopA proteins for the development of high-quality antibodies, and we employed two different methods for generating diagnostic antibodies of diverse sequences: the mouse-derived immune library screening method and the hybridoma screening method. The insect expression system has proven to be advantageous for antigen preparation, as it ensures a sufficient amount of protein while minimizing the likelihood of endotoxin-induced immunogenicity, which can occur when proteins are produced by microorganisms (Mamat et al., 2013; Tripathi and Shrivastava, 2019). In this study, we employed two methods for antibody screening: a hybridoma screening system, and an immune library screening method using phage displays. Although the hybridoma screening system is an effective method for developing high-affinity antibodies through natural affinity maturation, it has the disadvantage of low efficiency in cell fusion and hybridoma isolation, requiring considerable time to generate a cell line and select a specific hybridoma. Moreover, hybridoma cell lines can be genetically unstable and their cultures are at constant risk of contamination (Moraes et al., 2021). In contrast, the use of phage displays for immune library screening has proven to be a feasible approach for identifying a broad range of high-affinity antibodies. This method offers significant advantages, specifically by enabling the selection of numerous sequences during the panning process and facilitating the rapid isolation and characterization of monoclonal antibodies with high specificity. Additionally, it allows for easy modification of diverse antibody formats, making it a versatile tool for antibody discovery (Clementi et al., 2012; Moraes et al., 2021). Unfortunately, we encountered difficulties generating diagnostic-grade antibodies during the hybridoma screening process. The clones derived from the hybridoma process faced challenges in expressing a form of IgG antibodies, and even when additional cloning processes were applied, the resulting antibodies had a low affinity compared to those selected from the immune library.

We validated two antibody candidates that recognized distinct epitopes of FopA and can be utilized in a sandwich ELISA diagnosis test for *F. tularensis*. Therefore, it is essential to evaluate the diagnostic potential of these antibodies in various matrices to confirm their effectiveness. This sandwich ELISA method demonstrated exceptional performance in multiple matrices, including human sera, with detection limits of 0.062–0.074 ng/mL. This diagnostic method maintains high sensitivity and specificity regardless of sample contamination. Commercial immunodiagnostic kits evaluate *F. tularensis* infections by detecting IgG or IgM antibodies specific to the LPS antigen of the bacterium (Yanes et al., 2018). These methods are commonly used to identify antibodies in the blood of patients suspected of infection (Maurin, 2020). However, these diagnostic methods may result in false-positive outcomes due to the presence of anti-LPS antibodies from other gram-negative bacteria (Sharma et al., 2013). Furthermore, the diagnosis of infection before *F. tularensis* antibody generation can be difficult because of the limitations of these methods (Maurin, 2020). Additionally, when using anti-LPS detection antibodies, the possibility of false-positive results for other infectious bacteria and the low sensitivity of these antibodies when detecting infections in patient sera should be taken into account (Hannah et al., 2021). We have not been able to directly detect *F. tularensis* using the actual pathogen owing to its unavailability in Korea. However, our study suggests that novel anti-FopA antibodies could serve as a promising alternative for diagnosing *F. tularensis* infections, offering high sensitivity and specificity without inducing cross-reactivity.

It is important to identify highly specific antigens and acquire diverse antibody candidates to improve the sensitivity of early pathogen detection. Hybridoma technology is a highly effective antibody-screening method; however, it presents difficulties for high-throughput screening. Incorporating a technique that isolates single B cells to identify high-affinity antibodies against the antigen following mouse immunization could be a potential solution (Pedrioli and Oxenius, 2021). Additionally, the immune library screening method employs NGS-based antibody sequencing to obtain diverse sequences (Yang et al., 2017).

5 Conclusion

In conclusion, we have successfully developed a range of antibodies that specifically bind to FopA, an outer membrane protein of *F. tularensis*, a pathogen that poses a significant infective risk. These antibodies can be used for early detection and diagnosis of infections caused by this pathogen. Prompt diagnosis is crucial for controlling the rapid spread of infectious diseases and preventing instances of bioterrorism. Existing antibody-based diagnostic systems for *F. tularensis* rely on targeting LPS proteins; however, our system utilizes antibodies against FopA as a novel diagnosable antigen. The development of these diagnostic antibodies highlights the potential of immunodiagnostics based on antibodies targeting other outer membrane proteins, as well as those targeting LPS, for diagnosing pathogens. This finding could serve as a basis for future research exploring the therapeutic use of antibodies that bind to FopA in humans infected with *F. tularensis*.

Data availability statement

The original contributions presented in the study are included in the article/Supplementary Material. Further inquiries can be directed to the corresponding authors.

Author contributions

JJ: Data curation, Formal analysis, Investigation, Methodology, Validation, Writing – original draft. DK: Data curation, Formal analysis, Investigation, Methodology, Validation, Writing – original draft. J-HJ: Writing – review & editing, Investigation, Methodology, Validation. D-GL: Investigation, Methodology, Validation, Writing – review & editing. S-HC: Investigation, Methodology, Validation, Writing – review & editing. M-YJ: Investigation, Methodology, Validation, Writing – original draft. Y-SJ: Formal analysis, Resources, Writing – review & editing. D-HS: Writing – review & editing, Formal analysis, Resources. J-KM: Data curation, Methodology, Writing – review & editing. J-GP: Data

curation, Methodology, Writing – review & editing. M-SL: Data curation, Methodology, Writing – review & editing. B-SH: Data curation, Writing – review & editing, Methodology. WY: Conceptualization, Project administration, Writing – review & editing, Data curation, Writing – original draft. N-KL: Conceptualization, Project administration, Writing – review & editing. JL: Conceptualization, Funding acquisition, Project administration, Supervision, Writing – review & editing.

Funding

The author(s) declare financial support was received for the research, authorship, and/or publication of this article. This research was supported by the Defense Acquisition Program Administration (ADD-911255202).

Acknowledgments

We thank Seong Tae Jeong and Gyeung-Haeng Hur for their fruitful discussions.

Conflict of interest

The authors declare that the research was conducted in the absence of any commercial or financial relationships that could be construed as a potential conflict of interest.

Publisher's note

Supplementary material

The Supplementary Material for this article can be found online at: https://www.frontiersin.org/articles/10.3389/fcimb.2024.1455259/full#supplementary-material

References

Ahmed, I. M., Khairani-Bejo, S., Hassan, L., Bahaman, A. R., and Omar, A. R. (2015). Serological diagnostic potential of recombinant outer membrane proteins (rOMPs) from Brucella melitensis in mouse model using indirect enzyme-linked immunosorbent assay. *BMC Vet. Res.* 11, 1–10. doi: 10.1186/s12917-015-0587-2

Altman, G. B., and Wachs, J. E. (2002). Tularemia: A pathogen in nature and a biological weapon. *AAOHN J.* 50, 373–379. doi: 10.1177/216507990205000810

Babrak, L., Mcgarvey, J. A., Stanker, L. H., and Hnasko, R. (2017). Identification and verification of hybridoma-derived monoclonal antibody variable region sequences using recombinant DNA technology and mass spectrometry. *Mol. Immunol.* 90, 287–294. doi: 10.1016/j.molimm.2017.08.014

Bishop, A., Wang, H.-H., Donaldson, T. G., Brockinton, E. E., Kothapalli, E., Clark, S., et al. (2023). Tularemia cases increase in the USA from 2011 through 2019. *Curr. Res. Parasitol. Vector-Borne Dis.* 3, 100116. doi: 10.1016/j.crpvbd.2023.100116

Boisset, S., Caspar, Y., Sutera, V., and Maurin, M. (2014). New therapeutic approaches for treatment of tularaemia: a review. *Front. Cell. Infect. Microbiol.* 4, 40. doi: 10.3389/fcimb.2014.00040

Çelebi, G., Baruonu, F., Ayoglu, F., Çinar, F., Karadenizli, A., Ugur, M. B., et al. (2006). Tularemia, a reemerging disease in northwest Turkey: epidemiological investigation and evaluation of treatment responses. *Japan. J. Infect. Dis.* 59, 229. doi: 10.7883/yoken.JJID.2006.229

Chaignat, V., Djordjevic-Spasic, M., Ruettger, A., Otto, P., Klimpel, D., Müller, W., et al. (2014). Performance of seven serological assays for diagnosing tularemia. *BMC Infect. Dis.* 14, 234. doi: 10.1186/1471-2334-14-234

Clementi, N., Mancini, N., Solforosi, L., Castelli, M., Clementi, M., and Burioni, R. (2012). Phage display-based strategies for cloning and optimization of monoclonal antibodies directed against human pathogens. *Int. J. Mol. Sci.* 13, 8273–8292. doi: 10.3390/ijms13078273

Confer, A. W., and Ayalew, S. (2013). The OmpA family of proteins: roles in bacterial pathogenesis and immunity. *Vet. Microbiol.* 163, 207–222. doi: 10.1016/j.vetmic.2012.08.019

Cox, K. L., Devanarayan, V., Kriauciunas, A., Manetta, J., Montrose, C., and Sittampalam, S. (2019). Immunoassay methods. *Assay Guidance Manual [Internet]*. 223–262.

Genchi, M., Prati, P., Vicari, N., Manfredini, A., Sacchi, L., Clementi, E., et al. (2015). Francisella tularensis: no evidence for transovarial transmission in the tularemia tick vectors Dermacentor reticulatus and Ixodes ricinus. *PloS One* 10, e0133593. doi: 10.1371/journal.pone.0133593

Hannah, E. E., Pandit, S. G., Hau, D., Demers, H. L., Robichaux, K., Nualnoi, T., et al. (2021). Development of immunoassays for detection of Francisella tularensis lipopolysaccharide in tularemia patient samples. *Pathogens* 10, 924. doi: 10.3390/pathogens10080924

Hennebique, A., Gas, F., Batina, H., De Araujo, C., Bizet, K., and Maurin, M.. (2020). Evaluation of the biotoxis qPCR detection kit for Francisella tularensis detection in clinical and environmental samples. *Journal of Clinical Microbiology*, 59 (1), 10–1128. doi: 10.1128/JCM.01434-20

Hestvik, G., Warns-Petit, E., Smith, L., Fox, N., Uhlhorn, H., Artois, M., et al. (2015). The status of tularemia in Europe in a one-health context: a review. *Epidemiol. Infect.* 143, 2137–2160. doi: 10.1017/S0950268814002398

Hickey, A. J., Hazlett, K. R., Kirimanjeswara, G. S., and Metzger, D. W. (2011). Identification of Francisella tularensis outer membrane protein A (FopA) as a protective antigen for tularemia. *Vaccine* 29, 6941–6947. doi: 10.1016/j.vaccine.2011.07.075

Jang, J. H., Kim, S., Kim, S. G., Lee, J., Lee, D. G., Jang, J., et al. (2022). A sensitive immunodetection assay using antibodies specific to staphylococcal enterotoxin B produced by baculovirus expression. *Biosensors (Basel)* 12 (10), 787. doi: 10.3390/bios12100787

Jeon, M. Y., Han, J. E., Lee, D. G., Cho, Y. L., Jang, J. H., Lee, J., et al. (2023). Novel sandwich immunoassay detects a shrimp AHPND-causing binary PirAB(Vp) toxin produced by Vibrio parahaemolyticus. *Front. Cell Infect. Microbiol.* 13, 1294801. doi: 10.3389/fcimb.2023.1294801

Kim, J.-E., Seo, Y., Jeong, Y., Hwang, M. P., Hwang, J., Choo, J., et al. (2015). A novel nanoprobe for the sensitive detection of Francisella tularensis. *J. Hazard. Mater.* 298, 188–194. doi: 10.1016/j.jhazmat.2015.05.041

Kiliç, S., Celebi, B., and Yesilyurt, M. (2012). Evaluation of a commercial immunochromatographic assay for the serologic diagnosis of tularemia. *Diagnostic microbiology and infectious disease.* 74 (1), 1–5. doi: 10.1016/j.diagmicrobio.2012.05.030

Lamps, L. W., Havens, J. M., Sjostedt, A., Page, D. L., and Scott, M. A. (2004). Histologic and molecular diagnosis of tularemia: a potential bioterrorism agent endemic to North America. *Modern Pathol.* 17, 489–495. doi: 10.1038/modpathol.3800087

Lee, N.-K., Bidlingmaier, S., Su, Y., and Liu, B. (2018). Modular construction of large non-immune human antibody phage-display libraries from variable heavy and light chain gene cassettes. *Phage Display: Methods Protoc.* 1701, 61–82. doi: 10.1007/978-1-4939-7447-4_4

Lindgren, H., Liu, X., and Sjöstedt, A. (2024). Francisella tularensis-specific antibody levels in sera from Swedish patients with suspected tularemia during a 13-year period. *Front. Cell. Infect. Microbiol.* 14, 1381776. doi: 10.3389/fcimb.2024.1381776

Liu, H. Y., Hopping, G. C., Vaidyanathan, U., Ronquillo, Y. C., Hoopes, P. C., and Moshirfar, M. (2019). Polymerase chain reaction and its application in the diagnosis of infectious keratitis. *Med. Hypothesis Discov. Innov. Ophthalmol.* 8, 152.

Liu, Y., Zhan, L., Qin, Z., Sackrison, J., and Bischof, J. C. (2021). Ultrasensitive and highly specific lateral flow assays for point-of-care diagnosis. *ACS nano* 15, 3593–3611. doi: 10.1021/acsnano.0c10035

Mamat, U., Woodard, R. W., Wilke, K., Souvignier, C., Mead, D., Steinmetz, E., et al. (2013). *Endotoxin-free protein production—ClearColi™ technology* (US New York: Nature Publishing Group). doi: 10.1038/nmeth.f.367

Maurin, M. (2020). Francisella tularensis, tularemia and serological diagnosis. *Front. Cell Infect. Microbiol.* 10, 512090. doi: 10.3389/fcimb.2020.512090

Maurin, M., and Gyuranecz, M. (2016). Tularaemia: clinical aspects in Europe. *Lancet Infect. Dis.* 16, 113–124. doi: 10.1016/S1473-3099(15)00355-2

Maurin, M., Pondérand, L., Hennebique, A., Pelloux, I., Boisset, S., and Caspar, Y. (2024). Tularemia treatment: experimental and clinical data. *Front. Microbiol.* 14, 1348323. doi: 10.3389/fmicb.2023.1348323

Moraes, J. Z., Hamaguchi, B., Braggion, C., Speciale, E. R., Cesar, F. B. V., Da Silva Soares, G. D. F., et al. (2021). Hybridoma technology: is it still useful? *Curr. Res. Immunol.* 2, 32–40. doi: 10.1016/j.crimmu.2021.03.002

Nagaratnam, N., Martin-Garcia, J. M., Yang, J.-H., Goode, M. R., Ketawala, G., Craciunescu, F. M., et al. (2022). Structural and biophysical properties of FopA, a major outer membrane protein of Francisella tularensis. *PloS One* 17, e0267370. doi: 10.1371/journal.pone.0267370

Nelson, C. A., and Sjöstedt, A. (2024). Tularemia: A storied history, an ongoing threat. *Clin. Infect. Dis.* 78, S1–S3. doi: 10.1093/cid/ciad681

Pedrioli, A., and Oxenius, A. (2021). Single B cell technologies for monoclonal antibody discovery. *Trends Immunol.* 42, 1143–1158. doi: 10.1016/j.it.2021.10.008

Pelletier, N., Raoult, D., and La Scola, B. (2009). Specific recognition of the major capsid protein of Acanthamoeba polyphaga mimivirus by sera of patients infected by Francisella tularensis. *FEMS Microbiol. Lett.* 297, 117–123. doi: 10.1111/fml.2009.297.issue-1

Pillai, S. P., DePalma, L., Prentice, K. W., Ramage, J. G., Chapman, C., Sarwar, J., et al (2020). Comprehensive laboratory evaluation of a specific lateral flow assay for the presumptive identification of francisella tularensis in suspicious white powders and aerosol samples. *Health security*. 18 (2), 83–95. doi: 10.1089/hs.2019.0151

Savitt, A. G., Mena-Taboada, P., Monsalve, G., and Benach, J. L. (2009). Francisella tularensis infection-derived monoclonal antibodies provide detection, protection, and therapy. *Clin. Vaccine Immunol.* 16, 414–422. doi: 10.1128/CVI.00362-08

Sharma, N., Hotta, A., Yamamoto, Y., Fujita, O., Uda, A., Morikawa, S., et al. (2013). Detection of Francisella tularensis-specific antibodies in patients with tularemia by a novel competitive enzyme-linked immunosorbent assay. *Clin. Vaccine Immunol.* 20, 9–16. doi: 10.1128/CVI.00516-12

Sharma, R., Patil, R. D., Singh, B., Chakraborty, S., Chandran, D., Dhama, K., et al. (2023). Tularemia–a re-emerging disease with growing concern. *Vet. Q.* 43, 1–16. doi: 10.1080/01652176.2023.2277753

Tripathi, N. K., and Shrivastava, A. (2019). Recent developments in bioprocessing of recombinant proteins: expression hosts and process development. *Front. Bioeng. Biotechnol.* 7, 420. doi: 10.3389/fbioe.2019.00420

Walker, D. (2014). Principles of diagnosis of infectious diseases. *Pathobiol Hum. Dis.* 222–225. doi: 10.1016/B978-0-12-386456-7.01713-5

Wiesinger-Mayr, H., Vierlinger, K., Pichler, R., Kriegner, A., Hirschl, A. M., Presterl, E., et al. (2007). Identification of human pathogens isolated from blood using microarray hybridisation and signal pattern recognition. *BMC Microbiol.* 7, 1–17. doi: 10.1186/1471-2180-7-78

Yanes, H., Hennebique, A., Pelloux, I., Boisset, S., Bicout, D. J., Caspar, Y., et al. (2018). Evaluation of in-house and commercial serological tests for diagnosis of human tularemia. *J. Clin. Microbiol.* 56 (1), 10–1128. doi: 10.1128/JCM.01440-17

Yang, S., and Rothman, R. E. (2004). PCR-based diagnostics for infectious diseases: uses, limitations, and future applications in acute-care settings. *Lancet Infect. Dis.* 4, 337–348. doi: 10.1016/S1473-3099(04)01044-8

Yang, W., Yoon, A., Lee, S., Kim, S., Han, J., and Chung, J. (2017). Next-generation sequencing enables the discovery of more diverse positive clones from a phage-displayed antibody library. *Exp. Mol. Med.* 49, e308–e308. doi: 10.1038/emm.2017.22

Yao, M., Guo, X., Wu, X., Bai, Q., Sun, M., and Yin, D. (2022). Evaluation of the combined use of major outer membrane proteins in the serodiagnosis of brucellosis. *Infect. Drug Resist.* 15, 4093–4100. doi: 10.2147/IDR.S372411

Zellner, B., and Huntley, J. F. (2019). Ticks and tularemia: do we know what we don't know? *Front. Cell Infect. Microbiol.* 9, 146. doi: 10.3389/fcimb.2019.00146

frontiers | Frontiers in Cellular and Infection Microbiology

TYPE Review
PUBLISHED 24 September 2024
DOI 10.3389/fcimb.2024.1402941

OPEN ACCESS

EDITED BY
Stefano Stracquadanio,
University of Catania, Italy

REVIEWED BY
Jari Intra,
San Gerardo Hospital, Italy
Kurt G. Naber,
Technical University of Munich, Germany

*CORRESPONDENCE
Adline Princy Solomon
adlineprinzy@sastra.ac.in
John Bosco Balaguru Rayappan
rjbosco@ece.sastra.edu

RECEIVED 18 March 2024
ACCEPTED 02 September 2024
PUBLISHED 24 September 2024

CITATION
Sujith S, Solomon AP and Rayappan JBB (2024) Comprehensive insights into UTIs: from pathophysiology to precision diagnosis and management.
Front. Cell. Infect. Microbiol. 14:1402941.
doi: 10.3389/fcimb.2024.1402941

Comprehensive insights into UTIs: from pathophysiology to precision diagnosis and management

Swathi Sujith[1], Adline Princy Solomon[1*] and John Bosco Balaguru Rayappan[2*]

[1]Quorum Sensing Laboratory, Centre for Research in Infectious Diseases (CRID), School of Chemical and Biotechnology, SASTRA Deemed to be University, Thanjavur, India, [2]Nanosensors Laboratory, School of Electrical & Electronics Engineering, Centre for Nanotechnology & Advanced Biomaterials (CeNTAB), SASTRA Deemed to be University, Thanjavur, India

Urinary tract infections (UTIs) are the second most common infectious disease, predominantly impacting women with 150 million individuals affected globally. It increases the socio-economic burden of society and is mainly caused by *Escherichia coli*, *Proteus mirabilis*, *Klebsiella pneumoniae*, *Enterobacter* spp., and *Staphylococcus* spp. The severity of the infection correlates with the host factors varying from acute to chronic infections. Even with a high incidence rate, the diagnosis is mainly based on the symptoms, dipstick analysis, and culture analysis, which are time-consuming, labour-intensive, and lacking sensitivity and specificity. During this period, medical professionals prescribe empirical antibiotics, which may increase the antimicrobial resistance rate. Timely and precise UTI diagnosis is essential for addressing antibiotic resistance and improving overall quality of life. In response to these challenges, new techniques are emerging. The review provides a comprehensive overview of the global burden of UTIs, associated risk factors, implicated organisms, traditional and innovative diagnostic methods, and approaches to UTI treatment and prevention.

KEYWORDS

bacteria, diagnosis, POCT, sensors, UTI

1 Urinary tract infections: an insightful overview

Infection occurs when the pathogens coercively enter, multiply, and produce toxins in the host for their survival. UTIs, which reduce the quality of life of patients and increase the social burden on society, are the second most common type of infectious disease (after respiratory tract infections) in hospitals and communities (Sahu et al., 2018; Adegun et al., 2019; Danilo de Oliveira et al., 2021; Yang et al., 2022). UTIs are inflammatory reactions of the urinary tract mainly caused by multispecies microorganisms – including bacteria, fungi,

and viruses (Amdekar et al., 2011; Seifu and Gebissa, 2018; Wu et al., 2023). Annually, 150 million people worldwide are affected by UTIs in developed and emerging nations (Foxman, 2014; Flores-Mireles et al., 2015).

There is a lack of information on the global incidence and the long-term trends of UTIs, but due to their impact on policy-making and prevention efforts, the Institute of Health Metrics and Evaluation (IHME) conducted a systematic global epidemiological study named Global Burden of Disease (GBD), which used a DisMod-MR Bayesian meta-regression model that quantifies the incidence, mortality, disability, and 87 risk factors for 369 diseases by sex, age, location, and year for 204 countries and territories from 1990 to 2019 (Yang et al., 2022; Zeng et al., 2022). Globally, the total number of incidents, death rates, and DALY (Disability Adjusted Life Year) of UTIs grew significantly from 1990 to 2019, irrespective of gender, geography, and age. Population growth, particularly in the low and middle-income nations, was the driving force behind the sharp increase in the number of infections. The total number of UTI cases increased by 60.40%, from 252.25 million cases in 1990 to 404.61 million cases in 2019. There were 236,790 cases of UTI worldwide in 2019, an increase of 140.18% compared to 98,590 cases in 1990. India had a significant growth in the incident rates, more than doubling between 1990 and 2019, due to the burden on the healthcare system. In 2019, India accounted for 100.8 million incident cases, 55,558 deaths, and 1.59 million DALYs (Yang et al., 2022; Zeng et al., 2022). This review article aims to provide a comprehensive understanding of the various risk factors, and the organisms associated with UTI, conventional and emerging diagnostic methods, along with biomarkers and the management of UTI.

2 Understanding UTIs

2.1 Anatomy and pathophysiology of UTIs

2.1.1 Structural insights and infection routes

The urinary system is a contiguous hollow organ that includes kidney, ureter, urinary bladder, and urethra. The kidneys are the most important organs, acting as natural filters by clearing the undesired water-soluble debris and reabsorbing components like water, glucose, and amino acids. Through the ureter, urine is directed into the muscular, flexible structure called the urinary bladder until excreted and finally flushed out through the urethra. The urinary tract behaves as a closed system that is impenetrable to pathogens while it is not excreting urine, and the infections occur due to the invasion of the pathogens via the urinary tract, which leads to bladder infection and, subsequently, in some cases to kidney infection with possible kidney damage (Vasudevan, 2014; Hickling et al., 2015). Ascending, hematogenous, and lymphatic are the three ways bacteria use to penetrate and cause UTIs, in which the ascending route is the more prevalent route of infection. Females are more inclined to develop UTIs than males due to shorter urethras, hormonal fluctuations, and proximity to the anus. The progression of infection involves multiple steps. Uropathogens from the gastrointestinal tract or the fecal flora initially attach to the urethra, colonise the bladder, and subsequently spread to the kidneys through the ureters, resulting in cystitis and pyelonephritis, respectively. The enhancement of this route is associated with the use of urinary catheters or spermicidal agents, pregnancy, and ureteral blockage; however, their pathophysiology remains unknown (Foxman, 2002; Davis and Flood, 2011; Mancuso et al., 2023). The descending channel or the hematogenous route (blood-borne route), mainly caused by the *streptococcus* or *staphylococcu*s spp., comprises less than 5% of UTI cases and typically affects patients with ureteral blockages as well as immunocompromised individuals (Davis and Flood, 2011) (Davis and Flood, 2011). When UTI is severe and complicated, bacteria may enter the bloodstream (bacteremia) and potentially reach other organs or tissues, including the lymph nodes. However, it is not the direct route of UTI progression. Rarely, bacteria from nearby organs may enter the urinary tract through the lymphatics. Retroperitoneal abscesses and severe bowel infections are the conditions connected to the lymphatic pathway (Davis and Flood, 2011).

2.1.2 Prevalent microorganisms triggering UTIs

The healthy urine sample can contain non-culturable bacterial cells and the resident flora is polymicrobial, mainly consisting of *Lactobacillus, Prevotella* and *Gardnerella* in varying proportions. (Siddiqui et al., 2011; Wolfe et al., 2012; Kogan et al., 2015) During an infection, there is a disruption of the flora and severity of the infection correlates with the risk factors in the host (Vasudevan, 2014; Colella et al., 2023; Mancuso et al., 2023). Gram-negative bacteria *E.coli* is the most frequent organism causing UTI. Less common include *Proteus mirabilis, Klebsiella* spp., *Pseudomonas aeruginosa, Enterobacter* spp., and gram-positive species such as *Streptococcus* spp (Loh and Sivalingam, 2007; Pardeshi, 2020). Uropathogenic *E.coli* (UPEC) accounts for 80–90% and 30–50% of community-acquired and hospital-acquired UTIs respectively, and have been classified into four major UPEC phylogroups (A, B1, B2, and D) based on chromosomal Pathogenicity Islands (PAI) (Terlizzi et al., 2017; Shah et al., 2019; Katongole et al., 2020). The virulence factors determine the pathogenicity of the UPEC and can be broadly classified into two categories, i.e., bacterial cell surface and secreted virulence factors. Fimbriae, flagellum, capsular lipopolysaccharides, and outermost membrane proteins are commonly present in bacterial cell surface virulence factors. The secreted virulence factors are haemolysin and siderophores (Shah et al., 2019). *P. mirabilis*, isolated from 1–10% of all UTIs, is a gram-negative, rod-shaped motile bacteria with peritrichous flagella, characterised by swarming phenomena. Community-acquired urinary tract infections, catheter-associated urinary tract infections (CAUTI), and nosocomial UTIs are also known to be caused by *P.mirabilis*. The virulence factors, which include biofilms, adhesion molecules, urease, proteases, siderophores, and toxins, are correlated to the pathogenesis. These components relate to the interaction of surfaces with bacteria, invasion, injury to host tissues, immune system escape, and iron absorption (Danilo de Oliveira et al., 2021; Hayder et al., 2020; Tabibian et al., 2008; Tabatabaei et al., 2021). *K. pneumoniae*, regarded as the second most prevalent uropathogen, is an encapsulated facultative gram-negative anaerobic bacillus and ferments lactose (Flores-Mireles et al., 2015). The ability of *K.*

pneumoniae to attack the immune system and cause a range of diseases depends on virulence factors (Flores-Mireles et al., 2015; Davoudabadi et al., 2023). *P. aeruginosa*, an aerobic, gram-negative, non-fermentative rod-shaped bacterium, is the third most prevalent bacteria associated with hospital-acquired UTIs and accounts for 9% globally (Fu et al., 2013; Heidary et al., 2016). The epidemiology of *P. aeruginosa* infections is influenced by several factors associated with its virulence. The combination of virulence factors influences the severity of an infection. In the general population, *Staphylococcus aureus* accounts for 0.5–6% of urinary tract infections, making it a very infrequent cause of UTIs. Still, they can lead to potentially fatal invasive infections like bacteremia (Xu et al., 2023). Extended hospital stays are a result of MRSA urinary tract infections, which are linked to recent antibiotic usage and urinary catheterization. It is crucial to limit the use of urinary catheterization to necessary situations and remove the device as soon as clinically recommended because there is a strong correlation between catheters and urinary tract infections (Alshomrani et al., 2023).

However, the various bacterial virulent factors act as triggers for initiating infection in the dynamic urinary tract. The lipopolysaccharides on the outer membrane of the gram-negative bacteria are one of the host's potent inducers of inflammatory responses. Several adhesion proteins found on the cell surfaces of uropathogens are essential for the initial interactions between the host and the pathogen. Biofilms are clusters of microbial cells encased in a polysaccharide-based matrix and are permanently attached to a surface. By positioning themselves to efficiently exploit the available resources and block access to antimicrobials, antibodies, and white blood cells, biofilms provide bacteria with a chance to survive. To remove bacteria from the urinary tract, free urine outflow is required. Urinary stasis provides a more extended period of bacterial adherence and multiplication if bacteria are not mechanically cleared by normal urinary flow due to anatomical or functional conditions (Katongole et al., 2020) (Table 1).

2.2 Categories of UTIs: a differentiation

UTI classification is crucial for medical assessment, research, quality assurance, and education (Smelov et al., 2016). To develop more homogeneous study groups for the evaluation of novel anti-infective medications in clinical trials, the Infectious Diseases Society of America (IDSA) and the European Society of Clinical Microbiology and Infectious Diseases (ESCMID) introduced the concepts of uncomplicated UTI and complicated UTI in 1992 (Wagenlehner et al., 2020). Most individuals with uncomplicated UTIs are healthy, without structural or neurological abnormalities of the urinary system. A complicated UTI is an infection that occurs in conjunction with another condition, such as an abnormality of the genitourinary tract's structure or function, or the presence of an underlying disease, such as urinary obstruction, a neurological condition that causes urinary retention, renal failure, renal transplantation, pregnancy, or the presence of foreign bodies like calculi, indwelling catheters, or other drainage devices (Flores-Mireles et al., 2015; Pardeshi, 2020). The broad range of symptoms and the heterogeneous nature of the disease have raised concerns that the findings from the clinical studies on patients who were diagnosed with complicated UTI using one set of criteria would not be applicable to patients diagnosed using another set of criteria (Wagenlehner et al., 2020).

TABLE 1 Virulence Genes of Uropathogens.

Virulence Genes Of Uropathogens					
S.No.	Pathogen	Genes	Protein Encoding	Function	Reference
1	UPEC	*fim* operon	Type 1 Fimbriae	Adherence and colonization	(Mancuso et al., 2023; Whelan et al., 2023)
			Type 2 Fimbriae	Adherence and colonization	
		sfa	S Frimbriae	Adherence and colonization	
		dra	Dr Frimbriae	Adherence and colonization	
		foc operon	F1C Fimbriae	Adherence and colonization	
		pap operon	Pap Pilli	Adherence and colonization	
		csg	Curli	Adhesion, Colonization, Biofilm formation	
		afa	Afimbrial Adhesins	Adherence and colonization	(Terlizzi et al., 2017)
		hlyA	α-hemolysin	Tissue damage (Pore formation), Dysfunction of the local immune response	
		cnf 1	Necrotizing cytotoxic factor 1	Renal invasion	
		iutA	Aerobactin	Iron acquisition	

(Continued)

TABLE 1 Continued

Virulence Genes Of Uropathogens					
S.No.	Pathogen	Genes	Protein Encoding	Function	Reference
2	*Proteus mirabilis*	*MR/P* operon	Mannose-resistant/Proteus-like Fimbriae	Adherence and colonization	(Oliveira et al., 2021; Hayder et al., 2020; Tabibian et al., 2008; Tabatabaei et al., 2021)
		uca	Uroepithelial cell adhesion fimbriae	Adherence and colonization	
		atf operon	ATF	Adherence and colonization	(Zunino, 2000)
		pmfACDEF	PMF/*Proteus Mirabilis* Fimbriae	Adherence and colonization	(Oliveira et al., 2021; Hayder et al., 2020; Tabibian et al., 2008; Tabatabaei et al., 2021)
		pmp	*Proteus mirabilis* P-like pili	Adherence and colonization	(Bijlsma et al., 1995)
		zapA	ZapA metalloprotease	Protease activity	(Oliveira et al., 2021; Tabatabaei et al., 2021; Hasan et al., 2021; Tabibian et al., 2008)
		hpm	Hemolysin	Toxin generates pores in the target membrane	(Oliveira et al., 2021; Hayder et al., 2020; Tabibian et al., 2008; Tabatabaei et al., 2021)
		pta	Proteus toxic agglutinin (pta)	Colonization	
		ureRDABCEFG	Urease	Hydrolyze urea to ammonia and Carbon dioxide	
3	*K. pneumoniae*	*fimBEAICDFGH* Operon	Mannose-sensitive type 1 pili	Adherence and colonization	(Wilksch et al., 2011; Sarshar et al., 2020)
		mrkABCDF Operon	Type 3 pilli	Adherence and colonization	
			Capsule	Anti- phagocytic Activity	
4	*P. aeruginosa*	-	Flagellin	Motility	(Allison et al., 1985)
		toxA	Exotoxin A	Tissue necrosis.	(Newman et al., 2017)
		exoS	exoenzyme S	Inhibit eukaryotic cell function	
		lasB	Elastase	Prteolytic Enzyme act on connective tissue	
		plcH	Phospholipase C	Hydrolyzes phospholipids.	
		-	Pyoverdine, pyochelin	Siderophores- acquire Iron	
5	*Enterococci* spp.	*ace*	Collagen-binding protein,	Collagen and laminin adhesin	(Haghi et al., 2019)
		PAI	Pathogenicity islands,	Virulence factor	
		asa1	Aggregation substance	Aggregation, adherence	
		sprE	Serine protease	Proteolytic activity	
		cylA	Cytolysin	Toxin that aids virulence	
		esp	Enterococcal surface protein	Function unidentified	(Toledo-Arana et al., 2001)
		gelE	Gelatinase	Peptide hydrolysis	(Haghi et al., 2019)
		hyl	Hyaluronidase	Tissue damage	(Golińska, 2013)
6	*Streptococcus* spp.	*uafA*	Uro-adhesion factor A	adherence to the epithelial cells of the human bladder	(Rafiee and Ghaemi, 2023) (de Paiva-Santos et al., 2018)
		aas	Hemagglutinin Aas	adherence and autolytic characteristics	
		ureACD	urease	development of urinary infectious stones and is necessary for the effective	(Xu et al., 2023)

(Continued)

TABLE 1 Continued

Virulence Genes Of Uropathogens					
S.No.	Pathogen	Genes	Protein Encoding	Function	Reference
				colonization of the kidneys and bladder.	
		*dsd*A	D-serine deaminase	survival in the bladder environment	
		pvl	Pantone Valentine leucocidin	Toxin	(Baba-Moussa et al., 2008)
		(fnbPA	fibronectin binding protein A	adherence	(Baba-Moussa et al., 2008; Goudarzi et al., 2019)
		clf	clumping factor	Adhesion to fibrinogen	
		ebp	elastin binding protein	Adhesion	
		lbp	laminin binding protein	Adhesion	
		(icaABCD	polysaccharide intercellular adhesion	adhesion	
		spa	staphylococcal protein A	biofilm formation	
		hla	hemolysin	osmotic cytolysis, cellular depolarization and the loss of vital molecules	(Aubais aljelehawy et al., 2021)
		mecA	PBP2A protein	bacterial cell wall formation) and resistance to some antibiotics	

The ORENUC classification system developed by the European Association of Urology classifies UTIs based on clinical presentation, risk factors (RFs), and severity. This system classifies adults with uncomplicated UTIs as O (no known/associated RF), R (recurrent UTI RF, but no risk of severe outcome), and occasionally E (extraurogenital RF, with risk of more severe outcome), while complicated UTIs are classified as N (nephropathic disease, with risk of more severe outcome), U (urological RF, with risk of more severe outcome, which can be resolved during therapy), and C (permanent urinary catheter and non-resolvable urological RF, with risk of more severe outcome) (Smelov et al., 2016; Tan and Chlebicki, 2016; Gama et al., 2020; Johansen et al., 2011). Based on the site of infection, UTIs can be classified into urethritis, cystitis, and pyelonephritis (Wagenlehner et al., 2020). Cystitis is an infection in the urinary bladder that can be classified as uncomplicated or complicated (Li and Leslie, 2023).

Pyelonephritis affects the kidneys, can be classified as both uncomplicated and complicated. Uncomplicated cases typically appear with few symptoms and are curable. Pregnant women, people who have had kidney transplants, uncontrolled diabetes, urinary anatomical anomalies, acute or chronic kidney failure, immunocompromised patients, and having acquired bacterial infections from hospitals are all at risk for complicated pyelonephritis (Venkatesh, 2017; Belyayeva and Jeong, 2023).

2.3 UTI risk factors: identifying contributors

A clinical examination, record history, and request for more preoperative tests are common procedures to check for any diseases or ongoing treatments that may raise the risk of infection (Marmor and Kerroumi, 2016). UTI classification involves risk variables as a fundamental component. Physicians can effectively modify preventative treatments to lower the likelihood of recurrence by thoroughly understanding the risk factors linked with recurrent UTIs (Storme et al., 2019) (Figure 1; Table 2).

2.3.1 Age and gender

Urinary tract infections affect people of all ages, and their frequency rises with advancing age in both genders (Bardsley, 2017; Ünsal et al., 2019). Boys experience the highest prevalence of UTIs in the initial three months after birth, and it is common in girls after 6 months of age, which then holds a steady trend until late childhood and adolescence (Ünsal et al., 2019). UTI occurrence declines in middle age but again rises in elderly persons (Rowe and Juthani-Mehta, 2013; Akhtar et al., 2021). Compared to men, women are more prone to lower UTIs due to the presence of the short urethra as well as the proximity of the urethral opening to the anus and vagina which are considered as the reservoirs of bacteria. Lower UTI usually manifests in men after 60 years due to prostate syndrome.

Age-related immune function changes (progressive T-cell dysregulation and general deterioration of mucosal immunity), urinary incontinence, impaired emptying with residual urine, urethral catheters and instrumentation, obstructive uropathy from prostatic disease in older men, declining estrogen levels, diabetes, kidney stones, and greater exposure to nosocomial and environmental pathogens may contribute to the persistence or recurrent UTI (rUTI)older people (Gavazzi and Krause, 2002; Bardsley, 2017; Hsiao et al., 2020; Martischang et al., 2021; Dutta et al., 2022).

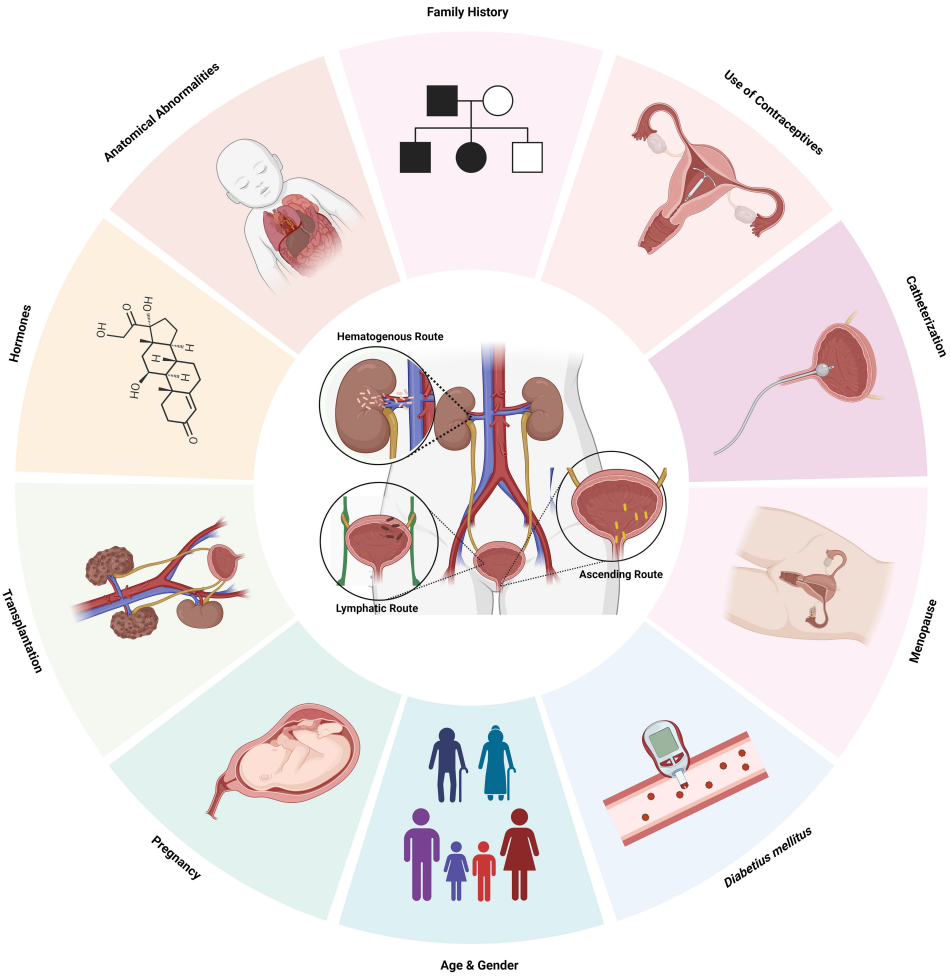

FIGURE 1
Risk Factors and routes of infection of UTI. *Created Using BioRender.com*.

TABLE 2 Risk Factors of UTI.

	Risk factors														
S. No	Types	Gender	Age	Diabetes	Menopause	Catheterization/Foreign Body	Frequent Sexual Intercourse	Use of Contraception	Family History	Anatomic Abnormalities	Antimicrobials/Antibiotic Use	Hormonal Changes	Transplantation	Pregnancy	Reference
1	Cystitis	+	+	+	+	+	+	+	+	+	+	+	+	+	(Schmiemann et al., 2010; Yoon et al., 2013)
2	Pyelonephritis	+	+	+	+	+	+	+	+	+	+	+	+	+	(Scholes et al., 2005; Bethel, 2012)

2.3.2 Diabetes mellitus

The risk of UTIs is correlated with more significant duration and severity of diabetes (Chen et al., 2009). Elevated levels of glucose in urine serve as a culture medium to encourage the growth of uropathogens and the decreased immune function, including humoral, cellular, and innate immunity, such as impaired migration, intracellular killing, phagocytosis, or chemotaxis in polymorphonuclear leukocytes (Chen et al., 2009; Wang et al., 2013; Saliba et al., 2015). Patients with type 2 diabetes have a higher incidence of all UTI types. In contrast to people without diabetes, patients with diabetes have lower amounts of IL-6 and IL-8 in their urine (Soo Park et al., 2006; Schneeberger et al., 2014; Saliba et al., 2015).

2.3.3 Menopause

UTI in premenopausal women and postmenopausal women have fundamentally different pathogenesis. *Lactobacillus* spp. colonize the healthy premenopausal vagina and maintain a protective vaginal microbiome, hindering the adherence of the uropathogens by the production of lactic acid from the glycogen produced by the vaginal epithelial cells. The women are vulnerable to developing both primary and rUTIs during menopause due to the drop in estrogen levels that thins the vaginal epithelium and reduces glycogen levels which indirectly increases the colonisation of pathogenic bacteria (Perrotta et al., 2008; John et al., 2016; Caretto et al., 2017; Jung and Brubaker, 2019).

2.3.4 Catheters/foreign body

Catheter-associated urinary tract infection accounts for 70–80% of infections because devices such as indwelling catheters act as the site of infection by introducing opportunistic organisms into the urinary tract at the junction of the catheter collecting tube or at the portal of the drainage bag (Nicolle, 2014). Insertion of the urinary catheter allows the organisms to ascend into the bladder and start to produce symptoms within 25-72 h due to the damage in the uroepithelial mucosa, which exposes new binding sites for bacterial adhesins and also interferes with the host mechanical defences such as incomplete voiding (Garibaldi et al., 1980; Hashmi et al., 2003; Jacobsen et al., 2008). Prolonged catheterization, disconnection of the catheter and drainage tube, and the absence of systemic antibiotic medication are all risk factors for catheter-associated urinary tract infections (John et al., 2016).

2.3.5 Contraceptive

The barrier methods of contraception are more predisposed to causing urinary tract infections than other types. Long-term complications can be avoided with health education on the hygienic and reliable use of family planning techniques (Fihn et al., 1985; Dienye and Gbeneol, 2011). The usage of contraceptives exacerbates the susceptibility of women to urinary tract infections due to the colonisation of the uropathogens in the vagina and periurethral area. Therefore, UTI among those who use barrier contraceptives may result from unhygienic conditions during condom application. The vaginal wall may be damaged by unlubricated condoms, leaving it open to infections. Additionally, it has been proposed that those who utilise barrier methods are susceptible to UTI as they encounter elevated vaginal fluid pH, changes to the normal vaginal flora, and greater rates of introital *E. coli* colonisation (Acton and O'Meara, 1997; Dienye and Gbeneol, 2011). The use of an IUD increases the risk of urinary tract infection, particularly in women who have rUTIs (Fallahian et al., 2005).

2.3.6 Chronicles of UTIs

Intraindividual variations in incidence and severity UTIs with intraindividual variations in incidence and severity are common among females with a genetic history due to the impact of several heritable genes which include *HSPA1B, CXCR1 and 2, TLR1,2,4,5, SIGIRR, TRIF, TRAM, MyD88 TIRAP, VEGF*, and *TGF-1* (Hagberg et al., 1985; Hopkins et al., 1999; Lundstedt et al., 2007; Zaffanello et al., 2010).

2.3.7 Structural or functional anomalies

Vesicoureteral reflux, which mainly affects children, impedes the flow of urine, and reduces the bladder emptying efficiency, which in turn serves as a medium for the uropathogen to adhere and multiply, thus causing an infection (Yuyun et al., 2004; Hickling et al., 2015; Kaufman et al., 2019). The study by Yuyun et al. found that, compared to males without urinary tract infections, men from Cameroon had a much higher prevalence of UTI due to anatomical and functional abnormalities (Yuyun et al., 2004). Ureteral obstruction caused by urinary calculi may serve as a surface for bacteria to attach to and proliferate, thus accounting for rUTIs (Hickling et al., 2015).

2.3.8 Transplantation

More than 75% of kidney transplant recipients acquire urinary tract infections. UTI lowers the quality of life associated with health and may affect transplant function, thereby lowering graft and patient survival. The risk of UTI is increased by recipient-related characteristics such as waiting time before transplantation, female gender, age, or a history of rUTI, diabetes mellitus, and urinary tract abnormalities or by organ factors such as re-transplantation, duplex ureters, and deceased donors and transplantation factors such as Foley catheters, ureteric catheters, transplant malfunction, and rejection. Additionally, the degree of immunosuppression correlates with the UTI (Giessing, 2012; Arabi et al., 2021).

2.3.9 Pregnancy

Pregnant women often experience urinary tract infections, especially pyelonephritis, that can be treated effectively in most cases. Women are more likely to acquire urinary tract infections due to alterations to the urinary system and immunologic changes during pregnancy. The ureter and renal calyces enlarge as a result of progesterone-related smooth muscle relaxation and ureteral compression from the gravid uterus, which are both physiological alterations of the urinary tract. Vesicoureteral reflux can be observed, and frequent urination is also caused due to decreased bladder capacity. Preterm labor, low birth weight, or systemic infection in the mother may be caused by pregnancy-related adaptive changes during UTI (Habak and Griggs, 2023).

3 Approaches for UTI detection

3.1 UTI biomarkers

A diagnostic biomarker validates the presence and severity of a disease and also helps to classify the disease, which helps in targeted diagnosis and treatment (Califf, 2018) (Figure 2).

3.1.1 Host- based biomarkers

Lipocalin 2, or Neutrophil gelatinase-associated lipocalin (NGAL), is a 25 kDa acute phase iron carrier protein, highly expressed by human monocytes/macrophages and neutrophils and acts as a modulator in the innate immune response along with the oxidative stress response by distinct cell types and epithelial development. The transcription is initiated due to the lipopolysaccharides, and it hinders the growth of the bacteria by inhibiting the siderophores. Under normal circumstances, the levels of NGAL in plasma(pNGAL) and urine (uNGAL) are low, but they quickly rise in response to cell injury, particularly in cases of gram-negative UTIs indicating it as a potential biomarker for UTI. pNGAL and uNGAL are released during systemic inflammation genitourinary epithelium infection, respectively, and the levels are correlated with the duration of infection; they may also be utilized for monitoring as they rise within 12 h and peak in 3 days. (Ichino et al., 2009; Horváth et al., 2020; Moon et al., 2021; Yamamoto et al., 2023) Acute pyelonephritis and UTI in children with fever can be distinguished using uNGAL, according to a study by Moon et al. Compared to the non-UTI individuals, the individuals with UTI had a higher uNGAL level (Moon et al., 2021). Urbschat et al., in their study with 97 individuals, concluded that NGAL can be used as a biomarker for UTI (Urbschat et al., 2014). Yilmaz et al. evaluated the ideal cutoff level for uNGAL to consider it as a biomarker for UTIs. ELISA technique was employed to quantify the uNGAL in 29 healthy controls and 60 UTI patients. With a 20 ng/ml limit for uNGAL, the sensitivity and specificity obtained were 97% and 76%, respectively (Yilmaz et al., 2009). In contrast, Lubell et al. identified the threshold uNGAL in newborns and children as 39.1 ng/ml with a sensitivity and specificity of 97.1% and 95.6%respectively (Lubell et al., 2017). Jagadesan et al. also validated that NGAL at a cutoff level of 27ng/mL, NGAL can be used as a biomarker with 79.4% and 68.2% sensitivity and specificity, respectively (Jagadesan et al., 2019). The study by Price et al. demonstrated the potential of urine NGAL as a biomarker for adult female UTI diagnosis. They reported that the women with UTI had greater urine NGAL levels than the control out of the 50 UTI patients and 50 control subjects that were included. NGAL showed 100% specificity and 98% sensitivity with a threshold of 23.9 ng/mL (Price et al., 2017).

YKL-40, also known as cartilage glycoprotein-39 or chitinase-3-like-1 (CHI3L1), is a member of the chitinase-like protein family found in mammals and is expressed by many different types of cells, including chondrocytes, fibroblasts, some cancer cells, and some primary immune cells like neutrophils and macrophages.YKL-40 has been linked to several biological processes, including extracellular matrix remodelling, fibrosis, angiogenesis, and inflammation, even though its exact functions are unknown. YKL-40 is produced locally in inflammatory sites and may serve as a site-specific inflammatory marker. On the other hand, not much information about the

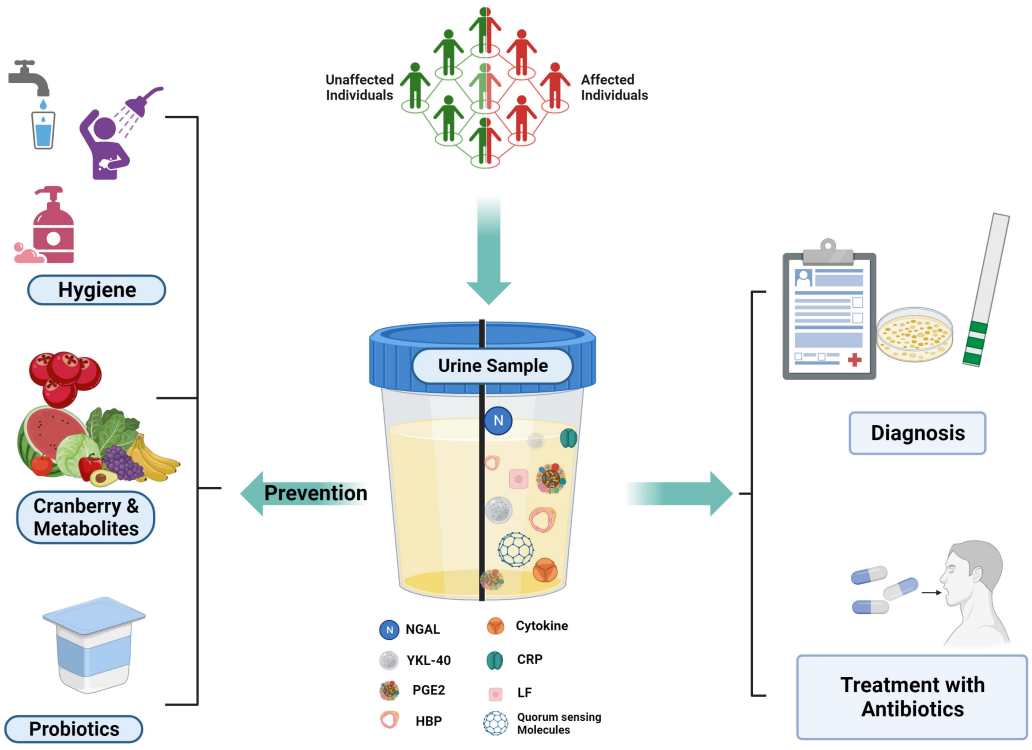

FIGURE 2
UTI Biomarkers and Prevention Strategies: Various host and pathogen markers for UTI Detection. *Created Using BioRender.com*.

connection between YKL-40 and UTI has been found (Kim et al., 2018; Mashaly et al., 2020). The study by Mashaly et al. compares the value of uYKL-40 to uNGAL in an attempt to evaluate it as a biomarker for UTI in children using ELISA. With a threshold value of 171.5 pg, 82% and 84% specificity and sensitivity, respectively, were obtained (Mashaly et al., 2020). Kim et al. used a sample size of 44 children with UTI and 35 children as controls to examine the association between fever and urinary tract infection in children. The concentration of YKL-40 in each sample was measured using ELISA. Urinary YKL-40/Cr levels were measured with a cut-off value of 125.23 pg mg^{-1} to detect UTIs. Of the nine children in the control group with pyuria, eight had levels less than 125.23 pg mg^{-1}, and the single child in the UTI group without pyuria or positive nitrite had a level more than 125.23 pg mg^{-1} (Kim et al., 2018). The inflammation caused by cyclooxygenase-2 (COX-2) makes rUTI more susceptible and converts arachidonic acid to Prostaglandin E2 (PGE2), eliciting different responses such as angiogenesis, inflammation, pain perception, and cell proliferation. PGE2 is secreted at higher levels when COX-2 expression is induced (Ebrahimzadeh et al., 2021). The study by Ganguly et al. shows that PGE2 is a useful biomarker for quick, label-free UTI testing in terms of both diagnosis and prognosis. The novel electrofluidic capacitor-based biosensor based on affinity capture by monoclonal PGE2 antibody can be employed in less than five minutes for small-volume urine samples and provide high accuracy at home for managing UTIs (Ganguly et al., 2022).

Human neutrophil is secretory and azurophilic granules secrete a heparin-binding protein (HBP), commonly known as azurocidin or cationic antimicrobial protein of 37 kDa (CAP37) causes vascular leakage, development of oedema, act as a chemoattractant and has a wide range of antibacterial activity. HBP is released when neutrophilic β2-integrins ligate resulting in vascular leakage. Research has demonstrated that it is elevated. HBP levels in plasma are present in patients with severe sepsis before the onset of hypotension (El-Refaey et al., 2020; Linder et al., 2010). The Kjolvmark et al. study showed that urine levels of heparin-binding protein produced from neutrophils can serve as a signal for pediatric UTIs with a sensitivity and specificity of 93.3% and 93.3%, respectively at a cut-off level of 32 ng mL^{-1} (Kjölvmark et al., 2012). Rafaey et al. concluded that urinary heparin-binding protein could be utilized as a reliable biomarker for the identification of UTI using ELISA in infants, and the sensitivity and specificity were confirmed as 72.2% and 81.2%, respectively, at a threshold level of 650 pg mL^{-1} (El-Refaey et al., 2020). Kjolmark et al. assessed adult U-HBP as a UTI marker and compared it to IL-6 urine levels and the dipstick test in two distinct healthcare settings. As a UTI marker, HBP in urine has a sensitivity of 89.2% and a specificity of 89.8%, respectively, and was superior at differentiating between cystitis and pyelonephritis (Kjölvmark et al., 2014).

Small soluble peptides called cytokines are produced by macrophages, glomerular endothelial cells, and intestinal epithelial cells in the presence of uropathogenic bacteria causing inflammatory reactions. Mononuclear phagocytes release IL-1, which comes in two forms and serves as the initial cytokine in the antigen recognition immunological cascade accounting for acute-phase reactions and fever development. Multifunctional cytokine IL-6 controls several bodily processes, including inflammation, organ development, and the acute phase response. Hepatocytes, podocytes, T-helper cells, neutrophils, and macrophages all express the IL-6 receptor. TNF-α, IL-1, and IL-2 cause macrophages to release the IL-8, which attracts the neutrophils. IL-6 and IL-8 are present in trace amounts in a healthy individual and are assumed to be biomarkers of urinary tract infections and to be indicative of the infection site (Al Rushood et al., 2020; Gedikbaşı et al., 2020). A study by Gedikbaşı et al. demonstrated using ELISA that the amount of IL-1β in urine could serve as a reliable marker for urinary tract infections. With a threshold value of 6.11 pg mL^{-1}, the sensitivity and specificity were 100% and 93.1%, respectively, IL-1β was expressed at a higher concentration in UTI patients compared to controls (Gedikbaşı et al., 2020). Using eighty serum samples and seventy-two urine samples taken from children with urinary tract infections, Abed et al. demonstrated that IL-8 is a good biomarker for urinary tract infection, while IL-6 is not. Their findings demonstrated that there was a considerable increase in IL-8 concentrations in both the serum and urine during UTI as compared to the control (abed et al., 2021).

In contrast, Abdelaal et al. demonstrated IL-6 as a UTI biomarker. The results of the study showed that patients with UTIs had considerably higher urinary IL-6 levels than the control group. The optimal cut-off value was 17 pg mL^{-1}, with a sensitivity, specificity, and diagnostic accuracy of 94.4%, 92.1%, and 92.8%, respectively. Furthermore, they showed that urine IL-6 levels were positively correlated with leukocyte count, fever, CRP, and that urinary IL-6 levels were significantly higher in instances of acute pyelonephritis APN compared to milder UTI cases (Abdelaal et al., 2019). According to the study conducted by Mazaheri et al, IL-6 and IL-8 are both sensitive biomarkers of UTI that can distinguish between lower urinary tract infections and acute pyelonephritis (Mazaheri, 2021). Acute-phase inflammatory protein (CRP) produced by the hepatocytes under the influence of IL-6 is homopentamer and shows upregulated expression during inflammatory disorders, rheumatoid arthritis, and cardiovascular illnesses. CRP levels are 0.3–0.6 mg dL^{-1} in healthy people, and due to the infection, the serum concentrations surpass 5 mg L^{-1} within approximately 6 h and peak at 48 h, which has a half-life of roughly 19 h (Agrawal et al., 2013; Narayan Swamy et al., 2022; Tang and Zhou, 2022).

The function of blood C-reactive protein levels in upper and lower urinary tract infections in adult patients was investigated by Agarwal et al. They discovered that the upper urinary tract infection cases had a mean C-reactive protein value of 127.33 mg L^{-1}, which is statistically substantially higher than the control (Mamatha, 2020). The majority of upper UTI patients diagnosed with acute pyelonephritis had CRP values >100 mg L^{-1}, and lower UTI patients diagnosed with cystitis had CRP levels between 3 and 50 mg L^{-1}, according to a study by Narayan Swamy et al (Narayan Swamy et al., 2022).

Lactoferrin, belonging to the transferrin family and a component of the innate immune system, is a single polypeptide chain glycoprotein that binds iron and has a molecular weight of about 78 kDa. Initially isolated from human breast milk and later it was discovered in bodily fluids such as saliva, tears, bile, pancreatic juice, and intestinal fluid. Being the initial line of defence against pathogens that enter through mucosal tissues, it is crucial in the identification of several clinical

conditions, including Parkinson, inflammatory bowel disease (IBD), Alzheimer's, and UTI (Fatah et al., 2016; Naseri et al., 2021).

The LF concentrations in the urine of 88 patient samples and 121 normal samples were measured using an ELISA in a study by Arao et al. The lactoferrin concentration in the UTI samples and healthy individuals was 3,300.0 ± 646.3 ng mL^{-1} and 30.4 ± 2.7 ng mL^{-1} respectively. With the threshold of 200 ng mL^{-1}, the efficacy of the immunochromatography was measured and the sensitivity, specificity, positive, negative predictive values were found to be 93.3, 89.3, 86.2, and 94.9%, respectively (Arao et al., 1999). In a study by Fatah et al., the urine samples of the control had a concentration of 670 ± 319 ng mL^{-1} while it was 1387 ± 509 ng/ml during the infection and 885 ± 268 ng mL^{-1} after two months indicating higher concentrations during the infection and the significantly lower concentrations following two months (Fatah et al., 2016).

To detect lactoferrin, Naseri et al. developed an electrochemical biosensor with a broad linear range of 10 to 1300 ng mL^{-1}, a LOD of 0.9 ng mL^{-1}, high selectivity, and reproducibility (Naseri et al., 2021).

Numerous disorders (chronic, metabolic, or malignant disease, recurrent infections, etc.) constantly affect the immune system and can have an impact on biomarker expression for UTI. Urine testing for volatile organic chemicals or bacterial metabolites should be preferred (Horváth et al., 2020). Trimethylamine (TMA), acetate, and xanthine oxidase (XO) were shown to be potential markers in the review by Karlsen et al. Trimethyl quaternary amines ($N(CH_3)_3$)) are dietary sources of a volatile tertiary amine with a "shy odour" absorbed by the gut bacteria through the stomach walls and transferred to the liver, where it is converted by the avin-containing monooxygenase (FMO) enzyme into the odourless trimethylamine-N-oxide (TMAO), finally expelled through urine. In healthy individuals, TMA is nearly entirely transformed into TMAO, with a urinary TMAO excretion rate of up to 60 mg per day (Karlsen and Dong, 2015). The study by Lam et al. revealed that trimethylamine, a human-microbial marker associated with *E. coli*, established a threshold of 0.0117mmol with 97.0% specificity and 66.7% sensitivity (Lam et al., 2015). At physiological pH, acetic acid mostly occurs as the conjugate carboxylate base acetate with a pKa of 4.76, and the concentrations are high in the majority of the infections. Gupta et al. identified acetate, lactate, succinate, and formate as markers capable of discriminating between UTI patients and healthy controls with high sensitivity and specificity.

3.1.2 Pathogen-based biomarkers

Small chemicals termed autoinducers diffuse into the environment, accumulate during the growth of the microbial population, and reach a certain threshold to mediate the cell-to-cell signalling system known as quorum sensing (QS) and attach to cytoplasmic or membrane-bound transcription factors to initiate gene expression and release additional signalling molecules. Clinical professionals can diagnose a disease if these signalling molecules are quickly detected and help curb the spread of antibiotic-resistant bacteria (Stapleton et al., 2011; Miller and Gilmore, 2020) (Table 3). Low molecular weight acyl-homoserine lactones (HSLs) and autoinducing peptides are secreted either passively or actively by Gram-negative and Gram-positive bacteria, respectively. HSLs are neutral lipid molecules that have a lactone ring with variable side chains of carbon, indicating the hydrophobicity of the compound (Miller and Gilmore, 2020). Among *P. aeruginosa* uroisolates, there were variations in the types and quantities of AHL generated. In these strains, several AHLs, C4-HSL, C6-HSL, oxo-C6-HSL, C8-HSL, C10-HSL, and C12-HSL families were identified (R. Kumar et al., 2011). N-octanoyl homoserine lactone and N-3-dodecanoyl-l-homoserine lactone are produced by *K.pneumoniae* isolates from human tongues (Miller and Gilmore, 2020). Montagut et al. produced antibodies directed against 2-heptyl-4-quinolone (HHQ), a signalling molecule from *P.aeruginosa* PQS QS system that is crucial for the synthesis of virulence components and the creation of biofilms. The ELISA that was developed has a LOD of 0.34 ± 0.13 nM (Montagut et al., 2020). To detect the quorum-sensing signalling molecules of gram-negative bacteria, N-acyl-homoserine lactones (AHLs), Sahana et al. developed a PL-based biosensor using ZnO nanoparticles functionalized with cysteamine (S. Vasudevan et al., 2020).

3.2 Diagnostic methods for UTIs

The term "diagnosis" has been defined as a classification scheme used by the medical community to group specific diseases that are pathological that aid in establishing a social order that identifies and diagnoses the disease promptly in healthcare and the pharmaceutical sector, suggesting the best course of treatment, and forecasting the results (Jutel, 2009; Chua et al., 2011; Balogh et al., 2015; Kumar et al., 2016). Even a slight delay enhances the risk of morbidity and mortality, necessitating early treatment that depends on rapid detection. (Arinzon et al., 2009; Fazly Bazzaz et al., 2021) The ideal test should be affordable, rapid, and accurate in the diagnosis of high-risk individuals. However, the diagnosis of UTI is challenging as the signs and symptoms can overlap with the risk factors (Mambatta et al., 2015) (Figure 3).

3.2.1 Urinalysis

An easy-to-use, quick, and cheap screening technique is urine analysis, which includes physical, chemical, and microscopic investigation (Mambatta et al., 2015) (Figure 4).

3.2.1.1 Dipstick analysis

Dipstick urinalysis is the first step in urine testing that checks the presence of leukocyte esterase (LE), nitrite, and red blood cells based on symptoms and other characteristics shown by the patient (Chu and Lowder, 2018). Leukocytes, which are elevated in urine during UTI, express LE with a threshold limit for the detection of 5-15 WBC/high-power fields. The LE in the sample interacts and hydrolyses the ester substrates in the dipstick, turning it blue (Mambatta et al., 2015; Chu and Lowder, 2018). The presence of nitrite in urine is typically undetectable, but if the bladder holds the dietary nitrates in the urine for more than four hours, bacteria get sufficient time to reduce them to nitrite and the threshold value being 0.1 g/ml for the test to be positive indicated by a colour change in the strip (Andriole, 1987; Mambatta et al., 2015). The hematuria dipstick test is a screening test for UTI indicated by a

TABLE 3 Various quorum sensing molecules used for diagnosis of different diseases.

S.No.	Probable QS system that can be used	Detection technique	Sample collection	LOD	Merits	References
1	Pyocyanin	Polyaniline/Au nanostructures modified ITO electrochemical sensor	Clinical samples	500 nM	• Fast • precise	(Elkhawaga et al., 2019)
		Silver nanorod array based SERS	Sputum samples	2.38 x 10^{-8} mol L^{-1}	• Multiple specimen • rapid	(Wu et al., 2014)
		Gold coated zein film SERS	Drinking water	25 μM	• Biodegradable	(Jia et al., 2019)
		ELISA immunochemical method	Sputum samples.	0.60 ± 0.01 nM	• Robust • reproducible • Multiple samples	(Pastells et al., 2016)
		Carbon fibre electrochemical sensor	–	0.030 μM	• Reagent free • Rapid • inexpensive consumables • performed by non-specialists	(Sharp et al., 2010)
		3D redox capacitor electrochemical sensors	Sputum	50 nM	• High sensitivity	(Kang et al., 2021)
			Wound fluid	100 nM		
			Urine	5 nM		
2	HQNO	Immunochemical approach	Clinical samples	0.60 ± 0.13 nM	• Fast • precise	(Montagut et al., 2022)
3	2-Heptyl-4-quinolone	Elisa immunochemical method	Sputum specimens	0.34 ± 0.13 nM	• Robust • Reproducible • specific	(Montagut et al., 2020)
4	4-hydroxy-2-heptylquinoline	Electrochemical method	Sputum	1.2 μM	• Low cost • easy to use instrumentation	(Burgoyne et al., 2020)
5	2-heptyl-3,4-dihydroxyquinoline	Electrochemical method	Sputum	1.1 μM	• Low cost • easy to use instrumentation	(Burgoyne et al., 2020)
6	2-heptyl-3-hydroxy-4-quinolone (PQS), and	Boron-doped diamond based electroanalysis	Sputum samples	0.15 μM	• Wide potential range • high current density • electrochemical stability • low background current • high resistance to fouling	(Buzid et al., 2016)
	2-heptyl-4-hydroxyquinoline (HHQ)			0.62 μM		
	pyocyanin			1.25 μM		
7	Quinolone	Elisa immunochemical approach	Sputum samples	0.36 ± 0.14 nM	• Robust • accurate	(Montagut et al., 2021)

(Continued)

10.3389/fcimb.2024.1402941

TABLE 3 Continued

S.No.	Probable QS system that can be used	Detection technique	Sample collection	LOD	Merits	References
8	1-hydroxyphenazine	ELISA immunochemical method	Sputum samples.	0.60 ± 0.01 nM	• Robust • Reproducible • Multiple sample detection	(Pastells et al., 2016)
9	3-oxo-C12-HSL	DNA-encoded biosensor	Sputum samples	1.56 nM	• Rapid • low-cost detection assays	(Wen et al., 2017)
10	AHL	Genetically engineered whole-cell sensing systems	Saliva samples	–	• minimal or no sample preparation • provide information regarding the bioavailability of the analyte.	(Kumari et al., 2008)
11	N-(3-oxo)-dodecanoyl-L-homoserine lactone	Electrochemical biosensor	Spiked saliva	2 pM	• High reproducibility • minimal sample preparation • rapid	(Baldrich et al., 2011)

colour change for a positive result due to the oxidation of a test-strip reagent. However, the microscopic analysis needs to be conducted for verification (Mambatta et al., 2015).

The purpose of a study by Mambatta et al. was to assess the sensitivity of urine dipstick analysis utilizing the Multistix 10 SG (Siemens) and Clinitek Advantus Analyzer. The sensitivity of nitrite, leukocyte esterase, and blood alone was found to be 23.31%, 48.5%, and 63.94%, respectively. When nitrite, leukocytes, and blood were taken into account collectively, the sensitivity turned out to be at its highest. They concluded that the nitrite test and LE test had low sensitivity and could not rule out UTIs in patients, and a urine culture needs to be performed for suspected patients with UTIs as the results of the Dipstick are unreliable in a few cases (Mambatta et al., 2015). Nitrite and red blood cell testing yield the results after one minute, and LE needs two minutes for the outcome. The interpretation of a dipstick urinalysis might be affected by several conditions.

3.2.1.2 Microscopic examination

Nephrologists frequently use the diagnostic technique of urinary microscopy by direct or indirect examination of the centrifuged or uncentrifuged samples (Fogazzi et al., 1998). The procedure for the staining of an uncentrifuged sample is simple in which a small amount of urine is placed on a glass microscope slide, let to air dry, stained with gram stain, and then studied under a microscope (Wilson and Gaido, 2004). To diagnose UTIs brought by *bacilli* spp., including *cocci*, the study by Hiraoka et al. evaluated the value of microscopic examination of 172 unspun urine samples using a disposable slide with counting chambers. The approach indicated bacteriuria with 94% and 88% accuracy, respectively. Pyuria had a 79% and 71% sensitivity and specificity, respectively (Hiraoka et al., 1993). Similar research revealed that the sensitivity and specificity for 89 urine samples were 91 and 98%, respectively. Both studies stated that the microscopic examination of urine on disposable counting chambers was quick and simple to do without the need to set up or clean the chambers—reliable, affordable, and time-efficient (Hiraoka et al., 1995).

An alternative quick test for the intended purpose that is often used in Danish general practice is point of care (POC) microscopy. The clinician may determine the number of bacteria seen per field of vision, ascertain the morphology of the organisms (rods or cocci), and describe their type of motility (non-motility, polar or nonpolar motility) using POC microscopy using either a conventional light microscope or a phase-contrast microscope. The benefit of phase-contrast microscopy is that the specimen does not need to be stained. To prevent overdiagnosis, immersion oil and phase contrast microscopy, which showed high clinical accuracy and specificity, may be helpful as a follow-up test for urine dipstick (Beyer et al., 2019). Pyuria can be identified and quantified microscopically utilizing the urinary leukocyte excretion rate, counting leukocytes either by haemocytometer or by Gram staining or in the centrifuged sample. The ability to see leukocytes, leukocyte casts, and other cellular components up close is a benefit of urine microscopy. Leukocytes quickly degrade in urine that is not fresh, or that has not been properly preserved, which is a drawback of urine microscopy. Urinary leukocyte

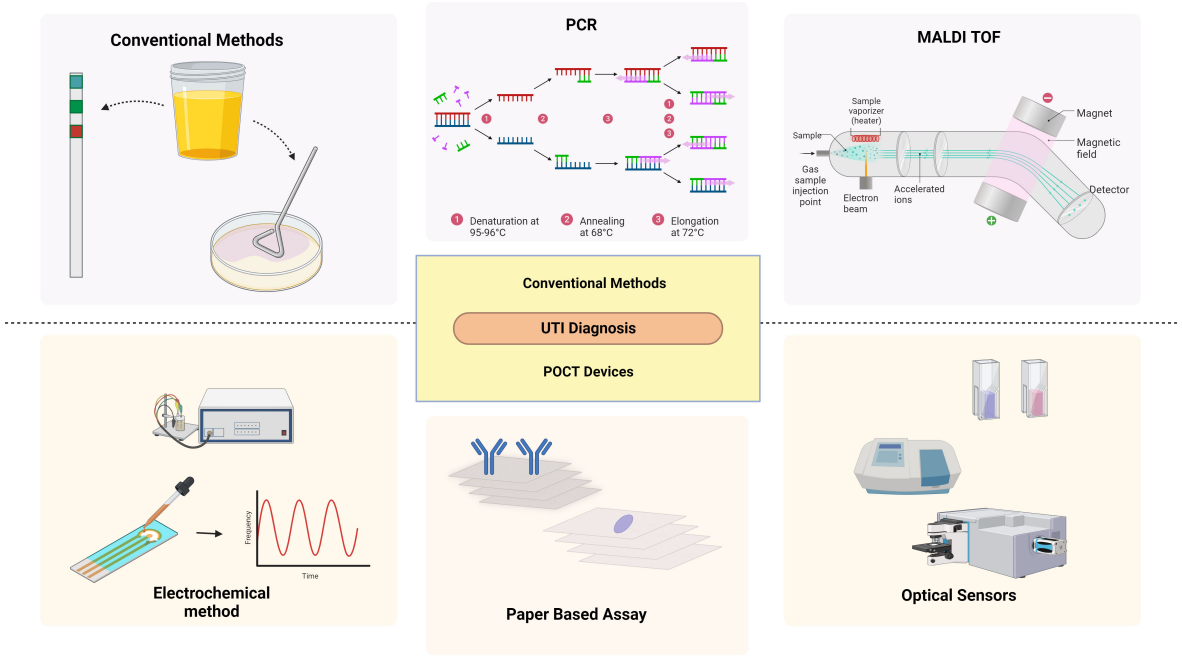

FIGURE 3
Diagnostic methods of UTI: Conventional and emerging methods. *Created Using BioRender.com*.

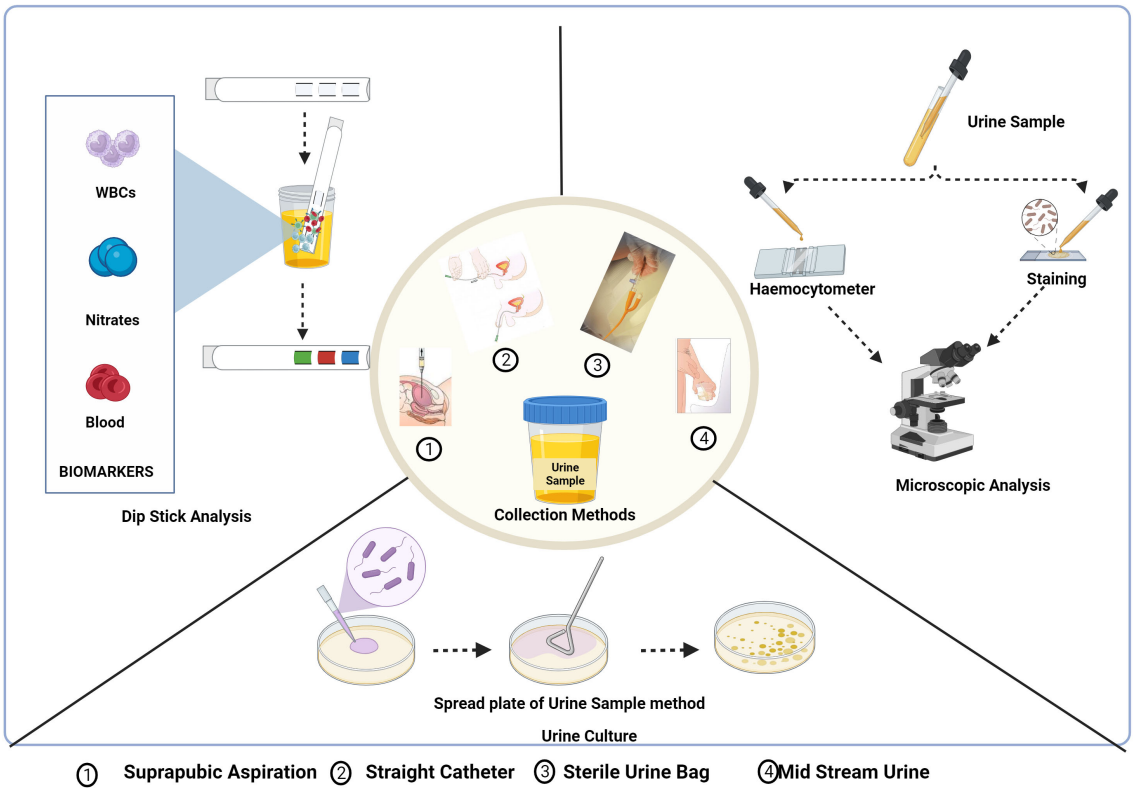

FIGURE 4
Urine collection methods and conventional diagnostic methods of UTI: Dipstick analysis, Microscopic analysis and urine culture test. *Created Using BioRender.com*.

excretion rates in patients with symptomatic UTIs are 400,000 leukocytes/h (Wilson and Gaido, 2004).

3.2.1.3 Urine culture and sensitivity

For urine culture, suprapubic aspiration, straight catheter technique, and mid-stream catch are the different collection methods that are influenced by the comfort of the patient, the capacity to void, and lowering the risk of iatrogenic infection. The most effective technique to prevent specimen contamination is to collect samples by suprapubical method. With the use of ultrasonography, a needle attached to a syringe is introduced through the lower abdomen into the bladder to collect the urine sample (Karacan et al., 2010). This procedure is rarely used as it is invasive, uncomfortable for the patient, and resources are utilized inappropriately. The next most suitable method is urine collection using a single catheter (straight catheter approach). However, this approach is rarely performed and only when necessary due to the labour intensiveness and probable risk of introducing bacteria into the bladder, which could potentially result in a UTI. A clean-catch midstream technique, which is neither intrusive nor painful, is the most typical way to obtain a urine sample for urine culture. The possible drawback of this method is that the sample can get contaminated with the commensal residing in the distal urethra. So, collecting midstream urine is recommended (Wilson and Gaido, 2004; Sinawe and Casadesus, 2023).

The test results are based on the urine collection method as well as its processing. The test requisition slip should include the date, time, and method of specimen collection, patient demographic information, and details regarding antimicrobial therapy, anatomic abnormalities, or indwelling urinary catheters. The Urine sample needs to be tested within 2 h of collection or should be refrigerated or preserved using a boric acid solution and is generally cultured in Blood agar, and MacConkey's agar media is incubated at 37°C for 24-48 h. Patient-related factors, such as the use of antibiotics or diuretics, reduce the presence of pathogens, leading to false results. Additionally, improper collection or handling of the specimen also affects the test results (Wilson and Gaido, 2004; Sinawe and Casadesus, 2023).

Suprapubic aspiration had the lowest contamination rate, while sterile urine bags had the highest, according to a study done to assess the reliability of the four urine sample collection techniques among children suspected of having urinary tract infections. Urine culture costs increased due to the necessity to repeat procedures on contaminated specimens (Karacan et al., 2010). In another study, the non-invasive method, the clean-catch urine stimulation approach was employed to collect urine from infants younger than three years of age for the diagnosis of UTI. Urinary catheterization has a reduced but comparable contamination rate to clean-catch urine stimulation (Herreros et al., 2021).

3.2.2 Imaging studies

Imaging can help make a diagnosis of UTI in newborns and infants as it is crucial when clinical and laboratory results are ambiguous or when atypical or vague clinical symptoms are present. The abnormalities elevate the risk for challenging treatment and long-term complications. Additionally, imaging aids in the detection of serious conditions, such as lobar nephronia, granulomatous pyelonephritis, pyonephrosis, necrosis/necrotizing pyelonephritis, and track the progression of the deformity in children who have had severe UTIs or malformations of the urinary system that are related to UTIs (Bjerklund Johansen, 2004; Riccabona, 2016). The most frequently used technique, named ultrasonography, is a non-invasive, adaptable, and affordable treatment that uses high-frequency sound waves to acquire real-time images of the area being scanned and allows the detection of urinary tract dilations and irregularities. Ultrasonography is prone to the appearance of artefacts caused by abnormal interactions between sound waves and tissues or air-filled cavities, which result in inaccurate reconstructions of their anatomical structures because it relies on the creation of images from rapid analysis and interpretation of data acquired by a transducer. The majority of these distortions are caused by abnormal interactions between sound waves and tissues or air-filled cavities, which result in inaccurate reconstructions of their anatomical structures.

3.2.3 Molecular diagnostic methods

3.2.3.1 Polymerase chain reaction

Molecular diagnostic techniques based on Polymerase Chain Reaction (PCR) are extensively employed in clinical laboratories and physician offices globally, leading to better medical treatment and patient outcomes for a variety of illnesses (Kelly, 2023). Wojno et al. assessed the use of multiplex PCR-based molecular testing to identify bacterial infections in 582 patients who exhibited symptoms. In 74% of cases, there was agreement between PCR and culture; in 34% of cases, both were positive, and in 40% of cases, both were negative. But in 26% of cases, there was a discrepancy between PCR and culture: in 22% of cases, PCR was positive, but culture was negative, and in 4% of cases, PCR was positive but culture was negative. They concluded that urine culture and multiplex PCR are equally effective at identifying and detecting bacteria (Wojno et al., 2020).

By employing 82 urine samples and a commercial real-time PCR blood pathogen test (SeptiFast®), Lehmann et al. assessed the viability of qualitative urine pathogen detection and compared the results with dipslide and microbiological culture. They discovered that the results of SeptiFast® pathogen identifications were available 43 h prior to that of the culture results, and 67 samples were dip slide culture positive while 61 samples tested positive for SeptiFast® indicating the test has a sensitivity and specificity of 0.82 and 0.60, respectively, for identifying infections (Lehmann et al., 2011).

The study by Hansen et al. demonstrated a real-time PCR technique for UTI diagnosis and uropathogen identification in 330 urine samples had a sensitivity and specificity of 97% and 80%, respectively. They concluded that this method could differentiate between bacteriuria and the absence of bacteriuria, identify the uropathogen implicated within 4 h of sampling, enable appropriate medication decisions to be made the same day, and significantly reduce the need for subsequent urine cultures (Hansen et al., 2013).

3.2.3.2 Mass spectroscopy

For the past few decades, mass spectrometry (MS) -based techniques—particularly matrix-assisted laser desorption ionization

time-of-flight mass spectrometry, or MALDI-TOF MS—have been effectively applied to routine clinical pathogen characterisation, including UTIs (Svetličić et al., 2022). Mass spectrometry involves ionizing chemical compounds into charged molecules by the addition or removal of one or more protons and measuring the mass-to-charge ratio (m/z) (Singhal et al., 2015). Ferreira et al. verified the MALDI-TOF using 206 samples by initially centrifuging the material at a low rpm and then at a higher rpm to exclude leukocytes and collect bacteria, respectively. In 94.2%, MALDI-TOF MS detected this microbe directly from the urine sample, indicating direct bacterial identification is possible in a short amount of time and with a high degree of accuracy, particularly when high concentrations of Gram-negative bacteria are present (Ferreira et al., 2010). Liu et al. showed that MALDI TOF can reduce the identification time (minimum 0.5 h) and AST (minimum 4 h) of the primary pathogens of UTI to 5–10 h. This significantly reduces inspection time and significantly aids in the timely diagnosis and treatment of UTI patients (Liu et al., 2022). The findings of a study by Oros et al. highlighted the critical role that sample preparation and storage conditions play in influencing the dependability of MS data analysis, and they suggest that it has great potential as a dependable high-throughput tool for microbial pathogen identification in human urine samples (Oros et al., 2020). Traditional methods for UTI diagnosis have their limitations, as shown in Table 4. Recognizing the importance of rapid and accurate diagnosis, new methods are emerging that aid in improving patient outcomes.

3.3 Emerging trends in UTI diagnosis

The term point of care testing (POCT) is used to describe tests that are carried out near the patient rather than at a central laboratory, which reduces the detection turnaround time (St-Louis, 2000; Luppa et al., 2011; Shaw, 2016). Point-of-care diagnostic devices are adopted by healthcare professionals, patients, and their families for their user-friendly features (Konwar and Borse, 2020). The POCT Device was first introduced in 1962 to rapidly analyse blood glucose levels, and later, in 1977, rapid pregnancy test kits were developed, which led to the development of a trend for personalised diagnostics. The use of POC diagnostics to cover a wide range of conditions promises benefits and helps improve the health status of a wide range of the population in a developing country like India, which is resource-constrained in terms of healthcare developments and advances (Clark and Lyons, 1962; Yetisen et al., 2013; Konwar and Borse, 2020). POC tests, which are quick, affordable, and suitable for remote locations, should replace the traditional expensive lab-based diagnostic approaches, and the devices need to follow the ASSURED criteria that include affordable, sensitive, specific, user-friendly, rapid and robust, equipment-free, and deliverable (Garcia et al., 2015; Konwar and Borse, 2020; Naseri et al., 2022) (Table 5).

3.3.1 New approaches for point of care devices

3.3.1.1 Paper-based assay

In the study conducted by Muljadi et al., the practicality of the MTT-PMS test strips was evaluated using *E.coli* as depicted in Figure 5A. The latter has a system of dehydrogenases capable of converting MTT to MTT-Formazan. The test strips were prepared by attaching the Whatman Fusion 5™ paper test pad to the MTT-PMS coated paper and then immersing it in a diagnostic reagent for five minutes, and storing it after drying it in the dark for 24 h. The assay was based on the colorimetric method, which involved dipping the strips for two minutes in the pretreated sample, letting it dry for twenty minutes, and recording the colorimetric data using a smartphone application, ColourPicker. They observed that the MTT-PMS strips could be used to differentiate the quantities of bacteria in a sample, and the correlation was calculated to be 98%. The strips might be employed as a quick and practical early alternative bacterium screening technique for a range of purposes (Muljadi et al., 2021). Wang et al. developed a turntable paper device consisting of three layers of paper, a wooden chopstick rotation axis in the centre, and an acrylic base at the bottom as depicted in Figure 5B. Blotting paper, Whatman® Grade 3 filter paper and Whatman® Grade 1 filter paper, respectively, comprised the first, second, and third layers. The filter paper in layer 2 in a rectangular shape is rotatable and was wax printed with a circular reactive zone. Six hydrophobic test zone sections were wax printed onto circular layer 3 and were fixed with pins. After loading a bacterial suspension onto the second layer of paper, it was given an hour to dry. Following the device assembly, reagents were gradually added to the third test zone, and the axis was adjusted to position the sample zone beneath the layer 3 reaction zone. Ultimately, after 2 minutes, the generated colorimetric reaction was captured on camera, and the images were analysed to determine the intensity of colour which correlated with the log scale of the bacterial cell concentrations (Y.-C. Wang et al., 2021).

A smartphone-integrated paper (SIP)- a device based on rapid on-site UTI screening- was proposed by Janev et al. as depicted in Figure 5C. A filtration system to separate the target cells WBCs from the heterogeneous components in the urine sample comprised of three layers of paper with various pore sizes. The sodium fluorescein dye in Layer 1 stains to the WBCs in the urine sample and is gathered in Layer 2 while the smaller cells are passed to Layer 3. Subsequently, the filter device is disassembled to acquire layer 2, and it is then positioned beneath a fluorescent microscope integrated with a smartphone. This microscope uses the rear lens of the smartphone to capture the fluorescence images of the WBCs, and the UTI is quantified by the processing of the image with a sensitivity and specificity of 96.67% and 100%, respectively. The use of smartphones enables to instantly share the collected data with the medical staff for real-time UTI patient monitoring and diagnosis and the whole detection process can be accomplished in less than ten minutes, which enables quick and precise UTI screening (Janev et al., 2023).

The study by Noiphung et al. was set out to develop a low-cost, portable paper-based analytical device (PAD) that quickly tests the presence of nitrite and simultaneously cultivates bacteria *in situ* as depicted in Figure 5D. A cotton sheet on top of Whatman No. 1 filter paper that had been wax-printed with a pattern to support the bacterial growth. The Griess reaction was utilized to sense nitrate, and X-GlcA, which was aliquoted into each PAD's growth area, served as a substrate for the identification of bacteria. It was determined that the linear detection range of nitrate was 0–1.6 mg/dL. *E.coli* produces a β-glucuronidase enzyme that converts

TABLE 4 Conventional Techniques and demerits.

Sl.No.	Method Of Detection	Probable Biomarker	Demerits of the Detection Method	References
1	Dip stick analysis	Nitrate	False negative results due to • diluted sample • presence of *Streptococcus* spp.	(Chu and Lowder, 2018)
		Leukocyte esterase	False negative results due to • Contamination of Urine sample • Consumption of Antibiotics • technical error	(Wilson and Gaido, 2004; Mambatta et al., 2015)
		RBCs	false-positive result due to • hemoglobinuria, • myoglobinuria, • menstrual blood, • concentrated urine, • vigorous exercise • presence of oxidising agents like hypochlorite and povidone, • exposure to air • the pH of the urine is less than 5.1	(Bacârea et al., 2021)
2	Microscopic Examination	Bacteria	Outcome affected by • proper patient guidance, • appropriate urine collection and handling, • adequate microscopic equipment	(Wilson and Gaido, 2004)
3	Urine Culture	Bacteria	• Contamination of urine sample, • Handling of Sample	(Wilson and Gaido, 2004)
4	Imaging Techniques		Lack of high quality images due to • patient's characteristics, • morbid obesity, • the presence of gas in the intestine, • lesions, and abnormalities	(Bjerklund Johansen, 2004; Riccabona, 2016)
5	PCR	Bacteria	• Preparation of Primers • Expensive • Skilled Personnel required	Yang and Rothman, 2004)
6	MALDI -TOF	Bacteria	Poor species discrimination due to • inherent similarities between organisms • misidentification due to a small number of spectra in the database	(Rychert, 2019)

colourless X-GlcA substrate into blue colour. In 6 h, under ideal circumstances, the suggested apparatus could quantify bacterial concentrations in the range of 10^4–10^7 CFU/mL (Noiphung and Laiwattanapaisal, 2019).

A paper-based ELISA point-of-care diagnostic tool was developed by Shih et al. to quickly identify *E.coli* as depicted in Figure 5E. This involved adding the sample to the paper surface, letting it dry for an hour, and then blocking it with BSA. After 30 minutes each, horseradish peroxidase (HRP)-conjugated streptavidin and anti-*E. coli* biotin conjugate antibodies were added such that they conjugate with the sample. Following the addition of the substrate solution, the colorimetric findings were captured using a smartphone after two minutes. In just five h, the paper-based colorimetric platform could identify *E. coli* contamination. The average colour intensity on this platform is 0.1187 ± 0.002 for samples containing 10^5 cells/mL and 0.01457 ± 0.003 for samples that are not contaminated (Shih et al., 2015). Adrover-Jaume et al. developed a portable origami cellulose immuno biosensor that can identify *E. coli*-caused UTIs at the bedside in less than seven minutes as depicted in Figure 5F. The device consists of a single piece of paper folded in an easy origami pattern and loaded with nanoparticles functionalized with antibodies. After the application of the urine sample in the paper in a reservoir containing polystyrene sulfonate (PSS), it is allowed to dry. The paper is then folded such that the nanoparticles are moved to the detection area and bind to the *E.coli*, causing coloured spots to appear on the paper strip due to the localized surface plasmon resonance (LSPR) of the gold nanoparticles at 531nm. The biospecific identification of the pathogen by the antibody is correlated with the pixel intensity of the spot measured using a smartphone app that operates in real time. They concluded that the assays exhibited high specificity and selectivity with other prevalent uropathogens as evidenced by the single false negative result they produced when tested using a panel of 57 patient urine samples (Adrover-Jaume et al., 2020).

3.3.1.2 Electrochemical sensors

The study by Ganguly et al. showed the quantification of urine prostaglandin E2 (PGE2) for UTI diagnosis using a lateral flow-based electrochemical biosensor, as shown in Figure 6A. The

TABLE 5 Commercially Available UTI Diagnosis POCT Devices.

Commercially available POCT Devices					
S.No.	POCT Device	Principle/working of the instrument	Method of Detection	Time taken	Reference
1	FLEXICULT SSI-Urinary Kit	Petridish is divided into 6 compartments in which 5 are of equal size for antibiotic susceptibility and 1 is larger for quantitative analysis. The urine sample is poured and the results are analysed the following day after incubation.	Culture based method	Approx. 24 hrs	(Blom et al., 2002)
2	Uricult Trio	It consists of a dip slide with CLED agar on one side and both colourless base agar incorporated with 8-hydroxyquinoline-b-D-glucuronide and [Fe(III)] as substrate and indicator molecule and MacConkey agar for the detection of the b-GCNDase enzyme on the other side. b-GCNDase splits the substrate into glucuronic acid and 8-hydroxyquinoline and the latter, in the presence of iron ions, produces an insoluble complex which, after incubation at 37°C for 24 h, dyes the colonies with a characteristic black colour. The base agar medium furthermore incorporates bile salts to inhibit the growth of gram-positive cocci.	Culture based method	Approx. 24 hrs	(Dalet and Segovia, 1995)
3	KAR® device	The device consists of the receiving and the dispensing part. The former consist of 9 different wells which contains the culture media, chromophore and the reagent. After the addition of the sample, the results are observed the after 24 hours with a colour change.	Culture based method	8 hours	(Jover-García et al., 2020)
4	Diaslide urine culture	The Diaslide is composed of two plastic sections and are filled with MacConkey agar and CLED. The inoculation and dilution streaking in both agars are made possible by dipping the V-shaped inoculator into the urine sample and pulling the sampler from the other end through the device. After the inoculation process, the sampler is disposed of and the case is placed in a tray for standing incubation. Without opening the device, growth is seen.	Culture based method	Approx. 24 hrs	(Rosenberg et al., 1992)
5	uriscreen	The basis of Uriscreen is the detection of the bacterial catalase enzyme. Urine is drawn into a test tube that has been filled with the powdered Uriscreen reagent and hydrogen peroxide is then added, and the mixture is gently shaken for five seconds. A successful outcome is demonstrated by the creation of enough foam within one to two minutes of the hydrogen peroxide addition to form a complete ring or layer on the surface.	Enzymatic method	2 minutes	(Waisman et al., 1999)
6	Dipstreak	Two different kinds of agar are affixed back to back to a plastic paddle in the DipStreak apparatus. The prong tips that are attached to the end of the paddle are dipped into the urine sample, that inoculate the agar. Colonies are isolated between the range 103 and 107 CFU/ml.	Culture based method	Approx. 24 hrs	(Scarparo et al., 2002)
7	Urisys 2400 automated urine analyser	The flow cell measures the specific gravity using refractometry.	urine analyser		(Chien et al., 2007)
8	Urisys 1100	The LED illuminates at three different wavelength and the detector measures the amount of light reflected by the test strip used for the computation of the results.	Colorimetry	1 min	(Harris and Fasolino, 2022)
9	Clinitek Status	The reflectance spectrophotometer, measures the colour and intensity of light reflected from the reagent area and generates the results.	Colorimetry	1 min	(Chien et al., 2007)
10	Aution Micro	Using the refractive index method, the specific gravity of the urine is measured and the values are adjusted based on the protein and glucose concentration.	Colorimetry	45 seconds	(Chien et al., 2007)
11	Urilyzer	The LEDs emit the light onto the test strips placed on the strip tray and then, the reflected light based on the concentration of the analyte is detected by the detector that provides the output.	Colorimetry	1 min	(Pernille et al., 2019)
12	MBS POCT	It uses mono-use, disposable reaction vials in which samples are inoculated and quantifies the catalytic activity of redox enzymes in the primary metabolic pathways of bacteria. The log of bacterial concentration is inversely correlated with the amount of time required to produce a colour change.	Enzymatic method	5.24 hours	(Arienzo et al., 2020)

affinity-based sensors were built by the deposition of the gold microelectrodes on the Cytiva Fusion 5 lateral flow membrane using a shadow mask in a cryo e-beam evaporator. The capture probe monoclonal PGE2 antibody was crosslinked to the gold electrode using DSP, and due to the interaction between the antibody and PGE2, the sensor detected the PGE2 using electrochemical impedance spectroscopy. The sensor predicts as UTI positive or negative in five minutes and offers a broad dynamic range of 100–4000 pg mL^{-1} (Ganguly et al., 2021).

The development of an electrochemical immunosensor using lactoferrin as the biomarker was reported, as shown in Figure 6B. A self-assembled monolayer (SAM) of alkanethiolate consisting of 6-mercapto-1-hexanol and 11-mercaptoundecanoic acid characterized with the help of electrochemical impedance spectroscopy was

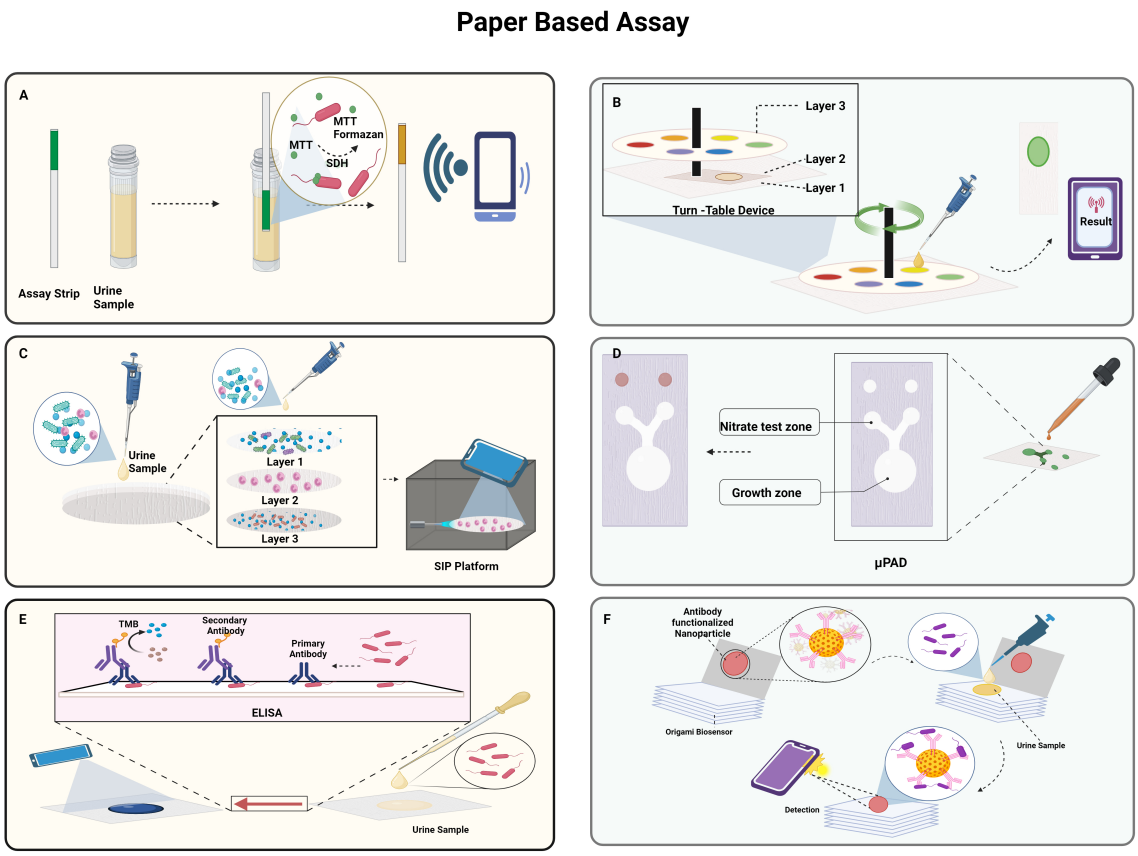

FIGURE 5
Paper-based approaches to detect UTI: **(A)**. Schematic representation of MTT-PMS test strips; **(B)**. Turn table paper-based device; **(C)**. Smartphone integrated paper (SIP)-based device; **(D)**. Paper-based analytical device (PAD) for detection of nitrate and *E.coli*; **(E)**. paper-based ELISA; **(F)**. Portable origami cellulose immunobiosensor. *Created Using BioRender.com*.

employed in an electrochemical biosensor array. Biotin was added once the sensor surface was activated which facilitated the binding of the streptavidin-attached antibody. The secondary antibody conjugated with HRP captures lactoferrin in the urine and the presence was detected with the help of amperometry measurements at -200 mV. The limit of detection determined through the analysis of 111 urine samples was found to be 145 pg mL^{-1} (Pan et al., 2010).

The fabrication of an immunosensor for sensitive and selective electrochemical detection of UPEC was described by Jijie et al. as shown in Figure 6C. Using the electrophoretic deposition approach, the gold electrodes were modified with thin active layers of reduced graphene oxide/polyethylenimine (rGO/PEI). Later, the electrode surface was again covalently modified with anti-fimbrial *E.coli* antibodies by amide bond formation that binds specifically to the *E.coli*. The decrease in the current due to the restriction of electron transfer from the redox probe potassium ferrocyanide to the modified electrode as a result of the immune complex formation served as the basis for the identification of *E.coli* and was measured using differential pulse voltammetry (DPV). The developed immunosensor had a detection limit of 10 CFU mL^{-1} and a linear range of 1×10^1–1×10^4 CFU mL^{-1} (Jijie et al., 2018).

An electrochemical biosensor was developed by Tseng et al. to detect leukocyte esterase and nitrate in clinical samples as shown in Figure 6D. The study was demonstrated by creating LE antibody conjugated to a modified glassy carbon electrode (GCE) with carboxylic acid-functionalized poly(3,4-ethylenedioxythiophene) (PEDOT-COOH), namely, LE antibody/Avidin/EDC-NHS/PEDOT-COOH/GCE. The presence of LE is indicated by the inhibition of the electron transfer by the [$Fe(CN_6)$] and that of the nitrate by the DPV. The constructed electrode demonstrated good performance under optimal conditions, with a linear range of 9.1–131 µM and 0.2–590 µg L^{-1}, and limits of detection for NIT and LE of 6.24 µM and 0.2 µg L–1, respectively. The outcomes from urine samples from thirteen patients showed 100% diagnostic sensitivity and 87.5% specificity when compared to the strip test (Tseng et al., 2023).

Capatina et al. developed an aptamer-based electrochemical sensor that could detect the 3-O-C12-HSL as shown in Figure 6E. The electrode surface was initially modified with gold nanoparticles, and then the C-SPE/AuNPs surface was immobilized with the aptamers, and later, the surface was blocked with MCH solution. After each modification step, the electrode surface was characterised using cyclic voltammetry, DPV, and electrochemical impedance spectroscopy using different redox probes. After the preparation of the electrode, the analyte 3-O-C12-HSL was added, and an electrochemical signal was determined. The presence of the analyte was also determined in spiked urine samples, spiked microbiological growth media, and microbiological cultures. The developed aptasensor had a LOD of 145 ng mL^{-1} (0.5 µM) and could detect the analyte between the range of 0.5–30 µM (Capatina et al., 2022).

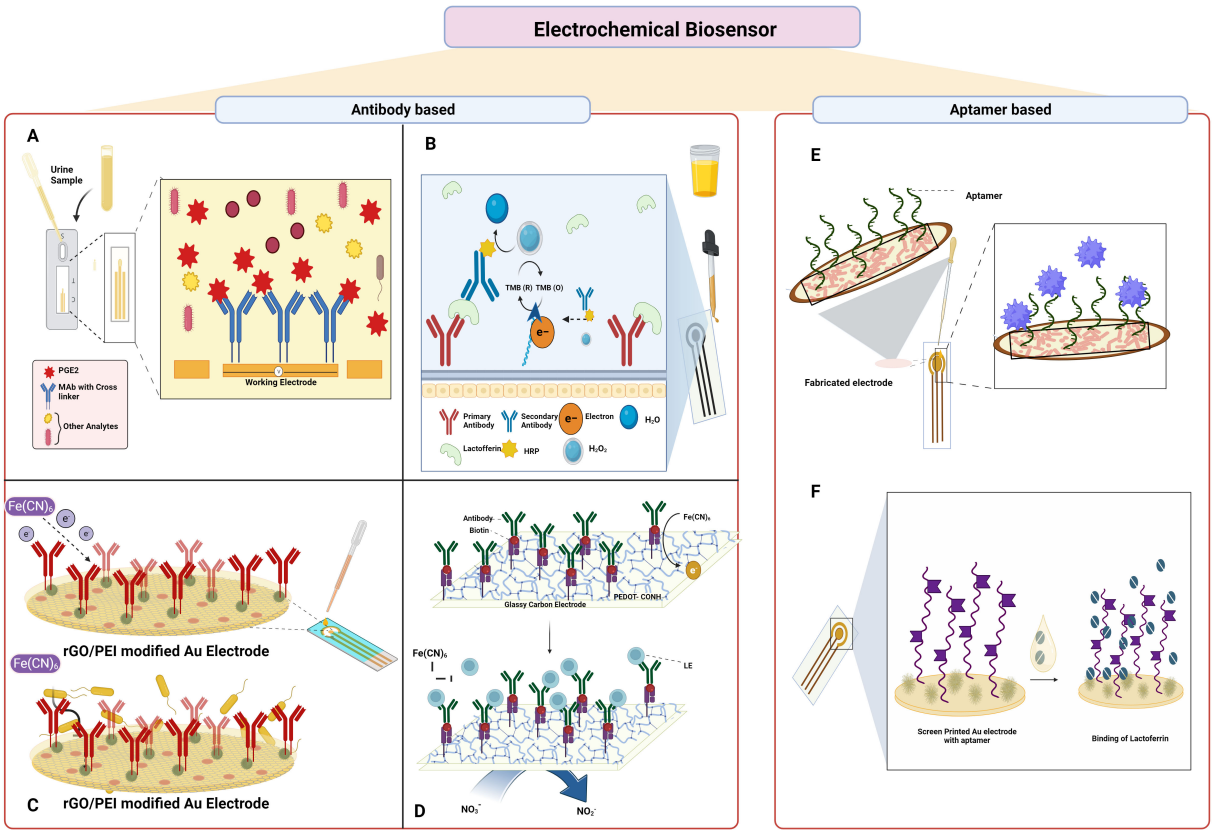

FIGURE 6
Electrochemical sensor-based approach to detect UTI: **(A)**. Lateral flow-based electrochemical biosensor for detection of urine PGE2; **(B)**. Electrochemical immunosensor for detection of Lactoferrin **(C)**. Electrochemical immunosensor for detection of UPEC; **(D)** electrochemical biosensor for detection of leukocyte esterase and nitrate; **(E)** Aptamer-based electrochemical sensor for detection of 3-O-C12-HSL; **(F)** electrochemical aptasensor for detection of lactoferrin. *Created Using BioRender.com.*

Naseri et al. developed a label-free electrochemical multivalent aptasensor for the detection of human lactoferrin in urine samples as shown in Figure 6F. The materials gold, silver, and gold served as the working, reference, and counter electrode in the screen-printed gold electrodes, and the polynucleotide multivalent aptamer sequence was immobilized on the electrode. DPV was performed using 0.1 M acetate buffer solution as a blank to check the presence of human lactoferrin using a spiked buffer or artificial urine medium. The multivalent aptamer exhibited excellent sensing performances against human lactoferrin and had strong affinity and specificity with a broad linear range of 10 to 1300 ng/mL and a LOD of 0.9 ng/mL (Naseri et al., 2021).

3.3.1.3 Optical sensors

Gomez-Cruz et al. developed a label-free nanoplasmonic sensing platform to detect UPEC in real-time at concentrations below the physiological limit for UTI diagnosis as shown in Figure 7A. The sensing platform consisted of a metallic flow-through nanohole array-based sensor in conjunction with a Raspberry Pi interface, lens assembly, CMOS detector, and red LED light source. The light from the LED, after passing through the nanohole containing the UPEC antibody complex, causes the variation in the intensity of the transmitted light that is measured using surface plasmon resonance imaging. With a detection limit of 100 CFU mL^{-1}, a resolution of approximately 10^{-6} RIU and a bulk sensitivity of 212 pixels per intensity unit (PIU)/refractive index unit (RIU) are observed (Gomez-Cruz et al., 2018).

Wu et al. described a multimodal CA-independent LFIA (MCI-LFIA) technique with adaptability and accuracy for the quick identification of bacterial UTIs as shown in Figure 7B. The Lateral Flow Assay employed *E.coli* as the model bacteria and AuNF – PMBA NMs (Gold nanoflower by p-mercaptophenylboronic acid nanomaterials) and AuNP-streptavidin nanoprobes as the test line (T-line) and control line (C-line) probes, respectively. The sample was initially incubated with AuNF – PMBA solution to obtain AuNF – PMBA – bacterium conjugates, and the conjugates, along with AuNP-streptavidin conjugates, were then applied to the test strip sample pad. Qualitative data was obtained by using high-accuracy visual observation to determine if the blue-green colour band of the T-line was present or absent within 45 minutes. The LOD for *E. coli* was 10^3 CFU/mL in the colorimetric mode, 10^2 CFU mL^{-1} in the Raman mode, and 10^2 CFU Ml^{-1} in the photothermal mode (Wu et al., 2023). Using the shift in surface plasmon resonance of aptamer-modified AuNPs (Apt-AuNP), Deb et al. created an aptasensor to rapidly, precisely, and accurately identify *K. pneumoniae* (Figure 7C). Aptamers were immobilized on the gold surface to form the Apt-AuNP. The

presence of the *K.pneumonia* bacteria in the urine sample causes the attachment of the Apt-AuNPs to their surface, and the UV–vis signal is intensified by producing a hyperchromic effect (Deb et al., 2023).

The ability of the glucose-responsive photonic crystal integrated optical sensor to measure glucose in urine for the diagnosis of UTI and glucosuria was demonstrated by Chowdhury et al. as shown in Figure 7D. Using incident electric polarized light, gold nanoparticles were chosen as the photonic crystal material and implanted into 36 blocks of a functionalized microgel matrix that was placed on top of a silicon substrate. A shift in the concentration of glucose resulted in wavelength shifting. The microgel swelled as the glucose concentration increased, increasing stack spacing and causing a rise in shift. On the other hand, as the concentration of glucose decreased, the microgel contracted. The sensor demonstrated enhanced sensitivity of less than 85.65 nm/mM at pH 7.4 and less than 110.60 nm/mM at pH 8.0 (Chowdhury and Zubair, 2022).

Vasudevan et al. developed a photoluminescence-based optical biosensor using cysteamine-capped Zinc Oxide (ZnO) nanoparticles that detects the AHL present in the sample. Prepared ZnO nanoparticles are functionalized with the linker molecule cysteamine as shown in Figure 7E. They can detect and bind to the quorum-sensing molecules, AHL, produced by the bacteria. The variations in the PL-based signals due to the surface defects allowed the detection of the analyte was validated using C4-HSL and 3-oxo-C12 HSL with a detection range of 10-120nM and a sensitivity of 97% (Vasudevan et al., 2020).

3.3.1.4 Other Devices

For the diagnosis of UTIs, Michael et al. developed an instrument-free lab on a disc platform named diagnostic fidget spinner (Dx-FS). The device preloaded with the FAST solution was filled with a raw urine sample. The device is spun twice to concentrate the bacterial cells, followed by the removal of the FAST solution and then after the addition of the detecting solution. The colour change observed after 45 minutes was determined using the rapid colorimetric WST-8 assay that involved the transfer of electrons from living bacterial cells to the WST-8 by the electron mediator, which led to the visualization of the colour change of the formazan dye. The device allowed the on-site detection of urine samples from 39 individuals suspected of having a urinary tract infection in Tiruchirappalli, India, within 50 minutes using the naked eye (Michael et al., 2020).

The Micro Biological Survey (MBS) method was developed by Roma Tre University in Rome, Italy, as a colorimetric technique for the quantification of bacteria in various samples. It uses mono-use, disposable reaction vials in which samples are inoculated without any prior treatment and quantifies the catalytic activity of redox enzymes in the primary metabolic pathways of bacteria. The log of

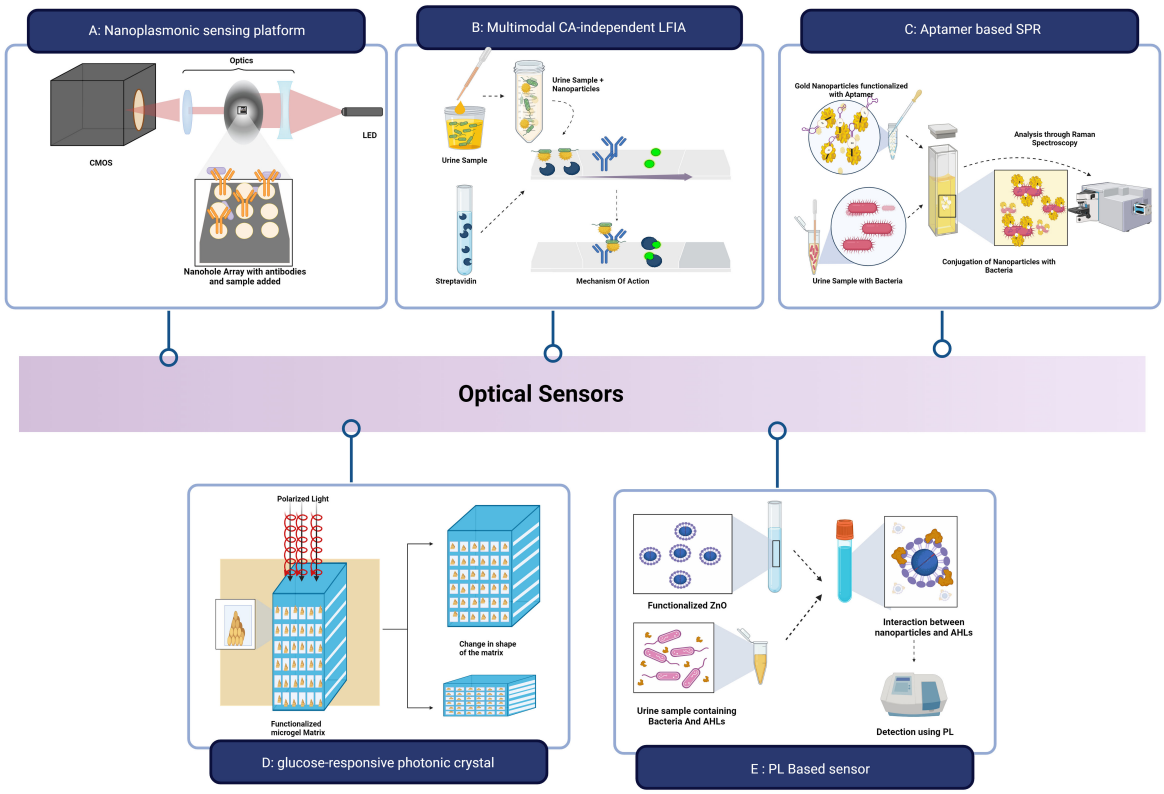

FIGURE 7
Optical sensors for UTI Detection: **(A)** Nanoplasmonic sensing platform for detection of UPEC; **(B)** Lateral Flow Assay for detection of *E.coli*; **(C)** Aptasensor to detect *K pneumoniae*; **(D)** Glucose-responsive photonic crystal integrated optical sensor; **(E)** Photoluminescence based optical biosensor. *Created Using BioRender.com*.

bacterial concentration is inversely correlated with the amount of time required to produce a colour change (Bottini, 2013). Arienzo et al. conducted a study to validate the MBS POCT. 1 ml urine sample was manually placed into a UBQ vial and was incubated in the MBS Multireader at 37°C and the bacteriuria is indicated by a colour change from blue to yellow. Positive results were indicated by a colour change that occurred within 5.24 h, whereas slower or no colour change occurred during the 24-h analytical timeframe. The MBS POCT urine analysis results were compared to the usual culture-based test results and the results showed 97% accuracy, 92% sensitivity, 100% specificity, 99% PPV, and 96% NPV within a 5-h analytical time threshold (Arienzo et al., 2020).

By using retrospective and prospective studies, Iseri et al. assessed the diagnostic accuracy of the UTI-lizer (digital dipstick), a culture-based detection POC device developed by UTIlizer AB, Stockholm, Sweden, that aids in the rapid identification and quantification of five distinct bacteria in the urine in under two minutes. The 180 microculture wells are filled with a three-step process that involves inserting the dipstick in urine to inoculate the sample, incubating it at 37°C, and then analysing the digital image with a smartphone or scanner in which the colour change indicates a positive result. Compared to clinical standards, the retrospective study demonstrated 100% sensitivity and specificity in detecting bacteriuria, 98.6% sensitivity and 96.8% specificity in identifying primary pathogens with UTI-lizer. Meanwhile, the prospective study showed 100% sensitivity and 89.6% specificity in detecting significant bacteriuria for in-panel microorganisms (Iseri et al., 2024).

4 Treatment and management of UTI

The antimicrobial usage guidelines published by IDSA, offer valuable information to medical professionals that can be used directly or serve as the foundation for the hospital guidelines on the treatment of a range of infectious disorders, including urinary tract infections (Nicolle et al., 2005; Weese et al., 2011). The National Institute for Health and Clinical Excellence recommends a course of oral antibiotics for a brief period of 7-10 days for acute UTIs, while it is 10 -14 days for pyelonephritis (Neu, 1992a; Novelli and Rosi, 2017 for effective treatment to prevent antimicrobial resistance and recurrence of the infection (Neu, 1992; Novelli and Rosi, 2017). Empirical antimicrobial treatment with broad-spectrum antibiotics is initiated experimentally prior to the availability of urine culture results considering factors such as patient characteristics (comorbidities, allergies, concurrent medication, and compliance), regional practice patterns, the incidence of resistance in the local community, product availability, and price (Neu, 1992; Novelli and Rosi, 2017; Alkhawaldeh et al., 2022; Ara et al., 2022).

Since 1940s, antimicrobial medicines have been utilized to treat UTI. The first-line treatment with nitrofurantoin, trimethoprim-sulfamethoxazole, fosfomycin trometamol, β-lactam medicines, and fluoroquinolones, and cephalosporins including cefuroxime, axetil, and cefixime are the preferred medications for uncomplicated UTIs (Jancel, 2002). Compared to nitrofurantoin and β -lactams, TMP and fluoroquinolones produce large quantities of vaginal secretions that might be more effective to completely remove uropathogens from the vagina (Nicolle, 2003).

Vellinga et al. showed that 56% of the patients received a prescription for an antimicrobial medication, while only 14% of them had the isolate identified. Trimethoprim, nitrofurantoin, fluoroquinolones, or co-amoxyclav, were commonly used for uncomplicated UTIs, but trimethoprim alone as an empirical treatment was less successful due to the increased resistance (Vellinga et al., 2011).

The study by Alkhawaldeh et al. showed that there was no correlation between the culture results and the treatment that could lead to antimicrobial resistance. The statistics of their study showed that out of 87.6% patients who got empirical treatment, only 10.5% of patients saw improvement in their management of UTIs once culture and sensitivity findings were known, while 0.8% of patients saw a worsening of their therapy (Alkhawaldeh et al., 2022). Studies shows that urine isolates are susceptible to fosfomycin, nitrofurantoin, amoxiclav, and meropenem and can be used to treat lower UTI (Sharmin et al., 2022 (Sharma et al., 2021). Pregnancy induces several physiological, hormonal, and functional changes in the urinary tract, demanding the need for urine culture. During pregnancy physiological hormonal and functional changes demand for the proper selection of antibiotic, with FDA category B antimicrobials such as penicillins, oral cephalosporins, and fosfomycin trometamol are advised for the lower urinary tract infections while parenteral cephalosporins, penicillins, or monobactams (aztreonam) are preferred for acute pyelonephritis. Some antibiotics can have effects like dysplasia and discolouration of teeth and bones, restrict the development of the neural tube, hemolysis and glucose-6-phosphate dehydrogenase (G6PD) impairment, obstruct the eighth nerve in foetus, and changes in the joint cartilages respectively (Krcmery et al., 2001) (Figure 2).

Synthetic and nylon innerwear increases UTI risk as they do not absorb sweat as cotton innerwear leading the urogenital area wet and prone to infection (Vyas, 2015). Hence, maintaining proper perineal cleanliness i.e., cleaning from genitalia to the anus, changing the soiled sanitary pad frequently needs to be considered (Das et al., 2015). According to a study by Jelly et al. there were fewer UTIs when women used peri-wash more frequently after urinating and during their menstrual cycle (Jelly et al., 2022).

Cranberries, in its various form, is used as prophylactic measure to treat lower and recurrent UTIs has no scientific evidence for therapeutics. The presence of various phytochemicals, especially, quinic acid and anthocyanidin/proanthocyanidin are thought to cause the urine to contain high levels of hippuric acid, triggering antibacterial properties and prevent type I and P-fimbriated uropathogens to adhere to the bladder wall (Kinney and Blount, 1979; Guay, 2009; Hisano et al., 2012; Jepson et al., 2012).

Probiotics, particularly *lactobacilli* spp., replenish the urogenital flora disrupted by antibiotics thus prevent UTIs. (Falagas et al., 2006; Akgul and Karakan, 2018) (Falagas et al., 2006 Lactin V (Osel), contains hydrogen peroxide-producing ($H_2O_2^+$) *Lactobacillus crispatus* strain CTV-05, which aids women who are susceptible to UTIs to regain a normal vaginal flora with treatment

leading to an intense and protracted colonization with *Lactobacillus crispatus* in women with rUTI (Stapleton et al., 2011).

5 Conclusion

UTI is one of the most common infectious diseases affecting women at a higher rate due to their anatomy and physiology and increases the socio-economic burden of society. Early disease diagnosis is crucial to combat AMR organisms. There are a large number of predisposing and lifestyle-related factors that lead to UTIs. The current diagnostic techniques are mainly culture tests and dipstick analysis, which are time-consuming. The emergence of user-friendly, cost-effective, and adaptable diagnostic approaches, including paper-based, electrochemical, and optical sensors, holds promise for early UTI detection. The use of bacterial biomarkers helps in the diagnosis, as the individual biomarkers can be affected by the immune condition. Also, medical professionals prescribe antibiotics for the treatment of UTIs, but proper diagnosis and treatment of UTIs are required to counter the infection. Proper hygiene, using plant sources like cranberry, and consuming probiotics effectively prevent UTIs. By embracing these advancements and working together to implement preventive measures, we can take a more comprehensive approach to tackling the challenges associated with UTIs.

Author contributions

SS: Data curation, Visualization, Writing – original draft. AS: Conceptualization, Writing – review & editing. JR: Writing – review & editing.

Funding

The author(s) declare that no financial support was received for the research, authorship, and/or publication of this article.

Acknowledgments

The authors are grateful to SASTRA University for providing us with an excellent infrastructure and facilitating access to diverse journals, and being a part of the Quorum Sensing Lab (QSL).

Conflict of interest

The authors declare that the research was conducted in the absence of any commercial or financial relationships that could be construed as a potential conflict of interest.

The author(s) declared that they were an editorial board member of Frontiers, at the time of submission. This had no impact on the peer review process and the final decision.

Publisher's note

References

Abdelaal, A. M., Salah, A. A., Alhamshary, A., Saad, O., Shaer, E., Mohamedyounes, A. Z., et al. (2019).Urinary Interleukin-6 as biomarker for diagnosis of acute pyelonephritis in children. Available online at: https://geget.journals.ekb.eg/.

Abed, H. A., Mohammed Ali, K. O., and Alrifai, S. B. (2021). Estimation of IL-6 and IL-8 in the urine and serum of children with urinary tract infection. *Indian J. Forensic Med. Toxicol.* 15. doi: 10.37506/ijfmt.v15i3

Acton, S., and O'Meara, Y. M. (1997). Urinary tract infection and contraceptive method. *Irish Med. J.* 90, 176.

Adegun, P. T., Odimayo, M. S., Olaogun, J. G., and Emmanuel, E. E. (2019). Comparison of uropathogens and antibiotic susceptibility patterns in catheterized ambulant middle-aged and elderly Nigerian patients with bladder outlet obstruction. *Türk Üroloji Dergisi/Turkish J. Urol.* 45, 48–55. doi: 10.5152/tud.2018.25588

Adrover-Jaume, C., Rojo-Molinero, E., Clemente, A., Russell, S. M., Arranz, J., Oliver, A., et al. (2020). Mobile origami immunosensors for the rapid detection of urinary tract infections. *Anal.* 145, 7916–7921. doi: 10.1039/D0AN01218A

Agrawal, P., Pandey, A., Sompura, S., and Pursnani, M. L. (2013). Role of blood C - reactive protein levels in upper urinary tract infection and lower urinary tract infection in adult patients (>16 years). *J. Assoc. Phys. India* 61, 462–463.

Akgul, T., and Karakan, T. (2018). The role of probiotics in women with recurrent urinary tract infections. *Türk Üroloji Dergisi/Turkish J. Urol.* 44, 377–383. doi: 10.5152/tud.2018.48742

Akhtar, A., Ahmad Hassali, M. A., Zainal, H., Ali, I., and Khan, A. H. (2021). A cross-sectional assessment of urinary tract infections among geriatric patients: prevalence, medication regimen complexity, and factors associated with treatment outcomes. *Front. Public Health* 9. doi: 10.3389/fpubh.2021.657199

Alkhawaldeh, R., Abu Farha, R., Abu Hammour, K., and Alefishat, E. (2022). Optimizing antimicrobial therapy in urinary tract infections: A focus on urine culture and sensitivity testing. *Front. Pharmacol.* 13. doi: 10.3389/fphar.2022.1058669

Allison, J. S., Dawson, M., Drake, D., and Montie, T. C. (1985). Electrophoretic separation and molecular weight characterization of *Pseudomonas aeruginosa* H-antigen flagellins. *Infect. Immun.* 49, 770–774. doi: 10.1128/iai.49.3.770-774.1985

Al Rushood, M., AL-Eisa, A., and AL-Attiyah, R. (2020). Serum and urine interleukin-6 and interleukin-8 levels do not differentiate acute pyelonephritis from lower urinary tract infections in children. *J. Inflammation Res.* 13, 789–797. doi: 10.2147/JIR.S275570

Alshomrani, M. K., Alharbi, A. A., Alshehri, A. A., Arshad, M., and Dolgum, S. (2023). Isolation of *Staphylococcus aureus* Urinary Tract Infections at a Community-Based Healthcare Center in Riyadh. *Cureus.* 15 (2), e35140. doi: 10.7759/cureus.35140

Amdekar, S., Singh, V., and Singh, D. D. (2011). Probiotic therapy: immunomodulating approach toward urinary tract infection. *Curr. Microbiol.* 63, 484–490. doi: 10.1007/s00284-011-0006-2

Andriole, V. T. (1987). Urinary tract infections: recent developments. *J. Infect. Dis.* 156, 865–869. Available at: https://about.jstor.org/terms.

Ara, R., Mohammad Nasrullah, S., Tasnim, Z., Afrin, S., Saif-Ur-Rahman, K. M., and Hawlader, M. D. H. (2022). Effective antimicrobial therapies of urinary tract infection among children in low-income and middle-income countries: protocol for a systematic review and meta-analysis. *BMJ Open* 12, e060568. doi: 10.1136/bmjopen-2021-060568

Arabi, Z., Al Thiab, K., Altheaby, A., Aboalsamh, G., Kashkoush, S., Almarastani, M., et al. (2021). Urinary tract infections in the first 6 months after renal transplantation. *Int. J. Nephrol.* 2021, 1–8. doi: 10.1155/2021/3033276

Arao, S., Matsuura, S., Nonomura, M., Miki, K., Kabasawa, K., and Nakanishi, H. (1999). Measurement of urinary lactoferrin as a marker of urinary tract infection. *J. Clin. Microbiol.* 37, 553–557. doi: 10.1128/JCM.37.3.553-557.1999

Arienzo, A., Cellitti, V., Ferrante, V., Losito, F., Stalio, O., Murgia, L., et al. (2020). A new point-of-care test for the rapid detection of urinary tract infections. *Eur. J. Clin. Microbiol. Infect. Dis.* 39, 325–332. doi: 10.1007/s10096-019-03728-3

Arinzon, Z., Peisakh, A., Shuval, I., Shabat, S., and Berner, Y. N. (2009). Detection of urinary tract infection (UTI) in long-term care setting: Is the multireagent strip an adequate diagnostic tool? *Arch. Gerontol. Geriat.* 48, 227–231. doi: 10.1016/j.archger.2008.01.012

Aubais aljelehawy, Q., Hadi Alshaibah, L. H., and Abbas Al- Khafaji, Z. K. (2021). Evaluation of virulence factors among *Staphylococcus aureus* strains isolated from patients with urinary tract infection in Al-Najaf Al-Ashraf teaching hospital. *Cell. Mol. Biomed. Rep.* 1, 78–87. doi: 10.55705/cmbr.2021.144995.1017

Baba-Moussa, L., Anani, L., Scheftel, J. M., Couturier, M., Riegel, P., Haïkou, N., et al. (2008). Virulence factors produced by strains of *Staphylococcus aureus* isolated from urinary tract infections. *J. Hosp. Infect.* 68, 32–38. doi: 10.1016/j.jhin.2007.10.010

Bacârea, A., Fekete, G., Grigorescu, B., and Bacârea, V. (2021). Discrepancy in results between dipstick urinalysis and urine sediment microscopy. *Exp. Ther. Med.* 21, 538. doi: 10.3892/etm.2021.9971

Baldrich, E., Muñoz, F. X., and García-Aljaro, C. (2011). Electrochemical detection of quorum sensing signaling molecules by dual signal confirmation at microelectrode arrays. *Anal. Chem.* 83, 2097–2103. doi: 10.1021/ac1028243

E. P. Balogh, B. T. Miller and J. R. Ball (Eds.) (2015). *Improving Diagnosis in Health Care* (Washington (DC): National Academies Press). doi: 10.17226/21794

Bardsley, A. (2017). Diagnosis, prevention and treatment of urinary tract infections in older people. *Nurs. Older People* 29, 32–38. doi: 10.7748/nop.2017.e884

Belyayeva, M., and Jeong, J. M. (2023). Acute pyelonephritis.

Bethel, J. (2012). Acute pyelonephritis: risk factors, diagnosis and treatment. *Nurs. Stand.* 27, 51–56. doi: 10.7748/ns2012.10.27.5.51.c9334

Beyer, A. K., Currea, G. C. C., and Holm, A. (2019). Validity of microscopy for diagnosing urinary tract infection in general practice – a systematic review. *Scandinavian J. Prim. Health Care* 37, 373–379. doi: 10.1080/02813432.2019.1639935

Bijlsma, I. G. W., Dijk, L., Kusters, J. G., and Gaastra, W. (1995). Nucleotide sequences of two fimbrial major subunit genes, *pmpA* and *ucaA*, from canine-uropathogenic *Proteus mirabilis* strains. *Microbiology* 141, 1349–1357. doi: 10.1099/13500872-141-6-1349

Bjerklund Johansen, T. E. (2004). The role of imaging in urinary tract infections. *World J. Urol.* 22, 392–398. doi: 10.1007/s00345-004-0414-z

Blom, M., Sørensen, T. L., Espersen, F., and Frimodt-Møller, N. (2002). Validation of FLEXICULTTM SSI-urinary kit for use in the primary health care setting. *Scandinavian J. Infect. Dis.* 34, 430–435. doi: 10.1080/00365540110080601

Bottini, G. (2013). A new method for microbiological analysis that could be used for point-of-care testing (POCT). *Open Emergency Med. J.* 5, 13–15. doi: 10.2174/1876542401305010013

Burgoyne, E. D., Molina-Osorio, A. F., Moshrefi, R., Shanahan, R., McGlacken, G. P., Stockmann, T. J., et al. (2020). Detection of *Pseudomonas aeruginosa* quorum sensing molecules at an electrified liquid|liquid micro-interface through facilitated proton transfer. *Anal.* 145, 7000–7008. doi: 10.1039/D0AN01245A

Buzid, A., Shang, F., Reen, F. J., Muimhneacháin, E.Ó., Clarke, S. L., Zhou, L., et al. (2016). Molecular Signature of *Pseudomonas aeruginosa* with Simultaneous Nanomolar Detection of Quorum Sensing Signaling Molecules at a Boron-Doped Diamond Electrode. *Sci. Rep.* 6, 30001. doi: 10.1038/srep30001

Califf, R. M. (2018). Biomarker definitions and their applications. *Exp. Biol. Med.* 243, 213–221. doi: 10.1177/1535370217750088

Capatina, D., Lupoi, T., Feier, B., Blidar, A., Hosu, O., Tertis, M., et al. (2022). Label-free electrochemical aptasensor for the detection of the 3-O-C12-HSL quorum-sensing molecule in *pseudomonas aeruginosa*. *Biosensors* 12, 440. doi: 10.3390/bios12070440

Caretto, M., Giannini, A., Russo, E., and Simoncini, T. (2017). Preventing urinary tract infections after menopause without antibiotics. *Maturitas* 99, 43–46. doi: 10.1016/j.maturitas.2017.02.004

Chen, S. L., Jackson, S. L., and Boyko, E. J. (2009). Diabetes mellitus and urinary tract infection: epidemiology, pathogenesis and proposed studies in animal models. *J. Urol.* 182, S51–6. doi: 10.1016/j.juro.2009.07.090

Chien, T.-I., Lu, J.-Y., Kao, J.-T., Lee, T.-F., Ho, S.-Y., Chang, C.-Y., et al. (2007). Comparison of three automated urinalysis systems—Bayer Clinitek Atlas, Roche Urisys 2400 and Arkray Aution Max for testing urine chemistry and detection of bacteriuria. *Clinica Chimica Acta* 377, 98–102. doi: 10.1016/j.cca.2006.08.033

Chowdhury, E., and Zubair, A. (2022). Triangular gold nanoplates integrated microgel-based sensor for urinary tract infection and glucosuria detection. *Opt. Mater. Express* 12, 2212. doi: 10.1364/OME.456759

Chu, C. M., and Lowder, J. L. (2018). Diagnosis and treatment of urinary tract infections across age groups. *Am. J. Obstet. Gynecol.* 219, 40–51. doi: 10.1016/j.ajog.2017.12.231

Chua, A., Yean, C. Y., Ravichandran, M., Lim, B., and Lalitha, P. (2011). A rapid DNA biosensor for the molecular diagnosis of infectious disease. *Biosensors Bioelectron.* 26, 3825–3831. doi: 10.1016/j.bios.2011.02.040

Clark, L. C., and Lyons, C. (1962). Electrode systems for continuous monitoring in cardiovascular surgery. *Ann. New York Acad. Sci.* 102, 29–45. doi: 10.1111/j.1749-6632.1962.tb13623.x

Colella, M., Topi, S., Palmirotta, R., D'Agostino, D., Charitos, I. A., Lovero, R., et al. (2023). An overview of the microbiota of the human urinary tract in health and disease: current issues and perspectives. *Life* 13, 1486. doi: 10.3390/life13071486

Dalet, F., and Segovia, T. (1995). Evaluation of a new agar in Uricult-Trio for rapid detection of *Escherichia coli* in urine. *J. Clin. Microbiol.* 33, 1395–1398. doi: 10.1128/jcm.33.5.1395-1398.1995

Das, P., Baker, K. K., Dutta, A., Swain, T., Sahoo, S., Das, B. S., et al. (2015). Menstrual hygiene practices, WASH access and the risk of urogenital infection in women from Odisha, India. *PloS One* 10, e0130777. doi: 10.1371/journal.pone.0130777

Davis, N. F., and Flood, H. D. (2011). "The Pathogenesis of Urinary Tract Infections," in *Clinical Management of Complicated Urinary Tract Infection* (InTech). doi: 10.5772/22308

Davoudabadi, S., Goudarzi, M., and Hashemi, A. (2023). Detection of Virulence Factors and Antibiotic Resistance among *Klebsiella pneumoniae* Isolates from Iran. *BioMed. Res. Int.* 2023, 1–7. doi: 10.1155/2023/3624497

Deb, A., Gogoi, M., Mandal, T. K., Sinha, S., and Pattader, P. S. G. (2023). Specific instantaneous detection of *klebsiella pneumoniae* for UTI diagnosis with a plasmonic gold nanoparticle conjugated aptasensor. *ACS Appl. Bio Mater.* 6, 3309–3318. doi: 10.1021/acsabm.3c00369

de Paiva-Santos, W., de Sousa, V. S., and Giambiagi-deMarval, M. (2018). Occurrence of virulence-associated genes among *Staphylococcus saprophyticus* isolated from different sources. *Microbial. Pathogen.* 119, 9–11. doi: 10.1016/j.micpath.2018.03.054

Dienye, P. O., and Gbeneol, P. K. (2011). Contraception as a risk factor for urinary tract infection in Port Harcourt, Nigeria: A case control study. *Afr. J. Prim. Health Care Family Med.* 3, 1–4. doi: 10.4102/phcfm.v3i1.207

Dutta, C., Pasha, K., Paul, S., Abbas, M. S., Nassar, S. T., Tasha, T., et al. (2022). Urinary tract infection induced delirium in elderly patients: A systematic review. *Cureus.* 14 (12), e32321. doi: 10.7759/cureus.32321

Ebrahimzadeh, T., Kuprasertkul, A., Neugent, M. L., Lutz, K. C., Fuentes, J. L., Gadhvi, J., et al. (2021). Urinary prostaglandin E2 as a biomarker for recurrent UTI in postmenopausal women. *Life Sci. Alliance* 4, e202000948. doi: 10.26508/lsa.202000948

Elkhawaga, A. A., Khalifa, M. M., El-badawy, O., Hassan, M. A., and El-Said, W. A. (2019). Rapid and highly sensitive detection of pyocyanin biomarker in different *Pseudomonas aeruginosa* infections using gold nanoparticles modified sensor. *PloS One* 14, e0216438. doi: 10.1371/journal.pone.0216438

El-Refaey, A., Hagar, A., Abo El kheir, N., and Zeid, M. (2020). Diagnostic value of urinary heparin binding protein in urinary tract infection in children. *GEGET* 15, 10–16. doi: 10.21608/geget.2020.19165.1010

Falagas, M. E., Betsi, G. I., Tokas, T., and Athanasiou, S. (2006). Probiotics for prevention of recurrent urinary tract infections in women. *Drugs* 66, 1253–1261. doi: 10.2165/00003495-200666090-00007

Fallahian, M., Mashhady, E., and Amiri, Z. (2005). Female urology asymptomatic bacteriuria in users of intrauterine devices. *Urol. J. UNRC/IUA* 2, 157–159. doi: 10.22037/uj.v2i3.240

Fatah, M., Waheda, N., and Kok, D. (2016). Detection of urinary lactoferrin as an indicator of urinary tract infection in girls. *Zanco J. Med. Sci.* 20, 1485–1489. doi: 10.15218/zjms.2016.0048

Fazly Bazzaz, B. S., Darvishi Fork, S., Ahmadi, R., and Khameneh, B. (2021). Deep insights into urinary tract infections and effective natural remedies. *Afr. J. Urol.* 27, 6. doi: 10.1186/s12301-020-00111-z

Ferreira, L., Sánchez-Juanes, F., González-Ávila, M., Cembrero-Fuciños, D., Herrero-Hernández, A., González-Buitrago, J. M., et al. (2010). Direct identification of urinary tract pathogens from urine samples by matrix-assisted laser desorption ionization-time of flight mass spectrometry. *J. Clin. Microbiol.* 48, 2110–2115. doi: 10.1128/JCM.02215-09

Fihn, S. D., Latham, R. H., Roberts, P., Running, K., and Stamm, W. E. (1985). Association between diaphragm use and urinary tract infection. *JAMA* 254, 240–245. doi: 10.1001/jama.1985.03360020072027

Flores-Mireles, A. L., Walker, J. N., Caparon, M., and Hultgren, S. J. (2015). Urinary tract infections: epidemiology, mechanisms of infection and treatment options. *Nat. Rev. Microbiol.* 13, 269–284. doi: 10.1038/nrmicro3432

Fogazzi, G. B., Grignani, S., and Colucci, P. (1998). Urinary microscopy as seen by nephrologists. *Cclm* 36, 919–924. doi: 10.1515/CCLM.1998.159

Foxman, B. (2002). Epidemiology of urinary tract infections: incidence, morbidity, and economic costs. *Am. J. Med.* 113, 5–13. doi: 10.1016/S0002-9343(02)01054-9

Foxman, B. (2014). Urinary tract infection syndromes. *Infect. Dis. Clinics North America* 28, 1–13. doi: 10.1016/j.idc.2013.09.003

Fu, X.-H., Zhou, W., Zhang, X.-M., Yin, Y.-B., Jing, C.-M., Liu, L., et al. (2013). Clinical analysis of 22 cases community-acquired *Pseudomonas aeruginosa* urinary tract infection. *Zhonghua Er Ke Za Zhi = Chin. J. Pediatr.* 51, 298–301.

Gama, C. R. B., Pombo, M. A. G., Nunes, C. P., Gama, G. F., Mezitis, S. G., Suchmacher Neto, M., et al. (2020). Treatment of recurrent urinary tract infection symptoms with urinary antiseptics containing methenamine and methylene blue: analysis of etiology and treatment outcomes. *Res. Rep. Urol.* 12, 639–649. doi: 10.2147/RRU.S279060

Ganguly, A., Ebrahimzadeh, T., Zimmern, P. E., De Nisco, N. J., and Prasad, S. (2021). Label free, lateral flow prostaglandin E2 electrochemical immunosensor for urinary tract infection diagnosis. *Chemosensors* 9, 271. doi: 10.3390/chemosensors9090271

Ganguly, A., Ebrahimzadeh, T., Zimmern, P., De Nisco, N. J., and Prasad, S. (2022). Label-free, novel electrofluidic capacitor biosensor for prostaglandin E2 detection toward early and rapid urinary tract infection diagnosis. *ACS Sensors* 7, 186–198. doi: 10.1021/acssensors.1c01951

Garcia, P. J., You, P., Fridley, G., Mabey, D., and Peeling, R. (2015). Point-of-care diagnostic tests for low-resource settings. *Lancet Global Health* 3, e257–e258. doi: 10.1016/S2214-109X(15)70089-6

Garibaldi, R. A., Burke, J. P., Britt, M. R., Miller, W. A., and Smith, C. B. (1980). Meatal colonization and catheter-associated bacteriuria. *New Engl. J. Med.* 303, 316–318. doi: 10.1056/NEJM198008073030605

Gavazzi, G., and Krause, K.-H. (2002). Ageing and infection. *Lancet Infect. Dis.* 2, 659–666. doi: 10.1016/S1473-3099(02)00437-1

Gedikbaşı, A., Şevketoğlu, E., Karyağar, S., Sağlampınar Karyağar, S., Hatipoğlu, S. S., and Yılmaz, A. (2020). Urine interleukin-1β Can be used for early prediction of urinary tract infection in children. *J. Child* 20, 1–6. doi: 10.26650/jchild.2020.1.0001

Giessing, M. (2012). Urinary tract infection in renal transplantation. *Arab J. Urol.* 10, 162–168. doi: 10.1016/j.aju.2012.01.005

Golińska, E. (2013). Virulence factors of *Enterococcus* strains isolated from patients with inflammatory bowel disease. *World J. Gastroenterol.* 19, 3562. doi: 10.3748/wjg.v19.i23.3562

Gomez-Cruz, J., Nair, S., Manjarrez-Hernandez, A., Gavilanes-Parra, S., Ascanio, G., and Escobedo, C. (2018). Cost-effective flow-through nanohole array-based biosensing platform for the label-free detection of uropathogenic E. *coli real time Biosensors Bioelectron.* 106, 105–110. doi: 10.1016/j.bios.2018.01.055

Goudarzi, M., Mohammadi, A., Amirpour, A., Fazeli, M., Nasiri, M. J., Hashemi, A., et al. (2019). Genetic diversity and biofilm formation analysis of *Staphylococcus aureus* causing urinary tract infections in Tehran, Iran. *J. Infect. Develop. Countries* 13, 777–785. doi: 10.3855/jidc.11329

Guay, D. R. P. (2009). Cranberry and urinary tract infections. *Drugs* 69, 775–807. doi: 10.2165/00003495-200969070-00002

Habak, P. J., and Griggs, J. R. P. (2023). Urinary tract infection in pregnancy.

Hagberg, L., Briles, D. E., and Edén, C. S. (1985). Evidence for separate genetic defects in C3H/HeJ and C3HeB/FeJ mice, that affect susceptibility to gram-negative infections. *J. Immunol.* 134, 4118–4122. doi: 10.4049/jimmunol.134.6.4118

Haghi, F., Lohrasbi, V., and Zeighami, H. (2019). High incidence of virulence determinants, aminoglycoside and vancomycin resistance in *enterococci* isolated from hospitalized patients in Northwest Iran. *BMC Infect. Dis.* 19, 744. doi: 10.1186/s12879-019-4395-3

Hansen, W. L. J., van der Donk, C. F. M., Bruggeman, C. A., Stobberingh, E. E., and Wolffs, P. F. G. (2013). A real-time PCR-based semi-quantitative breakpoint to aid in molecular identification of urinary tract infections. *PloS One* 8, e61439. doi: 10.1371/journal.pone.0061439

Hasan, T. H., Alasedi, K. K., and Jaloob, A. A. (2021). Proteus mirabilis virulence factors. *International Journal of Pharmaceutical Research* 13 (1), 2145–2149. doi: 10.31838/ijpr/2021.13.01.169

Harris, M., and Fasolino, T. (2022). New and emerging technologies for the diagnosis of urinary tract infections. *J Lab Med.* 46 (1), 3–15. doi: 10.1515/labmed-2021-0085

Hashmi, S., Kelly, E., Rogers, S. O., and Gates, J. (2003). Urinary tract infection in surgical patients. *Am. J. Surg.* 186, 53–56. doi: 10.1016/S0002-9610(03)00120-X

Hayder, T., Abusaiba, H., Alasedi, K., and Aljanaby, A. (2020). Proteus mirabilis virulence factors: review. *Int. J. Pharm. Res.* 13 (1), 2145–2149. doi: 10.31838/ijpr/2021.13.01.169

Heidary, Z., Bandani, E., Eftekhary, M., and Jafari, A. A. (2016). Virulence genes profile of multidrug resistant *pseudomonas aeruginosa* isolated from Iranian children with UTIs. *Acta Med. Iranica* 54, 201–210.

Herreros, M. L., Gili, P., del Valle, R., Barrios, A., Pacheco, M., and Sánchez, A. (2021). Urine collection methods for infants under 3 months of age in clinical practice. *Pediatr. Nephrol.* 36, 3899–3904. doi: 10.1007/s00467-021-05142-4

Hickling, D. R., Sun, T.-T., and Wu, X.-R. (2015). Anatomy and physiology of the urinary tract: relation to host defense and microbial infection. *Microbiol. Spectr.* 3, 1–25. doi: 10.1128/microbiolspec.UTI-0016-2012

Hiraoka, M., Hida, Y., Hori, C., Tsuchida, S., Kuroda, M., and Sudo, M. (1995). Urine microscopy on a counting chamber for diagnosis of urinary infection. *Pediatr. Int.* 37, 27–30. doi: 10.1111/j.1442-200X.1995.tb03680.x

Hiraoka, M., Hida, Y., Tuchida, S., Tsukahara, H., Yamashita, M., Kuroda, M., et al. (1993). Diagnosis of urinary tract infection by urine microscopy using a disposable counting chamber. *Scandinavian J. Clin. Lab. Invest.* 53, 705–709. doi: 10.3109/00365519309092575

Hisano, M., Bruschini, H., Nicodemo, A. C., and Srougi, M. (2012). Cranberries and lower urinary tract infection prevention. *Clinics* 67, 661–667. doi: 10.6061/clinics/2012(06)18

Hopkins, W. J., Uehling, D. T., and Wargowski, D. S. (1999). Evaluation of a familial predisposition to recurrent urinary tract infections in women. *Am. J. Med. Genet.* 83, 422–424. doi: 10.1002/(ISSN)1096-8628

Horváth, J., Wullt, B., Naber, K. G., and Köves, B. (2020). Biomarkers in urinary tract infections - which ones are suitable for diagnostics and follow-up? *GMS Infect. Dis.* 8. doi: 10.3205/id000068

Hsiao, C.-Y., Chen, T.-H., Lee, Y.-C., Hsiao, M.-C., Hung, P.-H., and Wang, M.-C. (2020). Risk factors for uroseptic shock in hospitalized patients aged over 80 years with urinary tract infection. *Ann. Trans. Med.* 8, 477–477. doi: 10.21037/atm.2020.03.95

Ichino, M., Kuroyanagi, Y., Kusaka, M., Mori, T., Ishikawa, K., Shiroki, R., et al. (2009). Increased urinary neutrophil gelatinase associated lipocalin levels in a rat model of upper urinary tract infection. *J. Urol.* 181, 2326–2331. doi: 10.1016/j.juro.2009.01.010

Iseri, E., Nilsson, S., van Belkum, A., van der Wijngaart, W., and Özenci, V. (2024). Performance of an innovative culture-based digital dipstick for detection of bacteriuria. *Microbiol. Spectr.* 12, e03613–23. doi: 10.1128/spectrum.03613-23

Jacobsen, S. M., Stickler, D. J., Mobley, H. L. T., and Shirtliff, M. E. (2008). Complicated Catheter-Associated Urinary Tract Infections Due to *Escherichia coli* and *Proteus mirabilis*. *Clin. Microbiol. Rev.* 21, 26–59. doi: 10.1128/CMR.00019-07

Jagadesan, I., Agarwal, I., Chaturvedi, S., Jose, A., Sahni, R., and Fleming, J. (2019). Urinary neutrophil gelatinase associated lipocalin – A sensitive marker for urinary tract infection in children. *Indian J. Nephrol.* 29, 340. doi: 10.4103/ijn.IJN_276_18

Jancel, T. (2002). Management of uncomplicated urinary tract infections. *Western J. Med.* 176, 51–55. doi: 10.1136/ewjm.176.1.51

Janev, A., Kang, J. S., and Park, S.-Y. (2023). A smartphone integrated paper (SIP)-based platform for rapid and on-site screening of urinary tract infections. *Sensors Actuators B: Chem.* 382, 133498. doi: 10.1016/j.snb.2023.133498

Jelly, P., Verma, R., Kumawat, R., Choudhary, S., Chadha, L., and Sharma, R. (2022). Occurrence of urinary tract infection and preventive strategies practiced by female students at a tertiary care teaching institution. *J. Educ. Health Promo.* 11, 122. doi: 10.4103/jehp.jehp_750_21

Jepson, R. G., Williams, G., and Craig, J. C. (2012). Cranberries for preventing urinary tract infections. *Cochrane Database System. Rev.* 2014. doi: 10.1002/14651858.CD001321.pub5

Jia, F., Barber, E., Turasan, H., Seo, S., Dai, R., Liu, L., et al. (2019). Detection of pyocyanin using a new biodegradable SERS biosensor fabricated using gold coated zein nanostructures further decorated with gold nanoparticles. *J. Agric. Food Chem.* 67, 4603–4610. doi: 10.1021/acs.jafc.8b07317

Jijie, R., Kahlouche, K., Barras, A., Yamakawa, N., Bouckaert, J., Gharbi, T., et al. (2018). Reduced graphene oxide/polyethylenimine based immunosensor for the selective and sensitive electrochemical detection of uropathogenic Escherichia coli. *Sensors Actuators B: Chem.* 260, 255–263. doi: 10.1016/j.snb.2017.12.169

Johansen, T. E. B., Botto, H., Cek, M., Grabe, M., Tenke, P., Wagenlehner, F. M., et al. (2011). Critical review of current definitions of urinary tract infections and proposal of an EAU/ESIU classification system. *Int J Antimicrob Agents.* 38, 64–70. doi: 10.1016/j.ijantimicag.2011.09.009

John, A. S., Mboto, C. I., and Agbo, B. E. (2016). A review on the prevalence and predisposing factors responsible for urinary tract infection among adults. *Eur. J. Exp. Biol.* 6 (4), 7–11. Available at: https://api.semanticscholar.org/CorpusID:52993535.

Jover-García, J., Gil-Tomás, J. J., Díaz-Lantada, A., Lafont-Morgado, P., Oliver-Sáez, P., and Colomina-Rodríguez, J. (2020). Validación de un dispositivo point-of-care para la detección rápida de infección urinaria y susceptibilidad antimicrobiana. *Rev. Chil. Infectol.* 37, 523–530. doi: 10.4067/S0716-10182020000500523

Jung, C., and Brubaker, L. (2019). The etiology and management of recurrent urinary tract infections in postmenopausal women. *Climacteric* 22, 242–249. doi: 10.1080/13697137.2018.1551871

Jutel, A. (2009). Sociology of diagnosis: a preliminary review. *Sociol. Health Ill.* 31, 278–299. doi: 10.1111/j.1467-9566.2008.01152.x

Kang, M., Jo, Y., Mun, C., Yeom, J., Park, J. S., Jung, H. S., et al. (2021). Nanoconfined 3D redox capacitor-based electrochemical sensor for ultrasensitive monitoring of metabolites in bacterial communication. *Sensors Actuators B: Chem.* 345, 130427. doi: 10.1016/j.snb.2021.130427

Karacan, C., Erkek, N., Senel, S., Akin Gunduz, S., Catli, G., and Tavil, B. (2010). Evaluation of urine collection methods for the diagnosis of urinary tract infection in children. *Med. Principles Pract.* 19, 188–191. doi: 10.1159/000273068

Karlsen, H., and Dong, T. (2015). Biomarkers of urinary tract infections: state of the art, and promising applications for rapid strip-based chemical sensors. *Anal. Methods* 7, 7961–7975. doi: 10.1039/C5AY01678A

Katongole, P., Nalubega, F., Florence, N. C., Asiimwe, B., and Andia, I. (2020). Biofilm formation, antimicrobial susceptibility and virulence genes of Uropathogenic *Escherichia coli* isolated from clinical isolates in Uganda. *BMC Infect. Dis.* 20, 453. doi: 10.1186/s12879-020-05186-1

Kaufman, J., Temple-Smith, M., and Sanci, L. (2019). Urinary tract infections in children: an overview of diagnosis and management. *BMJ Paedia. Open* 3, e000487. doi: 10.1136/bmjpo-2019-000487

Kelly, B. N. (2023). UTI detection by PCR: Improving patient outcomes. *J. Mass Spectrom. Adv. Clin. Lab.* 28, 60–62. doi: 10.1016/j.jmsacl.2023.02.006

Kim, H. H., Chung, M. H., Bin, J. H., Cho, K. S., Lee, J., and Suh, J.-S. (2018). Urinary YKL-40 as a candidate biomarker for febrile urinary tract infection in young children. *Ann. Lab. Med.* 38, 39–45. doi: 10.3343/alm.2018.38.1.39

Kinney, A. B., and Blount, M. (1979). Effect of cranberry juice on urinary pH. *Nurs. Res.* 28, 287–290. doi: 10.1097/00006199-197909000-00012

Kjölvmark, C., Åkesson, P., and Linder, A. (2012). Elevated urine levels of heparin-binding protein in children with urinary tract infection. *Pediatr. Nephrol.* 27, 1301–1308. doi: 10.1007/s00467-012-2132-x

Kjölvmark, C., Påhlman, L. I., Åkesson, P., and Linder, A. (2014). Heparin-binding protein: A diagnostic biomarker of urinary tract infection in adults. *Open Forum Infect. Dis.* 1, ofu004. doi: 10.1093/ofid/ofu004

Kogan, M. I., Naboka, Y. L., Ibishev, K. S., Gudima, I. A., and Naber, K. G. (2015). Human urine is not sterile - shift of paradigm. *Urol. Internation.* 94, 445–452. doi: 10.1159/000369631

Konwar, A. N., and Borse, V. (2020). Current status of point-of-care diagnostic devices in the Indian healthcare system with an update on COVID-19 pandemic. *Sensors Int.* 1, 100015. doi: 10.1016/j.sintl.2020.100015

Krcmery, S., Hromec, J., and Demesova, D. (2001). Treatment of lower urinary tract infection in pregnancy. *Int. J. Antimicrob. Agents* 17, 279–282. doi: 10.1016/S0924-8579(00)00351-4

Kumar, R., Chhibber, S., Gupta, V., and Harjai, K. (2011). Screening & profiling of quorum sensing signal molecules in *Pseudomonas aeruginosa* isolates from catheterized urinary tract infection patients. *Indian J. Med. Res.* 134, 208–213.

Kumar, M. S., Ghosh, S., Nayak, S., and Das, A. P. (2016). Recent advances in biosensor based diagnosis of urinary tract infection. *Biosensors Bioelectron.* 80, 497–510. doi: 10.1016/j.bios.2016.02.023

Kumari, A., Pasini, P., and Daunert, S. (2008). Detection of bacterial quorum sensing N-acyl homoserine lactones in clinical samples. *Anal. Bioanal. Chem.* 391, 1619–1627. doi: 10.1007/s00216-008-2002-3

Lam, C.-W., Law, C.-Y., Sze, K.-H., and To, K. K.-W. (2015). Quantitative metabolomics of urine for rapid etiological diagnosis of urinary tract infection: Evaluation of a microbial–mammalian co-metabolite as a diagnostic biomarker. *Clinica Chimica Acta* 438, 24–28. doi: 10.1016/j.cca.2014.07.038

Lehmann, L. E., Hauser, S., Malinka, T., Klaschik, S., Weber, S. U., Schewe, J.-C., et al. (2011). Rapid qualitative urinary tract infection pathogen identification by septiFast® Real-time PCR. *PloS One* 6, e17146. doi: 10.1371/journal.pone.0017146

Li, R., and Leslie, S. W. (2023). Cystitis.

Linder, A., Soehnlein, O., and Åkesson, P. (2010). Roles of Heparin-Binding Protein in Bacterial Infections. *J Innate Immun.* 2 (5), 431–438. doi: 10.1159/000314853

Liu, Z., Tang, H., Xu, H., Lu, G., Yang, W., Xia, Z., et al. (2022). Rapid identification and drug sensitivity test to urinary tract infection pathogens by DOT-MGA. *Infect. Drug Resist.* 15, 1391–1397. doi: 10.2147/IDR.S356045

Loh, K., and Sivalingam, N. (2007). Urinary tract infections in pregnancy. *Malay. Family Physician : Off. J. Acad. Family Phys. Malaysia* 2, 54–57.

Lubell, T. R., Barasch, J. M., Xu, K., Ieni, M., Cabrera, K. I., and Dayan, P. S. (2017). Urinary neutrophil gelatinase–associated lipocalin for the diagnosis of urinary tract infections. *Pediatrics* 140. doi: 10.1542/peds.2017-1090

Lundstedt, A., Leijonhufvud, I., Ragnarsdottir, B., Karpman, D., Andersson, B., and Svanborg, C. (2007). Inherited susceptibility to acute pyelonephritis: A family study of urinary tract infection. *J. Infect. Dis.* 195, 1227–1234. doi: 10.1086/512620

Luppa, P. B., Müller, C., Schlichtiger, A., and Schlebusch, H. (2011). Point-of-care testing (POCT): Current techniques and future perspectives. *TrAC Trends Anal. Chem.* 30, 887–898. doi: 10.1016/j.trac.2011.01.019

Mamatha, G. (2020). Role of C-reactive protein levels in differentiating upper urinary tract infection and lower urinary tract infection in adults. *J. Med. Sci. And Clin. Res.* 08, 269–274. doi: 10.18535/jmscr/v8i2.49

Mambatta, A., Jayarajan, J., Rashme, V., Harini, S., Menon, S., and Kuppusamy, J. (2015). Reliability of dipstick assay in predicting urinary tract infection. *J. Family Med. Prim. Care* 4, 265. doi: 10.4103/2249-4863.154672

Mancuso, G., Midiri, A., Gerace, E., Marra, M., Zummo, S., and Biondo, C. (2023). Urinary tract infections: the current scenario and future prospects. *Pathogens* 12, 623. doi: 10.3390/pathogens12040623

Marmor, S., and Kerroumi, Y. (2016). Patient-specific risk factors for infection in arthroplasty procedure. *Orthop. Traumatol.: Surg. Res.* 102, S113–S119. doi: 10.1016/j.otsr.2015.05.012

Martischang, R., Godycki-Ćwirko, M., Kowalczyk, A., Kosiek, K., Turjeman, A., Babich, T., et al. (2021). Risk factors for treatment failure in women with uncomplicated lower urinary tract infection. *PloS One* 16, e0256464. doi: 10.1371/journal.pone.0256464

Mashaly, G. E.-S., El-Kazzaz, S. S., and Zeid, M. S. (2020). Urine YKL-40 versus urine NGAL as potential markers for diagnosis of urinary tract infection in febrile pediatric patients. *Open J. Immunol.* 10, 10–20. doi: 10.4236/oji.2020.101002

Mazaheri, M. (2021). Serum interleukin-6 and interleukin-8 are sensitive markers for early detection of pyelonephritis and its prevention to progression to chronic kidney disease. *Int. J. Prev. Med.* 12, 2. doi: 10.4103/ijpvm.IJPVM_50_19

Michael, I., Kim, D., Gulenko, O., Kumar, S., Kumar, S., Clara, J., et al. (2020). A fidget spinner for the point-of-care diagnosis of urinary tract infection. *Nat. Biomed. Eng.* 4, 591–600. doi: 10.1038/s41551-020-0557-2

Miller, C., and Gilmore, J. (2020). Detection of quorum-sensing molecules for pathogenic molecules using cell-based and cell-free biosensors. *Antibiotics* 9, 259. doi: 10.3390/antibiotics9050259

Montagut, E. J., Martin-Gomez, M. T., and Marco, M. P. (2021). An immunochemical approach to quantify and assess the potential value of the pseudomonas quinolone signal as a biomarker of infection. *Anal. Chem.* 93, 4859–4866. doi: 10.1021/acs.analchem.0c04731

Montagut, E. J., Raya, J., Martin-Gomez, M.-T., Vilaplana, L., Rodriguez-Urretavizcaya, B., and Marco, M.-P. (2022). An immunochemical approach to detect the quorum sensing-regulated virulence factor 2-heptyl-4-quinoline N-oxide (HQNO) produced by *pseudomonas aeruginosa* clinical isolates. *Microbiol. Spectr.* 10, 3237–3246. doi: 10.1128/spectrum.01073-21

Montagut, E. J., Vilaplana, L., Martin-Gomez, M. T., and Marco, M. P. (2020). High-throughput immunochemical method to assess the 2-heptyl-4-quinolone quorum sensing molecule as a potential biomarker of *pseudomonas aeruginosa* infections. *ACS Infect. Dis.* 6, 3237–3246. doi: 10.1021/acsinfecdis.0c00604

Moon, J. H., Yoo, K. H., and Yim, H. E. (2021). Urinary neutrophil gelatinase-associated lipocalin: a marker of urinary tract infection among febrile children. *Clin. Exp. Pediatr.* 64, 347–354. doi: 10.3345/cep.2020.01130

Muljadi, M., Cheng, C.-M., and Shen, C.-J. (2021). Development of a tetrazolium-derived paper-based diagnostic device as an early, alternative bacteria screening tool. *Micromachines* 13, 44. doi: 10.3390/mi13010044

Narayan Swamy, S. N., Jakanur, R. K., and Sangeetha, S. R. (2022). Significance of C-reactive protein levels in categorizing upper and lower urinary tract infection in adult patients. *Cureus.* 14 (6), e26432. doi: 10.7759/cureus.26432

Naseri, M., Halder, A., Mohammadniaei, M., Prado, M., Ashley, J., and Sun, Y. (2021). A multivalent aptamer-based electrochemical biosensor for biomarker detection in urinary tract infection. *Electrochimica Acta* 389, 138644. doi: 10.1016/j.electacta.2021.138644

Naseri, M., Ziora, Z. M., Simon, G. P., and Batchelor, W. (2022). ASSURED-compliant point-of-care diagnostics for the detection of human viral infections. *Rev. Med. Virol.* 32. doi: 10.1002/rmv.2263

Neu, H. C. (1992). Optimal characteristics of agents to treat uncomplicated urinary tract infections. *Infection* 20, S266–S271. doi: 10.1007/BF01710012

Newman, J. W., Floyd, R. V., and Fothergill, J. L. (2017). The contribution of *Pseudomonas aeruginosa* virulence factors and host factors in the establishment of urinary tract infections. *FEMS Microbiol. Lett.* 364, fnx124. doi: 10.1093/femsle/fnx124

Nicolle, L. E. (2003). Urinary tract infection: Traditional pharmacologic therapies. *Disease-a-Month* 49, 111–128. doi: 10.1067/mda.2003.11

Nicolle, L. E. (2014). Catheter associated urinary tract infections. *Antimicrob. Resist. Infect. Control* 3, 23. doi: 10.1186/2047-2994-3-23

Nicolle, L. E., Bradley, S., Colgan, R., Rice, J. C., Schaeffer, A., and Hooton, T. M. (2005).Infectious diseases society of America guidelines for the diagnosis and treatment of asymptomatic bacteriuria in adults. Available online at: https://about.jstor.org/terms.

Noiphung, J., and Laiwattanapaisal, W. (2019). Multifunctional paper-based analytical device for *in situ* cultivation and screening of escherichia coli infections. *Sci. Rep.* 9, 1555. doi: 10.1038/s41598-018-38159-1

Novelli, A., and Rosi, E. (2017). Pharmacological properties of oral antibiotics for the treatment of uncomplicated urinary tract infections. *J. Chemother.* 29, 10–18. doi: 10.1080/1120009X.2017.1380357

Oliveira, W. D., Lopes Barboza, M. G., Faustino, G., Yamanaka Inagaki, W. T., Sanches, M. S., Takayama Kobayashi, R. K., et al. (2021). Virulence, resistance and clonality of *Proteus mirabilis* isolated from patients with community-acquired urinary tract infection (CA-UTI) in Brazil. *Microbial. Pathogen.* 152, 104642. doi: 10.1016/j.micpath.2020.104642

Oros, D., Ceprnja, M., Zucko, J., Cindric, M., Hozic, A., Skrlin, J., et al. (2020). Identification of pathogens from native urine samples by MALDI-TOF/TOF tandem mass spectrometry. *Clin. Proteomics* 17, 25. doi: 10.1186/s12014-020-09289-4

Pan, Y., Sonn, G. A., Sin, M. L. Y., Mach, K. E., Shih, M.-C., Gau, V., et al. (2010). Electrochemical immunosensor detection of urinary lactoferrin in clinical samples for urinary tract infection diagnosis. *Biosensors Bioelectron.* 26, 649–654. doi: 10.1016/j.bios.2010.07.002

Pardeshi, P. (2020). Prevalence of urinary tract infections and current scenario of antibiotic susceptibility pattern of bacteria causing UTI. *Indian J. Microbiol. Res.* 5, 334–338. doi: 10.18231/2394-5478.2018.0070

Pastells, C., Pascual, N., Sanchez-Baeza, F., and Marco, M.-P. (2016). Immunochemical determination of pyocyanin and 1-hydroxyphenazine as potential biomarkers of *pseudomonas aeruginosa* infections. *Anal. Chem.* 88, 1631–1638. doi: 10.1021/acs.analchem.5b03490

Pernille, H., Lars, B., Marjukka, M., Volkert, S., and Anne, H. (2019). Sampling of urine for diagnosing urinary tract infection in general practice - First-void or mid-stream urine? *Scand J Prim Health Care.* 37 (1), 113–119. doi: 10.1080/02813432.2019.1568708

Perrotta, C., Aznar, M., Mejia, R., Albert, X., and Ng, C. W. (2008). Oestrogens for preventing recurrent urinary tract infection in postmenopausal women. *Cochrane Database System. Rev.* doi: 10.1002/14651858.CD005131.pub2

Price, J. R., Guran, L., Lim, J. Y., Megli, C. J., Clark, A. L., Edwards, S. R., et al. (2017). Neutrophil gelatinase–associated lipocalin biomarker and urinary tract infections: A diagnostic case-control study (NUTI study). *Female Pelvic Med. Reconstruct. Surg.* 23, 101–107. doi: 10.1097/SPV.0000000000000366

Rafiee, M., and Ghaemi, E. A. (2023). Detection of virulence genes among *Staphylococcus saprophyticus* isolated from women with urinary tract infections: first report from Iran. *BMC Res. Notes* 16, 206. doi: 10.1186/s13104-023-06481-1

Riccabona, M. (2016). Imaging in childhood urinary tract infection. *La Radiol. Med.* 121, 391–401. doi: 10.1007/s11547-015-0594-1

Rosenberg, M., Berger, S. A., Barki, M., Goldberg, S., Fink, A., and Miskin, A. (1992). Initial testing of a novel urine culture device. *J. Clin. Microbiol.* 30, 2686–2691. doi: 10.1128/jcm.30.10.2686-2691.1992

Rowe, T. A., and Juthani-Mehta, M. (2013). Urinary tract infection in older adults. *Aging Health* 9, 519–528. doi: 10.2217/ahe.13.38

Rychert, J. (2019). Benefits and limitations of MALDI-TOF mass spectrometry for the identification of microorganisms. *J. Infectiol.* 2, 1–5. doi: 10.29245/2689-9981/2019/4.1142

Sahu, R., Sahoo, R. K., Prusty, S. K., and Sahu, P. K. (2018). Urinary tract infection and its management. *System. Rev. Pharm.* 10, 42–48. doi: 10.5530/srp.2019.1.7

Saliba, W., Nitzan, O., Chazan, B., and Elias, M. (2015). Urinary tract infections in patients with type 2 diabetes mellitus: review of prevalence, diagnosis, and management. *Diab. Metab. Syndr. Obes.: Targets Ther.* 129, 129–136. doi: 10.2147/DMSO.S51792

Sarshar, M., Behzadi, P., Ambrosi, C., Zagaglia, C., Palamara, A. T., and Scribano, D. (2020). FimH and anti-adhesive therapeutics: A disarming strategy against uropathogens. *Antibiotics* 9, 397. doi: 10.3390/antibiotics9070397

Scarparo, C., Piccoli, P., Ricordi, P., and Scagnelli, M. (2002). Evaluation of the dipstreak, a new device with an original streaking mechanism for detection, counting, and presumptive identification of urinary tract pathogens. *J Clin Microbiol.* 40 (6), 2169–2178. doi: 10.1128/JCM.40.6.2169-2178.2002

Schmiemann, G., Kniehl, E., Gebhardt, K., Matejczyk, M. M., and Hummers-Pradier, E. (2010). The diagnosis of urinary tract infection. *Deutsches Ärzteblatt Int.* 107 (21), 361–367. doi: 10.3238/arztebl.2010.0361

Schneeberger, C., Kazemier, B. M., and Geerlings, S. E. (2014). Asymptomatic bacteriuria and urinary tract infections in special patient groups. *Curr. Opin. Infect. Dis.* 27, 108–114. doi: 10.1097/QCO.0000000000000028

Scholes, D., Hooton, T. M., Roberts, P. L., Gupta, K., Stapleton, A. E., and Stamm, W. E. (2005). Risk factors associated with acute pyelonephritis in healthy women. *Ann. Internal Med.* 142, 20. doi: 10.7326/0003-4819-142-1-200501040-00008

Seifu, W. D., and Gebissa, A. D. (2018). Prevalence and antibiotic susceptibility of Uropathogens from cases of urinary tract infections (UTI) in Shashemene referral hospital, Ethiopia. *BMC Infect. Dis.* 18, 30. doi: 10.1186/s12879-017-2911-x

Shah, C., Baral, R., Bartaula, B., and Shrestha, L. B. (2019). Virulence factors of uropathogenic *Escherichia coli* (UPEC) and correlation with antimicrobial resistance. *BMC Microbiol.* 19, 204. doi: 10.1186/s12866-019-1587-3

Sharma, S., Verma, P. K., Rawat, V., Varshney, U., and Singh, R. K. (2021). Fosfomycin versus nitrofurantoin for the treatment of lower UTI in outpatients. *J. Lab. Phys.* 13, 118–122. doi: 10.1055/s-0041-1729141

Sharmin, S., Kamal, S. M. M., Md., A., Elahi, K. M. A., Elma, S. M. M., and Habib, B. (2022). Fosfomycin—A promising oral antibiotic for the treatment of urinary tract infection (UTI). *Open J. Urol.* 12, 257–270. doi: 10.4236/oju.2022.125026

Sharp, D., Gladstone, P., Smith, R. B., Forsythe, S., and Davis, J. (2010). Approaching intelligent infection diagnostics: Carbon fibre sensor for electrochemical pyocyanin detection. *Bioelectrochemistry* 77, 114–119. doi: 10.1016/j.bioelechem.2009.07.008

Shaw, J. L. V. (2016). Practical challenges related to point of care testing. *Pract. Lab. Med.* 4, 22–29. doi: 10.1016/j.plabm.2015.12.002

Shih, C.-M., Chang, C.-L., Hsu, M.-Y., Lin, J.-Y., Kuan, C.-M., Wang, H.-K., et al. (2015). Paper-based ELISA to rapidly detect *Escherichia coli*. *Talanta* 145, 2–5. doi: 10.1016/j.talanta.2015.07.051

Siddiqui, H., Nederbragt, A. J., Lagesen, K., Jeansson, S. L., and Jakobsen, K. S. (2011). Assessing diversity of the female urine microbiota by high throughput sequencing of 16S rDNA amplicons. *BMC Microbiol.* 11, 244. doi: 10.1186/1471-2180-11-244

Sinawe, H., and Casadesus, D. (2023). Urine culture.

Singhal, N., Kumar, M., Kanaujia, P. K., and Virdi, J. S. (2015).). MALDI-TOF mass spectrometry: an emerging technology for microbial identification and diagnosis. *Front. Microbiol.* 6. doi: 10.3389/fmicb.2015.00791

Smelov, V., Naber, K., and Bjerklund Johansen, T. E. (2016). Improved classification of urinary tract infection: future considerations. *Eur. Urol. Suppl.* 15, 71–80. doi: 10.1016/j.eursup.2016.04.002

Soo Park, B., Lee, S.-J., Wha Kim, Y., Sik Huh, J., Il Kim, J., and Chang, S.-G. (2006). Outcome of nephrectomy and kidney-preserving procedures for the treatment of emphysematous pyelonephritis. *Scandinavian J. Urol. Nephrol.* 40, 332–338. doi: 10.1080/00365590600794902

Stapleton, A. E., Au-Yeung, M., Hooton, T. M., Fredricks, D. N., Roberts, P. L., Czaja, C. A., et al. (2011). Randomized, placebo-controlled phase 2 trial of a *lactobacillus crispatus* probiotic given intravaginally for prevention of recurrent urinary tract infection. *Clin. Infect. Dis.* 52, 1212–1217. doi: 10.1093/cid/cir183

St-Louis, P. (2000). Status of point-of-care testing: promise, realities, and possibilities. *Clin. Biochem.* 33, 427–440. doi: 10.1016/S0009-9120(00)00138-7

Storme, O., Tirán Saucedo, J., Garcia-Mora, A., Dehesa-Dávila, M., and Naber, K. G. (2019). Risk factors and predisposing conditions for urinary tract infection. *Ther. Adv. Urol.* 11, 175628721881438. doi: 10.1177/1756287218814382

Svetličić, E., Dončević, L., Ozdanovac, L., Janeš, A., Tustonić, T., Štajduhar, A., et al. (2022). Direct identification of urinary tract pathogens by MALDI-TOF/TOF analysis and *de novo* peptide sequencing. *Molecules* 27, 5461. doi: 10.3390/molecules27175461

Tabatabaei, A., Ahmadi, K., Namazi Shabestari, A., Khosravi, N., and Badamchi, A. (2021). Virulence genes and antimicrobial resistance pattern in *Proteus mirabilis* strains isolated from patients attended with urinary infections to Tertiary Hospitals, in Iran. *Afr. Health Sci.* 21, 1677–1684. doi: 10.4314/ahs.v21i4.22

Tabibian, J. H., Gornbein, J., Heidari, A., Dien, S. L., Lau, V. H., Chahal, P., et al. (2008). Uropathogens and host characteristics. *J. Clin. Microbiol.* 46, 3980–3986. doi: 10.1128/JCM.00339-08

Tan, C., and Chlebicki, M. (2016). Urinary tract infections in adults. *Singapore Med. J.* 57, 485–490. doi: 10.11622/smedj.2016153

Tang, Y., and Zhou, Q. (2022). Changes in serum CRP and PCT levels in patients with acute simple lower urinary tract infection and evaluation of the efficacy of treatment with Shuangdong capsules. *Emergency Med. Int.* 2022, 1–7. doi: 10.1155/2022/9750237

Terlizzi, M. E., Gribaudo, G., and Maffei, M. E. (2017). UroPathogenic *escherichia coli* (UPEC) infections: virulence factors, bladder responses, antibiotic, and non-antibiotic antimicrobial strategies. *Front. Microbiol.* 8. doi: 10.3389/fmicb.2017.01566

Toledo-Arana, A., Valle, J., Solano, C., Arrizubieta, M. J., Cucarella, C., Lamata, M., et al. (2001). The enterococcal surface protein, esp, is involved in enterococcus faecalis biofilm formation. *Appl. Environ. Microbiol.* 67, 4538–4545. doi: 10.1128/AEM.67.10.4538-4545.2001

Tseng, W.-T., Chou, Y.-Y., Wu, J.-G., Wang, Y.-C., Tseng, T.-N., Pan, S.-W., et al. (2023). An electrochemical conducting polymer-based biosensor for Leukocyte esterase and nitrite detection for diagnosing urinary tract infections: A pilot study. *Microchem. J.* 188, 108493. doi: 10.1016/j.microc.2023.108493

Ünsal, H., Kaman, A., and Tanır, G. (2019). Relationship between urinalysis findings and responsible pathogens in children with urinary tract infections. *J. Pediatr. Urol.* 15, 606.e1–606.e6. doi: 10.1016/j.jpurol.2019.09.017

Urbschat, A., Obermüller, N., Paulus, P., Reissig, M., Hadji, P., Hofmann, R., et al. (2014). Upper and lower urinary tract infections can be detected early but not be discriminated by urinary NGAL in adults. *Int. Urol. Nephrol.* 46, 2243–2249. doi: 10.1007/s11255-014-0831-x

Vasudevan, R. (2014). Urinary tract infection: an overview of the infection and the associated risk factors. *J. Microbiol. Experiment.* 1, 00008. doi: 10.15406/jmen.2014.01.00008

Vasudevan, S., Srinivasan, P., Rayappan, J. B. B., and Solomon, A. P. (2020). A photoluminescence biosensor for the detection of N -acyl homoserine lactone using cysteamine functionalized ZnO nanoparticles for the early diagnosis of urinary tract infections. *J. Mater. Chem. B* 8, 4228–4236. doi: 10.1039/C9TB02243K

Vellinga, A., Cormican, M., Hanahoe, B., Bennett, K., and Murphy, A. W. (2011). Antimicrobial management and appropriateness of treatment of urinary tract infection in general practice in Ireland. *BMC Family Pract.* 12, 108. doi: 10.1186/1471-2296-12-108

Venkatesh, L. (2017). Acute pyelonephritis - correlation of clinical parameter with radiological imaging abnormalities. *J. Clin. Diagn. Res.* TC15–TC18. doi: 10.7860/JCDR/2017/27247.10033

Vyas, S. (2015). Role of behavioural risk factors in symptoms related to UTI among nursing students. *J. Clin. Diagn. Res.* 9 (9), LC15–LC18. doi: 10.7860/JCDR/2015/10995.6547

Wagenlehner, F. M. E., Bjerklund Johansen, T. E., Cai, T., Koves, B., Kranz, J., Pilatz, A., et al. (2020). Epidemiology, definition and treatment of complicated urinary tract infections. *Nat. Rev. Urol.* 17, 586–600. doi: 10.1038/s41585-020-0362-4

Waisman, Y., Zerem, E., Amir, L., and Mimouni, M. (1999). The validity of the uriscreen test for early detection of urinary tract infection in children. *Pediatrics* 104, e41. doi: 10.1542/peds.104.4.e41

Wang, Y.-C., Tsai, Y.-H., Shen, C.-F., He, M.-Y., Fu, Y.-C., Sang, C.-Y., et al. (2021). Turntable paper-based device to detect *escherichia coli*. *Micromachines* 12, 194. doi: 10.3390/mi12020194

Wang, M.-C., Tseng, C.-C., Wu, A.-B., Lin, W.-H., Teng, C.-H., Yan, J.-J., et al. (2013). Bacterial characteristics and glycemic control in diabetic patients with Escherichia coli urinary tract infection. *J. Microbiol. Immunol. Infect.* 46, 24–29. doi: 10.1016/j.jmii.2011.12.024

Weese, J. S., Blondeau, J. M., Boothe, D., Breitschwerdt, E. B., Guardabassi, L., Hillier, A., et al. (2011). Antimicrobial use guidelines for treatment of urinary tract disease in dogs and cats: antimicrobial guidelines working group of the international society for companion animal infectious diseases. *Vet. Med. Int.* 2011, 1–9. doi: 10.4061/2011/263768

Wen, K. Y., Cameron, L., Chappell, J., Jensen, K., Bell, D. J., Kelwick, R., et al. (2017). A cell-free biosensor for detecting quorum sensing molecules in P. aeruginosa -infected respiratory samples. *ACS Synth. Biol.* 6, 2293–2301. doi: 10.1021/acssynbio.7b00219

Whelan, S., Lucey, B., and Finn, K. (2023). Uropathogenic *escherichia coli* (UPEC)-associated urinary tract infections: the molecular basis for challenges to effective treatment. *Microorganisms* 11, 2169. doi: 10.3390/microorganisms11092169

Wilksch, J. J., Yang, J., Clements, A., Gabbe, J. L., Short, K. R., Cao, H., et al. (2011). MrkH, a Novel c-di-GMP-Dependent Transcriptional Activator, Controls *Klebsiella pneumoniae* Biofilm Formation by Regulating Type 3 Fimbriae Expression. *PloS Pathog.* 7, e1002204. doi: 10.1371/journal.ppat.1002204

Wilson, M. L., and Gaido, L. (2004). Laboratory diagnosis of urinary tract infections in adult patients. *Clin. Infect. Dis.* 38, 1150–1158. doi: 10.1086/383029

Wojno, K. J., Baunoch, D., Luke, N., Opel, M., Korman, H., Kelly, C., et al. (2020). Multiplex PCR based urinary tract infection (UTI) analysis compared to traditional urine culture in identifying significant pathogens in symptomatic patients. *Urology* 136, 119–126. doi: 10.1016/j.urology.2019.10.018

Wolfe, A. J., Toh, E., Shibata, N., Rong, R., Kenton, K., FitzGerald, M., et al. (2012). Evidence of uncultivated bacteria in the adult female bladder. *J. Clin. Microbiol.* 50, 1376–1383. doi: 10.1128/JCM.05852-11

Wu, X., Chen, J., Li, X., Zhao, Y., and Zughaier, S. M. (2014). Culture-free diagnostics of *Pseudomonas aeruginosa* infection by silver nanorod array based SERS from clinical sputum samples. *Nanomed.: Nanotechnol. Biol. Med.* 10, 1863–1870. doi: 10.1016/j.nano.2014.04.010

Wu, P., Zuo, W., Wang, Y., Yuan, Q., Yang, J., Liu, X., et al. (2023). Multimodal capture – antibody-independent lateral flow immunoassay based on AuNF – PMBA for point-of-care diagnosis of bacterial urinary tract infections. *Chem. Eng. J.* 451, 139021. doi: 10.1016/j.cej.2022.139021

Xu, K., Wang, Y., Jian, Y., Chen, T., Liu, Q., Wang, H., et al. (2023). Staphylococcus aureus ST1 promotes persistent urinary tract infection by highly expressing the urease. *Front. Microbiol.* 14. doi: 10.3389/fmicb.2023.1101754

Yamamoto, A., Nakayama, S., Wakabayashi, Y., Yoshino, Y., and Kitazawa, T. (2023). Urine neutrophil gelatinase-associated lipocalin as a biomarker of adult pyelonephritis. *J. Infect. Chemother.* 29, 508–512. doi: 10.1016/j.jiac.2023.01.001

Yang, X., Chen, H., Zheng, Y., Qu, S., Wang, H., and Yi, F. (2022). Disease burden and long-term trends of urinary tract infections: A worldwide report. *Front. Public Health.* 10. doi: 10.3389/fpubh.2022.888205

Yang, S., and Rothman, R. E. (2004). PCR-based diagnostics for infectious diseases: uses, limitations, and future applications in acute-care settings. *Lancet Infect. Dis.* 4, 337–348. doi: 10.1016/S1473-3099(04)01044-8

Yetisen, A. K., Akram, M. S., and Lowe, C. R. (2013). Paper-based microfluidic point-of-care diagnostic devices. *Lab. Chip* 13, 2210. doi: 10.1039/c3lc50169h

Yilmaz, A., Sevketoglu, E., Gedikbasi, A., Karyagar, S., Kiyak, A., Mulazimoglu, M., et al. (2009). Early prediction of urinary tract infection with urinary neutrophil gelatinase associated lipocalin. *Pediatr. Nephrol.* 24, 2387–2392. doi: 10.1007/s00467-009-1279-6

Yoon, B. I., Kim, S. W., Ha, U.-S., Sohn, D. W., and Cho, Y.-H. (2013). Risk factors for recurrent cystitis following acute cystitis in female patients. *J. Infect. Chemother.* 19, 727–731. doi: 10.1007/s10156-013-0556-2

Yuyun, M. F., Angwafo, F. F. III, Koulla-Shiro, S., and Zoung-Kanyi, J. (2004). Urinary tract infections and genitourinary abnormalities in Cameroonian men. *Trop. Med. Int. Health* 9, 520–525. doi: 10.1111/j.1365-3156.2004.01219.x

Zaffanello, M., Malerba, G., Cataldi, L., Antoniazzi, F., Franchini, M., Monti, E., et al. (2010). Genetic risk for recurrent urinary tract infections in humans: A systematic review. *J. Biomed. Biotechnol.* 2010, 1–9. doi: 10.1155/2010/321082

Zeng, Z., Zhan, J., Zhang, K., Chen, H., and Cheng, S. (2022). Global, regional, and national burden of urinary tract infections from 1990 to 2019: an analysis of the global burden of disease study 2019. *World J. Urol.* 40, 755–763. doi: 10.1007/s00345-021-03913-0

Zunino, P. (2000). Virulence of a *Proteus mirabilis* ATF isogenic mutant is not impaired in a mouse model of ascending urinary tract infection. *FEMS Immunol. Med. Microbiol.* 29, 137–143. doi: 10.1016/S0928-8244(00)00198-X

frontiers | Frontiers in Cellular and Infection Microbiology

TYPE Review
PUBLISHED 25 September 2024
DOI 10.3389/fcimb.2024.1402932

OPEN ACCESS

EDITED BY
Andrea Marino,
University of Catania, Italy

REVIEWED BY
Nejat Duzgunes,
University of the Pacific, United States
Yingwang Ye,
Hefei University of Technology, China
Ricardo Oliveira,
National Institute for Agrarian and Veterinariay Research (INIAV), Portugal

*CORRESPONDENCE
Adline Princy Solomon
adlineprinzy@sastra.ac.in
Helma David
helmadavid@scbt.sastra.ac.in

†These authors have contributed equally to this work

RECEIVED 18 March 2024
ACCEPTED 03 September 2024
PUBLISHED 25 September 2024

CITATION
Sujith S, Naresh R, Srivisanth BU, Sajeevan A, Rajaramon S, David H and Solomon AP (2024) Aptamers: precision tools for diagnosing and treating infectious diseases.
Front. Cell. Infect. Microbiol. 14:1402932.
doi: 10.3389/fcimb.2024.1402932

Aptamers: precision tools for diagnosing and treating infectious diseases

Swathi Sujith†, Rajalakshmi Naresh†, B. U. Srivisanth†, Anusree Sajeevan, Shobana Rajaramon, Helma David* and Adline Princy Solomon*

Quorum Sensing Laboratory, Centre for Research in Infectious Diseases (CRID), School of Chemical and Biotechnology, SASTRA Deemed to be University, Thanjavur, India

Infectious diseases represent a significant global health challenge, with bacteria, fungi, viruses, and parasitic protozoa being significant causative agents. The shared symptoms among diseases and the emergence of new pathogen variations make diagnosis and treatment complex. Conventional diagnostic methods are laborious and intricate, underscoring the need for rapid, accurate techniques. Aptamer-based technologies offer a promising solution, as they are cost-effective, sensitive, specific, and convenient for molecular disease diagnosis. Aptamers, which are single-stranded RNA or DNA sequences, serve as nucleotide equivalents of monoclonal antibodies, displaying high specificity and affinity for target molecules. They are structurally robust, allowing for long-term storage without substantial activity loss. Aptamers find applications in diverse fields such as drug screening, material science, and environmental monitoring. In biomedicine, they are extensively studied for biomarker detection, diagnostics, imaging, and targeted therapy. This comprehensive review focuses on the utility of aptamers in managing infectious diseases, particularly in the realms of diagnostics and therapeutics.

KEYWORDS

aptamers, SELEX, biosensor, therapeutics, diagnosis, bacteria, virus, infectious disease

1 Introduction

Pathogens, such as bacteria, fungi, viruses, or parasitic protozoa transmitted throughout populations, are typically the source of infectious diseases, some recognized as potentially fatal (Wan et al., 2021; Krüger et al., 2021; Zhang et al., 2021). Infectious diseases continue to be a significant global public health concern, representing the primary causes of morbidity and mortality (Cohen, 2000). Similar signs and symptoms are common among numerous diseases, and the diagnosis, treatment, and management of infectious diseases may face significant difficulties due to the emergence of novel pathogens as well as the reappearance and rise of previously identified pathogen variations (Chen et al., 2022b)

(Wan et al., 2021). The rise of antimicrobial resistance can be attributed to the improper or empirical use of antibiotics in the treatment of infections. This underscores the need for careful and evidence-based antibiotic management in addressing infectious diseases (Fair and Tor, 2014; Rahbi et al., 2023). While laboratory testing, imaging scans, and biopsies based on clinical signs and epidemiological data have been successfully used to identify infections, these conventional procedures are either labor-intensive or highly complex (Wan et al., 2021; Zhang et al., 2021).

Therefore, it is imperative to develop new, quick, and precise diagnostic and therapeutic techniques to address the issues of drug resistance and anti-microbial resistance (Krüger et al., 2021). Aptamer-based diagnostic technologies are among the diagnostic approaches that are rapidly being employed for molecular disease diagnosis due to their cost-effectiveness, sensitivity, specificity, and convenience (Wan et al., 2021). The Latin word "aptus", which means "to fit," and the Greek word "meros", which means "region," are the sources of the word "aptamer" (Ku et al., 2015). Aptamers, single-stranded RNA or DNA oligonucleotide sequences with a length of approximately 25–80 bases, are the nucleotide counterparts of monoclonal antibodies. They may bind target molecules with high affinity and specificity, demonstrating the nucleic acid's multifunctional nature (Ni et al., 2021). Aptamers offer a range of benefits, such as being cost-effective, exhibiting minimal batch-to-batch variation, demonstrating low immunogenicity, and possessing a small size for improved tissue penetration (Otte et al., 2022). Despite their potential, aptamers are constrained by their rapid clearance through renal filtration and susceptibility to nuclease hydrolysis, leading to a very short half-life *in vivo* (Kovacevic et al., 2018; Ni et al., 2021). In response to these limitations, several techniques have been developed to extend the half-life. These include PEGylation for sustained action, modification of sugar ring or base, phosphodiester linkage, and 3′ end capping with inverted thymidine (Ni et al., 2017). Due to their structural stability, aptamers can be manufactured in large quantities and stored for extended periods without significant activity loss (Srivastava et al., 2021).

Various aptamers have been developed against various targets such as hormones, viruses, metal ions, proteins, viruses, and bacteria (Zhou and Rossi, 2017; Shraim et al., 2022). These complexes form stable and specific targets with dissociation constants in the nanomolar range. Additionally, aptamers have a greater target range, it is easier to regenerate, substantially smaller, and is neither poisonous nor immunogenic (García-Recio et al., 2016; Zheng et al., 2015; Roxo et al., 2019). New aptamer reports are released nearly daily due to their broad applicability. A specific database has been built (https://sites.utexas.edu/aptamerdatabase) to classify the aptamer-related data and enable access to information about various existent aptamers (Askari et al., 2024). Aptamers have drawn a lot of interest in the biomedical community due to their unique qualities and wide applications in a variety of sectors, including drug screening, material science, and environmental monitoring (Chen et al., 2022a).

Aptamers have been extensively studied and developed over the past 20 years by researchers in several biomedical fields, including biomarker detection, diagnostics, imaging, and targeted therapy. Aptamers that are now utilized in cancer treatment can bind to and block the immunoregulatory components of carcinogenesis, which are particular to molecular targets that are characteristic of various diseases. In December 2004, the US Food and Drug Administration approved pegaptanib (Macugen), the first medication based on aptamer technology, for the treatment of age-related macular degeneration (Adachi and Nakamura, 2019). Despite the lack of new aptamers approved for clinical use, there is promising progress in the development of aptamers for blood disorders, with several of them currently undergoing different stages of clinical trials and proof-of-concept investigations (Aljohani et al., 2022). Aptamers demonstrate a wide range of applications, highlighting their versatile nature in the field of infectious diseases. Thus, the review provides an in-depth insight into the general mechanism of aptamer selection and its applications in the diagnostic and therapeutic fields. Furthermore, it addresses recent advances and challenges in the field of aptamers, aiming to inspire further exploration of aptamer-based approaches in combating infectious diseases.

2 Mechanisms of aptamer selection

The process of aptamer selection includes a range of methodologies designed to identify nucleic acid sequences that can bind specific target molecules with high affinity and specificity (Kinghorn et al., 2017). Both SELEX (Systematic Evolution of Ligands by Exponential Enrichment) and non-SELEX approaches are used to refine methods. SELEX employs iterative rounds of selection, in which a nucleic acid library interacts with the target molecule under controlled conditions, to enhance sequences with optimal binding properties (Uemachi et al., 2021). Contrastingly, Non-SELEX methods steer clear of traditional scaffold-based approaches, opting instead for innovative strategies to bolster aptamer stability, specificity, and interaction dynamics (Kong and Byun, 2013). These diverse methodologies empower researchers to confidently tailor aptamer selection processes according to the specific requirements of their applications, from diagnostics to therapeutic interventions.

2.1 Systematic evolution of ligands by exponential enrichment

SELEX is a method used to derive aptamers from a pool of nucleotide sequences that exhibit high affinity and selectivity (Chen et al., 2016). The process involves several key steps to select aptamers through a repetitive cycle of amplification and enrichment. Initially, a large and diverse library of nucleic acid sequences (DNA or RNA) is synthesized and incubated with the target molecule in an appropriate buffer at a specific temperature (Sun et al., 2014). The partitioning or the eluting steps involves removal of the unbound nucleotide by chromatography, electrophoresis or filtration (Dong et al., 2018). A low ratio of nucleic acid sequences to the target molecule is used, ensuring effective binding. The aptamer-target complexes are then separated from unbound sequences using techniques such as capillary

electrophoresis (Hamedani and Müller, 2016), magnetic bead separation (Yüce et al., 2015), and flow cell methodologies (Gopinath, 2007).

The bound sequences are eluted from the target and amplified using PCR for DNA aptamers or reverse transcription followed by PCR for RNA aptamers, creating a new, enriched library. These processes are repeated for several rounds, typically 8-15, to enhance the prevalence of high-affinity species, which eventually dominate the library (Zhou and Rossi, 2017) (Figure 1). After multiple rounds of selection, the enriched library is cloned and sequenced to identify individual aptamer sequences, which are then validated for their binding performance. Through these iterative rounds, SELEX effectively isolates aptamers that can bind to specific target molecules with high affinity and specificity. However, a common drawback of aptamers derived from traditional SELEX methods is poor or nonspecific detection performance in diagnostic applications (Bakhtiari et al., 2021). To overcome these shortfalls, different methodologies are incorporated over conventional SELEX, some of which are discussed below.

2.1.1 Magnetic beads SELEX

Magnetic SELEX is a method that is commonly employed as this method offers ease in the separation of the target and nucleotide sequence easily from the remaining reaction mixture by employing a magnet (Yüce et al., 2015). When the DNA sequence binds with the target molecule, the mixture is now added with magnetic beads coated with a molecule that can selectively bind with the nucleic acid sequence attached to the target molecule. The elution of the bound nucleic acid sequences from the magnetic beads is achieved by altering the buffer's properties, applying heat, or utilizing other methods that hinder the nucleic acids' binding to the magnetic beads (Komarova and Kuznetsov, 2019). In previous research, the isolation of Metamitron (MTM) aptamers using magnetic-bead SELEX has been successful. MTM, a widely used herbicide in agriculture, has been the subject of a thorough investigation. It is important to note that even with significant exposure, the negative health effects on humans are minimal. Following ten rounds of screening, high-throughput sequencing successfully identified six

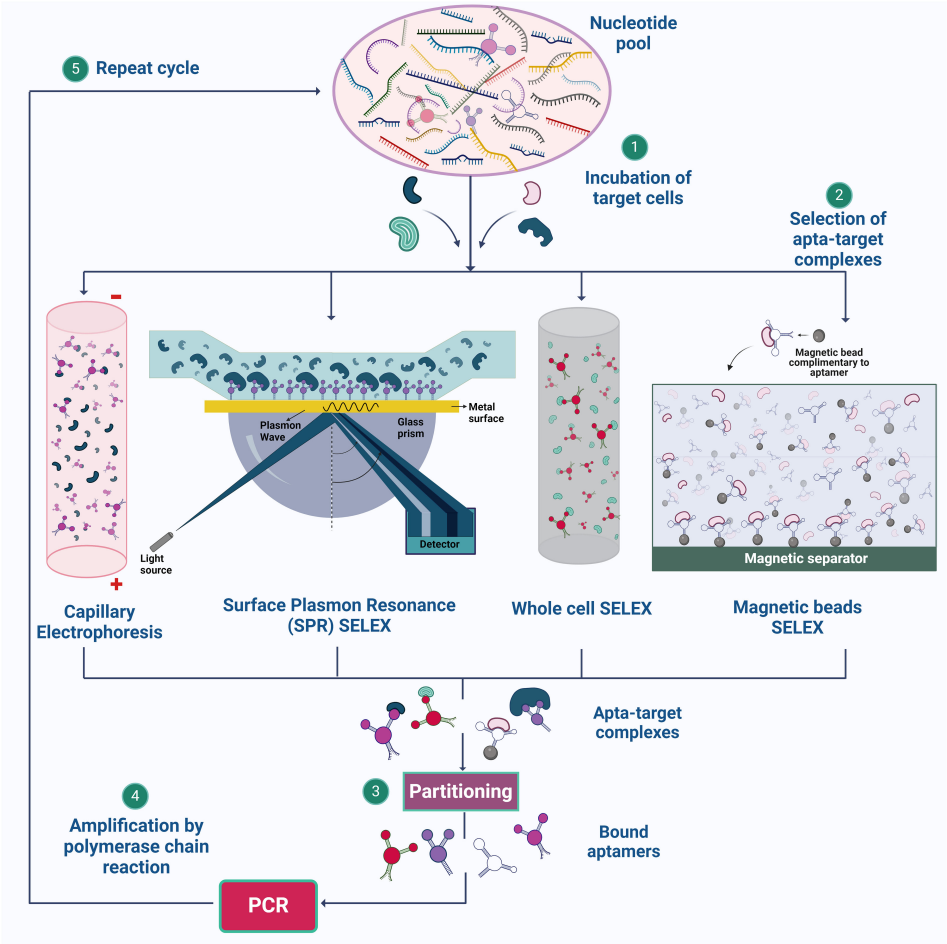

FIGURE 1
Illustration of SELEX strategies for aptamer synthesis. (1) The process begins with the preparation of a nucleotide pool, which is then incubated with target cells. (2) Various SELEX methods, such as Capillary Electrophoresis SELEX, SPR-SELEX, Whole Cell SELEX, and Magnetic Beads SELEX, are employed to facilitate the selection of aptamer-target complexes. (3) & (4) These complexes are isolated, and the bound aptamers are subsequently amplified by PCR. (5) The cycle is repeated multiple times to enhance the specificity and affinity of the aptamers for their targets. Created using Biorender.com.

outstanding candidate aptamers with remarkable affinity and specificity (Xie et al., 2022).

2.1.2 Capillary electrophoresis

Apart from using traditional gel electrophoresis, capillary electrophoresis (CE) is employed to derive aptamer candidates on the metrics of sizes and charge; under the electric field, capillary electrophoresis can separate molecules as tiny as porphyrin30 (Yüce et al., 2015). When performing CE-SELEX, the target molecules are subjected to incubation with the random library in free solution, and the resulting combination of free target molecules, target-ssDNA complexes, and free ssDNA is then fed into a capillary column, then split apart using a high voltage. Taking a sample of the output fraction at the designated retention time, target-bond ssDNA provides the chance to collect DNA aptamers that bind to a specific target (Hamedani and Müller, 2016). Demonstrating the perspective of CE-SELEX for small-molecule targets in just four rounds. Small-molecule targets are anticipated to alter the mobility of the complex only slightly from the nonbinding sequences, leading to only partial separation of the bound and unbound sequences. However, even if just a tiny amount of the complex can be recovered, adequate enrichment can be accomplished since nucleic acids can be exponentially amplified by polymerase chain reaction (PCR). Additionally, repeated recurrent rounds of enrichment can eventually lead to the evolution of an abundant pool with high quality, even in the situation of separation with poor resolution (Yang and Bowser, 2013).

When CE-SELEX and high throughput sequencing (HTS) gave higher efficiency with faster separation of target-ssDNA complex and free ssDNA in free solution, aptamers can be chosen with relatively fewer rounds of selection thanks to HTS, which offers insight into the sequence evolution during the CE-SELEX process and makes it possible to characterize the entire evolutionary path. This reduces the need for the pool to occupy a consensus sequence and increases selection efficiency (Zhu et al., 2021).

2.1.3 Whole cell SELEX

While the major targets for the other SELEX techniques are highly purified targets, whole cell-SELEX uses a complete cell as the target. The cell-SELEX procedure may aim for extracellular cell surface proteins or unidentified cell structures. This SELEX approach makes it possible to create whole-cell targeting aptamers without much prior information on the cell's surface proteins, which facilitates the identification of new biomarkers primarily for diagnosis and imaging (Yüce et al., 2015). The whole-cell SELEX method is used to create highly selective aptamers by different rounds of SELEX and counter SELEX. Aptamer can be separated using methods such as flow cytometry, Magnetic-Activated Cell Sorting, Differential Centrifugation, and Label-free methods. Whole-cell SELEX yields aptamers with high affinity and specificity when targeting bacterial surface compounds and live bacterial cells. Flow cytometry is a vital method for identifying target aptamers that bind selectively to cells. The technique overcomes the limitations of whole-cell SELEX by sorting, counting, and detecting fluorescence (Moon et al., 2013). Within flow cytometry techniques, fluorescence-Activated Cell Sorting (FACS) technique offers the ability to simultaneously differentiate and separate cell subpopulations, facilitating the identification of bound and unbound aptamers with specificity along with isolation of functional nucleic acids. By utilizing a sorting device that efficiently separates specific cells based on their fluorescence, FACS streamlines the process of finding aptamers that target different cell types contributing to a better yield of the aptamer candidates. The effectiveness of FACS in SELEX for functional aptamer selection is apparent in its successful separation of *E. coli* cells that produce RNA mimics (Nishimoto et al., 2007; Mayer et al., 2010; Zou et al., 2015). FACS is an effective method for large-scale aptamer screening because it is a fast and accurate technique that can process thousands of cells per second. It can sort cells based on multiple parameters and select aptamers based on their binding to live cells or complex mixtures, which may be more representative of physiological conditions than selections made *in vitro*. The possibility of obtaining high-quality aptamers is increased by the capacity to sort and enrich high-affinity binders from a huge library. FACS employs both positive and negative selection strategy, thereby reducing the experimental steps and experimental errors in the cell SELEX process, hence saves times. DNA Aptamers against Burkitt's lymphoma cells which exhibit a characteristic phenotype was chosen using positive selection methods (Ohuchi, 2012; Raddatz et al., 2008; Sola et al., 2020). Despite the benefits of the cell-SELEX system, the low aptamer enrichment performance of this technique is caused by the co-expression of several off-target surface indicators and compounds on the target cells (Sun et al., 2014).

2.1.4 Surface plasmon resonance or flow cell SELEX

SPR- SELEX utilizes SPR for the selection process, differentiating it from the other methods. A Randomized library is passed over a surface coated (gold surface) with the target molecule (Yüce et al., 2015). In the library, a diverse range of oligonucleotides interact with the target in various ways. Oligonucleotides demonstrating strong binding will firmly adhere to the target-coated surface, while those with weak binding or unbound sequences will be effectively washed away (Jia et al., 2018). In SPR the nucleic acid sequence bound to the target molecule will be monitored in real time by observing the change in the refractive index on the surface leading to the change in surface plasmon signal (Ferhan et al., 2016). With the help of the above-mentioned steps, specific aptamer candidates are carefully selected and amplified using PCR (Jia et al., 2018).

2.2 Non-SELEX methods

SELEX uses a nucleic acid scaffold to develop the aptamer; however, other techniques do not require scaffolds (Reverdatto et al., 2015). For instance, aptamers are produced in the RNase III-deficient *E. coli* HT115(DE3), and 5′- and 3′ ends of the RNA transcript are protected from the RNase using double stranded

spacers. This method only required fewer nucleotides than scaffold-based methods like the other different types of SELEX used to avoid RNase activity on the formed aptamer (Zou et al., 2023). PhotoSELEX, featuring photoreactive nucleic acids, confidently enhances control over the selection process. Upon exposure to light, the photoreactive groups confidently form covalent bonds between the selected aptamers and the target molecule, confidently providing a reliable method for identifying and capturing aptamer-target complexes (Brody et al., 1999). Graphene oxide (GO) is composed of carbon atoms arranged in a hexagonal lattice. Its unique properties allow for the immobilization of arbitrary DNA or RNA sequences on its surface, forming an oligonucleotide library with diverse sequences. During the GO-SELEX process, the target molecule interacts with the library-immobilized sequences. In the presence of the target molecule, the immobilized sequences on the GO surface are released and precisely interact with the target. This stage allows for the selection of aptamers with a high affinity for the target molecule (Nguyen et al., 2014; Ding and Liu, 2023). In the Capture-SELEX process, a DNA library is immobilized onto a substrate. The target of interest is then passed through to extract eluted aptamers. Aptamers are specifically chosen using this strategy for solute targets (Boussebayle et al., 2019). These non-SELEX methods provide versatile alternatives, overcoming challenges such as RNase degradation, and enhancing binding affinity through innovative selection techniques.

The aptamers that are selected can be used in various applications. One groundbreaking application is the use of apta-sensors for detecting infectious diseases. These biosensors use aptamers as recognition elements, and they provide fast, sensitive, and specific detection of pathogens. By incorporating aptamers selected through SELEX or Non-SELEX methods, apta-sensors can accurately detect infectious agents, greatly improving diagnostic capabilities. Their versatility and ability to detect a wide range of pathogens make aptasensors extremely valuable tools in epidemiology, healthcare settings, and biodefense (Brosseau et al., 2023).

3 Aptamers in diagnostics of infectious diseases

Traditional methodologies for detection encompass culture-based techniques and color culture medium approaches. However, these methodologies are encumbered by limitations, necessitating professional expertise, and demanding cumbersome labor and time commitments. The procedural intricacies include pre-enrichment, selective enrichment, and biochemical identification, typically leading to a confirmed outcome after 2-3 days (Bell et al., 2016). Due to the limitations present in these methods, there is a need for more efficient, rapid and accurate diagnostic methods. Immunological assays, such as ELISA and immunosensors, are commonly used for bacterial detection. However, their sensitivity is limited because proteins like immunoglobulins cannot be amplified. Furthermore, nucleic acid-based assays are unable to distinguish between viable and non-viable cells, as DNA can persist in the environment long after cell viability has been lost. This creates a need for a more specific, sensitive, and convenient diagnostic method that can bridge the gap between the detection. Aptamer-based assays are utilized for the detection of pathogens and biomarkers. Aptamers synthesis is rapid compared to the antibody production, and these rapid turnaround time helps in timely diagnosis. Furthermore, they have increased stability and shelf life compared to antibodies and reduced risk of immunogenicity due to ease of modifications that increase the stability, binding affinity and functionality (Ali et al., 2019). These assays enhance detection methods by providing improved specificity and sensitivity even at lower concentrations compared to traditional methods (Aslan et al., 2023). By delivering rapid results, which are ideal for point-of-care settings, this approach enhances diagnostic efficiency across various healthcare applications (Majdinasab et al., 2022). Further, the review delineates a comprehensive analysis of the diverse categories of apta-sensors. (Figure 2, Table 1).

3.1 Optical aptasensors

The components of an optical biosensor are an optical transducer system coupled with a biorecognition sensor. Optical biosensors are designed to generate a signal that is directly proportional to the concentration of the analyte (Damborský et al., 2016). Optical aptasensors are biosensors in which the biorecognition sensing element is an aptamer. The transduction method can be SPR, fluorescence, surface enhanced raman scattering (SERS) and chemiluminescence (Uniyal et al., 2023). Optical sensors are frequently used in aptasensors because of their high sensitivity, robustness, reliability, good temporal and spatial control, selectivity, simplicity, versatility, and wide linear range for biomolecule detection (Chen et al., 2021c).

3.1.1 Surface plasmon resonance based aptasensors

When a plane polarized light falls on a thin sheet of metal, plasmons (group of electrons that undergo oscillation due to energy absorption) are formed. In context of aptasensors, aptamer-functionalized metal particles are used. When the analyte binds to the aptamer, it causes changes in the refractive index at the interface, altering the resonance condition of the surface plasmons. These changes can be observed as variations in the angle or intensity of reflected light (Schasfoort, 2017). The sensitivity and selectivity of SPR-based sensors can be significantly improved by utilizing gold nanoparticles linked to ligands that are specific to the target. SPR assays are commonly used in dual-recognition biosensors and sandwich assays to enhance detection capabilities (Kim et al., 2018a).

3.1.2 Fluorescence based aptasensors

In this type of biosensing there are usually two probes involved-the capture probe that binds to the infectious agent and the signaling probe which is usually a nanoparticle that is tagged with a fluorophore. The interaction between the analyte and the

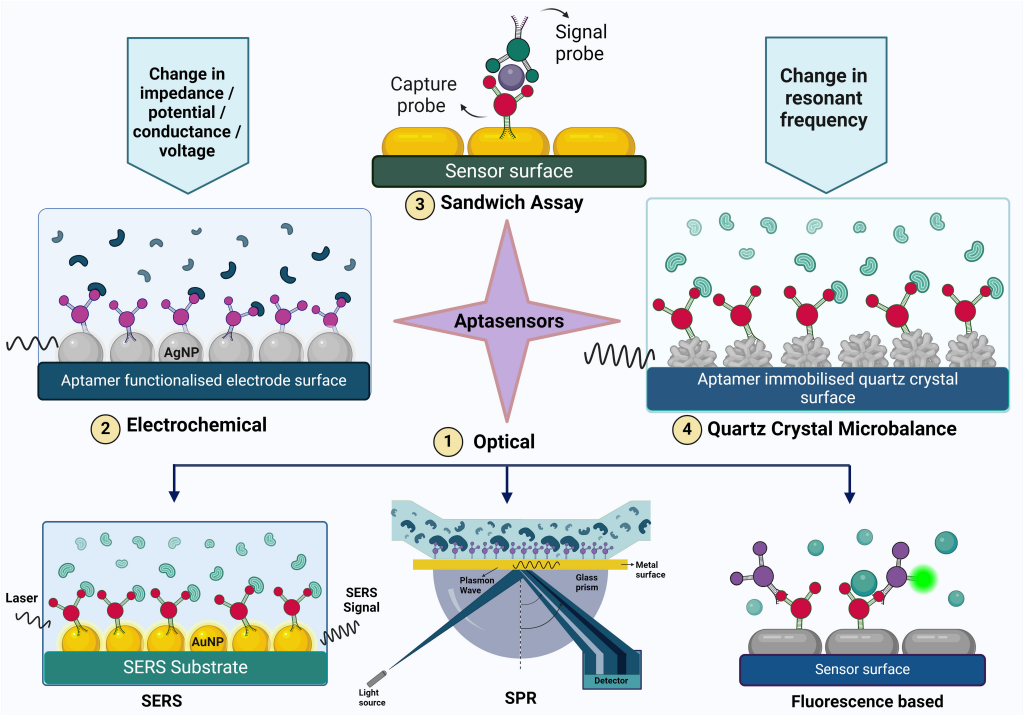

FIGURE 2
The figure illustrates various aptasensing mechanisms used for detecting target molecules. These mechanisms include (1) Optical sensors (such as Surface-Enhanced Raman Scattering (SERS), Surface Plasmon Resonance (SPR), and fluorescence-based methods), (2) Electrochemical sensors, (3) Sandwich assays, and (4) Quartz Crystal Microbalance (QCM). Each mechanism provides a unique approach to aptamer-based detection, highlighting the versatility and specificity of aptamers in biosensing applications.

aptamers leads to a rise in the fluorescence signal, which is detectable and can be analyzed in both qualitatively and quantitatively. Examples of fluorescent labels are Lanthanide-doped upconversion nanoparticles (UCNPs), silver nanoclusters (AgNCs) (Zhang et al., 2020), carbon quantum dots (CQDs) (Pebdeni et al., 2020), CdTe quantum dots and thiazole orange (Pang et al., 2015).

UCNPs have distinctive optical and chemical characteristics, including excellent photostability, low light scattering, low autofluorescence backgrounds, and low toxicity (Liu et al., 2021). AgNCs have the advantages of high quantum yield, strong photostability, low toxicity, adjustable fluorescence emission, and excellent biocompatibility (Zhang et al., 2020).

An important application of fluorescence spectroscopy is förster resonance energy transfer (FRET). It involves non-radiative transfer of energy from an excited donor fluorophore to an acceptor fluorophore that are in proximity. This phenomenon is also called quenching. Graphene oxide is a commonly used quencher molecule (Verma et al., 2023). For example, Pebdeni et al. discovered that CDQs emit blue-colored fluorescence, which is quenched in the presence of aptamers and gold nanoparticles. With the introduction of specific bacteria, the aptamer-target complex was effectively assembled, leading to the restoration of free CQD emission. The linear range of this aptasensor was 10^8 to 10^1 CFU/mL, with a detection limit as low as 10 CFU/mL for *S. aureus* (Pebdeni et al., 2020). Colorimetric aptasensors work by detecting changes in the color due to the binding of the aptamer to the analyte. This is done with the help of UV-visible spectroscopy. A peak is obtained at a specific wavelength and stokes shift takes place (Weerathunge et al., 2019).

3.1.3 SERS based aptasensors

Surface-enhanced Raman scattering (SERS) is a phenomenon in which the Raman scattering signals are amplified by enhancing the sensor surface. Nanostructured surfaces, usually made of metals such as gold or silver, are shaped into nanoparticles, nanorods, or nanostars. These structures demonstrate strong localized surface plasmon resonance (LSPR), resulting in the enhancement of Raman signals of nearby molecules through electromagnetic and chemical mechanisms. The SERS substrates are aptamers and when the infectious agent binds to the aptamer, there is a change in the raman signal that is detected (Zhou et al., 2020).

3.1.4 Chemiluminescence based aptasensors

Chemiluminescence-based aptasensors rely on the emission of light resulting from a chemical reaction between a luminophore (a molecule capable of emitting light) and a substrate or analyte, often facilitated by enzymatic reactions (Chen et al., 2021b). A DNA aptasensor to detect norovirus GII capsid was developed based on guanine chemiluminescence detection and the principle of intra chemiluminescent resonance transfer. The high-energy intermediates formed from the reaction of extra guanines and TMPG transferred the energy to 6-FAM which caused bright chemiluminescence (Kim et al., 2018a).

TABLE 1 Pathogen detection table: Pathogens, aptamer sequences, and detection mechanisms.

S.No.	Aptamer sequence (5′ to 3′)	Type	Organism	Target	Concentration range	LOD (limit of detection)	Methodology	Reference
Bacteria								
1.	S-S- ATCCGTCACACCTGCTCTGTCTGCGAGCGGGGC GCGGGCC CGGCGGGGGATGCGTGGTGTTGGCTCCCGTAT	DNA	*E. coli O157:H7*	Outer membrane proteins	10^1 to 10^5 CFU/mL	2.9×10^2 CFU/mL	Impedimetric aptasensor	(Brosel-Oliu et al., 2018)
2.	ATCCGTCACACCTGCTCTGTCTGCGAGCGGGGCGCGGGCCCGGC GGGGGATGCGTGGTGTTGGCTCCCGTAT	DNA	*E. coli O157:H7*	–	500 to $5x10^7$ CFU/mL	250 and 400 CFU/mL, for buffer and milk samples respectively	Eye-based microfluidic aptasensor (EA-Sensor)	(Li et al., 2020)
3.	CCATGAGTGTTGTGAAATGTTGGGACACTAGGTGGCATAGAGC CG-C_6-SH	DNA	*E. coli*	–	3.2×10^1 to 3.2×10^7 CFU/mL	3.46 CFU/mL	SERS aptasensor	(Ye et al., 2022)
4.	Apt1 (signal probe) A20-CCGGACGCTTATGCCTTGCCATCTACAGAGCAGGTGTGACGG Apt2 (capture probe) biotin-CCGGACGCTTATGCCTTGCCATCTACAGAGCAGGTGTGACGG-3	DNA	*E. coli O157:H7*	–	10 to 10000 CFU/mL	3 CFU/mL	Gold nanobones enhanced ultrasensitive SERS aptasensor	(Zhou et al., 2020)
5.	CAG TCC AGG ACA GAT TCG CGA G-N_{45}-CAC GTG GAT TTC ATT CAG CGA TT	ssDNA	*E. coli O157:H7*	–	–	1.46×10^3 CFU/mL	Aptamer-antibody sandwich assay	(Yu et al., 2018)
6.	ATCCAGAGTGACGCAGCA-(N45)- TGGACACGGTGGCTTAGT	DNA	*E. coli O78: K80:H11*	–	10^1 to 10^6 CFU/mL	10 CFU/mL	Bridged rebar graphene functionalized impedimetric aptasensor	(Kaur et al., 2017)
7.	ATCCAGAGTGACGCAGCA-(N45)-TGGACACG GTGGCTTAGT	ssDNA	*E. coli O157:H7*	–	10^0 to 10^5 CFU/mL	10 CFU/mL	Electrochemical aptasensor using boron-carbon nanorods decorated by nickel nanoparticles	(Kaur et al., 2020)
8.	P-CCG GAC GCT TAT GCC TTG CCA TCT ACA GAG CAG GTG TGA CGG	DNA	*E. coli O157:H7*	LPS of *E. coli* O157:H7	–	3 CFU/mL	Zirconium-based metal–organic framework$Ti_3C_2T_x$ nanosheet based faraday cage-type electrochemical aptasensor	(Dai et al., 2022)
9.	SH-ATC CGT CAC ACC TGC TCT GTC TGC GAG CGG GGC GCG GGC CCG GCG GGG GAT GCG TGG TGT TGG CTC CCG TAT	DNA	*E. coli O157:H7*	–	500 to 5000 CFU/mL	116 CFU/mL	MoS_2 nanosheets-based label-free colorimetric aptasensor	(Li et al., 2023)
10.	TATGGCGGCGTCACCCGACGGGGACTTGACA TTATGACAG	DNA	*Salmonella enterica*	–	10^8 to 10^1 CFU/mL	10^1 CFU/mL	Reduced graphene oxide-titanium dioxide nanocomposite-based electrochemical aptasensor	(Muniandy et al., 2019)
11.	–	dsDNA	*Salmonella typhimurium*	–	10 to 10^5 CFU/mL	6 CFU/mL	Aptasensor based immuno-HCR-SERS method with dual signal amplification capability	(Li et al., 2021)

(Continued)

10.3389/fcimb.2024.1402932

TABLE 1 Continued

S.No.	Aptamer sequence (5′ to 3′)	Type	Organism	Target	Concentration range	LOD (limit of detection)	Methodology	Reference
			Bacteria					
12.	C_6-NH_2-CTGTCATAAT GTCAAGTC	CdTe QD-labeled ssDNA2	*Salmonella typhimurium*	Outer membrane proteins	10 to 10^{10} CFU/mL	1 CFU/mL	Aptamer-based fluorescence assay	(Ren et al., 2019)
13.	ATTAGTCAAGAGGTAGACGCACATAAGGGGTCTGGTGTCGGGCCGC GGGTCAGGGGGGTAAGGGATTCTGGTCGTCGTGACTCCTAT	ssDNA	*Salmonella paratyphi A*	–	–	10 CFU/mL	FRET based aptasensor	(RM et al., 2020)
14.	Apt1 botin- GAGGAAAGTCTATAGCAGAGGAGATGTGTGAACCGAGTAA Apt2 CTCCTCTGACTGTAACCACGGAGTTAATCAATACAAGGCGGGAACA TCCTTGGCGGTGCCGCATAGGTAGTCCAGAAGCC	ssDNA	*Salmonella typhimurium*	–	3.3×10^1 to 3.3×10^6 CFU/mL	33 CFU/mL in pure culture and 95 CFU/mL in spiked milk	Colorimetric sensor based on dual aptamers - the absorbance intensity ratio (A_{523}/A_{650}) for quantitative analysis of various concentrations of bacteria	(Chen et al., 2021a)
15.	TAT GGC GGC GTC ACC CGA CGG GGA CTT GAC ATT ATG ACA G	DNA	*Salmonella typhimurium*	–	10 to 10^5 CFU/mL	4 CFU/mL	SERS using spiny gold nanoparticles (SGNPs)	(Ma et al., 2018)
16.	Apt 1 SH-AGTAATGCCCGGTAGTTATTCAAAGATGAGTAGGAAAAGA Apt2 ROX-AGTAATGCCCGGTAGTTATTCAAAGATGAGTAGGAAAAGA	DNA	*Salmonella typhimurium*		15 to 1.5×10^6 CFU/mL	15 CFU/mL	SERS-*S.typhimurium* specifically interacted with the aptamers to form Au@Ag-apt 1-target-apt 2-ROX sandwich-like complexes.	(Duan et al., 2016)
17.	HS-TATGGCGGCGTCACCCGACGGGGACTTGACATTATGACAG	ssDNA	*Salmonella enterica*		10 to 10^5 CFU/mL	1.223 CFU/mL	Competitive voltammetric aptasensor based on electrospun carbon nanofibers-gold nanoparticles modified graphite electrode	(Fathi et al., 2020)
18.	NH_2-TTT GGT CCT TGT CTT ATG TCC AGA ATG CGA GGA AAG TCT ATA GCA GAG GAG ATG TGT GAA CCG AGT AAA TTT CTC CTA CTG GGA TAG GTG GAT TAT	DNA	*Salmonella typhimurium*		10^1 to 10^8 CFU/mL	6 CFU/mL	Diazonium-based impedimetric aptasensor	(Bagheryan et al., 2016)
19.	NH_2-TAT GGC GGC GTC ACC CGA CGG GGA CTT GAC ATT ATG ACA-G	DNA	*Salmonella*		75 to 7.5×10^5 CFU/mL	25 CFU/mL	Impedimetric aptasensor using a glassy carbon electrode modified with an electrodeposited composite consisting of reduced graphene oxide and carbon nanotubes	(Jia et al., 2016)
20.	SH-GCA ATG GTA CGG TAC TTC CTC GGC ACG TTC TCA GTA GCG CTC GCT GGT CAT CCC ACA GCT ACG TCA AAA GTG CAC GCT ACT TTG CTA A	DNA	*S. aureus*		10^1 –10^7 CFU/mL	1 CFU/mL	Dual recognition aptasensor	(El-Wekil et al., 2022)

(Continued)

10.3389/fcimb.2024.1402932

TABLE 1 Continued

S.No.	Aptamer sequence (5′ to 3′)	Type	Organism	Target	Concentration range	LOD (limit of detection)	Methodology	Reference
				Bacteria				
21.	SH-TCG GCA CGT TCT CAG TAG CGC TCG CTG GTC ATC CCA CAG CTA CGT C	DNA	*S. aureus*		1.2×10^{1} to 1.2×10^{8} CFU/mL	1 CFU/mL	Electrochemical aptasensor using Au nanoparticles/carbon, nanoparticles/cellulose, nanofibers nanocomposite	(Ranjbar and Shahrokhian, 2018)
22.	GCG CCC TCT CAC GTG GCA CTC AGA GTG CCG GAA GTT CTG CGT TAT	DNA	*S. aureus*		10^{8} to 10^{1} CFU/mL	10 CFU/mL	Aptasensor based on the FRET between green carbon quantum dot and gold nanoparticle	(Pebdeni et al., 2020)
23.	ATACCAGCTTATTCAATTAGCAACATGAGGGGGATAGAGGGGGT GGGTTCTCTCGGCT	DNA	*S. aureus*	Targets protein A (surface bound virulence factor	–	10 CFU/mL	Impedimetric biosensor based on the protein A-binding aptamer	(Reich et al., 2017)
24.	–	DNA	*MRSA*	–	10^{2} to 10^{8} CFU/mL	Theoretical value = 2 CFU/mL Visual LOD <100 CFU/mL	Aptasensor swab designed for qualitative and quantitative detection, on contaminated non-absorbable surfaces.	(Raji et al., 2021)
25.	GCAATGGTACGGTACTTCCTC GGCACGTTCTCAGTAGCGCTCGCTGG TCATCCCACA GCTACGTCAAAAGTGCACGCTACTTTGCTAA	DNA	*S. aureus*	–	52 to 5.2×10^{7} CFU/mL	1 CFU/mL	An ultrasensitive sandwich–type electrochemical aptasensor using silver nanoparticle/titanium carbide nanocomposites	(Hui et al., 2022)
26.	–	–	*S. aureus*	–	7.6×10^{1} to 7.6×10^{7} CFU/mL	1.09 CFU/mL	Dual-recognition SERS biosensor based on teicoplanin functionalized gold-coated magnet NPs as capture probe and *S.aureus* aptamer functionalized silver coated gold NPs as signal probe	(Qi et al., 2022)
27.	NH_2- GCG CCC TCT CAC GTG GCA CTC AGA GTG CCG GAA GTT CTG CGT TAT	DNA	*S. aureus*	–	10^{2} to 10^{8} CFU/mL	80 CFU/mL	Aptamer and antibiotic-based dual detection sensor combining vancomycin-copper nanoclusters for the recognition and quantification using fluorescence	(Bagheri Pebdeni et al., 2021)
28	–	DNA	*S. aureus*	–	10 to 10^{8} CFU/mL	3 CFU/mL	Electrochemical aptasensor based on gold/nitrogen-doped carbon nano-onions	(Sohouli et al., 2022)

(Continued)

10.3389/fcimb.2024.1402932

TABLE 1 Continued

S.No.	Aptamer sequence (5′ to 3′)	Type	Organism	Target	Concentration range	LOD (limit of detection)	Methodology	Reference
				Bacteria				
29.	ATCCATGGGGCGGAGATGAGGGGGAGGAGGGCGGGTACCCGGTTGAT	ssDNA	*Listeria monocytogenes*	–	1.4×10^1 to 1.4×10^6 CFU/mL	4 CFU/mL	Solid-state electrochemiluminescence biosensing based on the quenching effect of ferrocene on ruthenium pyridine	(Chen et al., 2021c)
30.	NH2-ATC CAT GGG GCG GAGATG AGG GGG AGG AGG GCG GGT ACC CGG TTGAT	ssDNA	*Listeria monocytogenes*	–	10^1 to 10^8 CFU/mL	10 CFU/mL	Paper-based electrodes conjugated with tungsten disulfide nanostructure and aptamer for impedimetric detection	(Mishra et al., 2022)
31.	biotin-ATC CAT GGG GCG GAG ATG AGG GGG AGG AGG GCG GGT ACC CGG TTG AT	DNA	*Listeria monocytogenes*	–	1.0×10^1 to 1.0×10^5 CFU/mL	6 CFU/mL	Luminol-functionalized AuNF-labeled aptamer recognition and magnetic separation	(Chen et al., 2021b)
32.	–	–	*Listeria monocytogenes*	–	10^2 to 2×10^8 CFU/mL	2.8×10^2 CFU/mL	Sandwich fluorometric method for dual-role recognition was developed based on antibiotic-affinity strategy and fluorescence quenching effect	(Li et al., 2022)
33.	biotin-TAC TAT CGC GGA GAC AGC GCG GGA GGC ACC GGG GA	DNA	*Listeria innocua*	–	–	1.6×10^3 CFU/mL	Acoustic aptasensor	(Oravczová et al., 2020)
34.	TATCCATGGGGCGGAGATGAGGGGGAGGAGGGCGGGTACCCGGTTGAT	DNA	*Listeria monocytogenes*	–	4.6×10^2 to 4.6×10^7 $CFUmL^{-1}$in pure culture and 6.1×10^3 to 6.1×10^7 CFU/g in spiked fresh lettuce	4.6×10^2 $CFUmL^{-1}$ in pure culture and 6.1×10^3 CFU/g in spiked fresh lettuce	Competitive enzyme-linked aptasensor with rolling circle amplification (ELARCA) assay for colorimetric detection	(Zhan et al., 2020)
35.	TACTATCGCGGAGACAGCGCGGGAGGCACCGGGGA	–	*Listeria monocytogenes*	–	1.4×10^1 to 1.4×10^7 CFUmL	0.88 CFU/mL	Dual recognition and highly sensitive detection by fluorescence enhancement strategy	(Du et al., 2022)
36.	NH2(CH2)6GGGAGCTCAGAATAAACGCTCAA TACTATCGCGGGACAGCGC GGGAGGCACCGGGGATTCGACATGAGGCCCGGATC	DNA	*Listeria monocytogenes*	–	68 to 68×10^6 CFU/mL	8 CFU/mL	Fluorescence aptasensor	(Liu et al., 2021)
37.	NH2-C6-CCC CCG TTG CTT TCG CTT TTC CTT TCG CTT TTG TTC GTT TCG TCC CTG CTT CCT TTC TTG	DNA	*Pseudomonas aeruginosa*	–	3.1×10^2 to 3.1×10^7 CFU/mL	100 CFU/mL	Low-field magnetic resonance imaging aptasensor for the rapid and visual sensing	(Jia et al., 2021)
38.	NH2- CCC CCG TTG CTT TCG CTT TTC CTT TCG CTT TTG TTC GTT TCG TCC CTG CTT CCT TTC TTG	DNA	*P. aeruginosa*	Whole cell	10^2 to 10^6 CFU/mL	50 CFU/mL	A magnetic relaxation switch aptasensor	(Jia et al., 2017)

(Continued)

10.3389/fcimb.2024.1402932

TABLE 1 Continued

S.No.	Aptamer sequence (5′ to 3′)	Type	Organism	Target	Concentration range	LOD (limit of detection)	Methodology	Reference
				Bacteria				
39.	CCCCCG TTGCTTTCGCTTTTCCTTTCGCT TTTGTTCGTTTC GTCCCTGCTTCCTTTCTTG	ssDNA	*P. aeruginosa*	–	10^8 to 10^5 CFU/mL	10^5 CFU/mLfor colour change by the naked eye and 10^4 CFU/mL for UV–Vis spectrometry	Colorimetric detection by aptamer–functionalized gold nanoparticles	(Schmitz et al., 2023)
40.	GCA-ATG-GTA-CGG-TAC-TTC-CCG-GGG-CCC-GCT-TCT-GGT-GCG-GTG -TAC-TAG-TGA-CCG-CAA-AAG-TGC-ACG-CTA-CTT-TGC-TAA-(CH_2) 6-SH	DNA	*P. aeruginosa*	3-O-C12-HSL (Quorum-Sensing Molecule)	0.5 to 30 μM	0.5 μM	Label-free electrochemical aptasensor for the detection of the 3-O-C12-HSL	(Capatina et al., 2022)
41.	CCC CCG TTG CTT TCG CTT TTC CTT TCG CTT TTG TTC GTT TCG TCC CTG CTT CCT TTC TTG	DNA	*P. aeruginosa*	–	1.28×10^3 to 2.00×10^7 CFU/mL	100 CFU/mL	Graphene oxide quantum dots assisted construction of fluorescent aptasensor	(Gao et al., 2018)
42.	NH2-CCC CCG TTG CTT TCG CTT TTC CTT TCG CTT TTG TTC GTT TCG TCC CTG CTT CCT TTC TTG	DNA	*P. aeruginosa*	–	10^2 to 10^7 CFU/mL	33 CFU/mL	Impedimetric aptasensor by using a glassy carbon electrode modified with silver nanoparticles	(Roushani et al., 2019)
				Virus				
43.	AGC GGA TCC GAT GGG TGG GGG GGT GGG TAG GAT CCG CG	ssDNA	DENV	Non-structural protein 1	–	2.51 nM in buffer and 8.13 nM in serum	G-quadruplex (GQ)-based fluorescent aptasensor using one-shot detection of NS1	(Mok et al., 2021)
44.	HS_TAGGCAGTGTGGACGAGAGGGAGCTGTCCTGAGAGAGGCCTG TCAACCAGGGGTACCACAACCGAGGGCATA_SH	DNA	DENV-2	E-protein	–	100 infectious units per mL	Porous Au-seeded Ag nanorod networks conjugated with DNA aptamers for impedimetric sensing	(Kumar De et al., 2021)
45.	–	DNA	DENV	surface envelope proteins	10^{-6} to 10^6 $TCID_{50}$ /mL	1.74×10^{-7} $TCID_{50}$/mL	AC-electrothermal flow-based rapid biosensor	(Park et al., 2023)
46.	$HS(CH_2)_6$ – TTTTT – ACTAGGTTGCAGGGGACTGCTCGGGATTGCG GATCAACCTAGTTGCTTCTCTCGTATGAT	DNA	DENV-1 and DENV-4	NS1	10 pg to 1 μg/mL	22 pg/mL	Electrochemical aptasensor	(Bachour Junior et al., 2021)
47.	–	DNA	Hepatitis C virus (HCV)	HCV core protein	10 to 70 pg/mL and 70 to 400 pg/mL	3.3 pg/mL	Electrochemical detetction using GQD nanocomposite	(Bachour Junior et al., 2021)

(Continued)

10.3389/fcimb.2024.1402932

TABLE 1 Continued

S.No.	Aptamer sequence (5′ to 3′)	Type	Organism	Target	Concentration range	LOD (limit of detection)	Methodology	Reference
				Virus				
48.	GCGGATCCAGACTGGTGTGCCGTATCCCT CCCTTGTAATTATTTG TTCCATCCGTTCCGCCCTAAAGACAAGCTTC	ssDNA	HCV	HCV core protein	10^{-14} to 10^{-18} M	15.6 aM	Attomolar detection powered by molecular antenna-like effect in a graphene field-effect aptasensor	(Palacio et al., 2023)
49.	CACAGCGAACAGCGGCGGACATAATAGTGCTTACTACGAC	DNA	Hepatitis B virus (HBV)	HBsAg	–	0.05ng/mL	Chemiluminescent aptasensor based on rapid magnetic separation and double-functionalized gold nanoparticle	(Xi et al., 2018)
50.	NH_2- TTGGGGTTATTTGGGAGGGCGGGGGTT	DNA	Influenza A virus	H5N1 IAV hemagglutinin	0.2 to 12 ng/mL	114.7 pg/mL	FRET Aptasensors	(Zhao et al., 2021)
51.	GTG TGC ATG GAT AGC ACG TAA CGG TGT AGT AGA TAC GTG CGG GTA GGA AGA AAG GGA AAT AGT TGT CCT GTT G	DNA	H5N1 AIV	–	–	0.0128 hemagglutinin units (HAU)	An Impedance Aptasensor with Microfluidic Chips	(Lum et al., 2015)
52.	Cy3/GGG TTT GGG TTG GGT TGG GTT TTT GGG TTT GGG TTG GGT TGG GAA AAA	DNA	Influenza A/ H1N1 virus	–	–	97 PFU/mL	SERS imaging-based aptasensor	(Chen et al., 2020)
53.	Apt 1 H2N-GCT AGC GAA TTC CGT ACG AAG GGC GAA TTC CAC ATT GGG CTG CAG CCC GGG GGA TCC Apt 2 H2N-GTC TGT AGT AGG GAG GAT GGT CCG GGG CCC CGA GAC GAC GTT ATC AGG C Apt 3 H2N-CGT ACG GAA TTC GCT AGC ACG GGG CTT AAG GAA TAC AGA TGT ACT ACC GAG CTC ATG AGG ATC CGA GCT CCA CGT G Apt 4 H2N-CGT ACG GAA TTC GCT AGC CGA CGG TCA ATG CTC GTG AGC CAG TAC ACA CAA TAT ATG TGG ATC CGA GCT CCA CGT G	DNA	Norovirus	NoV capsid protein	–	70 aM	An Aptamer-aptamer Sandwich Assay with Nanorod-enhanced SPR for Attomolar Concentration	(Kim et al., 2018b)
54.	AGT ATA CGT ATT ACC TGC AGC CCA TGT TTT GTA GGT GTA ATA GGT CAT GTT AGG GTT TCT GCG ATA TCT CGG AGA TCT TGC	DNA	Norovirus	–	13 ng/mL to 13 μg/mL	4.4 ng/mL and 3.3 ngmL for MWCNT or GO respectively	Aptamer-based fluorometric determination using a paper-based microfluidic device	(Weng and Neethirajan, 2017)
55.	GCTAGCGAATTCCGTACGAAGGGCGAATTCCACATTGGGCT GCAGCCCGGGG GATCC	DNA	Norovirus	MNV virion	–	200 viruses/mL	Ultrasensitive colorimetric detection using NanoZyme aptasensor	(Weerathunge et al., 2019)

(Continued)

10.3389/fcimb.2024.1402932

TABLE 1 Continued

S.No.	Aptamer sequence (5′ to 3′)	Type	Organism	Target	Concentration range	LOD (limit of detection)	Methodology	Reference
Virus								
56.	CAG CAC CGA CCT TGT GCT TTG GGA GTG CTG GTC CAA GGG CGT TAA TGG ACA	DNA	SARS-CoV-2-RBD	–	0.5–250 ng/mL	32 ng/mL	Highly sensitive aptasensor using aptamer-gated methylene blue@mesoporous silica film/laser engraved graphene electrode	(Amouzadeh Tabrizi and Acedo, 2022)
57.	–	DNA	SARS-CoV-2	Nucleocapsid protein	–	0.77 to 1.94 ngmL	Fluorescent nanodiamond-based spin-enhanced lateral flow immunoassay and spike protein from different variants	(Wei-Wen Hsiao et al., 2022)
58.	Apt 1 biotin-GCT GGA TGT CAC CGG ATT GTC GGA CAT CGG ATT GTC TGA GTC ATA TGA CAC ATC CAG C Apt 2 biotin-GCT GGA TGT TGA CCT TTA CAG ATC GGA TTC TGT GGG GCG TTA AAC TGA CAC ATC CAG C	DNA	SARS-CoV2	Nucleocapsid protein	–	33.28 pg/mL	Aptamer/antibody sandwich method	(Ge et al., 2022)
59.	GCA ATG GTA CGG TAC TTC CGG ATG CGG AAA CTG GCT AAT TGG TGA GGC TGG GGC GGT	DNA	SARS-CoV-2	–	1 fM to 100 pM	0.389 fM	Aptasensing nucleocapsid protein on nanodiamond assembled gold interdigitated electrodes for impedimetric assessment	(Ramanathan et al., 2022)
60.	TGA CAC CGT ACC TGC TCT-N40-AAG CAC GCC AGG GAC TAT	DNA	Zika virus	–	100 pM to 10 µM	38.14 pM	Electrical biosensor	(Park et al., 2022)
61.	CTTCTGCCCGCCTCCTTCC-(39N)-GGAGACGAGATAGGCGGACACT	DNA	Zika virus	NS1 protein	0.01 to 1000 pg/mL	0.01 pg/mL	Aptasensor based on graphene FETs	(Almeida et al., 2022)

10.3389/fcimb.2024.1402932

3.2 Electrochemical biosensors

A variety of electrochemical transducer systems, including impedimetric, potentiometric, amperometric, voltammetric, conductometric, and FET-based biosensors, can be integrated with aptamers for enhanced functionality.

3.2.1 Impedimetric aptasensor

When the target analyte binds to the aptamer functionalized sensor surface, inducing changes in the electrical properties at the interface such as charge transfer kinetics, dielectric properties, or surface conductivity at the sensor interface. The change in impedance is converted into a measurable electrical signal. Impedance spectroscopy measures the impedance change of the sensor due to exposure to the target analyte and computes how the sensors electrical impedance changes over a range of frequencies. In a study conducted by Roushani et al. (2019) NH_2-aptamer was immobilized covalently on the surface of a glassy carbon electrode through electrodeposition modification of AgNPs. The conductivity and the charge transfer resistance before and after the addition of *P.aeruginosa* to the aptasensor was studied. The impedance increases on going from 10^2 to 10^7 CFU/mL concentrations of *P. aeruginosa*, and the detection limit was found to be 33 CFU/mL (for S/N=3). In a study conducted by Ramanathan et al. (2022) carbon nanodiamond enhanced gold interdigitated electrode was used to detect the nucleocapsid protein of SARS-CoV-2. The aptasensor which was portable, showed a good selectivity with a lower detection limit of 0.389 fM; at a linear detection range from 1 fM to 100 pM; showing 30 & 33% loss with stability & reusability. A rapid (30 mins) label-free aptasensor was constructed by Bagheryan et al., using screen-printed electrodes (SPEs) that were modified with diazonium salt for the detection of *Salmonella typhimurium* in spiked apple juice samples. The aptasensor had a linear detection range of 1×10^1 to 1×10^8 CFU mL^{-1} (Bagheryan et al., 2016).

3.2.2 Voltammetry based aptasensors

In a recent study, Fathi et al. (2020) developed a novel voltammetric aptasensor for detecting *Salmonella enterica* serovar. The sensor utilized a pencil graphite electrode modified with chitosan-coated electrospun carbon nanofibers and gold nanoparticles. The presence of the analyte on the electrode surface led to an increase in charge transfer resistance, with the change in current being measured as a function of voltage. Electrochemical detection of *Salmonella* was achieved using differential pulse voltammetry in a methylene blue solution. The aptasensor demonstrated a linear detection range of 10 to 10^5 CFU/mL, with a limit of detection (LOD) of 1.223 CFU/mL, outperforming the PCR technique.

3.2.3 Graphene FET based aptasensors

An aptamer with high affinity against HCV (hepatitis C virus) was functionalized on graphene solution-gated field-effect transistors (g-SGFET) and the developed aptasensor was used to amplify and detect the change in conductance caused by the interaction between the aptamer and the HCV core protein (Palacio et al., 2023). Similarly, Almeida et al., fabricated a graphene FET aptasensor to detect Zika virus (ZIKV). The aptamer (termed ZIK60), selected by CE-SELEX was complimentary to the Zika virus non-structural protein 1 (NS1) and counterselection against the NS1 proteins of DENV (serotypes 1, 2, 3, and 4) and YFV (Almeida et al., 2022).

3.2.4 Quartz crystal microbalance based aptasensors

QCM aptasensor is an acoustic (mass-based) piezoelectric biosensor that detect changes in mass on the aptamer immobilized surface of quartz crystal due to its interaction with the analyte molecules by detecting changes in the resonance frequency of the crystal. QCM-based aptasensors are highly sensitive, label free, portable and can be miniaturised and hence are suitable for point-of-care diagnostics. Aptamer selected using whole cell SELEX was utilized to fabricate a QCM sensor to detect *E. coli O157:H7*. The aptasensor had a LOD that was as low as 1.46×10^3 CFU/mL and outperformed most QCM-based immunosensors for pathogen detection. In addition, the quick response time of 50 min showed the possibility of using this aptamer in various other types of biosensors used for rapid detection and investigation of *E. coli* O157:H7 outbreaks (Yu et al., 2018). An interesting study conducted by Wang et al., demonstrates the use of QCM based SELEX to effectively select the ssDNA aptamer and subsequent construction of QCM based aptasensor which was able to detect 10^3 CFU/mL of *S. typhimurium* within 1 h (Wang et al., 2017a). Another example is a QCM aptasensor in which a nanowell based electrode effectively increased the immobilization capacity of aptamers for the detection of avian influenza virus. The result showed that the binding of target AIV H5N1 onto the immobilized aptamers decreased the sensor's resonant frequency, and the frequency change correlated to the virus titer. The detection range of 2^{-4} to 2^4 hemagglutination units (HAUs)/50 µL was obtained with a detection limit of 2^{-4} HAU/50 µL for AIV H5N1 with a detection time of 10 mins using a label free assay. (Wang et al., 2017a, 2017b)

3.3 Dual recognition aptasensor

As the name suggests, dual recognition sensors make use of two different recognition principles facilitating a highly specific detection. Li et al., developed an aptasensor for detecting *S. typhimurium* by combining the methods of immune hybridization chain reaction (HCR) with SERS achieving double amplification and high sensitivity with a limit of detection of 6 CFU/mL in 3.5 h (Li et al., 2021). Bagheri Pebdeni et al., proposed an aptamer and antibiotic-based dual detection sensor that combines copper nanoclusters (CuNCs) as an effective approach for the recognition and quantification of *S. aureus*. The use of dual receptors enhanced fluorescence signal linearly with *S. aureus* concentrations between 10^2 -10^8 CFU/mL, and the detection limit was 80 CFU/mL after 45 min (Bagheri Pebdeni et al., 2021).

Aptasensors like the electrochemiluminescence aptasensors come under both electrochemical and optical sensors. It works by detecting the luminescence that is produced due to the electrochemical interactions between the aptamer and the analyte molecules (Chen et al., 2021c; Chen et al., 2021b).

3.4 Sandwich assay based aptasensors

A sandwich assay involves two aptamers – the capture probe and the signal probe. The capture probe is immobilized on the surface of the sensor and after the analyte is added, the signal probe is added forming an aptamer-aptamer sandwich platform. This method is desirable because of the high sensitivity and selectivity that it offers. S. Kim et al., demonstrated a nanorod enhanced SPR with sandwich enzyme-linked immunosorbent assay (ELISA) for the attomolar detection of the norovirus (NoV) capsid protein (Kim et al., 2018b). RNA aptamer-based sandwich assays were used to detect the NS1 protein of dengue virus serotype 2 and a LOD of 2 nM was attained (Thevendran et al., 2023).

Another notable example is an aptamer/antibody sandwich constructed by Ge et al., for the digital detection of SARS-CoV2 nucleocapsid protein using fluorometry. The detection limit of this digital method for N protein was 33.28 pg/mL, which was 300 times lower than traditional double-antibody sandwich-based ELISA (Ge et al., 2022). Even though sandwich ELISA assay offers various advantages, it has a complex workflow, more optimization is required, is labor intensive and the time of detection is a little high.

3.5 Other aptasensors

There are aptasensors based on principles other than the above mentioned, for example, F. Jia et al. developed a low-field magnetic resonance imaging (LF-MRI) aptasensor based on the difference in magnetic behavior of two magnetic nanoparticles covalently immobilized with aptamers for the rapid detection of *P.aeruginosa*. Under optimum conditions, the LF-MRI platform provides both image analysis and quantitative detection of *P. aeruginosa*, with a detection limit of 100 CFU/mL (Jia et al., 2021).

Aptamer-based assays represent a significant advancement in the diagnostics of infectious diseases, addressing the limitations of traditional methods. Optical aptasensors, including surface plasmon resonance, fluorescence, and surface-enhanced Raman scattering, excel in sensitivity and specificity, ideal for detailed biomolecule detection. Electrochemical aptasensors, such as impedimetric, voltammetric, and graphene FET-based sensors, offer robust, portable solutions with high sensitivity for point-of-care applications. Meanwhile, dual-recognition and sandwich assay-based aptasensors combine multiple detection principles to enhance accuracy and detection limits. This comprehensive range of aptamer-based technologies demonstrates their potential to revolutionize diagnostic practices by providing versatile, efficient, and precise tools for infectious disease management. The most suitable method can be selected by understanding the strengths and limitations for each approach.

4 Notable aptasensor case studies

4.1 For the detection of methicillin resistant *Staphylococcus aureus*-*contaminated* surfaces

Methicillin-resistant Staphylococcus aureus (MRSA) is a well-known pathogen that causes healthcare-associated infections. Hospitals with contaminated environments are important sources for the spread of MRSA and other nosocomial infections. In a study, researchers have developed a new swab called a pathogen aptasensor which can specifically detect MRSA on contaminated non-absorbable surfaces. The visual detection limit of the MRSA aptasensor swab was less than 100 CFU/mL, and theoretically, using a standard curve, it was 2 CFU/mL. The assay has a short turnaround time of 5 minutes, with a linear range of quantitation from 10^2 to 10^5 CFU/mL. The MRSA aptamers bind to the swab's activated aldehyde group, and when exposed to an MRSA-contaminated surface, the activated nanobeads conjugate with the aptamer, causing the swab to turn blue. The intensity of the color change is proportional to the concentration of MRSA, allowing for both qualitative and quantitative detection (Raji et al., 2021).

4.2 Simultaneous detection of *E.coli* O157: H7 and *S.typhimurium*

Simultaneous detection of *E.coli* and *S.typhimurium* was achieved using an evanescent wave dual-color fluorescence aptasensor based on time resolved effect. Two fluorescence labeled aptasensors, Cy3-apt-E and Cy5.5-apt-S that were complimentary to *E.coli* O157:H7 and *S.typhimurium* were alternatively excited by evanescent waves originated from 520 nm to 635 nm excitation lights, respectively. The fiber nanoprobe with *in-situ* etched nanopores was used for distinguishing free aptamer and aptamers bound to pathogenic bacteria based on the limited penetrated depth of evanescent wave and the significant size difference of bacteria and nanopore. The *E. coli* O157:H7 and *S. typhimurium* were directly and simultaneously quantitated in less than 35 min without the requirement of the complex immobilization of biorecognition molecules and bacteria enrichment/separation processes. The limits of detection of *E. coli* O157:H7 and *S. typhimurium* were 340 CFU/mL and 180 CFU/mL, respectively (Fang et al., 2021).

4.3 Colorimetric aptasensor for detecting *Salmonella* spp., *Listeria monocytogenes*, and *Escherichia coli* in meat samples

Aptasensors are revolutionizing infectious disease detection by enhancing the specificity and sensitivity of aptamers. These biosensors provide versatile solutions for streamlining diagnostic processes in healthcare by rapidly and precisely identifying pathogens.

A recent study introduced a quick detection method that can simultaneously identify *Salmonella* spp., *Listeria monocytogenes*,

and *E. coli*. This method uses visual colorimetric detection with labeled colloidal gold nanoparticles and UV absorbance determination at optimized wavelengths of 625 nm and 525 nm. The aptasensor has a detection limit as low as 10^5 CFU/mL. Notably, this colorimetric aptasensor enables one-step detection without the need for pre-culture, DNA extraction, or amplification steps. As a result, it provides a simple, rapid, specific, and qualitative assay suitable for point-of-care testing, allowing for direct detection of multiple foodborne pathogens (Ledlod et al., 2020). Additionally, exploring virulence factors as potential targets for aptamers is helping us understand pathogen behavior and leading to the development of targeted therapeutic interventions.

5 Aptamer applications: targeting virulence factors and recent advances

5.1 Virulence factors and potential aptamer targets

Aptamer is one of the most promising therapeutic candidates because of its selectivity. In the field of therapeutics, they serve various crucial roles, including acting as a drug delivery vehicle (Ninomiya et al., 2014), functioning as a targeting molecule for genes or whole cells, thereby reducing the expression of virulent genes in pathogens and enhancing susceptibility to the immune system (Lai et al., 2014). Furthermore, it serves as a binding agent for toxins and specific proteins that contribute to increased pathogen virulence (Gribanyov et al., 2021). When it comes to treating viral infections that have no known treatment and drug-resistant microorganisms that cause infectious diseases, aptamers may be a useful therapeutic tool (Figure 3).

5.1.1 Bacteria

By removing important virulence components from bacteria, aptamers present a viable strategy for treating bacterial illnesses. (Tables 2, 3). The innovative technology enhance the treatment efficacy against pathogens such as *Staphylococcus aureus*, *Mycobacterium tuberculosis*, *Salmonella typhi*, *Listeria monocytogenes*, *Streptococcus pneumoniae*, and *Escherichia coli*. In the fight against *S. aureus* infections, aptamers AT-33 and AT-36 have been specifically engineered to target and neutralize the α-toxin, a key virulence factor. These aptamers effectively inhibit α-toxin-induced cell death and cytokine upregulation in human cells, offering a promising therapeutic approach (Ommen et al., 2022). Another set of aptamers targets *S. aureus* biofilms, binding to the biofilm matrix to enhance antibiotic delivery and significantly improve treatment outcomes by overcoming biofilm-associated resistance. This dual approach of targeting both toxins and biofilms represent a significant advancement in therapeutic strategies against *S. aureus* infections.

To identify and target important molecules connected to M. tuberculosis, aptamers have also been developed. For instance, mannose-capped lipoarabinomannan (ManLAM), a major glycolipid on the bacterial surface, serves as a target for specific aptamers, aiding in both diagnostic and therapeutic applications. Additionally, aptamers targeting the GlcB and HspX antigens disrupt bacterial metabolism and persistence, offering potential therapeutic benefits (Zhou et al., 2021). Furthermore, aptamers targeting ESAT-6, a critical virulence factor secreted by *M. tuberculosis*, can reduce the bacterium's virulence and increase its vulnerability to immune system attacks (Sreejit et al., 2014). *M. tuberculosis* produces a lipid called phthiocerol dimycocerosate (PDIM), which is essential to the pathogenicity and virulence of the bacteria (Augenstreich et al., 2020).

Researchers have developed an aptamer that interacts with and neutralizes the InvA gene of *S. typhi*, a crucial element in the bacterium's invasion process. Additionally, the S9 aptamer targets the outer membrane protein of *S. typhi*, further contributing to the bacterium's neutralization (Pathania et al., 2017; Yang et al., 2013). SPI1, or *Salmonella* pathogenicity island 1, is essential for *Salmonella's* interaction with host cells, facilitating penetration through the T3SS, also known as the needle complex, which assembles proteins to translocate effector proteins into host cells (Raffatellu et al., 2005; Lerminiaux et al., 2020). The pathogenicity of *S. typhi* is enhanced by the release of typhoid toxin and the Vi capsular antigen, which has anti-opsonic and antiphagocytic properties (Galán, 2016; Tran et al., 2010; Wain et al., 2005). These harmful factors can be targeted by specifically curated aptamers.

In order to prevent L. monocytogenes from invading host cells, aptamers that target InlB, one of the bacteria's virulence factors, have been created. By blocking this key infection pathway, these aptamers offer a promising therapeutic strategy for preventing *L. monocytogenes* infections (Chen et al., 2024). *L. monocytogenes* produces listeriolysin O (LLO), a pore-forming toxin dependent on cholesterol (Dramsi and Cossart, 2002). LLO damages the vacuolar membrane, facilitating bacterial escape into the cytosol (Petrišič et al., 2021). These vulnerable parts of the pathogen can be exploited by targeting them with protein-specific aptamers.

For *S. pneumoniae*, aptamers have shown good specificity; the Lyd-3 aptamer in particular has shown promise. Lyd-3 effectively inhibits biofilm formation, a critical factor in the pathogen's virulence and antibiotic resistance. By significantly reducing biofilm formation, Lyd-3 enhances treatment outcomes, especially when used in combination with antibiotics (Afrasiabi et al., 2020). The pneumococcus's polysaccharide capsule is a significant virulence component, aiding in immune evasion and colonization (Jonsson et al., 1985). PspK mediates adherence to human epithelial cells, independent of the pneumococcal isolate genetic background (Keller et al., 2013).

Four aptamers have demonstrated high affinity and specificity for *E. coli* cells, making them valuable tools for both diagnostic and therapeutic applications. These aptamers offer precise detection and effective targeting of *E. coli* (Marton et al., 2016). *E. coli* causes various infections, including urinary tract infections, and relies on colonization factors and toxins for virulence. Aptamers can target these virulent factors, disrupting *E. coli's* pathogenic mechanisms and enhancing treatment efficacy (Johnson, 1991; Kaper et al., 2004; Terlizzi et al., 2017).

By leveraging the specificity and affinity of aptamers, we can target key virulence factors in various bacterial pathogens, offering innovative and effective therapeutic strategies.

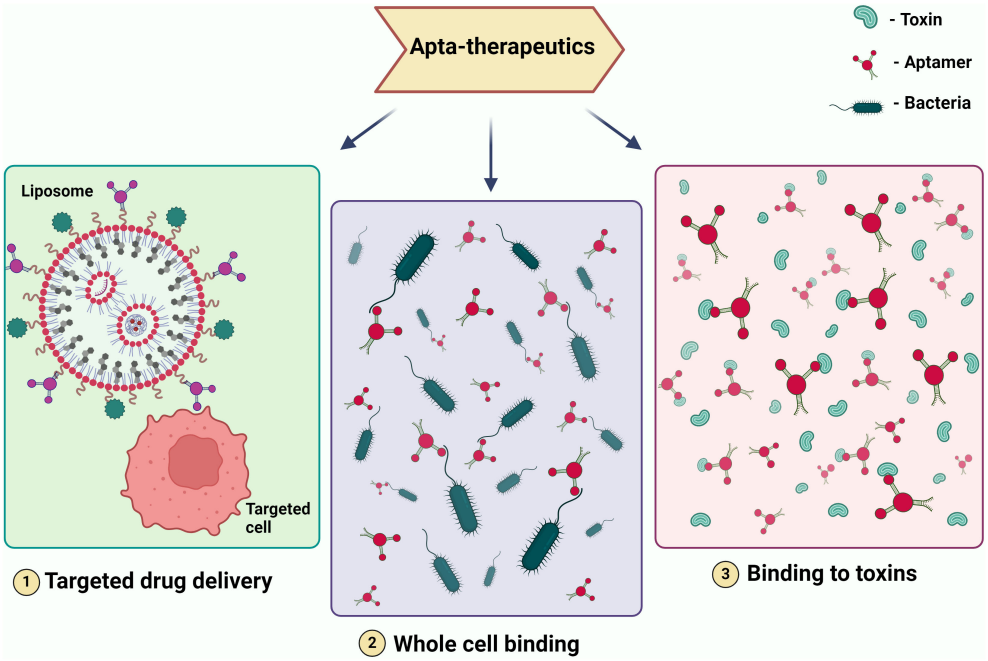

FIGURE 3
Illustrating Therapeutic Modalities Employing Aptamers. The figure depicts various therapeutic applications of aptamers, including (1) targeted drug delivery, where aptamers are used to direct drugs specifically to diseased cells; (2) whole cell binding, where aptamers bind to specific cells for therapeutic purposes; and (3)binding to toxins, where aptamers neutralize toxins by binding to them. These modalities showcase the potential of aptamers in precision medicine and targeted therapies.

TABLE 2 Therapeutic techniques and mechanisms of aptamers against bacteria.

Target	Conjugated With	Target site	Mechanism	Reference
		Salmonella species		
S. choleraesuis	Ampicillin	Flagella	■ Aptamer 3 targets flagella, causing loss of bacterial motility decreasing adherence to the matrix surface, and reinforces hydrodynamic and repulsive forces which inhibit biofilm formation. ■ Aptamer 3 may also serve as an antibiotic carrier helping ampicillin to penetrate biofilms to eradicate bacteria and to overcome biofilm tolerance to drugs	(Lijuan et al., 2017)
S. enteritidis	–	Sip A protein (SPI – *Salmonella* pathogenicity island)	■ Apt17, an aptamer targeting SipA an effector protein secreted by Type Three Secretion System (T3SS). ■ It facilitates the invasion of *Salmonella* cells by triggering membrane ruffling	(Shatila et al., 2020b)
S. Typhimurium and S. Enteritidis	–	Sip A protein (SPI – *Salmonella* pathogenicity island)	■ Targeting *Salmonella* invasion protein (SipA) ■ A type three secretory system effector protein blocking this helps in anti-adhesion and anti-invasion property against *Salmonella Enteritidis*	(Shatila et al., 2020a)
S. Typhimurium and S. Enteritidis	Using rolling circle amplification	-	■ Use complementary sequences of recently described (anti-ST and anti-SE) DNA aptamers as a template to develop RCA-p. ■ The use of RCP-p is done to increase the bacteriostatic effect on the bacteria	(Hameed et al., 2022)
Salmonella enterica serovar typhimurium	Gold nano particles	Membrane disruption, Intracellular interaction.	■ Involve the binding of the AMPs to lipopolysaccharide and lipoteichoic acid ■ With subsequent membrane disruption through pore formation or other processes ■ AMPs are drugs delivered by aptamer nanoparticle complex	(Yeom et al., 2016)
Salmonella enterica Serovar typhi	–	Preferentially bind type IVB pilli	■ RNA Aptamer is used to bind to IVB pilus operon and stops IVB PILUS formation	(Pan et al., 2005)

(Continued)

TABLE 2 Continued

Target	Conjugated With	Target site	Mechanism	Reference
			Salmonella species	
			■ Which helps *S.enterica serovar typhi* to attach to cells which increases its pathogenicity	
			Staphylococcus aureus	
S aureus	Teicoplanin and PLGA nanoparticles	D-Ala, D-Ala site in peptidoglycan	■ Aptamer is used to bind to the bacteria and is conjugated with teicoplanin encapsulated in PLGA ■ Which stops the cell wall synthesis by blocking the D-Ala, D-Ala site	(Ucak et al., 2020)
S. aureus	–	Alpha toxin and transcriptional activators of *TNF-alpha* and *IL 17* gene	■ Aptamers are specific to their targets through SELEX process, so they bind directly to the alpha toxin	(Vivekananda et al., 2014)
S .aureus (MRSA)	Magnetic graphene oxide	Whole-cell	■ The conjugated magnetic graphene oxide (MGO) benefits from the aptamer ■ When it is exposed to NIR light, it produces heat that aids in the death of MRSA.	(A Ocsoy et al., 2021)
S aureus (MRSA)	Anti-galactosyltransferase (anti-α-gal)	Whole-cell and help immune system enhance the fight against *MRSA*	■ Anti-galactosyltransferase, or anti-α-gal, is conjugated with MRSA specific aptamer. ■ Anti-α-gal alerts the immune system to the presence of bacteria and aids in its prompt elimination.	(Doherty et al., 2023)
S aureus	NaY0.28F4:Yb0.70, Er0.02 magnetic nanoparticle	As of now no targets but This can be used as a potential therapeutic	■ The magnetic nanoparticle NaY0.28F4:Yb0.70, Er0.02 coupled with aptamer is utilized to draw all of the bacterial cells into one location, offering it a possible therapeutic use.	(Duan et al., 2012)
			Mycobacterium tuberculosis	
Mycobacterium tuberculosis	–	Malate Synthase	■ Aptamer attaches itself to the Mtb's malate synthase, ■ Inhibiting adhesin function and preventing bacterial invasion.	(Dhiman et al., 2019)
Mycobacterium tuberculosis	–	HupB protein	■ Aptamer attaches itself to the HupB protein and prevents it from working.	(Kalra et al., 2018)
Mycobacterium tuberculosis	Biotin	DevR dimer	■ The DevR dimer becomes dysfunctional when an aptamer attaches to it, inhibiting transcription.	(Chauhan et al., 2022)
			Listeria monocytogenes	
Listeria monocytogenes	Porous silica Nanoparticles	Whole-cell	■ The aptamer is coupled to porous silica nanoparticles and loaded with benzalkonium chloride (BAC). ■ Because BAC is toxic, it cannot be utilized in treatment; instead, an appropriate antibiotic can be employed to effectively target the bacteria.	(Sudagidan et al., 2021)
Listeria monocytogenes	Antibody of *L. monocytogenes*	Antigen	■ When an aptamer and bacterial antibodies are conjugated The antigen found in the bacterium may be targeted therapeutically.	(Du et al., 2022)
Listeria monocytogenes	Bacteriocin (nisin with leucocin F10)	Cell membrane	■ Aptamer in connection with Nisin and Leucocin F10 Once it attaches to bacteria, the aptamer pores the bacteria's surface.	(Turgis et al)
			Streptococcus pnuemoniae	
Streptococcus pnuemoniae	α-Gal epitope	Whole cell	■ An aptamer is designed to attach to an α-Gal epitope, creating an alphamer that targets bacteria ■ Initiating opsonization and phagocytosing the pathogen by anti-α-Gal antibody.	(Kristian et al., 2015)
Streptococcus pnuemoniae	Graphene oxide (GO)		■ This aptamer has the potential to be a therapeutic tool when combined with drugs that are specific to this bacteria	(Bayraç and Donmez, 2018)
Streptococcus pnuemoniae	–	PavA and FHbp	■ Researchers created an aptamer that binds to the virulent proteins PavA and FHbp. ■ When the aptamer binds to PavA, it prevents the bacteria from attaching to fibronectin	(Escolano et al., 2017)

(Continued)

TABLE 2 Continued

Target	Conjugated With	Target site	Mechanism	Reference
Streptococcus pnuemoniae				
			■ When it binds to FHbp, it compromises the ability to evade the immune system and kills the bacteria.	
Escherichia coli				
E. coli	–	Targets adhesins and colonization factor eg: Afimbrial Adhesins	■ Aptamers were employed to lower the biofilm activity.	(Kusumawati et al., 2022)
E.coli	–	Cell membrane	■ Aptamer was designed to attach to the elements of the cell membrane. ■ It is also utilized to prevent from forming biofilms.	(Oroh et al., 2020)
E.coli	–	LPS	■ This paper's researchers have inferred that aptamer attaches to the LPS ■ This method may be exploited as a treatment option in addition to detection.	(Zou et al., 2018)
E.coli	AuNPs and Antimicrobial peptides	Cell membrane	■ Antimicrobial action is demonstrated by HPA3P, a derivative of HP(2-20) ■ AMP with substitutions of E9P connected with gold nanoparticles and aptamer pair (AuNPs-Apt).	(Lee et al., 2017)

TABLE 3 Virulence factors for aptamer-based targeting of bacterial pathogens.

Virulent factors	Bacteria						
	L. monocytogenes	*S.aureus*	*S.typhi*	*M.tuberculosis*	*E.coli*	*S.pnuemoniae*	Reference
LPS (Endotoxin)			+		+		(Chessa et al., 2014) (Somerville et al., 1999)
Colonization factor		+(adhesins)			+		(Gerlach et al., 2007) (Gerlach et al., 2007)
Listeriolysin O	+						(Portnoy et al)
Phospholipases	+	+					(Faucher et al., 2008) (Kadurugamuwa and Beveridge, 1995)
ACT A	+						(Pistor et al., 1994)
Capsules	+	+	+	+	+	+	(Bai et al., 2021)
Exotoxins	+(Listeriolysin O)	+ (hemolysin, leukotoxin, exfoliative toxin, enterotoxin, and toxic-shock syndrome toxin-1 (TSST-1).)	+(typhoid toxin)	+(necrotizing toxin)	+	+(pneuemolysin)	(Portnoy et al) (Otto, 2014) (Fowler and Galán, 2018) (Sun et al., 2015) (Kaper et al., 2004) (Nishimoto et al., 2020)
ESAT-6				+			(Sreejit et al., 2014)
Surface adhesins		+	+	+	+	+	(Gerlach et al., 2007) (Johnson, 1991)

(Continued)

TABLE 3 Continued

Virulent factors	Bacteria						
	L. monocytogenes	*S.aureus*	*S.typhi*	*M.tuberculosis*	*E.coli*	*S.pnuemoniae*	Reference
Protein A		+					(Palmqvist et al., 2002)
Salmonella pathogenicity island			+(SPI1, SPI2, SPI3)				(Lerminiaux et al., 2020)
Vi antigen			+				(Zhang et al., 2022)
Pneumococcal factors (*psp k , sir A, pmp A*)						+	(Brooks and Mias, 2018)
Flagella	+		+		+		(Winter et al., 2009) (Grü ndling et al., 2004)
Protein Kinases	+				+	+	(Wang & Koshland, 1978) (Canova and Molle, 2014)
Mannose capped lipoarabinomannan				+			(Turner and Torrelles)
Phthiocerol Dimycocerosate				+			(Augenstreich et al., 2020)

5.1.2 Virus

Aptamers are also increasingly recognized for their potential to combat viral infections by targeting and neutralizing specific viral components (Table 4). It can enhance the efficacy of existing antiviral treatments and provides new therapeutic avenues for diseases like Zika virus, Nipah virus, Ebola virus, and Influenza A virus.

Zika virus, a member of the Flaviviridae family transmitted by Aedes aegypti mosquitoes (Diagne et al., 2015), has been targeted with various antiviral strategies. Ribavirin has shown efficacy in suppressing viremia in ZIKV-infected STAT-1-deficient mice (Kamiyama et al., 2017), while favipiravir and BCX4430 inhibit viral RNA synthesis by targeting viral RNA-dependent RNA polymerase (Furuta et al., 2009; Eyer et al., 2017). The similarity between the envelope proteins of dengue and Zika viruses underscores their close evolutionary relationship (Lunardelli et al., 2023). NS1 protein plays critical roles in ZIKV replication (Valente and Moraes, 2019), and aptamer technology holds promise for enhancing antiviral drug efficacy by targeting specific virulence factors (Feng et al., 2011).

Nipah virus lacks specific antiviral treatments, making aptamer-based therapies a potential breakthrough by targeting its virulence factors, such as the F protein that mediates viral entry through ephrin B2/B3 receptors (Sun et al., 2018; Weis and Maisner, 2015). The Nipah virus V protein inhibits STAT proteins, crucial for interferon signaling, enhancing viral pathogenesis (Shaw et al., 2004). Aptamers designed to bind these proteins could mitigate infection severity.

Ebola virus VP35 and VP24 proteins are key virulence factors that disrupt host immune responses (Leung et al., 2010; Zhang et al., 2012), with aptamers identified to target VP35's interferon inhibitory domain (Binning et al., 2013). These aptamers offer potential therapeutic avenues against Ebola virus by restoring interferon response pathways.

Influenza A viruses, characterized by their surface proteins HA and NA, play crucial roles in viral entry and replication (Bouvier and Palese, 2008). Aptamers targeting HA have demonstrated significant antiviral effects in animal models, inhibiting viral replication and reducing infection rates across different influenza strains (Nobusawa, 1997; Gopinath et al., 2006; Jeon et al., 2004). Aptamer research continues to explore novel therapeutic strategies, addressing the challenges posed by viral mutation and enhancing treatment efficacy (Musafia et al., 2014; Sanjuán, 2012).

5.2 Recent advancements and case studies

5.2.1 Notable developments in aptamer research for infectious diseases

5.2.1.1 Gold nanoparticle-DNA aptamer conjugate-assisted delivery of antimicrobial peptide (CA2634987A1)

Gold nanoparticles are a durable and widely used delivery technology that offers various benefits over liposomes and PLGA. It was demonstrated that combining antimicrobial peptides with a gold nanoparticle-aptamer complex was effective in eliminating intracellular Salmonella enterica serovar Typhimurium (Yeom et al., 2016).

TABLE 4 Therapeutic techniques and mechanisms of aptamers against the virus.

Virulence factors of Viruses					
S. No.	Virus	Virulence factor	Function	Mechanism	Reference
1	Zika	NS1 (non-structural protein 1)	Immune evasion and modulation	■ NS1 prevents the synthesis of interferon-beta (IFN-β), ■ Essential for the antiviral immune response.	(Rastogi and Singh, 2020)
		NS2A and NS4B	Viral replication	■ The Zika virus's NS2A contributes to the suppression of NF-κB promoter activity. ■ NS2A is composed of a central region (the bridge) that passes through a cellular compartment (ER) & six arms (segments) that extend outward from the central region.	(Lee et al., 2020) (Nutho et al., 2019)
		Envelope protein	Entry into host cell and helps in assembly of new viral particles	■ E protein promotes the production of viral particles by interacting with apolipoprotein E, a protein involved in lipid metabolism. ■ C-type lectin receptors in the host cell are involved in receptor-mediated endocytosis.	(Nutho et al., 2019) (Agrelli et al., 2019)
		Capsid protein	Helps in formation of new virus particles	■ capsid protein forms overall positively charged dimers that bridge RNA and lipid membrane surfaces. ■ The protein exists as dimers with four α helices and a long pre-α1 loop, contributing to its unique structure	(Shang et al., 2018)
2	Ebola	Viral protein 24 (VP24)	Interferes in host interferon and evades host immune system	■ VP24 suppresses interferon-dependent signaling, of interferon alpha/beta (IFN-α/β). ■ The host's antiviral response is interfered, which makes it easier for the virus to multiply and propagate.	(Zhang et al., 2012)
		VP30	Helps in transcription and replication	■ Dynamic phosphorylation of VP30 occurs at six serine residues at the N-terminus. ■ This post-translational alteration affects VP30's function in viral transcription and replication by regulating its activity in conjunction with dephosphorylation.	(Lier et al., 2017)
		VP35	Interferes with host interferon regulatory factor (IRFs)	■ VP35 interacts with the PKA-CREB1 pathway, a set of intracellular chemical signals. ■ A biological protein known as AKIP1 is bound by VP35, starting a chain reaction. ■ PKA (Protein Kinase A) and CREB1 (cAMP Response Element-Binding Protein 1), two important participants, are activated by this binding. ■ Following activation, CREB1 is drawn to viral inclusion bodies, which are particular structures created when the Ebola virus infects a host.	(Zhu et al., 2022)
		VP40	Formation and release of viral particles from infected cells	■ SUMOylation is a post-translational modification that controls VP40. ■ Affects the stability, nucleocapsid recruitment, structure, and budding of the virus.	(Baz-Martnez et al., 2016)
		L Polymerase	RNA dependent RNA polymerase involved in replication and transcription	■ The process includes the polymerase starting RNA synthesis from scratch, or de novo, without the aid of an existing primer.	(Yuan et al., 2022)
3	Nipah	Nucleoprotein (N protein)	responsible for enclosure of viral RNA genome	■ The N protein facilitates the interchange of N-terminal (NTARM) and C-terminal subdomains (CTARM) and lateral interactions that lead to the creation of a stable homopolymer structure.	(Ker et al., 2021)

(Continued)

TABLE 4 Continued

Virulence factors of Viruses					
S. No.	Virus	Virulence factor	Function	Mechanism	Reference
				■ This particular structural configuration enhances the nucleocapsid's integrity.	
		Phosphoprotein (P protein)	Crucial for viral RNA synthesis and synthesis	■ Viral polymerase activity and viral RNA synthesis are regulated by overexpression of the Nipah virus nucleocapsid protein (N) ■ Which indicates the complex interaction between P and other viral components.	(Ranadheera et al., 2018)
		Matrix protein (M protein)	Involved in assembly and budding of new vial particles	■ The induction of interferon-beta (IFNβ) at the level of the TBK1/IKKε kinases is inhibited by the NiV matrix protein.	(Bharaj et al., 2016)
		Fusion protein (F protein)	Helps in viral entry into host cells	■ The attachment (G) protein and the NiV-F protein work together to mediate viral entry and syncytium formation. ■ Syncytium formation is the process by which adjacent and infected cells combine to promote the spread of the virus.	(Aguilar et al., 2006)
4	Influenza A virus	Hemagglutinin HA	Helps in adherence to host cell	■ Low pH inside endosomes causes HA to undergo a conformational shift after attachment. ■ The fusing of the viral and endosomal membranes can be mediated by HA ■ Conformational shift exposes a fusion peptide. ■ The viral genome must pass through this stage in order to enter the cytoplasm of the host cell.	(Brandenburg et al., 2013)
		Neuraminidase NA	Releases viral particles from infected cells	■ Neuraminidase is an exosialidase that breaks the α-ketosidic bond between the sugar residue next to the sialic acid on the surface of host cells that are infected. ■ The release of offspring viruses from the host cell membrane depends on this cleavage.	(McAuley et al., 2019)
		PB1, PB2, PA	Viral replication	■ The catalytic component responsible for RNA-dependent RNA polymerase (RdRP) activity is called PB1. ■ PB2 participates in the cap-snatching process, responsible for the start of viral transcription. To facilitate the production of viral mRNA, the viral polymerase snatches the 5' cap structure from host pre-mRNAs. ■ In the cap-snatching procedure, PA is an essential component. Sue to its endonuclease activity, host mRNA can be broken down close to the 5' cap structure. ■ Afterwards, PB2 uses this cleaved cap to start viral transcription.	(Binh et al., 2013) (Lerminiaux et al., 2020) (Ma et al., 2017)
		NP	Responsible for enclosure of viral RNA genome	■ The results show that NP serves a variety of purposes throughout the life cycle of the virus, and its requirement varies depending on the particular circumstances or context of the viral activities under investigation.	(Turrell et al., 2013)
		M1 M2	Involved in assembly and budding of new vial particles	■ M1's conformation may be affected by association with M2, which would promote the elongation of viral budding. ■ The effective release of new virus particles depends on this interaction.	(Roberts et al., 1998)
		NS1 NS2	Immune evasion	■ NS1 suppresses host's antiviral defenses by blocking several pathways, including interferon generation and activation of PKR	(Huang et al., 2017) (O'Neill et al., 1998)

(Continued)

TABLE 4 Continued

Virulence factors of Viruses					
S. No.	Virus	Virulence factor	Function	Mechanism	Reference
				(Protein Kinase R). ■ The nuclear export of viral ribonucleoprotein (vRNP) complexes is facilitated by NS2. ■ It controls the movement of NS2 mRNA that has been spliced and its precursor, NS1 mRNA, making it easier for vital viral components to be exported from the nucleus into the cytoplasm.	
5	Noro virus	VP1 (major capsule protein)	Formation of viral capsid, contributes to stability of virion	■ The capacity of the virus to reproduce in B cells is closely correlated with the projecting domain of VP1 ■ Potential function for this domain in determining norovirus virulence.	(Zhu et al., 2016)
		VP2 (minor structural protein)	Contributes for the stability of the virion	■ VP2 experiences coevolution and is the cause of most illnesses. Its significance in the infection process is shown by the coevolutionary dynamics.	(Hong et al., 2022)

5.2.1.2 Point-of-care SARS-CoV-2 salivary antigen testing with an off-the-shelf glucometer (WO2022016163A2)

An innovative test technique that combines a pre-conjugated aptamer with the enzyme invertase, which is then attached to a magnetic bead. Because the aptamer is highly specific to the antigen found in the corona virus, it goes through a confirmational change that releases the enzyme into the medium, where it is separated by magnetic separation. The medium's invertase then breaks down sucrose into glucose, and measuring the glucose yields an assay of the antigen present in the sample. This model operates on this concept (Singh et al., 2021).

5.2.1.3 Graphene aptasensor for the detection of hepatitis C virus (EP4124855A1)

Changes in their surroundings, particularly the attachment of bio-receptors to the graphene surface, cause Graphene Field-Effect Transistor Biosensors (gFET) to detect changes in electrical metrics, such as conductivity. Graphene's sensing potential is increased by chemical modification. As an example of how biological molecules can be sensed, researchers have created chemically functionalized gFETs that can detect negatively charged exosomes when they are bound to the graphene surface. In this particular case, researchers have created sgFETs with aptamer that can detect HCV protein even at lower concentrations making it an ultrasensitive aptasensor. Attomolar detection of the viral protein target is made possible by the enhanced sensitivity brought about by induced polarization at the graphene interface (Kwong Hong Tsang et al., 2019; Palacio et al., 2023).

5.2.1.4 Aptamer binding hemagglutinin of H7N7 subtype influenza virus (JP2014008002A)

An aptamer capable of differentiating between influenza A serotypes and interfering with the HA-glycan interaction was created by researchers. To ensure the aptamer's stability in the presence of endo-ribonucleases, 2′-fluoro cytidine is employed, which does not interfere with its binding to HA. This aptamer has applications in detecting and diagnosing H5N1 and H7N7 viruses, as well as in synthesizing virucidal drugs that selectively target these viruses, impeding their early interactions with hosts (Suenaga and Kumar, 2014). The glycoprotein known as hemaglutinin (HA), which is present on the influenza virus's surface, is essential to the virus's capacity to bind to and penetrate host cells. Aptamers work by specifically targeting HA, which stops the virus from attaching to host cell receptors and preventing it from entering the cells (Zou et al., 2019)

5.2.2 Case studies: aptamers that inhibit biofilm

Quorum sensing, a mechanism that enables signaling and communication within bacteria, plays a key role in the formation of *P.aeruginosa* biofilms. Three main QS systems in *P.aeruginosa*: *las* system, *rhl* system and *Pseudomonas quinolone signal* system (PQS) encode for various signaling molecules that act as regulator for the transcription of numerous virulence factor genes (Zhang et al., 2013; Chadha et al., 2022). Zhao et al., conducted a study in which they screened DNA aptamers complimentary to the signal molecule C4-HSL of the *rhl* system. Depressing the *rhl* system affects the formation and maintenance of the biofilm. It was observed that the biofilm formation of *P.aeruginosa* was efficiently reduced to about 1/3 by the aptamers compared with that of the groups without the aptamers in the *in vitro* biofilm inhibition experiments (Zhao et al., 2019) (Figure 4).

Matchawong et al., constructed a 2' -fluoropyrimidine modified nuclease-resistant RNA aptamersusing cell SELEX against *Streptococcus suis* serotype 2, strain P1/7. The R8-su12 RNA aptamer significantly reduced the *S. suis* biofilm formation and had the ability to bind to other pathogenic *S. suis* (serotype ½, 1, 9, and 14) (Matchawong et al., 2022). *Candida albicans* was grown in the exposure of condensed cigarette smoke (CSC), prepared from clove (CCSC) and non-clove (NCSC) cigarettes, for 48 h (Bachtiar et al., 2021).It was found that the presence of added CCSC or NCSC

significantly enhanced *C. albicans* biofilm development but when *C. albicans* was precoated with aptamer (Ca-apt1) there was a significant impairment in the biofilm development accelerated by the NCSC and CCSC. This could be attributed to the enhancement of the morphological changes of *C. albicans* (from yeast to hypha formation) due to CCSC or NCSC was reduced due to precoating the aptamer.

Ning et al.,conducted an interesting study in which a GO-loaded aptamer/berberine bifunctional complex specific to penicillin-binding protein 2a (PBP2a) significantly inhibited MRSA biofilm formation (Ning et al., 2022). The aptamer blocks the function of PBP2a, reducing surface-cell attachment and berberine attenuates the level of the accessory gene regulator (agr) system, which is essential for MRSA biofilm formation. Furthermore, GO also has the potential to disrupt cell membranes, attributing to the antibiofilm activity (Saravanan et al., 2023). Lijuan et al., developed an aptamer-ampicillin bifunctional conjugate that targeted bacterial flagella for treating biofilms (Lijuan et al., 2017).

6 Challenges and limitations

6.1 Stability and delivery concerns of aptamers

The term "steady state" describes the dynamic balance that results from consistent dosage between the total amount of a drug taken and its elimination. For aptamers, the steady-state or nearly steady-state concentration can be attained three to five times the half-life following aptamer administration, which has a steady-state duration of 17 to 29 hours (Lee et al., 2015). This emphasize on the importance of aptamer's stability i.e.,The longer the aptamer stays in circulation for the treatment of infectious disorders, the greater the likelihood that it may encounter pathogens. The pharmacokinetic profile of the aptamer must be determined to proceed with trials, firstly the aptamer's half-life *in vivo* is rather brief, lasting roughly 2 mins. Unmodified ssDNA oligonucleotides have a half-life of less than one minute (Griffin et al., 1993) (Sanjuán, 2012).

In conditioned media, HEK cells infected with *M. fermentans* exhibit ribonuclease activity that rapidly degrades RNA carrying 2′-fluoro- and 2′-O-methyl-modified pyrimidines. Similar ribonuclease activity was seen in a pure culture of *M.fermentans*, but not in a culture of uncontaminated HEK cells (Hernandez et al., 2012). RA-36, an aptamer with antithrombin properties, have shown rapid bloodstream elimination with a half life of 1 minute As opposed to 23 minutes in tissues (Zavyalova et al., 2017). The tissue type, aptamer sequence, and their formulation affects the outcomes of aptamer uptake ad distribution. A single bolus oral dose of aptamer was administered to mice, and after tissue contamination was eliminated with perfusion buffer, the aptamer was diffused into the bloodstream from the peritoneum and into multiple organs, including the brain and spinal cord, within minutes of oral administration. The uptake of the aptamer was reduced within a few hours (Perschbacher et al., 2015). When aptamer and nanoparticles are conjugated, the physiochemical properties including the size and distribution of the particles are altered (Ghassami et al., 2018).

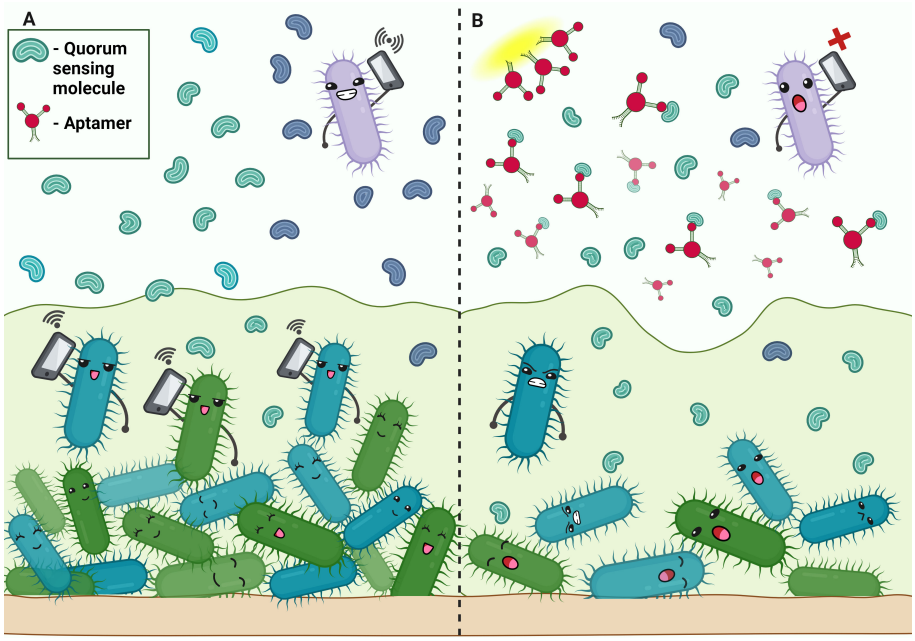

FIGURE 4
Aptamers disrupting quorum sensing in biofilm. **(A)** Communication in bacterial biofilm by quorum sensing molecule. **(B)** Aptamer binds to the quorum-sensing molecules, disrupting signaling.

6.2 Potential for off-target effects and safety issues

Drugs undergoing clinical trials may have side effects and safety problems of their own, but it is crucial to understand these effects in order to design a therapeutic version with less side effects. Investigations' findings by Zhao et.al., in the tested settings, the SGC8 aptamer exhibited neither mutagenicity nor genetic toxicity using total body-positron emitting tomography (TB PET) (D. Ding et al., 2023). When an aptamer-tagged radioactive element was injected intravenously, the kidney contained the highest quantities of radioactivity. This indicates that the pharmacokinetics profile of absorption from intravenous aptamer injection results in a relatively low absorption rate. However, giving aptamer was administered in many doses, but this did not cause aptamer to accumulate in plasma. The factor most likely limiting the drug's rate of disposal is its rate of absorption (Siddiqui and Keating, 2005).

Researchers discovered that the absence of conjugating cholesterol has certain undesirable effects, such as altering the expression of genes associated to innate immunity and cellular survival (Lee et al., 2015). In addition, the aptamer's overall negative charge causes it to attach to positively charged substances without being specific. As stated previously, the aptamer's short length and compact size promote bio clearance (Gholikhani et al., 2022).

6.3 Strategies to overcome challenges and ongoing research in the field

The aforementioned problems can be solved in a number of ways, and some of these tactics are (1) substituting sulfur for one of the monothio or dithio groups of the phosphoryl non-bridging oxygen atoms results in a number of benefits, including increased binding to the target, resistance to nuclease action, and faster absorption into the cells. However, there is a small drawback to this the aptamer may become less specific (Thiviyanathan et al., 2007; Keefe et al., 2010). (2) integrating aptamer into a larger molecular framework in the shape of a multivalent circle by offering nucleolytic stabilization that guards against exonucleases (Di Giusto et al., 2006). (3) the body's nuclease enzymes could not break down aptamers synthesized with an L nucleotide sequence. This type of sequence, called spigelmers, is the mirror image of an oligonucleotide but contains L nucleotide instead of R nucleotide (Maasch et al., 2008; Chen et al., 2017). (4) RNA sequences that have aldehyde derivatives appended to the 5' end, facilitate affinity purification and coupling with other molecules (Pfander et al., 2007). (5) producing the most stable hybrids by employing nucleoside analogues that have a methylene bond between the ribose ring's 2′-O and 4′-C in order to create a locked nucleic acid sequence. The sugar moiety is thus locked in a C3′-endo configuration (Lebars et al., 2007). (6) an aptamer was modified by adding PEG linkers to decrease stearic hinderance and 2'-fluoro-pyrimidines (2'F) (Derbyshire et al., 2012; Ni et al., 2021). (7) the highest tissue exposure was achieved by the aptamer, which was prepared as a 3′ biotin derivative coupled with tetrameric streptavidin (Perschbacher et al., 2015). To achieve this, a cholesterol moiety was linked to the 5' end of a 29-nucleotide RNA aptamer that had been modified with 2'-F against the HCV NS5B protein. This modification was chosen because previous studies have shown that conjugating oligonucleotide molecules with cholesterol can prolong their plasma half-life by associating with plasma lipoproteins and enhance their uptake by hepatic cells through receptor-mediated endocytosis. (8) An improved aptamer half-life results by conjugating cholesterol with the aptamer (Lee et al., 2015). (9) The aptamer attached to MetCyc, facilitating its interaction with other molecules helping evade attacks from nucleases (Borbas et al., 2007; Ni et al., 2021). (10) In some circumstances, we can employ liposomal conjugated aptamers to lengthen the drug's half-life and make it more covert (Jiang et al., 2020; Alameh et al., 2021; Kim et al., 2001). (11) To shield the RNA from exonuclease degradation, the derivative's two terminals are capped with an extended stem structure, allowing for the effective *in vivo* expression of the aptamer (Mori et al., 2012). Creating chimeric aptamers by combining segments from different aptamers or combining with other functional molecules for enhancing specificity (Cheng et al., 2023). In conclusion, these diverse strategies and modifications illustrate ongoing efforts to optimize aptamer technology, enhancing their stability, specificity, and therapeutic efficacy across various biomedical applications.

7 Conclusion and future perspectives

The diverse applications of aptamers in the realm of infectious diseases underscore their immense potential in diagnostics, therapeutics, and biosensing. The ability of aptamers to specifically recognize and bind to a wide range of pathogenic targets, including viruses, bacteria, and fungus, has paved the way for innovative solutions in disease detection and treatment. In diagnostics, aptamers have demonstrated exceptional sensitivity and specificity, enabling the development of rapid and accurate diagnostic assays. Their incorporation into biosensors has facilitated the detection of infectious agents at early stages, contributing to timely interventions and improved patient outcomes. Aptamer-based diagnostic platforms also offer the advantage of portability and cost-effectiveness, making them particularly valuable in resource-limited settings. Aptamers have proven their mettle in therapeutic applications, where they can be engineered to inhibit viral entry, replication, or modulate the host immune response. The versatility of aptamers allows for the design of tailored therapeutic interventions, offering a promising avenue for the development of antiviral and antibacterial agents. Moreover, the potential for aptamers to mitigate the emergence of drug-resistant strains adds another layer of significance to their therapeutic applications. Looking ahead, the future perspectives of aptamer research in infectious diseases are exciting and multifaceted. Advancements in aptamer selection technologies, such as SELEX, will likely enhance the discovery of aptamers with improved binding affinities and specificities. The integration of aptamers with emerging technologies, such as CRISPR-based diagnostics and gene editing, holds promise for the development of next-generation diagnostic and

therapeutic tools. Furthermore, the exploration of aptamer-nanoparticle conjugates and other delivery systems may enhance the targeted delivery of aptamers to infected tissues, improving their therapeutic efficacy. Collaborations between academia, industry, and healthcare providers will be crucial in translating aptamer-based technologies from the laboratory to clinical practice.

Author contributions

RN: Data curation, Visualization, Writing – original draft. BS: Visualization, Writing – original draft, Conceptualization. SS: Data curation, Visualization, Writing – original draft. AS: Data curation, Visualization, Writing – review & editing. SR: Data curation, Visualization, Writing – review & editing. HD: Conceptualization, Data curation, Supervision, Visualization, Writing – review & editing. AS: Conceptualization, Data curation, Supervision, Visualization, Writing – review & editing.

Funding

The author(s) declare that no financial support was received for the research, authorship, and/or publication of this article.

Acknowledgments

The authors are grateful to SASTRA University for providing us with an excellent infrastructure and for providing the opportunity to be a part of the Quorum Sensing Lab (QSL).

Conflict of interest

The authors declare that the research was conducted in the absence of any commercial or financial relationships that could be construed as a potential conflict of interest.

The author(s) declared that they were an editorial board member of Frontiers, at the time of submission. This had no impact on the peer review process and the final decision

Publisher's note

References

Adachi, T., and Nakamura, Y. (2019). Aptamers: A review of their chemical properties and modifications for therapeutic application. *Molecules* 24, 4229. doi: 10.3390/molecules24234229

Afrasiabi, S., Pourhajibagher, M., Raoofian, R., Tabarzad, M., and Bahador, A. (2020). Therapeutic applications of nucleic acid aptamers in microbial infections. *J. Biomed. Sci.* 27, 6. doi: 10.1186/s12929-019-0611-0

Agrelli, A., de Moura, R. R., Crovella, S., and Brandão, L. A. C. (2019). ZIKA virus entry mechanisms in human cells. *Infection Genet. Evol.* 69, 22–29. doi: 10.1016/j.meegid.2019.01.018

Aguilar, H. C., Matreyek, K. A., Filone, C. M., Hashimi, S. T., Levroney, E. L., Negrete, O. A., et al. (2006). N-Glycans on Nipah Virus fusion protein protect against neutralization but reduce membrane fusion and viral entry. *J. Virol.* 80, 4878–4889. doi: 10.1128/jvi.80.10.4878-4889.2006

Alameh, M.-G., Tombácz, I., Bettini, E., Lederer, K., Ndeupen, S., Sittplangkoon, C., et al. (2021). Lipid nanoparticles enhance the efficacy of mRNA and protein subunit vaccines by inducing robust T follicular helper cell and humoral responses. *Immunity* 54, 2877–2892.e7. doi: 10.1016/j.immuni.2021.11.001

Ali, M. H., Elsherbiny, M. E., and Emara, M. (2019). Updates on aptamer research. *Int. J. Mol. Sci.* 20, 2511. doi: 10.3390/ijms20102511

Aljohani, M. M., Cialla-May, D., Popp, J., Chinnappan, R., Al-Kattan, K., and Zourob, M. (2022). Aptamers: potential diagnostic and therapeutic agents for blood diseases. *Molecules* 27, 383. doi: 10.3390/molecules27020383

Almeida, N. B. F., Sousa, T. A. S. L., Santos, V. C. F., Lacerda, C. M. S., Silva, T. G., Grenfell, R. F. Q., et al. (2022). DNA aptamer selection and construction of an aptasensor based on graphene FETs for Zika virus NS1 protein detection. *Beilstein J. Nanotechnology* 13, 873–881. doi: 10.3762/bjnano.13.78

Amouzadeh Tabrizi, M., and Acedo, P. (2022). Highly sensitive aptasensor for the detection of SARS-CoV-2-RBD using aptamer-gated methylene blue@mesoporous silica film/laser engraved graphene electrode. *Biosensors Bioelectronics* 215, 114556. doi: 10.1016/j.bios.2022.114556

A Ocsoy, M., Yusufbeyoglu, S., Ildiz, N., Ulgen, A., and Ocsoy, I. (2021). DNA aptamer-conjugated magnetic graphene oxide for pathogenic bacteria aggregation: selective and enhanced photothermal therapy for effective and rapid killing. *ACS Omega* 6, 20637–20643. doi: 10.1021/acsomega.1c02832

Askari, A., Kota, S., Ferrell, H., Swamy, S., Goodman, K. S., Okoro, C. C., et al. (2024). UTexas Aptamer Database: the collection and long-term preservation of aptamer sequence information. *Nucleic Acids Res.* 52, D351–D359. doi: 10.1093/nar/gkad959

Aslan, Y., Atabay, M., Chowdhury, H. K., Göktürk, I., Saylan, Y., and Inci, F. (2023). Aptamer-based point-of-care devices: emerging technologies and integration of computational methods. *Biosensors* 13, 569. doi: 10.3390/bios13050569

Augenstreich, J., Haanappel, E., Sayes, F., Simeone, R., Guillet, V., Mazeres, S., et al. (2020). Phthiocerol dimycocerosates from *Mycobacterium tuberculosis* increase the membrane activity of bacterial effectors and host receptors. *Front. Cell. Infection Microbiol.* 10. doi: 10.3389/fcimb.2020.00420

Bachour Junior, B., Batistuti, M. R., Pereira, A. S., de Sousa Russo, E. M., and Mulato, M. (2021). Electrochemical aptasensor for NS1 detection: Towards a fast dengue biosensor. *Talanta* 233, 122527. doi: 10.1016/j.talanta.2021.122527

Bachtiar, B. M., Gani, B. A., Deviana, A., Utami, N. R., Andriyani, A. D., and Bachtiar, E. W. (2021). The discrepancy between clove and non-clove cigarette smoke-promoted *Candida albicans* biofilm formation with precoating RNA-aptamer. *F1000Research* 10, 372. doi: 10.12688/f1000research.52266.3

Bagheri Pebdeni, A., Mousavizadegan, M., and Hosseini, M. (2021). Sensitive detection of S. aureus using aptamer- and vancomycin -copper nanoclusters as dual recognition strategy. *Food Chem.* 361, 130137. doi: 10.1016/j.foodchem.2021.130137

Bagheryan, Z., Raoof, J.-B., Golabi, M., Turner, A. P. F., and Beni, V. (2016). Diazonium-based impedimetric aptasensor for the rapid label-free detection of *Salmonella typhimurium* in food sample. *Biosensors Bioelectronics* 80, 566–573. doi: 10.1016/j.bios.2016.02.024

Bai, X., Nakatsu, C. H., and Bhunia, A. K. (2021). Bacterial biofilms and their implications in pathogenesis and food safety. *Foods* 10, 2117. doi: 10.3390/foods10092117

Bakhtiari, H., Palizban, A. A., Khanahmad, H., and Mofid, M. R. (2021). Novel approach to overcome defects of Cell-SELEX in developing aptamers against aspartate β-hydroxylase. *ACS Omega* 6, 11005–11014. doi: 10.1021/acsomega.1c00876

Bayraç, A. T., and Donmez, S. I. (2018). Selection of DNA aptamers to *Streptococcus pneumonia* and fabrication of graphene oxide based fluorescent assay. *Analytical Biochem.* 556, 91–98. doi: 10.1016/j.ab.2018.06.024

Baz-Martnez, M., El Motiam, A., Ruibal, P., Condezo, G. N., de la Cruz-Herrera, C. F., Lang, V., et al. (2016). Regulation of Ebola virus VP40 matrix protein by SUMO. *Sci. Rep.* 6. doi: 10.1038/srep37258

Bell, R. L., Jarvis, K. G., Ottesen, A. R., McFarland, M. A., and Brown, E. W. (2016). Recent and emerging innovations in *Salmonella* detection: a food and environmental perspective. *Microbial Biotechnol.* 9, 279–292. doi: 10.1111/1751-7915.12359

Bharaj, P., Wang, Y. E., Dawes, B. E., Yun, T. E., Park, A., Yen, B., et al. (2016). The matrix protein of nipah virus targets the E3-ubiquitin ligase TRIM6 to inhibit the IKKε kinase-mediated type-I IFN antiviral response. *PLoS Pathog.* 12. doi: 10.1371/journal.ppat.1005880

Binh, N. T., Wakai, C., Kawaguchi, A., and Nagata, K. (2013). The N-terminal region of influenza virus polymerase PB1 adjacent to the PA binding site is involved in replication but not transcription of the viral genome. *Front. Microbiol.* 4. doi: 10.3389/fmicb.2013.00398

Binning, J. M., Wang, T., Luthra, P., Shabman, R. S., Borek, D. M., Liu, G., et al. (2013). Development of RNA aptamers targeting ebola virus VP35. *Biochemistry* 52, 8406–8419. doi: 10.1021/bi400704d

Borbas, K. E., Ferreira, C. S. M., Perkins, A., Bruce, J. I., and Missailidis, S. (2007). design and synthesis of mono- and multimeric targeted radiopharmaceuticals based on novel cyclen ligands coupled to Anti-MUC1 aptamers for the diagnostic imaging and targeted radiotherapy of cancer. *Bioconjugate Chem.* 18, 1205–1212. doi: 10.1021/bc0700741

Boussebayle, A., Groher, F., and Suess, B. (2019). RNA-based Capture-SELEX for the selection of small molecule-binding aptamers. *Methods* 161, 10–15. doi: 10.1016/j.ymeth.2019.04.004

Bouvier, N. M., and Palese, P. (2008). The biology of influenza viruses. *Vaccine* 26, D49–D53. doi: 10.1016/j.vaccine.2008.07.039

Brandenburg, B., Koudstaal, W., Goudsmit, J., Klaren, V., Tang, C., Bujny, M. V., et al. (2013). Mechanisms of hemagglutinin targeted influenza virus neutralization. *PLoS One* 8 (12), e80034. doi: 10.1371/journal.pone.0080034

Brody, E., Willis, M., Smith, J., Jayasena, S., Zichi, D., and Gold, L. (1999). The use of aptamers in large arrays for molecular diagnostics. *Mol. Diagnosis* 4, 381–388. doi: 10.1016/S1084-8592(99)80014-9

Brooks, L. R. K., and Mias, G. I. (2018). *Streptococcus pneumoniae*'s virulence and host immunity: Aging, diagnostics, and prevention. *Front. Immunol.* 9. doi: 10.3389/fimmu.2018.01366

Brosel-Oliu, S., Ferreira, R., Uria, N., Abramova, N., Gargallo, R., Muñoz-Pascual, F.-X., et al. (2018). Novel impedimetric aptasensor for label-free detection of *Escherichia coli* O157:H7. *Sensors Actuators B: Chem.* 255, 2988–2995. doi: 10.1016/j.snb.2017.09.121

Brosseau, N. E., Vallée, I., Mayer-Scholl, A., Ndao, M., and Karadjian, G. (2023). Aptamer-based technologies for parasite detection. *Sensors* 23, 562. doi: 10.3390/s23020562

Canova, M. J., and Molle, V. (2014). Bacterial serine/threonine protein kinases in host-pathogen interactions. *J. Biol. Chem.* 289, 9473–9479). doi: 10.1074/jbc.R113.529917

Capatina, D., Lupoi, T., Feier, B., Blidar, A., Hosu, O., Tertis, M., et al. (2022). Label-free electrochemical aptasensor for the detection of the 3-O-C12-HSL quorum-sensing molecule in *Pseudomonas aeruginosa*. *Biosensors* 12, 440. doi: 10.3390/bios12070440

Chadha, J., Harjai, K., and Chhibber, S. (2022). Revisiting the virulence hallmarks of Pseudomonas aeruginosa : a chronicle through the perspective of quorum sensing. *Environ. Microbiol.* 24, 2630–2656. doi: 10.1111/1462-2920.15784

Chauhan, P., Datta, I., Dhiman, A., Shankar, U., Kumar, A., Vashist, A., et al. (2022). DNA aptamer targets *Mycobacterium tuberculosis* DevR/DosR response regulator function by inhibiting its dimerization and DNA binding activity. *ACS Infect. Dis.* 8, 2540–2551. doi: 10.1021/acsinfecdis.2c00414

Chen, X., Chang, Y., Ye, M., Wang, Z., Wu, S., and Duan, N. (2024). Rational design of a robust g-quadruplex aptamer as an inhibitor to alleviate *Listeria monocytogenes* infection. *ACS Appl. Materials Interfaces* 16, 15946–15958. doi: 10.1021/acsami.4c00496

Chen, W., Cui, L., Song, Y., Chen, W., Su, Y., Chang, W., et al. (2021b). Detection of Listeria monocytogenes using luminol-functionalized AuNF-Labeled aptamer recognition and magnetic separation. *ACS Omega* 6, 26338–26344. doi: 10.1021/acsomega.1c03527

Chen, Z., Luo, H., Gubu, A., Yu, S., Zhang, H., Dai, H., et al. (2023). Chemically modified aptamers for improving binding affinity to the target proteins via enhanced non-covalent bonding. *Front. Cell Dev. Biol.* 11, 1091809. doi: 10.3389/fcell.2023.1091809

Chen, X., Ma, Y., Xie, Y., and Pu, J. (2022a). Aptamer-based applications for cardiovascular disease. *Front. Bioengineering Biotechnol.* 10. doi: 10.3389/fbioe.2022.1002285

Chen, H., Park, S.-G., Choi, N., Moon, J.-I., Dang, H., Das, A., et al. (2020). SERS imaging-based aptasensor for ultrasensitive and reproducible detection of influenza virus A. *Biosensors Bioelectronics* 167, 112496. doi: 10.1016/j.bios.2020.112496

Chen, W., Wu, J., Li, S., Zhang, H., Cui, L., Liu, J., et al. (2021c). Ultrasensitive detection of Listeria monocytogenes using solid-state electrochemiluminescence biosensing based on the quenching effect of ferrocene on ruthenium pyridine. *J. Food Saf.* 41. doi: 10.1111/jfs.12868

Chen, H., Xie, S., Liang, H., Wu, C., Cui, L., Huan, S.-Y., et al. (2017). Generation of biostable L-aptamers against achiral targets by chiral inversion of existing D-aptamers. *Talanta* 164, 662–667. doi: 10.1016/j.talanta.2016.11.001

Chen, M., Yu, Y., Jiang, F., Zhou, J., Li, Y., Liang, C., et al. (2016). Development of Cell-SELEX technology and its application in cancer diagnosis and therapy. *Int. J. Mol. Sci.* 17, 2079. doi: 10.3390/ijms17122079

Chen, X.-F., Zhao, X., and Yang, Z. (2022b). Aptasensors for the detection of infectious pathogens: design strategies and point-of-care testing. *Microchimica Acta* 189, 443. doi: 10.1007/s00604-022-05533-w

Chen, S., Zong, X., Zheng, J., Zhang, J., Zhou, M., Chen, Q., et al. (2021a). A colorimetric strategy based on aptamer-catalyzed hairpin assembly for the on-site detection of salmonella typhimurium in milk. *Foods* 10 (11), 2539. doi: 10.3390/foods10112539

Chessa, D., Spiga, L., de Riu, N., Delaconi, P., Mazzarello, V., Ganau, G., et al. (2014). Lipopolysaccharides belonging to different Salmonella serovars are differentially capable of activating toll-like receptor 4. *Infection Immun.* 82, 4553–4562. doi: 10.1128/IAI.02297-14

Cohen, M. L. (2000). Changing patterns of infectious disease. *Nature* 406, 762–767. doi: 10.1038/35021206

Dai, G., Li, Y., Li, Z., Zhang, J., Geng, X., Zhang, F., et al. (2022). Zirconium-based metal–organic framework and Ti3C2Tx nanosheet-based faraday cage-type electrochemical aptasensor for Escherichia coli detection. *ACS Appl. Nano Materials* 5, 9201–9208. doi: 10.1021/acsanm.2c01548

Damborský, P., Švitel, J., and Katrlík, J. (2016). Optical biosensors. *Essays Biochem.* 60, 91–100. doi: 10.1042/EBC20150010

Derbyshire, N., White, S. J., Bunka, D. H. J., Song, L., Stead, S., Tarbin, J., et al. (2012). Toggled RNA aptamers against aminoglycosides allowing facile detection of antibiotics using gold nanoparticle assays. *Analytical Chem.* 84, 6595–6602. doi: 10.1021/ac300815c

Dhiman, A., Kumar, C., Mishra, S. K., Sikri, K., Datta, I., Sharma, P., et al. (2019). Theranostic application of a novel G-quadruplex-forming DNA aptamer targeting malate synthase of Mycobacterium tuberculosis. *Mol. Ther. Nucleic Acids* 18, 661–672. doi: 10.1016/j.omtn.2019.09.026

Diagne, C. T., Diallo, D., Faye, O., Ba, Y., Faye, O., Gaye, A., et al. (2015). Potential of selected Senegalese Aedes spp. mosquitoes (Diptera: Culicidae) to transmit Zika virus. *BMC Infect. Dis.* 15, 492. doi: 10.1186/s12879-015-1231-2

Di Giusto, D. A., Knox, S. M., Lai, Y., Tyrelle, G. D., Aung, M. T., and King, G. C. (2006). Multitasking by multivalent circular DNA aptamers. *ChemBioChem* 7, 535–544. doi: 10.1002/cbic.200500316

Ding, Y., and Liu, J. (2023). Quantitative comparison of Capture-SELEX, GO-SELEX, and Gold-SELEX for enrichment of aptamers. *Analytical Chem.* 95, 14651–14658. doi: 10.1021/acs.analchem.3c02477

Ding, D., Zhao, H., Wei, D., Yang, Q., Yang, C., Wang, R., et al. (2023). The first-in-human whole-body dynamic pharmacokinetics study of aptamer. *Research* 6. doi: 10.34133/research.0126

Doherty, M. K., Shaw, C., Woods, L., and Weimer, B. C. (2023). Alpha-gal bound aptamer and vancomycin synergistically reduce *Staphylococcus aureus* infection *In vivo*. *Microorganisms* 11 (7), 1776. doi: 10.3390/microorganisms11071776

Dong, Y., Wang, Z., Wang, S., Wu, Y., Ma, Y., and Liu, J. (2018). "Introduction of SELEX and important SELEX variants," in *Aptamers for Analytical Applications: Affinity Acquisition and Method Design*, pp.1–pp25.

Dramsi, S., and Cossart, P. (2002). Listeriolysin O. *J. Cell Biol.* 156, 943–946. doi: 10.1083/jcb.200202121

Du, J., Chen, X., Liu, K., Zhao, D., and Bai, Y. (2022). Dual recognition and highly sensitive detection of *Listeria monocytogenes* in food by fluorescence enhancement effect based on Fe3O4@ZIF-8-aptamer. *Sensors Actuators B: Chem.* 360, 131654. doi: 10.1016/j.snb.2022.131654

Duan, N., Chang, B., Zhang, H., Wang, Z., and Wu, S. (2016). Salmonella typhimurium detection using a surface-enhanced Raman scattering-based aptasensor. *Int. J. Food Microbiol.* 218, 38–43. doi: 10.1016/j.ijfoodmicro.2015.11.006

Duan, N., Wu, S., Zhu, C., Ma, X., Wang, Z., Yu, Y., et al. (2012). Dual-color upconversion fluorescence and aptamer-functionalized magnetic nanoparticles-based bioassay for the simultaneous detection of *Salmonella Typhimurium* and *Staphylococcus aureus*. *Analytica Chimica Acta* 723, 1–6. doi: 10.1016/j.aca.2012.02.011

El-Wekil, M. M., Halby, H. M., Darweesh, M., Ali, M. E., and Ali, R. (2022). An innovative dual recognition aptasensor for specific detection of *Staphylococcus aureus* based on Au/Fe3O4 binary hybrid. *Sci. Rep.* 12, 12502. doi: 10.1038/s41598-022-15637-1

Escolano, J. M., Díaz-Durán, B., DeMiguel-Ramos, M., Olivares, J., Geday, M. A., and Iborra, E. (2017). Selection of aptamers to *Neisseria meningitidis* and *Streptococcus pneumoniae* surface specific proteins and affinity assay using thin film AlN resonators. *Sensors Actuators B: Chem.* 246, 591–596. doi: 10.1016/j.snb.2017.02.098

Eyer, L., Zouharová, D., Širmarová, J., Fojtíková, M., Štefánik, M., Haviernik, J., et al. (2017). Antiviral activity of the adenosine analogue BCX4430 against West Nile virus and tick-borne flaviviruses. *Antiviral Res.* 142, 63–67. doi: 10.1016/j.antiviral.2017.03.012

Fair, R. J., and Tor, Y. (2014). Antibiotics and bacterial resistance in the 21st century. *Perspect. Medicinal Chem.* 6, PMC.S14459. doi: 10.4137/PMC.S14459

Fang, S., Song, D., Zhuo, Y., Chen, Y., Zhu, A., and Long, F. (2021). Simultaneous and sensitive determination of *Escherichia coli* O157:H7 and *Salmonella typhimurium* using evanescent wave dual-color fluorescence aptasensor based on micro/nano size effect. *Biosensors Bioelectronics* 185, 113288. doi: 10.1016/j.bios.2021.113288

Fathi, S., Saber, R., Adabi, M., Rasouli, R., Douraghi, M., Morshedi, M., et al. (2020). Novel competitive voltammetric aptasensor based on electrospun carbon nanofibers-gold nanoparticles modified graphite electrode for salmonella enterica serovar

detection. *Biointerface Res. Appl. Chem.* 11, 8702–8715. doi: 10.33263/BRIAC112.87028715

Faucher, S. P., Viau, C., Gros, P. P., Daigle, F., and Le Moual, H. (2008). The prpZ gene cluster encoding eukaryotic-type Ser/Thr protein kinases and phosphatases is repressed by oxidative stress and involved in *Salmonella enterica* serovar Typhi survival in human macrophages. *FEMS Microbiol. Lett.* 281, 160–166. doi: 10.1111/j.1574-6968.2008.01094.x

Feng, H., Beck, J., Nassal, M., and Hu, K. (2011). A SELEX-Screened aptamer of human hepatitis B virus RNA encapsidation signal suppresses viral replication. *PLoS One* 6, e27862. doi: 10.1371/journal.pone.0027862

Ferhan, A. R., Jackman, J. A., and Cho, N.-J. (2016). Integration of quartz crystal microbalance-dissipation and reflection-mode localized surface plasmon resonance sensors for biomacromolecular interaction analysis. *Analytical Chem.* 88, 12524–12531. doi: 10.1021/acs.analchem.6b04303

Fowler, C. C., and Galán, J. E. (2018). Decoding a *Salmonella typhi* regulatory network that controls typhoid toxin expression within human cells. *Cell Host Microbe* 23, 65–76.e6. doi: 10.1016/j.chom.2017.12.001

Furuta, Y., Takahashi, K., Shiraki, K., Sakamoto, K., Smee, D. F., Barnard, D. L., et al. (2009). T-705 (favipiravir) and related compounds: Novel broad-spectrum inhibitors of RNA viral infections. *Antiviral Res.* 82, 95–102. doi: 10.1016/j.antiviral.2009.02.198

Galán, J. E. (2016). Typhoid toxin provides a window into typhoid fever and the biology of Salmonella Typhi. *Proc. Natl. Acad. Sci.* 113, 6338–6344. doi: 10.1073/pnas.1606335113

Gao, R., Zhong, Z., Gao, X., and Jia, L. (2018). Graphene oxide quantum dots assisted construction of fluorescent aptasensor for rapid detection of *Pseudomonas aeruginosa* in food samples. *J. Agric. Food Chem.* 66, 10898–10905. doi: 10.1021/acs.jafc.8b02164

García-Recio, E. M., Pinto-Díez, C., Pérez-Morgado, M. I., García-Hernández, M., Fernández, G., Martín, M. E., et al. (2016). Characterization of MNK1b DNA Aptamers that inhibit proliferation in MDA-MB231 breast cancer cells. *Mol. Ther. - Nucleic Acids* 5, e275. doi: 10.1038/mtna.2015.50

Ge, C., Feng, J., Zhang, J., Hu, K., Wang, D., Zha, L., et al. (2022). Aptamer/antibody sandwich method for digital detection of SARS-CoV2 nucleocapsid protein. *Talanta* 236, 122847. doi: 10.1016/j.talanta.2021.122847

Gerlach, R. G., Jäckel, D., Stecher, B., Wagner, C., Lupas, A., Hardt, W. D., et al. (2007). Salmonella Pathogenicity Island 4 encodes a giant non-fimbrial adhesin and the cognate type 1 secretion system. *Cell. Microbiol.* 9, 1834–1850. doi: 10.1111/j.1462-5822.2007.00919.x

Ghassami, E., Varshosaz, J., Jahanian-Najafabadi, A., Minaiyan, M., Rajabi, P., and Hayati, E. (2018). Pharmacokinetics and *in vitro/in vivo* antitumor efficacy of aptamer-targeted Ecoflex® nanoparticles for docetaxel delivery in ovarian cancer. *Int. J. Nanomedicine Volume* 13, 493–504. doi: 10.2147/IJN.S152474

Gholikhani, T., Kumar, S., Valizadeh, H., Mahdinloo, S., Adibkia, K., Zakeri-Milani, P., et al. (2022). Advances in aptamers-based applications in breast cancer: drug delivery, therapeutics, and diagnostics. *Int. J. Mol. Sci.* 23, 14475. doi: 10.3390/ijms232214475

Gopinath, S. C. B. (2007). Methods developed for SELEX. *Analytical Bioanalytical Chem.* 387, 171–182. doi: 10.1007/s00216-006-0826-2

Gopinath, S. C. B., Misono, T. S., Kawasaki, K., Mizuno, T., Imai, M., Odagiri, T., et al. (2006). An RNA aptamer that distinguishes between closely related human influenza viruses and inhibits haemagglutinin-mediated membrane fusion. *J. Gen. Virol.* 87, 479–487. doi: 10.1099/vir.0.81508-0

Gribanyov, D., Zhdanov, G., Olenin, A., Lisichkin, G., Gambaryan, A., Kukushkin, V., et al. (2021). SERS-Based colloidal aptasensors for quantitative determination of influenza virus. *Int. J. Mol. Sci.* 22, 1842. doi: 10.3390/ijms22041842

Griffin, L., Tidmarsh, G., Bock, L., Toole, J., and Leung, L. (1993). *In vivo* anticoagulant properties of a novel nucleotide-based thrombin inhibitor and demonstration of regional anticoagulation in extracorporeal circuits. *Blood* 81, 3271–3276. doi: 10.1182/blood.V81.12.3271.3271

Gründling, A., Burrack, L. S., Bouwer, H. A., and Higgins, D. E. (2004). *Listeria monocytogenes* regulates flagellar motility gene expression through MogR, a transcriptional repressor required for virulence. *Proc Natl Acad Sci.* 101 (33), 12318–12323.

Hamedani, N. S., and Müller, J. (2016). Capillary electrophoresis for the selection of DNA aptamers recognizing activated protein C. *Nucleic acid aptamers: selection, characterization, and application*. 1380, 61–75. doi: 10.1007/978-1-4939-3197-2_5

Hameed, S. S., Al-Ogaili, A. S., and Noori, N. (2022). Single-stranded DNA aptamer-based rolling circle amplification as anti-chicken *Salmonella* bacteriostatic. *Veterinary World* 15, 1171–1176. doi: 10.14202/vetworld.2022.1171-1176

Hernandez, F. J., Stockdale, K. R., Huang, L., Horswill, A. R., Behlke, M. A., and McNamara, J. O. (2012). Degradation of nuclease-stabilized RNA oligonucleotides in mycoplasma-contaminated cell culture media. *Nucleic Acid Ther.* 22, 58–68. doi: 10.1089/nat.2011.0316

Hong, X., Xue, L., Gao, J., Jiang, Y., and Kou, X. (2022). Epochal coevolution of minor capsid protein in norovirus GII.4 variants with major capsid protein based on their interactions over the last five decades. *Virus Res.* 319, 198860. doi: 10.1016/j.virusres.2022.198860

Huang, X., Zheng, M., Wang, P., Mok, B. W. Y., Liu, S., Lau, S. Y., et al. (2017). An NS-segment exonic splicing enhancer regulates influenza A virus replication in mammalian cells. *Nat. Commun.* 8 (1), 14751. doi: 10.1038/ncomms14751

Hui, Y., Peng, H., Zhang, F., Zhang, L., Liu, Y., Jia, R., et al. (2022). An ultrasensitive sandwich-type electrochemical aptasensor using silver nanoparticle/titanium carbide nanocomposites for the determination of *Staphylococcus aureus* in milk. *Microchimica Acta* 189, 276. doi: 10.1007/s00604-022-05349-8

Jeon, S. H., Kayhan, B., Ben-Yedidia, T., and Arnon, R. (2004). A DNA aptamer prevents influenza infection by blocking the receptor binding region of the viral hemagglutinin. *J. Biol. Chem.* 279, 48410–48419. doi: 10.1074/jbc.M409059200

Jia, F., Bai, X., Zhang, X., Fu, Y., Li, Y., Li, X., et al. (2021). A low-field magnetic resonance imaging aptasensor for the rapid and visual sensing of *Pseudomonas aeruginosa* in food, juice, and water. *Analytical Chem.* 93, 8631–8637. doi: 10.1021/acs.analchem.1c01669

Jia, F., Duan, N., Wu, S., Dai, R., Wang, Z., and Li, X. (2016). Impedimetric *Salmonella* aptasensor using a glassy carbon electrode modified with an electrodeposited composite consisting of reduced graphene oxide and carbon nanotubes. *Microchimica Acta* 183, 337–344. doi: 10.1007/s00604-015-1649-7

Jia, W., Li, H., Wilkop, T., Liu, X., Yu, X., Cheng, Q., et al. (2018). Silver decahedral nanoparticles empowered SPR imaging-SELEX for high throughput screening of aptamers with real-time assessment. *Biosensors Bioelectronics* 109, 206–213. doi: 10.1016/j.bios.2018.02.029

Jia, F., Xu, L., Yan, W., Wu, W., Yu, Q., Tian, X., et al. (2017). A magnetic relaxation switch aptasensor for the rapid detection of Pseudomonas aeruginosa using superparamagnetic nanoparticles. *Microchimica Acta* 184, 1539–1545. doi: 10.1007/s00604-017-2142-2

Jiang, L., Wang, H., and Chen, S. (2020). Aptamer (AS1411)-conjugated liposome for enhanced therapeutic efficacy of mirna-29b in ovarian cancer. *J. Nanoscience Nanotechnology* 20, 2025–2031. doi: 10.1166/jnn.2020.17301

Johnson, J. R. (1991). Virulence factors in *Escherichia coli* urinary tract infection. *Clin. Microbiol. Rev.* 4, 80–128. doi: 10.1128/CMR.4.1.80

Jonsson, S., Musher, D. M., Chapman, A., Goree, A., and Lawrence, E. C. (1985). Phagocytosis and killing of common bacterial pathogens of the lung by human alveolar macrophages. *J. Infect. Dis.* 152, 4–13. doi: 10.1093/infdis/152.1.4

Kadurugamuwa, J. L., and Beveridge, T. J. (1995). Virulence factors are released from pseudomonas aeruginosa in association with membrane vesicles during normal growth and exposure to gentamicin: a novel mechanism of enzyme secretion. *J. Bacteriol.* 177 (14), 3998–4008. doi: 10.1128/jb.177.14.3998-4008.1995

Kalra, P., Mishra, S. K., Kaur, S., Kumar, A., Prasad, H. K., Sharma, T. K., et al. (2018). G-Quadruplex-forming DNA aptamers inhibit the dna-binding function of HupB and *Mycobacterium tuberculosis* entry into host cells. *Mol. Ther. Nucleic Acids* 13, 99–109. doi: 10.1016/j.omtn.2018.08.011

Kamiyama, N., Soma, R., Hidano, S., Watanabe, K., Umekita, H., Fukuda, C., et al. (2017). Ribavirin inhibits Zika virus (ZIKV) replication in *vitro* and suppresses viremia in ZIKV-infected STAT1-deficient mice. *Antiviral Res.* 146, 1–11. doi: 10.1016/j.antiviral.2017.08.007

Kaper, J. B., Nataro, J. P., and Mobley, H. L. T. (2004). Pathogenic *escherichia coli*. *Nat. Rev. Microbiol.* 2, 123–140. doi: 10.1038/nrmicro818

Kaur, H., Shorie, M., and Sabherwal, P. (2020). Electrochemical aptasensor using boron-carbon nanorods decorated by nickel nanoparticles for detection of E. coli O157:H7. *Microchimica Acta* 187, 461. doi: 10.1007/s00604-020-04444-y

Kaur, H., Shorie, M., Sharma, M., Ganguli, A. K., and Sabherwal, P. (2017). Bridged rebar graphene functionalized aptasensor for pathogenic E. coli O78:K80:H11 detection. *Biosensors Bioelectronics* 98, 486–493. doi: 10.1016/j.bios.2017.07.004

Keefe, A. D., Pai, S., and Ellington, A. (2010). Aptamers as therapeutics. *Nat. Rev. Drug Discovery* 9, 537–550. doi: 10.1038/nrd3141

Keller, L. E., Jones, C. V., Thornton, J. A., Sanders, M. E., Swiatlo, E., Nahm, M. H., et al. (2013). PspK of *Streptococcus pneumoniae* increases adherence to epithelial cells and enhances nasopharyngeal colonization. *Infection Immun.* 81, 173–181. doi: 10.1128/IAI.00755-12

Ker, D. S., Jenkins, H. T., Greive, S. J., and Antson, A. A. (2021). CryoEM structure of the Nipah virus nucleocapsid assembly. *PLoS Pathog.* 17 (7), e1009740. doi: 10.1371/journal.ppat.1009740

Kim, B., Chung, K. W., and Lee, J. H. (2018a). Non-stop aptasensor capable of rapidly monitoring norovirus in a sample. *J. Pharm. Biomed. Anal.* 152, 315–321. doi: 10.1016/j.jpba.2018.02.022

Kim, S., Lee, S., and Lee, H. J. (2018b). An aptamer-aptamer sandwich assay with nanorod-enhanced surface plasmon resonance for attomolar concentration of norovirus capsid protein. *Sensors Actuators B: Chem.* 273, 1029–1036. doi: 10.1016/j.snb.2018.06.108

Kim, E. S., Lu, C., Khuri, F. R., Tonda, M., Glisson, B. S., Liu, D., et al. (2001). A phase II study of STEALTH cisplatin (SPI-77) in patients with advanced non-small cell lung cancer. *Lung Cancer* 34, 427–432. doi: 10.1016/S0169-5002(01)00278-1

Kinghorn, A., Fraser, L., Liang, S., Shiu, S., and Tanner, J. (2017). Aptamer bioinformatics. *Int. J. Mol. Sci.* 18, 2516. doi: 10.3390/ijms18122516

Komarova, N., and Kuznetsov, A. (2019). Inside the black box: what makes SELEX better? *Molecules* 24, 3598. doi: 10.3390/molecules24193598

Kong, H. Y., and Byun, J. (2013). Nucleic acid aptamers: new methods for selection, stabilization, and application in biomedical science. *Biomolecules Ther.* 21, 423–434. doi: 10.4062/biomolther.2013.085

Kovacevic, K. D., Gilbert, J. C., and Jilma, B. (2018). Pharmacokinetics, pharmacodynamics and safety of aptamers. *Advanced Drug Delivery Rev.* 134, 36–50. doi: 10.1016/j.addr.2018.10.008

Kristian, S. A., Hwang, J. H., Hall, B., Leire, E., Iacomini, J., Old, R., et al. (2015). Retargeting pre-existing human antibodies to a bacterial pathogen with an alpha-Gal conjugated aptamer. *J. Mol. Med.* 93, 619–631. doi: 10.1007/s00109-015-1280-4

Krüger, A., de Jesus Santos, A. P., de Sá, V., Ulrich, H., and Wrenger, C. (2021). Aptamer applications in emerging viral diseases. *Pharmaceuticals* 14, 622. doi: 10.3390/ph14070622

Ku, T.-H., Zhang, T., Luo, H., Yen, T., Chen, P.-W., Han, Y., et al. (2015). Nucleic acid aptamers: an emerging tool for biotechnology and biomedical sensing. *Sensors* 15, 16281–16313. doi: 10.3390/s150716281

Kumar De, S., Ray, S., Rawat, Y., Mondal, S., Nandy, A., Verma, P., et al. (2021). Porous Au-seeded Ag nanorod networks conjugated with DNA aptamers for impedimetric sensing of DENV-2. *Sensors Actuators B: Chem.* 348, 130709. doi: 10.1016/j.snb.2021.130709

Kusumawati, A., Mustopa, A. Z., Umami, R. N., Santoso, A., Wibawan, I. W. T., Setiyono, A., et al. (2022). Antibiofilm activity and binding specificity of polyclonal dna aptamers on *Staphylococcus aureus* and *Escherichia coli*. *Microbiol. Biotechnol. Lett.* 50, 328–336. doi: 10.48022/mbl.2206.06001

Kwong Hong Tsang, D., Lieberthal, T. J., Watts, C., Dunlop, I. E., Ramadan, S., del Rio Hernandez, A. E., et al. (2019). Chemically functionalised graphene fet biosensor for the label-free sensing of exosomes. *Sci. Rep.* 9, 13946. doi: 10.1038/s41598-019-50412-9

Lai, H.-C., Wang, C.-H., Liou, T.-M., and Lee, G.-B. (2014). Influenza A virus-specific aptamers screened by using an integrated microfluidic system. *Lab. Chip* 14, 2002–2013. doi: 10.1039/C4LC00187G

Lebars, I., Richard, T., Di Primo, C., and Toulmé, J.-J. (2007). LNA derivatives of a kissing aptamer targeted to the trans-activating responsive RNA element of HIV-1. *Blood Cells Molecules Dis.* 38, 204–209. doi: 10.1016/j.bcmd.2006.11.008

Ledlod, S., Areekit, S., Santiwatanakul, S., and Chansiri, K. (2020). Colorimetric aptasensor for detecting Salmonella spp., *Listeria monocytogenes*, and *Escherichia coli* in meat samples. *Food Sci. Technol. Int.* 26, 430–443. doi: 10.1177/1082013219899593

Lee, C. H., Lee, S.-H., Kim, J. H., Noh, Y.-H., Noh, G.-J., and Lee, S.-W. (2015). Pharmacokinetics of a cholesterol-conjugated aptamer against the Hepatitis C Virus (HCV) NS5B protein. *Mol. Ther. - Nucleic Acids* 4, e254. doi: 10.1038/mtna.2015.30

Lee, J. Y., Nguyen, T. T. N., and Myoung, J. (2020). Zika virus-encoded NS2A and NS4A strongly downregulate NF-κB promoter activity. *J. Microbiol. Biotechnol.* 30, 1651–1658. doi: 10.4014/JMB.2011.11003

Lee, B., Park, J., Ryu, M., Kim, S., Joo, M., Yeom, J. H., et al. (2017). Antimicrobial peptide-loaded gold nanoparticle-DNA aptamer conjugates as highly effective antibacterial therapeutics against Vibrio vulnificus. *Sci. Rep.* 7 (1), 13572. doi: 10.1038/s41598-017-14127-z

Lerminiaux, N. A., MacKenzie, K. D., and Cameron, A. D. S. (2020). *Salmonella* pathogenicity island 1 (spi-1): the evolution and stabilization of a core genomic type three secretion system. *Microorganisms* 8, 576. doi: 10.3390/microorganisms8040576

Leung, D. W., Prins, K. C., Basler, C. F., and Amarasinghe, G. K. (2010). Ebolavirus VP35 is a multifunctional virulence factor. *Virulence* 1, 526–531. doi: 10.4161/viru.1.6.12984

Li, Y., Chen, M., Fan, X., Peng, J., Pan, L., Tu, K., et al. (2022). Sandwich fluorometric method for dual-role recognition of *Listeria monocytogenes* based on antibiotic-affinity strategy and fluorescence quenching effect. *Analytica Chimica Acta* 1221, 340085. doi: 10.1016/j.aca.2022.340085

Li, T., Ou, G., Chen, X., Li, Z., Hu, R., Li, Y., et al. (2020). Naked-eye based point-of-care detection of *E.coli* O157: H7 by a signal-amplified microfluidic aptasensor. *Analytica Chimica Acta* 1130, 20–28. doi: 10.1016/j.aca.2020.07.031

Li, J., Yun, W., Zhang, H., Chen, L., Ho, H.-P., Pu, X., et al. (2023). MoS2 nanosheets based label-free colorimetric aptasensor for *Escherichia coli* O157: H7 detection. *Colloids Surfaces A: Physicochemical Eng. Aspects* 674, 131955. doi: 10.1016/j.colsurfa.2023.131955

Li, A., Zuo, P., and Ye, B.-C. (2021). An aptamer biosensor based dual signal amplification system for the detection of Salmonella typhimurium. *Analytical Biochem.* 615, 114050. doi: 10.1016/j.ab.2020.114050

Lier, C., Becker, S., and Biedenkopf, N. (2017). Dynamic phosphorylation of Ebola virus VP30 in NP-induced inclusion bodies. *Virology* 512, 39–47. doi: 10.1016/j.virol.2017.09.006

Lijuan, C., Xing, Y., Minxi, W., Wenkai, L., and Le, D. (2017). Development of an aptamer-ampicillin conjugate for treating biofilms. *Biochem. Biophys. Res. Commun.* 483, 847–854. doi: 10.1016/j.bbrc.2017.01.016

Liu, R., Zhang, Y., Ali, S., Haruna, S. A., He, P., Li, H., et al. (2021). Development of a fluorescence aptasensor for rapid and sensitive detection of Listeria monocytogenes in food. *Food Control* 122, 107808. doi: 10.1016/j.foodcont.2020.107808

Lum, J., Wang, R., Hargis, B., Tung, S., Bottje, W., Lu, H., et al. (2015). An impedance aptasensor with microfluidic chips for specific detection of H5N1 avian influenza virus. *Sensors* 15, 18565–18578. doi: 10.3390/s150818565

Lunardelli, V. A. S., Almeida, B. S., Apostolico, J. S., Rezende, T., Yamamoto, M. M., Pereira, S. S., et al. (2023). Diagnostic and vaccine potential of Zika virus envelope protein (E) derivates produced in bacterial and insect cells. *Front. Immunol.* 14. doi: 10.3389/fimmu.2023.1071041

Ma, X., Xie, L., Wartchow, C., Warne, R., Xu, Y., Rivkin, A., et al. (2017). Structural basis for therapeutic inhibition of influenza A polymerase PB2 subunit. *Sci. Rep.* 7 (1), 9385. doi: 10.1038/s41598-017-09538-x

Ma, X., Xu, X., Xia, Y., and Wang, Z. (2018). SERS aptasensor for *Salmonella typhimurium* detection based on spiny gold nanoparticles. *Food Control* 84, 232–237. doi: 10.1016/j.foodcont.2017.07.016

Maasch, C., Buchner, K., Eulberg, D., Vonhoff, S., and Klussmann, S. (2008). Physicochemical stability of NOX-E36, a 40mer L-RNA (Spiegelmer) for therapeutic applications. *Nucleic Acids Symposium Ser.* 52, 61–62. doi: 10.1093/nass/nrn031

Majdinasab, M., Badea, M., and Marty, J. L. (2022). Aptamer-based lateral flow assays: current trends in clinical diagnostic rapid tests. *Pharmaceuticals* 15, 90. doi: 10.3390/ph15010090

Marton, S., Cleto, F., Krieger, M. A., and Cardoso, J. (2016). Isolation of an aptamer that binds specifically to E. coli. *PLoS One* 11, e0153637. doi: 10.1371/journal.pone.0153637

Matchawong, A., Srisawat, C., Sangboonruang, S., and Tharinjaroen, C. S. (2022). The ability of nuclease-resistant RNA aptamer against *Streptococcus suis* Serotype 2, Strain P1/7 to reduce biofilm formation in *vitro*. *Molecules* 27, 3894. doi: 10.3390/molecules27123894

Mayer, G., Ahmed, M.-S. L., Dolf, A., Endl, E., Knolle, P. A., and Famulok, M. (2010). Fluorescence-activated cell sorting for aptamer SELEX with cell mixtures. *Nat. Protoc.* 5, 1993–2004. doi: 10.1038/nprot.2010.163

McAuley, J. L., Gilbertson, B. P., Trifkovic, S., Brown, L. E., and McKimm-Breschkin, J. L. (2019). Influenza virus neuraminidase structure and functions. *Front. Microbiol.* 10. doi: 10.3389/fmicb.2019.00039

Mishra, A., Pilloton, R., Jain, S., Roy, S., Khanuja, M., Mathur, A., et al. (2022). Paper-based electrodes conjugated with tungsten disulfide nanostructure and aptamer for impedimetric detection of *Listeria monocytogenes*. *Biosensors* 12, 88. doi: 10.3390/bios12020088

Mok, J., Jeon, J., Jo, J., Kim, E., and Ban, C. (2021). Novel one-shot fluorescent aptasensor for dengue fever diagnosis using NS1-induced structural change of G-quadruplex aptamer. *Sensors Actuators B: Chem.* 343, 130077. doi: 10.1016/j.snb.2021.130077

Moon, J., Kim, G., Lee, S., and Park, S. (2013). Identification of *Salmonella Typhimurium*-specific DNA aptamers developed using whole-cell SELEX and FACS analysis. *J. Microbiological Methods* 95, 162–166. doi: 10.1016/j.mimet.2013.08.005

Mori, Y., Nakamura, Y., and Ohuchi, S. (2012). Inhibitory RNA aptamer against SP6 RNA polymerase. *Biochem. Biophys. Res. Commun.* 420, 440–443. doi: 10.1016/j.bbrc.2012.03.014

Muniandy, S., Teh, S. J., Appaturi, J. N., Thong, K. L., Lai, C. W., Ibrahim, F., et al. (2019). A reduced graphene oxide-titanium dioxide nanocomposite based electrochemical aptasensor for rapid and sensitive detection of Salmonella enterica. *Bioelectrochemistry* 127, 136–144. doi: 10.1016/j.bioelechem.2019.02.005

Musafia, B., Oren-Banaroya, R., and Noiman, S. (2014). Designing anti-influenza aptamers: Novel quantitative structure activity relationship approach gives insights into aptamer – virus interaction. *PLoS One* 9, e97696. doi: 10.1371/journal.pone.0097696

Nguyen, V.-T., Kwon, Y. S., Kim, J. H., and Gu, M. B. (2014). Multiple GO-SELEX for efficient screening of flexible aptamers. *Chem. Commun.* 50, 10513–10516. doi: 10.1039/C4CC03953J

Ni, S., Yao, H., Wang, L., Lu, J., Jiang, F., Lu, A., et al. (2017). Chemical modifications of nucleic acid aptamers for therapeutic purposes. *Int. J. Mol. Sci.* 18, 1683. doi: 10.3390/ijms18081683

Ni, S., Zhuo, Z., Pan, Y., Yu, Y., Li, F., Liu, J., et al. (2021). Recent progress in aptamer discoveries and modifications for therapeutic applications. *ACS Appl. Materials Interfaces* 13, 9500–9519. doi: 10.1021/acsami.0c05750

Ning, Y., Wang, X., Chen, P., Liu, S., Hu, J., Xiao, R., et al. (2022). Targeted inhibition of methicillin-resistant Staphylococcus aureus biofilm formation by a graphene oxide-loaded aptamer/berberine bifunctional complex. *Drug Delivery* 29, 1675–1683. doi: 10.1080/10717544.2022.2079768

Ninomiya, K., Yamashita, T., Kawabata, S., and Shimizu, N. (2014). Targeted and ultrasound-triggered drug delivery using liposomes co-modified with cancer cell-targeting aptamers and a thermosensitive polymer. *Ultrasonics Sonochemistry* 21, 1482–1488. doi: 10.1016/j.ultsonch.2013.12.023

Nishimoto, K. P., Newkirk, D., Hou, S., Fruehauf, J., and Nelson, E. L. (2007). Fluorescence activated cell sorting (FACS) using RNAlater to minimize RNA degradation and perturbation of mRNA expression from cells involved in initial host microbe interactions. *J. Microbiological Methods* 70, 205–208. doi: 10.1016/j.mimet.2007.03.022

Nishimoto, A. T., Rosch, J. W., and Tuomanen, E. I. (2020). Pneumolysin: pathogenesis and therapeutic target. *Front. Microbiol.* 11. doi: 10.3389/fmicb.2020.01543

Nobusawa, E. (1997). Structure and function of the hemagglutinin of influenza viruses. *Nihon Rinsho* 55, 2562–2569. Japanese Journal of Clinical Medicine.

Nutho, B., Mulholland, A. J., and Rungrotmongkol, T. (2019). The reaction mechanism of Zika virus NS2B/NS3 serine protease inhibition by dipeptidyl

aldehyde: A QM/MM study. *Phys. Chem. Chem. Phys.* 21, 14945–14956. doi: 10.1039/c9cp02377a

O'Neill, R. E., Talon, J., and Palese, P. (1998). The influenza virus NEP (NS2 protein) mediates the nuclear export of viral ribonucleoproteins. *EMBO J.* 17 (1), 288–296. doi: 10.1093/emboj/17.1.288

Ohuchi, S. (2012). Cell-SELEX technology. *Biores. Open Access* 1, 265–272. doi: 10.1089/biores.2012.0253

Ommen, P., Hansen, L., Hansen, B. K., Vu-Quang, H., Kjems, J., and Meyer, R. L. (2022). Aptamer-targeted drug delivery for *Staphylococcus aureus* biofilm. *Front. Cell. Infection Microbiol.* 12. doi: 10.3389/fcimb.2022.814340

Oravczová, V., Tatarko, M., Süle, J., Hun, M., Kerényi, Z., Hucker, A., et al. (2020). Detection of Listeria innocua by acoustic aptasensor. In *Proceedings*. MDPI 60 (1), 8. doi: 10.3390/IECB2020-07079

Oroh, S. B., Mustopa, A. Z., Budiarti, S., and Budiarto, B. R. (2020). Inhibition of enteropathogenic *Escherichia coli* biofilm formation by DNA aptamer. *Mol. Biol. Rep.* 47, 7567–7573. doi: 10.1007/s11033-020-05822-8

Otte, D.-M., Choukeife, M., Patwari, T., and Mayer, G. (2022). "Nucleic acid aptamers: from basic research to clinical applications," in *Handbook of chemical Biology of Nucleic Acids* (Springer Nature, Singapore), 1–25. doi: 10.1007/978-981-16-1313-5_25-1

Otto, M. (2014). *Staphylococcus aureus* toxins. *Curr. Opin. In Microbiol.* 17, 32–37. doi: 10.1016/j.mib.2013.11.004

Palacio, I., Moreno, M., Náñez, A., Purwidyantri, A., Domingues, T., Cabral, P. D., et al. (2023). Attomolar detection of hepatitis C virus core protein powered by molecular antenna-like effect in a graphene field-effect aptasensor. *Biosensors Bioelectronics* 222, 115006. doi: 10.1016/j.bios.2022.115006

Palmqvist, N., Foster, T., Tarkowski, A., and Josefsson, E. (2002). Protein A is a virulence factor in *Staphylococcus aureus* arthritis and septic death. *Microbial Pathogenesis* 33, 239–249. doi: 10.1006/mpat.2002.0533

Pan, Q., Zhang, X. L., Wu, H. Y., He, P. W., Wang, F., Zhang, M. S., et al. (2005). Aptamers that preferentially bind type IVB pili and inhibit human monocytic-cell invasion by *Salmonella enterica* serovar typhi. *Antimicrobial Agents Chemotherapy* 49, 4052–4060. doi: 10.1128/AAC.49.10.4052-4060.2005

Pang, Y., Rong, Z., Wang, J., Xiao, R., and Wang, S. (2015). A fluorescent aptasensor for H5N1 influenza virus detection based-on the core–shell nanoparticles metal-enhanced fluorescence (MEF). *Biosensors Bioelectronics* 66, 527–532. doi: 10.1016/j.bios.2014.10.052

Park, G., Lee, M., Kang, J., Park, C., Min, J., and Lee, T. (2022). Selection of DNA aptamer and its application as an electrical biosensor for Zika virus detection in human serum. *Nano Convergence* 9, 41. doi: 10.1186/s40580-022-00332-8

Park, H., Lee, H., Lee, M., Baek, C., Park, J. A., Jang, M., et al. (2023). Synthesis of isolated DNA aptamer and its application of AC-electrothermal flow-based rapid biosensor for the detection of dengue virus in a spiked sample. *Bioconjugate Chem.* 34, 1486–1497. doi: 10.1021/acs.bioconjchem.3c00249

Pathania, P., Sharma, A., Kumar, B., Rishi, P., and Raman Suri, C. (2017). Selective identification of specific aptamers for the detection of non-typhoidal salmonellosis in an apta-impedimetric sensing format. *Microchimica Acta* 184, 1499–1508. doi: 10.1007/s00604-017-2098-2

Pebdeni, A. B., Hosseini, M., and Ganjali, M. R. (2020). Fluorescent turn-on aptasensor of *Staphylococcus aureus* based on the FRET between green carbon quantum dot and gold nanoparticle. *Food Analytical Methods* 13, 2070–2079. doi: 10.1007/s12161-020-01821-4

Perschbacher, K., Smestad, J. A., Peters, J. P., Standiford, M. M., Denic, A., Wootla, B., et al. (2015). Quantitative PCR Analysis of DNA aptamer pharmacokinetics in mice. *Nucleic Acid Ther.* 25, 11–19. doi: 10.1089/nat.2014.0515

Petrišič, N., Kozorog, M., Aden, S., Podobnik, M., and Anderluh, G. (2021). The molecular mechanisms of listeriolysin O-induced lipid membrane damage. *Biochim. Biophys. Acta (BBA) - Biomembranes* 1863, 183604. doi: 10.1016/j.bbamem.2021.183604

Pfander, S., Fiammengo, R., Kirin, S. I., Metzler-Nolte, N., and Jäschke, A. (2007). Reversible site-specific tagging of enzymatically synthesized RNAs using aldehyde–hydrazine chemistry and protease-cleavable linkers. *Nucleic Acids Res.* 35, e25. doi: 10.1093/nar/gkl1110

Pistor, S., Chakraborty, T., Niebuhr, K., Domann, E., and Wehland, J. (1994). The ActA protein of *Listeria monocytogenes* acts as a nucleator inducing reorganization of the actin cytoskeleton. *EMBO J.* 13, 758–763. doi: 10.1002/j.1460-2075.1994.tb06318.x

Portnoy, D. A., Jacks, P. S., and Hinrichs, D. J. (1988). Role of hemolysin for the intracellular growth of Listeria monocytogenes. *J Exp Med.* 167 (4), 1459–1471. doi: 10.1084/jem.167.4.1459

Qi, X., Ye, Y., Wang, H., Zhao, B., Xu, L., Zhang, Y., et al. (2022). An ultrasensitive and dual-recognition SERS biosensor based on Fe3O4@Au-Teicoplanin and aptamer functionalized Au@Ag nanoparticles for detection of *Staphylococcus aureus*. *Talanta* 250, 123648. doi: 10.1016/j.talanta.2022.123648

Raddatz, M. L., Dolf, A., Endl, E., Knolle, P., Famulok, M., and Mayer, G. (2008). Enrichment of cell-targeting and population-specific aptamers by fluorescence-activated cell sorting. *Angewandte Chemie Int. Edition* 47, 5190–5193. doi: 10.1002/anie.200800216

Raffatellu, M., Wilson, R. P., Chessa, D., Andrews-Polymenis, H., Tran, Q. T., Lawhon, S., et al. (2005). SipA, SopA, SopB, SopD, and SopE2 Contribute to *Salmonella enterica serotype typhimurium* invasion of epithelial cells. *Infection Immun.* 73, 146–154. doi: 10.1128/IAI.73.1.146-154.2005

Rahbi, F. A., Salmi, I. A., Khamis, F., Balushi, Z. A., Pandak, N., Petersen, E., et al. (2023). Physicians' attitudes, knowledge, and practices regarding antibiotic prescriptions. *J. Global Antimicrobial Resistance* 32, 58–65. doi: 10.1016/j.jgar.2022.12.005

Raji, M. A., Suaifan, G., Shibl, A., Weber, K., Cialla-May, D., Popp, J., et al. (2021). Aptasensor for the detection of Methicillin resistant *Staphylococcus aureus* on contaminated surfaces. *Biosensors Bioelectronics* 176, 112910. doi: 10.1016/j.bios.2020.112910

Ramanathan, S., Gopinath, S. C. B., Ismail, Z. H., Md Arshad, M. K., and Poopalan, P. (2022). Aptasensing nucleocapsid protein on nanodiamond assembled gold interdigitated electrodes for impedimetric SARS-CoV-2 infectious disease assessment. *Biosensors Bioelectronics* 197, 113735. doi: 10.1016/j.bios.2021.113735

Ranadheera, C., Proulx, R., Chaiyakul, M., Jones, S., Grolla, A., Leung, A., et al. (2018). The interaction between the Nipah virus nucleocapsid protein and phosphoprotein regulates virus replication. *Sci. Rep.* 8 (1), 15994. doi: 10.1038/s41598-018-34484-7

Ranjbar, S., and Shahrokhian, S. (2018). Design and fabrication of an electrochemical aptasensor using Au nanoparticles/carbon nanoparticles/cellulose nanofibers nanocomposite for rapid and sensitive detection of Staphylococcus aureus. *Bioelectrochemistry* 123, 70–76. doi: 10.1016/j.bioelechem.2018.04.018

Rastogi, M., and Singh, S. K. (2020). Zika virus NS1 affects the junctional integrity of human brain microvascular endothelial cells. *Biochimie* 176, 52–61. doi: 10.1016/j.biochi.2020.06.011

Reich, P., Stoltenburg, R., Strehlitz, B., Frense, D., and Beckmann, D. (2017). Development of an impedimetric aptasensor for the detection of *Staphylococcus aureus*. *Int. J. Mol. Sci.* 18, 2484. doi: 10.3390/ijms18112484

Ren, J., Liang, G., Man, Y., Li, A., Jin, X., Liu, Q., et al. (2019). Aptamer-based fluorometric determination of *Salmonella typhimurium* using Fe3O4 magnetic separation and CdTe quantum dots. *PLoS One* 14, e0218325. doi: 10.1371/journal.pone.0218325

Reverdatto, S., Burz, D., and Shekhtman, A. (2015). Peptide aptamers: Development and applications. *Curr. Topics Medicinal Chem.* 15, 1082–1101. doi: 10.2174/1568026615666150413153143

RM, R., Maroli, N., J, A., Ponmalai, K., and K, K. (2020). Highly adaptable and sensitive FRET-based aptamer assay for the detection of Salmonella paratyphi A. *Spectrochimica Acta Part A: Mol. Biomolecular Spectrosc.* 243, 118662. doi: 10.1016/j.saa.2020.118662

Roberts, P. C., Lamb, R. A., and Compans, R. W. (1998). The M1 and M2 proteins of influenza A virus are important determinants in filamentous particle formation. *Virology* 240 (1), 127–137. doi: 10.1006/viro.1997.8916

Roushani, M., Sarabaegi, M., and Pourahmad, F. (2019). Impedimetric aptasensor for Pseudomonas aeruginosa by using a glassy carbon electrode modified with silver nanoparticles. *Microchimica Acta* 186, 725. doi: 10.1007/s00604-019-3858-y

Roxo, C., Kotkowiak, W., and Pasternak, A. (2019). G-Quadruplex-forming aptamers—characteristics, applications, and perspectives. *Molecules* 24, 3781. doi: 10.3390/molecules24203781

Sanjuán, R. (2012). From molecular genetics to phylodynamics: evolutionary relevance of mutation rates across viruses. *PLoS Pathog.* 8, e1002685. doi: 10.1371/journal.ppat.1002685

Saravanan, H., Subramani, T., Rajaramon, S., David, H., Sajeevan, A., Sujith, S., et al. (2023). Exploring nanocomposites for controlling infectious microorganisms: charting the path forward in antimicrobial strategies. *Front. Pharmacol.* 14. doi: 10.3389/fphar.2023.1282073

Schasfoort, R. B. M. (2017). "Introduction to surface plasmon resonance," in *handbook of surface plasmon resonance* (The Royal Society of Chemistry), 1–26. doi: 10.1039/9781788010283-00001

Schmitz, F. R. W., Cesca, K., Valério, A., de Oliveira, D., and Hotza, D. (2023). Colorimetric detection of *Pseudomonas aeruginosa* by aptamer-functionalized gold nanoparticles. *Appl. Microbiol. Biotechnol.* 107, 71–80. doi: 10.1007/s00253-022-12283-5

Shang, Z., Song, H., Shi, Y., Qi, J., and Gao, G. F. (2018). Crystal structure of the capsid protein from zika virus. *J. Mol. Biol.* 430, 948–962. doi: 10.1016/j.jmb.2018.02.006

Shatila, F., Yalçın, H. T., Özyurt, C., Evran, S., Çakır, B., Yaşa, İ., et al. (2020a). Single-stranded DNA (ssDNA) Aptamer targeting SipA protein inhibits Salmonella Enteritidis invasion of intestinal epithelial cells. *Int. J. Biol. Macromolecules* 148, 518–524. doi: 10.1016/j.ijbiomac.2020.01.132

Shatila, F., Yaşa, İ., and Yalçın, H. T. (2020b). Inhibition of Salmonella enteritidis biofilms by *Salmonella* invasion protein-targeting aptamer. *Biotechnol. Lett.* 42, 1963–1974. doi: 10.1007/s10529-020-02920-2

Shaw, M. L., Garciía-Sastre, A., Palese, P., and Basler, C. F. (2004). Nipah Virus V and W proteins have a common stat1-binding domain yet inhibit STAT1 activation from the cytoplasmic and nuclear compartments, respectively. *J. Virol.* 78, 5633–5641. doi: 10.1128/JVI.78.11.5633-5641.2004

Shraim, A. S., Abdel Majeed, B. A., Al-Binni, M. A., and Hunaiti, A. (2022). Therapeutic potential of aptamer–protein interactions. *ACS Pharmacol. Trans. Sci.* 5, 1211–1227. doi: 10.1021/acsptsci.2c00156

Siddiqui, M. A. A., and Keating, G. M. (2005). Pegaptanib. *Drugs* 65, 1571–1577. doi: 10.2165/00003495-200565110-00010

Singh, N. K., Ray, P., Carlin, A. F., Magallanes, C., Morgan, S. C., Laurent, L. C., et al. (2021). Hitting the diagnostic sweet spot: Point-of-care SARS-CoV-2 salivary antigen testing with an off-the-shelf glucometer. *Biosensors Bioelectronics* 180, 113111. doi: 10.1016/j.bios.2021.113111

Sohouli, E., Ghalkhani, M., Zargar, T., Joseph, Y., Rahimi-Nasrabadi, M., Ahmadi, F., et al. (2022). A new electrochemical aptasensor based on gold/nitrogen-doped carbon nano-onions for the detection of *Staphylococcus aureus*. *Electrochimica Acta* 403, 139633. doi: 10.1016/j.electacta.2021.139633

Sola, M., Menon, A. P., Moreno, B., Meraviglia-Crivelli, D., Soldevilla, M. M., Cartón-García, F., et al. (2020). Aptamers against live targets: is *in vivo* SELEX finally coming to the edge? *Mol. Ther. - Nucleic Acids* 21, 192–204. doi: 10.1016/j.omtn.2020.05.025

Somerville, J. E. Jr., Cassiano, L., and Darveau, R. P. (1999). *Escherichia coli* msbB Gene as a virulence factor and a therapeutic target. *Infection Immun.* 67 (12), 6583–6590. doi: 10.1128/IAI.67.12.6583-6590.1999

Sreejit, G., Ahmed, A., Parveen, N., Jha, V., Valluri, V. L., Ghosh, S., et al. (2014). The ESAT-6 Protein of *Mycobacterium tuberculosis* interacts with Beta-2-Microglobulin (β2M) affecting antigen presentation function of macrophage. *PLoS Pathog.* 10, e1004446. doi: 10.1371/journal.ppat.1004446

Srivastava, S., Abraham, P. R., and Mukhopadhyay, S. (2021). Aptamers: An emerging tool for diagnosis and therapeutics in tuberculosis. *Front. Cell. Infection Microbiol.* 11. doi: 10.3389/fcimb.2021.656421

Sudagidan, M., Yildiz, G., Onen, S., Al, R., Temiz, Ş.N., Yurt, M. N. Z., et al. (2021). Targeted mesoporous silica nanoparticles for improved inhibition of disinfectant resistant *Listeria monocytogenes* and lower environmental pollution. *J. Hazardous Materials* 418, 126364. doi: 10.1016/j.jhazmat.2021.126364

Suenaga, E., and Kumar, P. K. R. (2014). An aptamer that binds efficiently to the hemagglutinins of highly pathogenic avian influenza viruses (H5N1 and H7N7) and inhibits hemagglutinin–glycan interactions. *Acta Biomaterialia* 10, 1314–1323. doi: 10.1016/j.actbio.2013.12.034

Sun, B., Jia, L., Liang, B., Chen, Q., and Liu, D. (2018). Phylogeography, transmission, and viral proteins of Nipah Virus. *Virologica Sin.* 33, 385–393. doi: 10.1007/s12250-018-0050-1

Sun, J., Siroy, A., Lokareddy, R. K., Speer, A., Doornbos, K. S., Cingolani, G., et al. (2015). The tuberculosis necrotizing toxin kills macrophages by hydrolyzing NAD. *Nat. Struct. Mol. Biol.* 22, 672–678. doi: 10.1038/nsmb.3064

Sun, H., Zhu, X., Lu, P. Y., Rosato, R. R., Tan, W., and Zu, Y. (2014). Oligonucleotide aptamers: New tools for targeted cancer therapy. *Mol. Ther. - Nucleic Acids* 3, e182. doi: 10.1038/mtna.2014.32

Terlizzi, M. E., Gribaudo, G., and Maffei, M. E. (2017). UroPathogenic *Escherichia coli* (UPEC) infections: Virulence factors, bladder responses, antibiotic, and non-antibiotic antimicrobial strategies. *Front. Microbiol.* 8. doi: 10.3389/fmicb.2017.01566

Thevendran, R., Rogini, S., Leighton, G., Mutombwera, A., Shigdar, S., Tang, T.-H., et al. (2023). The diagnostic potential of RNA aptamers against the NS1 protein of dengue virus serotype 2. *Biology* 12, 722. doi: 10.3390/biology12050722

Thiviyanathan, V., Somasunderam, A. D., and Gorenstein, D. G. (2007). Combinatorial selection and delivery of thioaptamers. *Biochem. Soc. Trans.* 35, 50–52. doi: 10.1042/BST0350050

Tran, Q. T., Gomez, G., Khare, S., Lawhon, S. D., Raffatellu, M., Baöumler, A. J., et al. (2010). The *Salmonella enterica* Serotype typhi Vi capsular antigen is expressed after the bacterium enters the ileal mucosa. *Infection Immun.* 78, 527–535. doi: 10.1128/IAI.00972-09

Turgis, M., Khanh, D. V., Majid, J., Behnoush, M., and Monique, L. (2016). Synergistic antimicrobial effect of combined bacteriocins against food pathogens and spoilage bacteria. *Microb. Res. Inter.* 4 (1), 1–5.

Turner, J., and Torrelles, J. B. (2018). Mannose-capped lipoarabinomannan in Mycobacterium tuberculosis pathogenesis. *Pathog Dis.* 76 (4), fty026. doi: 10.1093/femspd/fty026

Turrell, L., Lyall, J. W., Tiley, L. S., Fodor, E., and Vreede, F. T. (2013). The role and assembly mechanism of nucleoprotein in influenza A virus ribonucleoprotein complexes. *Nat. Commun.* 4 (1), 1591. doi: 10.1038/ncomms2589

Ucak, S., Sudagidan, M., Borsa, B. A., Mansuroglu, B., and Ozalp, V. C. (2020). Inhibitory effects of aptamer targeted teicoplanin encapsulated PLGA nanoparticles for *Staphylococcus aureus* strains. *World J. Microbiol. Biotechnol.* 36 (5), 69. doi: 10.1007/s11274-020-02845-y

Uemachi, H., Kasahara, Y., Tanaka, K., Okuda, T., Yoneda, Y., and Obika, S. (2021). Hybrid-Type SELEX for the selection of artificial nucleic acid aptamers exhibiting cell internalization activity. *Pharmaceutics* 13, 888. doi: 10.3390/pharmaceutics13060888

Uniyal, A., Srivastava, G., Pal, A., Taya, S., and Muduli, A. (2023). Recent advances in optical biosensors for sensing applications: a review. *Plasmonics* 18, 735–750. doi: 10.1007/s11468-023-01803-2

Valente, A. P., and Moraes, A. H. (2019). Zika virus proteins at an atomic scale: how does structural biology help us to understand and develop vaccines and drugs against Zika virus infection? *J. Venomous Anim. Toxins Including Trop. Dis.* 25. doi: 10.1590/1678-9199-jvatitd-2019-0013

Verma, A. K., Noumani, A., Yadav, A. K., and Solanki, P. R. (2023). FRET Based Biosensor: Principle applications recent advances and challenges. *Diagnostics* 13, 1375. doi: 10.3390/diagnostics13081375

Vivekananda, J., Salgado, C., and Millenbaugh, N. J. (2014). DNA aptamers as a novel approach to neutralize *Staphylococcus aureus* α-toxin. *Biochem. Biophys. Res. Commun.* 444, 433–438. doi: 10.1016/j.bbrc.2014.01.076

Wain, J., House, D., Zafar, A., Baker, S., Nair, S., Kidgell, C., et al. (2005). Vi Antigen Expression in *Salmonella enterica* Serovar *typhi* Clinical Isolates from Pakistan. *J. Clin. Microbiol.* 43, 1158–1165. doi: 10.1128/JCM.43.3.1158-1165.2005

Wan, Q., Liu, X., and Zu, Y. (2021). Oligonucleotide aptamers for pathogen detection and infectious disease control. *Theranostics* 11, 9133–9161. doi: 10.7150/thno.61804

Wang, J. Y., and Koshland, D. E. Jr. (1978). Evidence for protein kinase activities in the prokaryote Salmonella typhimurium. *J. Biol. Chem.* 253 (21), 7605–7608.

Wang, L., Wang, R., Chen, F., Jiang, T., Wang, H., Slavik, M., et al. (2017a). QCM-based aptamer selection and detection of Salmonella typhimurium. *Food Chem.* 221, 776–782. doi: 10.1016/j.foodchem.2016.11.104

Wang, R., Wang, L., Callaway, Z. T., Lu, H., Huang, T. J., and Li, Y. (2017b). A nanowell-based QCM aptasensor for rapid and sensitive detection of avian influenza virus. *Sensors Actuators B: Chem* 240, 934–940. doi: 10.1038/nature13027

Weerathunge, P., Ramanathan, R., Torok, V. A., Hodgson, K., Xu, Y., Goodacre, R., et al. (2019). Ultrasensitive colorimetric detection of murine norovirus using nanozyme aptasensor. *Analytical Chem.* 91, 3270–3276. doi: 10.1021/acs.analchem.8b03300

Weis, M., and Maisner, A. (2015). Nipah virus fusion protein: Importance of the cytoplasmic tail for endosomal trafficking and bioactivity. *Eur. J. Cell Biol.* 94, 316–322. doi: 10.1016/j.ejcb.2015.05.005

Wei-Wen Hsiao, W., Sharma, N., Le, T.-N., Cheng, Y.-Y., Lee, C.-C., Vo, D.-T., et al. (2022). Fluorescent nanodiamond-based spin-enhanced lateral flow immunoassay for detection of SARS-CoV-2 nucleocapsid protein and spike protein from different variants. *Analytica Chimica Acta* 1230, 340389. doi: 10.1016/j.aca.2022.340389

Weng, X., and Neethirajan, S. (2017). Aptamer-based fluorometric determination of norovirus using a paper-based microfluidic device. *Microchimica Acta* 184, 4545–4552. doi: 10.1007/s00604-017-2467-x

Winter, S. E., Winter, M. G., Thiennimitr, P., Gerriets, V. A., Nuccio, S. P., Rüssmann, H., et al. (2009). The TviA auxiliary protein renders the *Salmonella enterica* serotype Typhi RcsB regulon responsive to changes in osmolarity. *Mol. Microbiol.* 74, 175–193. doi: 10.1111/j.1365-2958.2009.06859.x

Xi, Z., Gong, Q., Wang, C., and Zheng, B. (2018). Highly sensitive chemiluminescent aptasensor for detecting HBV infection based on rapid magnetic separation and double-functionalized gold nanoparticles. *Sci. Rep.* 8, 9444. doi: 10.1038/s41598-018-27792-5

Xie, X., Huang, W., Shen, G., Yu, H., and Wang, L. (2022). Selection and colorimetric application of ssDNA aptamers against metamitron based on magnetic bead-SELEX. *Analytical Methods* 14, 3021–3032. doi: 10.1039/D2AY00566B

Yang, J., and Bowser, M. T. (2013). Capillary Electrophoresis–SELEX selection of catalytic dna aptamers for a small-molecule porphyrin target. *Analytical Chem.* 85, 1525–1530. doi: 10.1021/ac302721j

Yang, M., Peng, Z., Ning, Y., Chen, Y., Zhou, Q., and Deng, L. (2013). Highly specific and cost-efficient detection of *salmonella paratyphi* A combining aptamers with single-walled carbon nanotubes. *Sensors* 13, 6865–6881. doi: 10.3390/s130506865

Ye, Y., Qi, X., Wang, H., Zhao, B., Xu, L., Zhang, Y., et al. (2022). A surface-enhanced Raman scattering aptasensor for *Escherichia coli* detection based on high-performance 3D substrate and hot spot effect. *Analytica Chimica Acta* 1221, 340141. doi: 10.1016/j.aca.2022.340141

Yeom, J. H., Lee, B., Kim, D., Lee, J. K., Kim, S., Bae, J., et al. (2016). Gold nanoparticle-DNA aptamer conjugate-assisted delivery of antimicrobial peptide effectively eliminates intracellular *Salmonella enterica* serovar *typhimurium*. *Biomaterials* 104, 43–51. doi: 10.1016/j.biomaterials.2016.07.009

Yu, X., Chen, F., Wang, R., and Li, Y. (2018). Whole-bacterium SELEX of DNA aptamers for rapid detection of *E.coli* O157:H7 using a QCM sensor. *J. Biotechnol.* 266, 39–49. doi: 10.1016/j.jbiotec.2017.12.011

Yuan, B., Peng, Q., Cheng, J., Wang, M., Zhong, J., Qi, J., et al. (2022). Structure of the Ebola virus polymerase complex. *Nature* 610, 394–401. doi: 10.1038/s41586-022-05271-2

Yüce, M., Ullah, N., and Budak, H. (2015). Trends in aptamer selection methods and applications. *Analyst* 140, 5379–5399. doi: 10.1039/C5AN00954E

Zavyalova, E., Samoylenkova, N., Revishchin, A., Turashev, A., Gordeychuk, I., Golovin, A., et al. (2017). The evaluation of pharmacodynamics and pharmacokinetics of anti-thrombin DNA aptamer RA-36. *Front. Pharmacol.* 8. doi: 10.3389/fphar.2017.00922

Zhan, Z., Li, H., Liu, J., Xie, G., Xiao, F., Wu, X., et al. (2020). A competitive enzyme linked aptasensor with rolling circle amplification (ELARCA) assay for colorimetric detection of *Listeria monocytogenes*. *Food Control* 107, 106806. doi: 10.1016/j.foodcont.2019.106806

Zhang, A. P. P., Abelson, D. M., Bornholdt, Z. A., Liu, T., Woods, J. V. L., and Saphire, E. O. (2012). The ebolavirus VP24 interferon antagonist. *Virulence* 3, 440–445. doi: 10.4161/viru.21302

Zhang, X., Khan, I. M., Ji, H., Wang, Z., Tian, H., Cao, W., et al. (2020). A label-free fluorescent aptasensor for detection of staphylococcal enterotoxin a based on aptamer-functionalized silver nanoclusters. *Polymers* 12, 152. doi: 10.3390/polym12010152

Zhang, L. F., Lepenies, B., Nakamae, S., Young, B. M., Santos, R. L., Raffatellu, M., et al. (2022). The Vi Capsular polysaccharide of *Salmonella typhi* promotes macrophage phagocytosis by binding the human C-type lectin DC-SIGN. *MBio* 13 (6). doi: 10.1128/mbio.02733-22

Zhang, T., Lu, Y., Deng, S., and Deng, R. (2021). "Aptamers for the diagnosis of infectious diseases," in *Aptamers for Medical Applications* (Springer, Singapore), 207–238. doi: 10.1007/978-981-33-4838-7_8

Zhang, Y., Zhang, Y., Yang, Y., Wang, L., and Weng, L. (2013). Identification of a Pseudomonas sp. that inhibits rhl system of quorum sensing. *Indian J. Microbiol.* 53, 28–35. doi: 10.1007/s12088-012-0340-5

Zhao, Q., Du, P., Wang, X., Huang, M., Sun, L.-D., Wang, T., et al. (2021). Upconversion fluorescence resonance energy transfer aptasensors for H5N1 influenza virus detection. *ACS Omega* 6, 15236–15245. doi: 10.1021/acsomega.1c01491

Zhao, M., Li, W., Liu, K., Li, H., and Lan, X. (2019). C4-HSL aptamers for blocking qurom sensing and inhibiting biofilm formation in *Pseudomonas aeruginosa* and its structure prediction and analysis. *PLoS One* 14, e0212041. doi: 10.1371/journal.pone.0212041

Zheng, J., Tang, X., Wu, R., Yan, Q., Tang, H., Luo, J., et al. (2015). Identification and characteristics of aptamers against inactivated *Vibrio alginolyticus*. *LWT - Food Sci. Technol.* 64, 1138–1142. doi: 10.1016/j.lwt.2015.07.021

Zhou, S., Lu, C., Li, Y., Xue, L., Zhao, C., Tian, G., et al. (2020). Gold nanobones enhanced ultrasensitive surface-enhanced raman scattering aptasensor for detecting *Escherichia coli* o157:h7. *ACS Sensors* 5, 588–596. doi: 10.1021/acssensors.9b02600

Zhou, J., and Rossi, J. (2017). Aptamers as targeted therapeutics: current potential and challenges. *Nat. Rev. Drug Discovery* 16, 181–202. doi: 10.1038/nrd.2016.199

Zhou, Y., Xiong, H., Chen, R., Wan, L., Kong, Y., Rao, J., et al. (2021). Aptamer detection of *Mycobaterium tuberculosis* mannose-capped lipoarabinomannan in lesion tissues for tuberculosis diagnosis. *Front. Cell. Infection Microbiol.* 11, 634915. doi: 10.3389/fcimb.2021.634915

Zhu, L., Gao, T., Huang, Y., Jin, J., Wang, D., Zhang, L., et al. (2022). Ebola virus VP35 hijacks the PKA-CREB1 pathway for replication and pathogenesis by AKIP1 association. *Nat. Commun.* 13 (1), 2256. doi: 10.1038/s41467-022-29948-4

Zhu, C., Li, L., Yang, G., and Qu, F. (2021). Investigating the influences of random-region length on aptamer selection efficiency based on capillary electrophoresis–SELEX and high-throughput sequencing. *Analytical Chem.* 93, 17030–17035. doi: 10.1021/acs.analchem.1c03661

Zhu, S., Watanabe, M., Kirkpatrick, E., Murray, A. B., Sok, R., and Karst, S. M. (2016). Regulation of norovirus virulence by the VP1 protruding domain correlates with B Cell infection efficiency. *J. Virol.* 90, 2858–2867. doi: 10.1128/jvi.02880-15

Zou, Y., Duan, N., Wu, S., Shen, M., and & Wang, Z. (2018). Selection, identification, and binding mechanism studies of an ssdna aptamer targeted to different stages of *E. coli* O157:H7. *J. Agric. Food Chem.* 66, 5677–5682. doi: 10.1021/acs.jafc.8b01006

Zou, J., Huang, X., Wu, L., Chen, G., Dong, J., Cui, X., et al. (2015). Selection of intracellularly functional RNA mimics of green fluorescent protein using fluorescence-activated cell sorting. *J. Mol. Evol.* 81, 172–178. doi: 10.1007/s00239-015-9718-4

Zou, X., Wu, J., Gu, J., Shen, L., and Mao, L. (2019). Application of aptamers in virus detection and antiviral therapy. *Front. Microbiol.* 10, 1462. doi: 10.3389/fmicb.2019.01462

Zou, Z., Younas, T., Dumsday, G., Haritos, V. S., and He, L. (2023). Rapid production of multimeric RNA aptamers stabilized by a designed pseudo-circular structure in *E. coli*. *Biotechnol. J.* 18 (3). doi: 10.1002/biot.202200390

frontiers | Frontiers in Cellular and Infection Microbiology

TYPE Original Research
PUBLISHED 17 October 2024
DOI 10.3389/fcimb.2024.1464411

OPEN ACCESS

EDITED BY
Stefano Stracquadanio,
University of Catania, Italy

REVIEWED BY
William R. Schwan,
University of Wisconsin–La Crosse, United States
Humberto Barrios Camacho,
National Institute of Public Health, Mexico

*CORRESPONDENCE
Yi-Le Wu
wuyilebank@163.com
Wei Huang
whuang_sz@163.com

†These authors have contributed equally to this work

RECEIVED 14 July 2024
ACCEPTED 25 September 2024
PUBLISHED 17 October 2024

CITATION
Jiang Y-L, Lyu Y-Y, Liu L-L, Li Z-P, Liu D, Tai J-H, Hu X-Q, Zhang W-H, Chu W-W, Zhao X, Huang W and Wu Y-L (2024) Carbapenem-resistant *Klebsiella oxytoca* transmission linked to preoperative shaving in emergency neurosurgery, tracked by rapid detection via chromogenic medium and whole genome sequencing.
Front. Cell. Infect. Microbiol. 14:1464411.
doi: 10.3389/fcimb.2024.1464411

Carbapenem-resistant *Klebsiella oxytoca* transmission linked to preoperative shaving in emergency neurosurgery, tracked by rapid detection via chromogenic medium and whole genome sequencing

Yun-Lan Jiang[1†], Yi-Yu Lyu[2†], Li-Li Liu[1], Zhi-Ping Li[1], Dan Liu[1], Jie-Hao Tai[2], Xiao-Qian Hu[3], Wen-Hui Zhang[4], Wen-Wen Chu[2], Xue Zhao[4], Wei Huang[5,6*] and Yi-Le Wu[3*]

[1]Department of Hospital Infection Prevention and Control, Anqing First People's Hospital of Anhui Medical University, Anqing, Anhui, China, [2]Department of Clinical Laboratory, The Second Affiliated Hospital of Anhui Medical University, Hefei, Anhui, China, [3]Department of Hospital Infection Prevention and Control, The Second Affiliated Hospital of Anhui Medical University, Hefei, Anhui, China, [4]The Fourth Affiliated Hospital of Anhui Medical University, Hefei, Anhui, China, [5]Department of Laboratory Medicine, Shenzhen People's Hospital, The Second Clinical Medical College, Jinan University, Shenzhen, Guangdong, China, [6]The First Affiliated Hospital, Southern University of Science and Technology, Shenzhen, Guangdong, China

Objectives: This study describes the detection and tracking of emergency neurosurgical cross-transmission infections with carbapenem-resistant *Klebsiella oxytoca* (CRKO).

Methods: We conducted an epidemiological investigation and a rapid screening of 66 surveillance samples using the chromogenic selective medium. Two CRKO isolates from infected patients and three from the preoperative shaving razors had similar resistance profiles identified by the clinical laboratory.

Results: The whole genome sequencing (WGS) results identified all isolates as *Klebsiella michiganensis* (a species in the *K. oxytoca* complex) with sequence type 29 (ST29) and carrying resistance genes bla_{KPC-2} and bla_{OXY-5}, as well as IncF plasmids. The pairwise average nucleotide identity values of 5 isolates ranged from 99.993% to 99.999%. Moreover, these isolates displayed a maximum genetic difference of 3 among 5,229 targets in the core genome multilocus sequence typing scheme, and the razors were confirmed as the contamination source. After the implementation of controls and standardized shaving procedures, no new CRKO infections occurred.

Conclusion: Contaminated razors can be sources of neurosurgical site infections with CRKO, and standard shaving procedures need to be established.

Chromogenic selective medium can help rapidly identify targeted pathogens, and WGS technologies are effective mean in tracking the transmission source in an epidemic or outbreak investigation. Our findings increase the understanding of microbial transmission in surgery to improve patient care quality.

KEYWORDS

surgery, infections, *Klebsiella oxytoca*, carbapenems, whole genome sequencing

1 Introduction

Surgical site infections (SSIs), the most prevalent healthcare-associated infections, occur in approximately 0.5% to 3% of surgery patients (Seidelman et al., 2023). Post-neurosurgical infections are a common and very harmful complication requiring re-operation, prolonging hospital stay lengths, and increasing disability and mortality rates (Li et al., 2023). Infections with antibiotic-resistant bacteria after neurosurgery have become an important treatment challenge due to the low blood-brain barrier permeation rate of most antibiotics (Li et al., 2023). Carbapenems are a potent class of broad-spectrum antibiotics with strong antibacterial activity and are considered "last-line" antibiotics (Tompkins and van Duin, 2021). Carbapenem-resistant organisms have emerged and spread worldwide (Nordmann et al., 2011). The World Health Organization (WHO) has classified these organisms as an urgent public health threat (Wyres and Holt, 2022). Carbapenem-resistant organisms are usually multidrug-resistant, extensively drug resistant, and even pandrug-resistant bacteria (Li et al., 2023). The growing prevalence and the considerable morbidity and mortality of carbapenem-resistant organisms have attracted increasing attention in neurosurgery (Li et al., 2023).

Klebsiella species often cause respiratory, urinary tract, and wound infections, and they are increasingly recognized as pathogens of emerging nosocomial infections and outbreaks, following *Klebsiella pneumoniae* (Guzmán-Puche et al., 2021; Neog et al., 2021). *K. oxytoca* has been associated with neurosurgical procedures (Tang and Chen, 1995). Recently, with the emergence of bacterial resistance to carbapenems, carbapenem-resistant *K. oxytoca* (CRKO) has been identified as a species associated with neurosurgical procedures (Guanghui et al., 2020); however, transmission routes of CRKO in neurosurgery have rarely been reported.

Whole genome sequencing (WGS) technologies provide rich data and capture numerous features of isolates; data helpful for identifying resistance and virulence genes, mobilizable plasmids, and evolutionary information, as well as for epidemiological tracking and pathogen surveillance (Mustafa, 2024). This study investigated neurosurgical cross-transmission infections with CRKO by applying rapid chromogenic selective medium and WGS technologies to track the source of cross-transmission and improve surgical patient care.

2 Materials and methods

2.1 Setting and epidemiological investigation

This investigation was conducted in a tertiary teaching hospital with 1,460 beds in Anqing (Anhui Province of China). Two patients with SSIs were reported in the neurosurgical intensive care unit (ICU) on October 8, 2023 after emergency neurosurgery. Two CRKO isolates with similar resistance profiles were isolated from the neurosurgical sites of these two infected patients, and an cross-transmission was suspected. We investigated the transmission and conducted an active surveillance to detect the source of infections and control the spread. The Ethical Committee of The Second Affiliated Hospital of Anhui Medical University approved the study protocol (YX2023-102).

2.2 Active surveillance cultures and microbiological methods

According to information from epidemiological investigation and interviews of medical staff in the operating room and neurosurgical ICU, we collected active surveillance samples from the potential related patients, medical staff (healthcare workers, shaver, cleaners), neurosurgery disinfectants, shared environmental and device surfaces (hanging towers, bedrails, infusion pumps, cardiovascular monitors, etc.), and equipment for preoperative shaving (such as razors and shampoo) in the operating room and neurosurgical ICU involved. We inoculated CHROMagar mSuperCARBA (CHROMagar™, France) medium, a chromogenic selective medium with 95.6% to 96.5% sensitivity to detect carbapenemase producers, with surveillance samples to rapidly screen for carbapenemase-producing organisms (Alizadeh et al., 2018). After 24 h of culture at 35°C ± 2°C, the blue colonies growing on the selective agar

suggested the potential presence of CRKO. Then the suspected isolates were further identified via matrix-assisted laser desorption/ionization time-of-flight mass spectrometry (MALDI-TOF MS, Germany). Antimicrobial susceptibility was tested using the VITEK2 drug sensitivity analyzer (bioMérieux, Marcy L'Étoile, France), and *K. pneumoniae* ATCC BAA-1705 and *Escherichia coli* ATCC 25922 as quality control strains. Testing results were interpreted referring to the performance standards of the Clinical and Laboratory Standards Institute (CLSI) guidelines (Wayne, 2019).

2.3 Whole genome sequencing and genome-based analysis

WGS was performed for detected CRKO isolates from patients with SSIs and from surveillance samples. The concentration and quality of genomic DNA of these isolates extracted by the cetyltrimethylammonium bromide (CTAB) method were determined using a Qubit fluorometer (Invitrogen, USA) and a NanoDrop spectrophotometer (Thermo Scientific, USA). Sequencing libraries were generated using the TruSeq DNA Sample Preparation Kit (Illumina, USA) and the Template Prep Kit (Pacific Biosciences, USA). WGS was ran on an Illumina Novaseq platform at Personal Biotechnology Company (Shanghai, China). After using AdapterRemoval and SOAPec to remove adapter sequences and filter data (Lindgreen, 2012; Luo et al., 2012), the reads were assembled by the SPAdes and A5-miseq for constructing scaffolds and contigs (Bankevich et al., 2012; Coil et al., 2015). Finally, the genome sequences were obtained after correction using the Pilon software (Walker et al., 2014). Species was identified according to the PubMLST website (https://pubmlst.org/). Multilocus sequence typing (MLST) was performed via the MLST 2.0 at the Center for Genomic Epidemiology (https://cge.food.dtu.dk/services/MLST/). Resistance genes were determined using ResFinder (http://genepi.food.dtu.dk/resfinder). Plasmids were identified with PlasmidFinder (https://cge.food.dtu.dk/services/PlasmidFinder/). Virulence factors were determined in the virulence factor database (http://www.mgc.ac.cn/cgi-bin/VFs/v5/main.cgi). Pair-wise average nucleotide identity (ANI) values were calculated using the orthologous average nucleotide identity tool (OAT), using the proposed cut-off value of 95.0–96.0% for species demarcation (Lee et al., 2016). In addition, SeqSphere+ version 10.0 (Ridom, Münster, Germany) (https://www.ridom.de/news/) and the publicly available core genome MLST (cgMLST) scheme for *K. oxytoca* were used to calculate the minimum spanning tree (MST). A *Klebsiella michiganensis* isolate "Control", which was isolated from a patient in the ICU of the same hospital on October 21, 2023, was used as the reference strain in the cgMLST analysis. Isolates with less than 9 allelic differences from 5,229 targets of the cgMLST scheme were defined as highly related (Dabernig-Heinz et al., 2024).

3 Results

3.1 Transmission investigation

Surveillance data indicated that none of the 36 patients who underwent neurosurgery in August 2023 developed SSIs. However, two of 23 patients (8.7%) undergoing neurosurgery in the neurosurgical ICU developed SSIs due to CRKO in September 2023. The two CRKO isolates with similar resistance profiles were isolated from cerebrospinal fluid and wound effusion in patients who had undergone emergency neurosurgery on September 27, 2023. Detailed characteristics of the two patients are presented in Table 1.

We collected 66 samples through active surveillance and detected 10 isolates (Table 2). Among them, three CRKO isolates were obtained from a preoperative electric shaving razor, its charging cable, and an unused razor head with an incomplete packaging. The traditional preoperative shaving procedure in the hospital involved using a unique electric razor head for each patient, and disinfecting the handle of the electric razor before each use. Besides, any unused razor heads and disinfected handles were stored together. We discovered that the two patients with SSIs both had undergone preoperative shaving with these electric razors. Therefore, we suspected contaminated razors during preoperative shaving procedure as the source of transmission.

TABLE 1 Epidemiological and clinical characteristics of 5 Carbapenem-resistant *Klebsiella oxytoca* (*CRKO*) isolates from patients and razors.

No. of isolates	Sample source	Gender	Age	Clinical diagnosis	Admission /operation date	Invasive procedure	Sample date	Sequence type
P1	Patient1 (cerebrospinal fluid)	Male	75 y	Closed encephalon injury	27/09/2023	Ventriculostomy	04/10/2023	ST 29
P2	Patient2 (wound effusion)	Male	69 y	Ruptured cerebral aneurysm	27/09/2023	Intracranial aneurysm surgery	04/10/2023	ST 29
R1	An electric razor	–	–	–	–	–	08/10/2023	ST 29
R2	A charging cable of the electric razor	–	–	–	–	–	08/10/2023	ST 29
R3	An unused razor head [a]	–	–	–	–	–	08/10/2023	ST 29

[a]An unused razor head with incomplete packaging.

TABLE 2 Results of environment, healthcare worker, and patient sampling during this transmission investigation.

Sampling site	Sampling number	Culture positive (%)	Bacterial species
Healthcare workers (medical personnel, shavers, cleaners)			
Throat and rectal swabs	18	0 (0.0)	None
Hands	8	0 (0.0)	None
Telephone and watch of shaver	2	2 (100.0)	1 *Acinetobacter baumannii*, 1 *Klebsiella pneumoniae*
Patients and possible epidemiological link			
Rectal swabs	7	2 (28.6)	1 *Klebsiella pneumoniae*, 1 *Escherichia coli*
Dress for family visits	2	0 (0.0)	None
Environment and equipment			
Hand hygiene facilities in the nurse station	2	0 (0.0)	None
Disinfectant in the operating room	1	0 (0.0)	None
Instruments of bed surroundings (Infusion pumps, cardiovascular monitors, etc.)	7	2 (28.6)	1 *Acinetobacter baumannii*, 1 *Klebsiella pneumoniae*
Noninstruments of bed surroundings (hanging tower, bedrails)	2	0 (0.0)	None
Tools for shaving			
Electric razors	9	4 (44.4)	3 carbapenem-*resistant Klebsiella oxytoca*, 1 *Acinetobacter baumannii*
A container for razors, dress for shaver, and packaging of shampoo	8	0 (0.0)	None
Total	n=66	10 (15.2)	

3.2 Implementation of control measures

Upon confirmation of CRKO infections, the two patients were immediately isolated and treated with antibiotic therapy. While investigating the transmission, additional infection control procedures were strengthened including hand hygiene, cleaning, disinfection, sterilization, surveillance cultures, and re-education of healthcare staff. Following the detection of CRKO isolates solely on the razors, when necessary, trained nurses were instructed to use disposable clippers for preoperative shaving. These cut hair close to the skin, leaving a short stubble without touching the skin. Moreover, the department of hospital infection prevention and control regularly supervised standardized preparation procedures. Finally, after the implementation of these control measures, no other patients developed SSIs with CRKO. The two infected patients were successfully treated and discharged.

3.3 Analysis of antibiotic susceptibility, resistance and virulence genes, plasmids, and genetic relatedness

Two CRKO isolates from infected patients and three from razors had consistent resistance patterns based on the antibiotic susceptibility testing results identified by the clinical laboratory. All the isolates were resistant to ticarcillin/clavulanic acid, piperacillin/tazobactam, aztreonam, imipenem, and meropenem (Table 3). WGS results identified these isolates as *K. michiganensis* (a species in the *K. oxytoca* complex) with sequence type 29 (ST29). All isolates carried two resistance genes (bla_{KPC-2} and bla_{OXY-5}), as well as IncF plasmids (IncFIB(K) and IncFII(K)). Two isolates carried 67 virulence genes, and three isolates carried 66 virulence genes but lacked *stbA* (Table 4). The pairwise ANI values among the genomes of the 5 isolates ranged from 99.993% to 99.999% (Figure 1). Besides, the minimum spanning tree displayed a maximum difference of 3 among 5,229 targets in the core genome scheme between 5 isolates, whereas these 5 isolates had a significant allele difference (more than 92) to the reference strain "Control" (Figure 2), revealing the close relatedness between the isolates from patients and razors.

4 Discussion

Despite great advances in neurosurgical technology, SSIs after neurosurgery remain a common problem (Velnar et al., 2023). The incidence of SSIs post-craniotomy ranges between 5.1% and 6.2% (He et al., 2024; Lee et al., 2024). Post-craniotomy SSIs can significantly impact patients recovery and lead to increased morbidity, mortality, hospital stay lengths, pain, and costs, and require re-operation (Velnar et al., 2023). Cerebrospinal fluid leaks, infratentorial surgery, emergency surgery, re-operation, and other factors have been associated with post-craniotomy SSIs (Magni et al., 2023). SSIs can be cause by bacteria from the patients themselves or from medical staff, equipment, or the environment entering surgical incision sites (Tanner and Melen, 2021). One previous study has reported a carbapenemase-producing *K. pneumonia* outbreak caused by a barber's contaminated shaving razor (Dai et al., 2014). Despite *K. oxytoca* being the 2nd most clinically prevalent *Klebsiella* species, there is limited information about it, especially about the carbapenem-resistant species and its infectivity and epidemiology in neurosurgery (Neog et al., 2021). According to data from the worldwide bacterial collection of SENTRY program, the resistance rate of *K. oxytoca* to carbapenems is 1.8% with an alarming increasing rate (Yang et al., 2022). *K. oxytoca* is known to cause healthcare associated infections outbreaks (Yang et al., 2022). In this study, the CRKO isolates from infected patients and the razors shared the same resistance profiles, and had pairwise ANI values higher than

TABLE 3 Antimicrobial resistance phenotypes, resistance genes, and plasmids of 5 CRKO isolates from infected patients and razors.

Sample source	Antimicrobial susceptibility															Resistance gene		Plasmid	
	TIM	TZP	ATM	IMP	MEM	AMK	CAZ	CFP/SU	FEP	TOB	CIP	LEV	DO	MH	TGC	CT	SXT	KPC-2	OXY-5	IncFIB(K)	IncFII(K)
P1	R	R	R	R	R	S	S	S	S	S	I	I	S	S	S	S	S	+	+	+	+
P2	R	R	R	R	R	S	S	S	S	S	I	I	S	S	S	S	S	+	+	+	+
R1	R	R	R	R	R	S	S	S	S	S	I	I	S	S	S	S	S	+	+	+	+
R2	R	R	R	R	R	S	S	S	S	S	I	I	S	S	S	S	S	+	+	+	+
R3	R	R	R	R	R	S	S	S	S	S	I	I	S	S	S	S	S	+	+	+	+

P1, Patient 1; P2, Patient 2; R1, Razor1; R2, Razor 2; R3, Razor 3.

TIM, ticarcillin/clavulanic acid; TZP, piperacillin/tazobactam; ATM, aztreonam; IMP, imipenem; MEM, meropenem; AMK, amikacin; CAZ, ceftazidime; CFP/SU, cefoperazone/sulbactam; FEP, cefepime; TOB, tobramycin; CIP, ciprofloxacin; LEV, levofloxacin; DO, doxycycline; MH, minocycline; TGC, tigecycline; CT, colistin; SXT, trimethoprim/sulfamethoxazole; R, resistant; S, susceptible; I, intermediate.

99.993% and a maximum difference of 3 among 5229 targets in the core genome scheme, indicating strong relatedness. A cgMLST analysis may enhance the MLST analysis by assigning allele numbers correlated to the exact genetic sequence of thousands of coding regions throughout the genome, providing a very high resolution and facilitating transmission and outbreak investigations (Dabernig-Heinz et al., 2024). Our findings confirm that contaminated razors can be the sources of CRKO transmission. Thus, inadequate preoperative shaving procedures can cause neurosurgical site infections. Moreover, *K. oxytoca* seems well adapted to healthcare environments (Yang et al., 2022), and implementation of sanitation protocols, equipment handling, aseptic technique, and antibiotic stewardship strategies should be emphasized, especially in preparation of surgical procedures.

Although the benefits of hair removal for preventing SSIs remain controversial in the literature, preoperative shaving at the intended surgical incision site is a traditional practice that reduces the interference of hair at the surgical site and incision suture, promoting cleanliness and facilitating dressing applications (Kose et al., 2016; Tanner and Melen, 2021; Liu et al., 2022). Preoperative hair removal may result in skin trauma, which in turn contributes to SSIs (Tanner and Melen, 2021). A meta-analysis has indicated that, when compared to the SSIs risk in patients without hair removal, the risk increases in patients who undergo hair removal using a razor (RR: 1.82) (Tanner and Melen, 2021). WHO Guidelines recommend that hair should not be routinely removed in patients undergoing surgical procedures, and that it should be removed with a clipper if absolutely necessary (World Health Organization).

Numerous advanced techniques have been applied for the prevention and control of infections and for promoting patient care. Timely evaluation of transmission sources is critical for implementing intervention strategies to contain the spread. In this study, we successfully applied rapid chromogenic screening and WGS technologies to investigate and control the transmission, and these practicabilities were well confirmed. We used chromogenic-based selective medium to screen for carbapenemase-producing organisms from active surveillance samples, and rapidly detected three suspected CRKO isolates on the razors (within 24 hours) to help timely implementation of precise control measures. The range of available chromogenic culture medium has experienced a rapid expansion. Chromogenic medium are based on synthetic chromogenic enzyme substrates to target specific species (Perry, 2017). Compared with traditional culture medium, chromogenic medium often save costs by reducing labor time and reagents use, while contributing to rapid pathogens identifications (Perry, 2017).

WGS technologies have contributed to the diagnosis, treatment, surveillance, and epidemiological investigations of bacterial infections (Mustafa, 2024). Utilizing WGS and genome-based analysis, these *K. oxytoca* isolates were identified as the species of *K. michiganensis* with ST29. *K. oxytoca* is described as a complex of nine species including *K. michiganensis* (Yang et al., 2022). *K. michiganensis* was first recovered from a toothbrush holder in 2012 (Saha et al., 2013). However, the clinical significance including the prevalence, disease spectrum, and severity of each species in the *K. oxytoca* complex remains largely unknown (Yang et al., 2022). By applying a genome-based analysis, we achieved the precise species identification,

10.3389/fcimb.2024.1464411

TABLE 4 Virulence factors of 5 CRKO isolates from infected patients and razors.

Virulence factors class	Related genes	P1	P2	R1	R2	R3
Adherence	*mrkABCDFHIJ*	+	+	+	+	+
	fimABCDEFGHIK	+	+	+	+	+
Antiphagocytosis	*Capsule*	+	+	+	+	+
Efflux pump	*acrAB*	+	+	+	+	+
Iron uptake	*iutA*	+	+	+	+	+
	entABCDEFS	+	+	+	+	+
	fepABCDG	+	+	+	+	+
	fes	+	+	+	+	+
	iroE	+	+	+	+	+
Regulation	*rcsAB*	+	+	+	+	+
Secretion system	*clpV/tssH*	+	+	+	+	+
	hcp/tssD	+	+	+	+	+
	impA/tssA	+	+	+	+	+
	sciN/tssJ	+	+	+	+	+
	vipA/tssB	+	+	+	+	+
	vipB/tssC	+	+	+	+	+
	clpV	+	+	+	+	+
	dotU	+	+	+	+	+
	icmF	+	+	+	+	+
	impAFGHJ	+	+	+	+	+
	ompA	+	+	+	+	+
	sciN	+	+	+	+	+
	vgrG	+	+	+	+	+
	SCI-I T6SS	+	+	+	+	+
Serum resistance	*LPS rfb locus*	+	+	+	+	+
Biofilm formation	*adeG*	+	+	+	+	+
Cell surface components	*sugC*	+	+	+	+	+
Endotoxin	*lpxC*	+	+	+	+	+
Enzyme	*eno*	+	+	+	+	+
Fimbrial adherence determinants	*stbA*	–	–	+	–	+
	stbCD	+	+	+	+	+
	stiB	+	+	+	+	+
Magnesium uptake	*mgtB*	+	+	+	+	+
Protease	*pla*	+	+	+	+	+

P1, Patient 1; P2, Patient 2; R1, Razor 1; R2, Razor 2; R3, Razor 3.

providing comprehensive information on the species in the *K. oxytoca* complex as well as on patient treatment, surveillance, and infection control interventions (Yang et al., 2022). We found that the isolates carried bla_{KPC-2} and bla_{OXY-5} resistance genes and IncF plasmids. In addition to the intrinsic bla_{OXY} of *K. oxytoca*, a number of genes encoding β-lactamases have been reported, and bla_{KPC-2} is the most common carbapenemase gene and is often carried on IncF plasmids (Yang et al., 2022). The horizontal transmission of bla_{KPC-2}-carrying plasmids across different genera of bacteria has been demonstrated (Schweizer et al., 2019). We also identified virulence factors such as *mrk*, *fim*, *iutA*, and *iroE* genes in these isolates. The *mrk* gene cluster can encode mannose-resistant *Klebsiella*-like

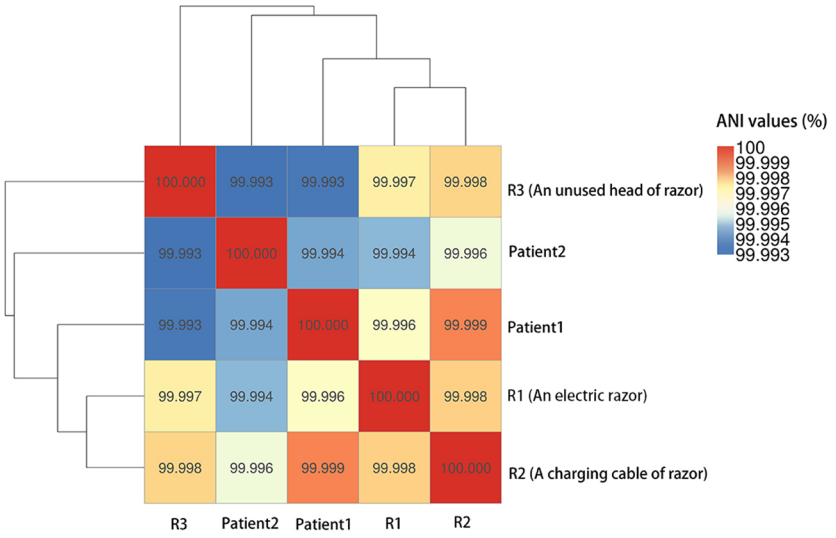

FIGURE 1
Pairwise average nucleotide identities (ANI) values among the genomes of the 5 CRKO isolates from infected patients and razors.

hemagglutinins, allowing *Klebsiella* spp. to attach to surfaces and form biofilms (Yang et al., 2022). Particularly, the *iut*A gene seems to be important for hypervirulence (Lee et al., 2017). Based on our findings, we believe that *K. oxytoca* can become a potential major threat to public health due to their ability to acquire resistance to antimicrobials and carry a large number of virulence genes (Yang et al., 2022). Supplemented with epidemiological data, we further validated cgMLST as a useful tool for investigating the source and route of pathogen transmission. cgMLST had been applied to guide interventions, determine durations, and evaluate effects of interventions strategies for other pathogens (Kjær Hansen et al., 2021; Knudsen et al., 2022). Also based on our results, WGS technologies are effective to precisely track transmission sources and provide abundant information on the complete genome of pathogens in an epidemic or outbreak investigation.

Increase in the numbers of multidrug-resistant bacteria, particularly of carbapenem-resistant organisms, have proved fatal to patients undergoing neurosurgery (Li et al., 2023). The surgical team and any professionals directly providing surgical care have an important responsibility to prevent SSIs (World Health Organization; Tvedt et al., 2017). The safety of surgical patients is of the utmost importance, and a list of evidence-based best practices including hand hygiene, preoperative skin antisepsis, antimicrobial irrigation, and others are routinely employed to promote a safe outcomes for surgical patients (Bashaw and Keister, 2019). Evidence-based information is needed to clarify the risk factors of SSIs and improve the quality of care (World Health Organization, 2018). With this study based on WGS, we demonstrated that contaminated razors can lead to SSIs with carbapenem-resistant organisms; therefore, a standard preoperative shaving procedure should be established and executed. Moreover, updated techniques such as chromogenic selective medium and WGS technology can be applied for prevention and control of SSIs and promoting surgical patient care.

We are aware of our study's limitations. First, although several virulence genes such as the hypervirulence *iut*A were detected via WGS, the virulence phenotypes were not tested. Second, although we confirmed that razors can transmit pathogens, including carbapenem-resistant organisms, and lead to SSIs, the survival time of these pathogens in the environment such as in razors

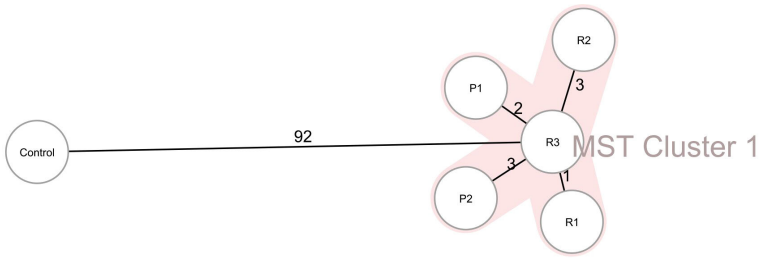

FIGURE 2
Ridom SeqSphere+ minimum spanning tree (MST) for 5 CRKO isolates from infected patients and razors based on 5,229 target genes (2536 cgMLST and 2693 accessory) with missing values are an own category. MST Cluster distance threshold: 9. P1, Patient 1; P2, Patient 2; R1, Razor 1; R2, Razor 2; R3, Razor 3.

needs to be further investigated. Finally, the cross-transmission involved a small number of isolates with the same sequence type. Therefore, further research is needed to account for the genetic diversity of CRKO complex bacteria.

To conclude, a cross-transmission of CRKO infections caused by contaminated preoperative shaving razors was confirmed during emergency neurosurgery, and revealed that contaminated shaving razors can transmit CRKO. Whenever hair removal is necessary, it should be removed in the proper area, and clippers may be a more proper alternative to razors (Knudsen et al., 2022; Seidelman et al., 2023). Chromogenic-based selective medium is a sensitive and convenient means to rapidly detect suspected isolates of carbapenem-resistant organisms in an epidemic or outbreak investigation (Alizadeh et al., 2018). We recommend applying WGS technology to track the microbial movement from the original to the infection site. Findings of this study will contribute to the understanding of microbial transmission in surgery and improving of infection prevention and control and patient care.

Data availability statement

The raw sequence data in this study can be found in the online repository. The name of the repository and accession number can be found below: NCBI Sequence Read Archive, PRJNA1171638.

Ethics statement

The studies involving humans were approved by Ethical Committee of The Second Affiliated Hospital of Anhui Medical University (YX2023-102). The studies were conducted in accordance with the local legislation and institutional requirements. The participants provided their written informed consent to participate in this study.

Author contributions

Y-LW: Conceptualization, Formal Analysis, Funding acquisition, Project administration, Supervision, Writing – original draft, Writing – review & editing. Y-LJ: Conceptualization, Funding acquisition, Investigation, Methodology, Writing – original draft. Y-YL: Conceptualization, Methodology, Writing – review & editing. L-LL: Data curation, Investigation, Writing – review & editing. Z-PL: Data curation, Investigation, Writing – review & editing. DL: Data curation, Investigation, Writing – review & editing. J-HT: Data curation, Formal Analysis, Investigation, Writing – review & editing. X-QH: Formal Analysis, Methodology, Writing – review & editing. W-HZ: Formal Analysis, Methodology, Writing – review & editing. W-WC: Formal Analysis, Funding acquisition, Methodology, Writing – review & editing. XZ: Funding acquisition, Methodology, Writing – review & editing. WH: Conceptualization, Formal Analysis, Project administration, Writing – original draft, Writing – review & editing.

Funding

The author(s) declare that financial support was received for the research, authorship, and/or publication of this article. This study was supported by the National Natural Science Foundation of the Republic of China (No. 82202572), the Anqing municipal medical category of science and technology project (No. 2023Z2019), and the Natural Science Research Project Funding of Higher Education Institutions of Anhui Province (No. KJ2021A0321, No. KJ2021A0332; No. 2023AH053175).

Conflict of interest

The authors declare that the research was conducted in the absence of any commercial or financial relationships that could be construed as a potential conflict of interest.

Publisher's note

References

Alizadeh, N., Rezaee, M. A., Kafil, H. S., Barhaghi, M. H. S., Memar, M. Y., Milani, M., et al. (2018). Detection of carbapenem-resistant Enterobacteriaceae by chromogenic screening media. *J. Microbiol. Methods* 153, 40–44. doi: 10.1016/j.mimet.2018.09.001

Bankevich, A., Nurk, S., Antipov, D., Gurevich, A. A., Dvorkin, M., Kulikov, A. S., et al. (2012). SPAdes: a new genome assembly algorithm and its applications to single-cell sequencing. *J. Comput. Biol.* 19, 455–477. doi: 10.1089/cmb.2012.0021

Bashaw, M. A., and Keister, K. J. (2019). Perioperative strategies for surgical site infection prevention. *AORN J.* 109, 68–78. doi: 10.1002/aorn.2019.109.issue-1

Coil, D., Jospin, G., and Darling, A. E. (2015). A5-miseq: an updated pipeline to assemble microbial genomes from Illumina MiSeq data. *Bioinformatics.* 31, 587–589. doi: 10.1093/bioinformatics/btu661

Dabernig-Heinz, J., Wagner, G. E., Prior, K., Lipp, M., Kienesberger, S., Ruppitsch, W., et al. (2024). Core genome multilocus sequence typing (cgMLST) applicable to the monophyletic Klebsiella oxytoca species complex. *J. Clin. Microbiol.* 62, e0172523. doi: 10.1128/jcm.01725-23

Dai, Y., Zhang, C., Ma, X., Chang, W., Hu, S., Jia, H., et al. (2014). Outbreak of carbapenemase-producing Klebsiella pneumoniae neurosurgical site infections associated with a contaminated shaving razor used for preoperative scalp shaving. *Am. J. Infect. Control.* 42, 805–806. doi: 10.1016/j.ajic.2014.03.023

Guanghui, Z., Jing, L., Guojun, Z., and Hong, L. (2020). Epidemiology and risk factors of neurosurgical bacterial meningitis/encephalitis induced by carbapenem resistant Enterobacteriaceae. *J. Infect. Chemother.* 26, 101–106. doi: 10.1016/j.jiac.2019.07.023

Guzmán-Puche, J., Jenayeh, R., Pérez-Vázquez, M., Manuel-Causse Asma, F., Jalel, B., Oteo-Iglesias, J., et al. (2021). Characterization of OXA-48-producing Klebsiella oxytoca isolates from a hospital outbreak in Tunisia. *J. Glob Antimicrob. Resist.* 24, 306–310. doi: 10.1016/j.jgar.2021.01.008

He, K., Li, Y. Y., and Liu, H. L. (2024). Risk and protective factors associated with wound infection after neurosurgical procedures: A meta-analysis. *Int. Wound J.* 21, e14699. doi: 10.1111/iwj.14699

Kjær Hansen, S., Andersen, L., Detlefsen, M., Holm, A., Roer, L., Antoniadis, P., et al. (2021). Using core genome multilocus sequence typing (cgMLST) for vancomycin-resistant Enterococcus faecium isolates to guide infection control interventions and end an outbreak. *J. Glob Antimicrob. Resist.* 24, 418–423. doi: 10.1016/j.jgar.2021.02.007

Knudsen, M. J. S., Rubin, I. M. C., Gisselø, K., Mollerup, S., Petersen, A. M., Pinholt, M., et al. (2022). The use of core genome multilocus sequence typing to determine the duration of vancomycin-resistant Enterococcus faecium outbreaks. *APMIS.* 130, 323–329. doi: 10.1111/apm.v130.6

Kose, G., Tastan, S., Kutlay, M., and Bedir, O. (2016). The effects of different types of hair shaving on the body image and surgical site infection in elective cranial surgery. *J. Clin. Nurs.* 25, 1876–1885. doi: 10.1111/jocn.2016.25.issue-13pt14

Lee, K. S., Borbas, B., Plaha, P., Ashkan, K., Jenkinson, M. D., and Price, S. J. (2024). Incidence and risk factors of surgical site infection after cranial surgery for patients with brain tumors: A systematic review and meta-analysis. *World Neurosurg.* 185, e800–e819. doi: 10.1016/j.wneu.2024.02.133

Lee, C. R., Lee, J. H., Park, K. S., Jeon, J. H., Kim, Y. B., Cha, C. J., et al. (2017). Antimicrobial resistance of hypervirulent klebsiella pneumoniae: epidemiology, hypervirulence-associated determinants, and resistance mechanisms. *Front. Cell Infect. Microbiol.* 7, 483. doi: 10.3389/fcimb.2017.00483

Lee, I., Ouk Kim, Y., Park, S. C., and Chun, J. (2016). OrthoANI: An improved algorithm and software for calculating average nucleotide identity. *Int. J. Syst. Evol. Microbiol.* 66, 1100–1103. doi: 10.1099/ijsem.0.000760

Li, C., Zhou, P., Liu, Y., and Zhang, L. (2023). Treatment of ventriculitis and meningitis after neurosurgery caused by carbapenem-resistant enterobacteriaceae (CRE): A challenging topic. *Infect. Drug Resist.* 16, 3807–3818. doi: 10.2147/IDR.S416948

Lindgreen, S. (2012). AdapterRemoval: easy cleaning of next-generation sequencing reads. *BMC Res. Notes.* 2, 337. doi: 10.1186/1756-0500-5-337

Liu, W. J., Duan, Y. C., Chen, M. J., Tu, L., Yu, A. P., and Jiang, X. L. (2022). Effectiveness of preoperative shaving and postoperative shampooing on the infection rate in neurosurgery patients: A meta-analysis. *Int. J. Nurs. Stud.* 131, 104240. doi: 10.1016/j.ijnurstu.2022.104240

Luo, R., Liu, B., Xie, Y., Li, Z., Huang, W., Yuan, J., et al. (2012). SOAPdenovo2: an empirically improved memory-efficient short-read *de novo* assembler. *Gigascience.* 1, 18. doi: 10.1186/2047-217X-1-18

Magni, F., Al-Omari, A., Vardanyan, R., Rad, A. A., Honeyman, S., and Boukas, A. (2023). An update on a persisting challenge: a systematic review and meta-analysis of the risk factors for surgical site infection post craniotomy. *Am. J. Infect. Control.* 52, 650–658. doi: 10.1016/j.ajic.2023.11.005

Mustafa, A. S. (2024). Whole genome sequencing: applications in clinical microbiology. *Med. Princ Pract.* 33, 185–197. doi: 10.1159/000538002

Neog, N., Phukan, U., Puzari, M., Sharma, M., and Chetia, P. (2021). Klebsiella oxytoca and emerging nosocomial infections. *Curr. Microbiol.* 78, 1115–1123. doi: 10.1007/s00284-021-02402-2

Nordmann, P., Naas, T., and Poirel, L. (2011). Global spread of carbapenemase-producing enterobacteriaceae. *Emerg. Infect. Dis.* 17, 1791–1798. doi: 10.3201/eid1710.110655

Perry, J. D. (2017). A decade of development of chromogenic culture media for clinical microbiology in an era of molecular diagnostics. *Clin. Microbiol. Rev.* 30, 449–479. doi: 10.1128/CMR.00097-16

Saha, R., Farrance, C. E., Verghese, B., Hong, S., and Donofrio, R. S. (2013). Klebsiella michiganensis sp. nov., a new bacterium isolated from a tooth brush holder. *Curr. Microbiol.* 66, 72–78. doi: 10.1007/s00284-012-0245-x

Schweizer, C., Bischoff, P., Bender, J., Kola, A., Gastmeier, P., Hummel, M., et al. (2019). Plasmid-mediated transmission of KPC-2 carbapenemase in enterobacteriaceae in critically ill patients. *Front. Microbiol.* 10, 276. doi: 10.3389/fmicb.2019.00276

Seidelman, J. L., Mantyh, C. R., and Anderson, D. J. (2023). Surgical site infection prevention: A review. *JAMA.* 329, 244–252. doi: 10.1001/jama.2022.24075

Tang, L. M., and Chen, S. T. (1995). Klebsiella oxytoca meningitis: frequent association with neurosurgical procedures. *Infection.* 23, 163–167. doi: 10.1007/BF01793857

Tanner, J., and Melen, K. (2021). Preoperative hair removal to reduce surgical site infection. *Cochrane Database Syst. Rev.* 8, CD004122. doi: 10.1002/14651858.CD004122.pub5

Tompkins, K., and van Duin, D. (2021). Treatment for carbapenem-resistant Enterobacterales infections: recent advances and future directions. *Eur. J. Clin. Microbiol. Infect. Dis.* 40, 2053–2068. doi: 10.1007/s10096-021-04296-1

Tvedt, C., Sjetne, I. S., Helgeland, J., Løwer, H. L., and Bukholm, G. (2017). Nurses' reports of staffing adequacy and surgical site infections: A cross-sectional multi-centre study. *Int. J. Nurs. Stud.* 75, 58–64. doi: 10.1016/j.ijnurstu.2017.07.008

Velnar, T., Kocivnik, N., and Bosnjak, R. (2023). Clinical infections in neurosurgical oncology: An overview. *World J. Clin. Cases.* 11, 3418–3433. doi: 10.12998/wjcc.v11.i15.3418

Walker, B. J., Abeel, T., Shea, T., Priest, M., Abouelliel, A., Sakthikumar, S., et al. (2014). Pilon: an integrated tool for comprehensive microbial variant detection and genome assembly improvement. *PloS One* 9, e112963. doi: 10.1371/journal.pone.0112963

Wayne, P. (2019). *Performance standards for antimicrobial susceptibility testing; 29th informational supplement. CLSI document M100-S29* (Maryland, USA: Clinical and Laboratory Standards Institute 2019).

World Health Organization *Global Guidelines for the Prevention of Surgical Site Infection. 2nd ed.* Available online at: https://www.who.int/publications/i/item/9789241550475 (Accessed 11 March 2024).

World Health Organization (2018). *Global Guidelines for the Prevention of Surgical Site Infection. 2nd ed.* (Geneva: World Health Organization).

Wyres, K., and Holt, K. (2022). Regional differences in carbapenem-resistant Klebsiella pneumoniae. *Lancet Infect. Dis.* 22, 309–310. doi: 10.1016/S1473-3099(21)00425-4

Yang, J., Long, H., Hu, Y., Feng, Y., McNally, A., and Zong, Z. (2022). Klebsiella oxytoca complex: update on taxonomy, antimicrobial resistance, and virulence. *Clin. Microbiol. Rev.* 35, e0000621. doi: 10.1128/CMR.00006-21

Frontiers in
Cellular and Infection Microbiology

Investigates how microorganisms interact with their hosts

Explores bacteria, fungi, parasites, viruses, endosymbionts, prions and all microbial pathogens as well as the microbiota and its effect on health and disease in various hosts.

Discover the latest Research Topics

See more →

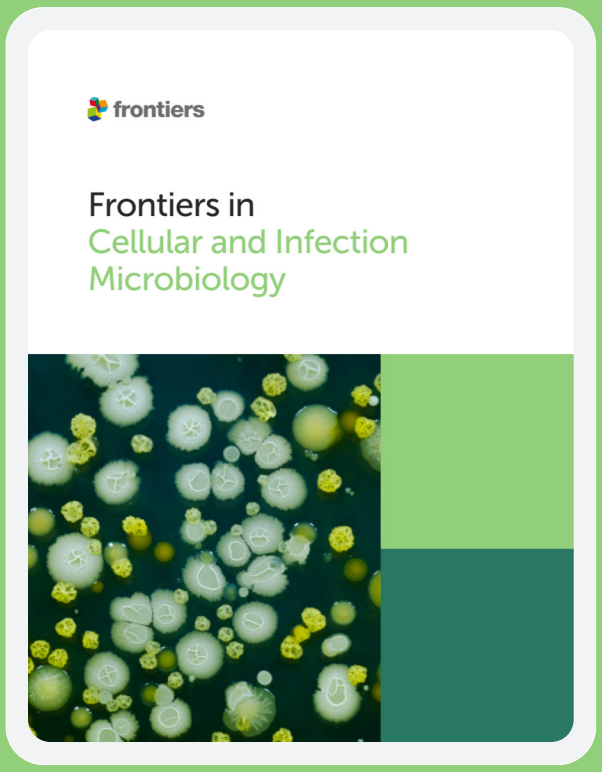

Frontiers

Avenue du Tribunal-Fédéral 34
1005 Lausanne, Switzerland
frontiersin.org

Contact us

+41 (0)21 510 17 00
frontiersin.org/about/contact